UNIVERSITY COLLEGE LONDON

UCL INSTITUTE OF NEUROLOGY

Department of Molecular Neuroscience

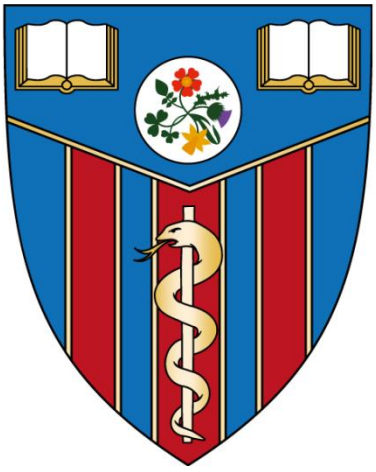

FULL GENOME ANALYSIS OF MICROGLIAL ACTIVATION; RAMIFICATIONS OF *TREM2*

Thesis submitted for the degree of Doctor of Philosophy

By,
Claudio N Villegas Llerena
2017

Supervisors,
Prof John Hardy
Dr Jennifer Pocock

DECLARATION

I, Claudio Nicolas Villegas Llerena, confirm that the work presented in this thesis is my own. Where information has been derived from other sources, I confirm that this has been indicated in the thesis.

ABSTRACT

Neuroinflammation is a pathological hallmark of Alzheimer's disease (AD) and it is well established that microglia, the brain's resident phagocytes, are pivotal for the immune response observed in AD. In the healthy brain, microglia attack and remove pathogens and cell debris, but have been shown to become reactive in AD. An apparent link between microglia and AD is Amyloid β (Aβ), which accumulates in the plaques observed in the brains of AD patients and has been reported as a microglia activator.

Genome Wide Association Studies (GWAS) have allowed the identification of more than 20 genetic risk associations to AD. Many of these associations highlight the importance of immune pathways (and others) in AD. More recently, the identification of mutations in *TREM2* (Triggering Receptor Expressed on Myeloid Cells 2), a gene exclusively expressed by microglia in the brain, has brought microglial activation and dysfunction back to the attention of the AD community.

The main focus of this study is to understand microglial activation elicited by different stimuli -including Aβ1-42 monomers, oligomers and fibrils- with regards to their inflammatory activation status (M1, M2 or other) and whole-genome expression profile. To this end, the mouse-derived BV2 cell line was used to assess gene expression changes during microglial activation. Data shows that M1 and M2 activators alter gene expression of AD-associated genes in a manner that is potentially detrimental for AD progression.

A second objective of this thesis was to use the CRISPR/Cas9 gene editing technology for the generation of *Trem2*-deficient BV2 cell lines. As a result, *Trem2 +/-* (haploinsufficient) and *Trem2 -/-* (knockout) BV2 cell lines were generated. Subsequently, these cell lines were characterised in terms of their phagocytic, proliferation, migration, cytokine release capacities and whole genome expression. In consequence, this study provides new and well-characterised *in vitro* models for the study of *Trem2* function.

ACKNOWLEDGEMENTS

I would like to wholeheartedly thank my supervisors, Prof John Hardy and Dr Jennifer Pocock, for giving me the opportunity to work in their groups. I am very grateful for their support and guidance throughout the course of my PhD. I would also like to thank the Pocock lab team; 'Dr Piers', Pablo, Kat, Matt, Anna and Alex. Many thanks for your help, scientific advice and for making the lab a fun place to work in. Alex, you have been a great PhD colleague/friend and I am terribly sorry about ever creating the B5 cells!

My sincere gratitude to all people who do science at 1 Wakefield Street and go to the Harrison's pub; including the Selina's, Guerreiro-Bras', Rohan's, Warner's and Patani's groups. Particular thanks go to Ellie, Bimali, Celia and Charlie. Their advice and friendship (and sometimes, reagents) have made my PhD a lot less stressful. I would also like to thank Prof Smith's lab for making the 2nd floor a friendly place, particularly Dimitra, Mario, Kim, Charlotte and Sharmeen. In addition, I would like to thank Mar and Seb, from the Molecular Neuroscience Dept., for their help with gene expression experiments and general advice.

My PhD, and my life, has been greatly enriched by the wonderful people, I was fortunate to meet during these past 4 years. Thank you, Alice, Vitaly, Mattia, Chris, Natalia, Martha, Khaled, Alastair and the ION's 5-a-side postgraduate team (Matt, Diego, Seb and all the others). A big thank you also to Sara, Eva and Leyla, your foodie-ness and friendship have made of London a familiar place. A collective thank you to all members of the University of London Archery Club, you have been pivotal in maintaining my sanity levels just about right (or maybe not); especially Bridget, Lifei, Dom, Richard, Aylish, Shabnam, Julie, Dr O'connell and Jay.

Friends are the family that we get to choose and in that I have chosen 12 brothers (you know who you are). I could not have finished my PhD without your constant cheering me on through difficult days and without the laughs we share. Gracias hermanos!

I am very grateful to my family, especially Tío Danny, Tía Dora, Tío Frank, Tía Luz and my grandparents as well. I am also super thankful to my ever-expanding nuclear family; Cuchi (that's my Mom), Dad, Javier, Martin, Mehnaz, Maria, Lyby, Abi, Laila and Alex. Thank you for your love and faith in me. I am also thankful to the Paredes-Moscosso family for their support and encouragement, especially to Anna-Lu.

The biggest of thank-yous goes to my wonderful girlfriend, Sol, whose love, patience, support and scientific advice have been fundamental in completing my PhD. Thank you for inspiring me to be a better person and laughing at my jokes. Finally, I thank God for the opportunities I have been given, for looking after my family and me, and for what comes next.

TABLE OF CONTENTS

LIST OF FIGURES

LIST OF TABLES

ABBREVIATIONS

7AAD	7-Aminoactinomycin D
APC	Antigen presenting cell
BMDMs	Bone-marrow-derived macrophages
BSA	Bovine serum albumin
Cas9	CRISPR associated protein 9 (wild type)
Cas9n	CRISPR associated protein 9 nickase mutant
cDNA	Complementary deoxyribonucleic acid
CFSE	Carboxyfluorescein succinimidyl ester
CRISPR	Clustered Regularly Interspaced Short Palindromic Repeats
CSF	Cerebrospinal fluid
CSF-1R	Colony stimulating factor-1 receptor
DAVID	Database for Annotation, Visualization and Integrated Discovery
DMSO	Dimethyl sulfoxide
DNA	Deoxyribonucleic acid
dNTP	Deoxyribonucleotide triphosphate
DSBs	DNA double stranded breaks
dsDNA	Double stranded DNA
EDTA	Ethylenediaminetetraacetic acid
EGFP	Enhanced Green Fluorescent Protein
ELISA	Enzyme-Linked Immunosorbent Assay
ER	Endoplasmic reticulum
FACS	Fluorescence activated cell sorting
FBS	Foetal bovine serum
FDR	False discovery rate
FTD	Frontotemporal dementia
GAPDH	Glyceraldehyde 3-phosphate dehydrogenase
gDNA	Genomic DNA
GFAP	Glial fibrillary acidic protein
GFP	Green fluorescent protein
HD	Huntington’s disease
HDR	Homology-directed Repair
IFN	Interferon
IL	Interleukin
Indel	Insertion and/or deletion genetic modification
ITAM	Immunoreceptor tyrosine-based activation motif
ITIM	Immunoreceptor tyrosine-based inhibitory motif
kDa	Kilodalton
KO	Knock out (gene modification)
LPS	Lipopolysaccharide (also known as Endotoxin)
MARCO	Macrophage receptor with collagenous structure
MCI	Mild cognitive impairment
MFI	Mean fluorescence intensity
MNoV	Murine noroviruses
mRNA	Messenger RNA
MS	Multiple sclerosis
NGS	Next Generation Sequencing
NHD	Nasu–Hakola disease

ABBREVIATIONS

NHEJ	Non-Homologous End-Joining
NMD	Nonsense-mediated decay
nt	Nucleotide
NTF	Neurofibrillary tangles
OMIM	Online Mendelian Inheritance in Man
OR	Odds ratio
PBS	Phosphate buffered saline
PCR	Polymerase Chain Reaction
PD	Parkinson's Disease
PGN	Peptidoglycan
PI	Propidium iodide
PRRs	Pattern Recognition Receptors
PS	Phosphatidylserine
q.s.p.	Quantité suffisante pour (quantity sufficient for)
qPCR	Quantitative PCR
RAGE	Receptor for advanced glycation end products
RFLP	Restriction Fragment Length Polymorphism
RFU	Relative Fluorescence Units
RNA	Ribonucleic acid
RNS	Reactive nitrogen species
ROS	Reactive oxygen species
RPMI	Roswell Park Memorial Institute medium
RT	Room temperature
RT-PCR	Reverse Transcriptase PCR
SDS-PAGE	Sodium Dodecyl Sulphate Polyacrylamide Gel Electrophoresis
sgRNA	Small guiding RNA
SNP	Single nucleotide polymorphism
ssDNA	Single stranded DNA
ssODN	Single-Stranded Oligo Donor
TALEN	Transcription activator-like effector nuclease
TBE	Tris/Borate/EDTA buffer
TMM	Trimmed mean of M-values
TNF	Tumour necrosis factor
TREM2	Triggering Receptor Expressed On Myeloid Cells 2
UV	Ultraviolet
WT	Wild type
ZFN	Zinc finger nuclease

1 CHAPTER 1: Introduction

1.1 Alzheimer's disease

Alzheimer's disease (AD) is a neurodegenerative disorder and is the most common cause of dementia, accounting for 60-80% of all cases (Alzheimer's Association, 2014). It is estimated to affect 35 million people worldwide and this number is expected to double in the next 20 years (Wimo et al., 2013). The total number of people with AD (or other dementias) in Western countries is expected to increase dramatically as the population aged 65 and over continues to grow (Alzheimer's Association, 2018). By 2050, it is estimated that one in every five people will be over 65 (United Nations, 2015). Demographic aging and improved healthcare over the last decades are the main reasons behind this dramatic increase (Brookmeyer et al., 2007). The largest rise in dementia prevalence is projected to take place in low and middle income countries, where cases of cardiovascular disease, hypertension and diabetes are increasing (Prince, 2014).

Dementia is an umbrella term used to describe diseases and conditions which show decline in memory and/or other cognitive abilities, compromising the patient's ability to carry out everyday activities (Alzheimer's Association, 2014). In this sense, AD is characterised by progressive neuronal degeneration and synaptic loss leading to memory and motor impairment, difficulties with language and an overall decline in cognitive function. It eventually leads to mental and functional incapacity followed by death (Mayeux, 2010). Currently, there is no treatment to slow or stop AD (Alzheimer's Association, 2014).

1.1.1 Clinical features of AD

Many clinical features are associated with AD, the most essential being, the decline in cognitive abilities. This feature has an insidious onset with a subsequent gradual progression throughout the different stages of disease development. AD's progression averages from 7 to 10 years since diagnosis and concludes with the patient's death. Loss of recent memory is the most well-known feature of AD, but other cognitive deficits are also apparent; executive dysfunction, language dysfunction, visuospatial difficulties, and loss of insight and personality changes. More advanced stages of the disease are characterised by obvious difficulties with memory (including long term memory), withdrawal from social activities and basic daily activities (e.g. bathing, dressing) and the need for supervision or assistance. In the final stages of the disease, patients are completely dependent on caregivers, become bedbound and unable to swallow or control bodily functions (Reviewed by Holtzman et al., 2011).

1.1.2 **Pathological features of AD**

At the macroscopic level, patients' brains present extensive atrophy. The most affected regions are those first affected by tau pathology (discussed in the next paragraphs), such as the entorhinal cortex, the hippocampus and the amygdala. The basal ganglia and cerebellum show no visible atrophy, although they may present some Aβ deposition (discussed in the next paragraphs). Both tau and Aβ pathologies are strongly associated with synapse loss, while neuronal loss is typically seen in the most affected areas. Cholinergic synapses are particularly affected by Aβ early neurotoxicity with cholinergic neurons located at the nucleus basalis of Meynert, which are the main neurons affected in AD (Wong et al., 1999, Bell et al., 2006, Whitehouse et al., 1981). Cholinergic synaptic loss has been shown to highly correlate with the cognitive impairment seen in AD patients (Selkoe, 2002). Said patients also show a consistent depigmentation of the locus coeruleus in the brainstem of AD brains (Calderon-Garciduenas and Duyckaerts, 2017). It is worth keeping in mind that since the original description by Alois Alzheimer (Moller and Graeber, 1998), and in the absence of fully validated biomarkers for the disease, AD definitive diagnosis continues to be dependent on the autopsy of the patients' brains (Perl, 2010).

At the microscopic level, there is accumulation of extracellular amyloid plaques, intracellular neurofibrillary tangles (NTF) and significant neuronal loss (Mayeux, 2010). Amyloid plaques are mainly composed of amyloid β (Aβ) peptides, which are 38-43 amino acid peptides derived from the amyloid precursor protein (APP) (Golde et al., 2000). Aβ peptides are produced mainly in neurons through sequential cleavage of APP by two proteases; β- and γ-secretases (O'Brien and Wong, 2011). Aβ 1-42 (Aβ42), is generally present in tissues and body fluids at levels 5–10% of those of Aβ40, yet it appears to be central to initiating Aβ aggregation as it is more hydrophobic and prone to aggregate (Holtzman et al., 2011). Within plaques, Aβ is found in insoluble conformations (both fibrillar and oligomeric). Accumulation of Aβ in the brain, due to imbalance between production and clearance of this peptide, is thought to be the driving force behind AD's neurodegenerative mechanisms. This postulate is known as the amyloid hypothesis (Hardy and Allsop, 1991, Hardy and Higgins, 1992, Selkoe, 1991). The exact mechanisms by which Aβ may drive neurodegeneration remain largely unknown, but accumulating evidence points to Aβ as the cause for overstimulation of the glutamatergic neurotransmission system, leading to considerable synaptic loss and cell death (Anggono et al., 2016, Wang and Reddy, 2017). Other mechanisms may also contribute to AD's neurodegeneration.

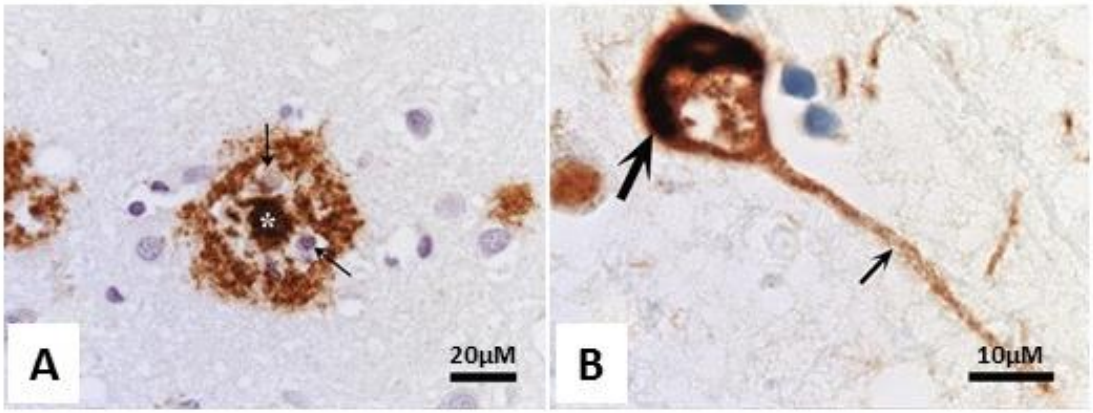

Figure 1.1 Aβ plaques and Neurofibrillary tangles (NTF). A) Aβ plaque in a brain section stained with 6F3D Dako antibody. The centre of the plaque is occupied by a dense focal deposit (asterisk). The surrounding clear area is occupied by macrophages (arrows). The outer halo is composed of less dense Aβ. B) Neurofibrillary tangle filling the cell body (thick arrow) and the apical dendrite (small arrow) of a neuron. Brain section stained with anti-tau AT8 antibody. Modified from Calderon-Garciduenas and Duyckaerts (2017).

In addition to Aβ plaque deposition in the extracellular space, intracellular neurofibrillary tangles (NTFs) are present in specific brain regions. NTFs are composed mainly of hyperphosphorylated tau protein. The latter is synthesised by neuronal and glial cells and its normal function is to bind to tubulin and stabilize microtubules, but becomes prone to self-aggregation following hyperphosphorylation (Holtzman et al., 2011). Another pathological hallmark of AD is the loss of synapses and selective neuronal death ocurring mainly in the hippocampus and the temporal, parietal and frontal neocortex (Holtzman et al., 2011), representing some of the most vulnerable brain areas in AD.

Inflammation in the brain is another pathological hallmark of AD (Rohn, 2013) and it is established that microglia, the brain's resident phagocytes, are pivotal for the inflammation/immune response in AD and other neurological diseases. Microglia act normally as sentinel cells, attacking and removing pathogens and cell debris (Wyss-Coray, 2006), but become reactive in AD (Pocock et al., 2002).

1.1.3 **AD diagnosis**

Patients are usually diagnosed by the primary care physician. In the US, there is no single test for the diagnosis of AD, and physicians (often with the help of specialists such as neurologists and geriatricians) use a myriad of approaches for diagnosis (Alzheimer's Association, 2018). In the UK, the National Institute for Health and Care Excellence (NICE) provides guidelines for the diagnosis of dementia. The diagnosis takes into account the patient's medical, family and psychiatric histories, as well as changes in cognition and behaviour (Cordell et al., 2013). Clinical assessment depends on the use of cognitive tests, such as the Mini-cog, the General Practitioner Assessment of

Cognition, the Memory Impairment Screen and the Informant Questionnaire on Cognitive Decline in the Elderly (Schaffer et al., 2015). The Mini-Cog asks the patient to remember a list of unrelated words, draw a clock and then recall the list of words. This test has a 99% sensitivity for AD diagnosis and it is not affected by confounding factors such as education level or language of the patient8. In the UK, the NICE guidelines recommend the use of any of the following standardised cognitive tests: the Mini Mental State Examination, the 6-item Cognitive Impairment test, the General Practitioner Assessment of Cognition or the 7-minute screen (NICE, 2018).

Changes in the brain of AD patients start almost 20 years before symptoms arise and can be used for clinical diagnosis. Therapeutic intervention during this asymptomatic phase could potentially slow or even prevent the progression of AD. Taking this early asymptomatic phase into account, in 2011, the Alzheimer's association (United States) proposed a new set of criteria for AD diagnosis which included two main additions. The first addition recognised three different stages in AD progression; preclinical AD (asymptomatic phase), mild cognitive impairment (MCI) due to AD, and dementia due to AD. The MCI stage of the disease starts when noticeable symptoms appear and precede the onset of dementia by 3-4 years. Lastly, the dementia stage starts when daily function is considerably compromised (Alzheimer's Association, 2013). The second addition to the criteria was the inclusion of biomarker tests for diagnosis, treatment monitoring and for research purposes. Nevertheless, more research will have to be carried out in order to validate the use of biomarkers in AD diagnosis (Bloudek et al., 2011).

1.2 **AD risk**

AD is a complex multifactorial disease influenced by several genetic and environmental (non-genetic) factors (Reitz and Mayeux, 2014). As such, this section will discuss the impact of many of the most important risk factors for AD.

1.2.1 **Genetic AD risk**

Classically, AD is classified into two groups according to the age of onset of the disease; Early Onset AD (EOAD, onset <65 years) which accounts for 2-10% of cases, and Late-Onset AD (LOAD, onset >65 years) which accounts for the majority of cases (Cacace et al., 2016). Clinical presentation in both groups is similar; nevertheless, EOAD is associated with a quicker disease progression and a Mendelian pattern of inheritance, although this is not true for the great majority of EOAD cases.

LOAD is a complex and heterogeneous disorder with an estimated heritability of 70-80%, while EOAD is almost entirely genetically determined with a heritability of 92-100%. Remarkably, 35-60% of EOAD patients have at least one first-degree relative who is also

affected. Interestingly, in 10-15% of those familial EOAD patients the mode of inheritance is autosomal dominant (reviewed by Cacace et al. (2016)). Autosomal-dominant forms of AD (also referred as familial AD) are considered rare as they account for less than 1% of all cases (Van Cauwenberghe et al., 2016).

Genetic linkage analysis of EOAD families has identified the only fully penetrant mutations to cause AD in three genes: amyloid precursor protein gene (*APP,* Goate et al. (1991)), presenilin 1 gene (*PSEN1,* Sherrington et al. (1995)) and presenilin 2 gene (*PSEN2,* Levy-Lahad et al. (1995)). Together, mutations in these three genes account for 5-10% of EOAD cases (Van Cauwenberghe et al., 2016). Moreover, these 3 genes have highlighted the relevance of Aβ production and processing in AD (Guerreiro et al., 2012).

LOAD is considered a multifactorial disease with a strong genetic predisposition component (Van Cauwenberghe et al., 2016). Genetic linkage analysis of LOAD families associated the *APOE* gene with an increased AD risk (Corder et al., 1993). APOE is a lipid-binding protein and it occurs in three different isoforms: *APOEε2*, *APOEε3* and *APOEε4*. The latter isoform has been associated with an augmented risk of LOAD (Figure 1.5), increasing the risk 3-fold for individuals carrying one copy of the allele and 12-fold if carrying two copies (Carmona et al., 2018).

The advent of new genetic screening technologies has allowed the identification of new genetic risk factors for AD. Genome Wide Association Studies (GWAS) have identified >20 genetic loci with low risk effects (Figure 1.5). Most of these genes can be broadly grouped according to their putative biological functions: immune response (*CR1, CD33, MS4A, CLU, ABCA7, EPHA1, INPP5D* and *HLA-DRB5-HLA-DRB1*), endocytosis (*BIN1, PICALM, CD2AP, EPHA1*, and *SORL1*) and lipid biology (*CLU, ABCA7* and *SORL1*) (Karch and Goate, 2015, Guerreiro et al., 2013a).

More recently, by using whole-exome and whole-genome sequencing strategies, two groups simultaneously reported a low frequency mutation in the *TREM2* (triggering receptor expressed in myeloid cells 2 protein) able to confer a moderate to high risk of developing AD (odds ratio ~4–5): p.Arg47His (R47H) (Guerreiro et al., 2013b, Jonsson et al., 2013). *TREM2* is almost exclusively expressed by microglial cells in the brain (Zhang et al., 2014, Colonna, 2003) and has been shown to regulate phagocytic activity and pro-inflammatory responses (Takahashi et al., 2005a, Colonna, 2003). The identification of rare coding variants in *TREM2* has provided further support for the involvement of immune response mechanisms and neuroinflammation in AD, and has pointed to microglia as main players in AD pathogenesis.

Similarly to *TREM2*, a recent study of LOAD families using a whole-exome sequencing approach identified genetic variants associated with AD risk in the phospholipase D3 (*PLD3*) gene. In this study, the *PLD3* variant V232M (rs145999145) increased the risk of AD by 2-fold (Cruchaga et al., 2014). In a recent communication report, Fazzari et al. (2017) showed that PLD3 is highly expressed in the pyramidal neurons of the cortex and hippocampus of mice using western blot analysis, while gene expression analysis carried out by Zhang et al. (2014) showed that this gene is expressed mainly in microglial cells. PLD3 is a non-classical phospholipase and is believed to be associated with pathways related to target cell innervation, neurotransmission and neuronal survival (Wang et al., 2015a). Its expression has been shown to inversely correlate with APP levels and Aβ secretion (Cruchaga et al., 2014). Nonetheless, further studies will be needed to validate this association as many studies have shown contradictory results (Carmona et al., 2018).

Down-syndrome, which is the most common chromosomal abnormality (Bayer et al., 1999), also confers a higher risk of developing AD. Down-syndrome is caused by the triplication of the chromosome 21, which carries the *APP* gene. Increased expression of this gene, results in increased production of Aβ, which is considered to be one of the initiators of neurodegeneration in AD. In the last decades, the lifespan of patients with down-syndrome has increased to 55-60 years and it is estimated that around 70% of them will suffer from EOAD (Hartley et al., 2015).

1.2.2 **Non-genetic AD risk**

Age is the strongest non-genetic risk factor for AD (Hickman et al., 2016). As mentioned before, the age of 65 is used to arbitrarily classify the disease as EOAD (onset before 65) or LOAD (onset after 65) (Carmona et al., 2018). The most common form of AD is LOAD (~90% of cases), with fewer cases of EOAD (~10%) being reported (Cacace et al., 2016). AD prevalence rise exponentially with age, increasing markedly after the age of 65. Between the ages 60 to 85 there is approximate 15-fold increase in the prevalence of dementias, mainly AD (Evans et al., 1989). Brookmeyer et al. (1998) estimated the age-specific incidence rates for AD based on studies carried out in different cities of the USA (Boston, Framingham, Rochester, and Baltimore). The reported rates doubled every 5 years after the age of 60, rising from 0.17% per year at age 65 to 0.71, 1.0, and 2.92% per year at 75, 80, and 85 years, respectively (Brookmeyer et al., 1998). Finally, in its most recent meta-analysis, Alzheimer's Disease International has reported that the incidence of dementia doubles with every 6.3 year increase in age, from 3.9 per 1000 person-years at age 60-64 to 104.8 per 1000 person-years at age >90 (Prince et al., 2015).

Other non-genetic risk factors include cardiovascular disease, hypertension, Type 2 diabetes and traumatic brain injury, among others. Patients that suffer with clinical or sub-clinical cardiovascular disease have been shown to have poorer cognitive function than healthy individuals (Breteler et al., 1994, Kuller et al., 1998). Nevertheless, studying the role of cardiovascular disease in AD is complicated by the existence of many confounding factors (Hickman et al., 2016). Regarding hypertension, many observational studies have shown that increased hypertension is associated with an accelerated cognitive decline and an increased risk of AD (Kalaria, 2010). Similarly, many observational studies have shown that type 2 diabetes (diabetes mellitus) can double the risk of AD (Leibson et al., 1997, Luchsinger et al., 2001, Ott et al., 1999). Another important non-genetic risk factor is traumatic brain injury, which is known to shorten the time to AD onset (Plassman et al., 2000). Traumatic brain injury is currently considered the strongest environmental risk factor for AD (Shively et al., 2012, Fleminger et al., 2003). Recent studies have proposed that chronic inflammation within the brain parenchyma may be a possible link between traumatic brain injury and AD (Johnson et al., 2013, Smith et al., 2013).

On the other hand, protective factors include cognitive stimulation and high educational achievement, both of which improve the cognitive reserve (Carlson et al., 2008, Fratiglioni and Wang, 2007). Physical exercise has also been reported to reduce the risk of developing dementia and to improve cognition in dementia patients (Groot et al., 2016, Akbaraly et al., 2009, Rovio et al., 2005). The protective effect of diets rich on antioxidants and polyunsaturated fatty acids has shown inconclusive results, with some studies showing a positive correlation and others showing no such association (Kalmijn et al., 1997, Roberts et al., 2010, Engelhart et al., 2002).

1.3 **Neuroinflammation in AD**

Inflammation, in a general sense, serves a protective role by eliminating pathogens and tumours as well as promoting tissue repair and clearance of debris. Nevertheless, inflammation can also be detrimental as a consequence of unintended side effects of the protective processes (Brown and Neher, 2010). Neuroinflammation, the inflammation of the CNS (Central Nervous System), is a pathological hallmark of many neurological conditions, including AD (Glass et al., 2010, Rohn, 2013).

The role of neuroinflammation in AD pathogenesis is supported by recent genetic findings which associate mutations in immune related genes –including *CR1, CD33, MS4A, CLU* and *TREM2* among others– with risk of AD (Heneka et al., 2015). Furthermore, epidemiological studies show that patients without dementia who take non-steroidal anti-inflammatory drugs (NSAIDs) have a lower risk of AD and PD (Parkinson's

disease) (Fernandes et al., 2014). Consequently, understanding the interaction between the immune and nervous systems may be pivotal for delaying or preventing AD and other neurodegenerative diseases (Heneka et al., 2015).

1.3.1 **Cellular mediators of Neuroinflammation in AD**

Neuroinflammation is characterised by microglial activation, changes in the BBB (Blood-Brain Barrier) permeability, infiltration of peripheral immune cells, secretion of inflammatory cytokines, neuronal cell damage and cell death. Microglial cells have been shown to be the major mediators of inflammation/immune response in AD progression; nonetheless, there is also indication that other cell types are involved, including astrocytes, neurons, endothelial cells and cells of the adaptive immune system (e.g. T-cells) (Gonzalez et al., 2014, Lucin and Wyss-Coray, 2009).

1.3.1.1 ***Microglia***

Microglia, the CNS resident phagocytes, are the predominant immune cell type of a healthy brain (Brown and Neher, 2010). These cells are important for normal brain development, maturation and homeostasis; they are also the first responders in case of CNS infection (Labzin et al., 2018). Microglia normally act as sentinel cells attacking and removing pathogens and clearing cell debris (Wyss-Coray, 2006). For instance, microglial cells are capable of up-taking and degrading myelin debris (composed of cholesterol and phospholipids) which can promote their immune activation (Safaiyan et al., 2016). Microglial cells are distributed throughout the brain and constantly survey their local brain areas, using their highly motile processes to look for pathogens and cell debris while simultaneously providing factors that support tissue maintenance.

Microglia also contribute to the protection and remodelling of synapses (Heneka et al., 2015, Gonzalez et al., 2014). For example, microglial cells are required for the complement-dependent synaptic pruning (through the recognition of C1q and C3 molecules) during development. They are also able to phagocyte apoptotic cells during neurogenesis (through the recognition of receptors Axl and Mer) and support synapsis formation by releasing neurotrophic factors (reviewed by Labzin et al. (2018)).

Microglial cells can be activated by several pathological triggers, including apoptotic cells or proteinaceous aggregates (such as Aβ plaques). Once the pathological trigger is detected, cells become activated, migrate to the lesion site and initiate the immune response. Recognition of pathological triggers by microglial cells is mediated by stimulation of membrane receptors that recognize Danger-associated molecular patterns (DAMPS) or Pattern-associated molecular patterns (PAMPS) (Heneka et al., 2015). TLR's (Toll-like receptors) are a family of receptors capable of recognizing these

pathological triggers, such as LPS (lipopolysaccharide), flagellin or double-stranded RNA (Sica and Mantovani, 2012). Remarkably, it has been shown that these receptors also recognize endogenous and oxidised proteins (Kim et al., 2013a, Reed-Geaghan et al., 2009). Activation of TLR's involves intracellular recruitment of adapter proteins, MyD88 and TRIF, and the subsequent expression of pro-inflammatory cytokines and enzymes (Gonzalez et al., 2014).

Upon activation, microglial cells have a similar response to that of peripheral macrophages. For instance, macrophages stimulated by LPS, TNFα and/or IFNγ become classically activated and acquire an M1 phenotype (discussed later) which promotes the expression of several pro-inflammatory cytokines and enzymes that stimulate tissue inflammation. In contrast, exposure of macrophages to IL4, IL3 or IL10 "alternatively" activates them and promotes conversion to an M2 phenotype (anti-inflammatory) (Gonzalez et al., 2014).

In AD, microglia are able to bind to Aβ peptide monomers, oligomers and fibrils (discussed later) via membrane receptors (SCARA1, CD36, CD14, α6β1 integrin, CD47 and TLR's), which cause microglia to become activated and produce pro-inflammatory cytokines and chemokines (Heneka et al., 2015). Nevertheless, there is evidence showing that microglial cells surrounding Aβ plaques have an anti-inflammatory phenotype characterised by enhanced phagocytosis (Jimenez et al., 2008). Yet, in the majority of cases, AD patients will show a mixture of activation phenotypes (pro- and anti-inflammatory) (Gonzalez et al., 2014).

1.3.1.2 ***Astroglia***

Astrocytes are also involved in the regulation of the inflammation/immune responses and damage/repair mechanism in the CNS. Typically, astrocytes participate in the control and formation of neuronal synapses, turnover of neurotransmitters, control of neuronal energy and regulation of the BBB permeability (Gonzalez et al., 2014). Astrocytes also fulfil neuroprotective functions, including clearance of ROS (Reactive Oxygen Species) from their local brain area.

Astrocytes become reactive in response to pathological triggers (e.g. CNS injury), migrate to the damaged site and form the glial scar, a response denominated astrogliosis (Pekny et al., 2014). Astrogliosis is a neuropathological characteristic surrounding Aβ plaques in AD patients and animal models (Medeiros and LaFerla, 2013, Olabarria et al., 2010). *In vitro* studies have shown that astrocytes are capable of migrating towards Aβ deposists and clearing them (Wyss-Coray et al., 2003). Additionally, astrocytes can contribute to soluble Aβ clearance by paravenous drainage (Iliff et al., 2012).

Similarly to microglia, astrocytes release cytokines, interleukins, nitric oxide (NO) and other cytotoxic molecules in response to Aβ, thus aggravating the inflammatory environment (Heneka et al., 2015). Reactive astrocytes are characterised by an upregulation of GFAP (Glial fibrillary acidic protein) and functional impairment. An important feature of astrocytic activation is the production of chemokines (e.g. CCL2, CCL5, CX3CL1, etc.) which are involved in the recruitment of microglia, monocytes/macrophages, and T-cells into the inflamed site (Gonzalez et al., 2014). Inflammatory mediators produced by astrocytes could stimulate microglial cells, thus exacerbating microglial activation and neuronal death. Likewise, microglial inflammatory mediators could intensify astrocyte activation, generating a positive feedback loop (Gonzalez et al., 2014).

1.3.1.3 ***Neuron-microglia interactions***

Classically the study of neuroinflammation is centred on glial cells (microglia and astrocytes); nevertheless, recent evidence has shown an active bi-directional crosstalk between neurons and microglia. In this sense, it has been shown that after neuronal injury, hsp60 (heat shock protein 60) is released from necrotic and apoptotic cells inducing the production of the neurotoxic mediator NO (nitric oxide) in microglial cells (Lehnardt et al., 2008). Not only are pro-inflammatory signals exchanged, anti-inflammatory signals have also been shown to be involved in this crosstalk. This is the case for cell surface protein CD200 (expressed by microglia) and its receptor CD200R expressed on the surface of neurons. Interaction between these two proteins favours the downregulation of pro-inflammatory mediators and upregulation of anti-inflammatory mechanisms in microglia (Lue et al., 2010).

Another example is the interaction between the chemokine CX3CL1 (expressed by neurons) and its receptor CX3CR1 (expressed by microglia). CX3CL1 (also known as fractalkine) is expressed as a transmembrane protein that can be cleaved to produce a soluble isoform. This soluble isoform binds to the CX3CR1 receptor and downregulates pro-inflammatory mechanisms (Morganti et al., 2012). This wealth of evidence suggests that microglial activation is a tightly regulated mechanism and that this regulation can be directly exercised by neurons (Gonzalez et al., 2014).

1.3.1.4 ***T-cells***

Typically, cells of the adaptive immune system are not found in healthy brains. However, after neuroinflammatory processes have commenced (usually initiated by microglia), peripheral T-cells can infiltrate the CNS parenchyma, where they play a crucial role in many neurodegenerative diseases (Lucin and Wyss-Coray, 2009, Gonzalez et al., 2014). The role of infiltrating T-cells in neurodegeneration depends on the functional

phenotype they acquire. For example, in the presence of IL12, T-cells differentiate into T-helper 1 cells (Th1), which are associated with inflammation and neuronal damage in AD mouse models (Browne et al., 2013). Another example of a T-cell inflammatory phenotype associated with neuroinflammation is the Th17 phenotype, which is promoted by the presence of IL23 (Dardalhon et al., 2008).

T-cells can also acquire an anti-inflammatory phenotype known as, T-regulatory (T-reg). This phenotype is capable of modifying the inflammatory role of other T-cell phenotypes, and has been shown to attenuate neuroinflammation (Yang et al., 2013, Reynolds et al., 2010). There is compelling evidence showing that different T-cell phenotypes, particularly Th1 and Th17, participate in AD neurodegeneration (reviewed by Gonzalez and Pacheco (2014)). Moreover, infiltrating T-cells can be found in the proximity of Aβ plaques in AD patients and mouse models of the disease (Togo et al., 2002, Monsonego et al., 2006). Recent studies have shown that infiltrating T-cells favour increased microglial activation, Aβ deposition and impaired cognitive functions in mice (Browne et al., 2013). In a recent paper, Mrdjen et al. (2018) noted a marked increase in the frequency of T-cells in the brains of adult mice compared to geriatric mice (from 1.5% to 11.1%), suggesting a profound change in the cellular landscape of the CNS with aging.

1.3.2 **Non-cellular mediators and modulators of neuroinflammation**

1.3.2.1 ***Cytokines***

Cytokines are proteins produced by many cell types involved in inflammatory and immune responses; they are the principal mediators of communication among immune cells. Cytokines are involved in every step of neuroinflammation, including pro- and anti-inflammatory responses, chemoattraction and response to Aβ deposits. In AD, both microglia and astrocytes are considered the major sources of cytokines (Heneka et al., 2015).

In mouse models of AD, an increased concentration of Aβ is associated with augmented levels of pro-inflammatory cytokines including; TNFα, IL6, IL1α and GM-CSF (Patel et al., 2005). Similarly, microglial cells exposed to pre-aggregated Aβ1-42 have increased production of pro-inflammatory cytokines (IL1β, IL6, TNFα, MIP-1α and M-CSF) (Lue et al., 2001a). These and other results suggest that production of pro-inflammatory cytokines is stimulated by exposure of microglial cells to Aβ peptides and is necessary for Aβ clearance (reviewed by Heneka et al., 2015). Conversely, increased expression of the anti-inflammatory cytokine IL4 resulted in increased Aβ deposition in a mouse model of AD (Chakrabarty et al., 2012).

TNFα and IL1β are of particular interest for AD neurodegeneration. Synthesis and release of these two cytokines by microglia and astrocytes has been shown to stimulate expression of APP by glial cells (Rogers et al., 1999, Rogers et al., 2002, Lahiri et al., 2003a) and the conversion of APP into the pathological forms of Aβ (Selkoe, 2001, Avramovich et al., 2002, Lahiri et al., 2003b). Furthermore, microglia and astrocytes can be activated by amyloid plaques and fibrillary Aβ, which in turn increases the production of TNFα and IL1β by microglial cells (Bamberger et al., 2003, Combs et al., 2001). In consequence, this series of events creates a self-propagating cycle of APP production, Aβ deposition and further neuroinflammation, which drives disease progression (Frankola et al., 2011).

Many studies have shown that TNFα levels are elevated in biological fluids of AD patients compared to cognitively normal controls (Brosseron et al., 2014, Tarkowski et al., 2003, Swardfager et al., 2010). Moreover, TNFα and its receptor TNFRI have been shown to be increased in the post-mortem analysis of brains from patients with early-stage AD (Zhao et al., 2003). TNFα can contribute to AD's neurodegeneration by many different mechanisms, including; excitotoxicity (Olmos and Llado, 2014), synaptic loss (Poon et al., 2013, Olmos and Llado, 2014), stimulation of astrogliosis and microgliosis (Wang et al., 2015b) and exacerbated amyloidogenesis (Liao et al., 2004, Lahiri et al., 2003a, Blasko et al., 1999).

IL1β has been shown to be overexpressed by microglia and astrocytes surrounding Aβ plaques in AD human brains and mouse models, relative to age-matched controls (Boutajangout and Wisniewski, 2013, Hunter et al., 2012). Overexpression of IL1β has been demonstrated to exacerbate tau phosphorylation, tangle formation and impair synaptic plasticity (Pickering and O'Connor, 2007). IL1β has also been shown to affect BBB permeability, which can promote Aβ accumulation in the brain (Wang et al., 2014). However, sustained overexpression of IL1β is also able to modulate microglia-dependent plaque degradation *in vivo* and in *vitro* (Shaftel et al., 2007, Ghosh et al., 2013, Tachida et al., 2008). The role of IL1β in AD is likely to be more complex that initially thought.

1.3.2.2 ***Chemokines***

Chemokines are low-molecular-weight cytokines that stimulate leukocyte movement and tissue infiltration. In the brain, chemokines promote microglial migration to sites of injury and inflammation. In AD, upregulation of chemokines and their receptors has been reported in activated microglia (CCL2, CCR3 and CCR5) and activated astrocytes (CCL4) (Xia et al., 1998, Ishizuka et al., 1997). Similarly, microglial cells cultured from AD patients' autopsies showed upregulation of *CXCL8* (known as *IL8*), *CCL2* and *CCL3*

in response to Aβ stimulation (Lue et al., 2001b). Mouse models of AD have revealed that chemokines could also be implicated in modulation of the course of the disease, neuronal survival, Aβ plaque load and cognition (reviewed by Heneka et al., 2015).

1.3.2.3 ***Caspases***

Caspases are intracellular proteases involved in enzymatic cascades that promote cell apoptosis; some (such as caspase-1) can also drive inflammation. Increased concentration of caspase-1 has been reported in the brains of AD patients and in a mouse model of Aβ deposition. Furthermore, deficiency of caspase-1 (or NLRP3) in the same AD mouse model seemed to promote the conversion of microglial cells from a pro-inflammatory to an anti-inflammatory phenotype (Heneka et al., 2013). Caspase activity (caspase-8 and caspase-3/7) has also been reported in activated microglial cells from AD patients (Burguillos et al., 2011). Additionally, inhibition of caspase activation has been shown to have neuroprotective effects in AD mouse models (Rohn et al., 2009, Biscaro et al., 2012).

1.3.2.4 ***Complement system***

The complement system is composed of many serum and cell surface proteins that are part of the innate immune system and are primarily involved in the protection against pathogens. Activation of the complement system occurs via one of three pathways (classical, alternative and lectin pathways) and concludes in the opsonisation and lysis of the invading microorganism.

In the brain, microglia and astrocytes are the main cell types involved in complement protein production. In AD, components of the complement system have been shown to be associated with Aβ deposits (Strohmeyer et al., 2002). *In vitro*, Aβ peptides are able to activate the complement system via the alternative and classical pathways (Bradt et al., 1998). Recent genetic studies have associated two complement system components with increased risk of AD: clusterin (known as *CLU* or *ApoJ*) and the complement receptor 1 (*CR1*) (Lambert et al., 2009, Harold et al., 2009). These findings highlight the potential importance of the complement system in AD pathogenesis.

1.3.2.5 ***Nitric Oxide (NO) and Reactive Oxygen Species (ROS)***

Among many other effects, cytokine stimulation of microglia and/or astrocytes can induce the expression of the inducible nitric oxide synthase (iNOS) protein. This protein produces large quantities of NO, which can be toxic to neurons (Heneka et al., 2015). There is evidence of *iNOS* upregulation in brains of AD patients (Vodovotz et al., 1996), and *iNOS* gene knockout has been shown to be protective in AD mouse models (Nathan et al., 2005). Increased expression of *iNOS* in AD brains produces post-translational

protein modifications as a result of nitric oxide activity (e.g. nitration, S-nitrosylation and dityrosine formation) (Butterfield et al., 2007). Nitration of the Aβ peptide has been shown to induce aggregation and has been identified in the core of Aβ plaques (Kummer et al., 2011).

Phagocytic cells, such as macrophages or microglia, express a specific NADPH oxidase, called PHOX (known as phagocytic oxidase). Normally, it is highly expressed by microglia in healthy brains (non-inflamed). However, PHOX does not become activated unless acutely stimulated by inflammatory stimuli such as LPS or Aβ. Once stimulated, this protein produces high levels of extracellular superoxide (a ROS molecule) which can either dismutate to hydrogen peroxide or react with NO to produce peroxynitrite (Bal-Price et al., 2002). Both of these oxidants contribute to pathogen killing, but can also damage neurons (Brown and Neher, 2010).

1.4 Microglia diversity and modulation of activation states: M1 vs M2, are there any boundaries?

Microglial activation is a tightly regulated and complex process that results in different cellular phenotypes (Heneka et al., 2015). The notion of microglial activation has been borrowed from macrophage research. As macrophage-like cells (some even consider them a sub-type of macrophage) of the brain, microglia are responsible for regulation of the innate immune response in the CNS (Cherry et al., 2014).

In the periphery, macrophages have been typically categorised into two groups according to their activation status. The M1 phenotype or pro-inflammatory activation which is associated with the expression of cytotoxic genes, and the M2 phenotype or alternative activation which is characterised by expression of anti-inflammatory and tissue repair genes (Tang and Le, 2016). These two activation states represent the extremes of inflammatory responses (Figure 1.2). A third phenotype (M0) could be that of deactivated cells (associated with corticosteroids or TGFβ) (Heneka et al., 2015).

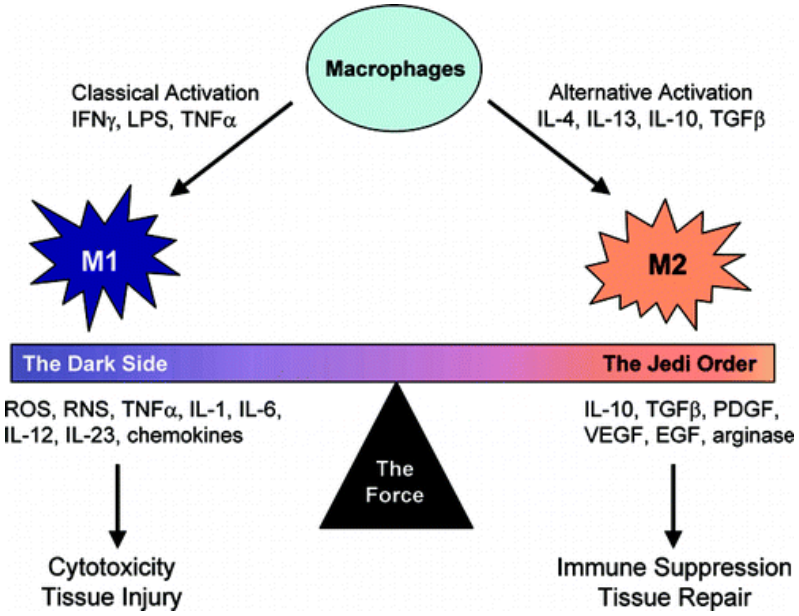

Figure 1.2 M1/M2 paradigm in macrophages. In response to inflammatory signals (e.g. IFNγ, LPS, IL4, etc.) macrophages have classically been regarded as acquiring one of two possible phenotypes: the M1 (pro-inflammatory) or M2 (anti-inflammatory). The M1 phenotype is associated with the release of cytotoxic and inflammatory mediators that contribute to tissue injury while the M2 phenotype promotes downregulation of inflammatory mediators and the initiation of tissue repair (Taken from Laskin, 2009).

The classical M1/M2 paradigm has been helpful to understand immune responses during acute infections, allergies, asthma and obesity (Chinetti-Gbaguidi and Staels, 2011). However, observations made during chronic inflammation, chronic infection and cancer progression suggest that macrophage activation has a more extensive repertoire than initially anticipated (Xue et al., 2014)(Figure 1.3).

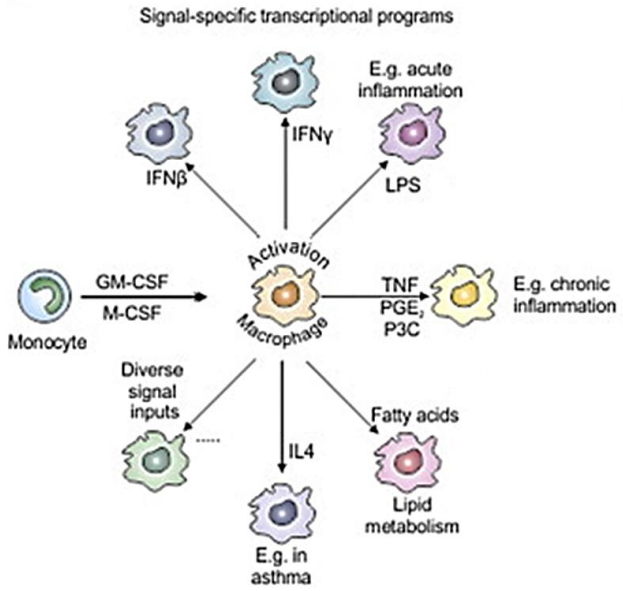

Figure 1.3 Spectrum model of human macrophage activation. Recent studies have suggested that macrophage activation states (and phenotypes) are more complex than the simplified M1/M2 paradigm and can be better modelled as a "spectrum" of phenotypes (Taken from Xue et al., 2014).

Recent studies have focused on the profound transcriptional reprogramming that macrophages undergo upon activation with different activation stimulus. In a recent study, Xue et al. (2014) provided evidence that extends the current M1/M2 polarization paradigm to a much wider spectrum with at least twenty-nine distinct macrophage activation programs (Xue et al., 2014).

In the same manner, the M1/M2 paradigm of microglial activation (Figure 1.4) has been increasingly studied in the context of many neurodegenerative diseases, including AD, in the hope of understanding how the immune response exerted by microglial cells contributes to neurodegeneration (Tang and Le, 2016). In order to model these activated phenotypes, microglial cells can be stimulated with LPS or IFNγ for M1 activation or IL4, IL10 or TGFβ for M2 activation (Figure 1.4). Accumulation of the Aβ peptides (and their different aggregate forms) further complicates this model of activation in microglia as there is no clear consensus on its effect on microglial activation (see Section 1.4.3).

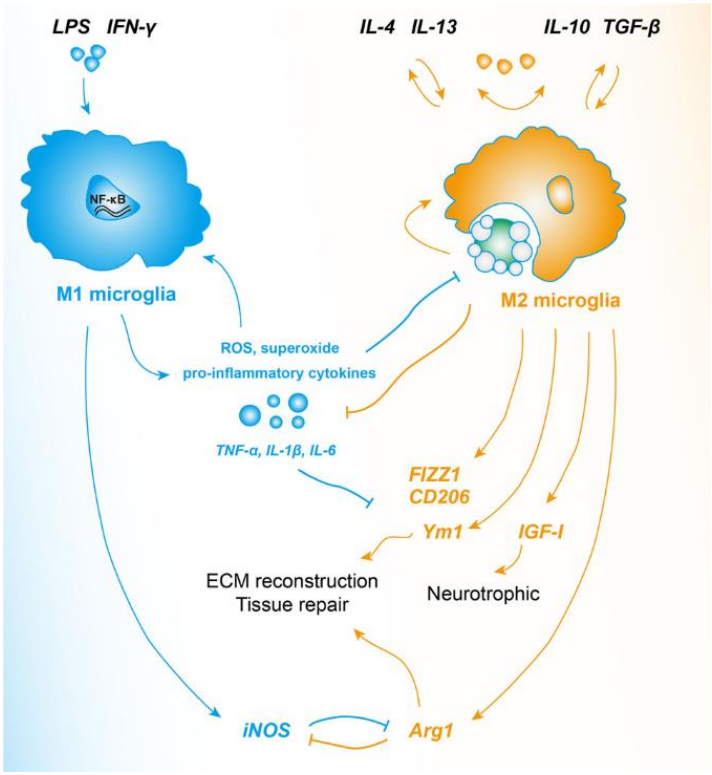

Figure 1.4 M1 and M2 microglia. Similar to macrophages, microglial cells are thought to possess two major activation states: M1 (pro-inflammatory) and M2 (inflammation resolution). M1 microglia are associated with the upregulation of pro-inflammatory cytokines TNFα, IL1β, IL6 and the production of superoxide, ROS and NO. M1 is also associated with the activation of the iNOS and NF-κB pathways. M1 state is induced by LPS and INFγ stimuli. M2 microglia (also known as alternative or acquired activation) are associated with increased phagocytosis, tissue repair, extracellular matrix (ECM) reconstruction as well as support of neuron survival. M2 state is induced by IL4/IL3 and IL10/TGFβ stimuli. M2 microglia antagonize M1 pro-inflammatory responses and promote inflammation resolution (Taken from Tang and Le, 2016).

1.4.1 **M1 state**

M1 microglial cells are stimulated by injury and infection, and are the first line of defence in promoting the destruction of invading pathogens (Tang and Le, 2016). Classic M1 activation is characterised by upregulation of pro-inflammatory cytokines, such as TNFα, IL1, IL6, IL12 and IL18 and is accompanied by impaired phagocytosis in macrophages (Mantovani et al., 2002). There is also an upregulation of MHCII (Major Histocompatibility Complex II), CD86 and Fcγ receptors to allow for antigen presentation and crosstalk with other cells of the immune system (Taylor et al., 2005). M1 microglia are also characterised by increased production of superoxide, NO and ROS (Tang and Le, 2016), and an upregulation of iNOS (Bagasra et al., 1995).

1.4.2 **M2 state**

The M2 phenotype is associated with resolution of inflammation. As such, M2 microglial cells have the potential to dampen pro-inflammatory responses and promote tissue repair (Tang and Le, 2016). The M2 state is characterised by secretion of anti-inflammatory cytokines IL4, IL10, IL13, TGFβ and increased phagocytic activity without toxic nitric oxide (Butovsky et al., 2005, Zhou et al., 2012). IL4 and IL13 are well-characterised cytokines which can supress the production of pro-inflammatory cytokines like IL8, IL6 and TNFα, and reduce NO release (Butovsky et al., 2005, Park et al., 2005, Zhao et al., 2006, Ledeboer et al., 2000).

The M2 state is also associated with increased secretion of neurotrophic factors such as IGF-1 (Insulin-Like Growth Factor 1) to dampen inflammation and promote neuronal survival (Suh et al., 2013). Typical M2 markers such as Arginase 1 (Arg1), Mannose receptor (CD206), Found in inflammatory zone 1 (FIZZ1), and Chitinase-3-Like-3 (Chi3l3 or YM1) are upregulated in response to the presence of apoptotic cells in the local milieu (Gordon, 2003).

1.4.3 **Microglial phenotypes in AD**

Activation of microglia can result in many different phenotypes; however, this could be further complicated by the presence of extracellular Aβ (in different conformations such as monomers, oligomers or fibrils) (Tang and Le, 2016). Aβ plaques (one of the major pathological hallmarks of AD) can attract and stimulate microglial cells *in vivo* (Meyer-Luehmann et al., 2008). Similarly, Aβ peptides have been shown to induce activation of primary microglia and to stimulate NO production *in vitro* (Maezawa et al., 2011, Walker et al., 2006).

Microglial cells can acquire an M2 phenotype (neuroprotective) as a response to the accumulation of Aβ peptides into plaques (Takata et al., 2010). Microglia surrounding Aβ

plaques generally express markers of M2 activation (i.e. YM1) (Jimenez et al., 2008). This agrees with the hypothesis stating that Aβ accumulation is the driving force in AD progression (known as the amyloid β hypothesis). However, age-dependent increases in the number and size of Aβ plaques suggest a decreased phagocytic capacity in senescent microglia (Mawuenyega et al., 2010, Jimenez et al., 2008).

Microglial phagocytic activity can be reduced by the presence of pro-inflammatory cytokines such as IFNγ, IL1 and TNFα, which shift microglia towards an M1 phenotype (Koenigsknecht-Talboo and Landreth, 2005). Stimulation with Aβ oligomers (and fibrils to a lesser extent) can shift microglial cells towards an M1 phenotype. Furthermore, an anti-inflammatory environment can diminish microglial reactivity towards oligomeric Aβ (Michelucci et al., 2009). Similarly, pro-inflammatory factors IL1β and IFNγ as well as LPS can suppress microglial phagocytosis of fibrillar Aβ. This effect can be antagonised by anti-inflammatory cytokines including IL4, IL13, TGFβ and IL10 both *in vitro* and *in vivo* (reviewed by Tang and Le, 2016).

Interestingly, inflammatory activation (M1) of microglial cells by TLR receptor agonists, TNFα or Aβ has been shown to cause slow neuronal loss via phagoptosis in *in vitro* co-culture systems (Neher et al., 2011, Neniskyte et al., 2016, Neniskyte et al., 2011). Phagoptosis refers to the cell death mechanisms by which viable cells dye as a consequence of being phagocytosed by another cell (Fricker et al., 2018). Once activated, microglia releases small amounts of ROS and reactive nitrogen species (RNS) that causes reversible phosphatidylserine (PS) exposure on viable neurons, which results in their phagocytosis by the activated microglia. Phagoptosis of neurons by microglia can be blocked by inhibition of PS (Neher et al., 2011, Neniskyte et al., 2016) and other signaling molecules or cellular receptors both *in vivo* and *in vitro* (for a review Fricker et al. (2018)). It is worth mentioning that to the best of our knowledge, there are currently no studies investigating the role of M2 activators during phagoptosis.

Using a mouse model of AD, it has been shown that the conversion of microglia from an M2 to M1 state is age-dependent and coincides with an increase in soluble Aβ peptide. Additionally, it was shown that YM1 positive (M2 marker) cells are exclusively located in close proximity to Aβ plaques with observed infiltration, and that this association was seen regardless of age (Jimenez et al., 2008). In a recent microarray study, immune gene expression correlated tightly with Aβ plaque load, although a distinction between M1 or M2 activation states was inconclusive (Matarin et al., 2015).

Colton et al. (2006), using quantitative RT-qPCR, showed that AD patients possess a mixed array of activated microglial phenotypes (M1 and M2). The same study found

similar results in two mouse models of AD (Colton et al., 2006). Microarray gene expression studies of AD brains have shown upregulation of apoptotic and pro-inflammatory signaling such as MHC-II, INFγ, IL1β (Blalock et al., 2004, Colangelo et al., 2002). The inconsistent results in gene expression patterns in different systems (mouse models and AD brains from patients) suggest that there is a very complex immune environment in the AD brain and that it can affect the role of microglia in different stages of AD neurodegeneration. To fully understand the role of microglia in neurodegeneration, it is imperative to understand their phenotypes and activation mechanisms (Tang and Le, 2016).

1.4.4 **Aging and microglial phenotypes**

AD is a disease that classically presents itself in middle-aged and elderly people. In the aged brain, microglia undergo a series of morphological and cellular changes that are indicative of senescence. Aged microglia are characterised by fragmented cytoplasmic processes, rendering them less efficient in their protective functions, (Streit et al., 2009, Luo and Chen, 2012) and altered inflammatory profiles (Lucin and Wyss-Coray, 2009).

In aging mouse models of Aβ accumulation, there is an increased expression of M2 related genes at the expense of M1 genes (Wilcock et al., 2011). Conversely, aging of the healthy brain is accompanied by upregulation of pro-inflammatory mediators including IL1β and IL6 and a downregulation of IL10 (Ye and Johnson, 2001, Lee et al., 2000). Age-associated normal inflammatory responses might favour the conversion of microglia to an M1 phenotype, which could render aging brains more susceptible to genetic or environmental inflammatory stimuli and subsequent neurodegenerative processes (Tang and Le, 2016).

1.5 **Microglial genes in AD risk**

Most of the AD risk loci identified by GWAS studies (>20 loci) can be broadly grouped according to their alleged biological functions into three main pathways: Immune response, endocytosis and lipid biology (Guerreiro et al., 2013a). From these pathways, immune response has motivated a renewed interest into the role of microglia in neurodegeneration as many of the associated genes are highly expressed in microglial cells (*TREM2, CR1, CD33, HLA-DRB5-HLA-DRB1, MS4A, CLU, ABCA7, EPHA1* and *INPP5D*). Furthermore, sequencing studies have identified low frequency mutations in the gene encoding *TREM2*, a gene almost exclusively expressed by microglia in the brain, which confers increased risk of AD with an effect size similar to *APOE* (Guerreiro et al., 2013b, Jonsson et al., 2013). Together, these findings have brought

neuroinflammation, and particularly the role of microglia, back at the centre of AD pathology. Figure 1.5 shows a list of AD-risk loci ordered according to their odds ratio (OR) value for AD and their relative expression in microglia compared to other brain cell types.

SNP	Odds ratio (OR)	Minor allele frequency (MAF)	Closest gene	Location	Cell type expression (RPKM), mouse[A]		
					Neurons	Astrocytes	Microglia
rs429358 (ε4)	4.89 (4.45 - 5.39)	0.12	*APOE*	Nonsynonymous	1.17	192	42.8
rs75932628	4.50 (1.7 - 11.9) 2.90 (2.2 - 3.9)	0.005	*TREM2*	Nonsynonymous	0	0.747	110
rs11218343	0.77 (0.72 - 0.82)	0.039	*SORL1*	Intronic	5.31	6.36	3.21
rs6733839	1.22 (1.18 - 1.25)	0.409	*BIN1*	Intergenic	15.6	7.24	74.7
rs6656401	1.18 (1.14 - 1.22)	0.197	*CR1*[B]	Intronic	4.13	4.19	3.46
rs4147929	1.15 (1.11 - 1.19)	0.19	*ABCA7*	Intronic	1.07	0.75	3.97
rs9331896	0.86 (0.84 - 0.89)	0.379	*CLU (APOJ)*	Intronic	2.62	117	2.63
rs17125944	1.14 (1.09 - 1.19)	0.092	*FERMT2*	Intronic	4.11	12.8	0.397
rs10792832	0.87 (0.85 - 0.89)	0.358	*PICALM*	Intergenic	6.74	4.05	22.7
rs7274581	0.88 (0.84 - 0.92)	0.083	*CASS4*	Intronic	0.115	0.335	1.96
rs9271192	1.11 (1.08 - 1.15)	0.276	*HLA-DRB1*[B]	Intergenic	0	0.077	20.3
rs11771145	0.90 (0.88 - 0.93)	0.338	*EPHA1*	Intergenic	0.48	0.625	1.45
rs983392	0.90 (0.87 - 0.92)	0.403	*MS4A6A*[C]	Intergenic	0	0	2.12
rs10948363	1.10 (1.07 - 1.13)	0.266	*CD2AP*	Intronic	4.97	3.36	5.67
rs28834970	1.10 (1.08 - 1.13)	0.366	*PTK2B*	Intronic	12.8	0.692	12.6
rs10498633	0.91 (0.88 - 0.94)	0.217	*SLC24A4*	Intronic	6.82	1.7	0.056
rs1476679	0.91 (0.89 - 0.94)	0.287	*ZCWPW1*	Intronic	0.791	0.627	2.69
rs10838725	1.08 (1.05 - 1.11)	0.316	*CELF1*	Intronic	8.54	3.37	4.56
rs35349669	1.08 (1.05 - 1.11)	0.488	*INPP5D*	Intronic	0.14	0.341	56.3
rs190982	0.93 (0.90 - 0.95)	0.408	*MEF2C*	Intergenic	11.3	2.03	15.3
rs2718058	0.93 (0.90 - 0.95)	0.373	*NME8*	Intergenic	0	0.043	0
rs3865444	0.94 (0. 91- 0.96)	0.307	*CD33*[B]	Intergenic	0.225	0.423	43.7

Key[A]:
= at least 10-fold higher than other cell types
= at least 3-fold higher than other cell types

Figure 1.5 AD-associated loci ordered from largest to smallest effect Odds Ratio (OR). Table showing AD-associated loci, their effect OR and relative gene expression in different brain cell types (modified from Yeh et al. (2017)). SNP identifier, MAF (Minor Allele Frequency) and OR data for most AD-associated loci are from the meta-analysis from Lambert et al. (2013). SNP, MAF and OR data for APOE are from Medway and Morgan (2014). For *TREM2*, SNP, MAF and OR data are from Jonsson et al. (2013) and Guerreiro et al. (2013b). Cell type expression data are from Srinivasan et al. (2016). **A)** Refer to key. **B)** Mouse lacks clear orthologous for CR1, HLA-DRB1 and CD33, instead expression data are for the homologous Cr1l, H2-Ab1 and Cd33 mouse genes respectively. **C)** Expression data are for the homologous mouse Ms4a6d gene.

1.5.1 ***TREM2***

TREM2 (Triggering receptor expressed on myeloid cells 2) is a transmembrane cell receptor selectively expressed in myeloid cells, including macrophages. In the brain, *TREM2* is highly and almost exclusively expressed by microglial cells (Klesney-Tait et

al., 2006). *TREM2* is thought to activate an ITAM (Immunoreceptor tyrosine-based activation motif) signalling pathway via the transmembrane adapter TYROBP (also known as DAP12). Upon activation, *TREM2* activates pathways that promote microglial cell activation (Wang et al., 2015c, Poliani et al., 2015), phagocytosis (Kleinberger et al., 2014a, Hsieh et al., 2009, Takahashi et al., 2005a) and microglial cell survival (Wang et al., 2015c).

Homozygous loss-of-function mutations in the *TREM2* gene (and its putative adapter protein *TYROBP*) are associated with a rare disease called polycystic lipomembranous osteodysplasia with sclerosing leukoencephalopathy (PLOSL), also known as Nasu-Hakola disease. This disease is characterised by development of bone cysts, pathological bone fractures and cognitive impairment at a young age (Paloneva et al., 2002). Interestingly, *Trem2* deficiency did not alter behaviour or cognitive function in *in vivo* mouse models (Kang et al., 2018). Remarkably, *TREM2* deficiency in mouse models leads to accelerated osteoclastogenesis *in vitro* and osteopenia *in vivo (Otero et al., 2012)*. However, *Trem2* deficient mice, do not develop bone lesions. There are many differences between the pathologies (bone deficiencies and osteoclast phenotypes) seen in mouse *TREM2* and DAP12 deficiency models and NHD patients that are not clearly understood at present. Nevertheless, it is thought that these discrepancies are the result of differences between the human and mouse proteins and/or the presence of alternative immunoreceptor and adapter proteins (Xing et al., 2015). Homozygous *TREM2* mutations (p.Q33X, p.Y38C and p.T66M) have also been identified in a pure dementia syndrome without bone involvement (Guerreiro et al., 2013c).

In 2013, two independent groups reported a low frequency mutation in the *TREM2* gene (rs75932628 also known as R47H) which increases the risk of AD. This mutation increases the risk of AD by 3-4 fold in humans (Guerreiro et al., 2013b, Jonsson et al., 2013). This increased AD risk is only second to that bestowed by the ε4 allele of the *APOE* gene, which is the strongest known genetic risk factor for AD (Corder et al., 1993, Holtzman et al., 2012, Kanekiyo et al., 2014). Since *TREM2* is almost exclusively expressed by microglia in the brain (Zhang et al., 2014b, Colonna, 2003), this finding sparked a renewed interest in neuroinflammation and the role that microglia play in Alzheimer's disease. Furthermore, many reports associate the AD risk variant *TREM2* R47H with other neurodegenerative diseases; including Parkinson's disease, frontotemporal dementia and amyotrophic lateral sclerosis (Guerreiro et al., 2013c, Lattante et al., 2013, Rayaprolu et al., 2013). Although the R47H variant has a low population frequency, the literature reports a very rare case of a patient carrying the R47H mutation in homozygosity. This patient exhibited features of both AD and NHD,

namely Aβ and tau protein deposition (AD hallmarks) and frontal brain atrophy (typical of NHD) (Slattery et al., 2014).

A second variant of *TREM2* (rs143332484 also known as R62H) has been linked with an increased risk of AD (Guerreiro et al., 2013b, Jin et al., 2014). Other *TREM2* variants may also be linked to AD (including rs142232675 and rs2234253 known as D87N and T96K respectively), but further studies need to be carried out to confirm these associations (for a review, see Yeh et al. (2017)).

Gene expression analysis of neuropathologically normal brains demonstrated that *TREM2* behaves as a hub gene in many brain regions, and it is suggested to play a key role in microglial cytoskeleton remodelling, phagocytosis and cell migration (Forabosco et al., 2013). Meanwhile, gene expression analysis of brains from *APP*, *PSEN* and *APP/PSEN* transgenic mice showed upregulation of *TREM2* (Matarin et al., 2015). Similarly, cells surrounding Aβ plaques in AD transgenic mice express high levels of *TREM2* (Frank et al., 2008).

TREM2 has been suggested to participate in Aβ clearance. Nevertheless, the role of TREM2 on Aβ clearance has proven controversial in many studies (Kleinberger et al., 2014a, Jay et al., 2015, Wang et al., 2015c). *TREM2* gene knockout in transgenic AD mice resulted in accumulation of Aβ, reduced microglial clustering around plaques and apoptosis (Wang et al., 2015c). *TREM2* has also been shown to sense negatively charged lipids; however, the R47H mutation (associated with increased risk of AD) impairs this function (Wang et al., 2015c). TREM2 can also be cleaved and shed from the cell membrane and secreted into the CSF (Wunderlich et al., 2013, Piccio et al., 2008). Mutations associated with Nasu-Hakola disease and the R47H variant impair TREM2 maturation and shedding (Kleinberger et al., 2014a).

Human *TREM2* sequence identity to mouse *Trem2* is 77.3% at the DNA level and 70.0% at the protein level. Sequence identity is particularly notorious at the Ig-like V extracellular domain (Figure 1.6). Similarly, human *DAP12* sequence identity to mouse *Dap12* is *75.6% at the DNA level and 75.0% at the protein level* (https://www.ncbi.nlm.nih.gov/homologene). This relatively high sequence identity between human and mouse TREM2 proteins allows the use of the mouse TREM2 protein as a model for the study of the human TREM2 protein.

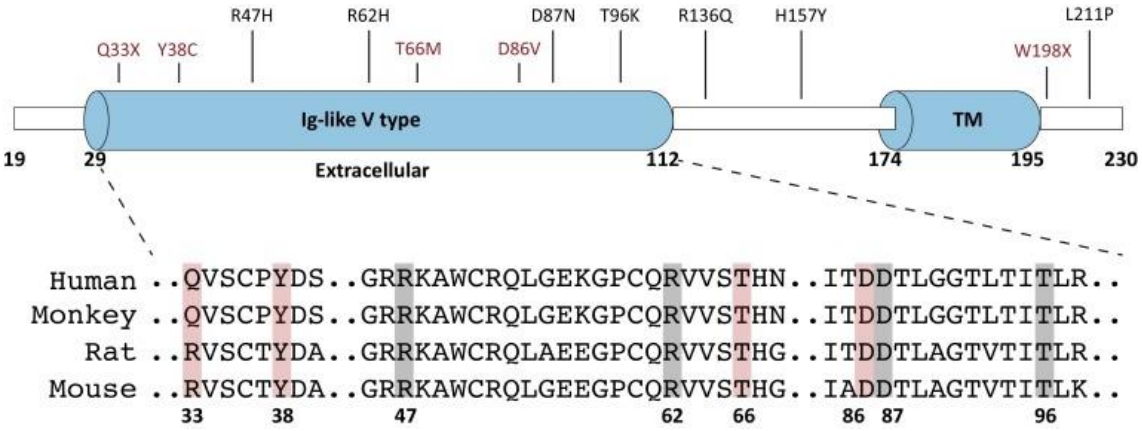

Figure 1.6. Human protein TREM2 sequence identity to monkey, rat and mouse TREM2 – Ig-like V domain. Human TREM2 protein has a relatively high sequence identity to the monkey, rat and mouse TREM2 proteins. The sequence identity is more notorious at the extracellular Ig-like V domain where the mutations that cause frontotemporal dementia (FTD), Nasu–Hakola disease (NHD) and AD are located. Mutations that cause FTD and NHD are marked in red while reported AD-related variants are shown in black, including the R47H and R62H mutations. Taken from Yeh et al. (2017).

1.5.1.1 **TREM2's ligands**

Early studies looking at possible TREM2 ligands found that the extracellular domain of the protein could bind to many different anionic molecules which are present in bacteria. These molecules include; LPS, lipoteichoic acid, peptidoglycans and dextran sulphates (Daws et al., 2003). Nevertheless, the importance of these interactions in the context of neurodegeneration remains uncertain (Yeh et al., 2017). Recent studies looking at possible endogenous TREM2 ligands have found that the mouse TREM2 extracellular domain is capable of binding to many different phospholipids, including; phosphatidylserine (PS) phosphatidylethanolamine (PE), cardiolipin (CL), phosphatidylglycerol (PG) and phosphatidic acid (PA) (Cannon et al., 2012). *TREM2* can also bind to glycolipids from cells and myelin, including; sulfatides, cerebrosides and sphingomyelins (Wang et al., 2015c, Poliani et al., 2015, Bailey et al., 2015).

Interestingly, the extracellular domain of TREM2 has also been found to bind to APOE, APOA1 and APOD in CSF from macaques (Bailey et al., 2015). A recent study found that the extracellular domain of TREM2 is capable of binding to low-density lipoprotein (LDL), very low density lipoprotein (VLDL), high-density lipoprotein (HDL) and lipoproteins (including CLU/APOJ and APOE) (Yeh et al., 2016). The same study also showed that Aβ binds to lipoproteins and that this complex is recognised and engulfed by microglia in a TREM2 dependent manner. This last finding links 3 important genetic risk factors for AD and suggests a possible mechanisms by which TREM2 contributes to AD pathology (Yeh et al., 2017).

Remarkably, binding of the human TREM2 receptor and its lipoprotein ligands (LDL, APOE and CLU) can be impaired by the*TREM2* AD-associated mutations R47H, R62H, D87N. Even further, the interaction can be completely abolished by the NHD/FTD-associated mutations (Bailey et al., 2015, Yeh et al., 2016, Atagi et al., 2015a). These findings support the idea that these mutations are loss-of-function mutations and that they may contribute to neurodegeneration by impairing microglial binding to lipoproteins. *TREM2* mutations have been shown to alter soluble TREM2 (sTREM2) levels in the CSF of carriers. For example, carriers of NHD-associated *TREM2* variants (*R136Q, D87N, Q33X or T66M*) had significantly lower sTREM2 levels in the CSF, supporting the idea that these mutations lead to reduced protein production and/or function. On the other hand, carriers of the AD-associated *TREM2* variant (*R47H*) showed significantly higher expression of sTREM2 in the CSF, compared to non-carriers (Piccio et al., 2016).

Although differences between the expression levels of sTREM2 in the CSF of patients carrying different TREM2 mutations is in itself interesting, it still remains a mystery how this differences may contribute to the different diseases' pathogenesis or progression. This is further complicated since the function of sTREM2 in the CSF (or anywhere else for that matter) remains unknown. Nevertheless, there is evidence suggesting that sTREM2 acts as a decoy receptor, opposing full-length membrane bound TREM2 function/signalling (Piccio et al., 2008, Kleinberger et al., 2014a). This idea has been inspired another member of the TREM family of proteins: TREM1. In this case, sTREM1 has been shown to compete with its membrane bound counterpart to block TREM1 signalling (Haselmayer et al., 2007). More recently, sTREM2 has been postulated to have its own biological function. Supplementation of BMDM cultures lacking *TREM2* expression with exogenous sTREM2 has been shown to promote cell survival (Wu et al., 2015a). Further studies will be needed to clarify sTREM2's function and its role in neurodegeneration (Jay et al., 2017).

Finally, the extracellular domain of TREM2 has been reported to bind to apoptotic neurons. This binding is thought to be mediated by TREM2's ability to detect the phosphatidylserine exposed in the plasma membrane of apoptotic neurons (Hsieh et al., 2009, Takahashi et al., 2005a, Takahashi et al., 2007).

1.5.2 ***CR1*** **(Complement Receptor 1)**

The identification of several *CR1* variants (SNPs) as risk-factors for AD further supports the link between immune dysfunction and AD (Lambert et al., 2009, Harold et al., 2009). The rs6656401 variant and its tagging SNPs have been shown to be strongly associated with AD. Likewise, carriers of the *APOE ε4* allele and the *CR1* rs3818361 variant have a higher LOAD risk (Lambert et al., 2009). CR1 is a multifunctional transmembrane

glycoprotein that forms part of the complement immune response. CR1 is expressed on phagocytic cells, including microglia, and its activation results in the ingestion and removal of complement activated particles (Liu and Niu, 2009). CR1 is a receptor of C3b (opsonin) and as such it participates in the regulation of both the classical and alternative complement pathways. C3b has been shown to bind and promote clearance of Aβ peptides therefore *CR1* variants may contribute to AD by altering Aβ clearance (Rogers et al., 2006).

The upregulation of CR1 (and other complement factors) has been reported in affected regions of AD brains (Shen et al., 1997). *CR1* upregulation is also associated with advanced cognitive decline in AD brains (Karch et al., 2012). Interestingly, material isolated from neurofibrillary tangles and Aβ plaques has been shown to activate the complement system (McGeer et al., 1989, Shen et al., 2001).

1.5.3 ***CD33***

CD33 is a transmembrane protein of the sialic acid-binding immunoglobulin-like lectins (SIGLECS) family and is expressed on phagocytic cells including microglia (Zhang et al., 2014, Griciuc et al., 2013). CD33 regulates innate immunity, Aβ clearance and other neuroinflammatory processes (Malik et al., 2013, Jiang et al., 2014). Upregulation of CD33 was noted in microglia in AD brains and is associated with a lowered AD risk. The CD33 polymorphisms associated with increased AD risk (e.g. rs3865444) are linked to increased CD33 expression, increased Aβ deposition and reduced Aβ uptake and degradation by microglia and monocytes (Griciuc et al., 2013, Bradshaw et al., 2013) It is worth mentioning that in a recent meta-analysis of AD cases and controls (including 74,046 individuals) the association of CD33 polymorphisms to AD did not reach genome wide significance (Lambert et al., 2013).

1.5.4 ***MS4A*** **cluster**

The MS4A locus associated with AD risk contains at least 5 genes implicated in immune modulation: MS4A3, MS4A2, MS4A6A, MS4A4A, MS4A4E, and MS4A6E (Karch and Goate, 2015). In humans, the MS4A gene family comprises more than 16 genes encoding membrane proteins. MS4A gene expression varies between tissues but is limited to haematopoietic cells (Zuccolo et al., 2010). Increased expression of MS4A6A in the parietal lobe is associated with more advanced brain pathology in AD patients (Karch et al., 2012), and elevated MS4A6A levels in blood and brain tissue are linked with AD risk (Proitsi et al., 2014). The SNPs rs670139 (near MS4A4) and rs610932 (near MS4A6E) have been associated with an increased AD risk. In contrast, the SNP rs983392 (near MS4A6A) was associated with a reduced AD risk (Lambert et al., 2013, Hollingworth et al., 2011).

1.5.5 *HLA-DRB5/HLA-DRB1* (Major Histocompatibility Complex, Class II, DR Beta 1/Major Histocompatibility Complex, Class II, DR Beta 5)

The HLA-DRB5/HLA-DRB1 locus is a part of the Major Histocompatibility Complex Class II (MHCII), a highly polymorphic region involved in the immune response and histocompatibility (Trowsdale and Knight, 2013). MHCII is expressed mainly in antigen-presenting cells (APCs) and is an essential regulator of the immune response. Its main role is the presentation of antigens to CD4 T-cells. HLA-DR, a component of MHCII, is highly expressed on reactive microglia in AD and PD brains (McGeer et al., 1988). The role of HLA-DRB5/B1 in microglial activation in the context of AD remains unknown.

1.5.6 *APOE* (Apolipoprotein E)

To date *APOE* remains the strongest genetic risk factor for LOAD. *APOE* is expressed in many tissues in the body and in the brain, it is expressed mainly by astrocytes and microglia (Zhang et al., 2014). *APOE* is the major cholesterol carrier in the brain. Classically, *APOE* has mainly been linked to lipid metabolism but recent studies have shown that in the CNS, *APOE* participates in lipoprotein metabolism, neuroplasticity and inflammation (Kim et al., 2009, Liu et al., 2013). Additionally, APOE can bind Aβ peptides and influence Aβ aggregation and clearance of soluble Aβ (Liu et al., 2013, Castellano et al., 2011).

APOE has three common alleles: *APOE ε2* (Cys112, Cys158), *APOE ε3* (Cys112, Arg158), and APOE ε4 (Arg112, Arg158). Of these three alleles, the APOE ε4 allele is associated increased LOAD risk. The risk is 3-fold higher for individuals carrying one copy and 12-fold for those carrying two copies of the *APOE ε4* allele (Corder et al., 1993). Overproduction of APOE, particularly isoform *APOE ε4*, can aggravate glial inflammatory response (Guo et al., 2004). In addition, *APOE* can modulate innate inflammatory responses through *TLR4* and *IL4R* receptor pathways, suggesting that it may have a more general role in inflammation (Tai et al., 2015).

Moreover, a recent study found correlation between reduced *TREM2* expression and the *APOE ε4/4* allele, in activated primary microglia (Li et al., 2015). At the protein level, the AD risk mutation *TREM2* R47H has been shown to reduce *TREM2*'s binding to cells (Kober et al., 2016) and the three common APOE isoforms (Bailey et al., 2015). Using a reporter cell line, Bailey et al. (2015) showed that APOE binding to *TREM2* is able to induce *TREM2* signalling in these cells, however the effect of such interaction *in vivo* remains to be determined. Interestingly, a recent study of pathologically confirmed cases of AD ((Murray et al., 2018)), the authors propose that *TREM2* R47H carriers are unlikely to develop AD without having an APOE ε4 allele, emphasizing the importance of exploring the function of APOE and its interaction with *TREM2* in a microglial context.

1.5.7 *CLU* (Clusterin or APOJ)

CLU is a chaperone protein involved in apoptosis, complement regulation, lipid transport and cell-to-cell interactions (Jones and Jomary, 2002). Similarly to APOE, CLU directly interacts with Aβ and modifies fibril formation *in vitro* (Reviewed by Li et al., 2014). *In vivo*, there is evidence that suggests both APOE and CLU may influence Aβ deposition and clearance (DeMattos et al., 2004). Additionally, CLU may modulate neuroinflammation by inhibiting the inflammatory response associated with complement activation (Nuutinen et al., 2009). In the CNS, CLU is more highly expressed in astrocytes and oligodendrocytes than in microglia (Zhang et al., 2014), but because of its similarity to APOE, its role in Aβ clearance and its association with the complement system, it could indirectly drive neuroinflammation in AD.

1.5.8 *ABCA7* (ATP-binding cassette transporter A7)

ABCA7 is a member of the ATP-binding cassette superfamily; it is involved in the transport of intracellular lipids to extracellular lipoproteins. *In vitro*, ABCA7 stimulates cholesterol efflux and inhibition of APP processing (Chan et al., 2008). It is also involved in phagocytosis of apoptotic cells through C1q complement pathway in macrophages (Jehle et al., 2006). Increased ABCA7 expression enhances microglial phagocytosis and Aβ uptake. APP transgenic mice that are ABCA7-deficient show increased Aβ deposition compared with controls (Kim et al., 2013b). Hence, ABCA7 may influence AD risk via cholesterol transfer to APOE or Aβ deposition (Karch and Goate, 2015). Despite low expression in most human brain cells, microglia and neurons show the highest expression of ABCA7 (Kim et al., 2006). The SNP rs3764650 (near ABCA7) has been associated with an increased LOAD risk (Hollingworth et al., 2011). On the other hand, the ABCA7 SNP rs72973581 has been shown to confer a modest but statically significant protection against AD (Sassi et al., 2016).

1.5.9 *INPP5D, MEF2C* and *EPHA1*

Many more loci, for which there is not much mechanistic evidence, were associated with elevated AD risk in the largest GWAS study to date (Lambert et al., 2013). Several of these gene associations fit into pathways that are known to be altered in AD, namely immune response mechanisms. That is the case for INPP5D, a negative regulator of myeloid cell proliferation and survival. This association is reinforced by the fact that INPP5D expression is restricted to myeloid cells. Another example is MEF2C, which is known to be involved in immune response and synaptic function pathways. Finally, EPHA1 has also been associated with immune response pathways in AD; however, it is better known for its role in cell and axonal guidance and synaptic plasticity (Reviewed by Karch et al., 2014, Karch and Goate, 2015).

As reviewed above, many of the genes associated with AD risk have been shown to participate or be involved in immune/inflammatory mechanisms. Nonetheless, their exact function and the role many of them play in microglial activation (M1/M2 or other) remains unknown.

1.6 **Genome editing – CRISPR/Cas9 tools**

The capacity to efficiently and precisely modify the genomes of model organisms is crucial for understanding the effect of specific genetic mutations in the context of normal and pathological processes. Traditionally, genome engineering of model organisms was achieved by random mutagenesis or low-efficiency targeting through homologous recombination (Peng et al., 2014).

During the last decade, programmable sequence-specific endonucleases have arisen as viable strategies for the precise editing of endogenous genomic DNA, allowing the systematic interrogation of specific genetic variations (Ding et al., 2013, Kim et al., 2014, Soldner et al., 2011). Many sequence-specific gene editing techniques have arisen in recent years, including Zinc-finger nucleases (ZFNs), Transcription activator-like effector nucleases (TALENS) and the RNA-guided CRISPR/Cas9 nuclease system (CRISPR/Cas9). Both ZFNs' and TALENS' strategies rely on the specific attachment of endonuclease catalytic domains to modular DNA-binding proteins for inducing DNA double stranded breaks (DSBs) at specific loci. Meanwhile, the CRISPR/Cas9 system relies on the specific Watson-Crick base pairing between a guiding RNA molecule and the target DNA site to produce DSBs. This last approach is distinctly easier to design, highly specific and efficient (Ran et al., 2013b).

In the present thesis, the CRISPR/Cas9 gene editing technique was used for the generation of *Trem2* and *Dap12* deficient cell models for the study of these genes' function during microglial activation and normal functioning. Similarly, this thesis describes the use of the CRISPR/Cas9 for the introduction of the AD-related risk mutation *Trem2 R47H* into BV2 cells. Once more, CRISPR/Cas9 was used to generate cell models for the study of the biological effects that the R47H mutation has on *Trem2*'s function.

1.6.1 **Genome editing: Hijacking the endogenous DNA repair systems.**

The advent of programmable endonucleases such as ZFNs, TALENS and CRISPR/Cas9 allows the targeted genetic manipulation of model organisms. Endonucleases achieve genetic disruption by causing DSBs on the gDNA which then can be repaired by multiple repairing systems. In mammals, there are two major repair

mechanisms: the predominant and error-prone Non-homologous end-joining (NHEJ) pathway and the high-fidelity homology-directed repair (HDR) pathway, both of which can be used to obtain the desired genetic modification (Figure 1.7).

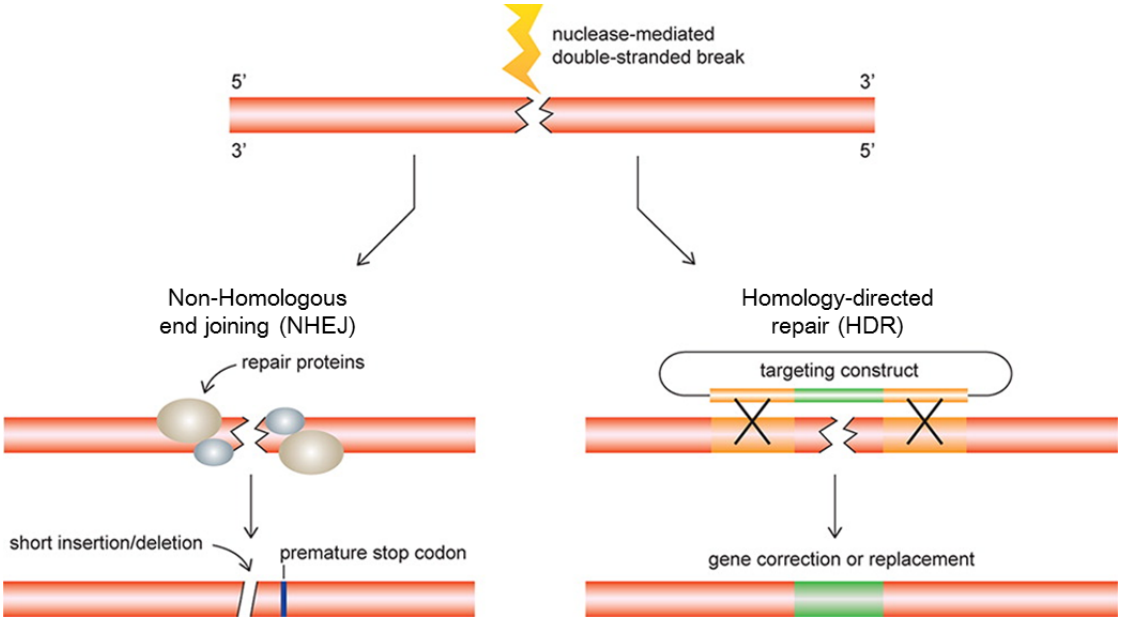

Figure 1.7 Programmable endonucleases hijack the endogenous DNA repair systems. Programmable endonucleases generate DSBs in the gDNA which can be repaired by two major repair mechanisms: Non-homologous end joining (NHEJ) and Homologous Directed repair (HDR). NHEJ directly binds the ends of the broken DNA in an error-prone process that can introduce small insertions or deletions (Indels) at the repair site, leading to the loss of gene function if targeted to protein coding regions of a gene. HDR allows more specific manipulation by using a repair template (i.e. plasmid or single-stranded DNA oligonucleotide) with homology arms flanking the DSB site (modified from Hsu and Zhang (2012)).

The error-prone nature of the NHEJ pathway leads to the accumulation of small deletions or insertions (Indels) that can shift the reading frame of the gene, producing premature stop codons. When NHEJ is combined with programmable endonucleases it is possible to generate genetic KO (knockouts) by targeting coding exons of a gene of interest (Hsu and Zhang, 2012).

The counterpart to NHEJ pathway is the HDR mechanism. This mechanism usually occurs at substantially lower rates than NHEJ and can be exploited to generate precise DNA modifications at the target locus. To this end, the HDR pathway requires the presence of a homologous repair template. To use HDR repair together with programmable endonucleases, co-transfection of a donor template containing homology arms and our desired mutation is required. This repair template can be a double-stranded DNA (i.e. plasmid) or a single-stranded DNA oligonucleotide (ssODN). Both kinds of template must have homology arms flanking the endonuclease target site (Ran et al., 2013b). HDR is more active in dividing cells and its efficiency depends on many

factors including cell type, cell cycle phase, target genomic locus and repair template (Saleh-Gohari and Helleday, 2004).

1.6.2 **Programmable genome editing tools: ZFNs, TALENS and CRISPRs**

Programmable endonuclease-based gene editing involves the generation of a DSB at the target region, resulting in the deletion, insertion or replacement of a genomic sequence using cellular repair pathways. As such, efficient genome editing depends on tools which can predictably and specifically recognize the target locus. Many naturally occurring proteins have the ability to bind DNA in a sequence-specific manner and by exploring how those proteins achieved this specific binding, researchers have been able to harness that capacity for genome editing. Currently, the major families of programmable endonucleases used are: ZFNs, TALENS and RNA-guided endonucleases (mainly CRISPR/Cas9) (Peng et al., 2014).

1.6.3 **Zinc-finger nucleases (ZFNs)**

Zinc-fingers are protein structural motifs that direct transcription factors to their specific genomic target sites. Zinc-finger domains are found in tandem arrays of “individual fingers”, where each finger is capable of recognizing a 3bp DNA sequence. Tandem repeats of zinc-fingers make up a larger zinc-finger protein wherein each finger (which can be modularly exchanged) recognizes distinct 3bp DNA sequences allowing the protein construct to recognize larger DNA sequences.

Proteins constructed with tandem repeats of zinc-fingers were the first custom-designed genome editing tool to successfully target specific DNA regions (Kim et al., 1996). By fusing tandem repeats of zinc-fingers with a sequence-independent endonuclease, like FokI, researchers were able to create targeted endonucleases to cut DNA in a sequence specific manner. Due to the dimeric nature of the FokI endonuclease domain, two individual ZFNs are required to induce a DBS at a single target site (Figure 1.8).

Despite their modularity and sequence specific targeting, ZFNs have some major drawbacks that hinder their widespread application. Limited binding selectivity conferred by the zinc-finger modules as well as altered binding affinity caused by complex context-dependent interactions among the adjacent fingers of the same ZFN and toxicity are notable drawbacks (Cornu et al., 2008). Moreover, ZFN design and construction is an arduous process, often requiring many rounds of test, which makes them less accessible for non-specialised laboratories (Carroll, 2011).

1.6.3.1 ***Transcription activator-like effector nucleases (TALENS)***

Transcription activator-like effectors (TALE) are a family of transcription factors found in the plant pathogenic bacteria *Xanthomonas,* which secrete TALEs to regulate specific

genes in their hosts (Bogdanove et al., 2010). TALEs contain DNA-binding domains consisting of 33-35 amino-acid modular repeats capable of recognizing a single DNA base pair. Two amino acids, at positions 12 and 13 on each tandem repeat (collectively known as repeat variable di-residue or RVD), confer binding specificity to each TALE (Bogdanove and Voytas, 2011).

By identifying each of the naturally occurring TALEs that bind to each of the four basic nucleotides, researchers have been able to assemble specific combinations of TALE monomers, with different RVDs, into synthetic TALE DNA-binding domains that target specific DNA sequences (Figure 1.8). Similar to zinc-fingers, TALE domains can also be fused to sequence independent endonucleases. TALENS (Transcription activator-like effector nucleases) are made by fusing TALE DNA-binding domains to the FokI catalytic domain to achieve precise genome editing (Christian et al., 2010, Mahfouz et al., 2011). TALENS are significantly easier to assemble and customize than zinc-finger proteins and can easily be implemented in non-specialised laboratories. TALENS have very few restrictions when it comes to sequence targeting and provide site-specific recognition in even the most complex genomes (Peng et al., 2014).

1.6.3.2 ***RNA-guided endonucleases for genome editing – CRISPRs***

Clustered regularly interspaced short palindromic repeats (CRISPRs) are a relatively new gene editing technology that has revolutionised the field of genome engineering since its introduction. This system has been adapted from the RNA-based adaptive immune mechanisms that defend bacteria (like *Streptococcus pyogenes*) and archaea from bacteriophage attacks (Horvath and Barrangou, 2010, Bhaya et al., 2011). The CRISPR adaptive immunity system functions by targeting and cutting invading nucleic acids (including DNA or RNA) using an array of proteins and RNA sequences.

So far, two main classes of CRISPR systems (1 and 2) have been described in bacteria and archaea based on their mechanisms of action and components, each class divided into three different sub-types (numbered I to VI). Class 1 systems use a complex of Cas proteins to degrade genetic materials. Class 2 systems use a single large Cas protein for the same purpose (Koonin et al., 2017).

Each CRISPR system is composed of three main components: a cluster of CRISPR-associated (Cas) genes, non-coding RNAs and an array of repeat sequences (known as direct repeats). Direct repeats are interspaced by short variable regions derived from exogenous DNA targets, known as protospacers, and together they form the CRISPR RNA (crRNA) array. Within the target DNA, each protospacer is associated with a

protospacer adjacent motif (PAM), which can vary its sequence depending on the CRISPR system (Koonin et al., 2017).

The type II CRISPR system (part of the Class II) is one of best characterised systems and consists of the nuclease Cas9 (capable of inducing a double strand break), the crRNA array (that encodes the guide RNAs) and the auxiliary trans-activating crRNA (tracrRNA), which helps the processing of the crRNA array into discrete units. Each crRNA contains a 20 nucleotide (nt) guide sequence and a partial direct repeat. The 20nt guide sequence is responsible for directing the Cas9 to the 20bp DNA target via classic Watson-Crick base pairing (Gasiunas et al., 2012)(Figure 1.8).

In the CRISPR/Cas9 system derived from the bacteria *Streptococcus pyogenes* (which was the first CRISPR system to be used as a genetic engineering tool); the target DNA sequence must lie directly upstream of a NGG nucleotide motif to act as a PAM site. Two key developments gave rise to the use of the CRISPR/Cas9 system as a genetic tool: First, the realization that the specificity conferred by the guiding RNA was not limited to only naturally occurring crRNA targets, but could be engineered to target almost any exogenous sequence as long as a PAM site was in the immediate vicinity of the target region. Second, crRNA and tracrRNA were fused to form a chimeric single-guide RNA (originally known as sgRNA, but commonly referred as gRNA). As a result, the nuclease Cas9 can be directed to virtually any target site, in the vicinity of a PAM sequence, by custom modifying the 20nt guide sequence within the gRNA (Panel C, Figure 1.8) (Jinek et al., 2012).

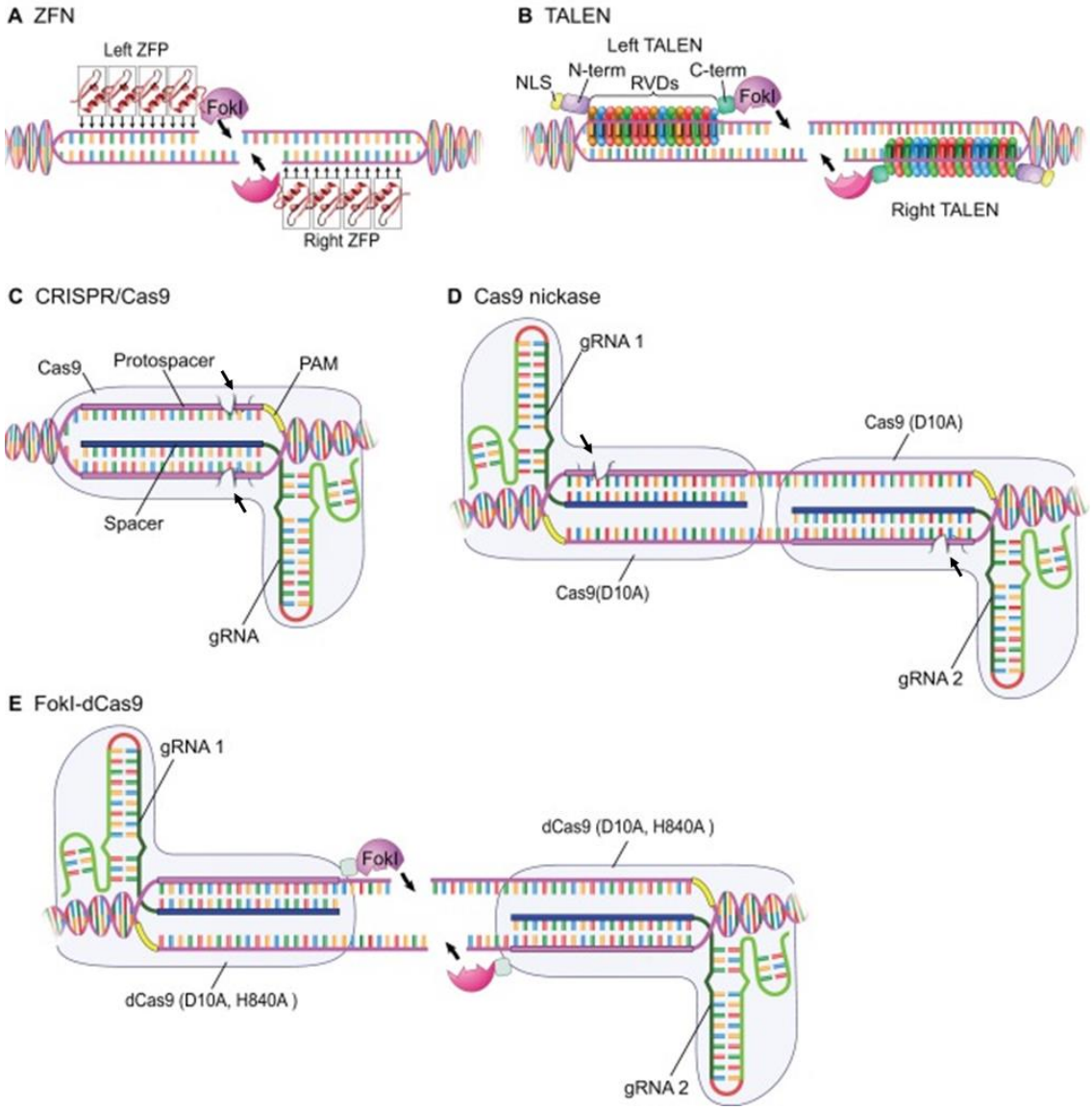

Figure 1.8 Programmable genome editing tools; ZNFs, TALENS and CRISPRs. Schematic of the mechanism of various genome engineering tools including: A) Zinc-finger nucleases (ZFNs) recognize DNA using three base pair recognition motifs (ZFPs); by fusing several ZFPs in tandem it is possible to specifically target specific genomic loci. The system uses two ZFNs recognizing adjacent sequences; each ZFN is fused to one *FokI* nuclease, these nucleases work as a dimer to produce a DSB in the target sequence. B) Transcription activator-like effector nucleases (TALENs) recognize DNA through amino acid modules that include repeat-variable di-residues (RVDs). Like ZFNs, two TALENs are needed that cut DNA using the *FokI* nuclease dimer. TALEN backbones have been engineered to include a specific NLS (nuclear localization signal) for better function. C) CRISPR/Cas9 system recognizes specific DNA using a guide RNA (gRNA)/DNA/Cas9 protein complex. This complex must be near a tri-nucleotide protospacer adjacent motif (PAM). Two Cas9 protein domains are responsible for DNA cleavage on each strand of the dsDNA: the HNH domain cleaves the complementary DNA strand, whereas the RuvC-like domain cleaves the non-complementary DNA strand. D) Cas9 nickase uses a molecularly modified Cas9 (known as D10A) protein that can only cut on one strand of the recognised gRNA/DNA complex. Analogous to ZFNs and TALENs, Cas9 nickases work in pairs to produce a DSB. E) Chimeric Nuclease-deficient Cas9/FokI fusion system. This approach utilizes the Cas9/gRNA complex for sequence-specific DNA binding, and the FokI dimer nuclease for DSB induction, similarly to the approach used by ZFNs and TALENs. NLS, nuclear localization sequence; N-term, protein N terminus; C-term, protein C terminus (modified from Peng et al. (2014))

Therefore, the CRISPR/Cas9 system has been widely adopted by many research laboratories for its simplicity of design (solely limited to the gRNA), efficiency,

robustness, amenability to multiplexing (targeting of two or more sequences of interest) and applicability to a wide range of organisms (Eid and Mahfouz, 2016). Nevertheless, the system still has some important drawbacks, including the off-target activities of the Cas9 protein (Fu et al., 2013), that hinder its clinical applications.

As such, many attempts and modifications of the system have been made in order to reduce the off-target effects. These include the generation of paired nickases (Panel D, Figure 1.8) or chimeras containing a catalytically inactive Cas9 (dCas9) and a catalytic domain *FokI* endonuclease (Panel E, Figure 1.8), similar to the design used for ZFNs and TALENs.

1.6.4 **Harnessing the power of the CRISPR/Cas9 system – More tools in the kit**

Several attempts to modify the CRISPR/Cas9 system have been made to date. Some of them have been oriented towards decreasing the off-target effects, whereas others have been focused on hacking the tools to send proteins to precise DNA targets to toggle genes on and off and even for the study of chromosomal dynamics (reviewed by Ledford (2016)) (Figure 1.9).

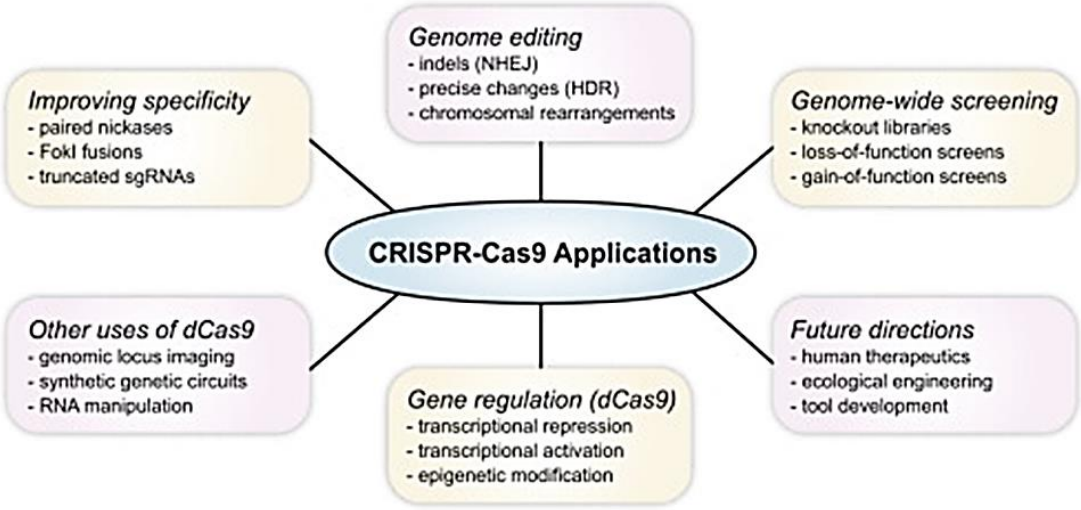

Figure 1.9 CRISPR/Cas9 applications. The capacity to specifically target DNA regions using the programmable RNA-guided Cas9 protein has been exploited in numerous applications. Some of these applications are oriented to improve the on-target/off-target genome editing efficiency of the system, while others are focused on harnessing its targeting capacity to control gene expression or even image specific chromosomal events/regions (taken from Sternberg and Doudna (2015)).

1.6.4.1 ***CRISPR/Cas9 nickases (CRISPR/Cas9n)***

The development of Cas9 protein variants that are capable of cutting one of the strands rather than both strands of the target DNA sequence (known as nickases) have been shown to be useful for genome editing. Nickases are capable of inducing DNA repair by both NHEJ or HDR mechanisms. Introduction of a D10A or H840A mutations into the RuvC1- or HNH-like nuclease domains in Cas9 protein results in nuclease protein

variants capable of generating single DNA nicks on either the complementary or non-complementary DNA target strands, respectively (Panel D, Figure 1.8). Similarly to what happens with ZFNs and TALENs systems, the use of two closely located Cas9 nickases (Cas9n) targeting opposite strands of DNA is able to generate DSBs (Ran et al., 2013a, Shen et al., 2014). Use of paired nickases show they are able to induce DSB at a frequency similar to the wild-type Cas9 protein with improved specificity (Shen et al., 2014), lowering the chances of possible off-target effects without compromising efficiency.

1.6.4.2 ***Cas9 and FokI fusion proteins***

Similar to the previous work done on ZFNs and TALENs, Cas9 can be fused with the catalytic domain of the FokI nuclease to generate chimeric proteins. fdCas9, fCas9 and RFNs are variants of chimeric fusions between the FokI catalytic domain and catalytically inactive Cas9 (dCas9) protein. These chimeric proteins have been shown to improve the precision of the Cas9 system for genome engineering (Guilinger et al., 2014, Aouida et al., 2015).

1.6.4.3 ***CRISPR interference (CRISPRi) and CRISPR activation (CRISPRa)***

Programmable RNA-guided DNA targeting by Cas9 has been exploited in numerous diverse applications, some of which are oriented towards gene expression disruption without gDNA alteration. The catalytically inactive dCas9 protein is still capable of binding DNA in a sequence based manner, without cutting its target. By co-expressing a gRNA and the dCas9 protein, Qi et al. (2013) were able to interfere with transcriptional elongation, RNA polymerase binding, or transcription factor binding of a target gene. This system is capable of repressing gene expression with no detectable off-target effects, is amenable for multiplexing and very importantly can be reversible. A step further using this same system saw the fusion of Cas9 to an activation domain (such as VP64 or the p65 subunit of nuclear factor kappa B; NF-κB) or a transcriptional repression domain (such as the Krüppel-associated box (KRAB) domain) to regulate the expression of endogenous human and mouse cells (reviewed by Sander and Joung (2014))

1.6.4.4 ***EGFP-dCas9 complex for imaging of specific genomic loci***

By fusing the dCas9 protein to the fluorescent EGFP (Enhanced green fluorescent protein) it is possible to visualize DNA loci containing repetitive sequences, such as telomeres, with a single gRNA or a non-repetitive loci using >26 gRNAs tiled across a large region of DNA (Chen et al., 2013a). This new use of the CRISPR/Cas9 system adds an extra tool for the study of chromosomal dynamics and expands the use of the Cas9 protein beyond gene expression-based applications (reviewed by Sander and Joung (2014)).

2 CHAPTER 2: Materials and Methods

2.1 Cell lines and culture

The murine microglia cell line BV2 was generated by transfecting the v-raf/v-myc oncogene into primary mouse microglia (Blasi et al., 1990). The cell line was obtained from Banca Biologica e Cell factory (Italy) and was checked regularly for mycoplasma contamination. BV2 cells were grown in T175cm^2 culture flasks (Appleton Woods, Bucks, UK) and maintained in Roswell Park Memorial Institute (RPMI) 1640 Medium (Life Technologies, Cat# 52400-025) supplemented with 10% (v/v) heat-inactivated Foetal Bovine Serum (FBS; Life Technologies) and 100U/mL penicillin, 100µg/mL streptomycin. Cells were maintained at 37°C in a humidified atmosphere with 5% CO_2. This batch of cells was used to carry out all experiments, with the exception of the microarray analysis of microglial activation.

Cells were karyotyped commercially (CELL Guidance Systems Genetics Service, Cambridge, UK) and were found to have a “Grossly abnormal mouse karyotype”, with 62-66 chromosomes. Mouse normal karyotype (2n) is made of 40 chromosomes (Nachman and Searle, 1995). Chromosome 17 (*Trem2*’s location) was found to have 2-4 copies in BV2 WT (wild type) cells. *Trem2* CRISPR/Ca9 clones C8 and G4 were also karyotyped commercially and found to possess the same “Grossly abnormal mouse karyotype”, with 62-66 chromosomes. Chromosome 17 had 3-4 copies on C8 clones and only 3 copies on G4 cells – see Supplementary Fig. 7.1, Supplementary Fig. 7.2 and Supplementary Fig. 7.3. These differences in the number of chromosomes can account for some of the variability (in gene or protein expression) seen during the characterization of the CRISPR/Cas9 models.

For the microarray experiment exclusively, a different batch of BV2 cells was used. This batch of cells was a kind gift from Dr Claudie Hooper (MRC Centre for Neurodegenerative Research, Institute of Psychiatry, King’s College London, UK) and was originally obtained from Dr F.S. Tzeng (Department of Life Sciences, National Cheng Kung University, Taiwan). This batch of cells was maintained in Dulbecco's modified Eagle's medium (Gibco, Cat# 41966-029) supplemented with 10% FBS, 100U/mL penicillin and 100mg/mL streptomycin.

BV2 cells were routinely frozen down and cryopreserved to increase longevity of the cell line. BV2 cells, 1x 10^{6}cells/mL, were suspended in freezing medium (RPMI, 50% FBS, 10% DMSO) and frozen down to -80°C, before putting them in long term storage in liquid nitrogen. To resuscitate the cells, frozen vials were thawed and added to 25mL of pre-warmed BV2 medium in a T175cm^2 culture flask (Corning, Cat# 353112, Germany).

Cells were maintained at 37°C in a humidified atmosphere with 5% CO_2 for 24h; medium was then changed to remove the cytotoxic components of the freezing medium.

For experimental procedures and passaging, BV2 cells were harvested from the culture flask when they reached 60-80% confluency. Firstly, media was removed and the attached cells were washed once with PBS ([-$CaCl_2$], [-Mg Cl_2]) (ThermoFisher, Cat# 14190144). Subsequently, cells were incubated for 10 min at 37°C with 25mL of PBS ([-$CaCl_2$], [-$MgCl_2$]). After incubation, most cells were floating in the PBS, but the flask was also vigorously shaken to completely detach all loosely attached cells. Floating cells were then pelleted by centrifugation at 2000rpm (460*g*) for 5 minutes at room temperature (Eppendorf 5804R) and re-suspended in 5mL of fresh warm medium (serum containing or serum-free). Cells were subsequently counted using a haemocytometer (Improved Neubauer Chamber, HawksleyVet).

For experimentation, BV2 cells were routinely seeded on 6-well plates at a density of 80 000 cells/well in 2mL of Serum-free RPMI medium (Life Technologies) supplemented with 100U/mL penicillin and 100µg/mL streptomycin. Cells were left to grow (deactivate) for at least 24h hours prior to any stimulation. BV2 cells grown in serum-free medium appear to be more ramified and respond better to stimuli. It is common practice to serum starve BV2 cells before and during stimulation as this relaxes and downregulates these cells (Li et al., 2016, Mairuae and Cheepsunthorn, 2018). There is evidence that points to autophagy, triggered by different cell stressors such as nutrient starvation, as the cause for this immune downregulation (Netea-Maier et al., 2016, Bussi et al., 2017). Serum starvation of BV2 cells is also used to reduce the mitogenic effect of serum (Li et al., 2016), which could affect the results of the stimulations.

2.2 Generation of *Trem2* and *Dap12* Knockdown BV2 cell lines using the CRISPR/Cas9 technology

2.2.1 Plasmid transfection of BV2 cells with Double Nickase plasmids

Trem2 (SC-429903-NIC) and *Dap12* (SC-423568-NIC) double nickases were bought from Santa Cruz Biotechnologies (Texas, USA). Double Nickase plasmids (Figure 4.1) consist of a pair of plasmids each encoding a D10A mutated Cas9 nuclease and a target-specific 20nt (nucleotide) guide RNA (gRNA) designed to knockout gene expression with greater specificity than the wild-type CRISPR/Cas9 protein. The sgRNAs contained in each of the nickase pairs used in this experiment were specifically designed to target the second and third exons of the mouse *Trem2* and *Dap12* genes, respectively.

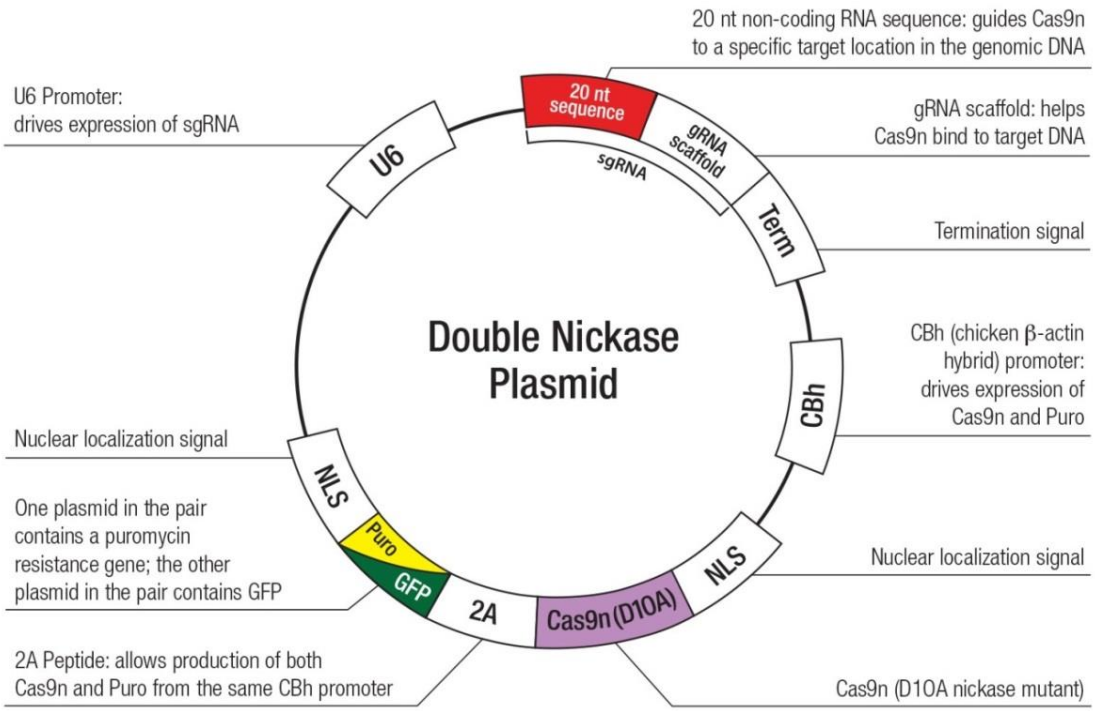

Figure 2.1 Double Nickase plasmids. Both *Trem2* (SC-429903-NIC) and *Dap12* (SC-423568-NIC) double nickase plasmids consist of a pair of plasmids each encoding a D10A mutated Cas9 nuclease and a target-specific 20nt guide RNA (gRNA) designed to knockout *Trem2* or *Dap12* mouse genes. One plasmid in the pair contains a puromycin-resistance gene while the other plasmid in the pair contains a GFP gene, both of which can be used for selection of positively transfected cells. In our experiment, expression of the fluorescent GFP protein was used for the selection of positively transfected clones.

BV2 cells were transfected with the 3µg of Double nickase plasmids using the D-Nucleofector™ System according to the manufacturer's instructions. Firstly, $0.5x10^6$ BV2 cells per sample were suspended in 100µl of P3 Primary Cell Nucleofector™ Solution containing 3µg of each Double nickase combination. Three nucleofections were prepared for the *Dap12 KO* ($1.5x10^6$ BV2 cells in total); two nucleofections were prepared for the *Trem2 KO* ($1.0x10^6$ BV2 cells in total) and one control transfection (no plasmid). Cells were nucleofected with the pre-set programme CM158 (standardization of the transfection programme and plasmid dose was done in house, data not shown). After transfection, cells were plated directly to 6-well plates (Corning, Cat# 3506, Germany) containing 2mL of pre-warmed RPMI 1640 medium (Gibco, Cat# 52400-025) supplemented with 10% foetal bovine serum (FBS), 100U/mL penicillin and 100mg/mL streptomycin. Cells were left to expand for 48 hours before single cell sorting. The sgRNA sequences can be found in Table 2-1.

Table 2-1 Double Nickase Plasmid's sgRNA sequences

Name of the nickase plasmid	Sequence	
	Strand A	Strand B
SC-423568-NIC Dap12 Double Nickase Plasmid (m)	TGAGCCCTGGTGTACTGGCT	CGGAAGAACAGTCGCATCTT
sc-429903-NIC Trem2 Double Nickase Plasmid (m)	GAAGCACTGGGGGAGACGCA	ATAAGTACATGACACCCTCA

2.2.2 **Clone sorting and expansion**

Nickase plasmids contained two selection markers for the isolation of positively transfected cells; 1) Puromycin resistance cassette and 2) Green Fluorescent protein (GFP). In this study, only the expression of the fluorescent GFP protein was used as a selection marker. To this end, 48 hours after transfection, plated cells were detached from the flasks using PBS ([-$CaCl_2$], [-$MgCl_2$]). Briefly, BV2 cells were incubated in 2mL PBS (Gibco, Cat # 14190-094) for 10 min and harvested from culture by pipetting the PBS up and down until most cells were detached. Cells were then pooled together and pelleted by centrifugation at 1600rpm (460*g*) for 5 minutes at room temperature (Eppendorf 5804R) and re-suspended in 400ul of PBS supplemented with 2% serum. Cells were transported on ice to the cell sorting facility.

Cells were FACS (Fluorescence-activated cell sorting) sorted on the FACSAria III Cell Sorter (BD Biosciences) to enrich for GFP+ cells. Only those cells with a high GPF expression (<1.0% of the original population) were sorted as individual cells into 3 96-well plates (per plasmid combination). Each well of the 96-well plates contained 200µl RPMI 1640 medium (Gibco, Cat# 52400-025) supplemented with 10% foetal bovine serum (FBS), 100U/mL penicillin and 100mg/mL streptomycin. Single cell sorting was carried out by Dr Ayad Eddaoudi at the UCL Great Ormond Street Institute of Child Health, Flow Cytometry Core Facility.

Cells were left to expand for 1 week and were inspected regularly, to ensure that cells were present. After the expansion period, 30 clones survived for the *Dap12 Ko* and 41 clones survived for the *Trem2 KO*. Clones were re-seeded into two identical 96-well plates (two plates for *Dap12* and two plates for *Trem2*) and left to grow until they were confluent. Once confluent, one duplicate 96-well plate was frozen down in complete RPMI 1640 medium supplemented with 10% DMSO and 50% FBS.

2.2.3 **Selection of CRISPR/Cas9 mutated cell clones by Next Generation Sequencing (NGS)**

2.2.3.1 ***Genomic DNA plate extraction***

Meanwhile, the clones from the second duplicate plate were re-seeded into a 48-well plate and left to grow until confluent. Once confluent, supernatants of each cell line were recover for detection of s*TREM2* by ELISA (see Section 2.2.4) and the cells were used for DNA extraction. DNA from all clones was extracted using the ZR-96 Quick-gDNA™ extraction Kit (Zymo Research, Cat# D3011, Germany) according to manufacturer's recommendations and finally eluted in 32µl of DNase/RNase free water. DNA concentration was then measured with Qubit® dsDNA BR Assay Kit (Life Technologies, Cat# Q32853).

2.2.3.2 ***PCR primer design for NGS (Next Generation Sequencing)***

Forward and reverse locus specific PCR primers were designed 60-165bp either side of the gRNAs' target site of both *Trem2* and *Dap12* double nickase plasmids (Figure 2.2).

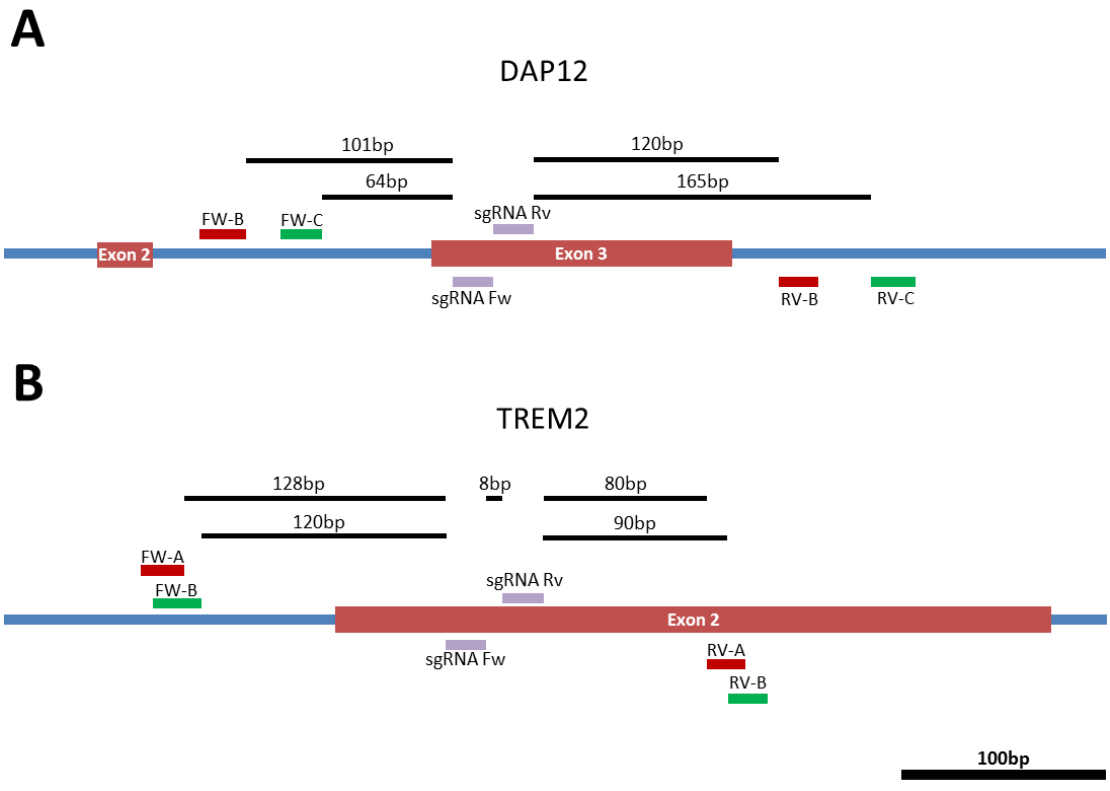

Figure 2.2 PCR primer and gRNA localization. Both *Trem2* (SC-429903-NIC) and *Dap12* (SC-423568-NIC) double nickase plasmids contain 2 target-specific 20nt guide RNAs (gRNA) that direct Cas9-mediated double nicking of *Trem2* or *Dap12* mouse genes. **(A, B)** PCR locus specific primers were designed 60-165bp either side of the gRNAs to allow efficient PCR amplification of the CRISPR/Cas9n edited genomic sequences for later NGS sequencing.

Subsequently, Illumina adapter overhang nucleotide sequences are added to the 5' end of the gene specific primers;

Forward overhang: 5' TCGTCGGCAGCGTCAGATGTGTATAAGAGACAG - [locus specific sequence]

Reverse overhang: 5' GTCTCGTGGGCTCGGAGATGTGTATAAGAGACAG - [locus specific sequence]

The full-length primer sequences (including the overhangs) are shown in Table 2-2.

Table 2-2 PCR primers For NGS sequencing

Name	Sequence	Size gene-specific primer, bp	Size (+Illumina overhang), bp	Amplicon product size (+Illumina overhang), bp
TREM2-FW-A	TCGTCGGCAGCGTCAGATGTGTATAAGAGACAGACCCAAGGACCAGAACTTATC	21	54	296 (363)
TREM2-RV-A	GTCTCGTGGGCTCGGAGATGTGTATAAGAGACAGTCCCATTCCGCTTCTTCAG	19	53	
TREM2-FW-B	TCGTCGGCAGCGTCAGATGTGTATAAGAGACAGAGGACCAGAACTTATCCTAATGAC	24	57	301 (368)
TREM2-RV-B	GTCTCGTGGGCTCGGAGATGTGTATAAGAGACAGATGACTGTGCTCCCATTCC	19	53	
TYROBP-FW-B	TCGTCGGCAGCGTCAGATGTGTATAAGAGACAGCTTTCTCTCTTCCTCTCAAAGAC	23	56	303 (370)
TYROBP-RV-B	GTCTCGTGGGCTCGGAGATGTGTATAAGAGACAGGTCCCAAAGTGTTCCAGAC	19	53	
TYROBP-FW-C	TCGTCGGCAGCGTCAGATGTGTATAAGAGACAGTCTCCTTCTAGCCCTCTTTG	20	53	311 (378)
TYROBP-RV-C	GTCTCGTGGGCTCGGAGATGTGTATAAGAGACAGTTTGATATTTGTGACCTTGACG	22	56	

After standardization of the PCR amplification protocol, the *TREM2* FW-A, *TREM2* RV-A, *DAP12* FW-B and *DAP12* RV-B were selected to amplify the CRISPR/Cas9 edited genomic regions.

2.2.3.3 ***First PCR amplification***

Prior to PCR amplification all genomic DNA (gDNA) samples were aliquoted and diluted to a final concentration of 5ng/µl; 2,5µl of gDNA from each clone was added into a 96-well plate to which was then added 22.5µl of PCR master mix. PCR mix was composed of the following; 5µl 1µM Forward and Reverse primers, 12.5µl 2x KAPA HiFi HotStart Ready Mix (KAPA Biosystems, Cat# KK2601) in a final volume of 22.5µl. PCR was conducted in a Mastercycler benchtop thermocycler (Eppendorf, Hamburg, Germany). Cycling conditions were as follows: 3 min at 95°C, followed by 35 cycles of amplification (30 sec at 95°C, 30 sec at 55°C and 30 sec at 72°C) and 5 min at 72°C.

After, amplification, 1µl of the PCR product was run on a Bioanalyzer DNA 1000 chip (Agilent Technologies, Cat # 5067-1504) to verify the size of the product. Expected size for both *Trem2* and Dap12 amplicons was 363bp and 370bp respectively (Table 2-2).

2.2.3.4 ***First Clean up***

PCR products were cleaned using AMPure XP beads (Beckman Coulter Genomics, Cat# A63881). Briefly, 20µl of AMPure XP beads was added to each well of the PCR amplicon plate and mixed gently by pipetting up and down. Then, the beads were left to incubate with the PCR products for 5 min at room temperature before placing the PCR plates on a magnetic stand for 2 min. Supernatants were discarded and the beads were washed twice with 200µl of freshly prepared 80% ethanol. After washes, the beads were

left to air-dry for 10 min on the magnetic stand. Once the beads were dry, the PCR plate was removed from the magnetic stand and the beads were resuspended in 53µl of 10mM Tris pH 8.5. Beads were left in 10mM Tris solution for 2 min before placing the plate on the magnetic stand. The plate was left on the magnetic stand until the supernatant was clear. Finally, using a multichannel pipette, supernatants were transferred from the amplicon PCR plate to a new 96-well plate, being careful not to carry over any beads to the new plate.

2.2.3.5 ***Second PCR amplification: Index PCR***

In this step, dual indices (for library identification) and Illumina sequencing adapters are added to the PCR products using the Nextera XT Index Kit (Illumina, Cat# FC-131-1002). Barcoded index primers (12 forward and 8 reverse) allow the unique barcoding of 96 PCR samples (or libraries). Briefly, 5µl of each cleaned-up PCR product was transferred into a new 96-well plate and the following was added: 5µl Nextera XT index Primer 1 (N7xx), 5µl Nextera XT index Primer 2 (S5xx), 25µl 2x KAPA HiFi HotStart Ready Mix (KAPA Biosystems, Cat# KK2601) and 10µl of PCR grade water, in a final volume of 50µl. Indices were added to each sample according to Figure 4.3. PCR was carried out in a Mastercycler benchtop thermocycler (Eppendorf, Hamburg, Germany). Cycling conditions were as follows: 3 min at 95°C, followed by 20 cycles of amplification (30 sec at 95°C, 30 sec at 55°C and 30 sec at 72°C) and 5 min at 72°C.

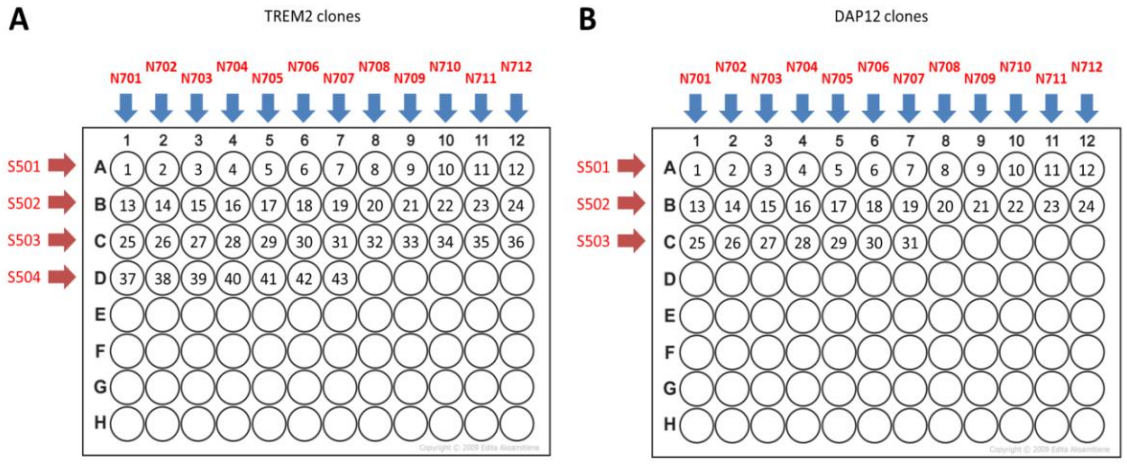

Figure 2.3 2nd PCR amplification: Index PCR. Dual indexing of PCR products is enabled by adding a unique Index 1 (i7) and Index 2 (i5) to each sample. The 96-sample Nextera XT Index Kit uses 12 different Index 1 adapters (N701-712) and 8 Index 2 adapters (S501-S508). **(A)** PCR products using *Trem2* specific primers were indexed using 43 different index combinations (41 clones + 1 positive (WT) control + 1 negative control). **(B)** PCR products using Dap12 specific primers were indexed using 31 different index combinations (30 clones + 1 control sample).

2.2.3.6 ***Second Clean up***

Like the first clean up, PCR products were cleaned using AMPure XP beads (Beckman Coulter Genomics, Cat# A63881). This time, 56µl of AMPure XP beads were added to each well of the 2nd PCR amplicon plate and mixed gently by pipetting up and down. Then, the beads were left to incubate with the PCR products for 5 min at room temperature before placing the PCR plates on a magnetic stand for 2 min. Supernatants were discarded and the beads were washed twice with 200µl of freshly prepared 80% ethanol. After washes, the beads were left to air-dry for 10 min on the magnetic stand. Once the beads were dry, the PCR plate was removed from the magnetic stand and the beads were re-suspended in 28µl of 10mM Tris pH 8.5. Beads were left in 10mM Tris solution for 2 min before placing the plate on the magnetic stand. The plate was left on the magnetic stand until the supernatant was clear. Finally, using a multichannel pipette, supernatants were transferred from the amplicon PCR plate to a new 96-well plate being careful not to carry over any beads.

Then, 1µl of a 1:50 dilution of the PCR products (libraries) was run on a Bioanalyzer DNA 1000 chip (Agilent Technologies, Cat# 5067-1504) to verify the size of the product. Expected size for both *Trem2* and Dap12 amplicons was ~450bp.

2.2.3.7 ***Library quantification, Normalization and pooling***

Concentration of PCR products, after the 2nd clean-up, was measured with Qubit® dsDNA BR Assay Kit (Life Technologies, Cat# Q32853). Concentration of the PCR products in nM was calculated based on the size of amplicons determined by the Bioanalyzer DNA 1000 chip and the following formula:

$$\frac{(\text{concentration in } \frac{\text{ng}}{\mu\text{l}})}{(660\,\frac{\text{g}}{\text{mol}}\ \text{x PCR product size in bp})} = \text{concentration in nM}$$

Once molarity was calculated for all PCR products, products were diluted to a final concentration of 4nM using Tris pH 8.5. Then, 5µl of each diluted product was pooled together in a single pooled library in a 1,5mL Eppendorf. The pooled library was kept at -20°C and used within 48h after preparation.

2.2.3.8 ***Library denaturing and sample preparation for NGS***

In preparation for NGS sequencing samples were denatured and mixed with an internal control for sequencing. Final sample preparation and sample loading was performed by Dr Deborah Hughes at the Molecular Neuroscience Department sequencing facility. Pooled libraries were sequenced using paired 300-bp reads on the Illumina MiSeq (San Diego, CA) and using MiSeq V3 reagents (Illumina, Cat# MS-102-3003). After

sequencing, trimming of adaptor sequences and indexes as well as alignment was completed by Dr Alan Pittman using R. Sequencing results were then visualised and aligned to the reference genome using Integrative Genomics Viewer (IGV) 2.3 (Thorvaldsdottir et al., 2013).

2.2.4 **Selection of CRISPR/Cas9 mutated cell clones – detection of s*TREM2* by ELISA (enzyme-linked immunosorbent assay)**

Conditioned medium from all clones (*Trem2* and *Dap12* CRISPR/Cas9 clones) was collected and tested for presence of soluble *TREM2* (s*TREM2*) using an ELISA assay. Conditioned medium from each cell line was collected when cells were confluent (see Section 2.2.3.1) and 24 hours after the last medium change. Cell medium was used immediately after recovery. Before performing the ELISA assay using the culture media, it was centrifuged at 2000 g for 5 min, to remove cells or cell debris.

Briefly, 96-well plates (Nunc MaxiSORP, ThermoFisher, Cat# DIS-971-010P) were coated overnight at 4°C with capture antibody: 100µl/well [1µg/mL] of anti-mouse *Trem2* mAb (R&D Systems; MAB17291) dissolved in PBS. Next day, plates were washed once with 1X PBS/0.1% Tween-20 and wells were blocked for 45 min with 100µl of 1% BSA dissolved in PBS. Plates were washed 3 times with 1X PBS/0.1% Tween-20. Subsequently, 50µl of neat supernatants was added in triplicate to the plates. At this point, 50µl of PBS was added into each well to reach a volume of 100µl. Concentration standards were prepared using recombinant murine *Trem2*-Fc (R&D Systems, Cat# 1729-T2-050) dissolved in 1X PBS, and added into the same plates.

Samples and standards were incubated in the plates for 2h at room temperature. Plates were then washed 3 times with 1X PBS/0.1% Tween before the detection antibody was added. 100µl [0.2µg/mL] of anti-mouse *TREM2* pAb-biotinylated (R&D Systems, Cat# BAF1729) was added to each well and incubated for 2h. Plates were washed again 3 times with 1X PBS/0.1% Tween. Then, 100µl [0.1µg/mL] of streptavidin-HRP (Invitrogen, Cat# SNN2004) was added to each well and incubated at room temperature for 45 min. Plates were washed 3 times with 1X PBS/0.1% Tween. Finally, 100µl/well of substrate solution TMB (Invitrogen, Cat# 00-2023) was added and left to react. Reaction was stopped with 50µl [0.5M] H_2SO_4 in H_2O. Absorbance was read at 450nm in a TECAN Spark 10M plate reader (TECAN, Switzerland). Values of the 3 technical replicates were averaged for analysis and graphical representation.

2.2.5 **Selection of CRISPR/Cas9 mutated cell clones by *Trem2* Western blotting**

2.2.5.1 ***Cell lysis***

In order to show that the expression of *Trem2* and Dap12 protein expression had been abolished in the CRISPR/Cas9 modified BV2 cells, a Western blot analysis was carried out using whole cell lysates from the gene-edited clones. Firstly, all clones BV2 clones were seeded into 25cm^2 flasks until they reached confluency. Confluent cells were harvested and divided into two 15mL falcons (approximately 1.5million cells/tube): one for genomic DNA extraction (kept at 4°C for 2-4h) and one for total protein extraction (processed immediately). For protein extraction, cells were spun down at 1600rpm (460*g*) for 5 min. Supernatants were discarded and pellets were dissolved in 200µl RIPA lysis buffer (150 mM sodium chloride, 1% Triton X-100, 0.5% sodium deoxycholate and 0.1% SDS, supplemented with 1mM of the protease inhibitor benzamidine, 4µg/mL of the protease inhibitor leupeptin, 1µM of phosphatase inhibitor microcystine LR and 0.1% of the reducing agent β-mercaptoethanol, pH 7.4) and transferred into 1.5mL Eppendorf tubes. Cell lysates were left rotating at 4°C for at least 30 min before centrifuging them at 14000*g* for 10 min to pellet the insoluble fractions. Supernatants were transferred to new Eppendorf tubes and all samples were stored at -20°C until they were quantified and analysed.

2.2.5.2 ***Bradford assay***

Protein concentration of the cell lysates was determined by means of a Bradford protein assay (Bradford 1976). Briefly, 1µl of each sample was added in triplicate into a 96-well plate. Then 200µl of Bradford assay reagent (Sigma, Cat# B6919) were added into each well. Parallel to the samples, a standard curve of BSA (bovine serum albumin) of known concentrations was constructed on the same plate. Samples were shaken and left at room temperature for 5 min before the absorbance was measured at 595nm on a Tecan X Fluor 4 plate reader. The BSA standard curve was used to calculate the protein concentration of each lysate.

2.2.5.3 ***Sodium Dodecyl Sulphate Polyacrylamide Gel (SDS-PAGE) Electrophoresis***

Proteins contained in the cell lysates were separated using SDS-PAGE gels. To this end, the Mini-PROTEAN Tetra Cell apparatus (BioRad, Cat# 1658005EDU) and 12% Mini-PROTEAN TGX Pre-cast gels (BioRad, Cat# 456-1044) were used. Firstly, the pre-cast gels were placed in their holders and into the tank filled with running buffer (25mM Tris-base, 192mM glycine and 0.1% SDS).

A volume equivalent to 45µg of total protein from each lysate was mixed with 4X Laemmli Sample Buffer (BioRad, Cat# 161-0747, supplemented with 10% β-mercaptoethanol). Before loading samples into gels, sample mixes were denatured by boiling them for 5 min. Denatured samples were then loaded into the gels together with a molecular weight marker (BioRad, Cat# 1610373). Gels were run at 160V (constant voltage) until the dye front was near the end of the gel (approximately 1 hour).

Following the separation of the proteins the gel was carefully removed from the casts and equilibrated for 20 min in cold transfer buffer (25mM Tris, 192mM glycine, 20% methanol, 0.01% SDS). Proteins were then transferred from the gel into a nitrocellulose membrane (BioRad, Cat# 1620112) which was previously equilibrated in transfer buffer. Transfer cassette (sandwich) was prepared as follows; one fibre pad, one 3MM chromatography paper, the run gel, a nitrocellulose membrane, one 3MM paper and another fibre pad, all soaked in ice-cold transfer buffer (25mM Tris-Base, 192mM glycine, 20% methanol, 0.01% SDS). The cassette was inserted into a BioRad mini gel transfer tank (BioRad, Cat# 1703930) for wet transfer. Proteins were transferred for 1.5 hours at 100V.

Transferred nitrocellulose membranes were subsequently blocked in PBS containing 5% milk for 1h at room temperature. Membranes were incubated with primary antibody (according to Table 2-3) in PBS containing 5% milk overnight at 4°C in an orbital shaker. Blots were developed with secondary antibody according to Table 2-3 (1:60 000 dilution in PBS) and visualised using an Odyssey Infrared Imaging System (Li-Cor Biosciences). Blots were re-probed for β-actin (Table 2-3) as a loading control to ensure equal loading of protein.

Table 2-3 Western Blot Antibodies

Target protein (weight kDa)	Antibody (Supplier)	Host, Isotype	Dilution
Primary			
Mouse TREM2 (25-40kDa)	AF1729 (R&D Systems)	Polyclonal sheep, IgG	1:500
Mouse DAP12 (10-12kDa)	12492 (Cell Signalling)	Monoclonal rabbit, IgG	1:500
Mouse β-actin (45kDa)	A5441 (Sigma)	Monoclonal mouse, IgG	1:10,000
Secondary			
Sheep IgG	713-655-147, Alexa Fluor® 790 conjugated (Jackson ImmunoResearch)	Polyclonal donkey, IgG	1:60,000
Rabbit IgG	A-11367, Alexa Fluor® 790 conjugated (Life Technologies)	Polyclonal goat, IgG	1:20,000
Mouse IgG	A-21058, Alexa Fluor® 680 conjugated (Life Technologies)	Polyclonal goat, IgG	1:30,000

2.2.6 **Sanger sequencing of *Trem2* and Dap12 CRISPR/Cas9 target regions**

A second genomic DNA extraction from each of the selected clones was performed using approximately 1.5million cells, harvested from the 25cm^2 flasks, and the DNeasy Blood & Tissue Kit (Qiagen, Cat# 69504). Once extracted, gDNA was used to amplify the *Trem2* and *Dap12* CRISPR/Cas9 target regions. Each clone was amplified using the same PCR primers (Table 2-2) and the same PCR conditions used for the NGS sample preparation (described above). The PCR amplification programme was modified as follows: 3 min at 95°C, followed by 35 cycles of amplification (30 sec at 95°C, 30 sec at 62°C and 30 sec at 72°C) and 5 min at 72°C.

Once the *Trem2* and *Dap12* CRISPR/Cas9 target regions were amplified, PCR products were cleaned using the QIAquick PCR Purification Kit (Qiagen, Cat# 28106). Cleaned samples were diluted in 30µl and quantified with the NanoDrop 1000 Spectrophotometer (Thermo Scientific). Finally, samples were diluted to 3.5ng/µl and sent to SourceBioscience (Cambridge, UK) to be Sanger sequenced.

2.2.7 **PCR product cloning and Single colony Sanger sequencing**

As an alternative to the NGS, PCR products for the *TREM2* CRISPR/Cas9 target region were cloned into plasmid vectors for sequencing and genotyping (Figure 2.4) – an approach known as Single colony Sanger sequencing. The same PCR products which were sent to be Sanger sequenced were cloned into plasmids using the Zero Blunt® TOPO® PCR Cloning Kit (ThermoFisher, Cat# K2895-20), as per manufacturers

recommendations. PCR products cloned into plasmids (TOPO® vector) corresponded to the *Trem2* CRISPR/Cas9 clones: A03, A04, A06, A07, A08, A10, B03, B04, B05, B08, B09, B11, B12, C04, C06, C08, C09, C10, C11, D01 and D05. These clones were selected based on the ELISA, Western blot and Sanger sequencing results.

Figure 2.4. Sequencing of cloned PCR products – Colony PCR. Single colony Sanger sequencing was used as an alternative to NGS (modified from Singh et al. (2015). To this end PCR products from the *Trem2* CRISPR/Cas9 target region were cloned into a TOPO® vector and transformed into DH5α-T1R E. coli cells. Plasmid DNA was extracted from at least 10 bacterial clones, for each initial PCR product, and sent for Sanger sequencing.

All the TOPO® vectors containing the PCR products were transformed into competent DH5α-T1R *E. coli* cells (ThermoFisher, Cat# 12297016) as per manufacturer's instructions. Briefly, a vial of competent cells was thawed on ice for each transformation. Each vial contained 50ul of competent cells. Next, 5µl of the cloned plasmids were added into each vial of chemically competent cells and tapped gently. The mixture was left to incubate 30 min on ice before heat-shocking the cells at 42°C for 30 sec. Cells were immediately returned to ice for 2 min. Subsequently, 250µl of SOC medium was added to each transformation and incubated at 37°C for 1 hour at 225rpm. After incubation, only 20µl of the bacterial suspension was streaked onto 10cm plates containing LB agar medium (Sigma Aldrich, Cat# L2897) supplemented with 100µg/mL ampicillin. Plates were incubated overnight at 37°C.

After transformation of DH5α-T1R *E. coli* cells, up to 12 colonies per CRISPR/Cas9 clone were selected for screening of positive clones. Single cell colonies were grown overnight in 3mL of LB medium (supplemented with ampicillin) at 37°C. Plasmid DNA was

extracted from the expanded single cell colonies using the QIAprep Spin Miniprep Kit (Qiagen, Cat# 27106). Purified plasmids were then digested using EcoRI restriction enzyme (Promega, Cat# R6011). Enzyme restriction reaction was as follows: 1µl of plasmid DNA, 6.5µl of DNase/RNase free water, 1µl of Buffer H 10X, 1µl of Bovine Serum Albumin acetylated and 0.5µl (6U) of EcoRI enzyme. Restriction was carried out at 37°C for 1h.

Restriction products were subsequently run in 1.5% agarose (Sigma, Cat# A9539) gels at 100v for approximately 45 min. Agarose gels were stained using the SYBR Safe DNA stain (Life Technologies, Cat# S33102) and DNA bands were visualised on a UV transilluminator (MiniBIS Pro, DNR Bio-Imaging Systems). Expected band size was 380bp (363bp+17bp) for the insert and 3939bp for the vector. The TOPO® vector possess 2 EcoRI restriction sites (17bp apart) on both sides of the insertion site. HypperLadder 100bp and HypperLadder 1kb (Bioline) were used to estimate the size of the inserted/cloned fragments.

Only those vectors which had an insert band of around 380bp were selected and sent for Sanger sequencing. Plasmids were sequenced using the standard M13F and M13R sequencing primers. Sequencing was outsourced and carried out by SourceBioscience (Cambridge, UK). At least 5 clones were used for alignment and analysis of each PCR product. Alignment of sequences and analysis was done using BioEdit Sequence Alignment Editor V7.2.5 (Hall, 1999).

2.2.8 **Second round of CRISPR/Cas9 gene editing on BV2 C8 cells**

Since the first round of CRISPR/Cas9 gene editing only produced heterozygous *Trem2* KO (*Trem2 +/-*, haploinsufficient cells), a second round of CRISPR/Cas9 editing was planned to produce homozygous *Trem2* KO (*Trem2 -/-*). Using the BV2 clone C8 as a starting point a 2nd round of CRISPR/Cas9 editing was performed. The rationale being that by targeting the WT allele in the clone C8 (*Trem2 +/-*), the HDR mechanisms will use the affected allele of the gene (34bp deletion) for repair, producing a homozygous knockout clone (*Trem2 -/-*). The same protocol as described in method sections 2.2.1 and 2.2.2 was used. Briefly, for the transfection step 3 simultaneous electroporations were performed using $0.5x10^6$ BV2 C8 cells each. After transfection cells were pooled together and seeded in a single well of a 6-well plate and incubated for 48h before cell sorting.

300 single cell clones were obtained after sorting of GFP positive cells. Following sorting, cells were left to expand for 1 week and inspected regularly. After the expansion period, 60 clones survived. Clones were re-seeded into two identical 96-well plates and left to

grow until they were confluent. Once confluent, one duplicate 96-well plate was frozen down in RPMI 1640 medium supplemented with 10% DMSO and 50% FBS.

2.2.8.1 ***Selection of homozygous Trem2 KO clones.***

The 34bp deletion of the BV2 C8 cells created a new restriction site for the enzyme AciI. This enzyme specifically cleaves the mutated allele of the C8 clone and spares its wildtype allele. In order to identify those BV2 cells which carried the 34bp deletion in homozygosity, the screening of the expanded clones used the AciI enzyme to unambiguously select clones which carried the 34bp in all alleles of the *Trem2* gene. To do this, the CRISPR/Cas9 target site was PCR amplified and subsequently amplicons were restricted using the AciI enzyme. Finally, restricted products were run on agarose gels for detection of cleaved products.

2.2.8.2 ***Plate genomic DNA extraction***

Firstly, DNA from the 60 BV2 C8 clones was extracted using the QuickExtract™ DNA Extraction Solution (Epicentre, Cat# QE09050) as per manufacturer's recommendations. Briefly, BV2 C8 clones were left to grow until >80% confluent in a 96-well plate. Once ready, cells were washed once with PBS ([+$CaCl_2$], [+$MgCl_2$]). After washing, 50µl of the QuickExtract™ DNA extraction solution was added into each well. Cell lysis was carried out by pipetting the solution up and down several times on each well, followed by incubation with the cells for 5 min before being transferred into a 96-well PCR plate and sealed. The sealed plate was vortexed and spun down before incubating it at 65°C for 15 min in a thermal cycler. The plate was vortexed and spun down again before incubating it at 95°C for 15 min in a thermal cycler. After extraction, an aliquot from each well (20µl) was diluted with nuclease free water (80µl). The diluted aliquot was used for downstream analysis.

2.2.8.3 ***PCR amplification and enzyme restriction selection***

Genomic DNA from each clone was subsequently used for the amplification of the CRISPR/Cas9 target region. 5µl of gDNA from each clone was added into a 96-well plate, to which was then added 20µl of PCR master mix. PCR mix was composed of the following; 2.5µl 10X Standard Taq Reaction buffer (New England Biolabs, Cat# M0273L), 0.5µl 10mM dNTPs (Thermo Fisher, Cat# 18427013), 0.5µl 10µM Forward and Reverse primers (Fw_Long_*Trem2*: GAGGTTCTTCAGAGTGATGGTG and Rv_Long_*Trem2*: CACCAAAGAACTGAGTCCAGATAG), 0.125µl Taq DNA Polymerase (New England Biolabs, Cat# M0273L) and 15.875µl of nuclease-free water. PCR was conducted in a Mastercycler benchtop thermocycler (Eppendorf, Hamburg, Germany). Cycling conditions were as follows: 3 min at 95°C, followed by 35 cycles of amplification (30 sec at 95°C, 15 sec at 62°C and 30 sec at 68°C) and 5 min at 68°C.

10µl of each PCR amplicon was subsequently visualised on a 1.5% agarose gel to verify the size of the amplicon (539bp). The remaining 15µl of PCR amplicon were enzyme restricted using the AciI nuclease (New England Biolabs, Cat# R0551L). Restriction reaction was prepared as follows: 15µl of PCR amplicon, 1.8µl 10X CutSmart® Buffer, 0.5µl AciI (5U) and 0.7µl of nuclease free water. Restriction was carried out at 37°C for 1h and 65°C for 20 min. Restriction fragments were visualised on a 2% agarose.

2.2.8.4 ***Sanger sequencing of Trem2 KO CRISPR/Cas9 candidates***

For Sanger sequencing of *Trem2* KO CRISPR/Cas9 candidates, a new PCR amplification using a high fidelity Taq polymerase was performed. The same gDNA samples used in the screening process were used to prepare the Sanger sequencing reactions. Each candidate clone was amplified using the same PCR primers (Fw_Long_*Trem2* and Rv_Long_*Trem2*) and the following conditions: 5µl of gDNA from each clone was added into a 96-well plate plus 20µl of PCR master mix. PCR mix was composed of the following: 1.5µl 1µM Forward and Reverse primers (Fw_Long_*Trem2* and Rv_Long_*Trem2*), 12.5µl 2x KAPA HiFi HotStart Ready Mix (KAPA Biosystems, Cat# KK2601) and 4.5µl of nuclease free water. PCR was conducted in a Mastercycler benchtop thermocycler (Eppendorf, Hamburg, Germany). Cycling conditions were as follows: 3 min at 95°C, followed by 35 cycles of amplification (20 sec at 98°C, 15 sec at 62°C and 15 sec at 72°C) and 1 min at 72°C.

PCR products were visualised in a 1.5% agarose gel to check the size of amplicons. Amplicons were then cleaned using the QIAquick PCR Purification Kit (Qiagen, Cat# 28106). Samples were diluted in 30µl of nuclease-free water and quantified with the NanoDrop Spectrophotometer (Thermo Scientific, NanoDrop 1000). Finally, samples were diluted to ~6ng/µl and then sent to be sequenced commercially (Source Bioscience, Nottingham, UK). Alignment of sequences and analysis was carried out using BioEdit Sequence Alignment Editor V7.2.5 (Hall, 1999).

2.2.9 **CRISPR/Cas9 off-target screening**

Detection of off-target damage on the CRISPR/Cas9 altered clones is important in the context of directed genetic manipulation. Using the nucleotide sequences for the 2 gRNAs employed to target *Trem2* and an online tool (http://crispr.mit.edu/), it was possible to find a list of likely off-target sites for the gRNAs used in our CRISPR/Cas9n system. In the case of the Strand B sgRNA targeting *Trem2,* the online tool predicted 219 possible off-target cuts, of these only 16 (7.3% of the total) were located in a gene coding region. None of these were among the top 5 most probable sites. For the Strand A sgRNA targeting *Trem2*, the online tool predicted 301 possible off-target cuts, of these 49 (16.3% of the total) were located in a gene coding region. Two of the top 5 most likely

off-target cuts were located in Ttll3 (NM_001142732) and Topbp1 (NM_176979) genes. In order to screen for possible off-target effects, PCR primers were designed for the top 5 off-target sites for each *Trem2* gRNA (Strand A or B) at least 80pb to each side (Table 2-4).

Table 2-4 PCR primers for amplification and sequencing of CRISPR/Cas9 off-target candidate sites

Primer Name	Sequence	Target sequence	Amplicon size, bp
TremOff_LEFT_1Fw	CCTGAGCTGCTTCCTGTATT	ATGTTTACATGACACCCTCAGAG	321
TremOff_LEFT_1Rv	ACCTCCATAGACCAGAGTATCA		
TremOff_LEFT_2Fw	AGATCAGCGTAGCTCTGTATTTA	ACAATTACATGCCACCCTCACAG	265
TremOff_LEFT_2Rv	TGAAGGGTAGCAGGGTTTG		
TremOff_LEFT_3Fw	GTCATATCTCACACTTCTACCCTATC	AGAAGTACTTAACACCCTCAGAG	278
TremOff_LEFT_3Rv	GGCAGCCTAAGAGTTGTTACT		
TremOff_L4new_Fw	CAGCGTGACTTGTCCTGTTAAG	TCCAGTTCATGACACCCTCAGGG	332
TremOff_L4new_Rv	TCACTGAGAGTGTCTCCATCAC		
TremOff_LEFT_5Fw	CCCTACTGTCAGAACAAGCATAG	ATACGTGCATGGCACCCTCATGG	295
TremOff_LEFT_5Rv	TGGAGAGAGCCAGCTTCATA		
TremOff_RIGHT_1Fw	GGGCTCTGCAAGTCATGTAA	GAAGGACTCGGGGAGACGCACAG	245
TremOff_RIGHT_1Rv	GGCTCTCTCTCTCTTTGGAATC		
TremOff_RIGHT_2Fw	TGAAGTGAGCTTGGTCTTTAGG	AAATGACTGGGGGAGACGCACAG	270
TremOff_RIGHT_2Rv	CTCATGGTAGTTGGGTGATGTATAG		
TremOff_RIGHT_3Fw	AAAGGAAAGAAGGGAGGGAAG	GAAGCACAGGGGGAGACTCATGG	275
TremOff_RIGHT_3Rv	CCCGCCTGGATCATCTATAAC		
TremOff_RIGHT_4Fw	GGTTGAGAGCCACTGAACTATAA	GAAGCACCGGGGGAGACCCACAG	277
TremOff_RIGHT_4Rv	GGTAGCATCGTGGGAAGAAA		
TremOff_RIGHT_5Fw	TGCAGCAGGCTCATCAC	GAAACACAGGAGGAGACGCACAG	267
TremOff_RIGHT_5Rv	AGTCTTTAATCAGGCGACAGTAA		

PCR amplification of off-target sites was carried out using gDNA from all CRISPR/Cas9 modified clones. Firstly, 5µl of gDNA from each clone was added into a 96-well plate and then added 45µl of PCR master mix. PCR mix was composed of the following; 1.5µl [1µM] Forward and Reverse primers (as per Table 2-4), 25µl 2x KAPA HiFi HotStart Ready Mix (KAPA Biosystems, Cat# KK2601) and 17µl of nuclease-free water. PCR was conducted in a Mastercycler benchtop thermocycler (Eppendorf, Hamburg, Germany). Cycling conditions were as follows: 3 min at 95°C, followed by 35 cycles of amplification (30 sec at 98°C, 30 sec at 62°C and 30 sec at 72°C) and 1 min at 72°C. The only exceptions to this programme were primers TremOff_L4new_FW and RV which had an annealing temperature of 68°C.

Once the off-target regions were amplified, PCR products were run in a 1.5% agarose gel to verify the size of the amplicons. PCR products were subsequently cleaned up using the QIAquick PCR Purification Kit (Qiagen, Cat# 28106). Cleaned samples were diluted in 30µl DNAse/RNAse free water and quantified with the NanoDrop spectrophotometer (Thermo Scientific, Nanodrop 1000). Finally, samples were diluted to ~6ng/µl and sent to SourceBioscience (Cambridge, UK) to be Sanger sequenced.

2.3 Generation of *Trem2* R47H BV2 cells using the CRISPR/Cas9 technology

This section describes the strategy and results used to introduce the *Trem2* R47H mutation into BV2 cells. The protocol used for generating *Trem2* R47H BV2 cells was the same as described by Ran et al. (2013b), with minor modifications.

2.3.1 Design of gRNAs and Single-strand DNA oligonucleotides (ssODN)

The design of the gRNAs was carried out using the CRISPR/Cas9 design online tool (http://tools.genome-engineering.org) and the DNA sequence of the second exon of the mouse *Trem2* gene. Using this web tool 5 different gRNAs (2 for the nickase plasmids and 3 for the WT nuclease plasmids) were designed. These gRNAs will direct the Cas9n or Cas9 enzymes to produce nicks or double strand breaks in the proximity of the codon that codes for the Argine 47 of the gene as shown in Figure 3.8. Sequences for the 5 gRNA are shown in Table 2-5.

Table 2-5 gRNA and ssODN used to introduce the *Trem2* R47H mutation on BV2 cells

Strategy/Purpose	Name	Sequence (5' -> 3')
Nickase plasmid construct (PX461)	gRNA Nickase Sense (S) gRNA Nickase Antisense (AS)	CAAGGCCTGGTGTCGGCAGC ATAAGTACATGACACCCTCA
WT nuclease plasmid construct (PX458)	1st gRNA 3rd gRNA 4th gRNA (AS)	ATGACGCCTTGAAGCACTGG AAGGCCTGGTGTCGGCAGCT CTCACCCAGCTGCCGACACC
Repair Template	ssODN (Single-Stranded Oligo Donor)	GCCCTCAACACCACGGTGCTGCAGGGCATGGCCGGCCAGTCCTTGA GGGTGTCATGTACTTATGACGCCTTGAAGCACTGGGGGAGAC**A**CA AGGCCTGGTGTCGGCAGCTGGGTGAGGAGGGCCCATGCCAGCGTG TGGTGAGCACACACGG

In order to introduce a mutation in the codon that corresponds to the 47th amino acid of the *Trem2* gene, an ssODN (single-stranded DNA oligonucleotides) carrying the R47H mutation was designed as a template for HDR. The ssODN was 152bp in length and had homology arms of 88bp and 63bp to each side of the nucleotide to be mutated (Figure 3.8) as recommended by Ran et al. (2013b).

To clone the sgRNA into the Cas9 expression vectors, two semi-complementary DNA oligonucleotides (named top and bottom respectively) had to be designed and synthesised for every sgRNA. As described in the paper by Ran et al. (2013b), these oligonucleotides had to be flanked by “extra” sequences to facilitate their base pairing and insertion to the CRISPR/Cas9 plasmids. Table 2-6 shows the sequences for those oligonucleotides; the “extra” flanking sequences are shown in red for each sgRNA. Since the sequences for both the sgRNA Nickase AS and the 2nd sgRNA were identical, the same oligonucleotide pairs were used to introduce the sgRNA into both the PX458 and PX461 CRISPR/Cas9 plasmids. The 5 pairs of oligonucleotides for sgRNA cloning and

the ssODN were synthesised commercially by Integrated DNA Technologies (IDT, Belgium).

Table 2-6 Oligonucleotides designed for the introduction of the targeting sgRNA into the CRISPR plasmids

Nucleotide name	Sequence 5' ->3' (bottom sequences are shown 3' -> 5')
sgRNA Nickase S Top	CACCGCAAGGCCTGGTGTCGGCAGC
sgRNA Nickase S Bottom	CGTTCCGGACCACAGCCGTCGCAAA
sgRNA Nickase AS Top	CACCGATAAGTACATGACACCCTCA
sgRNA Nickase AS Bottom	CTATTCATGTACTGTGGGAGTCAAA
1st sgRNA Top	CACCGATGACGCCTTGAAGCACTGG
1st sgRNA Bottom	CTACTGCGGAACTTCGTGACCCAAA
2nd sgRNA Top	CACCGATAAGTACATGACACCCTCA
2nd sgRNA Bottom	CTATTCATGTACTGTGGGAGTCAAA
3rd sgRNA Top	CACCGAAGGCCTGGTGTCGGCAGCT
3rd sgRNA Bottom	CTTCCGGACCACAGCCGTCGACAAA

2.3.2 Preparation of gRNA expression constructs

Each oligonucleotide was first dissolved with nuclease-free water to a final concentration of 100µM. In their corresponding pairs, the oligonucleotides were subsequently phosphorylated and annealed as follows: 1µl 100µM sgRNA top and bottom, 1µl 10X T4 ligation buffer, 1µl T4 PNK (New England Biolabs, Cat# M0201S) and 6µl nuclease-free water. The oligonucleotides were phosphorylated and annealed in a thermocycler using the following programme: 37°C for 30 min, 95°C for 5 min and a ramp down cycle to 25C at 5°C/min.

The annealed oligonucleotides were then diluted 1:200 using nuclease-free water. Subsequently, annealed oligonucleotides were ligated into the pSpCas9(BB)-2A-GFP WT Nuclease plasmid (Addgene, also known as PX458, Cat# 48138) or the pSpCas9n(BB)-2A-GFP nickase plasmid (Addgene, known also as PX461, Cat# 48140).

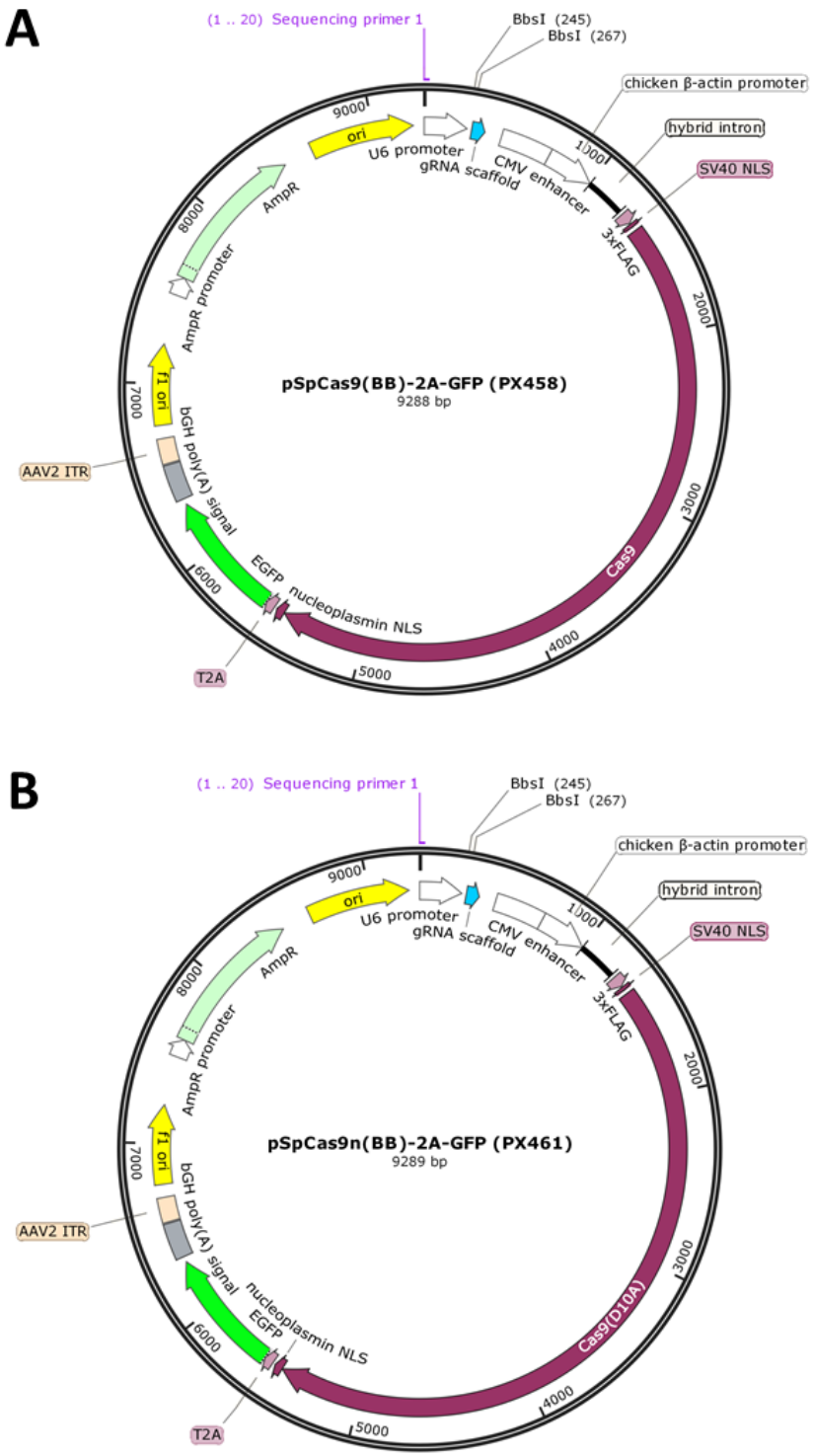

Figure 2.5 CRISPR/Cas9 plasmid backbones used to clone sgRNA for the introduction of the *Trem2* R47H mutation. sgRNAs were cloned into two different plasmids depending on the approach selected for introduction of the R47H mutation; (A) pSpCas9(BB)-2A-GFP WT Nuclease plasmid (also known as PX458) or (B) the pSpCas9n(BB)-2A-GFP nickase plasmid (also known as PX461). Both plasmids share the same architecture and more than 99.99% of their sequence identity, they only differ by 6 SNPs.

One ligation reaction was prepared for each sgRNA plus a negative control containing only the PX458 or PX461. Ligation reaction was prepared as follows: 2,5µl 100ng PX458 or PX461, 2µl 1:200 dilution annealed oligonucleotides, 2µl 10X tango buffer, 1µl 10mM

DTT (1,4-Dithiothreitol, Thermo Fischer, Cat# R0862), 1µl 10mM ATP (Adenosine 5'-triphosphate, New England Biolabs, Cat# P0756S), 1µl FastDigest BbsI (BpiI) (Thermo Fischer, Cat# FD1014), 0.5µl T7 ligase (New England Biolabs, Cat# M0318S) and 10µl nuclease-free water. Ligation was performed in a thermocycler for 1h; 6 cycles at 37°C for 5 min and 21°C for 5 min.

Ligation products were then treated with an exonuclease to destroy any non-ligated products. The exonuclease reaction was prepared as follows: 11µl of the ligation product, 1.5µl 10X PlasmidSafe buffer, 1µl PlasmidSafe ATP-dependent DNase (Epicentre, Cat# E3101K) and 1.5µl 10mM ATP (Adenosine 5'-triphosphate, New England Biolabs, Cat# P0756S). The reaction was incubated at 37°C for 30 min and 70°C for 30 min.

Treated ligation products were then transformed into One Shot Stbl3 chemically competent *E.coli* (ThermoFisher, Cat# C7373-03) as per manufacturer's instructions. Briefly, 2µl of the exonuclease treated ligation was added into 20µl of chemically competent Stbl3 cells on ice, the mixture was left to incubate 10 min on ice before heat-shocking the cells at 42°C for 30 sec. Cells were immediately returned to ice for 2 min. Subsequently, 100µl of SOC medium was added to each transformation and only 30µl of the bacterial suspension was streaked onto 10cm plates containing LB agar medium (Sigma Aldrich, Cat# L2897) supplemented with 100µg/mL ampicillin. Plates were incubated overnight at 37°C.

After overnight incubation, plates were inspected and colonies picked (5 per sgRNA plasmid construct) and seeded into a 15mL falcon containing 3mL of LB medium (Sigma Aldrich, Cat# L3022) supplemented with 100µg/mL ampicillin. Cultures were left incubating overnight at 37°C with moderate shaking.

The next day, 400µl of each bacterial growth were used to prepare glycerol stocks for long-term storage. The 400µl of bacterial growth were mixed with 600µl of 50% sterile glycerol (Sigma Aldrich, Cat# G5516) and frozen down to -20°C. The remaining bacterial culture was used for plasmid isolation using the QIAprep spin miniprep kit (Qiagen, Cat# 27106) as per manufacturer's instructions. Isolated plasmids were then sent to be commercially sequenced by SourceBioscience (Cambridge, UK) to verify that the correct insert had been cloned into the construct. The primer used for sequencing was U6-Fwd (GAGGGCCTATTTCCCATGATTCC). The sequenced region was then compared with the pSpCas9(BB)-2A-GFP cloning vector sequence to check that sgRNAs had been inserted in the correct position of the sgRNA scaffold.

2.3.3 **Production and isolation of sgRNA expression constructs**

For this step, glycerol stocks generated in the previous section (Section 2.3.2) were used. Firstly, starter cultures from each of the verified bacterial clones containing the correct sgRNA construct and the unmodified pSpCas9(BB)-2A-GFP vector were prepared. Starter cultures were pre-incubated in a 15mL falcon containing 5mL of LB medium (plus 100µg/mL ampicillin) with moderate shaking. After 6 hours, each starter culture was seeded in 1.2L of LB medium (plus 100µg/mL ampicillin) in conical flasks and left to grow overnight at 37°C with moderate shaking (200rpm). The next day, bacteria were harvested by centrifuging the LB medium at 6000*g* for 15 min at 4°C.

Pellets of harvested bacteria (one per each sgRNA construct) weighting between 4.2gr and 6.5gr were then processed with the EndoFree Plasmid Maxi Kit (Qiagen, Cat# 12362) as per manufacturer's instructions. The final isolated plasmid was diluted in 250µl of Endo-free water and stored at -20°C for later use.

2.3.4 **Optimization of transfection of plasmids PX458/461 into BV2 cells using the Cell Line Optimization 4D-Nucleofector™ X Kit**

Optimization of BV2 cells transfection was carried out using the Cell Line Optimization 4D-Nucleofector™ X Kit, the Cell Line 4D-nucleofector™ solution SF, the 4D-Nucleofector™ System (LONZA, Cambridge, UK) according to the manufacturer's instructions and the unmodified pSpCas9(BB)-2A-GFP (PX458) vector isolated as described in section 2.3.3. Briefly, BV2 cells were cultured as mentioned above in RPMI medium containing 10% (v/v) heat inactivated FBS and 100U/mL penicillin, 100µg/mL streptomycin at 37°C, 5% CO2. Once cells were 60-80% confluent, they were harvested using Trypsin and stopped trypsinization with 10mL of serum containing RPMI medium. Cell suspension was transferred to a 50mL falcon and cells were then pelleted at 2000rpm (460*g*) for 5 minutes at room temperature. Cells were re-suspended in PBS and counted using a haemocytometer.

In order to prepare the transfection master mix, 3.5 million cells were then pelleted at 2000rpm (460*g*) for 5 minutes at room temperature and re-suspended in 350µl of the Cell Line 4D-nucleofector™ solution SF (containing the supplement solution). Additionally, 7µg of the pSpCas9(BB)-2A-GFP vector was added to the master mix (final concentration was 20ng/µl).

Subsequently, 20µl of the master mix were transferred into each of the 16 wells of the 16-well Nucleocuvette™ Strip (200 000 cells and 400ng of construct per well). Once loaded with the cells and plasmids, the Nucleocuvette™ Strip was closed and placedinto the retainer of the 4D-Nucleofector™ X Unit, ensuring the correct orientation of the strip.

Nucleofection was performed using the Cell Line SF Opt1 pre-loaded programme. This programme tests 15 different nucleofection conditions, plus an extra untransfected control.

After transfection, cells were left to incubate on the Nucleocuvette™ Strip for 10 min at room temperature. Cells in each well were then resuspended using 100µl of RPMI complete medium and seeded into 6-well plates containing pre-warmed RPMI complete medium. Cells were left to grow at 37°C, 5% CO2 for 24h. In addition to the 16 conditions assayed in this optimization, a positive control transfection using the pmaxGFP plasmid was carried out at the same time. The positive control transfection was prepared using $1x10^6$ BV2 cells suspended in 100µl of SF solution containing 2µg of pmaxGFP plasmid, transfection was carried out using the pre-loaded programme CM-158.

2.3.5 **Functional validation of gRNA expression constructs: Surveyor assay.**

In order to assess the cutting efficiency of each of the gRNAs, BV2 cells had to be first transfected with the gRNA plasmids, GFP FACS sorted (to evaluate the efficiency of the gRNA only on transfected cells), DNA extracted and tested with the Surveyor assay.

Briefly, BV2 cells were cultured in complete RPMI medium until they reached 60-80% confluency. Cells were then harvested using PBS ([-$CaCl_2$], [-$MgCl_2$]) and washed once and re-suspended in PBS. Cells were counted using a haemocytometer and suspended with SF solution to a final concentration of $10x10^6$cells/mL. At this point, 4 different aliquots of the cell suspension were made. Each aliquot was supplemented with a different gRNA plasmid to a final concentration of 7µg of plasmid per 100µl of cell suspension (for the nickase constructs, 3.5µg of each plasmid was added).

Transfection was carried out using the 100µl single Nucleocuvettes™ as described in Section 2.3.4. After transfection, cells were left to grow for 48h before they were FACS sorted using their GFP signal. Cells were directly sorted (at least 10 000 events per gRNA) into a single well (per gRNA) of a 6-well plate and left to grow for 5 days before DNA was extracted. gDNA from each transfected population was extracted using the DNeasy Blood & Tissue Kit (Qiagen, Cat# 69504) as per manufacturer's instruction. gDNA was quantified using a NanoDrop 1000 Spectrophotometer (Thermo Scientific).

The Surveyor assay is an enzymatic cleavage assay used to detect single base mismatches or small indels. This assay is routinely used to identify mutations and confirm genome modifications like those introduced by CRISPR/Cas9 technology. For this experiment, the Surveyor® Mutation Detection kit (IDT, Cat #706020) was chosen for the identification of mutations in the CRISPR/Cas9 modified clones. The first step in this assay is the PCR amplification of the target region. PCR amplification was carried

out using the Fw_Long_*Trem2* (GAGGTTCTTCAGAGTGATGGTG) and Rv_Long_*Trem2* (CACCAAAGAACTGAGTCCAGATAG) primers and 2µl of gDNA (~50ng). The PCR master mix was prepared as follows: 25µl 2X KAPA HiFi HotStart Ready Mix (KAPA Biosystems, Cat# KK2601), 1.5µl 10µM forward and reverse primers and 20ul of nuclease-free water. PCR was conducted in a Mastercycler benchtop thermocycler (Eppendorf, Hamburg, Germany). Cycling conditions were as follows: 3 min at 95°C, followed by 35 cycles of amplification (20 sec at 98°C, 15 sec at 62°C and 15 sec at 72°C) and 1 min at 72°C.

5µl of each PCR product was subsequently visualised on a 1.5% agarose gel to verify the size of the amplicon (539bp). The remaining PCR amplicon was cleaned using the QIAquick PCR Purification Kit (Qiagen, Cat# 28106). Cleaned samples were diluted in 30µl and quantified with the Nanodrop 1000 spectrophotometer (Thermo Scientific). Finally, clean PCR products were diluted to 20ng/µl.

The next step was the formation of DNA heteroduplexes with the PCR products. The heteroduplex formation reaction was performed as follows: 2µl 10X Standard Taq Reaction buffer (New England Biolabs, Cat# M0273L) and 18µl 20ng/µl PCR product. The DNA heteroduplex mix was then incubated as per Table 2-7 to facilitate heteroduplex formation.

Table 2-7 Cycling programme for heteroduplex formation of PCR products

Cycle number	Cycling programme
1	95°C, 10min
2	95-85°C, -2°C/s
3	85°C, 1min
4	85-75°C, -0.3°C/s
5	75°C, 1min
6	75-65°C, -0.3°C/s
7	65°C, 1min
8	65-55°C, -0.3°C/s
9	55°C, 1min
10	55-45°C, -0.3°C/s
11	45°C, 1min
12	45-35°C, -0.3°C/s
13	35°C, 10min
14	35-25°C, -0.3°C/s
15	25°C, 1min
16	25-4°C, -0.3°C/s
17	4°C, hold

After heteroduplex formation, annealed products were digested with the SURVEYOR nuclease. Digestion reaction was prepared as follows: 20µl of heteroduplex product, 2.5µl 0.15M $MgCl_2$ (final concentration 15mM), 0.5µl Nuclease free water, 1µl SURVEYOR nuclease S (final concentration), 1µl SURVEYOR enhancer S (final concentration 1X). Digestion was carried out at 42°C for 30 min. After incubation, digestion was stopped by adding 2µl of the kit's Stop Solution to each well; samples were then either stored at -20°C for later analysis or run immediately in a 1.5% agarose gel. Positive (kit's control) and negative (no SURVEYOR) controls were also run in the same gels.

Gel was imaged using the MINIBIS gel doc system (DNR Bio-Imaging Systems) and estimation of the cleavage intensity was done using ImageJ software. Calculation of the fraction of PCR product cleaved (f_{cut}) and Indel occurrence (Indel%) estimation were performed as described by Ran et al. (2013b). The two formulas used for this estimation are shown in Equation 1. For the f_{cut} calculation, *a* represents the integrated intensity of the undigested PCR product while *b* and *c* are the integrated intensities of each cleavage product.

Equation 1 Formulas used for the estimation of Indel occurrence.

A

$$f_{cut} = \frac{(b + c)}{(a + b + c)}$$

B

$$indel\ (\%) = 100 \times \left(1 - \sqrt{(1 - f_{cut})}\right)$$

2.3.6 **Plasmid and ssODN transfection, cell sorting and expansion**

Plasmid and ssODN transfection were carried out as described in Methods section 2.2.1. Transfection conditions (transfection programme EN-150 and plasmid concentration of 7µg per 10^6cells) were as per the optimised conditions obtained from Methods section 2.3.4. Co-transfection of the CRISPR/Cas9 plasmids and the ssODN (10pmol per transfection) used the same optimised conditions from Methods section 2.3.4.

Cell sorting (based on GFP fluorescence) and cell expansion were carried out as described in Methods section 2.2.2.

2.3.7 **Screening of R47H CRISPR/Cas9 modified clones by RFLP (Restriction Fragment Length Polymorphism)**

Screening of the *R47H* positive clones was done using RFLP analysis. Firstly, total gDNA extraction and PCR amplification of the CRISPR/Cas9 targeted region were carried out as described in methods sections 2.2.8.2 and 2.2.8.3. Once amplified, 10µl of each PCR amplicon was run and visualised on a 1.5% agarose gel to verify their correct size (539bp).

The remaining 15µl of PCR amplicon was enzyme restricted using the BsmBI nuclease (New England Biolabs, Cat# R0580L). Restriction reaction was prepared as follows: 15µl of PCR amplicon, 1.8µl 10X NEBuffer 3.1, 0.5µl BsmBI (5U) and 0.7µl of nuclease free water. Restriction was carried out at 55°C for 1h and 80°C for 20 min. Restriction fragments were visualised on a 2% agarose gel using the MINIBIS gel doc system (DNR Bio-Imaging Systems).

2.3.8 **Sanger sequencing of *Trem2 R47H* CRISPR/Cas9 modified candidates**

For Sanger sequencing of the target sequence of the *Trem2 R47H* CRISPR/Cas9 candidates, a second PCR amplification was performed. This second PCR was prepared with a high fidelity Taq polymerase and the same gDNA used for the screening step. PCR reaction preparation (using primers Fw_Long_*Trem2* and Rv_Long_*Trem2*) and cycling were carried out as described in method section 2.2.8.4.

PCR products were visualised in a 1.5% agarose gel to check the size of the amplicon. Amplicons were subsequently cleaned up with the QIAquick PCR Purification Kit (Qiagen, Cat# 28106). Purified PCR products were diluted in 30µl of nuclease-free water and quantified with the NanoDrop 1000 spectrophotometer (Thermo Scientific). Finally, samples were diluted to ~6ng/µl and sent to be sequenced commercially (Source Bioscience, Nottingham, UK). Alignment of sequences and analysis was carried out using SnapGene V4.0.2 software (GSL Biotech). TIDE (Tracking of Indels by DEcomposition) analysis was performed using .ab1 files obtained from Sanger sequencing and the online tool (https://tide-calculator.nki.nl/) (Brinkman et al., 2014).

2.4 **Characterization of *Trem2* +/- and -/- BV2 clones**

2.4.1 **Cell treatments**

WT, A7, C8, B5 and G4 cell lines were plated in serum-free media 24h prior to treatment to ensure they were down-regulated and in a resting state. For mRNA gene expression experiments, treatments were done in triplicate (3 wells of a 6-well plate, each containing 80 000cells in 2mL of serum-free medium) for each biological replicate (n). For mRNA extraction, lysates from the triplicate wells were pooled together before RNA extraction.

Cells were activated with 1µg/mL LPS (Sigma, Cat# L2762, serotype: 026:B6, Dorset, UK), 10% FBS or a combination of both for 24h. For cytokine release analysis, cells were treated with 100ng/mL LPS (Sigma, Cat# L2762, serotype: 026:B6, Dorset, UK), mouse IL4 (Peprotech, Cat# 214-14) and Mouse Transforming Growth Factor β1 (TGFβ, New England Biolabs, Cat# 5231LC). For Western blot analysis, 463 000 cells were seeded in 10cm plates (approx. 12 000cells/cm^2) and left untreated for 24h before cell lysis and protein extraction.

2.4.2 **qPCR analysis of gene expression of clones A7, C8 (*Trem2* +/-), B5 and G4 (*Trem2* -/-)**

2.4.2.1 ***RNA extraction***

After treatment, cells were lysed directly on the plate. Briefly, medium from each well was discarded and 350µl of Qiazol Lysis Reagent (Qiagen, Cat# 79306) was added into each well. Lysis reagent was left to incubate for 5 min at room temperature and plates were subsequently vortexed for 10 sec. At this point, the 3 replicates of each treatment were pooled together into a single 2mL Eppendorf (total volume 1.05mL). Lysates were then frozen at -20°C or -80°C and processed later.

Total RNA from the stimulated BV2 WT, A7, C8, B5 and G4 clones was isolated using the RNeasy Mini Kit (Qiagen, Cat# 217004) according to manufacturer's recommendations with minor modifications to allow for the set-up of the experiment (see section 2.6.2). All total RNA samples were treated with DNAse in column according to manufacturer's recommendations. Extracted RNA was eluted in 32µl of DNase/RNase free water. The concentration and quality of the total RNA was determined using a NanoDrop 1000 spectrophotometer (Thermo Scientific) and the A260:280 and 260:230 ratios.

2.4.2.1 ***Reverse-transcription and quantitative PCR (qPCR)***

cDNA was synthesised from total RNA (0.5µg), using a High-Capacity cDNA Reverse Transcription Kit (Life Technologies, Cat# 4368813) in a total volume of 20µl. The reverse transcription (RT) master mix contained the following: q.s.p 0.5µg total RNA, 2µl 10X RT buffer, 0.8µl (100mM) dNTP mix, 2.0µl 10X RT Random primers, 1µl MultiScribe™ Reverse Transcriptase, q.s.p 9µl Nuclease free water. Reverse transcription was performed in a Mastercycler benchtop thermocycler (Eppendorf, Hamburg, Germany). Cycling parameters were as follows: 10 min at 25°C, 120 min at 37°C, 5 min at 85°C and held at 4°C.

qPCR amplification and data acquisition was performed in Mx3000P multiplex PCR System (Stratagene, California, USA), using Taqman probes (see Table 2-8). The use

of Taqman probes with two different fluorophores (FAM and VIC) allowed the gene expression quantification of two genes in a single tube, reducing assay cost and improving accuracy. This approach is termed “multiplex qPCR” and was used for the gene expression analysis of *Trem2* and *ApoE* (both associated with FAM, 494/518nm), relative to the normalizer gene *Gapdh* (associated with VIC, 538/554nm).

Table 2-8 Taqman probes used for the relative gene expression quantification of microglial genes

Gene Name (amplicon length)	Normalizer gene	Assay name (Thermo Fischer)	Fluorescent dye - quencher
Actb (115bp)	GAPDH	Mm00607939_s1	FAM-MGB
Apoe (79bp)	GAPDH (multiplex)	Mm01307193_g1	FAM-MGB
Arg1 (65bp)	Tbp	Mm00475988_m1	FAM-MGB
Cd33 (71bp)	GAPDH	Mm00491152_m1	FAM-MGB
Cd40 (68bp)	GAPDH	Mm00441891_m1	FAM-MGB
IL1b (90bp)	Tbp	Mm00434228_m1	FAM-MGB
Plxna1 (111bp)	Tbp	Mm00501110_m1	FAM-MGB
Tnf (81bp)	GAPDH	Mm00443258_m1	FAM-MGB
Trem2 (90bp)	GAPDH (multiplex)	Mm04209424_g1	FAM-MGB
Tyrobp/Dap12 (64bp)	GAPDH	Mm00449152_m1	FAM-MGB
GAPDH (107bp - for multiplex)	-	Mm99999915_g1	VIC-MGB
GAPDH (107bp)	-	Mm99999915_g1	FAM-MGB
Tbp (73bp)	-	Mm00446973_m1	FAM-MGB

The qPCR master mix for multiplex contained: 10µl 2X TaqMan® Universal Master Mix II, with UNG (Applied Biotechnologies, Cat 4440038), 1µl of each 20X TaqMan®Gene Expression Assay (Table 2-8), 6µl Nuclease free water and 2µl of diluted cDNA (1:10 dilution) in a final volume of 20µl. Samples were run in triplicate (technical replicates) in the same plate. Cycling conditions were as follows: activation of DNA polymerase 2 min at 50°C, cDNA denaturation 10 min at 95°C, followed by 40 cycles of amplification (15 sec at 95°C and 1 min at 60°C). To ensure there was no reagent or DNA contamination in the RNA samples, no RT (reverse transcriptase) and NTC (no-template control) controls were used in all experiments.

For the relative quantification of the mRNA expression, two main endogenous controls were utilised: *Gapdh* and *Tbp*. The use of one particular endogenous control over the other depended on their correlation coefficient (R^2), dynamic range and amplification efficiency. To this end, a standardization step was performed in control samples (data not shown) according to the Taqman probes’ manufacturer recommendations

(ThermoFischer, Real-time PCR handbook). *Actin* was not used as the endogenous control gene, because of concerns regarding its accuracy as a normalizer at the mRNA level. Piehler et al. (2010) have shown that of RT-qPCR normalization using *Gapdh* or *Actb* alone lead to inaccurate gene expression measurements in LPS-stimulated monocytes. However in our set up, *Actin* was the only normalizer gene shown to have variability related to cells' stimulations. As shown in Figure 5.9, *Actin* mRNA expression is upregulated during LPS in a dose dependent manner at 24h. Furthermore, the RNAseq experiment showed a statically significant upregulation of *Actb* (β-actin) at the 6h timepoint by both IL4 and LPS stimulations, something that was not seen in the case of *Tbp* or *Gapdh*, the two normalizer genes selected for mRNA experiments in this thesis (data not shown).

2.4.2.2 ***qPCR relative quantification and statistical analysis***

Relative quantification of mRNA expression was calculated using the ΔΔCT (Livak) method (Livak and Schmittgen, 2001). Ct (cycle threshold) values were normalised to the housekeeping genes *Gapdh* or *Tbp* (normalizer genes). Ct values for the 3 technical replicates were averaged before normalization. Gene expression levels are expressed relative to the untreated control, unless indicated differently. qPCR experiments on the 5 cell lines were performed in at least twice (biological replicates or n≥2) and statistical significance was calculated using a 2-way ANOVA with Dunnett's correction.

2.4.3 **Western blot analysis of TREM2 protein expression in A7, C8 (*Trem2 +/-*), B5 and G4 (*Trem2 -/-*)**

2.4.3.1 ***Cell lysis and protein quantification***

All 5 clones were seeded in serum-free conditions in a 10cm dish at a density of 463 000cells/plate (approx. 12 000cells/cm^2). Cells were left to grow/attach for 24h at 37ºC, 5% CO_2. Whole cellular protein extracts were obtained from all 5 clones 24h after seeding. Cells were lysed using 80µl of modified RIPA buffer (50mM Tris pH 8.0, 150mM NaCl, 1% NP40, 0.5% deoxycholate, 0.1% SDS) supplemented with 1X Halt™ Protease Inhibitor Cocktail (ThermoFisher, Cat# 78430). Lysis buffer was added on top of the washed cells and cells were scrapped using a rubber policeman. Lysates were incubated 30 min at 4°C and subsequently spun down at 14 000*g* for 10 min at 4°C. Supernatants were recovered and used immediately or stored at -20°C for later use.

A Bradford protein determination assay (Bradford, 1976) was carried out to determine the protein concentration of the whole cellular extracts as mentioned in Section 2.2.5.2.

2.4.3.2 **TREM2 *deglycosylation of whole cellular protein extracts from the Trem2 clones***

An appropriate volume of each whole cell extract containing 15µg of total protein was used for deglycosylation of the TREM2 protein using the PNGase F digest kit (New England Biolabs, Cat# P0704L). Firstly, the proteins were denatured by adding the kit's denaturing buffer to a final concentration of 1X and incubating at 100°C for 10 min. Samples were then left to cool down at room temperature. Finally, the deglycosylation reaction was prepared as follows: 15µg of denatured protein extract, 1X G7 reaction buffer, 1% NP-40 and 500U PNGaseF enzyme. Deglycosylation was carried out at 37°C for 1 hour.

2.4.3.3 ***SDS-PAGE Electrophoresis***

Deglycosylated whole cell protein extracts (15µg) were separated by SDS-PAGE gel electrophoresis. Samples were first mixed with 4X Laemmli Sample Buffer (BioRad, Cat# 161-0747) and then loaded onto a premade 12% SDS-PAGE gel (BioRad, Cat# 456-1044) together with a molecular weight marker (BioRad, Cat# 1610373). Gels were run at 150V until the dye front was near the end of the gel (approximately 75 min).

After migration, the gel was carefully removed from the casts and wet transferred (tank) onto a 0.2µM nitrocellulose membrane. The transfer solution was composed of 1X Tris/Glycine Transfer buffer (Biorad, Cat# 1610734) and 20% Methanol dissolved in water. Transfer was completed on ice at 100V for 60 min. After transfer, the nitrocellulose membrane was washed with PBS-T (0.1% Tween-20) for 10 min and subsequently blocked with 5% non-fat milk solution in PBS-T for 30 min to prevent non-specific binding of the antibody. The membranes were then ready for immunoblotting.

Membranes were incubated with anti-*TREM2* primary antibody (according to Table 2-3) in PBS-T containing 5% milk overnight at 4°C in an orbital shaker. The anti-*TREM2* primary antibody used for the detection was the sheep polyclonal antibody AF1729 (R&D, sheep polyclonal). This antibody was generated using the recombinant mouse protein *TREM2*b, amino acids 19 to 168 (150aa in total). The nitrocellulose membranes were then washed 3 times (10 min each) with PBS -T (0.1% Tween-20).

Blots were developed with secondary antibody according to Table 2-3 (1:10 000 dilution in 1:1 mix of PBS-T and Odyssey PBS blocking buffer). Nitrocellulose membranes were washed 3 times (10 min each) with PBS-T (0.1% Tween-20). Results were visualised using an Odyssey Infrared Imaging System. Blots were re-probed for β-actin (Table 2-3) as a loading control. β-actin was chosen as loading control for the western blot experiment as only one *TREM2* measurement was performed (24h after seeding). At the

mRNA level, *Actin* (and *Gapdh*) is not recommended to be used as the sole gene normaliser as it may lead to imprecise expression results in LPS stimulated monocytic cells (Piehler et al., 2010). However, since TREM2 protein quantification was done at a single timepoint and under immunologically down-regulated conditions (serum-free media) this is not likely to affect the experimental result.

Three independent biological replicates (n=3) were performed for this experiment

2.4.4 **Detection of sTREM2 by ELISA**

Cells of the 5 clonal lines (WT, A7, C8, B5 and G4) were seeded into a 6-well plate at a density of 80 000cells/well under serum-free conditions. Cells were left to grow for 24h at 37°C, 5% CO_2 prior to any treatments. Treatments were carried out for 24h and supernatants were recovered immediately after. Supernatants were centrifuged at 2000*g* for 5 min to remove cell debris. Subsequently, cell pellets were discarded and supernatants were recovered in a new 1.5mL Eppendorf. At this point, supernatants were stored at -80°C for later analysis or used immediately. Detection of sTREM2 was performed on the supernatants of the 5 cell lines according to the same protocol described in Section 2.2.4. Three independent biological replicates (n=3) were performed for this experiment

2.4.5 **Immunostaining: TREM2 and Golgi apparatus.**

Cells were seeded into coverslips at a density of 20 000 cells per coverslip in serum-free medium. After 24h in culture, cells were washed once with PBS and then fixed with ice cold methanol for 20 minutes at -20°C. Subsequently, cells were washed 3 times (10 min each) with PBS and blocked with 3% BSA in PBS for 30 min at room temperature. For staining, two primary antibodies were used: 1) Anti-*Trem2* (polyclonal sheep IgG, R&D Systems, Cat# AF1729) and 2) Anti-Golgin (monoclonal rabbit IgG, Cell Signalling Technologies, Cat# CST 13192). Anti-*TREM2* was used at a final concentration of 10µg/mL and Anti-Golgin was used at a dilution of 1:100 in 3% BSA (in PBS). Primary antibodies were incubated for 2h at RT. After incubation with primary antibodies, cells were washed 3 times (10 min each) with PBS. Two secondary antibodies were used: Donkey anti-sheep IgG conjugated with Alexafluor 568 and Goat anti-rabbit IgG conjugated with Alexafluor 488 (both from ThermoFisher). Secondary antibodies were added at a dilution of 1:1000 for 1h at RT. Following incubation, cells were washed 3 times (10 min each) with PBS. Coverslips were gently dabbed on paper and mounted into glass slides using Vectashield containing DAPI. Slides were stored protected from light and kept at 4°C until they were imaged. Image acquisition was performed in a confocal microscope (Zeiss LSM 880 with AiryScan) and image processing was done using the ZEN 2.3 software (CarlZeiss). For image analysis, fluorescence thresholds

were set using WT cells stained only with the secondary antibodies as negatives. Two independent biological replicates (n=2) were performed for this experiment.

2.4.6 **Phagocytosis assays**

To assess the impact of *Trem2* deficiency on phagocytosis, two different phagocytosis assays were utilised; the pHrodo™ Green Zymosan A Bioparticles® Conjugate (ThermoFisher, Cat# P35365) and the pHrodo™ Green E. coli BioParticles® Conjugate (ThermoFisher, Cat# P35366). For experimentation, cells were seeded at $1x10^5$ per well of a 24-well plate in 1% serum RPMI medium 24h hours before stimulation. 2h prior to adding the pHrodo™ Bioparticles, a group of cells was treated with Cytochalasin D (final concentration of 10µM) as a negative control for phagocytosis in the experiment. Cytochalasin D is an actin-polymerization inhibitor, its addition into the medium can reveal whether the uptake of particles is reliant on actin-dependent mechanisms or not. The experiment was not performed under serum-free conditions because cells grown without serum firmly attach to the culture plate; making them unrecoverable in enough numbers for FACS analysis. To avoid this problem, cells were grown in 1% serum medium (very-low serum concentration). It is worth mentioning that, in a recent paper by Bohlen et al. (2017), the authors showed that serum supplementation of microglial cells increases their phagocytic capacity *in vitro,* probably adding an extra confounding factor into the experimental design.

Two hours after stimulation with Cytochalasin D, all cells were treated with either 50µl (0.5mg/mL) of the Zymosan Bioparticles or 50-25µl (1mg/mL) of the *E. coli* Bioparticles. At this point, one group of cells was left “untreated”, meaning neither Cytochalasin D nor fluorescent beads were added to its culture medium, in order to be used as a “no beads” negative control for the experiment. Once the fluorescent beads were added, cells were left to incubate for 30 min. Once the 30 min passed, cell supernatants were removed and cells were detached from the plates and re-suspended in 2% BSA solution in PBS. Analysis of the cells was done by flow cytometry using a FACSCalibur cell sorter (BD Biosciences, USA) at the appropriate excitation/emission maxima (509/533nm). Results (at least 10 000 events were acquired per condition) were analysed using the FlowJo V10 software (FlowJo LLC). Two independent biological replicates (n=2) were performed for each of the *E. coli* particle concentrations (50µg and 25µg), while three independent biological replicates (n=3) were performed for the zymosan particles.

2.4.7 **Migration assay**

The effect of *TREM2* deficiency on migration was assessed using the Cell Migration/Chemotaxis Assay Kit (PromoKine, Cat# PK-CA577-K906) as per manufacturer’s recommendations, with some modifications to allow for our set up.

Briefly, $1.5x10^6$cells from each cell line were seeded in $175cm^2$ flask, 48h before experimentation in 10% FBS RPMI medium. 24 hours prior to the experiment, the medium on the flasks was changed to 0.5% FBS RPMI medium. On the day of experimentation, cells were harvested with trypsin and pelleted at 2000rpm (460*g*) for 5 minutes at room temperature (Eppendorf 5804R) and re-suspended in the assay's Wash buffer. Cells were counted and re-suspended at $1x10^6$cells/mL in serum-free medium.

The bottom chamber of the migration assay plate was then filled with 150µl of medium containing the desired chemoattractant. Treatments were applied in triplicate (technical replicates). The kit's Control Migration inducer was used as a positive control chemoattractant. The manufacturer recommends to use a no-chemoattractant well as negative control for the experiment, as this will only allow basal migration of cells between chambers. This a control was used in our experiment (untreated). Cells were seeded in the top chamber of the migration assay plate, 50µl per well (50 000cells); volume was completed to 100µl with serum-free medium. Cells in the Cell Migration Chamber were left to incubate for 12h at 37°C in 5% CO_2 incubator.

Simultaneously, a cell number standard curve was prepared in a separate clear 96-well plate. Standard curve was prepared by serially diluting the cells 1:1 in Wash buffer (from 50 000 to 781 cells per well) in a final volume of 100µl/well. Once seeded, 10µl of the Cell Migration Dye was added to each well and the plate was incubated at 37°C for 1h. Fluorescence was read at 530/590nm (Ex/Em) in a plate reader. Finally, the number of cells was plotted against the RFU (Relative Fluorescence Units) results obtained from the plate reader.

After 12h of incubation in the Cell Migration Chamber, media was aspirated from the top chamber. Cells that had did not migrate in the top chamber were removed carefully with a cotton swab. After this, the top chamber was set aside. The plate, containing only the bottom chamber, was then centrifuged at 1000*g* for 5 min at room temperature. Medium was aspirated from the bottom chamber and wells were washed with 200µl of wash buffer. Cells were centrifuged again at 1000*g* (rpm) for 5 min and the wash buffer was aspirated. Subsequently, 110µl of the Cell Dissociation Solution (containing 10% v/v Cell Dye) was added to each well and the Cell migration was reassembled by placing the top chamber back into the bottom chamber. The Cell Migration Chamber was then left to incubate for 1h at 37°C in 5% CO_2 incubator. Finally, the top chamber was removed and fluorescence was acquired from the bottom chamber 530/590nm (Ex/Em) in a plate reader. Technical replicates (triplicates) were averaged together for analysis. The number of migrated cells was meant to be calculated using the aforementioned standard curve, nevertheless, the fluorescence results obtained after the experiment were outside

the standard curve range (higher values than the highest value of the standard curve). For this reason the standard curve was not used and only the fluorescence values (in Arbitrary units, AU) obtained from each well (condition) are reported. A single biological replicate (n=1) was performed for this experiment.

2.4.8 **Proliferation assays**

2.4.8.1 **KI67 *assay***

To analyse the proliferative capacity of each of the CRISPR/Cas9 clones, cells were stained with an Anti-KI-67 antibody (MACS, Milteny Biotec, Cat# 130-100-340). The KI-67 antigen is a nuclear protein associated with cell proliferation and is often used to identify the growth fraction of a given cell population.

For experimentation, cells were seeded normally in 75cm^2 flasks, 632 000 cells per flask (final density of 8 426cells/cm^2), in serum-free, 1% or 10% FBS medium. Cells were incubated for 24h and 48h, at which point they were harvested using trypsin 1X (Gibco, Cat# 25300-062). Cells were fixed using 80% ethanol added in a dropwise manner while vortexing. Fixed cells were left at -20°C for at least an hour before being used for staining. If cells were not to be used immediately, they were stored at -20°C for up to 4 weeks.

Fixed cells were then stained as per manufacturer's protocol in a V-bottom 96-well plate. To rule out unspecific binding of the KI-67 antibody, an isotype antibody (MACS, Milteny Biotec, Cat# 130-104-611) was used in control samples. Samples were analysed using a flow cytometer (at least 10000 events were acquired per condition) and the FlowJo V10 software (FlowJo LLC). Three independent biological replicates (n=3) were performed for this experiment

2.4.8.2 ***CellTrace^{TM} CSFE dye***

CellTrace^{TM} dyes allow following up multiple generations of dividing cells using dye dilution by flow cytometry. For experimentation, the CellTrace^{TM} CSFE dye (ThermoFischer, Cat# C34554) was used as per the manufacturer's protocol, with some minor modifications.

BV2 cell lines were harvested normally, using PBS and counted with a haemocytometer. 3 million cells per cell line were stained for each experiment. Cells were firstly pelleted and re-suspended in 1mL PBS containing 0.75µM of the CSFE dye (initial stock solution was 5mM). Cells were left to incubate with the dye for 10 min at 37°C protected from light. After incubation, 5mL of 1% serum containing medium was added to the cells. Cells were pelleted once more and re-suspended in 3mL of serum-free medium. At this point cells were counted again and subsequently seeded at 80 000 cells/well in triplicate (3

wells per condition in a 6-well plate). Cells were seeded in serum-free, 1% and 10% FBS RPMI medium and left to grow for 24h and 48h.

Finally, cells were harvested using trypsin 1X (Gibco, Cat# 25300-062). Triplicate wells were pooled together at this point. Analysis was carried out using a flow cytometer (at least 10000 events were acquired per condition) and the FlowJo V10 software (FlowJo LLC). Three independent biological replicates (n=3) were performed for this experiment.

2.4.9 **Proteome profiling – Mouse cytokine array kit**

The Proteome Profiler Mouse XL Cytokine Array (R&D Systems, Cat# ARY028) was used to investigate the effect of *Trem2*'s deficiency in BV2 cells, in terms of their cytokine secretion capacity. This kit is capable of determine the relative abundance of 111 mouse cytokines in a membrane-based antibody array. Protocol was performed as per manufacturer's recommendations using cell-free supernatants from cells treated with LPS, IL4, TGFβ and an untreated control group (serum-free) for the wild-type, C8 (*Trem2* +/-) and B5 (*Trem2* -/-) cell lines. Treatments were performed for 24h, after the usual 24h serum-starvation period. After membrane development, the Streptavidin-HRP chemiluminescent signal was captured with autoradiography film. Densitometric analysis was performed using the ImageJ. Optical densities were normalised using the mean of the positive control points (reference spots) and analysis was performed as recommended by the manufacturer. Briefly, the average signal (pixel density) of the pair of duplicate spots representing each cytokine was normalised by subtracting an averaged background signal (negative control spots). Positive control spots were used for overlay alignment. Hierarchical clustering analysis and plotting of results as a heat map was done using MORPHEUS (https://software.broadinstitute.org/morpheus/). A single biological replicate (n=1) was performed for this experiment.

2.5 **Preparation and characterization of Aβ1-42 species**

2.5.1 **Aβ1-42 fibrils preparation (Microarray experiment)**

Fibrils of Aβ1-42 were produced as previously described by Lorenzo and Yankner (1994). Briefly, the Aβ1-42 peptide (Sigma, Cat# A-9810) was dissolved in double-distilled water (ddH_2O) to a final concentration of 350μM and incubated at 37°C for 5 days. After 5 days, the fibrils were resuspended with ddH_2O to a final concentration of 20μM. Aliquots of 20μl were stored at -80°C for later use. When an aliquot was needed for cell stimulation, it was first dissolved with ddH_2O to a final concentration of 20μM. All experiments were carried out within six months of fibril preparation.

2.5.2 **Preparation and characterization of Aβ1-42 species (RNAseq experiment)**

2.5.2.1 ***Preparation of monomeric Aβ1-42***

Aβ1-42 was purchased from AnaSpec (Cat# AS-24224). The peptide was first dissolved at a concentration of 1mg/mL in 100% HFIP (1,1,1,3,3,3-hexafluoro-2-propanol [Sigma Aldrich, Cat# 52517]). The resulting solution was then left to incubate for 1h at room temperature with occasional vortexing at moderate speed. After incubation, the peptide solution was sonicated for 10 min in a water bath sonicator. The solution was subsequently dried using a gentle stream of Nitrogen gas (approximately 30 min). The dried pellet was re-suspended in 100% DMSO to a concentration of 1mM. The pellet was incubated with DMSO at room temperature for 15 min with occasional vortexing. This preparation facilitates the solubilisation of the Aβ1-42 peptide in a solution that contains predominantly monomers. The final solution was then distributed into 5µl aliquots using 0.5mL Eppendorf® LoBind microcentrifuge tubes (Sigma-Aldrich, Cat# Z666491) and stored at -80°C until needed to prepare oligomers or fibrils.

2.5.2.2 ***Preparation of oligomeric and fibrillar Aβ1-42 species***

For oligomeric Aβ1-42, one 5µl aliquot of monomeric Aβ1-42 [1mM] was dissolved with DPBS –Ca/-Mg to a final concentration of 25µM. Monomeric Aβ1-42 was left to oligomerize at room temperature (21-28°C) for 20-24h with moderate agitation. Similarly, for fibrillary Aβ1-42, one 5µl aliquot of monomeric Aβ1-42 [1mM] was dissolved with DPBS –Ca/-Mg to a final concentration of 25µM. The solution was then left to incubate at 37°C for 7 days with occasional mixing.

2.5.2.3 ***Morphological characterization of Aβ1-42 species - TEM imaging and analysis***

Characterization of the different Aβ1-42 species was carried out by Transmission Electron Microscopy (TEM) as described by Jan et al. (2010). Briefly, 5µl of any of the three Aβ1-42 species conformations was deposited on top of a Formvar/carbon-coated TEM grid (Electron Microscopy Sciences, Cat# FCF200-Cu-50, 25-50nm Formvar and 1nm Carbon). These TEM grids had been glow discharged before sample fixation using a Mini Sputter Coater/Glow Discharge System (Electron Microscopy Systems, Cat# EMS 7620). Aβ1-42 samples were deposited as a droplet and left to settle on the grid for 1 min. After deposition, the TEM grids were gently dried by wicking their edges with a piece of blotting paper. Once dried, 10µl of a 2% (wt/vol) Uranyl Acetate (Agar Scientific Ltd., Cat# AGR1260A) was put on top of the grids and was left to settle for 90 sec. After settling, the excess solution was removed by gently wicking the edge of the grids with a piece of blotting paper. Grids were then left to dry at room temperature for 5 min before they were stored for later analysis. Grids were stored at room temperature.

Grids containing Aβ1-42 samples were examined using an Electron Emission Microscope (Philips CM12, FEI Tecnai G2 F20, USA) operating at 80kV. The microscope used was located at TEM facility at Queen Square house laboratories. Images were acquired using the Radius electron microscopy imaging software (Olympus Soft Imaging Solutions) and image analysis was carried out using ImageJ software. Image acquisition was performed by Dr Natalia Zanetti, Clinical & Experimental Epilepsy, UCL Institute of Neurology.

2.6 Gene expression analysis of microglial activation

2.6.1 Cell treatments

BV2 cells were routinely plated 24h prior to treatment in serum-free media, to ensure cells were downregulated and in a resting state. Treatments were carried out in serum-free medium unless stated otherwise. Cell stimulations were performed in triplicate (3 wells of a 6-well plate, each containing 80 000cells in 2mL of serum-free medium); 3 technical replicates. Technical replicates were pooled together at the cell lysis step before RNA extraction. Timing of sample collections represents different states of microglial activation. The 6h timepoint represents the acute phase of microglial activation, while the later timepoints, 24h and 48h, represent the chronic states of inflammation (Gao et al., 2011). Chronic inflammation is a pathological hallmark of neurodegeneration in diseases such as AD (Plaza-Zabala et al., 2017). Moreover, it has been shown that excessive acute or chronic activation of microglial cells can promote neuronal damage by the release of cytotoxic factors, including NO, ROS, TNFα, and IL1 (Dai et al., 2015).

For the microarray experiment, cells were stimulated with 1µg/mL LPS (Sigma L2762, serotype: 026:B6, Dorset, UK), 1mg/mL fibrinogen (Sigma, Cat# F4883, fibrinogen from human plasma), 1µg/mL and 100µg/mL Dextran Sulfate (Sigma, Cat# D6001, average MW >500,000 from *Leuconostoc spp.*) and 20nM Aβ1-42 fibrils (Sigma, Cat# A-9810) for 6h, 24h and 48h. The experiment also included a 0 hour untreated control per biological replicate, totalling 19 samples per experiment. The experiment was repeated 3 times; biological replicates (n=3). In addition to these treatments, the qPCR validation of microarray results used: ATP Adenosine Triphosphate Sodium salt, Tacris, Cat# 3245) and mouse INFγ (Interferon-γ, Peprotech, Cat# 315-05) (Table 2-9).

For the RNAseq experiment, cells were activated with 100ng/mL LPS (Sigma L2762, serotype: 026:B6, Dorset, UK), 100ng/mL mouse IL4 (Peprotech, Cat# 214-14), 100ng/mL mouse TGFβ (Cell Signalling Technologies, Cat# 5231LC) and 500nM Aβ1-

42 monomers or oligomers (for preparation see section 2.5) for 6h, 24h and 48hrs. The experiment was performed using 3 separate biological replicates (n=3).

All compounds with concentrations used to treat cultures are provided in Table 2-9. The concentrations selected are justified in the corresponding results chapter and were determined by concentration dependent analysis, from previous experiments in the laboratory or from the literature.

Table 2-9 Compounds and concentrations used for BV2 stimulation

Treatment	Final Concentration	Effect/Response
Aβ1-42 fibrils	20nM (microarray)	Fibrillar Aβ is the major component of Aβ plaques and can activate microglia (Resende et al., 2008). In microglia, scavenger receptors SCARA1 and SCARA2 have been shown to have high affinity for fibrillary and soluble Aβ (Wilkinson and El Khoury, 2012). Other microglial receptors capable of recognizing fibrillar Aβ include; TL2, CR3 and Mac1 (Doens and Fernandez, 2014). Aβ receptors have been reviewed extensively by (Jarosz-Griffiths et al., 2016). Dose determined by observations made in our group (Crehan et al., 2013) and others (Dahlgren et al., 2002).
Aβ1-42 monomers and oligomers	500nM	Oligomeric Aβ has been shown to activate microglia (Zheng et al., 2016). In our study, monomers are used as a control. In microglia, scavenger receptors SCARA1 and SCARA2 have been shown to have high affinity for fibrillary and soluble Aβ (Wilkinson and El Khoury, 2012). Microglial cells are capable of recognizing monomers via the macrophage receptor with collagenous structure (MARCO, Brandenburg et al. (2010)) and the Receptor for advanced glycation end products (RAGE, Origlia et al. (2010)). Similarly, Aβ oligomers can be recognised by pattern recognition receptors (PRR) in microglia (reviewed by Salminen et al. (2009). *TREM2* has also been shown to act as a receptor for oligomeric Aβ (Zhao et al., 2018). Dose determined by unpublished observations made in our group and others (Zheng et al., 2016).
ATP	100μM	Extracellular ATP activates macrophages through stimulation of purinergic receptors (Cauwels et al., 2014). Upon activation cells produce IL1β and IL18. Dose was established by unpublished observations made in our group.
Dextran Sulfate	1 and 100μg/mL	Putative ligand of *TREM2* ((Daws et al., 2003). Dose was determined by unpublished observations made in our group.
Fibrinogen	1mg/mL	Promotes production and release of pro-inflammatory cytokines in mononuclear cells (Jensen et al., 2007). Fibrinogen has been shown to bind to Macrophage-1 antigen (also known as Mac-1, CR3 or CD11b/CD18) receptor in activated microglia (Ryu and McLarnon, 2009, Flick et al., 2004, Adams et al., 2007). Dose was determined by unpublished observations made in our group.
IL4	100ng/mL	It is a well-known macrophage/microglia activator (M2) capable of promoting inflammation resolution (Chang et al., 2017). The receptor for IL4 is known as IL4Rα. IL4 has been also shown to upregulate *Trem2* expression (Turnbull et al., 2006). Dose was determined by a dose response curve (Section 2.6).
IL10	-	Promotes M2 activation of monocytes (Avdic et al., 2013) and microglia (Zhou et al., 2017). The receptor for IL10 is IL10R. Dose was determined by a dose response curve (Section 2.6).
LPS	1μg/mL (microarray) or 100ng/mL (RNAseq)	Activates microglia via TLR4 and promotes the expression of pro-inflammatory cytokines. LPS is a classical M1 activator. Dose was determined by observations made in our group and others (Nakamura et al., 1999, Qin et al., 2004).
TGFβ	100ng/mL	Promotes the conversion of activated microglia to an anti-inflammatory phenotype (Paglinawan et al., 2003). TGFβ is recognised by the TGFβ receptors in different tissues (Dore et al., 1998). Dose was determined by a dose response curve (Section 2.6).

2.6.2 **RNA extraction**

RNase-free consumables were used throughout and surfaces and gloves were frequently sprayed with RNaseZap® (Life Technologies, Cat# AM9780M). Total RNA from the stimulated BV2 cells was isolated using the RNeasy Mini Kit (Qiagen, Cat# 217004) according to manufacturer's recommendations, with minor modifications to allow for the set-up of the experiment. Briefly, medium from each well was discarded (or saved for later analysis) and cell lysis was performed directly on the plates by adding 350µl of Qiazol Lysis Reagent (Qiagen, Cat# 79306). Lysis reagent was left to incubate for 5 min at room temperature and plates were subsequently vortexed for 10 sec. At this point, the 3 technical replicates of each treatment were pooled together into a single 2mL Eppendorf (total volume 1.05mL). Technical replicates were pooled together to increase the concentration of final total mRNA needed for experimentation. Serum-starvation reduces the mitotic rate of cells, avoiding increase proliferation and reducing the amount of RNA synthesised (Li et al., 2016). Pooling of technical replicates was particularly important for the microarray experiment, where mRNA concentration needed to be at least 50ng/µl. Lysates were then frozen at -20°C for short periods of time (1 or 2 days) or -80°C for longer storage (up to six months) and processed later.

After this step, the protocol was followed according to manufacturer's recommendations and the RNA was finally eluted in 32µl of DNase/RNase free water. The concentration and quality of the total RNA was determined using a NanoDrop Spectophotometer (Thermo Scientific, Nanodrop 1000) and the A260:280 and 260:230 ratios.

For the RNAseq experiment, the concentration and the RIN (RNA Integrity Number) Quality Metric of the total RNA was determined using a TapeStation System (Agilent). RIN values of all samples sent for NGS were above 7.

2.6.3 **Microarray analysis**

Sample preparation and microarray hybridization was performed by AROS Applied Biotechnology (Denmark). RNA samples from all 3 biological replicates were sent to AROS in a single shipment; 56 samples in total. Although we had 57 samples (19 samples in each of the 3 biological replicates), only 56 were analysed since the microarray chips only analysed gene expression in batches of 8 samples; one of the 0h untreated controls was not included in the experiment. Before sending the samples to AROS, they were diluted in 10µl at a final concentration of 50ng/µl. Samples were then shipped to AROS Applied Biotechnology (Denmark) in dry ice, where microarray analysis was carried out using the Illumina MouseRef-8 v2.0 Expression Arrays. The MouseRef-8 v2 bead chips have the capability of analysing >22,000 probes targeting genes and known alternative splice variants. Experimental procedures (cDNA labelling and

hybridization) were performed according to manufacturer's instructions by AROS Applied Biotechnology. BeadArrays were scanned using the Illumina BeadStation 500X, and raw intensity values were saved in Illumina's Bead Studio program manager. For array hybridization, all samples were distributed among different arrays (avoiding the possibility that the same treatment or timepoint could be found in the same array) to minimize batch effect.

2.6.3.1 ***Microarray data analysis***

Gene expression analysis was performed using Partek Genomics Suite 6.6 (Partek, Inc., St. Louis, USA) and Lumi R package (Bioconductor, Du et al. (2008)). Raw expression data were log2 transformed, and all samples were quantile normalised together. To check data quality was optimal for gene expression analysis, normalised data was compared, using different QC (quality control) plots, before and after normalization. Individual probes were excluded from analysis if the detection pvalue was >0.05 in more than 2 out of the 3 repeats (or 1 repeat in the case of the 0h untreated control) for any condition.

Also, samples were excluded if <95% of the probes were detected (none of the samples were excluded due to this reason for this experiment). After these quality control steps, data were available for 56 samples representing 10,130 genes. Treatment, timepoint, the interaction treatment and timepoint, as well as hybridization batch accounted for most of the data variance and were therefore included in the regression model. A conservative statistical threshold of FDR <0.05 and minimum fold difference ≥1.5 between sample groups was used in all comparisons and to generate gene lists.

Identification of enriched biological pathways in the generated lists of differentially expressed genes was performed using the DAVID (Database for Annotation, Visualization and Integrated Discovery) database 6.7 (http://david.abcc.ncifcrf.gov). The EASE (Expression Analysis Systematic Explorer) (Hosack et al., 2003) was used to identify enriched pathways in the gene lists. EASE allocates each gene to Gene Ontology (GO), Kyoto Encyclopedia of Genes and Genomes (KEGG), and other experimentally derived gene categories, and then tests for statistically significant overrepresentation of genes within each category using a modified Fisher's exact test (Miller et al., 2013). An EASE Score ranges from 0 to 1, where a value equal to 0 represents perfect enrichment. Typically, an EASE Score ≤0.05 is considered as strongly enriched in the annotation categories. For our experiment, the EASE score was 0.1 and the minimum number of genes per pathway was set to 3. Only those functional categories with a Benjamini value (Benjamini and Hochberg, 1995) of <0.05 were considered as significantly enriched in the analysis.

2.6.3.2 ***Validation of genes by RT-qPCR***

2.6.3.2.1 Reverse -transcription and quantitative PCR (RT-qPCR)

cDNA synthesis from mRNA and relative quantification gene expression of *Trem2* and ApoE was carried out as described in section 2.4.2 with an independent set of samples. Multiplex qPCR reactions were prepared for these two probes.

2.6.3.2.2 qPCR relative quantification and statistical analysis

The relative expression of mRNA was calculated using the ΔΔCT method (Livak and Schmittgen, 2001). Gene expression levels were expressed relative to the untreated control for each timepoint. qPCR validation of the microarray data was performed in five independent experiments (n=5) and statistical significance was evaluated using a 2-way ANOVA (Bonferroni corrected).

2.6.4 **RNAseq analysis**

RNAseq library preparation (TruSeq Stranded Total RNA HT Sample Prep, polyA capture), Illumina (HiSeq. 2500) sequencing (paired end, 2×100bp cycle run) and de-multiplexing were all carried out by AROS Applied Biotechnology (Germany). At least 1.350µg of total RNA from each of the samples (72 in total, 24 samples in each of the 3 biological replicates) was sent to AROS Applied Biotechnology (Denmark) in dry ice for library preparation and sequencing.

2.6.4.1 ***RNAseq data analysis***

Raw RNA sequencing data was sent to us in FASTQ format for examination. Analysis of this data was performed using the Partek Flow Software (Partek, Inc., St. Louis, USA). The general workflow for RNA-Seq analysis used in this study, including adapter trimming, alignment, quantitation, normalization, and differential gene expression analysis is shown in Figure 2.6.

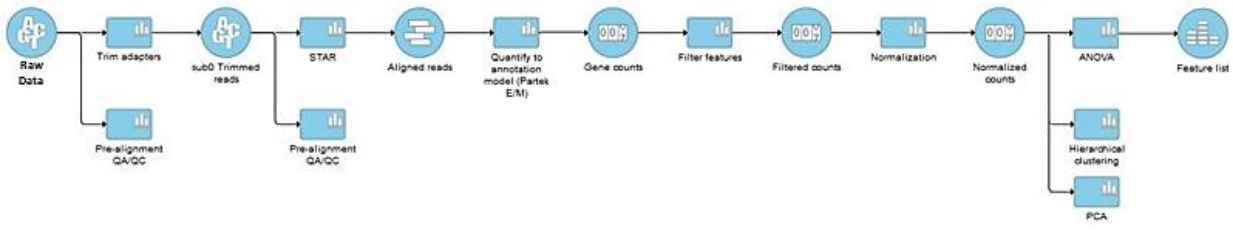

Figure 2.6 RNAseq data processing workflow. Schematic of pipeline used for evaluating mRNA expression in the present study. Raw FASTQ files were processed using Partek Flow (Partek Inc., St. Louis, USA) for (A) trimming adapter sequences, (B) aligning reads, (C) quantitating these reads to reference database, (D) normalizing read counts, and (E) identifying differentially expressed genes (mRNA expression).

Figure 2.6 shows the key steps for the data pipeline used for RNAseq analysis in this study

2.6.4.1.1 Alignment and Quantification

Firstly, FASTQ files were uploaded into the Partek Flow software (Partek Inc., St. Louis, USA) for analysis. Subsequently, sequencing Adapter sequences were trimmed out from the unaligned reads using Cutadapt tool (part of the Partek Flow software). A minimum read length filter retaining reads greater than 10 bases in length was used in this study.

Trimmed reads were aligned to the Whole Genome (latest human genome assembly, hg38) using the STAR 2.5.3a aligner. A seed mismatch limit of 1 and minimum seed length of 10 were used. A seed mismatch of 1 was chosen to avoid discarding reads potentially containing inaccurate base calls made by the sequencer. These settings are consistent with the standard recommendations provided by Partek Flow software (Sakaram et al., 2018). Raw read counts were obtained by quantitating aligned reads to either RefSeq Transcripts 80 using a modified version of the E/M algorithm implemented in the Partek Flow software.

2.6.4.1.2 Normalization

Raw read counts were normalised using the Total Count. Since mRNAs with 0 read counts would hinder statistical calculations when performing differential expression analysis, an offset of 0.0001 was added to all normalised read counts. The offset did not result in inclusion of genes with near zero read counts in the final differentially expressed lists since these lists were filtered to include only those genes with minimum read count values greater than or equal to 10 reads in each of the profiled samples.

2.6.4.1.3 Differential Expression (DE) Analysis

Normalised read counts for each gene were statistically modelled using Partek Flow's ANOVA analysis. A conservative statistical threshold of FDR <0.05 and minimum fold difference ≥1.5 between sample groups was used in all comparisons and to generate gene lists.

2.6.4.1.4 Gene Ontology and pathway analysis

The ToppFun application, part of the ToppGene Suite (https://toppgene.cchmc.org/), was employed for the identification of enriched biological GO terms and pathways in the generated lists of differentially expressed genes. Default thresholds were kept and an FDR B&H (Benjamini-Hochberg) value of <0.05 was considered as statistically significant for our analysis.

2.7 **Statistical Analysis**

Almost all statistical analysis –with the exception of the microarray and RNAseq experiments, which used Partek Software- was carried out using GraphPad Prism software (Version 7.00, Graphpad). Unless otherwise stated, 2-way ANOVA analysis with post-tests, such as Dunnett's multiple comparison test, was used as indicated in figures' legend. Dunnet's test compares the means from several experimental groups against a control group mean to see if there is a difference.

3 CHAPTER 3: Generation of BV2 CRISPR/Cas9 edited microglial cell lines for the study of *Trem2*'s role in microglial function and neurodegenerative diseases

This chapter describes the protocols used and the experimental results obtained during the CRISPR/Cas9 gene editing of the BV2 cell line for the study of *Trem2* function in microglia.

3.1 Introduction

Results from many GWAs studies suggest that neuroinflammation and microglia play a key role in AD pathogenesis and progression (Lambert et al., 2009, Lambert et al., 2013, Harold et al., 2009, Naj et al., 2011, Seshadri et al., 2010, Hollingworth et al., 2011). These human genetic studies have identified >20 genetic loci that show significant associations with increased or decreased risk of developing AD. Many of the associated genes (including CR1, CD33, INPP5D (SHIP1), ABCA7, MS4A gene cluster, HLA-DR1, CASS4, PICALM, and BIN1) show enriched expression in microglial cells relative to other brain cell types (Zhang et al., 2014) (see Figure 1.5), suggesting that microglial cells play an important role in AD.

The discovery that the rare variant rs75932628 in the *TREM2* gene –known as the *TREM2* R47H mutation– increases the risk of AD by 3-4 fold in humans (Guerreiro et al., 2013b, Jonsson et al., 2013) further strengthens the view that microglia play an active role in AD. Other *TREM2* variants have been linked to AD – including R62H (rs143332484), D87N (rs142232675) and T96K (rs2234253)– but further studies will be necessary to confirm these results (Guerreiro et al., 2013b, Jin et al., 2014, Song et al., 2017).

In the brain (human or mouse), *TREM2* is highly and almost exclusively expressed by microglial cells; consequently, the discovery of the *TREM2* AD risk variants in genetic studies triggered a renewed interest in the role of microglia in AD. *TREM2* is considered to be a microglial surface receptor, similar to other members of the *TREM* family of genes, and as such it has been suggested to interact with the tyrosine kinase-binding protein TYROBP (also known as DAP12). This adaptor is believed to initiate the signal transduction that promotes microglial activation (Wang et al., 2015c), phagocytosis (Kleinberger et al., 2014a, Hsieh et al., 2009) and survival (Wang et al., 2015c).

Insight into the properties and function of *TREM2* has stemmed from the study of another genetic disease: the Nasu-Hakola disease (NHD). Loss-of-function mutations in *TREM2* and its putative adapter protein *DAP12* have been shown to cause this autosomal

recessive disorder. Prominent outcomes from this disease in patients are: development of bone cysts, progressive dementia, behavioural changes and gait disturbances with the death of the patients occurring during the 4th or 5th decade of life (Paloneva et al., 2000, Klunemann et al., 2005). Recent studies have suggested that heterozygous carriers of the loss-of-function mutations that cause NHD may have an increased risk of AD (Guerreiro et al., 2013b, Jin et al., 2014). Furthermore, rare coding variants in the *DAP12* gene have been suggested to predispose to early-onset AD in an autosomal dominant manner (Pottier et al., 2016).

The very low frequency of the *TREM2 R47H* mutation (see Figure 1.5) has hampered the study of the mutation in a homozygous state. In fact, just one case of a homozygous R47H carrier has been reported so far. This patient presented features of both AD (amyloid and tau pathology) and NHD (frontal brain atrophy) (Slattery et al., 2014). There is clearly a need to develop and establish disease models that allow the study of loss-of-function and AD related mutations in both *TREM2* and TYROBP (Yeh et al., 2017). In this respect, *in vitro* signalling and functional studies have largely relied on monocytes, macrophages and microglia isolated from *Trem2* deficient animals (Yeh et al., 2017, Turnbull et al., 2006), siRNA gene interference (Zheng et al., 2016) and cell models stably transfected with *TREM2* constructs expressing the WT or mutated versions of the gene (Yeh et al., 2017, Daws et al., 2003).

The advent of the CRISPR/Cas9 genome editing has allowed the simple and effective genomic manipulation of nearly any cell type. As a result, research laboratories across the world have adopted this relatively new technique to mutate, silence, induce and replace genomic elements to interrogate gene function and the biology of disease. The CRISPR/Cas9 revolution has greatly impacted research both *in vivo* and *in vitro* (reviewed by Kato and Takada (2017) and Dow (2015)).

This chapter describes the methodology used for knocking-out the *Trem2* and *Dap12* genes in the murine microglial cell model BV2, as well as the various attempts to introduce the *R47H* mutation in these same cells using the CRISPR/Cas9 system for gene editing. To date, and to the best of our knowledge, only a single study has reported the genetic modification of a microglial cell line using the same approach. In a recent paper by Xiang et al. (2016a), N9 cells (a rat microglial cell line) were genome edited to knockout *Trem2*. As a result, the authors obtained a single clone with a 1bp insertion on the 2nd exon of the *Trem2* gene which caused a frameshift of the reading frame that consequently created a premature stop codon.

3.2 Aims

The aims of the following chapter are:

1. To generate *Trem2* and *Dap12* gene knockout (and haploinsufficient) BV2 cell lines using commercially available CRISPR/Cas9n (nickase mutant) plasmids.
2. To generate homozygous and heterozygous *Trem2* R47H BV2 cell lines using the CRISPR/Cas9 (wild type) or CRISPR/Cas9n technologies.

3.3 Results

3.3.1 Generation of *Trem2* and *Dap12* knockout (-/-) and knockdown (+/-) BV2 cell lines by CRISPR/Cas9 technology

3.3.1.1 ***Clone expansion***

Single cell colonies were expanded after CRISPR/Cas9n plasmid transfection and cell sorting in 96-well plates for at least 2 weeks. After this period, all surviving clones were re-seeded into two duplicate 96-well plates. Only 30 *Dap12* CRISPR/Cas9 and 41 *Trem2* CRISPR/Cas9 clones survived clonal expansion.

3.3.1.2 ***DNA sequencing of Trem2 and Dap12 CRISPR/Cas9n clones***

DNA from all *Trem2* and *Dap12* CRISPR/Cas9n clones was extracted, gRNAs' target sequences were PCR amplified and prepared for NGS. After sequencing, raw results were trimmed of adaptor sequences and indexes and aligned by Dr Alan Pittman, UCL Institute of Neurology, Dept. of Molecular Neuroscience. Analysis of the sequences using the IGV 2.3 software showed inconclusive results as it was not possible to identify mutations in any of the sequenced clones (either *Trem2* or *Dap12*). This could have been due to a technical error in sample preparation or CRISPR/Cas9 transfection not working.

To rule out any of those possibilities, gRNAs target regions were re-sequenced. To do this, all clones (*Trem2* and *Dap12*) were re-seeded into 25cm^2 tissue culture flasks and grown until confluent. Harvested cells were used for DNA and total protein extractions. DNA was used for PCR amplification of the CRISPR/Cas9 targeted sequences (using the same primers used for NGS) and sent to be commercially Sanger-sequenced (SourceBioscience, Cambridge, UK).

Results were analysed using BioEdit Sequence Alignment Editor V7.2.5 (Hall, 1999). In the case of *Dap12* CRISPR/Cas9 clones, all 30 PCR products aligned perfectly to the unmodified *Dap12* target sequence. This could be due to the fact that either the *Dap12* CRISPR/Cas9n-gRNA complex did not produce any cuts on the genomic sequence or that DAP12 is an essential molecule for the survival of microglial cells. *Dap12* deficiency

is not embryonic lethal in mice, although it has been shown to alter immune function (Kaifu et al., 2003), Bakker et al. (2000), (Tomasello et al., 2000). In humans, *DAP12* deficiency is not embryonic lethal either (Paloneva et al., 2000), even though it has been shown that some of its associated receptors are capable of promoting cellular activation and survival upon ligand binding (reviewed by Turnbull and Colonna (2007)).

For *Trem2* CRISPR/Cas9 clones, 22 PCR products aligned entirely to the unmodified *Trem2* CRISPR/Cas9 target reference sequence. The remaining 19 *Trem2* CRISPR/Cas9 clones showed evidence of being gene-edited. This represents a modification (Indel) efficiency of 46.3%, which is in line with other studies using CRISPR/Cas9 nickases (Ran et al., 2013a).

Table 3-1. Screening and selection of *Trem2* CRISPR/Cas9 clones

Clone name	ELISA (sTREM2)	Western Blot (total TREM2)	Sanger sequencing CRISPR/Cas9 target locus	Single colony Sanger sequencing
A01	+	+	WT Homozygous	
A02	+	+	WT Homozygous	
A03	-	+	Heterozygous	3+ alleles (including WT allele)
A04	-	-	Heterozygous	3+ alleles (including WT allele)
A05	+	+	WT Homozygous	
A06	-	-	Heterozygous	3+ alleles (including WT allele)
A07	-	-	Heterozygous	2 alleles (5bp deletion + WT allele)
A08	-	+	WT Homozygous	2 alleles (25bp deletion + WT allele)
A09	+	+	WT Homozygous	
A10	-	-	WT Homozygous	2 alleles (1bp deletion + WT allele)
A11	-	+	WT Homozygous	Not cloned
A12	+	+	WT Homozygous	
B01	+	+	WT Homozygous	
B02	+	+	WT Homozygous	
B03	-	-	Heterozygous	3+ alleles (including WT allele)
B04	-	+	Heterozygous	2 alleles (27bp deletion + 10bp deletion)
B05	-	+	Heterozygous	3+ alleles (including WT allele)
B06	+	+	WT Homozygous	
B07	+	+	WT Homozygous	
B08	+	+	Heterozygous	2 alleles (15bp deletion + WT allele)
B09	-	+	Heterozygous	3+ alleles (including WT allele)
B10	+	+	WT Homozygous	
B11	-	+	Heterozygous	3+ alleles (including WT allele)
B12	+ (low expression)	+	Heterozygous	3+ alleles (including WT allele)
C01	+ (low expression)	+	WT Homozygous	
C02	+	+	WT Homozygous	
C03	+	+	WT Homozygous	
C04	-	+	Heterozygous	1 WT allele
C05	+	+	WT Homozygous	
C06	-	-	Heterozygous	3+ alleles (including WT allele)
C07	+	+	WT Homozygous	
C08	-	+	Heterozygous	2 alleles (34bp deletion + WT allele)
C09	-	+	Heterozygous	3+ alleles (including WT allele)
C10	-	+	Heterozygous	3+ alleles (including WT allele)
C11	-	+	Heterozygous	3+ alleles (including WT allele)
C12	+	+	WT Homozygous	
D01	+ (low expression)	+	Heterozygous	3+ alleles (including WT allele)
D02	+	+	WT Homozygous	
D03	+	+	WT Homozygous	
D04	+	+	WT Homozygous	
D05	-	+	Heterozygous	2 alleles (46bp deletion + 42bp deletion)

(+) = Detection of (s)TREM2 protein

(-) = No detection of (s)TREM2 protein

3.3.1.3 ***sTREM2 ELISA***

To confirm the *Trem2* knockout at the protein level, an ELISA assay using supernatants from the *Dap12* and *Trem2* CRISPR/Cas9 clones was carried out. Quantification of the ELISA results showed reduction in the levels of s*TREM2* in any of the *Dap12* clones. Meanwhile, out of 41 clones, 22 *Trem2* CRISPR/Cas9 clones shed s*TREM2* into the cell

culture medium (3 of which had very low expression). The remaining 19 clones had no s*TREM2* in their supernatants (see Figure 3.1).

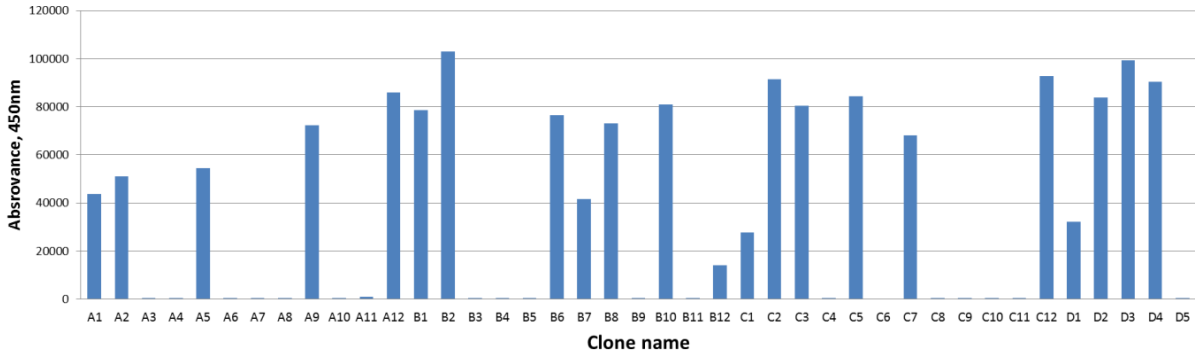

Figure 3.1. sTREM2 ELISA for the identification of *Trem2* KO BV2 clones. Supernatants (conditioned medium) from all 41 *Trem2* CRISPR/Cas9 clones were tested for the presence of s*TREM2*. 19 clones were found not to shed any s*TREM2* in the medium as a result of the suspected genetic KO. Meanwhile, clones B12, C1 and D1 were classified as low shedders. Finally, 22 clones were still able to secrete s*TREM2*. Absorbance is reported as arbitrary units.

3.3.1.4 TREM2 and DAP12 *Western Blot*

Whole cell lysates were obtained from all *Trem2* and *Dap12* CRISPR/Cas9 clones and used for western blotting and identification of intracellular TREM2 and DAP12 proteins. Cell lysates were not quantified prior to western blotting analysis, and as a result expressions are not comparable among samples. The purpose of this experiment was to show whether or not TREM2 was being expressed intracellularly and not to quantify this expression. In this experiment, ACTIN was used as a loading control (but not as a normalizer gene) in order to check that lysates had enough protein to be detectable by western blot.

In the case of the *Dap12* CRISPR/Cas9 clones, all lysates seemed to have the characteristic band corresponding to DAP12 (approximately 10-12kDa, Supplementary Fig. 7.10). These results complement the Sanger sequencing results and confirms that the *Dap12* CRISPR/Cas9 genome editing did not work in this experiment.

In a similar way, 35 *Trem2* CRISPR/Cas9 clones had bands that corresponded to *TREM2*'s molecular weight (approximately 25-40kDa). As TREM2 protein was not deglycosylated, *TREM2* was detected in multiple bands corresponding to the different glycosylated states of the protein, which are seen in the range of 25 to 49kDa. Only 6 clones did not seem to have the characteristic *TREM2* bands; A04, A06, A07, A10, B03 and C06 (Figure 3.2). Interestingly, 5 out of these 6 clones had been found to be heterozygous by Sanger sequencing of PCR products (except for clone A10).

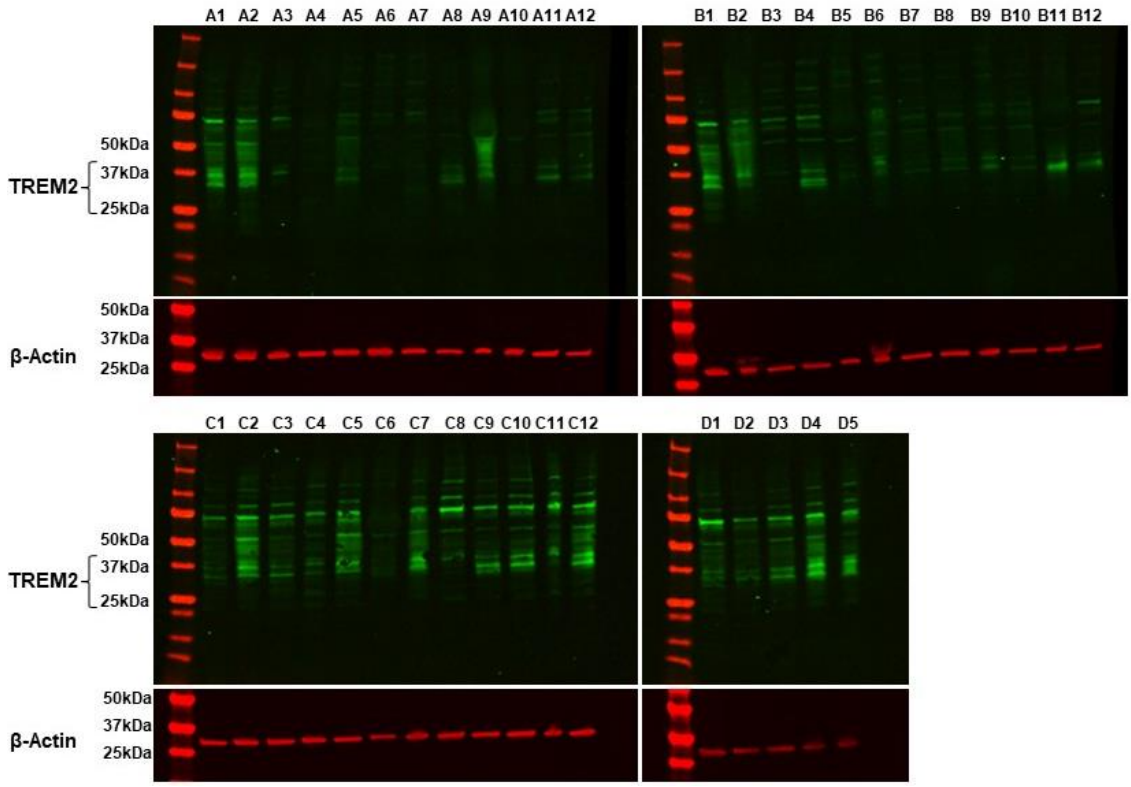

Figure 3.2. TREM2 Western blot for the identification of *Trem2* KO BV2 clones. All *Trem2* CRISPR/Cas9 clones were analysed by Western blot to identify if there was a reduction on the expression of TREM2 protein (25-40kDa). The amount of protein lysate in each lane varies (approximately 20ug) as protein content was not quantified prior to electrophoresis.*TREM2* was detected using a sheep polyclonal anti-*TREM2* antibody (R&D Systems, Cat# AF1729, 1:500 dilution). Only 6 clones seemed to have lost expression of *TREM2* on whole cell lysates. β-actin (45kDa) was used as a loading control and was detected using a mouse monoclonal anti-β-actin antibody (Sigma, Cat# A5441, 1:10 000 dilution).

Subsequently, ELISA, Western Blot and Sanger sequencing results were compared in order to select clones for PCR product cloning and sequencing. *Trem2* CRISPR/Cas9 clones were selected if there was any evidence from any of the assays (ELISA, Western blot or Sanger sequencing) that suggested *Trem2* had been knocked-out or knocked-down. After analysis, 22 *Trem2* CRISPR/Cas9 clones were selected for PCR cloning. Clones A3, A4, A6, A7, A8, A10, A11, B3, B4, B5, B8, B9, B11, B12, C4, C6, C8, C9, C10, C11, D1 and D5.

3.3.1.5 ***Single colony Sanger sequencing***

The *Trem2* CRISPR/Cas9 target region was PCR amplified in the 22 selected clones and cloned into plasmid vectors (only A11 was not cloned) for sequencing. After alignment and analysis of the cloned PCR sequences, none of the clones had the *Trem2* gene knocked-out on both alleles. Most clones (13 out of 21) had more than two *Trem2* alleles, which suggested a contamination during the cell expansion or cell sorting steps. Only 7 clones were found to possess just two alleles of the *Trem2* target region (Figure 3.3). Clones which possessed two alleles invariably had either a wild-type (WT, unmodified) allele or a deletion that allowed the protein to go back into its correct reading frame in one of their two alleles.

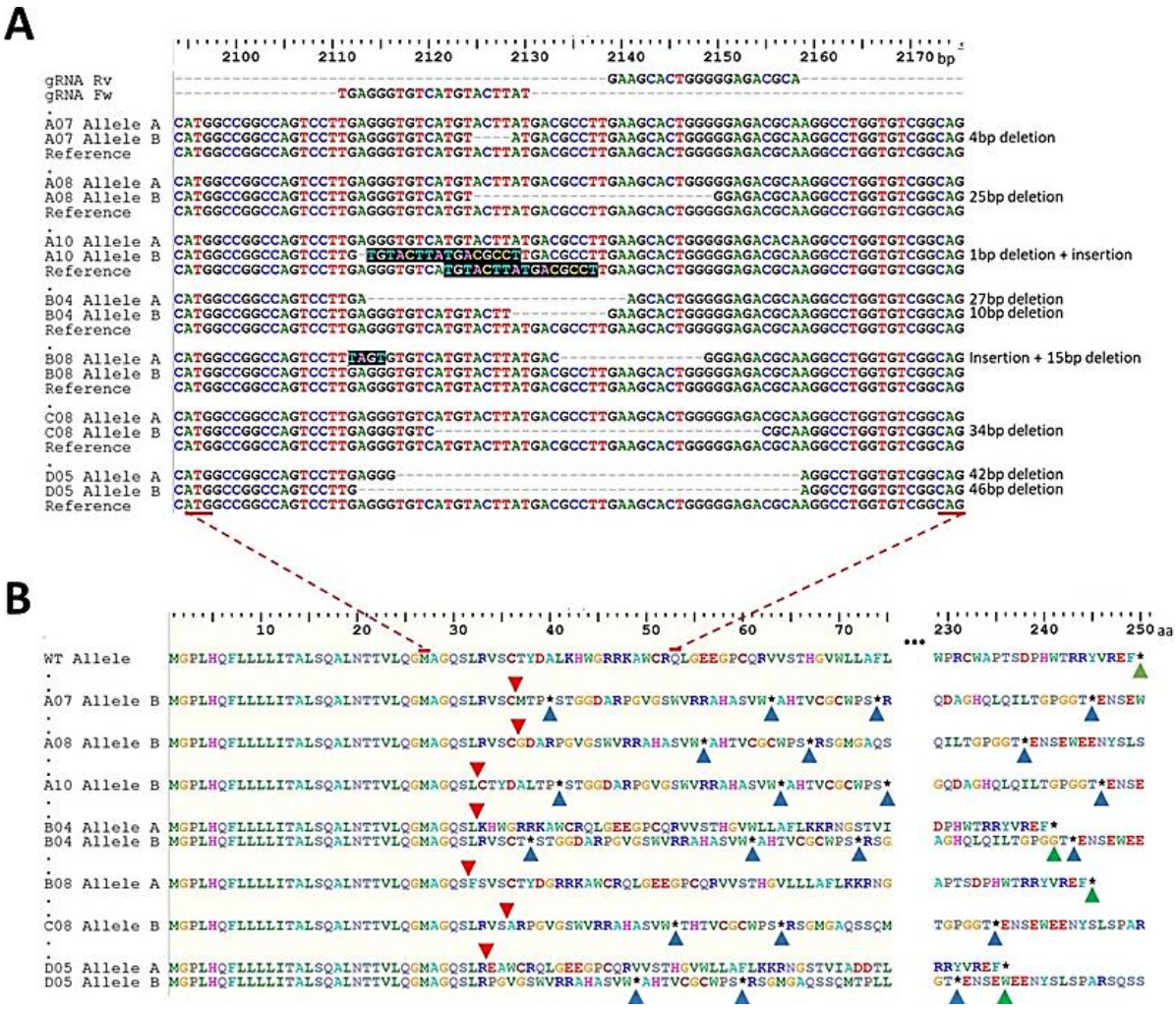

Figure 3.3. *Trem2* CRISPR/Cas9n target sequence alignment and protein sequence products obtained from *Trem2* CRISPR/Cas9n mutated clones. A) Alignment of the *Trem2* CRISPR/Cas9 target sequences from the 7 clones which presented only two alleles are shown. The sequences of both *Trem2* CRISPR/Cas9 gRNAs are also shown to serve as a reference (top). Most mutations found were deletions, as shown in the figure, nevertheless there were also insertion/deletion (indels) events and base pair changes (shown in black background). **B)** Protein sequence alignment of the expected translation products obtained from the 7 *Trem2* CRISPR/Cas9n mutated clones (panel A). The correct (wild type -WT) sequence of the protein (249aa) is found at the top of the panel and the correct stop codon (*) is indicated with a green arrow head. Protein products show perfect alignment from the 1st amino acid (M - Methionine) up to the 31st amino acid of the TREM2 protein (S - Serine). The indel events produced by CRISPR/Cas9n editing (indicated with a red arrowhead) have different effects on the translation of the TREM2 protein. For example, mutations in the clones A7 (allele B), A8 (allele B), A10 (allele B), B4 (allele B), B8 (allele A), C8 (allele B) and D05 (allele B), caused a shift on the reading frame of the protein, with the concomitant formation of premature stop codons (indicated with blue arrowheads). On the other hand, mutations in the clones B4 (allele A), B8 (allele A) and D5 (allele A) did not cause a frame shift in protein sequence or the formation of premature codons, preserving the correct stop codon at the end of the protein sequence (indicated with green arrowheads). However, these mutations produced small amino acid changes and deletions. Therefore, these three alleles produced shorter *TREM2* products (B04 allele B [241aa], B08 [244aa] and D05 allele A [235aa]) with small differences in the amino acid sequence of the protein.

As shown in Figure 3.3 (panel A), there were both insertion and deletion events in the 7 selected clones. Insertion/inversion events were less predominant (clones A10 and B08), while deletions, ranging from 1bp (clone A10) to 46bp (clone D05, allele B), were present in all 7 clones. Figure 3.3 (panel B) shows the predicted protein products

obtained from each of the 7 modified clones in panel A. As seen in this figure, Indel events have different effects on the protein sequence. For example, deletion events did not always result in a disruption of the TREM2 protein reading frame, like in the case of clones B04, B08 and D05 (27bp, 15bp and 42bp respectively), where the correct reading frame was re-established after the deletion. Only 4 clones effectively disrupted the reading frame of the protein (A07, A08, A10 and C08) ensuring efficient gene knockdown (KD) in at least one allele of the gene. This gene knockdown is the product of the introduction of short Indel events which are not a multiple of three. These Indels are able to shift the reading frame of the gene and introduce premature stop codons (Figure 3.3), resulting in mRNA degradation by nonsense-mediated decay (NMD) before the mRNA has a chance to be translated in abundant quantities. NMD is a eukaryotic mRNA quality control and regulatory process by which a premature stop codon that would lead to a truncated protein product triggers mRNA degradation (Popp and Maquat, 2016).

At this point, two haploinsufficient clones were chosen (at random) for further experimentation and characterization of the *Trem2* gene knockdown; A07 (4bp deletion) and C08 (34bp deletion).

3.3.1.6 ***RT-qPCR analysis of Trem2 expression of clones A7 and C8***

To verify that the gene knockdown of clones A7 and C8 was genuine, the effect of their mutations in the gene expression of *Trem2* was assessed using RT-qPCR.

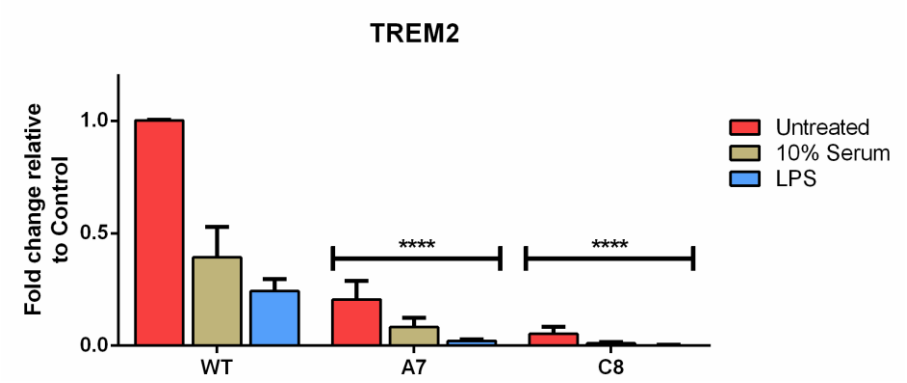

Figure 3.4 *Trem2* mRNA expression in clones A7 and C8. *Trem2* gene expression profiles obtained by RT-qPCR carried out on A7 and C8 clones compared to unmodified WT BV2 cells. Results represent mean ± SD of five independent biological replicates (n=5), ****p<0.0001.

Figure 3.4 shows the fold change variation of *Trem2* expression on A7 and C8 clones (which have one *Trem2* allele knocked-out) with respect to WT BV2 cells. *Trem2* expression is greatly reduced in the two selected clones under untreated conditions. Only 21% and 5% of the *Trem2* WT expression is conserved in the clones A7 and C8, respectively. Additionally, the expression profiles of both clones seem to correlate with WT BV2 cells when stimulated with LPS or 10% serum. Interestingly, 10% FBS

stimulation of WT BV2 cells reduces *Trem2* expression to 39% whereas LPS stimulation reduces this same expression to 24%. *Trem2* expression in clones A7 and C8 was also reduced by the LPS and 10% FBS treatments.

3.3.2 **2nd round of CRISPR/Cas9n modification on C8 (*Trem2* +/-) cells**

A 2nd round of CRISPR/Cas9n modification was carried out on clone C8 (*Trem2* +/-). This clone was chosen because of its long deletion (34bp) produced during the 1st CRISPR/Cas9n round. This deletion interfered with both sgRNAs (Sense and Antisense), ensuring that the second CRISPR/Cas9 round will only target the remaining unmodified allele of *Trem2*.

The same protocol as in the 1st round of CRISPR/Cas9n modification was used for transfection, single cell sorting and colony expansion. Single cell sorting produced 300 single cell colonies (3 full 96-well plates and 12 wells). After expansion, only 60 clones survived. Cells were compiled together in a single plate, of which two copies were made; one for DNA extraction and one for cryogenic banking.

For the identification of *Trem2* -/- clones, an RFLP (Restriction Fragment Length Polymorphism) approach was employed. Primers Fw_Long_*Trem2* and Rv_Long_*Trem2* were used to PCR amplify the CRISPR/Cas9 target region and PCR products were subsequently digested with a restriction enzyme. The enzyme employed for the RFLP screening was AciI. This enzyme specifically cuts the new junction created by the 34bp deletion on the *Trem2* knockout allele of the C8 clone (Figure 3.5). This enzyme has a second restriction site inside the PCR amplicon sequence but this site is present in both the WT and the C8 allele, as shown in Figure 3.5. As a result, if after electrophoresis of the restriction products a single lane presented 3 clear bands (2 AciI cuts) of 343bp, 93bp and 69bp, those cells were considered to be homozygous for the 34bp deletion seen in clone C8 (as shown in Figure 3.5, panel B). Conversely, if 4 bands were observed in a single lane, it was certain that the new restriction site had not been introduced and that the WT (or other) allele was still present in those cells (Figure 3.5, panel B).

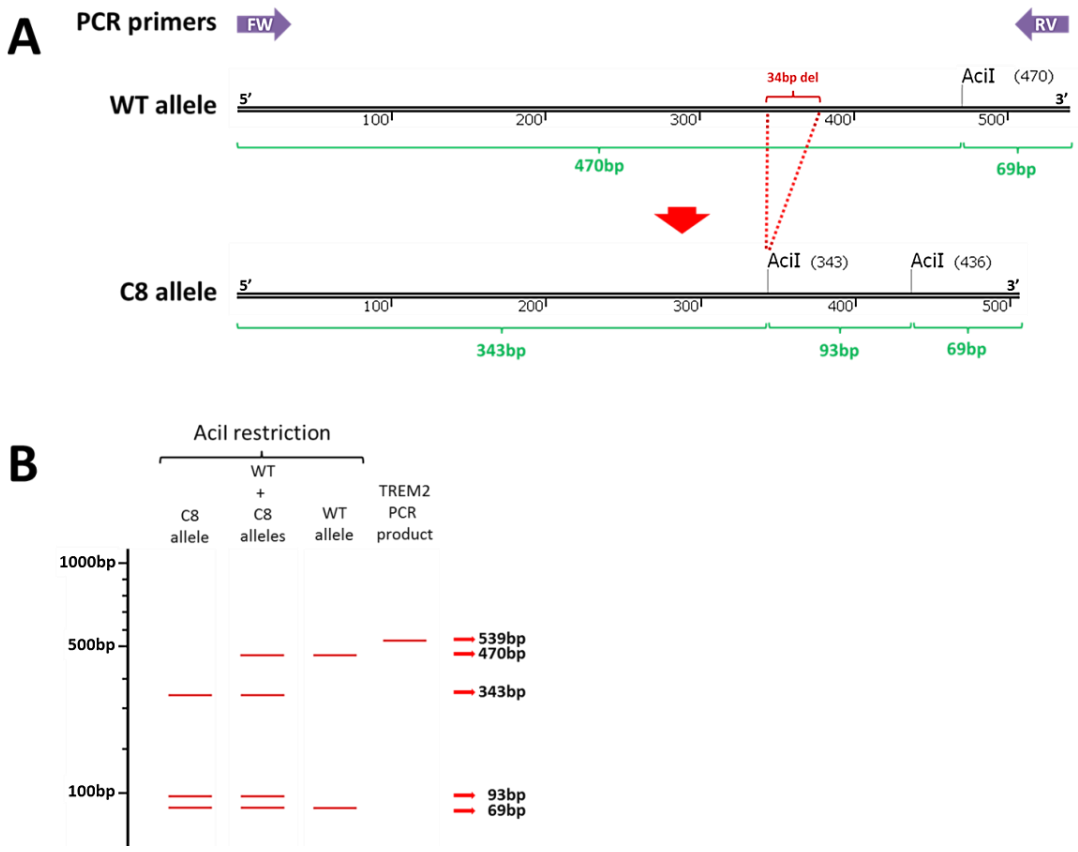

Figure 3.5 34bp deletion generated by CRISPR/Cas9n on the BV2-C8 clone creates a new AciI restriction site. (A) Schematic illustrating the WT and C8 alleles as amplified by the Fw_Long_*Trem2* and Rv_Long_*Trem2* primers. The schematic shows how the 34bp deletion generated by CRISPR/Cas9n modification created a new restriction site for the AciI enzyme. It also shows a second restriction site near the 3' end of the PCR product for AciI, which is conserved in both WT and C8 alleles. The expected sizes for digested fragments are shown in green below each allele. **(B)** Schematic showing the expected results for the RFLP analysis of expected C8 homozygous allele (*Trem2 -/-*), C8 clone (*Trem2 +/-*) and WT cells (*Trem2 +/+*) compared to the unrestricted PCR amplicon (539bp). Sizes of the restricted fragments are shown marked with arrows to the left of the figure.

All 60 surviving clones from the 2nd round of CRISPR/Cas9n were PCR amplified and the products were restricted with AciI. Figure 3.6 shows a representative image of 36 clones screened with this method. PCR amplicon size was as expected (539bp) and in the case of three of the samples (line 10, 34 and 60 in Figure 3.6), the amplicon was very clear and well defined. All PCR amplicons showed an unspecific artefact at around 180bp, except for the aforementioned samples 10, 34 and 60.

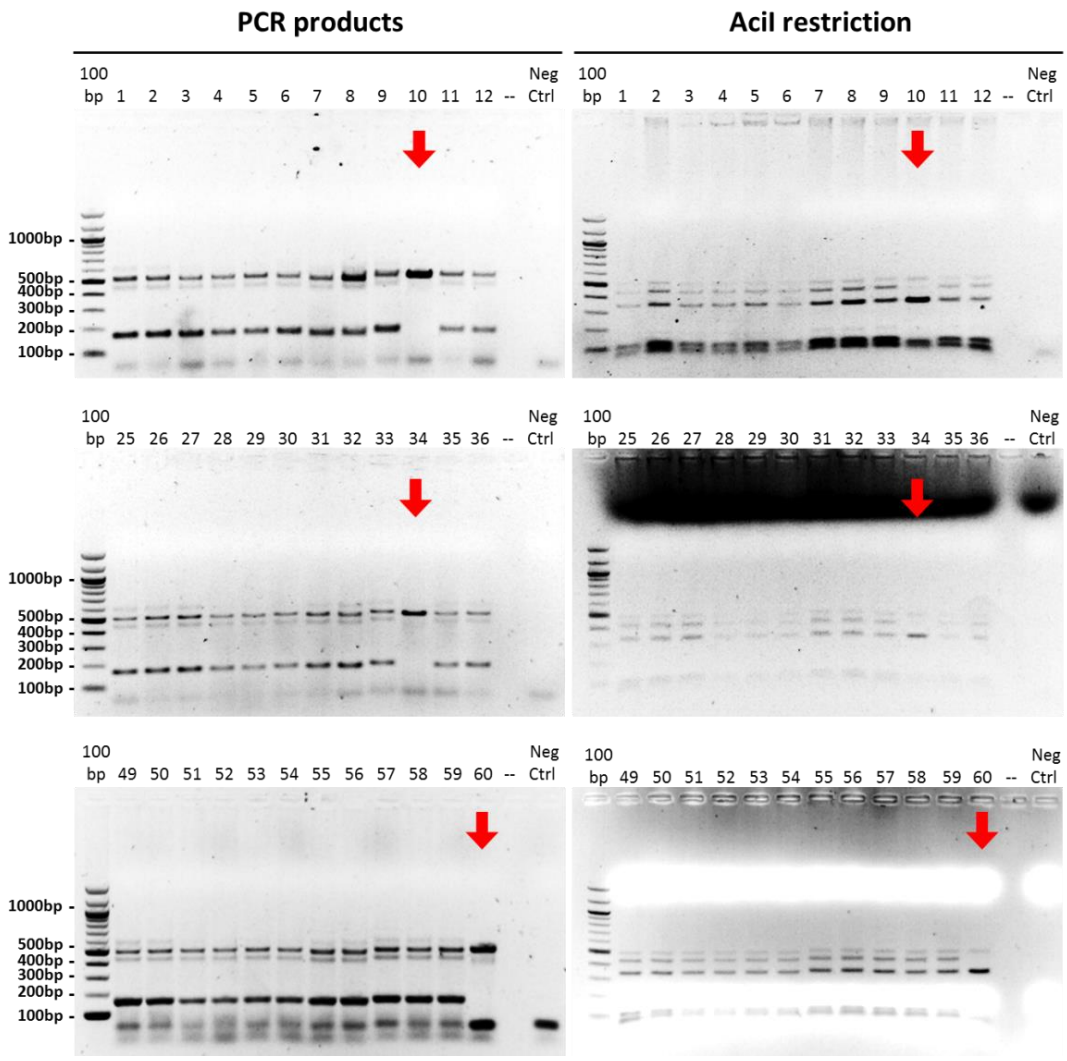

Figure 3.6 Identification of *Trem2 KO* clones by RFLP analysis. Identification of *Trem2 KO* clones containing a 34bp deletion in both alleles of the gene was carried out using RFLP analysis; PCR amplicons of the CRISPR/Cas9 target region were restricted using the enzyme AciI. This enzyme specifically detects the new restriction site created by the 34bp deletion present in one allele of the C8 clone. **Left panels** show PCR products from 36 clones (1-12, 25-36 and 49-60). PCR amplicons not only show the expected 539bp band but also an unspecific product of around 180bp. This artefact was not present in samples 10, 34 and 60 (indicated with red arrows). The **right panels** show PCR products after restriction with AciI. As shown, most samples showed 4-5 bands, including a 470bp band, which corresponds to the WT allele. Only samples 10, 34 and 60 (indicated with red arrows) did not show the band at 470bp. Negative controls had no gDNA in them. Ladder was the Quick-Load Purple 100bp DNA Ladder (New England Biolabs).

After restriction, three samples (10, 34 and 60) were chosen as candidates for carrying the C8 allele in homozygosity, as their restriction products only showed the expected three bands at 343bp, 96bp and 63bp. All other samples showed strong bands at around 470bp (WT allele), 343bp (C8 allele) and 2 bands below 100bp. Samples 10, 34 and 60 were PCR amplified again with a High-fidelity Taq (using the same primers) and sent for Sanger sequencing. Sequencing data (Figure 3.7) confirmed the results obtained by the RFLP screening regarding the 3 samples. Samples 10, 34 and 60 were renamed B5, G4 and G6 respectively. Only lines B5 and G4 were chosen (at random) and used for further characterization.

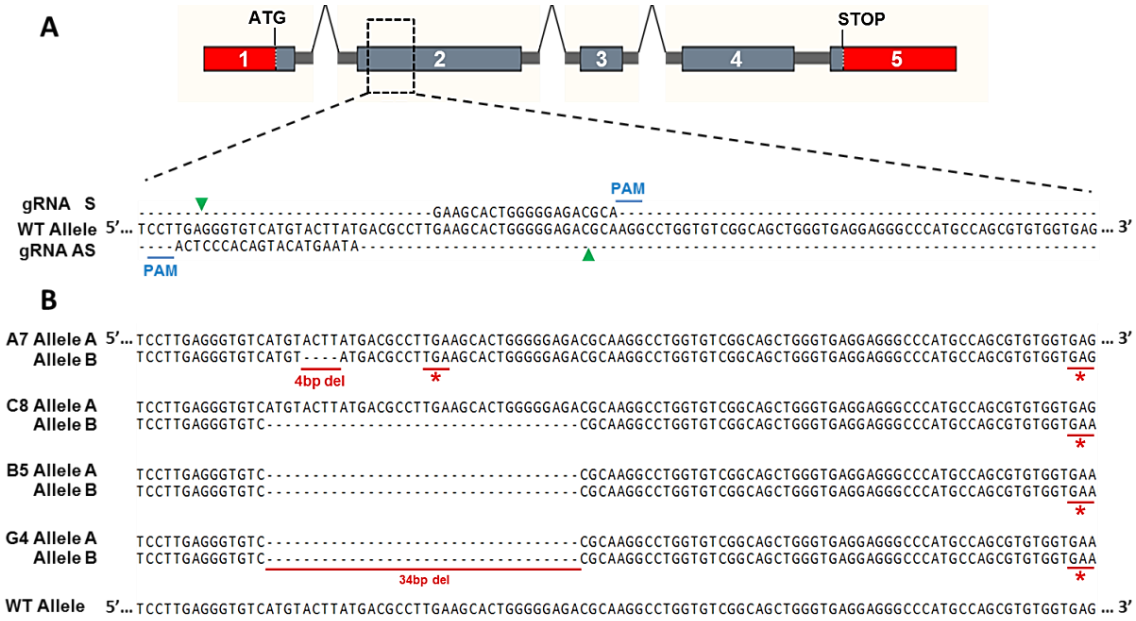

Figure 3.7 CRISPR/Cas9n modification of the *Trem2* gene in BV2 cells. (A) Schematic of the mouse *Trem2* locus and CRISPR/Cas9n modification strategy. gRNAs are aligned to their target sequences on exon 2 of *Trem2*. Protospacer-adjacent motifs (PAM) for each gRNA are marked with a blue line and nicking sites are indicated with green arrows. **(B)** Sequence alignment of the WT *Trem2* sequence and *Trem2* CRISPR/Cas9 mutants. Clones A7 and C8 were obtained during a first round of CRISPR/Cas9n modification, while clones B5 and G4 were obtained during a second round of CRISPR/Cas9n modifications using the clone C8 as the starting cell line. Nucleotide deletions are underlined in red as well as the newly generated stop codons (*).

Figure 3.7 shows a schematic of CRISPR/Cas9n gene editing strategy and the sequencing results obtained for the previously obtained clones A7 and C8, and the newly generated B5 and G4 cells. As observed in panel B, all generated clones have frameshifting deletion mutations near the sgRNA target sites, which create new stop codons for the translation of *Trem2* (marked with red asterisks). After verifying that all the genome edited BV2 clones carried deletions that rendered them either *Trem2* +/- or *Trem2* -/-, they were molecularly, biochemically and functionally characterised (Chapter 4).

3.3.2.1 ***Off-target Screening***

The top 5 potential off-target sites for each of the 2 *Trem2* gRNAs used in this experiment were amplified and sequenced. After sequencing and alignment to the reference sequences, none of the CRISPR/Cas9 modified cell lines (A7, C8, B5 or G4) was found to have any off-target mutations in any of the 5 screened sites. Although these results demonstrate that there have been no off-target modifications in the screened sites and we can extend that assumption to all other least likely off-target sites, a more thorough study (whole genome sequencing) will be needed to ensure that no off-target sites were affected by either small indels or other larger genetic modifications -chromosomal

rearrangements- which are not detectable by Sanger sequencing (Barrangou et al., 2015).

3.3.3 **Generation of BV2 cell lines carrying the *Trem2* R47H mutation by CRISPR/Cas9 technology**

In light of the results obtained during the generation of the *Trem2* KO clones, the next step was the introduction *Trem2* R47H mutation, associated with increased risk of AD (Guerreiro et al., 2013b, Jonsson et al., 2013), into BV2 cells. To this end, two different strategies were utilised: 1) CRISPR/Cas9 nickases (CRISPR/Cas9n) and CRISPR/Cas9 wild-type nucleases (CRISPR/Cas9). Although the double nickase approach greatly increases the target specificity (minimizing off-target effects), it also reduces the on-target efficiency (Chiang et al., 2016). Hence, both approaches (Figure 3.8) were used to increase the chances of stimulating HDR mechanisms needed to introduce targeted mutations.

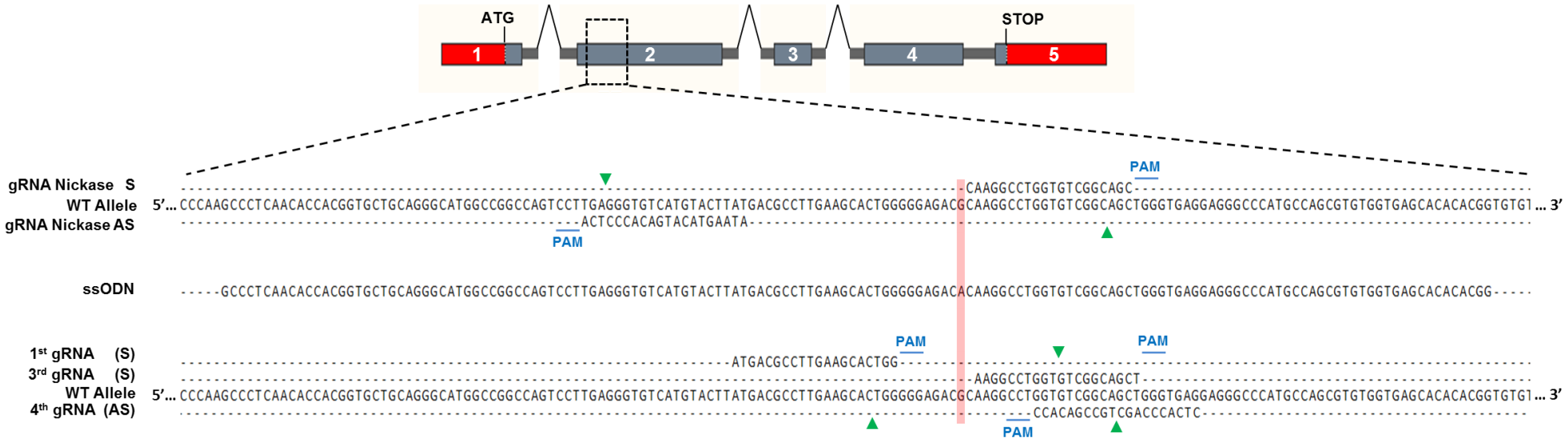

Figure 3.8 CRISPR/Cas9 Nickase and CRISPR/Cas9 strategies for the introduction of the *Trem2* R47H mutation into BV2 cells. Schematic of the *Trem2* mouse gene and the 2 strategies used for introduction of the R47H mutation into BV2 cells. The first approach involved the use of nickases. As shown in the top part of the figure, two nickases were designed to generate single strand nicks in opposite strands of the gDNA, one in the sense (S) orientation and one in an antisense (AS) orientation. The lower part of the graph shows the three sgRNA designed to be used with the WT CRISPR/Cas9 nuclease. Two of the sgRNA were in a sense orientation (1st and 3rd sgRNA), while just one was in the antisense orientation (2nd sgRNA). The schematic also shows the full length (152bp) ssODN used as a template to introduce the R47H mutation. Highlighted in red is the SNP that causes the change of the 47th amino acid of TREM2 protein from an arginine (CGC) 47 into a histidine (CAC). PAM sites for all sgRNAs are shown in light blue and the expected cleavage sites (nicks or double strand breaks accordingly) with green arrowheads.

3.3.3.1 ***Design of sgRNAs and ssODN***

Using the CRISPR/Cas9 Online tool (http://tools.genome-engineering.org), two sgRNAs for the nickase approach and 3 sgRNAs for the WT nuclease approach were chosen. The selection of the sgRNAs was based on their proximity to the nucleotide which needed to be mutated and the number of predicted off-target cuts. In this case, the nucleotide that needed to be mutated was a guanidine for an adenosine (GxA transition) at position 2156 of the *Trem2* gene, which corresponds to the 47th amino acid of the protein. Based on these criteria, 5 sgRNAs were chosen (sequences are shown in Table 2-5) for cloning into the CRISPR/Cas9 plasmids.

A single ssODN was designed for the introduction of the R47H mutation as recommended by Ran et al. (2013b). Since many sgRNAs were going to be tested in this experiment, the homology arm was designed to have homology arms of at least 45bp to both the 5' and 3' side of any sgRNA sequence, as recommended by Ran et al. (2013b). To increase the likelihood of stimulating the HDR, the ssODN contained homologous flanking sequences of 88bp (to the 5' end) and 63bp (to the 3' end), one each side of the target nucleotide (Figure 3.8).

3.3.3.2 ***Preparation of sgRNA expression constructs***

As shown in Figure 3.8, two different approaches were used to introduce the R47H mutation into the BV2 cell line. As such, one plasmid construct was prepared for each one of the sgRNAs (5 in total). Depending on the approach used, two different plasmid backbones were used: the PX458 (WT nuclease) and PX461 (nickase). Both plasmid backbones share the same essential architecture and sequence (Figure 2.5) and differ in only 6 SNP (one of them is a 1bp deletion on the nucleotide 1017 of the PX458), which makes them relatively comparable when assessing their transfection efficiencies.

Once cloned into their respective CRISPR/Cas9 plasmids, the insertion and sequence of the sgRNAs was verified by Sanger sequencing (Figure 3.9).

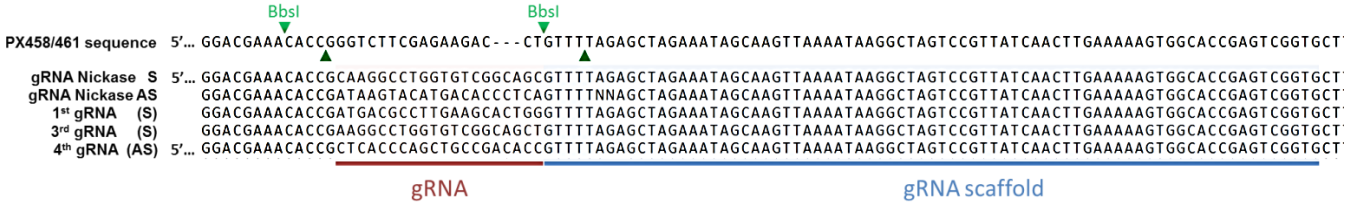

Figure 3.9 sgRNAs correctly inserted into the PX458 and PX461 backbones. sgRNAs were inserted into two different backbones (PX458 or PX461) depending on the approach to be used for the introduction of the *Trem2* R47H mutation. Sequences of all 5 resulting plasmids have been aligned to the PX458/461 plasmid. sgRNAs (underlined in red) are inserted next to the gRNA scaffold (underlined in blue). The BbsI restriction sites (enzyme used to cleave the plasmids for the insertion of the gRNAs) are shown with green arrowheads (this enzyme generates sticky ends). Once the plasmids are cleaved by the BbsI enzyme, the DNA fragment between the two restriction sites of the enzyme is replaced by the gRNAs.

As shown in Figure 3.9, all 5 gRNAs were correctly inserted into their respective plasmid backbones and to the 5' side of the gRNA scaffold. Once the gRNA expression constructs were ready, they were transformed into bacterial cells for amplification. Subsequently, all plasmids were extracted in Endotoxin-free conditions for their functional validation.

3.3.3.3 ***Functional validation of gRNAs: transfection optimization in BV2 cells***

In order to validate the cleaving capacity of each of the gRNAs, it was first necessary to optimise the transfection efficiency of the plasmid backbones. Since both backbones share the same basic architecture, standardisation of the transfection efficiency was only performed in one of the two; in this case the PX458. Both CRISPR/Cas9 plasmids used express the EGFP (Enhanced Green Fluorescent Protein) protein, which has an excitation/emission of 488/509. Expression of the EGFP protein can be used both for measuring transfection efficiency (percentage of transfected cells) and for single cell sorting of positively transfected cells by FACS.

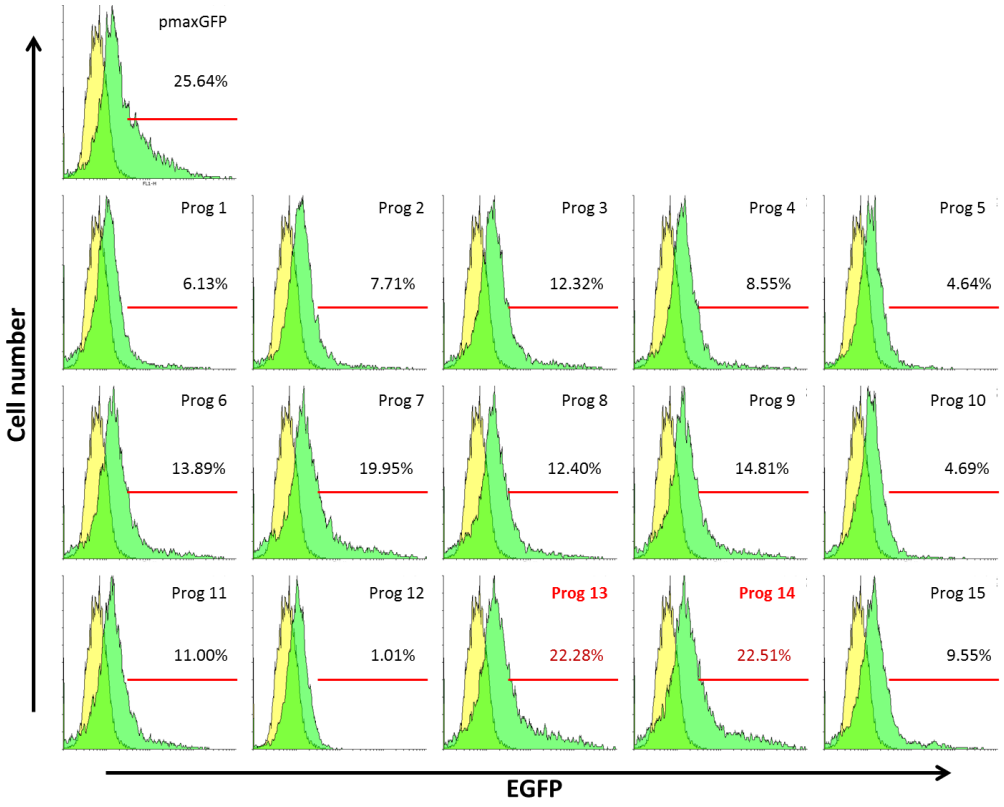

Figure 3.10 PX458/461 transfection efficiency optimization on BV2 cells. 15 Different electroporation protocols were tested for the transfection of the PX458 plasmid into BV2 cells. 200 000 cells were transfected with 400ng of the PX458 plasmid and left to grow for 48h before expression of the EGFP protein was measured by FACS. Untransfected control cells (GFP negative) are shown as a yellow histogram, which was used to set GFP positive gate. BV2 cells were transfected with the pmaxGFP™ vector (using programme CM-158) as a positive control for the experiment (top left corner). The percentage of EGFP positive cells for each programme as well as the programme identifier (1-16) are shown in each histogram (green). Programmes 13 and 14 (in red) show the highest percentage of transfected cells (higher transfection efficiency). Cells were transfected with the Cell Line Optimization 4D-NucleofectorTM X Kit and the Cell Line 4D-nucleofectorTM solution SF (LONZA).

As shown in Figure 3.10, transfection of the plasmid PX458 was optimised using the Cell Line Optimization 4D-NucleofectorTM X Kit and the Cell Line 4D-nucleofectorTM solution SF (LONZA). Expression of the protein EGFP was used to quantify the transfection efficiency of the plasmid into BV2 cells. Efficiency was calculated as the percentage of cells expressing the EGFP protein. As Figure 3.10 shows, the programmes with the highest efficiency are programmes 13 and 14 (22.28% and 22.51%).

A second parameter to consider when optimizing the transfection efficiency of most transfection methods, and particularly electroporation, is cell death. The kit's optimization guidelines recommend choosing the programme that achieves the highest percentage of transfected cells (GFP positive) with the lowest mortality. Mortality was assessed by PI (Propidium Iodide) staining and FACS analysis.

Table 3-2 Optimization of the PX458 plasmid transfection – Transfection efficiency vs. cell mortality

Programme identifier	GFP positive cells, %	Dead cells, %
CM158 (positive control)	25.64	6.77
14	22.51	24.51
13	22.28	22.99
7	19.95	22.08
9	14.81	20.77
6	13.89	22.23
8	12.40	18.84
3	12.32	20.40
11	11.00	22.17
15	9.55	23.07
4	8.55	18.19
2	7.71	15.81
1	6.13	21.63
10	4.69	20.87
5	4.64	18.13
12	1.01	6.83
Unstransfected (negative control)	0.09	3.72

As shown in Table 3-2, programmes 13 and 14 not only had the highest transfection efficiencies, but also the highest mortality of cells (22.99% and 24.51% respectively). Although the transfection efficiencies reached with said programmes (22.28% and 22.51%) are comparable to the transfection efficiency of the control plasmid (25.64%), the cell mortality is notably lower for the control plasmid. Based on both sets of data, programmes 13 and 14 were taken forward. Of note, the chosen programmes correspond to protocols EN-138 and EN-150 of the Nucleofector™ pre-set programmes.

There is evidence that supports a correlation between the total mass of DNA transfected and transfection efficiency for plasmids shorter than 4275bp (Hornstein et al., 2016); as such, the amount of plasmid to be transfected into BV2 cells was optimised using programmes EN-138 and EN-150. Optimization of the total mass of plasmid to be transfected was carried out using 1x10^6 cells per transfection and 100ul Single Nucleocuvettes™, keeping the rest of the protocol as before. Three different amounts of transfected plasmid were tested: 3µg, 5µg and 7µg.

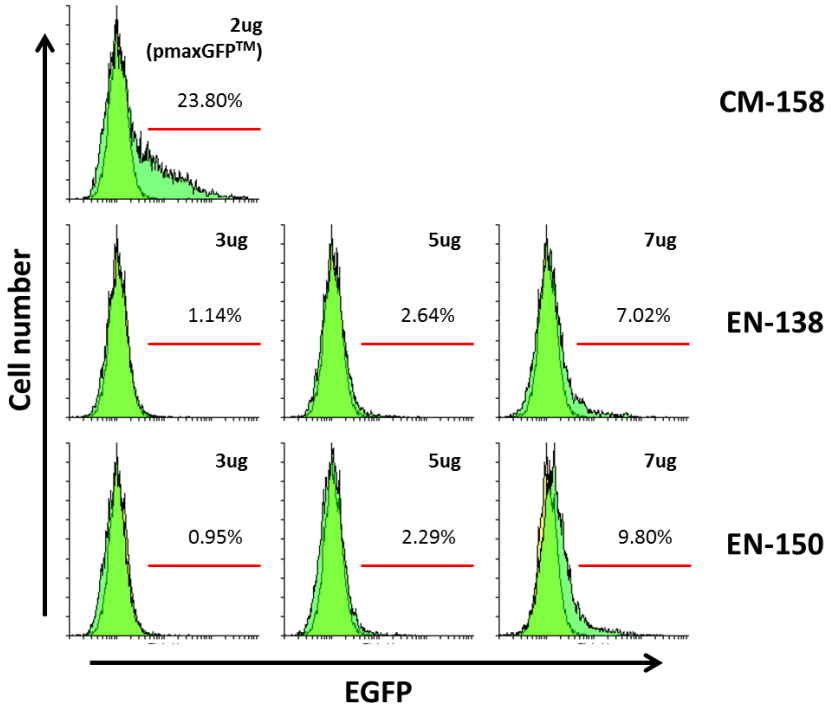

Figure 3.11 PX458/461 plasmid dose optimization for transfection into BV2 cells. Using programmes EN-138 and EN-158, three different amounts of the PX458 plasmid were tested: 3, 5 and 7µg total plasmid. 10^6 cells were transfected with the PX458 plasmid and left to grow for 48h before expression of the EGFP protein was measured by FACS. Untransfected control cells (GFP negative) are shown as a yellow histogram, which was used to set GFP positive gate. BV2 cells were transfected with the pmaxGFP™ vector (using programme CM-158) as a positive control for the experiment (top left corner). The percentage of EGFP positive cells for each transfection is shown in each histogram. As observed, a dose of 7µg, irrespective of the programme used, shows the highest percentage of transfected cells (higher transfection efficiency). Cells were transfected using the 100µl single Nucleocuvette and the Cell Line 4D-nucleofector™ solution SF (LONZA).

Figure 3.11 shows the results of the plasmid dose optimization for transfection of the plasmid PX458 into BV2 cells. As seen in the figure, there was a very small shift on the transfected population with respect to the untransfected controls. In fact, the shift is only noticeable for the highest dose tested (7µg – right panels). According to the manufacturer's recommendations, transfections conditions optimised using the Cell Line Optimization 4D-Nucleofector™ X Kit and the Cell Line 4D-nucleofector™ solution SF (LONZA) are transferable to the 100µl single Nucleocuvette™. Nevertheless, in our experiment there was a big drop in the transfection efficiency when both systems were

compared. However, the optimization was performed as per the kit's guidelines paying close attention to the cell mortality of each programme.

Table 3-3 Optimization of the PX 458 plasmid dose for electroporation of BV2 cells using programmes EN-150 and EN-138 – Transfection efficiency vs. cell mortality

Programme + plasmid dose	GFP positive cells, %	Dead cells, %
CM158 + 2ug (positive control)	23.8	3.85
EN-150 + 7ug	9.8	8.38
EN-138 + 7ug	7.02	5.97
EN-138 + 5ug	2.64	4.49
EN-150 + 5ug	2.29	4.34
EN-138 + 3ug	1.14	2.88
EN-150 + 3ug	0.95	2.85
Untransfected (negative control)	0.52	3.78

Table 3-3 shows the results of the optimization of the plasmid dose for BV2 transfection. The plasmid dose with the better transfection efficiency is 7µg regardless of the programme used, although programme EN-150 (9.80%) is almost 3% more efficient than EN-138 (7.02%). It should be noted that transfection efficiencies fell drastically (from 22.28 and 22.51% to 7.02 and 9.8% respectively) as well as the cell mortality (from 22.99 and 24.51% to 5.97 and 8.38% respectively) when compared to programme optimization step. Based on these results, programme EN-150 was chosen for the functional validation of the gRNAs.

The capacity to cleave the CRISPR/Cas9 target region by the 5 gRNA expression constructs was evaluated using the SURVEYOR assay. For this, 10^6 BV2 cells were transfected with 7µg of each gRNA expression vector (the two nickase plasmids were transfected together at 3.5µg each) and the optimised programme EN-150. After transfection, cells were grown for 48h. Subsequently, GFP positive cells were FACS sorted and left to expand for 5 days before gDNA was extracted from each transfected population. The CRISPR/Cas9 target region was amplified by PCR and amplicons were used for analysis with the SURVEYOR assay.

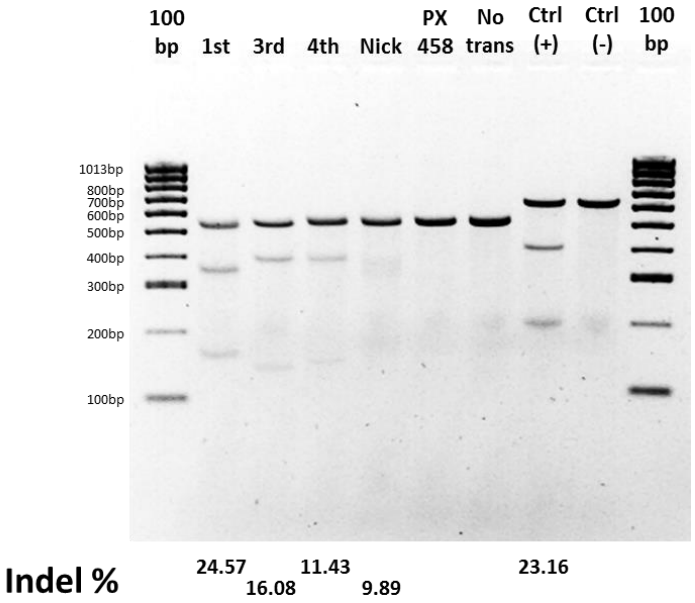

Figure 3.12 Estimation of cleavage efficiency - Functional testing of gRNAs designed for the introduction of the *Trem2* R47H mutation in BV2 cells. Functional testing of the cleavage efficiency of the 5 gRNA expression constructs designed for the introduction of the *Trem2* R47H mutation was carried out using the SURVEYOR assay. 6 different transfections were compared in this experiment: 3 transfections for each of the expression constructs with backbone PX458 (1st, 3nd and 4th), 1 transfection for the expression constructs with backbone PX461 (Nickase), 1 transfection for the plasmid backbone PX458 carrying no gRNA (PX458) and 1 untransfected control (No trans). The SURVEYOR assay kit provides two further controls: 1 positive control containing a single SNP (Ctrl(+)) and one negative control with identical sequences (Ctrl(-)). Indel% for each of the gRNA expression constructs are shown in the bottom part of the figure. Ladder used was the Hyperladder™ 100bp (Bioline).

As shown in Figure 3.12, the gRNA with the highest cleavage efficiency is 1st in the PX458 backbone (24.57%). The other two gRNAs (3rd and 4th) with the same backbone obtained cleavage efficiencies of 16.08% and 11.43% respectively. The nickase approach using the PX461 backbone and two gRNA (S and AS) obtained a cleavage efficiency just below 10%. This was expected given the fact that both nickases have to act at the same time in order to generate a double strand break and that the 7µg of plasmid dose had to be split between the two nickase constructs (3.5µg each). The SURVEYOR assay positive control showed an Indel% of 23.16; this result is unexpected as theoretically the control should have been 50%. To prepare this control, equal amounts of the two PCR control products, containing a single SNP, were mixed and assayed. Given that a 1:1 mixture of PCR products with a single SNP (equal to 50% sequence mismatch) gives an Indel% of 23.16, it can be presumed that an Indel% of 24.57 represents more than 50% sequence mismatch for the first sgRNA sample.

In light of the results obtained in this optimization and functional testing, all the transfections (CRISPR/Cas9n and CRISPR/Cas9 expression constructs) were carried out using 7µg of plasmid per $1x10^6$ cells and with the pre-loaded programme EN-150.

3.3.3.4 ***Introducing the Trem2 R47H mutation using the CRISPR/Cas9n (nickase) approach***

CRISPR/Cas9n nickases were used as first approach for the introduction of the *Trem2* R47H mutation in BV2 cells, due to our previous experience in their use and their low incidence of off-target effects. The plasmids containing the Antisense and sense sgRNAs were co-transfected with the ssODN for the experiment. Transfection of the nickase plasmids was done in $1x10^6$ BV2 cells and only 300 single cell colonies were obtained after FACS sorting. Of these, only 168 colonies survived. Clones were compiled into three 96-well plates for RFLP screening of the R47H mutation.

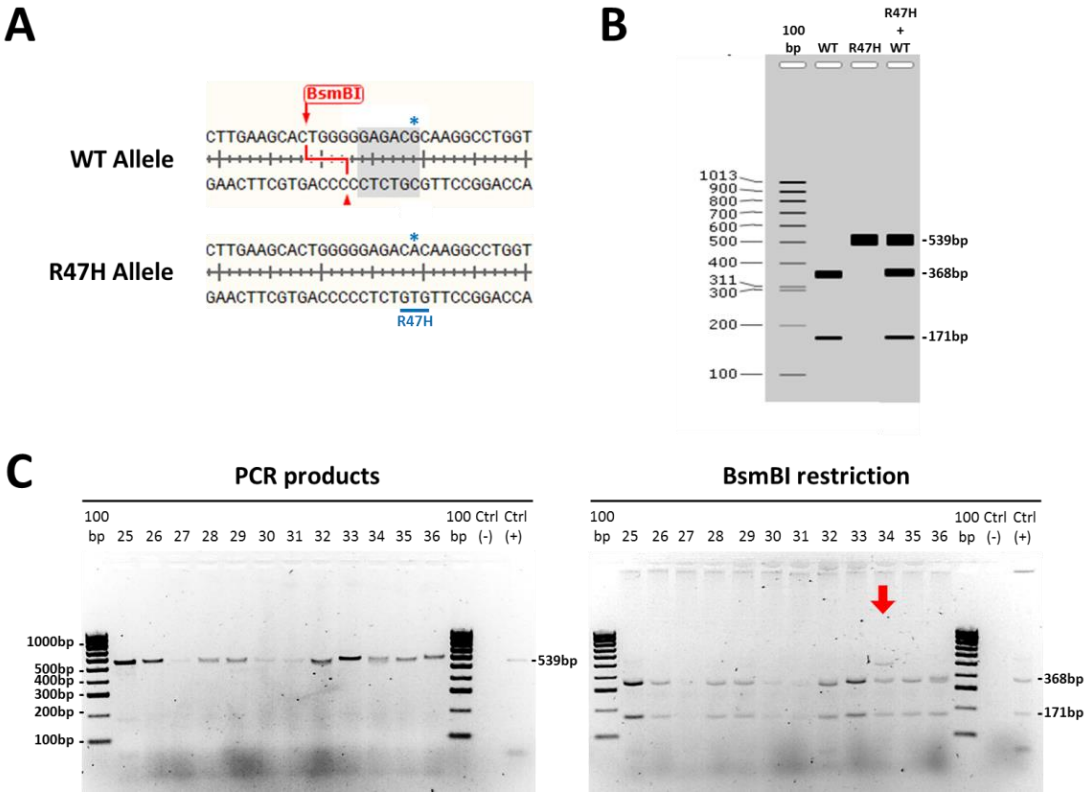

Figure 3.13 Screening methodology and RFLP analysis of single cell colonies for the identification of candidates carrying the *Trem2 R47H* mutation - Cas9n (nickase) approach. A) Schematic showing the cleavage site of the BsmBI enzyme within the PCR amplicon of the WT and R47H alleles. BsmBI specifically identifies the nucleotide sequence CGTCTC and cleaves the DNA downstream of the recognition site. The BsmBI recognition site is highlighted in grey on the WT allele and the cleavage sites are marked with red arrow heads. The codon corresponding to the R47H mutation is underlined in blue in the R47H allele and the mutation that has to be introduced is marked with a blue asterisk over the sequence. As it can be seen the R47H mutation (GxA) alters the BsmBI recognition site, inhibiting the enzyme's activity. **B)** Schematic showing the expected RFLP fragments after restriction of PCR amplicons (539bp) with BsmBI. Restriction enzyme BsmBI specifically cleaves the WT allele of the *Trem2* gene generating two small fragments of 368 and 171bp. Introduction of the R47H mutation impedes the cleavage of the PCR product by BsmBI. **C)** Representative image showing PCR amplification and screening of 12 single cell colonies by RFLP. BV2 cells were transfected with nickase expression vectors containing the S and AS gRNAs and the ssODN (repair arm) comprising the R47H mutation. Single cell colonies were screened for the R47H mutation using RFLP analysis. Left panel shows the PCR products of the nickases' target region (539bp) in 12 single cell colonies as well as negative (no DNA) and positive (untransfected BV2 DNA) controls. Right panel shows the restriction products of the 12 PCR amplicons (and controls) digested with the BsmBI enzyme. The red arrow points to a possible candidate carrying the R47H mutation (clone 34).

Figure 3.13 shows the selection strategy for the identification of BV2 clones carrying the R47H mutation. The BsmBI enzyme was used for selection as it specifically cleaves the WT allele (1 cut producing 2 fragments of 368 and 171bp) of the *Trem2* gene (Panel A, Figure 3.13) allowing selection of candidate clones which may have the R47H mutation (no cut). It is worth mentioning that the BsmBI is not able to cut the DNA if any of the 6 nucleotides in its recognition sequence is modified – this includes the R47H mutation and others. This consideration is important given the fact that selection based on this enzyme restriction does not guarantee the presence of the mutation, but helps to discard all clones in which the WT allele is kept in homozygosity. In order to confirm the presence of the mutation PCR products were sent for Sanger sequencing.

Figure 3.13 also shows a representative image of the selection process in cells transfected with the nickase expression plasmids. As shown in the figure, clone 34 was a possible candidate for carrying the mutation as it showed one uncut PCR product (top band) after BsmBI restriction. Sanger sequencing of this sample confirmed that this clone did not have the R47H mutation. Screening of the 168 expanded colonies rendered 10 possible candidates of which none carried the R47H mutation. As a result, insertion of the R47H mutation using Cas9n was deemed unsuccessful.

3.3.3.5 ***Introducing the Trem2 R47H mutation using the wild type Cas9 approach***

Having tried the CRISPR/Cas9 nickases with no success, the next approach involved the use of the wild type CRISPR/Cas9 nuclease for the introduction of the *Trem2* R47H. The use of the wild type Cas9 protein for CRISPR editing substantially increases the efficiency of HDR modification compared to the Cas9n. In contrast, the Cas9 strategy has a higher rate of off-target modifications (Ran et al., 2013a). Three independent transfections were carried out using BV2 cells, the 1st gRNA expression vector and the ssODN carrying the R47H mutation.

The first transfection was performed in $1x10^6$ cells which were subsequently GFP FACS-sorted. Of this first transfection, only 60 single cell clones were recovered. These clones were not expanded or screened for the R47H mutation. As seen in previous transfections, roughly 50% of the cells survive the sorting/expansion period, which reduces the number of viable candidates to 30 clones. Furthermore, Ran et al. (2013a) report, using HEK293T cells, that HDR efficiency for the Cas9 is ~9% of the total transfected population. Although our population has already been enriched for cells expressing the GFP protein encoded in the CRISPR/Cas9 construct, the same efficiency reported by Ran et al. (2013) was used to estimate that 30 single cell colonies will produce only 3 candidate colonies. As a result, the 60 single cell clones which were

recovered from the FACS sorting, were not expanded or screened for the R47H mutation.

A second genome editing experiment was performed using two simultaneous transfections of $1x10^6$ cells each. Cells from both transfections were pooled together in a single well of a 6-well plate and left to recover before being FACS sorted and expanded. 300 clones were obtained from the sorting step. After expansion only 50 single cell colonies survived. Of those, 11 were chosen as candidates for carrying the R47H mutation. All candidates were sent for Sanger sequencing; none of them was a carrier of the mutation.

A third and final transfection was prepared. This time, three simultaneous transfections of 10^6 cells each were performed. Cells from the three independent transfections were pooled together in a $75cm^2$ flask and left to recover before cell sorting. After single cell sorting, 2592 single cell colonies were obtained (27x 96-well plates). Of these, only 774 clones survived the clonal expansion stage (8x 96-well plates and 6 single wells). After BsmBI screening, 280 clones were chosen as candidates for carrying the R47H mutation. Finally, samples from all 280 clones were sent for Sanger sequencing. After analysis of sequencing results, none of the candidates were identified as carriers of the R47H mutation. Nevertheless, 2 homozygous *Trem2* KO (*Trem2* -/-) clones were identified. The remaining 278 clones are potential *Trem2* heterozygous knockdowns (*Trem2* +/-) clones, but further characterization will be needed.

Figure 3.14 shows a representative image of the RFLP screening on the single cell clones obtained from the third transfection. Results correspond to the 5^{th} plate (out of 9). Both PCR amplicons and BsmBI restriction fragments are shown side by side. As shown in the figure, there were 34 possible carriers of the R47H mutation on this plate (1/3 of the plate).

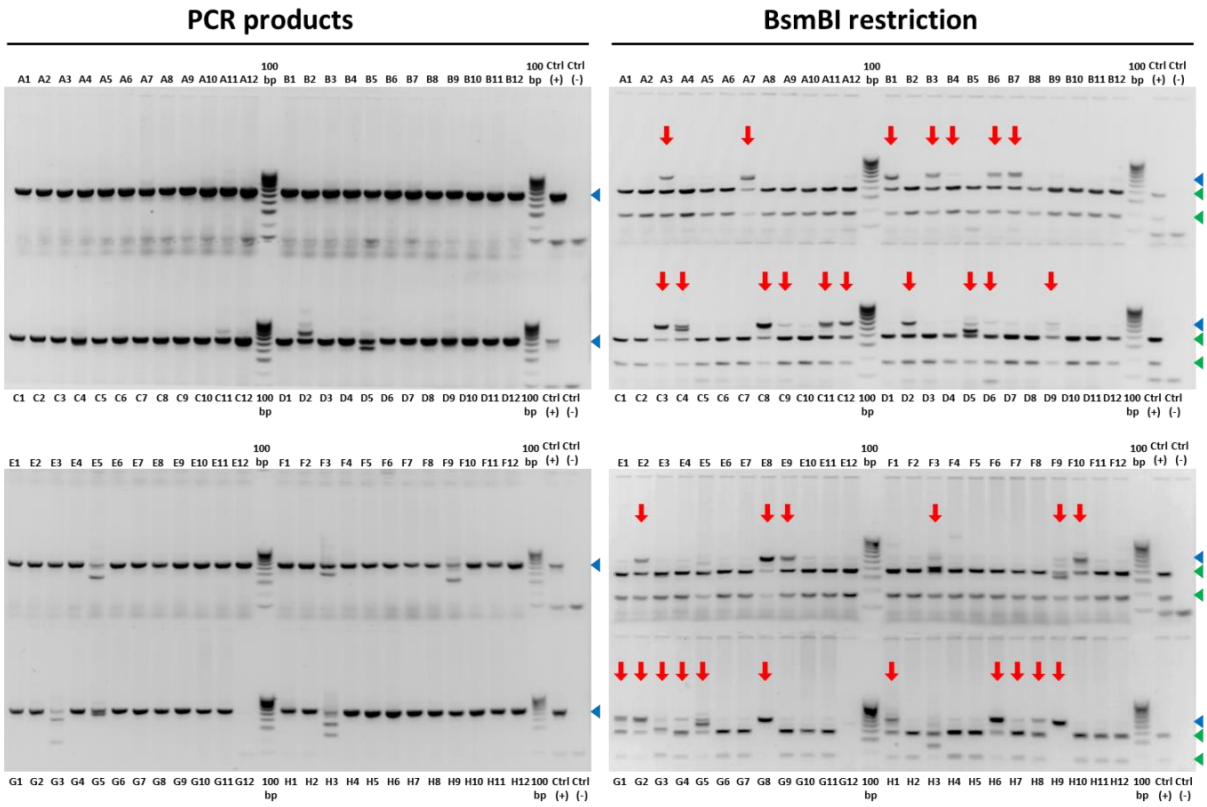

Figure 3.14 RFLP analysis of single cell colonies for the identification of candidates carrying the *Trem2* R47H mutation – Cas9 approach. Selection of possible candidates carrying the R47H mutation was done using RFLP screening on PCR amplicons of the CRISPR/Cas9 target region. The left panel shows the PCR amplicons of 96 single cell colonies (Plate #5, out of 9) at the expected size (539bp – blue arrowheads). The right panel shows the same PCR amplicons after BsmBI restriction. Selection of candidate clones was based on the presence of the uncut PCR product (539bp), complete digestion of the PCR amplicons by BsmBI (generating two fragments at 368 and 171bp – green arrowheads) discarded them as possible candidates. Candidate clones for this plate (Plate #5) are indicated with red arrows, a total of 34 out of 96 clones. The molecular weight marker used was HyperLadder™ 100bp. gDNA extracted from unmodified BV2 cells was used as positive control for PCR amplification and BsmBI restriction, while the PCR negative control used nuclease-free water instead of gDNA for amplification.

Analysis of the Sanger sequencing results for clone 5-G2 is shown in Figure 3.15. Clone 5-G2 was picked as a possible candidate based on the RFLP screening (Figure 3.14). Sequence alignment analysis revealed that the R47H mutation had not been introduced into clone 5-G2. Nonetheless, the Indel event (or events) in this clone was investigated further.

Alignment of the clone 5-G2 forward and reverse sequences was good to either side of the expected cleavage site; however, the quality of the sequencing trace was very poor near to the expected cut site of the Cas9 endonuclease. Because of the poor trace quality, it is not possible to identify the exact Indel event. Analysis of the same sequencing traces using the web tool TIDE (Brinkman et al., 2014) identified two different Indel events for this clone: i) a 5bp deletion (pvalue $3.9x10^{20}$) and ii) a 1bp insertion (pvalue $2.8x10^{11}$). Both mutations can shift the reading frame of the gene (as they are not a multiple of 3) and producing a premature stop codon. The TIDE web tool can predict

this sort of Indel events; nevertheless, Next-generation sequencing or Single colony Sanger sequencing strategies will be needed to confirm this observation. Similar analysis was carried out for all 280 R47H candidate clones chosen from the RFLP screening. After analysis, it was concluded that none of the screened clones was a carrier of the R47H mutation.

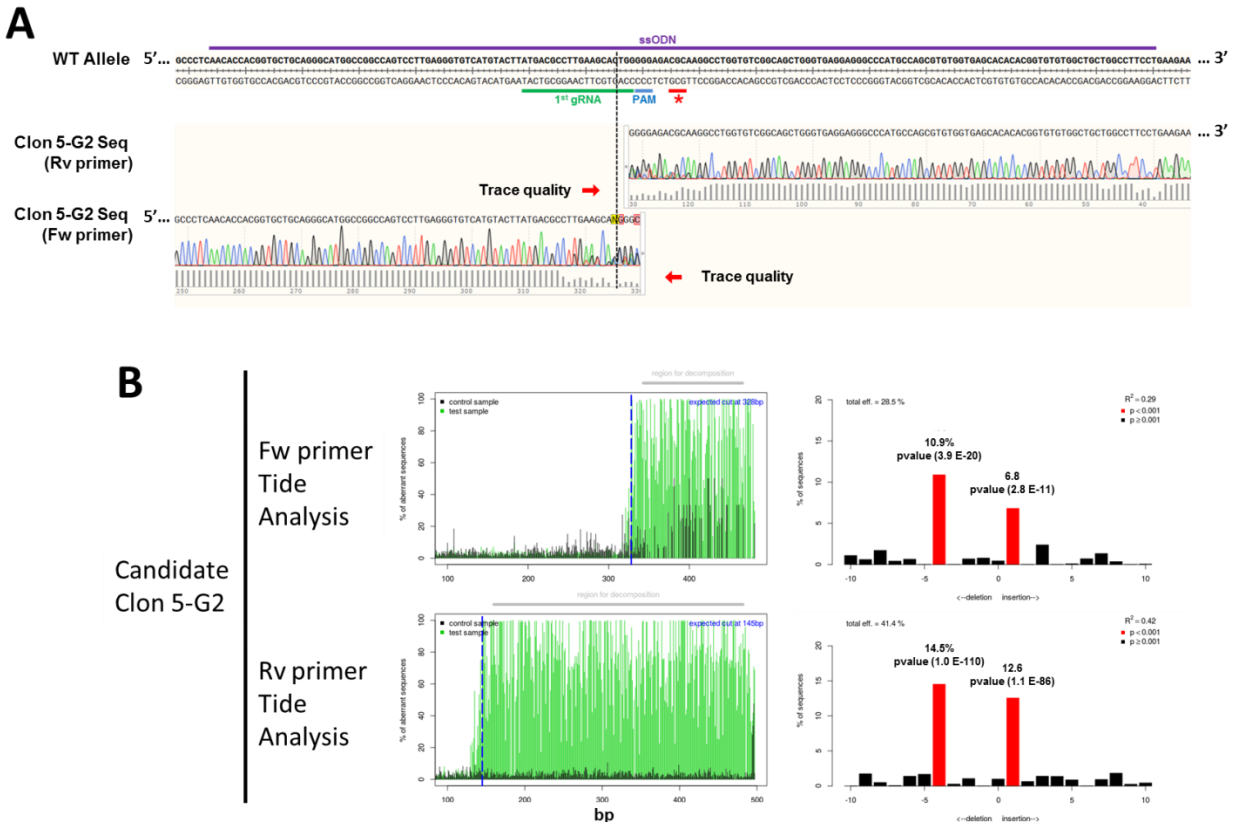

Figure 3.15 Analysis of Sanger sequencing results for chosen candidates (possible carriers of the R47H mutation) – Selected clone Clone 5-G2. Clone 5-G2 was selected as a possible carrier of the R47H mutation during the RFLP screening, as such PCR products of the Cas9 target region were sent for Sanger sequencing. A) Alignment of the reference sequence (WT allele) and the Sanger sequencing results obtained by sequencing of the PCR products with the Forward (Fw) and Reverse (Rv) primers. Sequencing traces (chromatogram) are shown as well as the trace quality of the reads (below the chromatogram). There was good alignment of the sequencing results at either side of the expected cleavage site of the Cas9 exonuclease (marked with a dashed vertical line). Nonetheless, sequencing alignment became poor (as well as the trace quality) as the reads got closer to the cleavage site. The poor quality of the reads did not allow identification of the exact mutation event (SNP or Indel), but because the sequencing results were not consistent with the presence of a single SNP mutation at the R47H mutation site, this clone was deemed as negative for the mutation. B) Further analysis of the sequencing results was done using the Tide web tool (Brinkman et al., 2014), which can predict Indel events based on sequencing traces. As shown in the top part of panel B, Tide analysis predicts the presence of two independent Indel events in the 5-G2 sequence; a 4bp deletion and a 1bp insertion. Same analysis was carried out using the Rv primer, which obtained similar results (bottom panel).

Table 3-4 shows the summary of the results obtained from the 4 attempts to insert the R47H mutation into BV2 cells. In total, 992 single cell colonies were screened (obtained using different Cas9 enzymes and transfections). After RFLP analysis the total number of possible clones carrying the R47H mutation was 301. Sanger sequencing of the possible carriers rendered zero positive clones carrying the R47H mutation.

Table 3-4 Summary of the CRISPR/Cas9(n) genome editing attempts to introduce the *Trem2* R47H into BV2 cells.

Strategy used	gRNA	Transfection (number of transfected cells)	Number of FACS sorted single cell colonies	Number of colonies after expansion	Number of candidate clones after RFLP screening	Number of clones carrying the R47H mutation	Observations
Cas9n Nickase (PX461)	S and AS	1st transfection (1 x 10^6 cells)	300	168	10	0	10 candidates are probable Trem2 heterozygous knockdowns (Trem2 -/+)
		1st transfection (1 x 10^6 cells)	60	-	-	0	Single cell colonies were not expanded or screened.
Cas9 WT endonuclease (PX458)	1st	2nd transfection (2 x 10^6 cells)	300	50	11	0	11 candidates are probable Trem2 heterozygous knockdowns (Trem2 -/+)
		3rd transfection (3 x 10^6 cells)	2592	774	280	0	2 candidates were Trem2 KO (Trem2 -/-) 278 candidates are probable Trem2 heterozygous knockdowns (Trem2 -/+)

Considering the negative results obtained from the 4 attempts to introduce the R47H mutation into BV2 cells, it was concluded that BV2 cells (and microglia in general) are a difficult cell type to genome edit and that future attempts should use different approaches/techniques for their genetic modification.

3.4 Discussion

The relatively recent development of the CRISPR/Cas9 genome editing system, derived from the microbial adaptive immune system, has revolutionised the fields of genome engineering and genetic research, particularly in mammalian model organisms (Jinek et al., 2012, Jinek et al., 2013, Mali et al., 2013). The CRISPR/Cas9 system is poised to transform biological research at all levels and is currently being considered for its use in human gene therapy (Singh et al., 2017, Fellmann et al., 2017, Schneller et al., 2017, Mout et al., 2017). Nonetheless, many argue that the real revolution has been on the bench (Ledford, 2016), where it has allowed many research groups to investigate the effect of particular mutations in diverse pathways and diseases (Singh et al., 2017).

In this study, the CRISPR/Cas9 gene editing technology was employed to better understand the role of gene *Dap12* and *Trem2* in microglial cells and the effect of the *Trem2* R47H mutation (associated with an increased risk of AD) on microglial function. As such, our first objective was to knockdown and knockout *Dap12* and *Trem2* from the

murine microglial cell model BV2. A second objective was the introduction of *Trem2* R47H mutation on this same cell line.

3.4.1 Generation of *Trem2* and *Dap12* knockout (-/-) and knockdown (+/-) BV2 cell lines by CRISPR/Cas9n genome editing

Our first aim was to genetically modify the BV2 cell line to generate isogenic *Trem2* and *Dap12* KO cells (*Trem2 -/-* and *Dap12 -/-*). Commercially available CRISPR/Cas9n plasmids targeting the exon 2 of *Trem2* and the exon 3 of the *Dap12* were used to this end. No construction, validation or functional evaluation of these commercial constructs was necessary and optimization of the transfection efficiency of the plasmid backbone was done previously in our lab.

After transfection and single cell sorting of our first attempt to knockout the *Trem2* and *Dap12* genes, it was evident that single cell survival and expansion of colonies were limiting factors for clone selection. In this first attempt, 288 single cell clones for each transfection were recovered in 96-well plates and left to expand for subsequent screening. Nevertheless, only 30 *Dap12* and 41 *Trem2* transfected clones survived the expansion period, which represents 10.4 and 14.2% survival of single cell clones selected by FACS sorting, respectively.

There is little mention in the literature regarding the rates of single cell colony survival, although it is a known limiting factor for CRISPR/Cas9 modification in iPSC. It is a problem mostly addressed by laboratories who seek to commercialise single cell expansion kits that promote increased viability of single cell colonies (Clontech Laboratories, 2016). For future studies, viability of single cell colonies must be considered as an important parameter as it directly affects the success rate of any CRISPR/Cas9 experiment by reducing the number of positively edited clones (as well as the non-edited clones). Methodologies dedicated to increasing the number of single cell colonies after genome editing have been shown to enhance the number and quality of mutated clones (Feng et al., 2014, Asplund et al., 2016). Our attempts to genome edit the BV2 cells, either for gene KO or introduction of the R47H mutation, showed single cell colony surviving rates between 16.6 and 56%, depending on the Cas9 approach used and the number of cells transfected. Future attempts to genetically modify BV2 cells should take this factor into account in the planning stages.

High transfection efficiency and CRISPR/Cas9 activity are other factors that contribute to successful genome editing experiments. Mali et al. (2013) made some of the most significant modifications to the bacterial Cas9 system that allowed their use in mammalian cells, particularly in human cells. By designing a human codon-optimised

Cas9 and fusing its C-terminus with the SV40 (Simian virus 40) nuclear localization signal they allowed higher localization of the Cas9 to the cell nucleus with the concomitant increase in Cas9 nuclease function. Moreover, by fusing the crRNA and the tracrRNA into a single RNA molecule (gRNA), they reduced the number of components of the Cas9 system (from 3 to only 2) that needed to be transfected into cells for gene editing. They also laid some foundational work by noting that the CRISPR/Cas9 system works at variable rates in different cell types.

Mali et al. (2013) observed that the same components of the CRISPR/Cas9 system worked at different rates of cleavage in 293T cells (10-25%), in K562 cells (8-13%), and in induced pluripotent stem cells (iPSCs, 2-4%), an observation that has been confirmed by other groups (Ran et al., 2013a). Numerous studies have examined the diverse elements that affect the CRISPR/Cas9 system efficiency, such as; Cas9 activity, target site selection, sgRNA design, delivery methods, off-target effects and the incidence of HDR (reviewed by Peng et al. (2016)). By addressing these potential pitfalls, researchers hope to improve the system's efficiency and specificity.

In this sense, it is well known that transfection efficiency highly correlates with the delivery method used and the target cell type. In this study, nucleofection (a variation of electroporation) was used because of its high transfection efficiency as phagocytes (microglial cells included) are well known for being "hard-to-transfect" cells. This "hard-to-transfect" status of BV2 cells is dependent on the transfection method and cargo utilised. For example, transfection experiments using siRNA and Lipofectamine have been shown to reach silencing efficiencies of up to 88.96% at the mRNA level and 65% reduction at the protein level (Yao et al., 2013). In this study, the use of lipofectamine for the transfection of the CRISPR/Cas9 plasmids was not considered as it has been shown that electroporation, if available, is a far better transfection method in "hard-to-transfect" cells, such as iPSC and THP-1 (human monocytes) cells (Yu et al., 2016). In our study, the use of CRISPR/Cas9n commercial plasmids and the recommended protocols for transfection invariably achieved transfection efficiencies lower than 5%, as measured by flow cytometry. This limitation was noted and efforts were made to optimise our own CRISPR/Cas9 constructs for the insertion of the R47H mutation.

The real cleavage efficiency obtained for the Cas9n plasmids targeting *Trem2* was 51% (21 modified clones out of 41 surviving colonies), whereas in the same experiment the cleavage efficiency obtained for the Cas9n plasmids targeting *Dap12* was 0% (0 modified clones out of 30 surviving colonies). These divergent results are the product of a variety of factors affecting CRISPR/Cas9 system efficiency, including but not limited to the

sgRNA design and delivery methods (Peng et al., 2016). Given the poor results obtained during our first attempt to gene edit the *Dap12* gene, the modification of the *Dap12* gene was not pursued any further. This was made under the assumption that the design of sgRNAs was not optimal, although their cleavage efficiency was not checked experimentally in this study. Another possibility for the failure of our attempt to knockout *Dap12* is that this gene is pivotal for the survival of microglial cells. Although *Dap12* deficiency is not embryonic lethal either in humans (Paloneva et al., 2000) or mice (Kaifu et al., 2003, Bakker et al. 2000, Tomasello et al., 2000), it has been associated with receptors that promote cellular activation and survival upon ligand binding (reviewed by Turnbull and Colonna (2007)). This partially rules out the possibility that *Dap12* is necessary for microglial survival, although more in-depth studies on the effect of *Dap12* deficiency on mature microglia survival are lacking.

Previous studies using the CRISPR/Cas9 genome editing technology on BV2 cells have rendered valuable tools for the study of microglial activation. In a recent paper by Kichev et al. (2017), the authors successfully managed to generate a BV2 cell line lacking RANK (Receptor Activator of NF-κB). Using this new model, they were able to demonstrate the importance of RANK signalling in modulating inflammatory activation of microglial cells and its modulatory effect on TLR3 and TLR4 signalling. Nonetheless, there is no mention of the exact backbone of the plasmid used for transfection or transfection reagents. They do not mention the total amount of screened clones, but they do mention that after their first transfection they were able to isolate 4 clones which carried one KO allele and one WT (*RANK +/-*) of the gene. Kichev et al. (2017) investigation was only focused on the effects of the absence of the gene, whereas our study was interested in both the possible effects that a genetic knockdown and knockout could have in overall microglial activation. As such, and similarly to our study, they set out to perform a second round of genome editing in one of the *RANK +/-* BV2 clones to completely abolish expression of the targeted gene. After the second round, they managed to obtain the complete gene knockout of RANK (RANK -/-).

One important limitation of this study was the difficulty to efficiently transfect BV2 cells. It is challenging to compare the work carried out by Kichev et al. (2017) to the work carried out in the present study, not only because of the lack of information regarding transfection, expansion and screening procedures, but also for the differences in the CRISPR/Cas9 approaches used. Nevertheless, it is clear that there are some similarities that confirm the "hard-to-transfect" status of BV2 cells (or microglial cells in general) (Maess et al., 2014). First among these is the fact that they only managed to isolate/pick 4 clones after the first round of CRISPR/Cas9 editing. It is not clear if this was a random

selection or if the 4 clones were the only survivors after the clonal expansion step. If the latter were the case, it highlights the necessity to use a methodology that increases single cell colony survival after clonal isolation. A second similarity is that in both studies, gene knockout was only achieved after 2 rounds of CRISPR/Cas9 editing. As discussed later in this chapter, during our 3rd attempt to introduce the R47H mutation, the rate at which homozygous knockout mutants were obtained was of 0.26% (only 2 clones out of 774 surviving colonies). These results are in stark contrast with other studies where homozygous mutants were obtained at rates of 15% (Bell et al., 2014) using Cas9 or 5-10% using Cas9n (Ran et al., 2013a).

To the best of our knowledge, there has only been one publication in which the *Trem2* gene was knocked-out on microglial cells using the CRISPR/Cas9 system, to date. In a recent study by Xiang et al. (2016a), the authors managed to knockout *Trem2* using the CRISPR/Cas9 system on the N9 cell line (rat microglia). In this study, Cas9 modification was achieved using a different CRISPR/Cas9 plasmid (PX459) containing the Cas9 and gRNA scaffold sequences and a puromycin resistance gene to use as selection marker for positively transfected clones. The Cas9n plasmids used for the gene editing of *Trem2* and *Dap12* contained both the puromycin resistance gene and the GFP gene. Only the latter was used for selection of positively transfected cells in our study. By using puromycin selection rather than GFP based single cell sorting, selection of genome edited clones is less stressful for the surviving clones, increasing viability. However, this selection process requires more laborious procedures for the isolation of single cell colonies after expansion. The study then goes on to demonstrate that *Trem2* deficient N9 cells have a reduced phagocytic capacity. To this end, the authors used a single homozygous *Trem2 KO* (containing a 1bp insertion) and no heterozygous clones, which may raise concerns regarding clonal variability and reproducibility.

In our study, it was only after two rounds of CRISPR/Cas9n genome editing that it was possible to obtain several homozygous and heterozygous *Trem2* knockouts. Of these clones, only 4 were used for further characterization and study of the *Trem2* function on microglial activation; A7, C8 (*Trem2* +/-), B5 and G4 (*Trem2* -/-). In this study, it is argued that similarly to studies carried out using iPSC cells, at least two (preferably more) CRISPR/Cas9 edited cell lines should be used for the study of specific mutations or gene KO. Although the CRISPR/Cas9 system offers the possibility to genome edit cells with high specificity, it is possible that clonal variations caused by several factors during the genome editing process, including single cell isolation and clonal expansion, can affect the genetic/epigenetic background of individual cells, similarly to what occurs in iPSC

cell differentiation (Kim et al., 2014). The use of multiple genome edited cell lines will provide higher confidence to study the effects of specific mutations.

In a recent paper Orchard et al. (2016) investigated the infection capabilities of Murine noroviruses (MNoV) using BV2 cells stably expressing the Cas9 protein in order to identify host molecules essential for virus binding and replication. In this study, the authors do not report any transfection problems and used up to 4 different gRNA libraries (transfected into BV2 cells using lentiviral transfection) for the screening of candidate proteins. The use of a BV2 cell line that constitutively expresses the Cas9 protein and gRNA libraries using lentiviral transduction evades all the difficulties observed in our study when using transient transfection of both Cas9 and gRNA. This same approach has been used by other studies where BV2 genome editing was required (Qin et al., 2017). It is worth mentioning that although the lentiviral route is a way of ensuring efficient CRISPR/Cas9 cleavage, it can also cause a chronic immune response in the transfected BV2 cells, a problem that can be avoided by the use of transient CRISPR/Cas9 and gRNA transfections (Rao et al., 2015).

Finally, during the last steps of validation of the A7 and C8 clones as haploinsufficient clones (*Trem2* +/-), *Trem2* mRNA expression was quantified by RT-qPCR (a further validation of these results in a new set of samples can be found in Chapter 3). A priori, it was expected that *Trem2* mRNA expression would be reduced by about 50%, given that only one of the alleles was functional. Surprisingly, the reduction in gene expression was markedly higher than expected. Only 21% of the expression was conserved in the A7 clone, while only 5% was conserved in the C8 clone. This drop could be explained by various mechanisms: a) epigenetic regulation of the gene – this would also account for the difficulty in targeting both alleles of the gene at the same time; b) feedback mechanism regulating gene expression – it is possible that the TREM2 protein promotes expression of the *Trem2* gene. In their study, Kichev et al. (2017) managed to knocked-out the RANK gene in BV2 cells, and the authors report a drop of 60% in RANK gene expression on the haploinsufficient RANK clones. Although this drop is much closer to the expected 50% reduction, it is still a bigger drop than anticipated.

3.4.2 **Generation of BV2 cell lines carrying the *Trem2* R47H mutation using the CRISPR/Cas9(n) technology**

The second aim of the chapter was to generate BV2 modified cell lines that carried the *Trem2* R47H mutation. To this end, two different approaches for genome editing were used: CRISPR/Cas9n (nickases mutant) and CRISPR/Cas9 (wild type nuclease). The use of Cas9 nickases offers a greater ratio of on- to off-target modification levels

compared to the wild type Cas9 (>100-fold greater specificity), while maintaining similar cleavage efficiencies. Nevertheless, the Cas9 nuclease still possesses a higher cleaving capacity, albeit with a higher risk of off-target effects (Ran et al., 2013a).

Construction of the gRNA plasmids (carrying the Cas9 or Cas9n), validation and functional testing was done in-house according to previously described protocols (Ran et al., 2013b). During the transfection optimization of the plasmids, there was a sharp drop in the transfection efficiencies when the transfection protocol was scaled up from 20µl to 100µl transfection cuvettes, from ~22% to 7-10% respectively. The same drop also affected cell mortality, which was reduced from 23-24% to 6-8%. This reduction in transfection efficiency and cell mortality was not seen in the positive control (pmaxGFP plasmid), discarding the possibility of a cell batch-specific effect. Based in our experience, it is still premature to venture and give an explanation for this unexpected effect of the scaling-up process as no similar observation has been made in the literature, but it is a subject that deserves attention in future experiments aimed at introducing plasmid DNA (CRISPR/Cas9 plasmids in particular) into BV2 cells.

Estimation of the cleavage efficiency of all the constructed CRISPR/Cas9 plasmids was carried out using the SURVEYOR assay. Generally, the efficiency of Cas9-mediated gene editing in mice via NHEJ can reach 20-60%, whereas the efficiency of HDR is only 0.5-20% (Maruyama et al., 2015). As such it was pivotal for our study to find the Cas9(n)/gRNA complex with the highest cleavage efficiency for the insertion of the R47H mutation. Functional validation of the gRNAs, showed that the 1st gRNA had the highest cutting efficiency in our experiment. The Indel% for this gRNA was 24.57%, which ensured that at least 1 in every 4 selected clones had some kind of genetic mutation near the CRISPR/Cas9 target site. The two gRNAs used for the nickase approach (A and AS) gave a combined cleavage efficiency of 9.89% at the CRISPR/Cas9 target site. Although Ran et al. (2013a) have demonstrated that Cas9 nickases can have cleavage efficiencies comparable to those of the wild-type Cas9 nucleases, in our study, nickases seemed to have a much lower efficiency. The comparison between the Cas9 nickase and the Cas9 nucleases in our study is hindered by the use of different sgRNA target sequences, unlike Ran et al. (2013a).

Despite their low Indel%, Cas9 nickases were selected as first approach for our 1st attempt at introducing the R47H mutation, given that nickases have a higher ratio of on- to off-target effects. A single stranded nucleotide (ssDNA) was used as HDR template for repair. Unfortunately, this approach did not bear any positive results (see Table 3-4). Consequently, a second approach involving the use of wild-type Cas9 nucleases was

utilised to increase the on-target cleavage, albeit with a higher risk of off-target effects. Three attempts to introduce the R47H mutation, using the wild-type Cas9 nuclease, were made with no positive results. Personal communications with two other research groups trying to introduce this same mutation into BV2 cells have confirmed that, to date, similar attempts to introduce this mutation in these cells have not been successful.

Considering these results, it is reasonable to question whether it is possible to genome edit BV2 cells using the HDR pathway. In a recent study, Kichev et al. (2017) managed to insert a piece of DNA (containing a LoxP/RFP/Puro/LoxP sequence) via HDR mechanisms in BV2 cells. Their approach was slightly different to the one used in our study, and it is worth taking into consideration for future attempts to genome edit BV2 cells. In their study, the introduction of the mutation was achieved by using a HDR plasmid (double stranded donor) containing homology arms flanking the sgRNA targeting site. Although, again, there is no information regarding the backbone of the HDR plasmid or its size, it is encouraging to have experimental evidence of HDR mechanisms working normally on BV2 cells. In light of these results, and contrary to what was used in this chapter, it may be necessary to use double-stranded DNA (dsDNA) donors, rather than ssODN, to stimulate HDR in BV2 cells.

Our research group still envisions introducing the R47H mutation into BV2 cells. To that end, it will be necessary to change the gene editing approach to enhance HDR pathways. In addition to the use of a dsDNA donor, like the HDR plasmid used by Kichev et al. (2017), it would be advantageous to use other approaches to shift the balance between the NHEJ/HDR pathways. By inhibiting components of the NHEJ pathway, Singh et al. (2017) managed to increase the efficiency of the HDR pathway by 19-fold in mammalian cells (reviewed by Salsman and Dellaire (2017)). Another way to favour the HDR pathway over the NHEJ pathway is controlling the cell cycle phase during the genome editing process. It has been reported that the frequency of HDR repair is 39-fold higher during the S-phase of the cell cycle, compared to the M-phase and 24-fold higher than in G1/G0 phases (Saleh-Gohari and Helleday, 2004). Finally, some studies have used the purified Cas9 nuclease protein and a gRNA molecule as a pre-formed ribonucleoprotein (RNP) complex for genome editing (reviewed by DeWitt et al. (2017)). This approach avoids many of the limitations faced by transient plasmid transfections, used in this study, or viral transductions. This method has also been shown to have reduced off-target effects and produce lower levels of cell toxicity when compared to plasmid mediated transfection (Lin et al., 2014, Liang et al., 2015). One final consideration for future work aimed at modifying the *Trem2* gene in BV2 cells, is the fact that these cell model has a karyotype that has been designated as 'Grossly abnormal'

(Section 2.1), particularly because the chromosome 17, where the *Trem2* gene is located, has 2-4 copies in BV2 cells. Polyploidy is known to greatly increase the difficulty of CRISPR/Cas9 mediated modifications (Scharf et al., 2018, Boettcher and McManus, 2015) and is a factor that need to be taken into consideration for future experiments.

Taken together, CRISPR/Cas9 genome editing on BV2 cells remains an obstacle for the study of microglial associated genes in AD and other neurodegenerative diseases. In this study, the use of the CRISPR/Cas9 technology allowed to knockdown and knockout the *Trem2* gene; nevertheless, efforts to insert the R47H mutation into the *Trem2* gene have rendered negative results. Future attempts to gene edit BV2 cells will have to use different variations of the CRISPR/Cas9 system to increase the chances of specific and targeted gene modifications being achieved.

4 CHAPTER 4: Characterization of the *Trem2* CRISPR/Cas9 gene-edited BV2 cell lines

In the previous chapter, different BV2 clones which had the *Trem2* gene either knockdown (*Trem2* +/-) or knockout (*Trem2* -/-) were generated using the CRISPR/Cas9 technology. While these new models will help us understand the function of *Trem2* both in normal microglial function and activation, it is imperative that these models are characterised before they can be used for further experimentation. After characterization, BV2 *Trem2* mutant cells will be challenged with different stimuli to study the effect of *TREM2* deficiency on normal microglial activation. This chapter will describe both the characterization of the *Trem2* mutant models as well as some functional studies on these cells (cytokine release, migration and phagocytosis).

4.1 Introduction

Microglial cells are the sentinel cells of the brain and, as such, upon activation they are prepared to quickly respond to neuronal insults and pathological protein deposits by increasing their cytokine release, phagocytosis, chemotactic migration and proliferation (Walter, 2016).

TREM2 has been shown to inhibit cytokine and chemokine expression, reduce pro-inflammatory responses to TLR ligands and to promote phagocytosis of neuronal cell debris and bacteria. These immunoregulatory roles of *TREM2* have been investigated using many *in vivo, ex vivo* and *in vitro* models (reviewed by Lue et al. (2015)). Early studies in *Trem2* deficiency using mouse models, revealed that bone marrow-derived macrophages which lacked *Trem2* expression released more inflammatory cytokines such as TNF and Interleukin-6 (IL-6) upon stimulation with TLR's agonists (LPS, CpG and zymosan) compared to wild-type cells (Turnbull et al., 2006, Hamerman et al., 2006). Similar results were found in *Dap12*-deficient mice, suggesting that the *TREM2*-DAP12 signalling pathway may have an anti-inflammatory function by counteracting the TLR pathway (Hamerman et al., 2005, Yeh et al., 2017).

Phagocytosis (of apoptotic cells, cell debris and microorganisms) is an essential part of the innate immune response and is fundamental for maintaining homeostasis. Phagocytosis involves many coordinated steps, including ACTIN reorganization, pseudopodia extension, plasma membrane expansion and uptake of the particles. Initiation of phagocytosis is mediated by specific interactions (recognition and binding) of phagocytic particles and cell surface proteins expressed by phagocytes (Groves et al., 2008). As a microglial membrane receptor, *Trem2* deficiency has been associated with

reduced phagocytic capacity in microglial cells. Knockdown of *Trem2* in primary microglia (transfected with a lentiviral vector carrying a shRNA targeting *Trem2*) has been shown to reduce the phagocytosis of microbeads and apoptotic cells (Takahashi et al., 2005a).

Similar studies using *Trem2* KO macrophages and microglia have also shown reduced ability to phagocyte apoptotic neurons, cell debris, bacteria and Aβ1-42 (Kleinberger et al., 2014a, N'Diaye et al., 2009b, Atagi et al., 2015a). In their study, N'Diaye et al. (2009b) show that *Trem2* is responsible for approximately 30% of the phagocytosis of *E. coli* by macrophages. Furthermore, by knocking-out *Dap12* they also managed to reduce phagocytosis of *E. coli* by approximately 60%. Reintroduction of DAP12 or a chimeric *TREM2*/DAP12 construct partially restored bacterial phagocytosis.

Clearance of apoptotic cells is another essential function of microglia in the brain. Microglial cells whose *Trem2* expression was knocked-down and subsequently exposed to apoptotic neurons showed increased levels of TNFα, IL1β and nitric oxide synthase 2 (NOS2) when compared to wild-type cells. Phagocytosis of apoptotic neurons was also reduced in the *Trem2* knockdown cells compared to wild-type (Takahashi et al., 2005a). In addition, gain-of-function studies have shown that expression of *Trem2* in non-phagocytic cells can enable the uptake of apoptotic cells and bacteria (Kleinberger et al., 2014a, N'Diaye et al., 2009b).

TREM2 is also implicated in the internalization of apolipoproteins and lipoproteins. By using HEK-293 cells with inducible *TREM2* expression, Yeh et al. (2016) showed that cells were able to internalise acetylated LDL and lipidated APOE and CLU (APOJ). Conversely, primary microglia from *Trem2* KO mice showed a reduced uptake of LDL and CLU. Interestingly, Aβ aggregates complexed with LDL or lipidated CLU were more efficiently taken by wild-type microglia than free Aβ. Primary microglia from *Trem2 -/-* and *Trem2* +/- mice showed reduced Aβ uptake in a *Trem2* dose-dependent manner (Yeh et al., 2016).

Microglia quickly respond to neuronal insults and pathological protein deposits in the brain by increasing chemotactic migration, cytokine release, phagocytosis and proliferation (reviewed by Ransohoff (2016)). Migration of microglia to the site of brain injury is pivotal for restoring tissue homeostasis (Streit, 2005). Microglial chemotaxis is regulated mainly by secreted factors, including chemokines (MCP-1, M-CSF, MIP-1), complement factors (C3a and C5a), growth factors (NGFβ and TGFβ), purine derivatives (ATP) and several cytokines. Using a FLAG-tagged-*Trem2* construct transduced into microglial cells, Takahashi et al. (2005a) demonstrated that *Trem2* stimulation does not alter the expression of inflammatory cytokines, but instead increased the chemotactic

responses of microglial cells towards CCL19 and CCL21. They also showed that this increased chemotactic response is mediated by CCR7, which is upregulated as a consequence of *TREM2* stimulation. In their study, they observed an enhanced phagocytic capacity in cells overexpressing *Trem2*.

In our study, we used C5a and NGFβ as chemoattractants. C5a is part of the complement cascade and is a well characterised mediator of inflammation through recruitment of inflammatory cells to the site of injury or infection (Robertson et al., 2018). It exerts its pro-inflammatory effect via the G-protein-coupled receptor C5a anaphylatoxin chemotactic receptor 1 (C5aR1, also known as CD88), which is expressed on myeloid cells (Klos et al., 2013). Its function is associated with diseases such as sepsis, rheumatoid arthritis, Crohn's disease and ischaemia-reperfusion injuries (Woodruff et al., 2011). More recently, C5a has been associated with neurodegenerative conditions, such as AD (Landlinger et al., 2015) and is being explored as a therapeutic target. The use of this chemoattractant will give us some clues about the effect of *Trem2* deficiency on innate immune response. Meanwhile NGFβ is the best characterised Neurotrophin (neurotrophic factor) and exerts its function on growth and survival of peripheral sensory and sympathetic neurons and other brain neurons, particularly forebrain cholinergic neurons. The latter are NFGβ's major target-cells in the CNS, where it activates two different receptors: TrkA (a tyrosine kinase receptor) and p75 (a member of the tumour necrosis factor receptor superfamily). Functional studies on NGF on brain target neurons has focused on the role that this protein plays in learning and memory during degeneration in age-related disorders, neurodegenerative disorders and AD (reviewed by Aloe and Rocco (2015)). Interestingly, development of Aβ pathology is accompanied by an impaired metabolism of NGF both in Down's syndrome and Alzheimer's disease. Similarly to C5a, NGF it is currently being explored as a therapeutic target for AD (Iulita and Cuello, 2016). The use of this chemoattractant in our study will provides with some clues about the role that *Trem2* deficiency has on the migration of microglia to the sites where maintenance, proliferation and survival of target neurons is required.

A recent study by Mazaheri et al. (2017) investigated the effect of *Trem2* deficiency on the microglial response to chemotactic stimuli. Firstly, they used a recently developed *ex vivo* model (Daria et al., 2017) to investigate the chemotactic migration of young microglia towards injured and dying tissue. As shown in their study, cells lacking *TREM2* migrated less readily towards injured tissue when compared to wild-type cells, suggesting that dying tissue provides chemotactic signals, which are detected by wild-type but not *TREM2* deficient cells. As a next approach, they used a CRISPR/Cas9-

modified N9 line – which completely lacks *Trem2* expression – to study the microglial response to C5a and CCL2. *TREM2* deficient N9 cells showed significantly decreased migration towards C5a or CCL2 chemotactic stimuli, while re-expression of the *Trem2* gene in the deficient cells rescued the response to C5a but not CCL2. The authors then assessed the capacity of microglial cells to migrate towards apoptotic cells injected in the cortex of wild-type and *Trem2 -/-* mice. They observed a significant reduction in the number of microglial cells clustered around apoptotic cells in the absence of *TREM2*, providing further evidence for the critical role of *TREM2* in the attraction of microglia to the sites of brain injury.

The role of *Trem2* in cell proliferation has been much less studied in comparison to its role in immune related responses. Migration, expansion and activation of microglial cells surrounding Aβ deposits (a process known as reactive microgliosis) is one of the pathological hallmarks associated with AD and is a well-known response of microglial cells to Aβ accumulation (reviewed by Ransohoff and Cardona (2010)). In a recent study, Wang et al. (2015c) found that both *Trem2* deficiency and haplodeficiency contributed to Aβ accumulation, partly due to a dysfunctional microglial response and apoptotic microglial death rather than cell activation and proliferation seen in wild-type cells. Similarly, the authors showed that *TREM2* is capable of sustaining microglial survival by synergizing with the CSF-1R (colony stimulating factor-1 receptor) signalling pathway. Similar studies have also shown that *Trem2* deficient microglia showed deficits in proliferation, polarization towards plaque, barrier formation and amyloid compaction (Yuan et al., 2016). Lastly, *Trem2* deficiency has also been linked to decreased proliferation of osteoclast precursor cells, a cell type that normally expresses *Trem2*, *in vitro* (Otero et al., 2012).

In this chapter, BV2 cells were serum-starved in order to immune downregulate them before stimulation/activation, and FBS supplementation (alone or in combination with LPS) was used to ‘stimulate’ and elicit responses from microglia. Serum contains a high amount of metabolites and growth factors, reason why it is used to supplement *in vitro* cell cultures, including microglial cells. Nevertheless, it contains blood-borne molecules that are actively excluded from the CNS and are not available to microglia. Serum supplementation of microglial cultures has been shown to alter their proliferative and phagocytic capacities, as well as their gene expression profile and morphology (Bohlen et al., 2017). For this reason, it is common practice to serum-starve microglial cells before stimulation/activation. Interestingly, Bohlen et al. (2017) showed that addition of serum in microglial cultures upregulated pathways involved in proliferation, amino acid metabolism and the complement immune system, while cytokine and lipid metabolism

pathways are downregulated. Furthermore, Wang et al. (2017) have shown that addition of 5% human serum (from healthy individuals or systemic lupus erythematosus patients) into BV2 cultures immune activate these cells.

4.2 Aims

The aims of the following chapter are:

1. To characterize the *Trem2* +/- (A7 and C8) and *Trem2* -/- (B5 and G4) cell lines generated by using the CRISPR/Cas9 technology, described in the previous chapter.
2. To characterize the effect of the *Trem2* knockdown and knockout in normal microglial cell function (proliferation, migration and phagocytosis) of microglial cells.
3. To characterize the *Trem2* knockdown and knockout cell lines in response to different stimuli (10% serum, LPS, IL4 and TGFβ).

4.3 Results

4.3.1 Characterization of *Trem2 (+/-)* and *Trem2 (-/-)* BV2 cell lines

4.3.1.1 *Trem2 mRNA expression*

To confirm that the *Trem2* CRISPR/Cas9 clones had reduced or no *Trem2* RNA expression, *Trem2* mRNA was quantified by RT-PCR and qPCR (RT-qPCR). All cell lines were seeded as per usual in 6-well plates and left to grow for 24h prior to all treatments. Treatments (untreated, LPS 1µg/mL, 10% FBS and LPS+10% FBS) were carried out for 24h before cells were lysed. mRNA was extracted from cell lysates as described in the Materials and Methods section, and purified mRNA from each clone was used to assess *Trem2* mRNA expression using Taqman probe Mm04209424_g1. This Taqman probe amplifies the exon junction between exons 4 and 5 of the *Trem2* gene and is capable of detecting expression of the 2 known isoforms of the mouse *Trem2* gene.

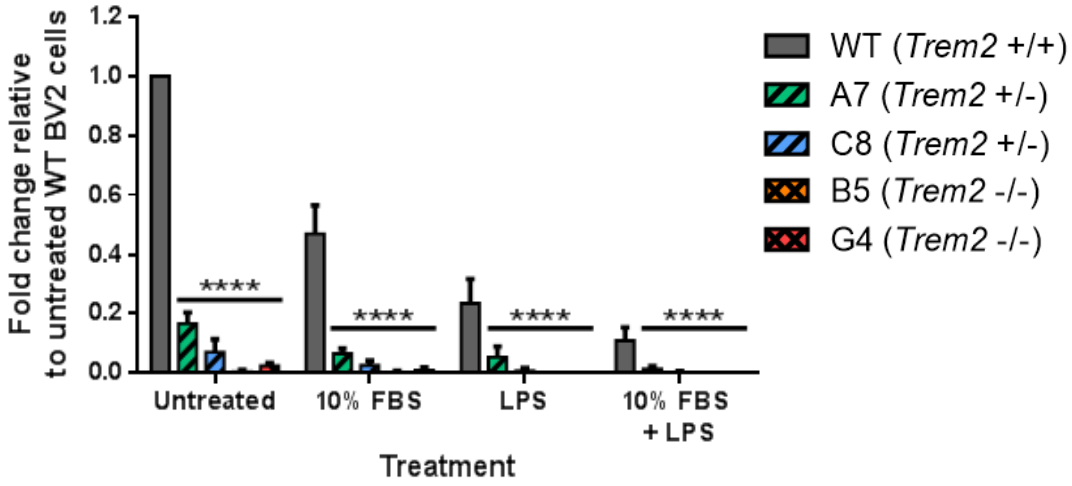

Figure 4.1 *Trem2* mRNA expression in CRISPR/Cas9 BV2 cell lines; A7, C8, B5 and G4. All 5 cell lines (WT, A7, C8, B5 and G4) were simultaneously seeded in serum-free medium for 24h prior to treatment. Cells were subsequently left untreated or treated with LPS 1µg/mL, 10% FBS or a combination of both. After 24h of treatment cells were lysed and *Trem2* mRNA expression profiles were obtained by RT-qPCR. *Trem2* expression was normalised to *Gapdh* expression and results are shown relative to untreated (serum-free) WT BV2 cells. Results represent mean ± SD of five independent biological replicates (n=5). Statistical differences were calculated relative to the WT cell line response for each treatment by 2-way ANOVA with Dunnett's correction for multiple comparisons, ****p<0.0001.

Gene expression analysis of Trem2 in the CRISPR/Cas9 BV2 cell lines is shown in Figure 4.1. So far, it has only been possible to positively modulate Trem2 gene expression by serum starving BV2 cells. Serum deprivation of BV2 cells has been shown to "relax" cells and immune downregulate them. Consistent with this observation, stimulation with LPS, FBS or both decreases Trem2 expression in a reproducible manner. The same trend in Trem2 expression reduction can be seen across all cell lines. Interestingly, addition of FBS into the medium of BV2 cells reduces Trem2 expression to approximately 47%, while LPS stimulation reduces this same expression to 23.4% in WT cells. Furthermore, when both treatments are used together Trem2 expression is reduced to only 11%. Since both FBS and LPS stimulation can increase BV2 proliferation/activation, a reduction of Trem2 could be linked to a higher level of cell activation.

As seen previously in a different set of experiments (Figure 3.4), *Trem2* expression in clones A7 and C8 (both *Trem2* +/-) is not reduced by the expected 50%, as a result of having just one allele of the gene. In fact, expression of *Trem2* is 16.6% and 7% of the WT expression for clones A7 and C8 respectively (untreated group). These results suggest that there might be an extra control mechanism (i.e. epigenetic) for the expression of *Trem2* or that maybe the cells have some other genetic anomaly. It is also worth considering that not all microglia express *Trem2*, (supporting the notion that there

is a variety of microglial phenotypes similar to the diversity of macrophages and dendritic cells) (Schmid et al., 2002). This possibility will be explored in a future chapter.

Trem2 expression in clones B5 and G4 (both *Trem2 -/-*) is almost non-existent, fluctuating between 2.5% for the untreated condition and 0% for all the other conditions. These results confirm the successful *Trem2* gene knockout in the BV2 cell line. Detection of 2.5% *Trem2* expression in clone G4 can be the result of the transcription of a degenerated (untranslatable) *Trem2* mRNA. However, RNAseq quantification of the *Trem2* mRNA expression (total transcripts) in the B5 (Chapter 5) showed fold changes between -11.05 to -13.70 in its expression compared to WT BV2 cells. This reduction in *Trem2's* expression means that only 9.05-7.30% of the *Trem2* expression is conserved in this clone, compared to WT BV2 cells. Detection of higher *Trem2* expression could be due to the improved sensitivity of the RNAseq technology compared to microarrays. This higher level of *Trem2* expression can also be the consequence of the detection of new splicing variants generated as a consequence of the CRISPR/Cas9 induced mutations (Sharpe and Cooper, 2017) or the presence of truncated/degenerated *Trem2* mRNA transcripts which have not been degraded by the NMD. These results warrant further verification of the loss of *Trem2* at the protein level.

4.3.1.2 **TREM2 *protein expression***

To verify that the TREM2 protein was either downregulated or untranslated, in the BV2 CRISPR/Cas9 clones, three different approaches were used: i) western blot of whole cell lysates, ii) soluble TREM2 (sTREM2) detection by ELISA using cell supernatants and iii) immunofluorescence studies for intracellular localization of TREM2.

4.3.1.2.1 Western blot

Western blot analysis of the TREM2 protein was carried using whole cell lysates to quantify its expression in the CRISPR/Cas9 clones. TREM2 expression was assessed 24 hours after seeding the cells in 6-well plates in serum-free medium.

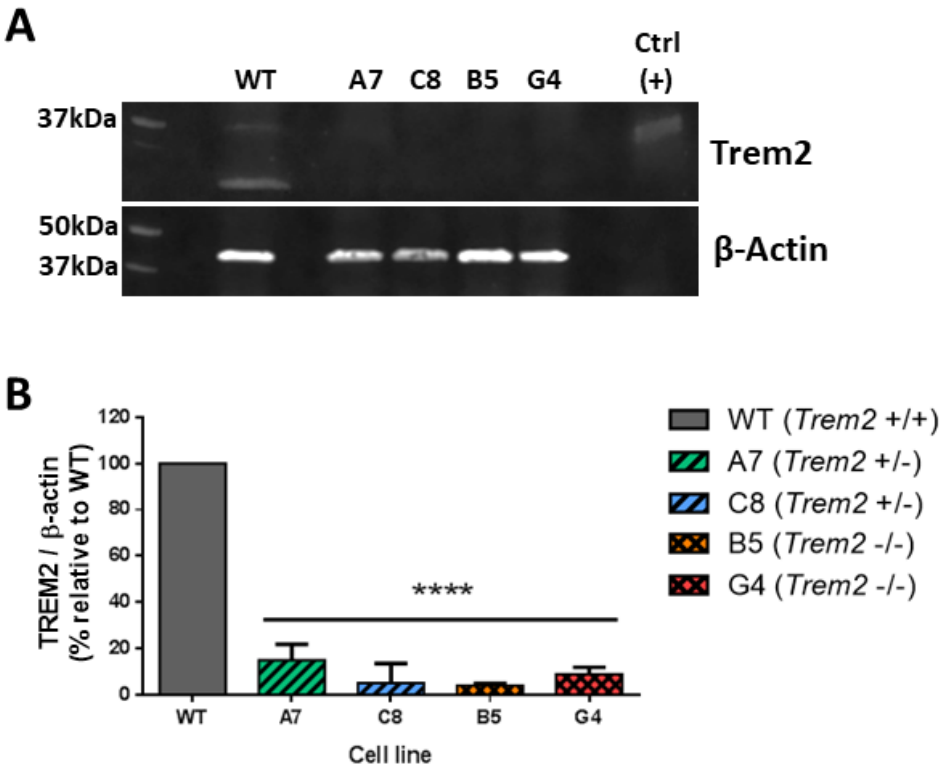

Figure 4.2 Intracellular TREM2 protein expression on CRISPR/Cas9 clones. All 5 cell lines (WT, A7, C8, B5 and G4) were seeded in serum-free medium for 24h hours prior to cell lysis. Each lane contains 15ug of deglycosylated whole cell lysate and samples were run under denaturing conditions. A) Representative image of the western blot detection of TREM2 (~25-37kDa) and β-Actin (~42kDa). TREM2 was detected using a sheep polyclonal anti-TREM2 antibody (R&D Systems, Cat# AF1729, 1:500 dilution). β-actin was used as a loading control and was detected using a mouse monoclonal ant-β-actin antibody (Sigma, Cat# A5441, 1:10 000 dilution). As a positive control for the experiment (far right lane), recombinant TREM2 protein was used (R&D Systems, Cat# 1729-T2-050) not deglycosylated. B) TREM2 protein expression quantification. TREM2 expression was normalised to β-Actin and results are shown relative to TREM2 expression in WT cells. Results represent mean ± SD of three independent experiments (n=3). Statistical differences were calculated by 1-way ANOVA with Dunnett's correction, ****p<0.0001.

Figure 4.2 shows the results from the intracellular TREM2 protein quantification in the CRISPR/Cas9 clones and WT BV2 cells. Before western blot analysis, whole cell lysates were treated with PNGaseF to deglycosylate TREM2. The TREM2 protein has been shown to exist with varying degrees of glycosylation (Wunderlich et al., 2013, Kleinberger et al., 2014a, Park et al., 2015), which can be seen as multiple bands of different protein sizes on western blot (25-45kDa). These multiple bands difficult protein quantification. Thus, samples must be deglycosylated to generate one single TREM2 protein band (~28kDa) for quantification. As shown in panel A, TREM2 (~28kDa) can only be seen clearly in the WT cell lysate and in the positive control (mouse recombinant TREM2 [~43kDa], not deglycosylated). The A7 lysate also has a distinguishable blurry band at the expected size for the protein. Panel B shows the quantification of the western blotting relative to the WT BV2 cells. The A7 cells have the highest TREM2 protein expression (14.97 ± 5.6% of WT) of all CRISPR/Cas9 clones, while clone C8 also shows a relatively

low TREM2 protein expression (5.10 ± 6.94% of WT). Both those results are in accordance with the results reported in Section 3.3.1.6.

Quantification of TREM2 protein in clones B5 and G4 (*Trem2* -/-) showed very low expression of the protein (4.05 ± 0.76% and 8.89 ± 2.51%, respectively). These low levels of TREM2 protein detected in the KO clones were attributed to the high background signal of the blots obtained with the anti-TREM2 antibody used. Other reason that explains the detection of TREM2 in the B5 and G4 clones, could be the translation of a truncated TREM2 protein by these clones. As seen in Figure 3.3, the 34bp deletion present in clones B5 and G4 (which is the same seen in their parental line C8) causes disruption of the *Trem2* reading frame, which in turn alters the amino acid sequence of the protein from the 35th amino acid onwards (the predicted protein product for clones C8, B5 and G4 has 53aa in total). This means that the detection antibody AF1729 (whose immunogen is the amino acid sequence 19-168 of the TREM2 protein) could potentially detect the truncated protein expressed by this clones, specifically the sequence 19 to 35 that is still conserved. In the case of clone A7, the predicted protein product is 40aa long and shares the same amino acid sequence with the wild typo protein up to the 36th amino acid. Taking this into consideration, further experiments were carried out to ensure that the protein was not being expressed in clones B5 and G4 (*Trem2* -/-).

For the quantification and normalization of the TREM2 protein, ACTIN was used as the endogenous control gene, despite concerns regarding its accuracy as a normalizer at the mRNA level. Piehler et al. (2010) have shown that normalization of RT-qPCR data to *Gapdh* or *Actb* alone leads to imprecise gene expression results in LPS-stimulated monocytes. However in our set up, ACTIN was used to normalize protein expression of immunologically downregulated cells (seeded in serum-free conditions for 24h) at a single timepoint, which reduces the likelihood of inaccurate normalization. Nonetheless, as shown in Figure 5.9, *Actin* mRNA expression is clearly upregulated during LPS stimulation in a dose dependent manner (24h stimulation). Moreover, the RNAseq experiment showed statically significant upregulation of *Actb* (β-actin) at the 6h timepoint by both IL4 and LPS stimulations, something that was not seen in the case of *Tbp* or *Gapdh*, which are the two normalizer genes used for mRNA experiments in this thesis.

4.3.1.2.2 sTREM2 ELISA

TREM2 can also be produced as a soluble protein: soluble TREM2 (sTREM2) (Figure 4.3). Full-length TREM2 undergoes proteolytic cleavage by ADAM (Disintegrin And Metalloproteinase Domain-Containing) proteases, specifically ADAM10, which results in the shedding of the protein's ectodomain into the extracellular space (Jay et al., 2017).

After sTREM2 shedding by ADAM10, the membrane-associated TREM2 C-terminus is cleaved by γ-secretase to release its intracellular domain (Wunderlich et al., 2013). In mouse, alternative splicing of 5' end of exon 4 of the *Trem2* gene can also generate a soluble protein that contains the Ig-like domain (Srinivasan et al., 2016). In our experiment CRISPR/Cas9 editing took place in exon 2 of the *Trem2* gene, this exon is present in all mouse *Trem2* isoforms and splicing variants known to date.

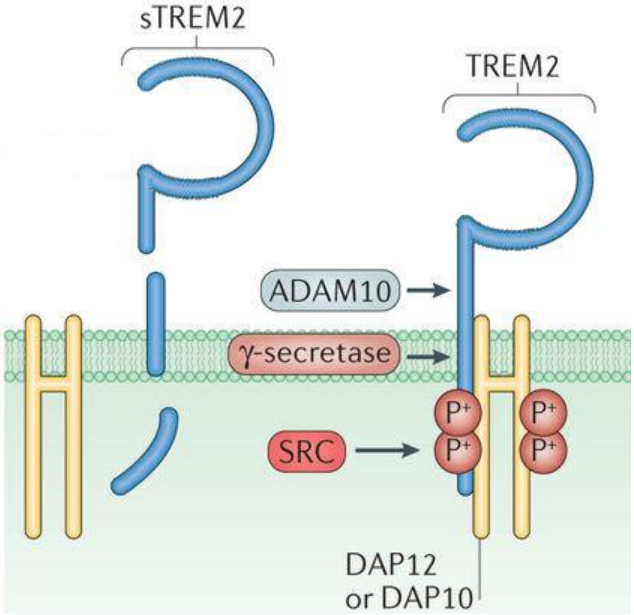

Figure 4.3 sTREM2 production. TREM2 can be cleaved from the cell surface by ADAM10 (a Disintegrin and Metalloproteinase Domain-containing protein 10) and γ-secretase, thereby releasing soluble TREM2 (sTREM2) (modified from Colonna and Wang (2016)).

In our study, sTREM2 quantification was carried out using a sTREM2 protein ELISA.

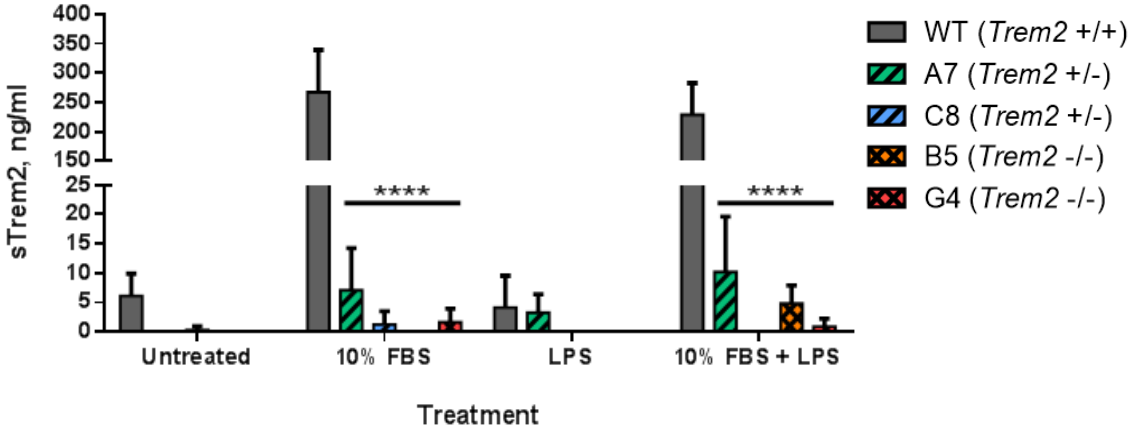

Figure 4.4 sTREM2 shedding by CRISPR/Cas9 clones. The extracellular domain of the TREM2 protein was quantified on the supernatants of all 5 cell lines (WT, A7, C8, B5 and G4) using an ELISA assay. Cells were seeded in serum-free medium for 24h hours prior to any treatments. Treatments were carried out for 24h before collecting supernatants. sTREM2 protein quantification was performed using a standard curve, which was made using recombinant human TREM2 protein. Results represent mean ± SD of three independent experiments (n=3), results are compared to the WT cells response for each treatment. Statistical differences were calculated by 2-way ANOVA with Dunnett's correction for multiple comparisons, ****p<0.0001.

sTREM2 function remains largely unknown but its shedding has been studied as a possible disease marker for AD (Henjum et al., 2016, Piccio et al., 2016). In human, its concentration in the CSF can be quantified by different methods, and for our experiment it was quantified in the supernatants of each cell line. Much to our surprise, the condition in which sTREM2 was released in higher amounts was 10% FBS or 10% FBS + LPS. This is an interesting finding since previous RT-qPCR *Trem2* quantification has shown that 10% FBS or 10% FBS + LPS treatments greatly reduce *Trem2* mRNA expression (Figure 4.1). These results imply that when exposed to a culture medium that contains 10% FBS, microglial cells not only have a reduced *Trem2* mRNA expression but also release a high amount of sTREM2. These two simultaneous events would mean that TREM2 is depleted on microglial cells cultured in serum-containing conditions.

In contrast, cells grown in serum-free conditions not only have a higher expression of Trem2 mRNA (as seen in Figure 4.1) but also shed very little sTREM2 into their supernatants (as seen in Figure 4.4), which may lead to an accumulation of the protein both intracellularly and on the cell membrane.

Analogous to the results obtained in the mRNA and Western blot experiments, CRISPR/Cas9 clones A7 and C8 (both *Trem2* +/-) showed reduced secretion of the sTREM2 protein. Meanwhile, clones B5 and G4 (both *Trem2* -/-) show negligible levels of sTREM2 which are at the limit of detection (~5ng/mL) of the ELISA assay, further confirming the effect of the *Trem2* gene knockout. It is worth mentioning again, that identification of sTREM2 in *Trem2* -/- clones can be the result of the detection of truncated protein products by the detection antibody AF1729.

4.3.1.2.3 Immunofluorescence: TREM2 accumulation in the cytoplasm.

It has been shown that TREM2 accumulates inside the Golgi apparatus in the cytoplasm (Sessa et al., 2004, Prada et al., 2006). Therefore, accumulation of the TREM2 protein inside BV2 cells was investigated as means to study any possible defects in TREM2 transport in clones A7 and C8. Expression and accumulation of the TREM2 protein (if any) was also studied on the B5 and G4 clones. It also worth mentioning at this point, that evaluation of the morphology of the *Trem2* deficient clones found no major differences compared to the WT cells, at the macroscopic level. In general, *Trem2* deficient cell lines seemed more round (which can be associated with immune activation) and less ramified regardless of the growth medium (serum-free or serum containing) and timepoint. Additionally, *Trem2* deficient cell lines seemed to be more complex (cytoplasm seem to be full of “granules”) intracellularly (see Supplementary Fig 7.11).

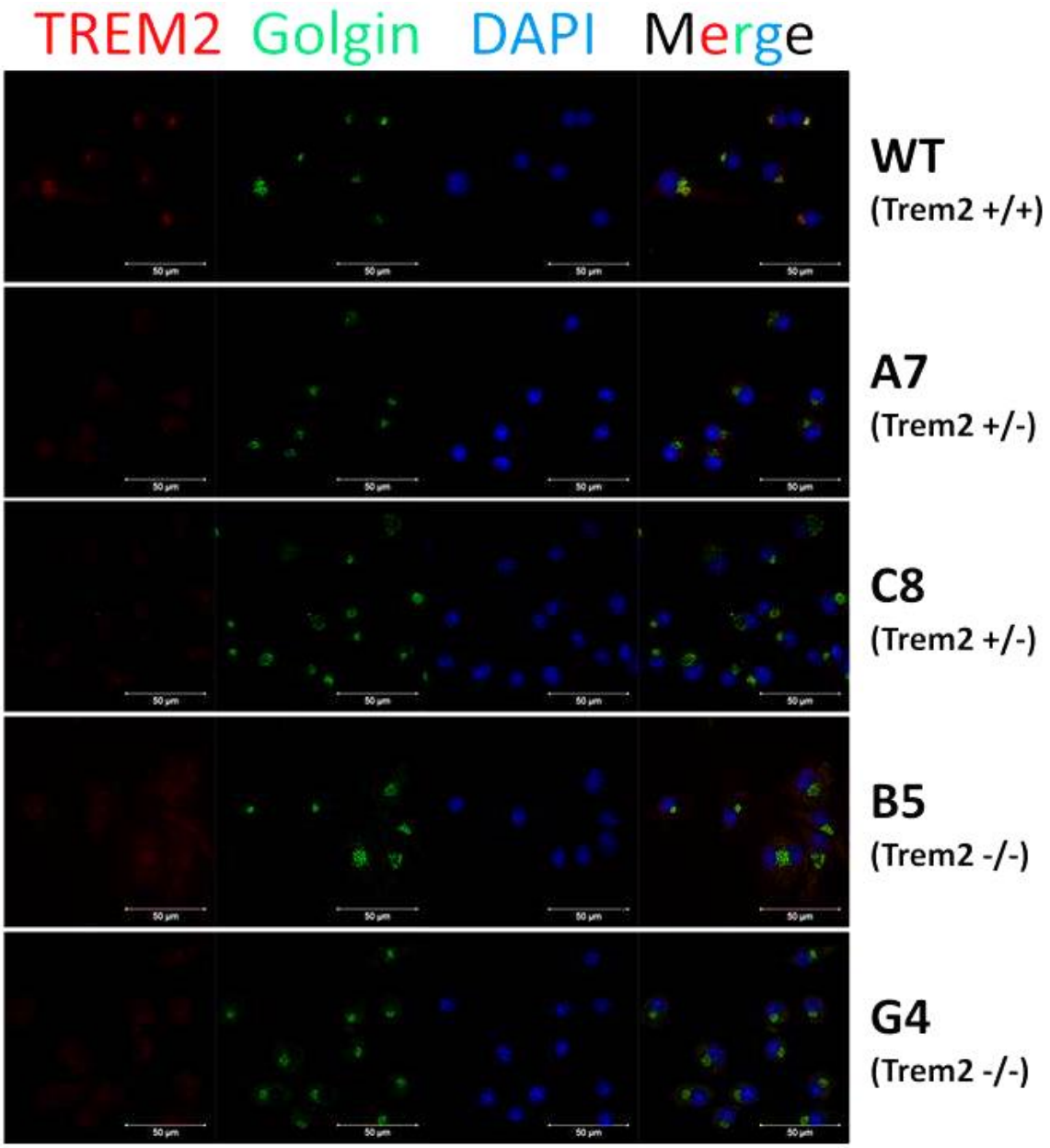

Figure 4.5 TREM2 co-localises with the Golgi apparatus. TREM2 protein expression and accumulation was evaluated in all 5 cell lines (WT, A7, C8, B5 and G4) using immunostaining. Cells were seeded in serum-free medium for 24h hours prior to fixation and staining. Fixed cells were stained for both TREM2 (red) and Golgin (green). Expression and accumulation of *Trem2* correlates very closely to the spatial expression of Golgin on WT BV2 cells, all other cell lines have negligible *Trem2* signal. DAPI (blue) stain the nuclei of cells. Representative images shown were obtained from one of two biological replicate (n=2). Scale bars represent 50µm.

TREM2 has been shown to contain large numbers of N-glycosylation sites and is processed as it passes through the Endoplasmic reticulum (ER) and the Golgi apparatus (where it accumulates) before being trafficked to the cell membrane (Park et al., 2015). As seen in Figure 4.5, TREM2 protein signal very closely overlays with Golgin (a Golgi apparatus associated protein) in the WT cells. This overlay is almost completely vanished in all CRISPR/Cas9 clones, although C8 cells seem to keep some TREM2 in co-localization with Golgin. It is interesting to note clones B5 and G4 (both *Trem2* -/-) have a higher background signal than WT, A7 and C8 cell lines. This is likely due to using

WT negative controls to set the fluorescence thresholds, rather than doing it in a cell by cell line fashion. Nonetheless, it is clear from the image analysis that TREM2 is almost absent in the intracellular space of the CRISPR/Cas9 clones. Another interesting observation is the fact that even on WT cells it is very difficult to identify any TREM2 protein in the cell membrane. Although the staining protocol is specifically optimised to allow staining of intracellular ligands, it should be possible to find some TREM2 receptor staining delimiting the cell's cytoplasm. Although the microscope used in this experiment (Zeiss LSM 880 with AiryScan) is theoretically able to detect single fluorophore molecules and consequently single protein targets; the acquisition set up used in our experiment was not the appropriate for this kind of detection. Nonetheless, the microscope should be able to detect small clusters of TREM2 protein in the cell membrane. However, in this experiment it was not possible to detect TREM2 protein attached to the cellular membrane.

4.3.1.3 ***Functional characterization of Trem2 CRISPR/Cas9 clones***

Once *Trem2* expression was shown to be downregulated or non-existent (both at the mRNA and protein levels) in the *Trem2* CRISPR/Cas9 clones, these newly developed models were used to study the effect of *Trem2* deficiency on BV2 cells. Firstly, functional characterization of the CRISPR/Cas9 models was performed in those cell processes in which TREM2 has been shown to participate: phagocytosis, proliferation, migration, cell activation and cytokine release. The expression of microglial activation and *Trem2* related genes in these cells was also characterised by RT-qPCR analysis.

4.3.1.3.1 Effect of *Trem2* deficiency on microglial phagocytosis

Many studies have shown that TREM2 controls phagocytosis in both macrophages and microglial cells. To date, the exact mechanism by which TREM2 regulates phagocytosis remains unknown. However, there is evidence that suggests that TREM2 binding to DAP12 triggers the reorganization of ACTIN and phosphorylation of ERK/MAPK, which may in turn mediate the clearance of apoptotic neurons (Fu et al., 2014). Nonetheless, a clear link between TREM2 deficiency and decreased phagocytic capacity of microglial cells has been established (Kleinberger et al., 2014a, Sieber et al., 2013, Atagi et al., 2015a, Yeh et al., 2016). As such, the phagocytic capacity of our 4 CRISPR/Cas9 cell lines (A7, C8, B5 and G4) was investigated. To this end, their ability to engulf pHrodo tagged *E. coli* and Zymosan particles was evaluated. The pHrodo dye is a novel, fluorogenic dye which increases its fluorescence as the pH of its surroundings acidifies. Such pH changes can occur inside phagosomes and endosomes. This dye allows to discriminate phagocytosed and endocytosed from adherent and extracellular particles.

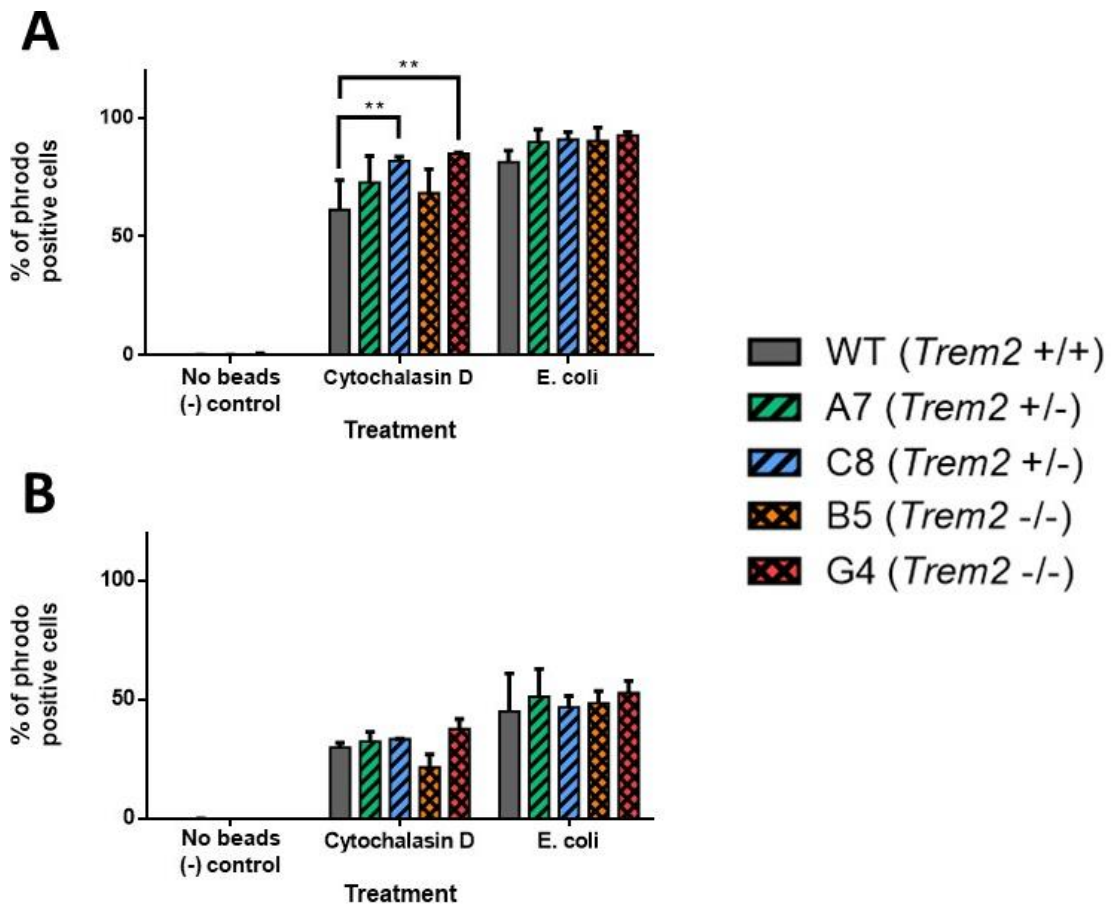

Figure 4.6 Effect of *Trem2* deficiency on the phagocytic capacity of *E. coli* particles by *Trem2* CRISPR/Cas9 clones. The capacity to engulf pHrodo *E. coli* particles by all 5 cell lines (WT, A7, C8, B5 and G4) was evaluated by flow cytometry. Cells were seeded in 1% FBS culture medium at a density of 10 000cells/well in 24-well plates and left to adhere for 24h. Cells were subsequently incubated for 30 min with two different amounts of *E. coli* particles; A) 50µg per 10 000cells and B) 25µg per 10 000cells. In both experiments, Cytochalasin D (10mM) was used as a negative control to inhibit phagocytosis. The No beads (-) control was used to control for autofluorescence changes in each of the cell lines. Results represent mean ± SD of two independent experiments (n=2) for each particle concentration. Statistical differences were calculated by 2-way ANOVA with Dunnett's correction for multiple comparisons, **p<0.01.

As a first approach, the phagocytic capacity of the *Trem2* CRISPR/Cas9 clones was evaluated using *E. coli* particles. Two different amounts of bacterial particles were used: 50µg and 25µg per 10 000 seeded cells. As shown in Figure 4.6, in both experiments with *E. coli* particles, there was no reduction of the phagocytic capacity in the *Trem2* +/- (A7 and C8) or *Trem2* -/- (B5 and G4) clones, clearly contradicting previous reports in the literature for *Trem2* -/- cells (Kleinberger et al., 2014b, N'Diaye et al., 2009a, Atagi et al., 2015b, Xiang et al., 2016b). In fact, there was an upward trend in the phagocytic capacity of all *Trem2* CRISPR/Cas9 clones. This upward trend was maintained even when cells were pre-treated with Cytochalasin D (used as a negative control to inhibit ACTIN-dependent particle uptake), and in the case of the 50µg dose of *E. coli* particles, this trend became statically significant for clones C8 and G4. Further studies will be needed to resolve these increasing trends on the phagocytic capacity of *Trem2* +/- and -/- BV2 cells with what has already been reported in the literature.

An interesting observation is that pre-treatment with Cytochalasin D in our experimental setting had very little effect over the phagocytic capacity of all cell lines, including WT. In a recent publication, Kleinberger et al. (2014a) report a ~50% decrease in phagocytic capacity of *E. coli* particles by primary mouse microglia (cultured in DMEM/F12 medium supplemented with 10% FBS) when treated with Cytochalasin D. In our study, the reduction was ~20% for the 50µg particle dose and ~15% for the 25µg particle dose. Bohlen et al. (2017) have shown that microglial cells grown in serum-free conditions have a reduced phagocytic capacity for different "model" prey particles conjugated with pHrodo. In our particular experimental setting, it was not possible to use serum-free conditions as the cells attached very strongly to the culture plates, reason why the phagocytic experiment was carried out under very-low serum conditions (1%). This reduced phagocytic capacity could be the reason why Cytochalasin D has a limited effect on the phagocytic ability of cells. It could be the case that under very-low serum or serum-free conditions, uptake of *E. coli* particles switches from an ACTIN-dependent mechanism to an ACTIN-independent one (endocytosis). Nonetheless, *E. coli* phagocytosis has been shown to be ACTIN-dependant and can be abolished by Cytochalasin D in a dose dependent manner in bone marrow-derived macrophages cultured in serum-free conditions (Kapellos et al., 2016). To the best of our knowledge, no similar experiment has been attempted in microglial cells (primary or established cell line) to evaluate the effect of Cytochalasin D in serum-free cultures.

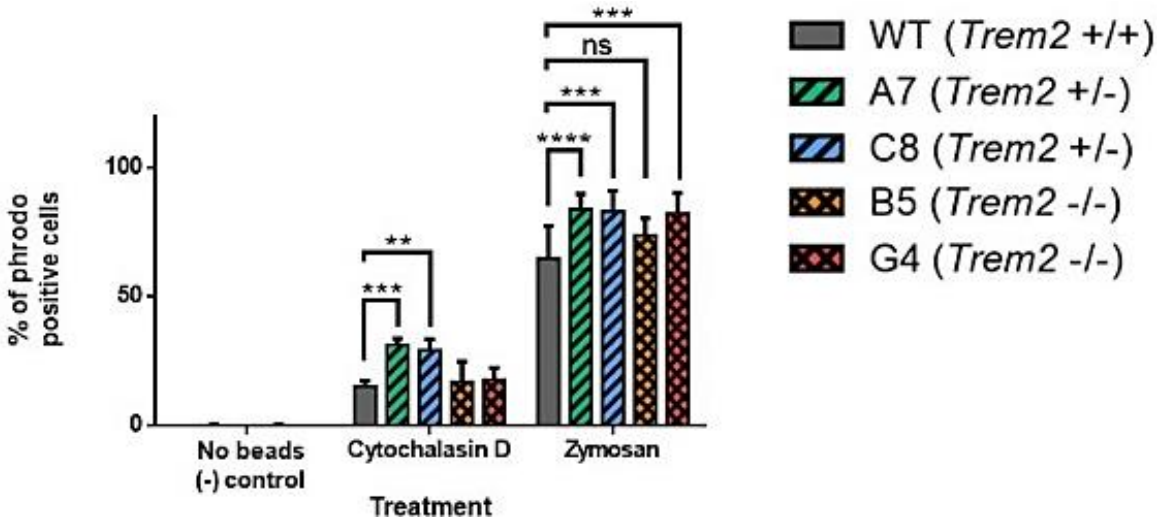

Figure 4.7 Effect of *Trem2* deficiency on the phagocytic capacity of Zymosan particles by *Trem2* CRISPR/Cas9 clones. The capacity to engulf pHrodo Zymosan particles by all 5 cell lines (WT, A7, C8, B5 and G4) was evaluated by flow cytometry. Cells were seeded in 1% FBS culture medium at a density of 10,000cells/well in 24-well plates and left to adhere for 24h. Cells were subsequently incubated for 30 min with 25µg Zymosan particles per 10,000cells. Cytochalasin D (10mM) was used as a negative control to inhibit phagocytosis. The No beads (-) control was used to control for autofluorescence changes in each of the cell lines. Results represent mean ± SD of 4 independent experiments (n=4). Statistical differences were calculated by 2-way ANOVA with Dunnett's correction for multiple comparisons, **p<0.01, ***p<0.001, ****p<0.0001, ns=non-statistically significant.

The capacity to phagocyte Zymosan particles in our CRISPR/Cas9 clones was evaluated by flow cytometry and compared to WT BV2 cells. As shown in Figure 4.7, CRISPR/Cas9 clones (either *Trem2* +/- or -/-) show an increased phagocytic capacity of Zymosan particles. The increase is statistically significant for clones A7, C8 and G4. In these three clones, the increase was of ~18% (~83% of pHrodo positive cells) compared to WT cells (65% of pHrodo positive cells). Clone B5 also shows an upward trend in its phagocytic capacity; nonetheless it is not statistically significant. The increase in this cell line is only ~8% (73% of pHrodo positive cells) compared to WT cells (65% of pHrodo positive cells). Interestingly, Cytochalasin D phagocytic inhibition of zymosan particles was more pronounced than what was previously seen for *E. coli* particles. Addition of Cytochalasin D reduces the percentage of pHrodo positive WT cells from ~65% to ~15%, but it does not abolish phagocytosis completely. Remarkably, Bohlen et al. (2017) showed that primary microglia grown in serum-free conditions engulfed almost no zymosan particles in comparison with cells cultured with serum, which was not the case in our experimental set up, where BV2 cells readily engulfed zymosan in an ACTIN-dependent (and independent) manner.

The increase in the phagocytic capacity of CRISPR/Cas9 clones was noticeable even when the phagocytosis inhibitor Cytochalasin D was used. Clones A7 and C8 showed a statistically significant higher capacity to engulf zymosan particles when cells were pre-treated with the inhibitor, while clones B5 and G4 show a modest increasing trend.

Our results of the phagocytic capacity of the *Trem2* CRISPR/Cas9 clones indicate a modest and sometimes statistically significant increase in the ability to engulf *E. coli* and Zymosan particles. *E. coli* phagocytosis studies have shown that there is an upward trend in phagocytic capacity of CRISPR/Cas9 clones that became statistically significant only when using the phagocytosis inhibitor Cytochalasin D. Zymosan phagocytosis experiments showed the same upward trend in the phagocytic capacity of the *Trem2* CRISPR/Cas9 clones. Differences with respect to the unmodified BV2 cells were significant for clones A7, C8 and G4, while clone B5 only showed a modest non-statistically significant increase. The same trend was observed in these cell lines when Cytochalasin D was used, particularly clones A7 and C8 showed an increased phagocytic capacity that was significantly higher than WT cells.

4.3.1.3.2 Effect of *Trem2* deficiency on microglial proliferation

TREM2 has been positively associated with increased cell proliferation (Otero et al., 2012, Otero et al., 2009, Wang et al., 2016b). As such, the proliferative capacity of our 4 CRISPR/Cas9 clones was investigated using two different flow cytometry assays: i)

staining of the KI67 proliferation associated protein and ii) staining with CFSE (Carboxyfluorescein succinimidyl ester). KI67 is a nuclear protein that is associated with cellular proliferation and is present during all active phases of the cell cycle (G1, S, G2, and mitosis), but is absent in resting cells (quiescent, G0) (Darzynkiewicz et al., 2015). Meanwhile, CFSE is a fluorescent cell staining dye which is cell permeable and covalently couples to intracellular molecules (lysine residues and other amine sources). Due to its covalent binding, CFSE can be retained within cells for long periods of time. Originally developed as a cell tracker dye, it can also be used to monitor cell proliferation, due to the progressive halving of CFSE fluorescence within daughter cells following each cell division (Lyons and Parish, 1994). By measuring the rate at which CFSE MFI (Mean Fluorescence intensity) diminishes because of cell doubling, it is possible to estimate the cells' proliferation rates.

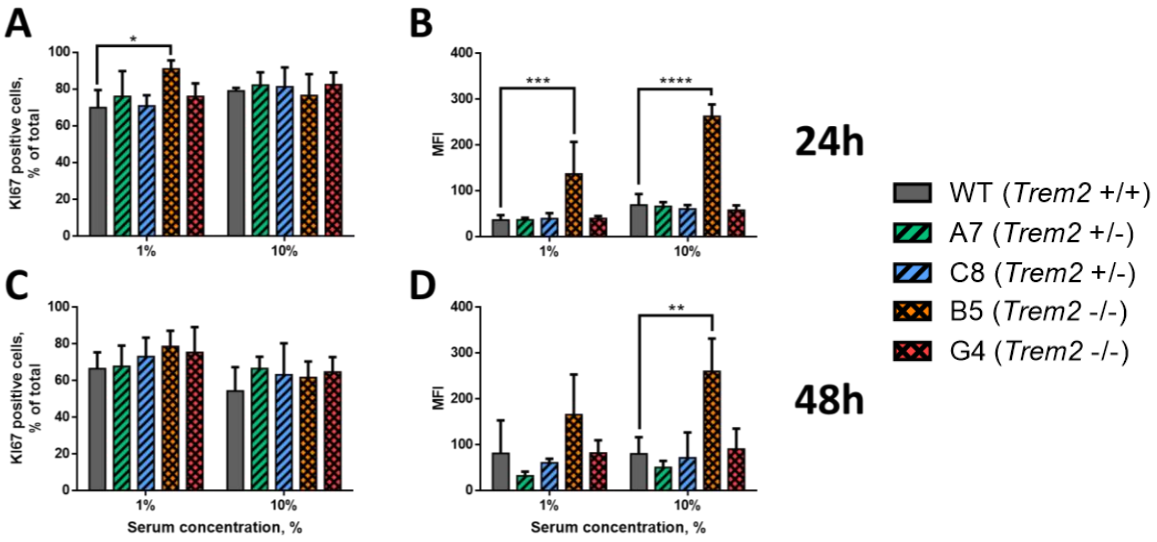

Figure 4.8 Effect of *Trem2* deficiency on the proliferation of BV2 cells - KI67 staining. The effect of *Trem2* deficiency on microglial proliferation was measured using the expression of the cell proliferation marker KI67. Cells were seeded in 1% or 10% FBS culture medium and left to grow for 24h and 48h. Cells were subsequently stained with an anti-KI67 antibody and protein expression levels were assessed by flow cytometry. Panel **A** and **B** show results of percentage of KI67 positive cells and MFI (Mean Fluorescence Intensity) values for cells grown for 24h, respectively. Panels **C** and **D** show the same results for cells incubated for 48h. MFI values were calculated for the entire alive cell population. An isotype control antibody (MACS, Milteny Biotec, Cat# 130-104-611) was used as negative control for KI6 staining. Results represent mean ± SD of three independent experiments (n=3). Statistical differences were calculated by 2-way ANOVA with Dunnett's correction for multiple comparisons, *p<0.05, **p<0.01, ***p<0.001, ****p<0.0001.

For the evaluation of the proliferative capacity of WT BV2 cells and *Trem2* CRISPR/Cas9 clones, the number of cells showing KI67 expression in the nucleus was quantified by flow cytometry. As seen in panel A and C of Figure 4.8, all CRISPR/Cas9 clones show a slightly higher number of KI67 positive cells at 24h and 48h hours. This difference in

the number of KI67 positive cells only reached statistical significance for the B5 clone cultured in 1% FBS at 24h.

MFI is a way to express/quantify the shift in fluorescence intensity of a population of cells in cases where the population of cells expresses different levels of an antigen or marker. This means that while % of KI67 positive cells give us an idea of the number of cells that express this marker, the MFI value tells us about the mean level of expression of the marker (intensity) in this population. MFI values for clones A7, C8 and G4 clones did not show any noticeable trends on the expression of KI67. MFI values of these three CRISPR/Cas9 cell lines remained close to the values of the WT cells. The clone B5 was the only cell line that showed a higher MFI value for the expression of KI67 in both assayed conditions (1% or 10% serum) and timepoints (24h and 48h) when compared to WT cells. Measurement of both parameters (% of KI67 positive cells and MFI) indicate that B5 cells have an increased proliferation rate compared to WT BV2 cells. All other cell lines have proliferation rates similar to that of WT cells.

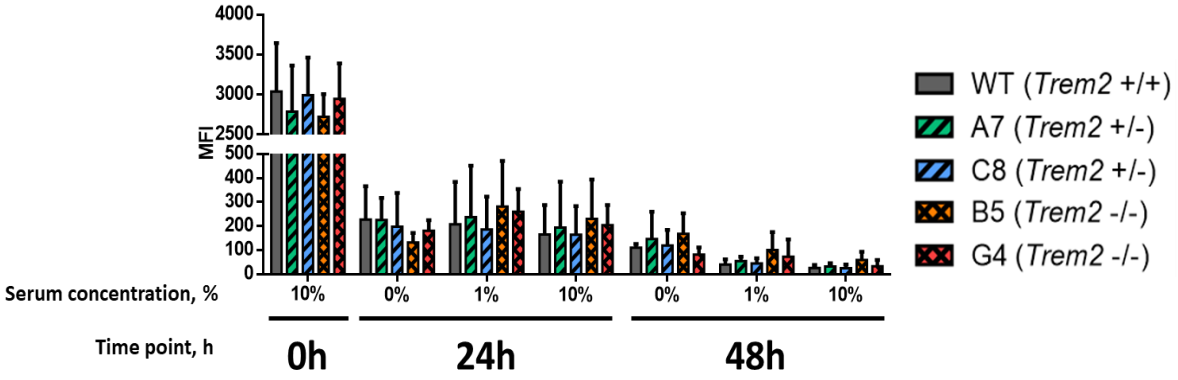

Figure 4.9 Effect of *Trem2* deficiency on BV2 cell proliferation - CFSE staining. The effect of *Trem2* deficiency on microglial proliferation was studied by measuring the changes on the MFI of CFSE staining by flow cytometry. Firstly, cells were stained with the CFSE marker (0h) and subsequently cultured in 0%, 1% or 10% FBS culture medium at a density of 632 000cells per 75cm2 flask. All cell lines were left to grow for 24h and 48h. CFSE staining was measured by flow cytometry at each timepoint. MFI values were calculated for the entire alive cell population and values were compared to the WT group for each condition. Results represent mean ± SD of three independent experiments (n=3). Statistical differences were calculated by 2-way ANOVA with Dunnett's correction for multiple comparisons, no statistically significant differences were found.

As a second approach for the assessment of the proliferative capacity of the *Trem2* CRISPR/Cas9 clones, changes in the MFI values of cells stained with CFSE were monitored and evaluated. Figure 4.9 shows the analysis and comparison of MFI of all CRISPR/Cas9 clones with respect to WT BV2 cells. In this experiment, it was not possible to detect any differences or trends between the *Trem2* CRISPR/Cas9 clones and the WT cell line in any of the tested conditions. These results suggest that doubling

times in WT and all *Trem2* CRISPR/Cas9 clones are similar in each of the tested conditions. Nonetheless, there were some expected differences in doubling speed according to the serum concentration used in the cell growth medium. In general, cells grown in 1% and 10% serum-containing medium seem to have lower MFI values than those cells grown in serum-free conditions (0% FBS). This difference is more noticeable in the 48h group.

Cell proliferation studies carried out on the *Trem2* CRISPR/Cas9 clones showed little or no evidence of differences in the proliferation capacity of the mutated cell lines. Overall, KI67 staining showed no differences in the percentage of KI67 expressing cell (panels A and C, Figure 4.8), while MFI values showed a higher expression of KI67 in the nuclei of B5 cells (panels B and D, Figure 4.8). Similarly, CFSE staining showed no differences in the doubling proliferation capacity of the *Trem2* CRISPR/Cas9 clones (Figure 4.9). Both studies, suggest that there are no differences in the proliferation capacity of *Trem2* deficient BV2 cells with respect to WT BV2 cells.

4.3.1.3.3 Effect of *Trem2* deficiency on microglial migration

Another cell function that has been linked to *Trem2* is migration. Many studies report that *Trem2* deficiency reduces migration of microglial cell models (Melchior et al., 2010, Mazaheri et al., 2017). Therefore, the migration capacity of the 4 *Trem2* CRISPR/Cas9 clones was evaluated using the Cell Migration/Chemotaxis Assay Kit (PromoKine, Cat# PK-CA577-K906). This system employs a Boyden chamber, where the cells migrate through a semi-permeable membrane in response to stimulatory or inhibitory compounds. The Boyden chamber has three main parts; 1) Top Chamber (where cells are seeded), 2) semi-permeable bottom membrane (through which cells migrate in response to chemoattractant) and 3) bottom chamber (containing the chemoattractant and where cells migrate during the assay).

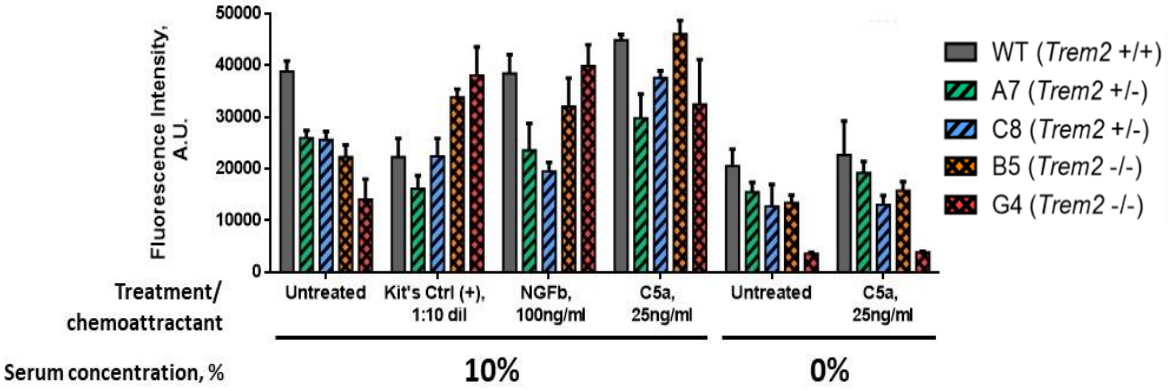

Figure 4.10 Effect of *Trem2* deficiency on BV2 cell migration. The effect of *Trem2* deficiency on microglial migration was studied using a Migration/Chemotaxis Assay Kit (PromoKine, Cat# PK-CA577-K906). The number of migrated cells was evaluated directly by using the kit's cell migration reagent and reading the fluorescence (Ex/Em = 530/590nm) in a plate reader. Cells were seeded in the top chamber in serum free-medium, while the bottom chamber was filled with serum-containing medium (or serum-free medium) plus the indicated chemoattractant. For our test 6 different conditions were assayed; A) untreated (containing serum-containing medium only) B) Kits positive control (1:10 dilution), C) NGFβ (Nerve growth factor-beta, 100ng/mL) and D) C5a (Complement component C5, 25ng/mL), E) Serum-free medium only and F) Serum-free medium plus C5a (25ng/mL). After the experiment, fluorescence intensity results were outside the standard curve's range, reason why raw intensity values are reported (in Arbitrary Units, AU) instead of cell numbers. Higher fluorescence intensities correlate with higher cell numbers in this experiment. Each treated group was compared to the WT group for each condition. Results represent mean ± SD of 3 technical replicates of 1 biological replicate (n=1).

Trem2 deficiency has been linked to a reduced cell migration capacity, as such the migration capacity of the 4 CRISPR/Cas9 was evaluated, particularly their ability to migrate towards chemoattractants such as NGFβ (Nerve growth factor-beta) (De Simone et al., 2007) and C5a (Complement component C5) (Mazaheri et al., 2017). As seen on the left-hand side of Figure 4.10, under untreated conditions (migration from serum-free towards serum-containing medium), BV2 cell migration correlated with the *Trem2* expression of the cells. Wild type cells migrated the most, followed by clones A7 and C8 (both *Trem2* +/-) and finally clones B5 and G4 (both *Trem2* -/-).

The untreated group (either in 10% or serum-free conditions) served as a negative control for the experiment (as recommended by the kit's manufacturer) since no chemoattractant was added into the lower chamber of the plate. Serum-free conditions seemed to reduce basal BV2 migration compared with the 10% condition regardless of the *Trem2* genotype, this difference in the migration capacity deserves to be explored further in the future. Other negative controls could have been used in this experiment. Remarkably, some migration experiments have suggested the use of Cytochalasin D to reduce cell migration. Cytochalasin D inhibits microfilament function and polymerization by blocking the elongation of the actin filament (Schliwa, 1982). Use of Cytochalasin D as in this experiment would have provided limited information about the migration capacity of the cell lines, as it has been shown to severely impair the chemotaxis of many

different cell lines (Glenn et al., 2016). A more informative control in our study would have been the inhibition of SYK activation, since *TREM2* is known to act via phosphorylation and activation of this protein (Paradowska-Gorycka and Jurkowska, 2013). Mazaheri et al. (2017) showed that N9 microglia response to chemoattractants was almost entirely blocked when cells were pre-incubated with a general tyrosine kinase inhibitor (genistein) or a SYK-selective inhibitor (piceatannol). Using a similar experimental paradigm to this study, the authors also showed that *Trem2*-deficient N9 microglia significantly reduced their response to chemotactic stimuli (including C5a and CCL2).

Surprisingly, when cells were stimulated with the kit's positive control (unknown composition) there was an inverse trend to the one seen in the untreated condition. For the kit's positive control, WT, A7 and C8 cells migrated at a similar rate (migration was even reduced when compared to the untreated condition), while B5 and C8 cells migrated noticeably more. It is difficult to speculate about the reason why WT cells did not migrate when stimulated by the Kit's positive control since its composition is not known (it is a proprietary formulation).

Similarly, NGFβ treatment had no effect on WT, A7 and C8 cell migration, when compared to the untreated group (same trends were maintained). WT are expected to have an increased migration in response to NGFβ as reported by De Simone et al. (2007). However, B5 and G4 cells increased their migratory capacity and were able to migrate at a rate similar to WT cells when treated with NGFβ. C5a treatment had a more complex response in BV2 cells. C5a increased the migratory capacity of all cell types (compared to the untreated condition), nonetheless all *Trem2* CRISPR/Cas9 clones continued to show a reduced migratory capacity compared to WT cells, with the exception of the B5 cells, which migrated at a similar rate to WT cells.

The migration capacity of BV2 cells was also tested in a serum-free system (from serum-free to serum-free) - right hand side of Figure 4.10. Untreated cells (serum-free to serum-free) presented reduced migration compared to the untreated group in 10% medium (serum-free to serum-containing), although showing the same trends. All CRISPR/Cas9 cell lines migrated less than WT and this difference was more noticeable in G4 cells. Stimulation of all 5 cell lines with C5a in serum-free medium had a similar effect to the untreated serum-free condition. Migration was marginally increased in the CRISPR/Cas9 cell lines exposed to C5a, although all cells kept the same trend seen in the untreated condition. G4 cells were the cells whose migration/invasion capacity was most seriously impaired by the lack of serum and/or chemoattractant (C5a).

The preliminary study of the migration capacity of the *Trem2* CRISPR/Cas9 clones (only 1 repetition was carried out) using the Boyden chamber system has shown some deficiencies in the migration capacity of *Trem2* +/- and *Trem2* -/- clones. CRISPR/Cas9 clones exhibited a reduced migration capacity in almost all conditions assayed, particularly clone G4 seemed to be severely impaired. Nonetheless, some of the treatments restored some functionality to these cells. Particularly, the kit's positive control (unknown composition) and NGFβ promoted cell migration of the CRISPR/Cas9 clones, sometimes surpassing the WT cells (particularly the Kit's control). NGFβ expression has been shown to be induced in BV2 cells exposed to LPS (Li et al., 2013). Interestingly, there seems to be similar responses in the CRISPR/Cas9 clones which share the same genotype (either *Trem2* +/- or -/-), pointing to the *Trem2* deficiency as the primary cause for the impaired responses.

4.3.1.3.4 Effect of *Trem2* deficiency on microglial cytokine release

One of the aims of this thesis is to understand the effect that *Trem2* deficiency has on microglial activation and immune response. Cytokines are small signalling proteins that work as immune-modulators capable of fine-tuning the humoral and cell-based immune responses. They are also capable of modulating the growth, maturation and response of specific cell types. Cytokines are produced by a wide range of cell types including immune cells (such as macrophages and microglia), endothelial cells, fibroblasts and stromal cells. In this section, the effect of *Trem2* deficiency on BV2 cells' cytokine release capacity was evaluated. To this end, BV2 cells were stimulated with LPS, TGFβ or IL4. LPS is a classical immune activator known to stimulate macrophage/microglial M1 activation, while TGFβ and IL4 are known to trigger M2 activation (Gonzalez et al., 2014).

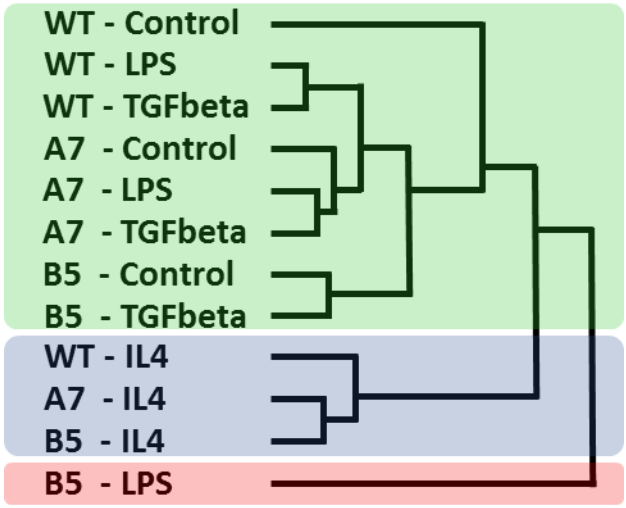

Figure 4.11 WT, A7 (*Trem2* +/-) and B5 (*Trem2* -/-) cell lines' cytokine release responses to different stimuli - Hierarchical clustering analysis. BV2 WT and *Trem2* CRISPR/Cas9 cell lines (A7 and B5) were exposed to different treatments (LPS, IL4 and TGFβ) for 24h. Cytokine release responses were quantified using Proteome Profiler Antibody Arrays (R&D; ARY028). These arrays can analyse up to 111 different cytokines simultaneously. The dendrogram is divided into three coloured zones, showing three sub-clusters; green, blue and red. Metric used, One minus Pearson's correlation; Linkage method, averages.

Figure 4.11 shows the hierarchical clustering of the cytokine release responses by BV2 WT and *Trem2* CRISPR/Cas9 clones. The figure is colour coded in three main zones; Green, Blue and Red. The Green zone is made up mainly of the responses of the three cell lines (WT, A7 and B5) to only three treatments: Control (untreated), LPS and TGFβ. Although this sub-cluster shows higher similarity between the responses between these three treatments, it is also clear that the WT Control condition is markedly different to all other responses in the sub-cluster. Another particularity of this sub-cluster is that LPS and TGFβ responses seem to cluster together for both WT and A7 (*Trem2* +/-) cell lines, which is not the case for B5 cells (*Trem2* -/-).

The Blue sub-cluster in Figure 4.11 is made up of the cytokine release responses of the three cell lines to IL4 stimulation. This shows a consistent and powerful capacity of IL4 to modulate cytokine responses in these cell lines. It also suggests that BV2 cell response to IL4 stimulation is not affected by *Trem2* genotype/expression. The last sub-cluster, Red, is made up of a single cytokine response; B5 LPS. This response is dissimilar to all others and suggests that cytokine release response to LPS stimulation is greatly influenced by the *Trem2* genotype/expression. After comparing the cytokine release responses of each cell line, the behaviour of individual cytokine responses was studied for each treatment.

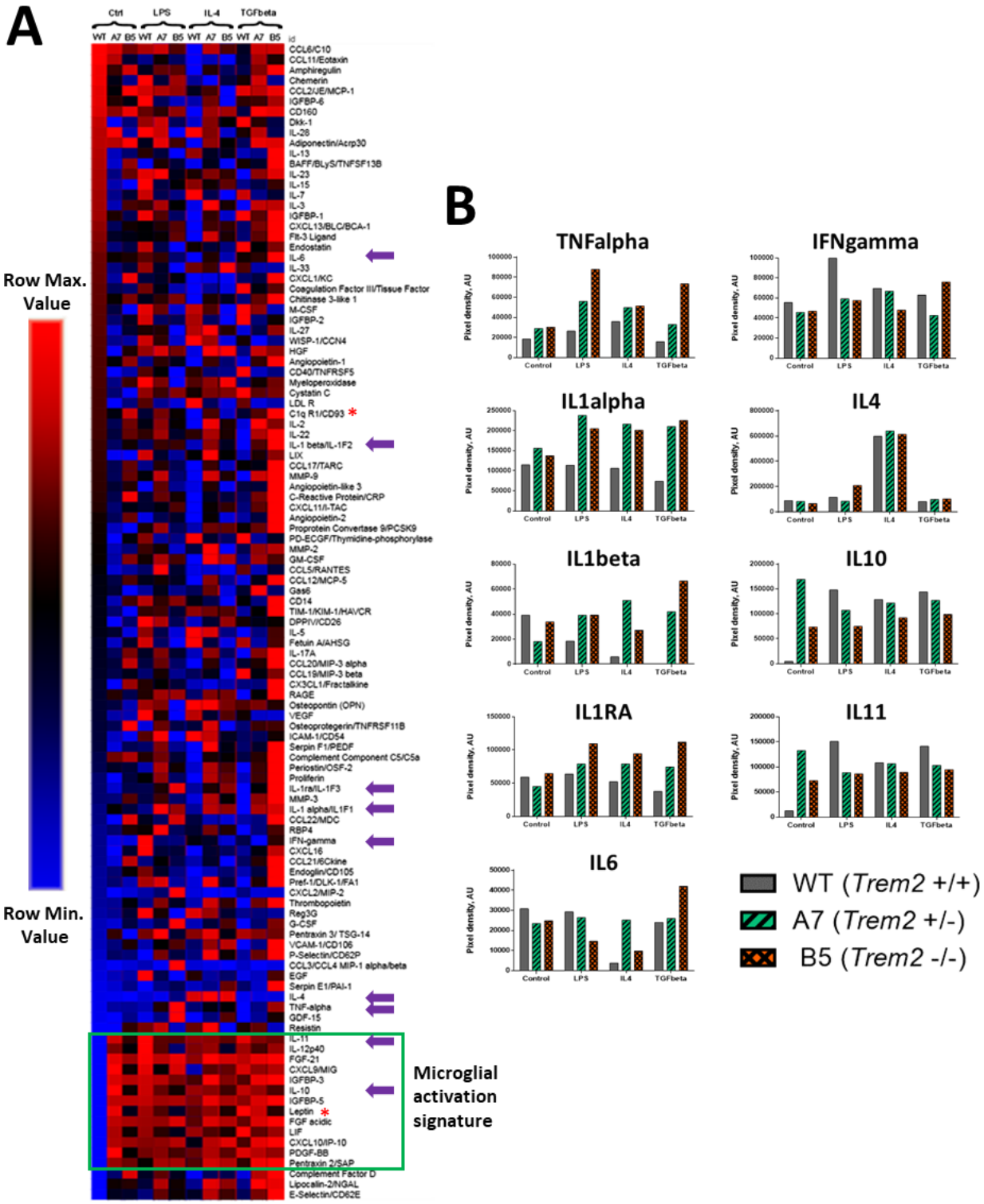

Figure 4.12 Effect of *Trem2* deficiency on BV2 cytokine release. Semi-quantitative cytokine detection was performed using Proteome Profiler Antibody Arrays (R&D; ARY028) for 111 different analytes according to manufacturer's instructions. Only 3 cell lines were used for this experiment; WT, A7 (*Trem2* +/-) and B5 (*Trem2* -/-). Cell lines were grown under serum-free conditions and exposed to 4 different treatments; Control (untreated), LPS, IL4 and TGFβ for 24h. Supernatants from each treatment were collected, spun down and analysed with antibody arrays. **A)** Heat map of the 111 cytokines present in the Proteome Profiler Antibody Arrays. Colour code indicates relative expression compared with the highest and lowest cytokine concentration for each row. Purple arrows mark specific cytokines that are plotted in panel B. Red asterisks indicate cytokines of importance which are plotted on Supplementary Fig. 7.4. Green square in panel A highlights a group of cytokines which are upregulated when the cells become activated (Microglial activation signature). **B)** Individual plots of M1 (TNFα, IL1β, IL1RA and IL6) and M2 (IL4, IL10, IL11) activation state associated cytokines. Results represent mean of a single biological replicate (n=1).

As shown in Figure 4.12, cytokine release responses are markedly different between cell lines (different *Trem2* genotypes) and treatments. In our experiment, each of the cell lines had a distinctive response to the different stimuli employed. Nevertheless, Panel A shows a group of cytokines (marked by a green rectangle) which are upregulated in all conditions and cell lines compared to the untreated WT control condition. These results are similar to those obtained during the hierarchical clustering of the cytokine release responses. In both cases, the cytokine release profile for unstimulated WT cells was markedly dissimilar to all other conditions. WT cell stimulation by any of three stimuli used (LPS, IL4 and TGFβ) increases the release of this group of cytokines (green rectangle), suggesting that these are upregulated by a common microglial cell activation pathway. Consequently, this group of cytokines was named “Microglial activation signature”. Upregulation of these cytokines in the A7 and B5 cell lines under unstimulated conditions implies that these cell lines are already activated even when left untreated, which points to a possible role for TREM2 in microglial activation. This signature included the following cytokines; IL11, IL12, FGF-21, CXCL9, IGFBP-3, IL10, IGFBP-5, leptin, FGF acidic, LIF, CXCL10, PDGF-BB and Pentraxin 2. Further studies on the expression of these cytokines during microglial activation (discussed in the next chapter) will need to be carried out to validate their significance in the context of microglial activation.

As observed in Figure 4.12 panel A, it is difficult to identify differences in cytokine release responses, when they are all assessed at the same time. Nonetheless, when individual cytokine release responses are observed more closely, trends among conditions become more obvious (Panel B). Figure 4.12 panel B shows the plots for the semi-quantitative evaluation of 9 cytokines associated with M1 (TNFα, IL1α, IL1β, IL1RA and IL6) and M2 (IL4, IL10, IL11) activation states. These same cytokines are marked by purple arrows in Panel A. One of the most striking results for this experiment is the effect of the *Trem2* genotype on TNFα release. As shown in Figure 4.12 panel B, all cell lines have similar levels of this cytokine under unstimulated (control) conditions, but its concentration increases upon LPS stimulation. WT cells marginally increase the level of TNFα after 24h of LPS stimulation, while A7 cells (*Trem2* +/-) increases TNFα levels 3-fold and B5 cells (*Trem2* -/-) by more than 4-fold. The release of TNFα by BV2 cells in response to LPS stimulation (classic M1 activator) seems to be inversely correlated to *Trem2* gene dose in the cells. IL4 stimulation has a more moderate effect on TNFα secretion; nevertheless, concentration of the cytokine seems to be higher in the CRISPR/Cas9 clones. TGFβ stimulation shows a similar trend to the LPS stimulation on the three CRISPR/Cas9 cell lines, supporting the correlation between TNFα release and *Trem2* genotype.

Release of IL1α, IL1β and IL1RA is associated with M1 activation (reviewed by Jay et al. (2017)). As seen in Figure 4.12 panel B, release of these cytokines is modulated not only by the treatment used but by the *Trem2* genotype as well. Results show upregulation of these cytokines in *Trem2* deficient cells under untreated conditions and in response to activating stimuli. Of particular interest are IL1α and IL1β, which has been linked to AD (Shaftel et al., 2008). IL6 is also linked to M1 activation. Proteome array analysis shows that IL6 is released at similar levels when cells are left unstimulated, regardless of their *Trem2* genotype. Upon LPS stimulation, A7 and B5 cells show a reduced level of IL6 compared to WT cells. On the other hand, TGFβ stimulation only upregulates IL6 secretion on A7 and B5 cells. Surprisingly, IL4 stimulation of cells reduces IL6 levels in both WT and B5 but not in A7 cells.

Release of M2 associated cytokines (IL4, IL10 and IL11) was also disrupted by *Trem2* deficiency in our experiment. As seen in Figure 4.12 panel B, IL4 secretion is similar between WT and CRISPR/Cas9 clones when cells are unstimulated. Meanwhile, LPS stimulation increased IL4 release in WT and B5 cells; this effect is more pronounced in the latter. Detection of high levels of IL4 in the IL4 stimulated condition is probably caused by the recognition of the same IL4 used to stimulate cells, or it could also be a product of the cytokine's own feedback loop. TGFβ stimulation does not seem to affect the expression of this cytokine. IL10 release was also disrupted by *Trem2* deficiency in our experiment. WT cells under untreated conditions show a very low level of this cytokine, compared to A7 and B5 cells. In all other conditions, WT cells release more IL10 than A7 and B5 cells; the latter showed the lowest levels of IL10 release for all conditions. IL11 shows similar responses to IL10 in all conditions, although differences between A7 and B5 responses are less marked.

IFNγ is a cytokine critical for innate and adaptive immunity. This cytokine is a major activator of macrophages and inducer of Class II major histocompatibility complex (MHC) expression. In our experiment, its expression/release was kept at almost a constant level for all conditions and cell types. This cytokine was only elevated in the LPS-treated WT cells, which almost doubled the secretion of this cytokine. Being that this cytokine was not upregulated by the LPS treatment in A7 and B5 cells, it could be said *Trem2* deficient cells have a less potent response to LPS stimulation.

The Proteome Profiler Antibody arrays also allowed to study the behaviours of cytokines which are not directly related to the M1 and M2 activation states. These cytokines are marked with red asterisks on Figure 4.12 panel A, and their plots can be found in Supplementary figure 7.4. Given that GWAS studies have found associations between

components of the complement system (such as CR1 and CLU) and AD, our experiment also tried to identify any evidence of disruption of this system. Nonetheless, the cytokine array used in this experiment can detect only three cytokines which are members of the complement system: C5a, Complement factor D and C1qR1.

C5a is a highly inflammatory cytokine able to activate the complement system, promote the formation of the Membrane Attack complex (MAC) and attract innate immune cells. In our experiment, release of C5a was upregulated in the two *Trem2* CRISPR/Cas9 clones in almost all conditions when compared to the WT control condition. Particularly interesting are the responses seen in IL4 and TGF treatments. IL4 treatment reduced the secretion of C5a in WT cells, while A7 and B5 cells showed no reduction on this cytokine's levels. TGFβ treatment, on the other hand, did not reduce the C5a levels in WT cells, but rather increased its release in A7 and B5 cells. Likewise, release of Complement Factor D was very similar to C5a's release. Once more, *Trem2* deficient clones showed higher release of this cytokine, with LPS and TGFβ conditions being the conditions that showed the highest releases. C1qR1 (CD93) was the third member of the complement system found in the arrays. This cytokine was once thought to be a receptor for C1q, but now is known to be involved in intercellular adhesion and apoptotic cell clearance. This cytokine is also elevated in *Trem2* deficient clones, when compared to the WT cells, and behaves similarly to C5a and Complement Factor D. Taken together these results reveal a disruption of the complement system, particularly upregulation of the complement associated cytokines C5a, Complement factor D and C1qR1.

Supplementary Figure 7.4 also shows the cytokine release profile of Leptin, a protein known to be involved in bone mass regulation (Ducy et al., 2000) and cognitive changes in AD (Lieb et al., 2009). Release of this cytokine is increased in the *Trem2* CRISPR/Cas9 clones under control conditions. The increase in Leptin release under unstimulated conditions is markedly higher for the A7 (*Trem2* +/-) cells. Stimulation of WT cells with LPS, lL4 or TGFβ increases leptin's release. This increase in leptin release is impaired by *Trem2* deficiency, with A7 showing a slightly lower release compared to WT cells. B5 cells on the other hand show a much lower release of Leptin in response to the three treatments when compared to A7 and WT cells.

The analysis of the effect of *Trem2* in the cytokine release capacity of BV2 cells clearly shows that *Trem2* deficiency disrupts the cytokine secretion/production of these cells under unstimulated conditions and in response to different stimuli such as LPS, IL4 and TGFβ. Furthermore, hierarchical clustering analysis of the responses showed that LPS stimulation of B5 cells is markedly different to all other conditions assayed and evaluated

with the cytokines arrays. This was partly corroborated by semi-quantitative analysis of individual cytokines associated with M1 and M2 activation states and the complement system. Additionally, the use of the cytokine arrays allowed the identification of a group of cytokines whose release is upregulated upon BV2 cell activation either by classic M1 (LPS) or M2 (IL4 or TGFβ) activators. This group of cytokines was named Microglial activation signature. Further studies will have to be carried out to verify these results as they are a product of a single biological replicate (n=1).

4.3.1.3.5 Effect of *Trem2* deficiency on mRNA expression of microglia associated genes

It is well known that microglial and macrophage acute pro-inflammatory activation, both *in vivo* and *in vitro*, results in the sharp decline in expression of *Trem2* mRNA expression (reviewed by Yeh et al. (2017)). As such, this section investigates the effect that *Trem2* deficiency (either *Trem2* -/- or +/-) has in the mRNA expression of different inflammation associated genes (TNFα and CD40). At the same time, this section examines the effect that *Trem2* deficiency could have in other microglial genes associated with AD risk (*ApoE* and *CD33*) and in the mRNA expression of proteins that have been shown to directly interact with the TREM2 protein (*Dap12* and *Plxna1*).

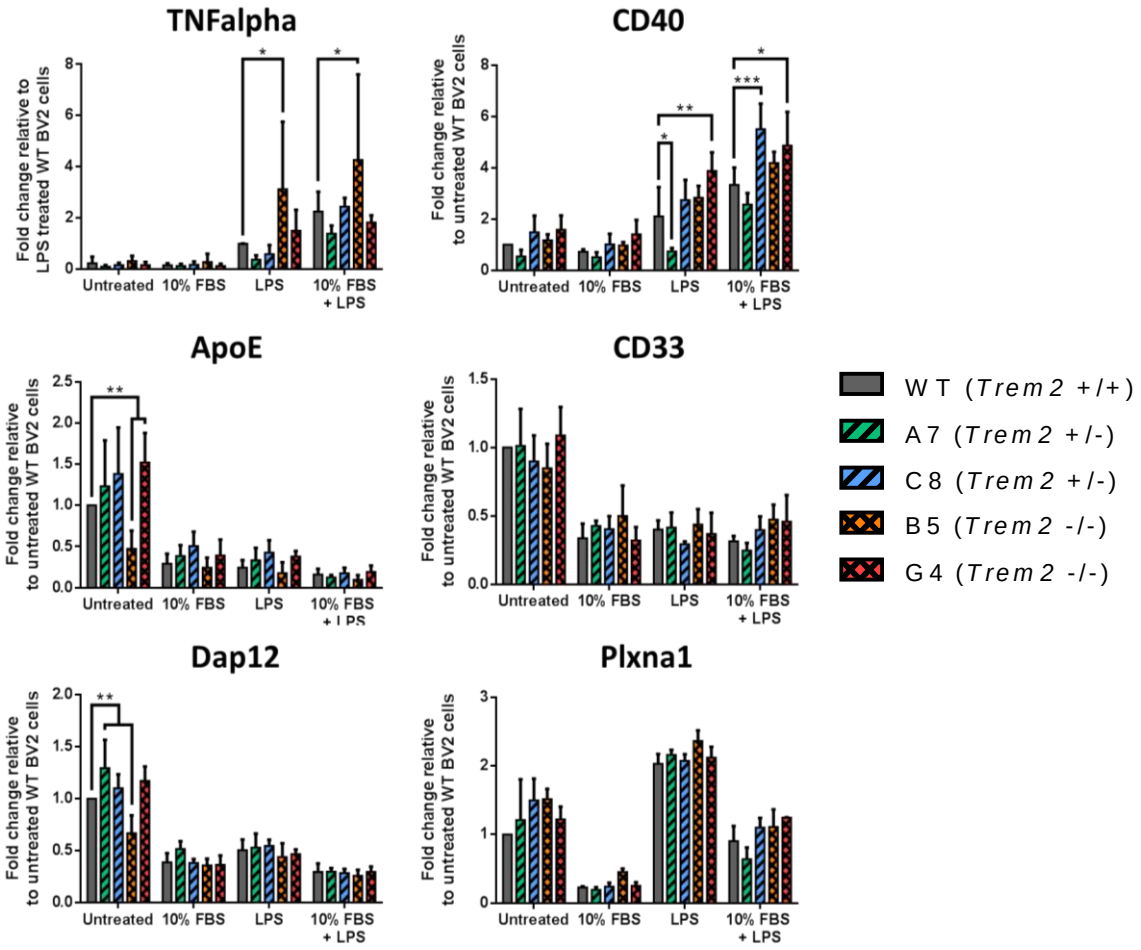

Figure 4.13 Effect of *Trem2* deficiency on the mRNA expression of microglial genes. Cell lines (WT, A7, C8, B5 and G4) were seeded in serum-free medium for 24h hours prior to treatment. Subsequently, cells were left untreated or stimulated with LPS 1µg/mL, 10% FBS or a combination of both. After 24h of treatment cells were lysed and mRNA expression profiles were obtained by RT-qPCR. mRNA expression was normalised to *Gapdh* (or *Tbp*) expression and results are shown relative to untreated (serum-free) WT BV2 cells, except in the case of *TNFα*, where results are normalised to LPS-treated WT cells. Results represent mean ± SD of five independent experiments (n=5). Statistical differences were calculated by 2-way ANOVA with Dunnett's correction for multiple comparisons, *p<0.05, **p<0.01, ***p<0.001.

Figure 4.13 shows the mRNA expression profiles of 6 genes of interest expressed by microglial cells: *Tnfα, Cd40, ApoE, Cd33, Dap12* and *Plxna1*. *Tnfα* and *Cd40* are two genes whose expression is upregulated during M1 activation (Martinez and Gordon, 2014, Becker et al., 2012). Consequently, upregulation of both mRNAs was expected in cells treated with LPS treated. Certainly, there was an increase in the TNFα mRNA levels in WT cells treated with LPS compared to WT untreated cells (almost 3-fold). This upregulation was more modest in the case of A7 and C8 cells (*Trem2* +/-) when compared to their unstimulated counterparts. A7 and C8 cells did not managed to upregulate the expression of TNFα to the same level that WT cells and in fact looked downregulated in comparison. B5 and G4 cell lines (*Trem2* -/-), on the other hand, showed a greater upregulation of TNFα both compared to their unstimulated counterparts and to the LPS treated WT cells, reaching statistical significance only for

the B5 cell line. A similar expression profile was observed when the LPS treatment was combined with the 10% FBS condition. The combination of both conditions increased the expression, although marginally, in all cell lines, suggesting that cells grown in 10% FBS are primed for the upregulation of TNFα.

As expected, WT cells stimulated with LPS alone or in combination with 10% FBS show upregulation of *CD40* mRNA. Increased expression of CD40 is associated with increased microglial activation (Ponomarev et al., 2006), and as seen in the next chapter, it was highly upregulated by LPS in our microarray experiment (Table 5-4). Surprisingly, A7 cells did not upregulate the expression of this gene under LPS stimulation alone, but only in combination with 10% FBS. In contrast, C8, B5 and G4 cell lines show a non-significant upregulation of *CD40* mRNA in all conditions assayed, including the unstimulated condition. Upregulation of *CD40* mRNA by the LPS treatment is statistically higher in G4 cells (*Trem2* -/-) compared to LPS treated WT cells. Similarly, *CD40* upregulation was statistically higher for C8 and G4 cells under LPS plus 10% FBS conditions compared to WT cells under the same conditions. These results show a clear tendency of the CRISPR/Cas9 clones, except for A7 cells, to upregulate the expression of CD40 in all conditions assayed.

Although much of the current research on the role of microglia in the initiation/progression of AD is centred on *Trem2*, microglial cells are also capable of expressing other AD-related genes; two of these are *ApoE* and *CD33*. Under unstimulated conditions, expression of *ApoE* by BV2 cells showed very heterogeneous results. Clones A7 and C8 (*Trem2* +/-) showed *ApoE* expression levels similar to unstimulated WT cells, whereas clones B5 and G4 (*Trem2* -/-) showed statistically significant up- and down-regulation of *ApoE* expression, respectively. All treatments reduced the expression of *ApoE* to less than 50% of the untreated WT cell expression, in all cell lines, although maintaining the same trends seen in the untreated condition. Expression of *CD33* was not affected by the *Trem2* genotype in any of the conditions assayed and *Trem2* CRISPR/Cas9 clones responded to the treatments similarly to WT cells.

Even though there are no defined pathways in which *Trem2* is involved, there is evidence of its interaction with other proteins, namely Dap12 (reviewed by Yeh et al. (2017)) and Plxna1 (Hayashi et al., 2012). Therefore, the effect of *Trem2* deficiency on the mRNA expression of both genes was assessed. Expression of *Dap12* under untreated conditions was significantly upregulated in A7 cells (*Trem2* +/-) and significantly downregulated in B5 cells (*Trem2* -/-). C8 and G4 clones had *Dap12* mRNA

expression levels comparable to the untreated WT cells. All assayed treatments reduced the mRNA expression of *Dap12* by 50% or more. Expression of *Dap12* in *Trem2* CRISPR/Cas9 clones and WT cells was similar for all treatments. *Plxna1* expression was not affected by the *Trem2* genotype of the cell lines. Nonetheless, under untreated conditions CRISPR/Cas9 clones seemed to have a slightly upregulated expression of the gene, which was not statistically significant. Expression of *Plxna1* was markedly downregulated (to less than 30% of the untreated WT expression) by 10% FBS, while LPS treatment upregulated its expression by more than 2-fold. The combination of both treatments brought *Plxna1* mRNA expression to an intermediate level which was similar to the expression of the gene under untreated conditions.

Analysis of the effect of *Trem2* deficiency on the expression of *TNFα, CD40, ApoE, CD33, Dap12* and *Plxna1* has shown some unexpected results. In the case of *TNFα, Trem2* deficiency does not seem to affect its expression. *TNFα* mRNA was only affected (upregulated) when B5 cells (*Trem2 -/-*) were treated with LPS alone or in combination with 10% FBS. On the other hand, *CD40* mRNA expression was affected by the *Trem2* genotype of cells. Upon LPS stimulation, A7 cells (*Trem2 +/-*) were not able to upregulate *CD40* expression, whereas C8 and B5 cells (*Trem2 +/-* and *Trem2 -/-* respectively) had a response that was similar to WT cells. Meanwhile, G4 cells (*Trem2 -/-*) showed a statistically significant upregulation of *TNFα*. Stimulation with both LPS and 10% FBS, showed a statistically significant upregulation of *TNFα* in both C8 and G4 cells.

ApoE, CD33, Dap12 and *Plxna1* were not overly affected by the *Trem2* deficiency. Just in the case of *ApoE* and *Dap12* mRNA expression was affected and only under basal (untreated) conditions. These results suggest that *Trem2* deficiency does not affect the expression of AD related genes or genes that have been shown to directly interact with it, but rather affects genes involved in microglial activation such as *TNFα* and *CD40*.

4.4 **Discussion**

The recent explosion of genetic data which implicate microglia as a crucial cell type and *TREM2* as a critical gene in AD, has led to a renewed interest in the role of *TREM2* in microglial normal function and in response to different stimuli. Important insights into the role of *TREM2* in the modulation of the microglial functions in the CNS come from the study of genetic conditions. Before the association between the *TREM2* R47H mutation and a higher risk of AD was discovered (Guerreiro et al., 2013b, Jonsson et al., 2013), much of our knowledge about *TREM2* function came from studies related to Nasu-Hakola disease. This genetic disease is caused by loss-of-function mutations in *TREM2* and its putative adapter protein DAP12. Patients affected by this disease develop bone

cysts, white matter degeneration and progressive dementia (Paloneva et al., 2002). Given that both *TREM2* and DAP12 are expressed in myeloid cells, it is reasonable to suppose that deficits or aberrations in these genes affect microglia and osteoclasts, which are the myeloid cell types in the brain and bone respectively. While the role of *TREM2* in osteoclast function and bone maintenance has been extensively studied (reviewed by Humphrey and Nakamura (2016)), *TREM2*'s role in microglial cells and in the brain remains a matter of debate (Mazaheri et al., 2017).

Gene Knockout models are a simple yet elegant way to study gene function by observing a biological system that lacks the gene of interest. In the previous chapter, the CRISPR/Cas9 technology was used to gene edit BV2 cells and obtain *Trem2* knockout cell models, with the aim to study its function in a microglial context. The present chapter describes the functional characterization of *Trem2* deficient BV2 cell models; A7, C8 (*Trem2* +/-), B5 and G4 (*Trem2* -/-).

Characterization of the *Trem2* deficient clones was carried out using the 4 CRISPR/Cas9 edited cell lines (A7, C8, B5 and G4) and only one WT control. Many gene editing protocols using CRISPR/Cas9 mediated modification, advise the use of the aggregate parental population and/or other non-edited subclones as phenotypic controls to compare with the edited cell lines (Olive et al., 2018). In our study, the unmodified WT control used was the parental BV2 cell line from which all CRISPR/Cas9 cell lines were derived, an approach used by other studies too (Harrod et al., 2017, Neggers et al., 2015). The rationale for using the parental cell line as phenotypic control for downstream characterization and experimentation was heavily influenced by the fact that singe cell isolation and clonal expansion has been shown to alter the genetic profile of the subcloned cell lines (edited or not). In fact, it has been previously reported that functional heterogeneity can arise within a 'clonal' cellular populations as a result of cell plasticity and/or epigenetic alteration (Kreso et al., 2013). The use of the parental cell line as phenotypic control for characterization of the introduced mutation gives us the opportunity to compare the single cell colonies with an "averaged" population of cells that represents various phenotypes within its population. Whereas the use of a subcloned non-edited WT cell line could introduce artifactual differences when compared with the edited subcloned populations. A solution to this problem will require the use of many subcloned WT and edited cell lines in order to clearly distinguish the phenotype produced by the introduced mutation. This strategy will be more time consuming and expensive.

Remarkably, the BV2 cell line is known to have highly heterogeneous genetic characteristics (i.e. karyotyping analysis of the BV2 WT cells showed that single cells

from the parental population have variable numbers of chromosomes, see Section 2.1). Therefore, single cell colonies derived from this heterogeneous population are likely to have very distinct phenotypes, which can be further exacerbated during single cell isolation and expansion. In a recent paper, Olive et al. (2018) show that in order to generate appropriately matched control cell lines that account for functional and phenotypic heterogeneity seen in certain cell lines (such as BV2 cells), it is necessary to carry out an initial single cell colony isolation on the parental cell line before subjecting the cells to CRISPR/Cas9 modification and downstream characterization. This approach is also time consuming and presents its own caveats as discussed by Olive et al. (2018)

4.4.1 **Characterizing the expression of *Trem2* in the CRISPR/Cas9 modified cell lines**

Firstly, *Trem2* expression was characterised at the mRNA and protein level. As expected, *Trem2* mRNA expression was reduced in the CRISPR/Cas9 clones. Clones A7 and C8, both of which are *Trem2* +/-, conserved just a fraction of the mRNA expression of *Trem2*: 17 and 8% respectively. This result is surprising, as the expected reduction on *Trem2* mRNA expression is of roughly 50% given that these clones still have a normal *Trem2* allele. One possible explanation for this phenomenon is the formation of a negative feedback loop which reduces *Trem2* mRNA expression in these two clones. As commented in the next chapter and by previous studies (Chen et al., 2008, Gawish et al., 2015b), immune cell activation reduces the expression of *Trem2*. Our hypothesis assumes that the *Trem2* deficiency alone is capable of activating microglia, which in turn downregulates *Trem2* expression generating a negative feedback loop that reduces *Trem2* mRNA expression.

Trem2 mRNA expression in B5 and G4 clones was reduced to 1 and 2.8% respectively. *Trem2* mRNA expression in these two clones was expected to be 0%,.It is likely that the detection of mRNA transcripts which contain premature stop codons, created by the CRISPR/Cas9 editing, can explain the low levels of *Trem2* mRNA detected in these clones. Additional mRNA sequencing experiments (or re-analysis of the results obtained in the Chapter 5) will need to be carried out to confirm this hypothesis.

In the same experiment, the effect of 10% FBS, LPS or the combination of both have on *Trem2* expression was investigated. In this study, supplementation of the culture medium with 10% FBS was considered as a treatment, since observations made in our group and others have suggested that addition of serum to the culture medium of BV2 cells can prime cells for immune activation. In a recent study, Wang et al. (2017) showed that supplementation of BV2 culture medium with 10% serum from healthy human donors

can upregulate the protein expression of MHCII, a protein associated with M1 activation, and can elevate secretion TGFβ, an immunoregulatory cytokine. This same study did not show any changes in the secretion of IL1β, TNFα, IL6, INFγ or IL10. Although the results obtained by Wang et al. (2017) were modest, they clearly show immune activation of BV2 cells when serum was added to the cultures medium. FBS could have a similar effect on BV2 cells, but further studies are needed to validate this observations.

To our surprise, supplementation of the culture media with 10% FBS reduced *Trem2* mRNA expression by ~50%, while LPS reduced *Trem2* expression by ~75% on WT cells. The combination of both treatments reduced *Trem2* expression even further (~90%). Addition of FBS to the culture medium is typically used to promote cell survival and proliferation of cells *in vitro*. The reduction of *Trem2* mRNA by FBS supplementation is intriguing since *Trem2* expression is also associated with increased survival and proliferation (Wang et al., 2016a, Cantoni et al., 2015, Wu et al., 2015b). In particular, *Trem2* has been shown to promote cell proliferation and survival in response to CSF-1 (macrophage colony-stimulating factor) *in vitro* (Otero et al., 2012). Similarly, *Trem2* mRNA reduction by LPS treatment is startling since microglia treated with LPS (M1 activated) have been shown to have increased proliferation (Gomes et al., 2013), which is also correlated with *Trem2* expression. Since *Trem2* expression is reduced in cells exposed to 10% FBS, it is reasonable to hypothesize that BV2 cells become activated as a result of their exposure to FBS or any of its components. This activation could potentially cause the reduction of *Trem2* mRNA, analogous to the reduction of *Trem2* mRNA caused by LPS activation of microglia. Finally, expression of *Trem2* in the A7 and C8 cell lines showed the same pattern of reduction when stimulated by FBS, LPS and their combination.

After confirming that *Trem2* mRNA levels were reduced in the CRISPR/Cas9 clones, intracellular TREM2 protein expression was investigated under serum-free conditions. Serum-free conditions were used because in previous experiments it has been shown that cells grown with no FBS have the highest *Trem2* mRNA expression (Figure 4,1). As shown in Figure 4.2, TREM2 protein levels in clones A7 and C8 correlate well with the mRNA expression seen in Figure 4,1. Nevertheless, it was possible to detect small amounts of TREM2 protein in the B5 and G4 clones. Since both clones have the same *Trem2* sequence, a 34bp deletion which disrupts the gene's reading frame and adds premature stop codons to its sequence, it was not possible that *Trem2* was being translated.

Although the detected levels of TREM2 protein are less than 10% in the B5 and G4 clones, this level of expression is considered the result of unspecific binding of the detection antibody used and high background levels in the blots. The anti-TREM2 antibody used (AF1729) is recommended for its use in immunocytochemistry staining, although it can be used for western blot analysis as well. A second reason that may explain the identification of TREM2 protein signal in clones B5 and G4, is the possibility that the detection antibody (AF1729, whose immunogen is the amino acid sequence 19-168 of the TREM2b protein) may be detecting the truncated protein expressed by these clones. Clones B5 and G4 can potentially express a truncated protein (assuming some of the *Trem2* mRNA escapes de NMD degradation) whose sequence would be exactly the same as the wild-type protein up to the 35th amino acid (MGPLHQFLLLLITALSQALNTTVLQGMAGQSLRVS). Immediately after this sequence, the frame shift caused by the CRISPR/Cas9 modification changes the protein sequence of the next 17 amino acids (ARPGVGSWVRRAHASVW) before the first premature stop codon appears. In consequence, clones B5 and G4 could potentially still express a 52 amino acid-truncated TREM2 protein (see Figure 3.3Figure 1.1). Amino acids 19th to 35th of these truncated TREM2 protein could is still be detected by the AF1729 antibody, provided that some of the epitopes lie within this region. Nonetheless, this truncated protein will have a predicted molecular weight of 5.6kDa (calculated using the ExPASy web tool), which was not detected in any of the blots analysed (mouse TREM2 protein has a molecular weight of ~25kDa). Analysis of the mouse TREM2 protein expression with a different anti-TREM2 antibody might reduce the background signal and/or not detect TREM2 proteins in B5 and G4 clones.

Subsequently, the effect of LPS, FBS and their combination on the shedding of sTREM2 was also investigated. The shedding of the soluble fraction of the TREM2 protein is of great interest as it has the potential to be used as a biomarker for AD and other neurodegenerative diseases. In AD patients, sTREM2 levels correlate with tau and phospho-tau in CSF, but not with Aβ1-42 (Henjum et al., 2016, Piccio et al., 2016). Furthermore, CSF levels of sTREM2 have been found to be elevated 5 years prior to disease onset in familial cases of AD (Suarez-Calvet et al., 2016). It has also been suggested that sTREM2 might act as a decoy receptor and that preventing its shedding may increase Trem2 levels on the cell membrane (Kleinberger et al., 2014b). Importantly, BMDMs (bone-marrow-derived macrophages) treated with recombinant sTREM2 showed decreased apoptosis induced by CSF-1 withdrawal. This protective effect of sTREM2 was dose-dependent and was consistent irrespective of *Trem2* and *Dap12* genotype of cells (WT, *Trem2* -/-, or *Dap12* -/-). This effect was shown to be due to

attenuated apoptotic signalling rather than an artefact of cell proliferation. These results point to sTREM2 as having an active role in promoting macrophage survival (Wu et al., 2015a).

In our experiment, sTREM2 levels were most abundant in WT cells, as expected, treated with 10% FBS alone or in combination with LPS. This increase in TREM2 shedding was almost 50-fold higher in the FBS treated conditions compared to the control or LPS conditions. Again, these results are particularly interesting since FBS treatment not only instigated a higher sTREM2 release but also reduced *Trem2* mRNA expression, as seen previously in Figure 4,1. FBS supplementation in microglial cultures both reduced *Trem2* mRNA expression and increased sTREM2 shedding which could potentially deplete microglial cells of TREM2 protein, disrupting any TREM2 associated pathway and impairing their response. More importantly, and considering that most studies investigating the microglial TREM2 function are carried out using cultured cells, the use of FBS in *in vitro* experiments may not be suitable for the study of TREM2 function since it can deplete TREM2 in cultured cells. The mechanisms by which FBS alters *Trem2* expression and shedding need to be further studied.

In vitro studies in human and mouse cell lines have shown that sTREM2 is produced by the cleavage of extracellular domain of TREM2 (Figure 4.3) by ADAM10 (a Disintegrin and Metalloproteinase Domain-containing protein 10) (Wunderlich et al., 2013, Kleinberger et al., 2014b). In BV2 cells, a broad-spectrum ADAM inhibitor has been shown to reduce sTREM2 shedding by ~50%. At the same time, BV2 cells increased their bacterial phagocytosis by ~25%; however, the connection between this two effects was not clearly established (Kleinberger et al., 2014b). The use of this inhibitor for the study of sTREM2 shedding in response to LPS and FBS will add great value to future studies using our same experimental paradigm and will shed some light about the mechanisms involved. Shedding of sTREM2 by the CRISPR/Cas9 clones followed the same response pattern seen in the WT cells. Unexpectedly, low levels of sTREM2 were detected in the supernatants of B5 and G4 cells treated with FBS and LPS together. Although, detection of these responses was very close to the detection limit of the ELISA assay used for quantification (~5µg/mL), it does not rule out the possibility that the assay may have been detecting an unspecific product in the supernatants of these two cell lines. As in the case of the western blot analysis, detection of sTREM2 in the B5 and G4 clones can also be the result of the detection of truncated TREM2 protein products in these clones. Future studies may require the use of more specific detection techniques such as Mass-spectrometry, which has been successfully used on CSF studies (Heslegrave et al., 2016).

Next, the intracellular accumulation of the TREM2 protein in BV2 cells was investigated by antibody staining and confocal microscopy. Although it is possible to detect some cell surface expression of TREM2, most TREM2 protein is stored in intracellular pools that can be rapidly translocated to the cell surface. Previous reports have shown that in microglial cells TREM2 is stored intracellularly in two distinct pools: the Golgi complex (which seems mostly a storage pool) and cytoplasmic vesicles (distinct from endosomes and lysosomes and able to exocytose) (Sessa et al., 2004, Prada et al., 2006). Upon stimulation with Ionomycin (a Ca^{2+} ionophore) microglial cells can rapidly redistribute the intracellular pool, although transiently, to the cell surface (Sessa et al., 2004). In our study, Golgin was used as a marker of the Golgi complex and was found intracellularly superimposed with TREM2 protein accumulations in WT BV2 cells (Figure 4.5). There were no signs of the presence of TREM2 on the cytoplasmic membrane. The methanol fixation method used for this experiment is known to be harsh and is not recommended for the detection of membrane bound antigens; nonetheless, it was not possible to spot any signs of membrane accumulation of TREM2 in any of the samples analysed. Maybe the use of Ionomycin and a different cell fixation method will be necessary to identify membrane-bound TREM2 in future studies. CRISPR/Cas9 clones on the other hand, showed expression of the Golgin protein and reduced (A7 and C8) or no expression (B5 and G4) of TREM2 intracellularly, again with no presence of membrane bound protein. This is consistent with other reports that have shown that TREM2 primarily accumulates intracellularly (Varnum et al., 2017). It is worth keeping in mind that to function as cellular receptors and be activated, members of the immunoglobulin and lectin-like superfamily – like TREM2 – must be on the cell surface (Colonna, 2003).

Interestingly, in our study *Trem2* +/- clones (A7 and C8) showed reduced TREM2 presence in the cytoplasm and negligible co-localization with Golgin, while *Trem2* -/- cells (B5 and G4) had the highest background signal for TREM2 intracellularly. In these cells, the weak TREM2 signal marginally co-localised with Golgin and was present in the cells' cytoplasm. TREM2 signals in these clones could be the result of the detection of the truncated protein product of the truncated *Trem2* gene. Since this truncated product may not be shed into the extracellular space, it could accumulate in the cytoplasm, waiting for degradation. This signal could also be caused by the cells' high auto-fluorescence signal, which was also seen during the flow cytometry experiments (phagocytosis and proliferation). This could explain why no TREM2 protein was detected in the western blot analysis of B5 and G4 whole cell lysates (Figure 4.2).

4.4.2 **Functional studies in *Trem2* +/- and *Trem2* -/- BV2 cells**

AD associated mutations in *Trem2* have been shown to inhibit its maturation and transport to the cell membrane as well as reducing its phagocytosis capacity, lipid sensing ability and ApoE binding (Kleinberger et al., 2014a, Sieber et al., 2013, Atagi et al., 2015a, Yeh et al., 2016). Consequently, these mutations suggest a *Trem2* loss of function. This hypothesis is supported by the association of null mutations in TREM2 and DAP12 with the Nasu-Hakola disease. However, the exact mechanisms by which these cellular functions are disrupted remain unknown. The study of the effect of *Trem2* deficiency on microglial cells will surely shed some light into these disrupted mechanisms, and may even open possibilities for therapeutic intervention. The CRISPR/Cas9 modification of the *Trem2* gene in BV2 cells (performed and discussed in the previous chapter) offers the possibility of studying microglial responses in a stable and well characterised system.

Functional characterization of the effects that *Trem2* deficiency on the CRISPR/Cas9 edited cell lines started only after it was established that *Trem2* expression was reduced at the mRNA and protein levels in these cells. Firstly, the effects of *Trem2* deficiency on phagocytosis were studied. To this end, pHrodo tagged *E. coli* and Zymosan particles were used to assess the phagocytic capacity of the gene-edited cells. Zymosan is a yeast cell wall derivative that is recognised by immune cells through TLR2 (Gantner et al., 2003) and Dectin-1, a lectin receptor for β-glucans (Brown and Gordon, 2001, Brown et al., 2002). TLR2 cooperates with TLR6 and CD14 in response to zymosan (Ozinsky et al., 2000). *E. coli* is a gram negative bacteria whose cell wall components include peptidoglycan (PGN) and lipopolysaccharide (LPS). These cell wall components are recognised by TLR2 and TLR4 (Takeuchi et al., 1999), inducing the production of pro-inflammatory cytokines (van Riet et al., 2009).

In vivo studies in *Trem2* KO mouse models (*Trem2* -/-) reported a reduced phagocytic capacity of microsphere beads and apoptotic neurons by microglia (Takahashi et al., 2005b). Similarly, *in vitro* studies using *Trem2* KO macrophages and microglia showed reduced phagocytic capacity of apoptotic neurons, cellular debris, Aβ1-42 and bacteria (Kleinberger et al., 2014b, N'Diaye et al., 2009a, Atagi et al., 2015b, Xiang et al., 2016b). Additionally, gain of function studies in non-phagocytic cells showed that expression of TREM2 can enable uptake of apoptotic neurons and bacteria (Kleinberger et al., 2014b, N'Diaye et al., 2009a). Furthermore, in a recent study Xiang et al. (2016b) demonstrated that the N9 cells (rat microglial cell line) lacking *Trem2* (knocked-out using CRISPR/Cas9 technology) had a reduced uptake capacity of pre-aggregated Aβ1-42. Unfortunately,

this study does not mention anything about the bacterial phagocytic capacity of this cell line.

In the present study, *Trem2* CRISPR/Cas9 clones (either *Trem2* +/- or -/-) do not show a reduced phagocytic capacity, neither when *E. coli* nor Zymosan particles were used (Figure 4.6 and Figure 4.7). This is particularly surprising in the case of *E. coli* particles, since knockdown and knockout of *Trem2* in BMDMs have been shown to reduce binding and uptake of these particles in 25% and 30%, respectively, compared to wild-type cells (N'Diaye et al., 2009b). Contrary to the report by N'Diaye et al. (2009b), our study shows that *Trem2* deficient cells do not have any impairment in their uptake of *E. coli* particles at the evaluated timepoints (Figure 4.6). Furthermore, increased phagocytosis of Zymosan particles was observed in the CRISPR/Cas9 clones (Figure 4.7), which reaches statistical significance for A7, C8 and G4 cell lines ($p<0.0001$, $p<0.001$ and $p<0.001$ respectively). To our knowledge, this is the first report where *Trem2* deficiency does not cause a decrease in the phagocytic capacity of cells. Although the increase seen in the uptake of Zymosan is modest compared to WT cells (~18%), there is no decreasing trend in any of the CRISPR/Cas9 cell lines.

It is important to consider that Bohlen et al. (2017) showed that primary microglial cells grown in serum-free conditions have a reduced phagocytic capacity of different 'prey' pHrodo tagged particles compared to their serum supplemented counterparts. The work done by Bohlen et al. (2017) clearly shows differences in the phagocytic capacities of microglial cells cultured at different serum concentrations, and could explain our contradicting results. Bohlen et al. (2017) demonstrated that cells grown in serum-containing medium for 72 hours prior to the phagocytic experiment are far more phagocytic than those kept in serum-free conditions. As seen in

Figure 4.1, addition of 10% FBS into the medium of BV2 cells for 24 hours reduces the expression of *Trem2* by more than 50% compared to those cells kept in serum-free conditions (from 100% expression to 47.8% after exposure). This difference in the expression of a cell receptor like TREM2 (and others) could potentially affect the engulfment of 'prey' particles by microglia. Additionally, in our experimental set up Cytochalasin D had very little effect over the phagocytic capacity of *E. coli* particles and a modest effect on the uptake of zymosan particles. Again, this could be a result of the reduced levels of phagocytosis seen in microglial cells grown in serum-free conditions. Furthermore, the lack of effect of Cytochalasin D point out to a shift in the phagocytic/endocytic capacities of microglia, which could be switching from an ACTIN-

dependant to an ACTIN-independent mechanism, especially in the case of *E. coli* particles.

Kleinberger et al. (2014b) showed that *Trem2* -/- primary microglia had a reduced phagocytic capacity of *E. coli* particles using a similar experimental paradigm. In that study, the reduction of phagocytic capacity of *Trem2* -/- cells was ~15%, which is also a modest effect. These small increases and decreases in the phagocytic capacity of *Trem2* deficient cells could mean that TREM2 has a limited influence over the uptake of bacterial particles. Kleinberger et al. (2014b) speculated that a reduced phagocytic capacity of microglial cells can contribute to neurodegeneration by many different mechanisms (including reduced Aβ and/or apoptotic cell uptake). In light of our results, it could be argued that the opposite could also be said; increased phagocytosis capacity could inadvertently eliminate endangered but viable neurons, a phenomenon termed "phagoptosis" (Brown and Neher, 2012). Interestingly, a recent study by Wang et al. (2015c) found that microglial cells isolated from *Trem2* -/- 5XFAD and 5XFAD mice engulfed apoptotic cells equally well. These conflicting results supporting a beneficial or detrimental role of phagocytosis need to be further investigated and validated. It is also worth mentioning that the phagocytosis experiments were repeated only twice instead of the typical ≥3 repeats, further validation of these results will give us a clearer picture of the experimental results found in this thesis.

Cell proliferation has also been positively associated with *Trem2* (and *Dap12*) expression (Otero et al., 2012, Otero et al., 2009, Wang et al., 2016b). Wang et al. (2016b) showed that plaque-associated microglial proliferation is affected by *Trem2* deficiency *in vivo*. Nevertheless, this study – like many others – has a caveat; they used IBA1 as a marker for microglia. As will be discussed in the next chapter, *Iba1* expression is reduced by microglial activation (particularly M1-like activation), which could lead to an underestimation of the number of microglial cells in immunohistochemistry studies. In a recent study, Zheng et al. (2016) showed that siRNA downregulation of *Trem2* reduced the proliferation of primary mouse microglia. In the same study, the authors used primary cells from *Trem2* -/- mice to study cytokine release alterations in microglia, but proliferation results were not reported.

For the study of the impact of *Trem2* deficiency on microglial proliferation, two different methods were used: i) KI67 staining and ii) CellTrace™ CSFE dye staining. KI67 protein is highly expressed in the nuclei of dividing cells and serves as a marker of proliferation. KI67 staining showed the same number of proliferating cells in WT and *Trem2* CRISPR/Cas9 clones treated with two different concentrations of FBS (1 and 10%) at 24

and 48h; with the exception of B5 cells, which showed a higher number of proliferating cells at 24h and 1% FBS (*p<0.05) (Figure 4.8). Similar results were obtained when the MFI values for KI67 (staining intensity) were compared. Once more, B5 cells were the exception, showing a higher MFI in 1% and 10% FBS at 24h and in 10% at 48h (***p<0.001, ****p<0.0001 and **p<0.01 respectively).

CellTrace™ analysis of *Trem2* deficient BV2 cells showed similar result to the KI67 staining. There were no differences in the proliferation rates (speed) between WT or the *Trem2* CRISPR/Cas9 clones (Figure 4.9). Taken together, these results show that the lack of TREM2 has little or no effect on the proliferation of BV2 cells and could even increase its proliferative capacity, as in the case of B5 cells. Considering these results, it is possible to speculate that the proliferation variations seen in other studies involving *Trem2 -/-* cells could be the result of their altered microglial activation (discussed below and in the next chapter) rather than a direct effect on the proliferation mechanisms/pathways of the cells. Interestingly, Wang et al. (2017) showed that addition of 5% human serum into BV2 cultures was able to immune activate cells and can be considered as a pro-inflammatory stimulus. Coincidentally, downregulation of *TREM2* by LPS and other classically pro-inflammatory molecules is a well-documented phenomenon (Jay et al., 2017), while classically anti-inflammatory molecules (such as vasoactive intestinal peptide and IL4) increase *TREM2* expression (reviewed by Jay et al. (2017)). These results suggest that *TREM2* expression is dependent on the immune activation state of cells in response to pro- and anti-inflammatory stimuli.

Migration has also been linked to *Trem2* expression. In a recent report Mazaheri et al. (2017) showed that microglial cells lacking *Trem2* had an impaired migration response towards chemo-attractants (C5a and CCL2) and apoptotic cells. Furthermore, the authors identified the downregulation of a gene cluster associated with chemotactic motility in *Trem2* deficient cells. In our study, the potential impact of *Trem2* deficiency on microglial migration was assessed using a modified transwell assay and previously reported chemoattractants. Two of these chemoattractants were C5a and NGFβ. C5a is a potent chemoattractant involved in the recruitment of immune cells (such as neutrophils, eosinophils, monocytes and T lymphocytes) and in the activation of phagocytic cells (such as macrophages and microglia)(Guo and Ward, 2005). NGFβ on the other hand, has been shown to induce microglial chemotaxis through the activation of the TrkA receptor (De Simone et al., 2007).

As seen in Figure 4.10, *Trem2* deficiency reduced microglial migration. The reduction was more pronounced when cells were left untreated (either in 10% serum or in serum-

free conditions). Nevertheless, there were some conditions that partially restored the migration capacity of *Trem2* deficient cells, such as C5a in 10% serum. The migration capacity of B5 and G4 clones was noticeably affected under untreated conditions (in 10% serum and serum-free conditions) and under C5a (serum-free). However, these clones seem to respond very well to NGFβ, C5a and the kit's positive control (all in 10% serum). Remarkably, *Trem2* haploinsufficient clones A7 and G8 had modest responses to these chemoattractants. These results are in agreement with the literature which supports a role of *Trem2* in microglial migration (reviewed by Jay et al. (2017)). Nevertheless, these results must be taken cautiously as this experiment was carried out only once (n=1).

Interestingly, the functional assays showed some degree of variability between the clones expressing the same *Trem2* genotype; A7 and C8 (*Trem2* +/-) or B5 and G4 (*Trem2* -/-). This variability could be the result of many interplaying factors related to the process of expansion and selection of CRISPR modified clones. The first and more obvious source of variability between clones could be the generation of unspecific cuts/modifications introduced during the CRISPR/Cas9 genome editing. In our experiment, only the top 5 more-likely off-target sites for each gRNA were screened, finding that none of them was modified by the Cas9 protein (Section 3.3.2.1). The great majority of papers where CRISPR experiments are reported have identified very few to no off-target mutations that can be attributed to the CRISPR/Cas9 modification, similar to what is reported in this thesis. This has led researchers to conclude that clonal artefacts (variability) resulting from the isolation of CRISPR/Cas9 modified cells could be a more important factor in downstream experimentation (Barrangou et al., 2015). Evaluation of this variability (caused by intrinsic genetic clonal variability or by un-screened off-target cuts) can only be achieved by Next-generation sequencing of the whole target genome, which remains a costly and analysis intensive examination. Karyotyping of selected clones can give us information on mayor genetic rearrangements and can help discard clones with gross genetic abnormalities. In this study, karyotyping was performed on WT, C8 (*Trem2* +/-) and G4 (*Trem2* -/-). Karyotypes for these cells were found to be "Grossly abnormal mouse karyotype", with 62-66 chromosomes (mouse normal karyotype (2n) has 40 chromosomes) including WT cells (Section 2.1). Moreover, chromosome 17 (*Trem2's* location) was found to have 2-4 copies in WT cells, 3-4 copies in C8 and only 3 copies in G4 cells. These differences in the chromosomal number of cells could account for some of the variability seen in the experiments.

In order to ensure redundancy of phenotype, it is advised that CRISPR experiments use multiple sgRNAs targeting the same locus to ensure that the phenotype is due to on-

target rather than off-target effects (Barrangou et al., 2015). This is the case with the approach used in this study, the use of CRISPR/Cas9 paired nickases increased the gene targeting specificity, thus lowering concerns about off-target effects (Ran et al., 2013a). This redundancy of phenotype can also be achieved by using 2 or more CRISPR/Cas9 modified clones for downstream experimentation, as was the case in the present study. This will ensure that the phenotypes seen are product of genetic manipulation and not individual clonal variation.

4.4.3 *Trem2* deficiency affects microglial activation

One of the main aims of this thesis is to understand how *Trem2* deficiency affects microglial activation. To this end, the full gene expression response of microglial cells during different activation states (M1, M2 or others) will be studied in the next chapter. In this section, the effect of *Trem2* deficiency on the cytokine release capacity of BV2 cells is studied as part of the microglial activation mechanisms.

Cytokine release capacity (and production) has been shown to be impaired in *Trem2* -/- models. Early work in BMDMs showed that *Trem2* -/- cells released more inflammatory cytokines, such as TNFα and IL6, upon stimulation with TLR agonists (LPS, CpG and Zymosan) compared to wild type cells (Turnbull et al., 2006, Hamerman et al., 2006). This increased cytokine response was also seen in *Dap12* -/- BMDMs, suggesting that both TREM2 and DAP12 play an anti-inflammatory role in response to TLR agonist's stimulation (Turnbull et al., 2006, Hamerman et al., 2005). In our experiment, the repertoire of cell activators used was bigger; not only the classical M1 activator LPS was used, but also the M2 activator IL4, and the alternative M2 activator TGFβ (Colonna and Butovsky, 2017). In order to appreciate microglia's role in neurodegenerative diseases, it is important to understand their activation range, including both inflammatory and anti-inflammatory responses; however, response to these M2 activators has been poorly studied.

The first step in our examination of the cytokine release responses was the hierarchical clustering analysis of such responses (Figure 4.11). The first thing that sprung to our attention was that B5 (*Trem2* -/-) cells' response to LPS was the most different response, suggesting that cytokine release was severely impaired in this clone compared to WT and A7 (*Trem2* +/-) cells. A second cluster of interest was the IL4 cluster, which was composed of the IL4 responses from the three cell lines; this suggests that IL4 activation of microglia is not affected by *Trem2*. A third cluster – composed of WT, A7 and B5 responses to the untreated, LPS and TGFβ treatments – showed that although LPS and TGFβ treatments have similar cytokine release responses, these seem to be

differentially affected by the *Trem2* genotype. Additionally, this third cluster shows that the cytokine release response under untreated (control) conditions is markedly different to the cytokine releases responses elicited by LPS or TFGβ and is also affected by the *Trem2* genotype.

Subsequently, the release of individual cytokines associated with M1 or M2 activation was studied; as well as their relationship with *Trem2* deficiency. Microglial M1 activation is characterised by an upregulated production of TNFα, IL1α, IL1β, and IL6 among many others (reviewed by Colonna and Butovsky (2017)). As reported previously in mouse *Trem2* -/- BMDMs and dendritic cells (Wang et al., 2015c, Takahashi et al., 2005a, Ito and Hamerman, 2012), *Trem2* deficient cell lines A7 and B5 had an exaggerated TNFα response to LPS. This response inversely correlated with *Trem2* expression (B5>A7>WT). TNFα was also upregulated in A7 and B5 cells in all other conditions, highlighting the importance of *Trem2* expression in TNFα production and release. Release of IL1β was also upregulated in A7 and B5 cells when stimulated with LPS. This upregulation was also seen when CRISPR/Cas9 clones were stimulated with IL4 or TGFβ. Increased microglial release of both TNFα and IL1β has been shown to promote neuronal damage when present in excessive amounts (Monif et al., 2010, Rossi et al., 2014).

Surprisingly, IL6 release was downregulated in the CRISPR/Cas9 clones after LPS stimulation. This result contradicts the findings made by Zhong et al. (2015). In their study, knockdown of *Trem2* (or *Dap12*) in BV2 cells significantly increased IL1β and IL6 following LPS stimulation. Importantly, overexpression of full-length *Trem2* (or *Dap12*) was able to suppress the disproportionate pro-inflammatory cytokine production. Similarly to our results, Gawish et al. (2015b) found an augmented early inflammatory response in *Trem2* -/- animals, which was followed by an accelerated resolution and ultimately improved survival. This accelerated resolution of inflammation could explain why IL6 is downregulated in our experiment. Further work will be needed to understand IL6 (and other inflammatory cytokines) regulation and dynamics in a *Trem2* deficient context. As seen in this experiment, *Trem2* deficient clones (either A7 or B5) have an altered inflammatory cytokine response when treated with LPS (M1 activator). Defining the effect of TLR4 stimulation (LPS receptor) on the production and release of pro-inflammatory cytokines has become pivotal for the AD research community since Aβ peptides have been shown to activate signal transduction cascades via TLR4 binding (reviewed by Painter et al. (2015))

The release of cytokines associated with M2 activation (IL4, IL10 and IL11) was also investigated in this experiment. Activation of peritoneal macrophages with IL4 has been shown to upregulate TREM2 protein expression, suggesting that IL4's anti-inflammatory effect is associated with a *Trem2* related pathway (Turnbull et al., 2006). Moreover, *Trem2* overexpression induced the transcription of IL10 and inhibited the production of inflammatory cytokines (IL1 and IL6) in BMDMs (Chen et al., 2013b). In our study, IL4 release did not seem to be greatly affected by *Trem2* genotype of cells. Its secretion was only marginally increased by LPS stimulation in all cell lines but particularly in B5 cells (*Trem2* -/-). Meanwhile, IL10 was readily released in all conditions except in unstimulated WT cells. Nonetheless, expression of IL10 correlated with *Trem2* in a dose dependent manner (WT>A7>B5) in all conditions except unstimulated, suggesting that *Trem2* might regulate IL10's release.

Similarly to IL10 expression, IL11 was stimulated in all conditions except for the untreated WT cells. The highest expression levels of IL11 were found in WT cells stimulated with LPS or TGFβ, while the A7 and B5 cell lines treated with these same stimuli had lower levels of this cytokine. These results show a modest impairment of the production/release of this cytokine in *Trem2* deficient clones. Studies on the effect of IL11 in microglial activation (using a mouse model of demyelination) have shown that local overexpression of IL11 can reduce microgliosis and microglial activation (Maheshwari et al., 2013), suggesting that this cytokine participates in immune deactivation on microglia. Interestingly, our results show that under untreated conditions WT cells had very little secretion of IL10 and IL11, while the CRISPR/Cas9 clones (A7 and B5) had an elevated release of both cytokines even without stimulation. The increased levels of IL10 and IL11 seen in the *Trem2* deficient clones were variable depending on the different stimuli used (LPS, IL4 or TGFβ) and were usually present at lower levels than in WT cells. Meanwhile, stimulation of WT cells with any of the three selected stimuli, dramatically increased the release of both cytokines compared with the untreated condition. These observations suggest that TREM2 may modulate IL10 and IL11 production/release mechanisms and microglial immune activation (Orihuela et al., 2016, Opal and DePalo, 2000).

Comparison of the cytokine release capacities of WT, A7 and B5 cells has shown that *Trem2* expression influences cytokine production. A7 and B5 cells have shown an increased release of M1-related cytokines in response not only to LPS, but also IL4 and TGFβ. Moreover, A7 and B5 cells showed an impaired secretion of M2-associated cytokines IL10 and IL11 in most conditions compared to WT cells. From this analysis, it can be concluded that *Trem2* expression not only contributes to an exaggerated M1

response in microglia (as has been widely reported by others), but can also alter the M2 response. Interestingly, *TREM2 R47H* AD carriers show: a) upregulation of *TREM2* and *DAP12* mRNA; b) downregulation of TREM2 protein; c) upregulation of pro-inflammatory cytokines (RANTES and IFNγ); d) downregulation of protective cytokines/markers (IL4, α2 macroglobulin, and ApoA1) (Roussos et al., 2015).

Analysis of the cytokine release response of WT and *Trem2* deficient clones allowed the identification of a microglial activation signature: IL11, IL12, FGF-21, CXCL9, IGFBP-3, IL10, IGFBP-5, leptin, FGF acidic, LIF, CXCL10, PDGF-BB and Pentraxin 2. This group of cytokines seems to be upregulated during the activation of BV2 cells by any of the three immune activators used (LPS, IL4 and TGFβ) or *Trem2* deficiency (either downregulation or depletion). The inclusion of M2 associated cytokines IL11 and IL10 in this microglial activation signature suggest a complex role of these cytokines in microglial activation. Another interesting result is the finding that leptin, a protein known for its role in the regulation of energy expenditure and inflammatory responses, is also upregulated during M1 or M2 activation, although this upregulation was less pronounced in the *Trem2* deficient clones. This cytokine has been shown to play a pro-inflammatory role, in synergy with IL1β, by inducing production of NOS2, IL6, IL8 and Prostaglandin E2 (Otero et al., 2005, Vuolteenaho et al., 2009). It is important to remember that leptin also participates in bone mass regulation (Ducy et al., 2000), which is consistent with a possible role in Nasu-Hakola disease, and cognitive changes in AD (Lieb et al., 2009).

Finally, analysis of cytokine release capacities of WT and *Trem2* deficient cells showed an increase on the expression of the complement system (C5a, C1qR1 and Complement Factor D) in A7 and B5 cells in response to all treatments. Particularly interesting is the observation that IL4 seems to downregulate the expression of C5a in WT cells but not in *Trem2* CRISPR/Cas9 clones. Similar responses, although less pronounced, are seen for the expression of C1qR1 and Complement Factor D. These observations are important, since GWAS studies have also associated CR1 with and increase AD risk (Lambert et al., 2009, Harold et al., 2009).

The results obtained during the evaluation of the cytokine release capacity of BV2 cells have to be taken as preliminary results as the experiment was performed just once (n=1). More biological repeats of the experiment will be needed to confirm our findings and validate the existence of the “microglial activation signature”. Moreover, the cytokine arrays used for the experiment are only capable of relative quantification of the cytokines. Follow-up experiments should be performed using a different quantification method that allows absolute quantification of cytokines (i.e. ELISA, mass spectrometry, etc.).

4.4.4 *Trem2* deficiency disturbs the mRNA expression of pro-inflammatory genes but not the expression of AD associated genes or genes whose protein products directly interact with the TREM2 protein.

Figure 4.13 shows the effect of *Trem2* deficiency on the mRNA expression of microglial genes. As seen in this figure, there was upregulation of *TNFα* mRNA by LPS in B5 cells (*Trem2* -/-), which is consistent with the results observed in the cytokine array (Figure 4.11). This exaggerated response was also seen in the LPS+10% FBS condition. Meanwhile, expression of the *CD40* mRNA was upregulated by LPS in G4 cells (*Trem2* -/-), but not A7 (where it was actually downregulated), C8 or B5. Expression of *CD40* was also upregulated under LPS+10% FBS conditions in C8 and G4 cells, but not A7 or B5. These results suggest that *Trem2* plays a role on the expression of pro-inflammatory genes *TNFα* and *CD40*, although there is no direct correlation between their expression levels. TNFα secretion is known to be increased after treatment of *Trem2* -/- BMDM with LPS for 24h, but whether increased cytokine release levels correlate with the peak mRNA expression of the gene remains unclear (Turnbull et al., 2006). The accelerated resolution of inflammation seen in *Trem2 -/-* animals (Gawish et al., 2015b) could explain why both *CD40* and *TNFα* did not show an exaggerated response to LPS in all *Trem2* deficient clones.

Next, the effect of *Trem2* deficiency on other AD related genes was examined, namely *ApoE* and *CD33*. mRNA expression of these genes in response to different stimuli was not affected by *Trem2* deficiency. The only observable differences were between the expression of WT cells and the *Trem2* CRISPR/Cas9 clones under unstimulated conditions. Nonetheless, these differences (upregulation and downregulation) were not consistent with a specific *Trem2* genotype (i.e. *ApoE* expression is significantly downregulated in B5 and upregulated in G4 cells). The mRNA expression of 2 genes whose protein products have been shown to directly interact with *TREM2* was also studied in the CRISPR/Cas9 clones; 1) *Dap12* (Yeh et al., 2017) and 2) *Plxna1* (Hayashi et al., 2012). Expression of these two genes was not affected by *Trem2* genotype under any of the conditions assayed. Remarkably, small differences in the mRNA expression of *Dap12* were only seen between WT and the *Trem2* CRISPR/Cas9 clones under unstimulated conditions. Changes on the expression of this gene under basal conditions were not consistent with the *Trem2* genotype. Taken together, these results suggest that *Trem2* genotype (and the resulting protein dose) do not affect gene expression of *Dap12* or *Plxna*. Although *Trem2* genotype did not seemed to affect the expression of these 2 genes, this experiment showed some interesting trends in their expression in response to specific treatments. For example, Dap12 expression was clearly downregulated to

~50% by every stimuli used in this experiment, including 10% FBS alone. These results are interesting for the study of the TREM2 function, since the same stimuli reduced *Trem2* mRNA expression by 50% or more in WT cells (see Figure 4.1). Similarly, *Plxna1* expression was downregulated by 10% FBS alone, while LPS upregulated this expression by almost 2-fold (compared to untreated). Remarkably, stimulation of cells with both 10% FBS and LPS (simultaneously) recovered the expression of *Plxna1* and brought it almost to basal levels. Further exploration of these changes, in future studies, may provide some clues about their interactions with TREM2.

5 CHAPTER 5: Gene expression analysis of microglial activation

Chapter 5 describes the gene expression response of BV2 cells, a mouse microglial cell model, to different activating stimuli. These stimuli include the classical M1 activator LPS, and the alternative M2 activators; IL4, IL10 and TGFβ. Importantly, the response of BV2 cells to different Aβ1-42 conformations (monomers, oligomers and fibrils) was also investigated. To this end, 2 different genome expression platforms were used: i) gene expression arrays (microarrays) and ii) RNA sequencing (RNAseq), both of which will be described in detail. The decision to use these 2 platforms for gene expression studies was taken after the completion of the microarray experiment. At this point, our group was informed that the microarrays used (MouseRef-8 v2.0 Expression Arrays) had been discontinued and were no longer being manufactured. For this reason, a change in platform -to NGS RNAseq- was decided in order to finish the activation experiment. This change in platform, allowed the comparison of two different gene expression techniques in our study.

Lastly, this chapter also reports the study of the effect that *Trem2* deficiency (*Trem2 -/-*) has on normal gene expression and activation of BV2 cells.

5.1 Introduction

In recent years, and due partly to the many advances in the field of genomics, it has been become increasingly clear that neuroinflammation plays a pivotal role in the pathogenesis and development of many neurodegenerative disorders including AD, PD, Huntington's disease (HD), and Multiple sclerosis (MS). Microglial cells are the main immune cell in the CNS and comprise 5-12% of brain cells. These cells coordinate the innate immunity responses in the brain, control neuronal homeostasis and are involved in most neuroinflammatory pathologies (reviewed by Tang and Le (2016)).

Microglia becomes quickly activated in response to infection, inflammation or brain injury. Classically activated microglia (M1) release various inflammatory mediators including TNFα, IL1β, IL6, NO, ROS and Prostaglandin E2 (PGE2), all of which have been linked to various neurodegenerative disorders (Streit et al., 2004, More et al., 2013, Lue et al., 2015). Non-classically activated microglia (M2) can be induced by cytokines including IL4, IL10, IL13 and TGFβ among others (Tang and Le (2016)). IL4 and IL13 are known to "alternatively" activate microglial and promote anti-inflammation, tissue repair and extracellular matrix reconstruction. Whereas, IL10 and TGFβ are known to "deactivate" microglia in order to alleviate acute inflammation (Colton and Wilcock, 2010). However,

the precise mechanisms controlling transcriptional microglial inflammatory activation and resolution are not well characterised.

Over the past two decades, phenotypic responses to different stimuli in macrophages have been linked to dramatic changes in transcriptional regulation. As a result, many studies have used both microarray (Martinez et al., 2006, Gustafsson et al., 2008, Lacey et al., 2012, Heng et al., 2008) and RNAseq (Xue et al., 2014) for gene expression profiling of such responses. Although both techniques are highly informative, RNAseq is becoming the method of choice for gene expression profiling studies, as it provides a series of advantages over microarrays, such as; broader dynamic range, increased specificity and sensitivity and allows the identification of novel transcripts (Marioni et al., 2008, Raghavachari et al., 2012, Schultze et al., 2015). Similarly, many studies are trying to unveil the microglia activation transcriptional changes using these same techniques (Beins et al., 2016, Hickman et al., 2013).

In this chapter, the classical M1 activator LPS was used to stimulate BV2 cells and their response was compared to the response of BV2 cells to other alternative microglial activators, namely IL4, IL10 and TGFβ (M2 activators). These 4 stimuli were used to study the spectrum of microglial activation (M1, M2 or other), and we do not suggest that any of them is directly implicated in AD´s pathogenesis or progression. On the other hand, the effect of Aβ1-42 (fibrils, oligomers and monomers) on microglial activation was also studied. Aβ1-42 is believed to be the cause or at least be implicated in AD pathogenesis and progression, and was included in our study for that reason. Finally, using the created B5 (*Trem2* -/-) cell line, it was possible to study the effect of *Trem2* deficiency on the microglial gene expression and in response to LPS. To explore the microglial response to the different stimuli, two different whole genome expression approaches were employed: i) microarrays and ii) RNAseq.

5.2 **Aims**

The aims of the following chapter are:

1. To study the BV2 activation response to LPS, Aβ1-42 (fibrils), dextran sulphate (putative TREM2 ligand) and fibrinogen at three different timepoints (6, 24 and 48h) using microarrays.
2. To characterize BV2 response to LPS, Aβ1-42 (monomers and oligomers), IL4 and TGFβ at three different timepoints (6h, 24h and 48h) using RNA sequencing.
3. To evaluate the transcriptional changes of the *Trem2* knockout cell line B5 in response to LPS and under basal (untreated) conditions.

5.3 Microarray analysis of microglial activation in response to LPS, Aβ1-42 (fibrils), dextran sulphate and fibrinogen.

5.3.1 Normalization and quality control

BV2 wild type (unmodified) cells were exposed to 6 different conditions under serum-free conditions; 1) Aβ1-42 fibrils 20nM, 2) untreated control (no stimulus), 3) Dextran 1µg/mL, 4) Dextran 100µg/mL, 5) fibrinogen 1mg/mL and 6) LPS 1µg/mL. Total mRNA was recovered from the stimulated cells 0h (only control samples), 6h, 24h and 48h after treatment and prepared for microarray analysis by AROS Applied Biotechnology (described in Sections 2.6.1 and 2.6.2).

After microarray analysis by AROS Applied Biotechnology, raw expression values were sent back to us for analysis. Raw expression values were normalised and quality control (QC) examined. After QC, only 10134 genes (out of ~19 100 genes unique genes present in the microarray chip) were included in the analysis. Principal component analysis (PCA) and unsupervised hierarchical clustering (Supplementary Fig. 7.5) were used to identify outliers and to visualize the clustering of all arrayed samples; Partek® Genomics Suite™ software was used for this step.

PCA is linear transformation method that transforms the data to a new coordinate system. PCA seeks a linear combination of variables such that the maximum variance is extracted from the variables and plots it on the first coordinate (called the first principal component). It then removes this variance and seeks a second linear combination which explains the maximum proportion of the remaining variance, and so on. PCA is used to emphasize variation and bring out strong patterns in a dataset. It makes data easy to explore and visualize (Jollife, 2002).

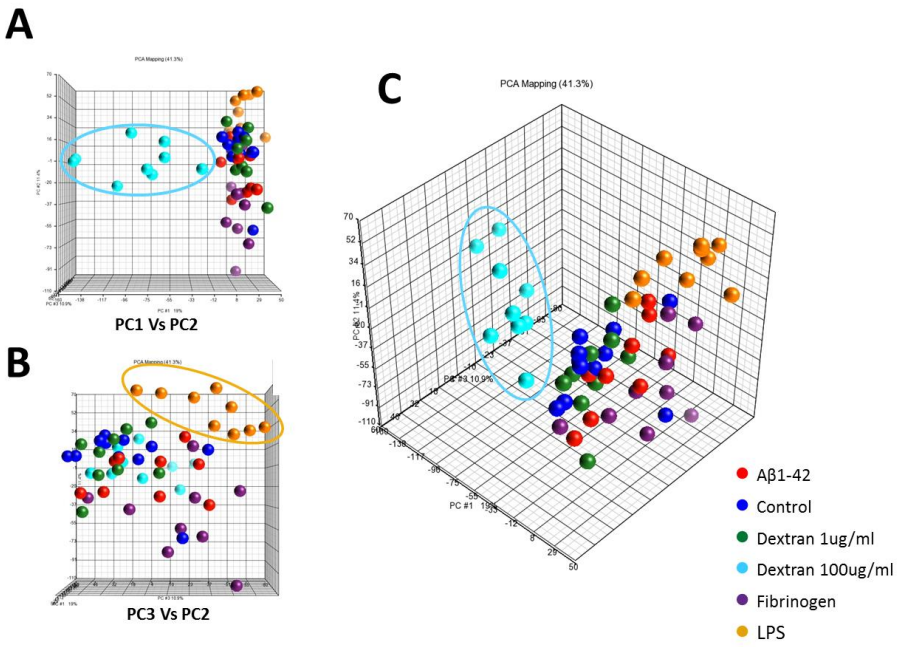

Figure 5.1 PCA scatter plot of data. Principal component analysis (PCA) was used to identify outliers and to visualize the clustering of all arrayed samples. Samples are colour coded according to their respective treatments. No samples were excluded as a result of this analysis and it was possible to distinguish some clustering of samples. Panels **(A)** and **(B)** show 2D lateral views of the PC1 vs PC2 and PC3 vs PC2 scatter plots. Panel **(C)** shows the 3D representation of scatter plot for the 3 principal components. In Panels **A** and **B**, it is possible to distinguish two clearly segregated clusters of samples: Dextran 100µg/mL (sky blue spheres and circle) and LPS 1µg/mL (orange spheres and circle). Apart from those two clusters, all other samples (Aβ1-42 fibrils, Dextran 10µg/mL, fibrinogen and control samples) were mixed up together in an undefined third cluster **C**. Samples in this representation are coloured according to their correspondent treatment.

The PCA scatter plot in Figure 5.1 shows samples coloured according to their treatment. In it, it is possible to distinguish 3 small clusters of samples which correspond to; 1) Dextran 100µg/mL (sky blue spheres) 2) LPS 1µg/mL (orange spheres) and 3) an undefined cluster with samples of many colours. This third cluster is made of Aβ1-42 fibrils, Dextran 10µg/mL, fibrinogen 1mg/mL and control samples, which seem to cluster together in a bigger group with no clear difference. Similar analyses were performed on the samples using different colouring patterns; according to timepoint, Microarray chip location and biological repeat (not shown). None of these factors seemed to reveal any clustering of the samples as in in the case of treatment.

5.3.2 **Identification of Differentially Expressed (DE) Genes**

A multi-factor ANOVA (Analysis of Variance) was set up for the identification of differentially expressed genes. Firstly, the main sources of variation that effected gene expression in our samples were identified. To this end, all probable sources of variation were plotted using Partek® Genomics Suite™ software (Figure 5.2). The source of variation plot is a graphical representation of the relative contribution of each factor (variable) to the variation in gene expression (intensity values) across the whole array.

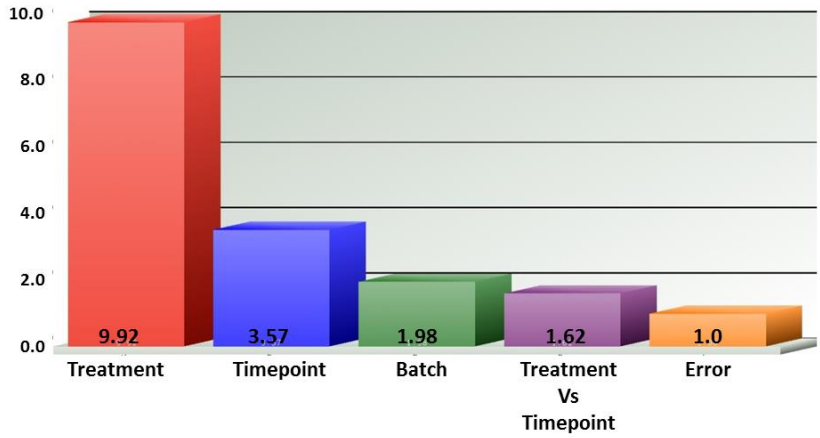

Figure 5.2 Sources of Variation. All probable sources of variation for gene expression changes in the experiment were plotted together. The most important source of variation is the Treatment, followed by Timepoint. Batch effect and the interaction Treatment Vs Timepoint had a less significant effect on gene expression. The Y-axis represents the Mean F-ratio (signal-to-noise) of all genes.

Based on the sources of variation plot, the ANOVA model included the following factors: Treatment, Timepoint, their interaction (Treatment x Timepoint) and Batch effect. At this point, contrasts (comparisons among samples) were set up to assess the effect of treatment, timepoint or their interaction in the experiment. In our case, 21 contrasts (Table 5-1) were set up together with the multi-factor ANOVA analysis.

Table 5-1 Contrasts (comparisons) used for the multi-factor ANOVA – Microarray experiment

	Control, 0h	Control, 6h	Control, 24h	Control, 48h
Control, 6h	X			
Abeta fibrils, 6h		X		
Dextran 1ug/ml, 6h		X		
Fibrinogen, 6h		X		
LPS, 6h		X		
Dextran 100ug/ml, 6h		X		
Control, 24h	X	X		
Abeta fibrils, 24h			X	
Dextran 1ug/ml, 24h			X	
Fibrinogen, 24h			X	
LPS, 24h			X	
Dextran 100ug/ml, 24h			X	
Control, 48h	X	X	X	
Abeta fibrils, 48h				X
Dextran 1ug/ml, 48h				X
Fibrinogen, 48h				X
LPS, 48h				X
Dextran 100ug/ml, 48h				X

Contrasts allow to identify differences (or similarities) among samples. In a first instance, all controls were compared with each other to determine whether genetic expression fluctuated depending on the elapsed time (timepoint). Likewise, each treatment (i.e. LPS 6h) was compared with their own control (i.e. Control 6h) to identify how different treated samples were with respect to untreated controls.

5.3.3 Creating gene lists of Differentially Expressed genes

Gene lists were created using the Partek® Genomics Suite™ software. A conservative FDR (False Discovery Rate) of 0.01 and a minimum fold change of ±1.5 were used to generate gene lists. Gene lists were created for all 21 contrasts; nevertheless 11 of the contrasts had no genes in the generated lists. Table 5-2 shows which contrasts generated gene lists (in red) compared to all contrasts set up for the experiment (in black).

Table 5-2 Contrasts (comparisons) used for the multi-factor ANOVA which generated (or not) gene lists of differentially expressed genes - Microarray experiment

	Control, 0h	Control, 6h	Control, 24h	Control, 48h
Control, 6h	X			
Abeta fibrils, 6h		X		
Dextran 1ug/ml, 6h		X		
Fibrinogen, 6h		X		
LPS, 6h		X		
Dextran 100ug/ml, 6h		X		
Control, 24h	X	X		
Abeta fibrils, 24h			X	
Dextran 1ug/ml, 24h			X	
Fibrinogen, 24h			X	
LPS, 24h			X	
Dextran 100ug/ml, 24h			X	
Control, 48h	X	X	X	
Abeta fibrils, 48h				X
Dextran 1ug/ml, 48h				X
Fibrinogen, 48h				X
LPS, 48h				X
Dextran 100ug/ml, 48h				X

X = Didn't generate a list of differentially expressed genes
X = Generated a list of differentially expressed genes

From the 10 generated gene lists, just one corresponded to differences among controls; Control 48h x Control 0h. In this list, only two genes were identified; Gpr84 and Lcp1. Gpr84 is a receptor for medium-chain free fatty acids and has been has been implicated

in fatty acid metabolism and regulation of the immune system. Lcp1 is an Actin-binding protein and has been shown to play a role in the activation of T-cells.

The other 9 gene lists corresponded to differences between the fibrinogen, LPS and dextran sulphate 100µg/mL treatments compared to their respective timepoint controls. Figure 5.3 shows the total number of differentially expressed genes for all the generated gene lists.

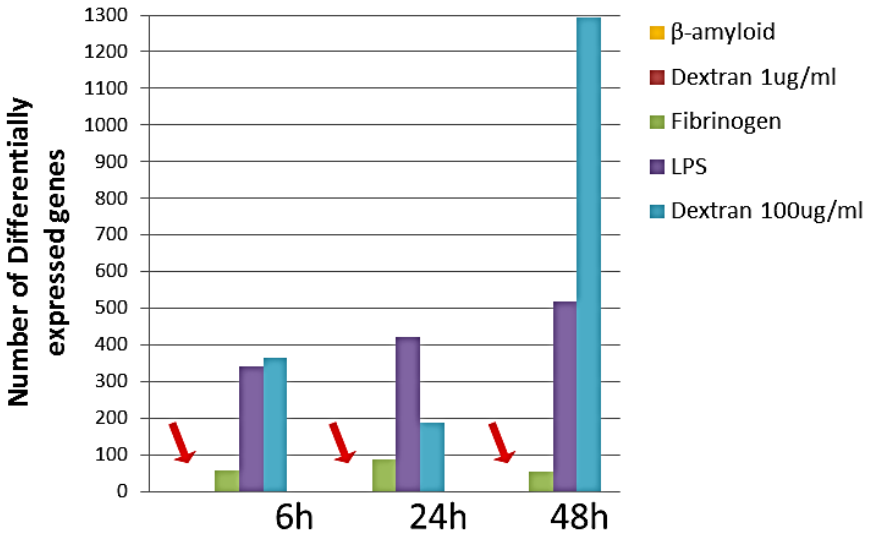

Figure 5.3 Number of differentially expressed genes in BV2 cells treated with Aβ1-42 fibrils, Dextran sulphate 1µg/mL, fibrinogen, LPS and Dextran sulphate 100µg/mL – Microarray experiment. After ANOVA analysis, the number of genes whose expression was affected by the different treatments was identified. As shown, only fibrinogen, LPS and Dextran Sulphate 100µg/mL treatments had an effect over the gene expression of BV2 cells at different timepoints. Surprisingly, Aβ1-42 fibrils and dextran sulphate 1µg/mL did not alter gene expression of any genes at any timepoint (red arrows).

As shown in Figure 5.3, only fibrinogen, LPS and dextran sulphate 100µg/mL treatments caused differential gene expression at all timepoints. Surprisingly, Aβ (fibrils) and dextran sulphate 1µg/mL did not alter gene expression of any genes at any timepoint (red arrows). This indicates that these two treatments are similar to the untreated control for each timepoint. This is an unexpected result as Aβ1-42 (fibrils and other conformations) have been shown to activate microglia (Pan et al., 2011).

For the next step of the analysis, gene lists were further divided into downregulated and upregulated genes (compared to their respective controls) as per the ANOVA analysis.

5.3.4 **Identification of enriched biological pathways – GO (Gene Ontology) Analysis**

The identification of enriched pathways and gene ontology analysis of the generated gene lists was carried out using the DAVID (Database for Annotation, Visualization and

Integrated Discovery) database 6.7 (http://david.abcc.ncifcrf.gov). For our analysis, a conservative EASE Score of 0.1 was used (minimum number of genes per pathway was set to 3). Figure 5.4, 5.5 and 5.6 show the top 5 GO terms for each generated list of differentially expressed genes.

Fibrinogen 6h Vs Control 6h (58 genes)					
Category	**Term**	**Category**	**Term**	**Category**	**Term**
---	No genes to analyze	GOTERM BP	regulation of transcription factor activity	GOTERM BP	regulation of transcription factor activity
		GOTERM BP	regulation of DNA binding	GOTERM BP	regulation of DNA binding
		GOTERM BP	regulation of binding	KEGG PATHWAY	Allograft rejection
		KEGG PATHWAY	Allograft rejection	GOTERM BP	regulation of binding
		---	---		
Fibrinogen 24h Vs Control 24h (87 genes)					
Category	**Term**	**Category**	**Term**	**Category**	**Term**
---	No significative BP, MF, MF or Pathway	GOTERM CC	nucleolus	GOTERM BP	nitrogen compound biosynthetic process
		GOTERM BP	nucleobase biosynthetic process		
		GOTERM BP	nucleobase, nucleoside, nucleotide and nucleic acid biosynthetic process		
		GOTERM BP	ribonucleoside monophosphate biosynthetic process		
		GOTERM BP	ribosome biogenesis		
Fibrinogen 48h Vs Control 48h (54 genes)					
Category	**Term**	**Category**	**Term**	**Category**	**Term**
---	No significative BP, MF, MF or Pathway	---	DAVID did not find any functinal group or pathway within this list	---	No significative BP, MF, MF or Pathway

Downregulated genes Upregulated genes Complete list

Figure 5.4 Microarray experiment - Top-5 most significant GO categories - Fibrinogen treated samples. GO analysis reveals that those genes whose expression was downregulated by the fibrinogen treatment at any timepoint do not group to any particular GO category or pathway (red panel). Meanwhile, upregulated genes (green panel) seem to be involved in functions related to transcription factor binding, allograft rejection and nucleic acid biosynthesis. When all differentially expressed genes were analysed together (up- and down-regulated genes) similar pathways and processes were overrepresented (blue panel). GO analysis was carried out using the lists of differentially expressed genes obtained from the microarray experiment, where wild-type BV2 cells were stimulated with Aβ1-42 fibrils, dextran 1µg/mL, dextran 100µg/mL, fibrinogen 1mg/mL and LPS (n=3).

According to the GO analysis fibrinogen treatment seems to activate cellular processes related to DNA binding and transcription (Figure 5.4). There was enrichment of an Allograft rejection pathway, but it was only seen in the upregulated genes at 6h.

LPS 6h Vs Control 6h (341 genes)					
Category	**Term**	**Category**	**Term**	**Category**	**Term**
---	No significative BP, CC, MF or Pathway	GOTERM BP	immune response	GOTERM BP	immune response
		KEGG PATHWAY	Toll-like receptor signaling pathway	KEGG PATHWAY	Cytosolic DNA-sensing pathway
		KEGG PATHWAY	Cytosolic DNA-sensing pathway	KEGG PATHWAY	Toll-like receptor signaling pathway
		GOTERM MF	cytokine activity	GOTERM BP	regulation of cytokine production
		KEGG PATHWAY	NOD-like receptor signaling pathway	GOTERM BP	defense response
LPS 24h Vs Control 24h (420 genes)					
Category	**Term**	**Category**	**Term**	**Category**	**Term**
GOTERM BP	DNA replication	GOTERM BP	immune response	GOTERM BP	immune response
GOTERM BP	cell cycle	GOTERM BP	regulation of cytokine production	GOTERM BP	DNA replication
GOTERM BP	cell division	KEGG PATHWAY	Toll-like receptor signaling pathway	GOTERM BP	regulation of cytokine production
GOTERM MF	DNA binding	GOTERM BP	inflammatory response	GOTERM BP	response to wounding
KEGG PATHWAY	Nucleotide excision repair	KEGG PATHWAY	Cytosolic DNA-sensing pathway	KEGG PATHWAY	Toll-like receptor signaling pathway
LPS 48h Vs Control 48h (516 genes)					
Category	**Term**	**Category**	**Term**	**Category**	**Term**
GOTERM MF	structural constituent of ribosome	GOTERM BP	immune response	GOTERM MF	structural constituent of ribosome
GOTERM CC	ribosome	KEGG PATHWAY	Toll-like receptor signaling pathway	GOTERM CC	ribosome
KEGG PATHWAY	Ribosome	KEGG PATHWAY	NOD-like receptor signaling pathway	KEGG PATHWAY	Ribosome
GOTERM BP	translation	KEGG PATHWAY	Cytokine-cytokine receptor interaction	GOTERM BP	translation
GOTERM MF	structural molecule activity	GOTERM BP	inflammatory response	GOTERM BP	immune response
KEGG PATHWAY	AD (Benjamini 0.073; 9 genes)			KEGG PATHWAY	AD (Benjamini 0.012; 15 genes)

Downregulated genes Upregulated genes Complete list

Figure 5.5 Microarray experiment - Top-5 most significant GO categories - LPS treated samples. Genes downregulated by LPS treatment seem to be involved in cell division and translation pathways at 24 and 48h (red panel). Upregulated genes were associated with GO categories related to immune response and inflammation at all timepoints (green panel). Finally, when the full list of downregulated and upregulated genes was analysed, a similar enrichment of the same GO categories was appreciated. Remarkably, there was a non-significant enrichment (Benjamini 0.073) of an Alzheimer's disease Pathway at 48h for the downregulated genes (bottom red panel). This enrichment became statistically significant when the full list was analysed (Benjamini 0.012) for the 48h timepoint (bottom blue panel). GO analysis was carried out using the lists of differentially expressed genes obtained from the microarray experiment, where wild-type BV2 cells were stimulated with Aβ1-42 fibrils, dextran 1µg/mL, dextran 100µg/mL, fibrinogen 1mg/mL and LPS (n=3).

GO analysis of the genes downregulated by LPS treatment showed an enrichment of processes related to cell cycle progression and cell division as well as ribosomal function and translation at 24h and 48h (Figure 5.5). Genes upregulated by the LPS treatment, on the other hand, were clearly associated to processes related to the immune and inflammatory responses at all timepoints. Similar trends were seen when the full list of genes (up- and down-regulated) were used for the analysis (Figure 5.5). Of note was the statistically significant enrichment (Benjamini 0.012) of an Alzheimer's disease associated pathway at 48h (Figure 5.5).

Dextran 100ug/ml 6h Vs Control 6h (362 genes)					
Category	**Term**	**Category**	**Term**	**Category**	**Term**
GOTERM MF	nucleotide binding	GOTERM CC	nuclear lumen	GOTERM MF	nucleotide binding
GOTERM MF	ribonucleotide binding	GOTERM MF	RNA binding	GOTERM MF	ribonucleotide binding
GOTERM MF	ATP binding	GOTERM CC	membrane-enclosed lumen	GOTERM MF	ATP binding
KEGG PATHWAY	MAPK signaling pathway	---	---	KEGG PATHWAY	Long-term depression
KEGG PATHWAY	Long-term depression			KEGG PATHWAY	MAPK signaling pathway
Dextran 100ug/ml 24h Vs Control 24h (186 genes)					
Category	**Term**	**Category**	**Term**	**Category**	**Term**
---	No significative BP, CC, MF or Pathway	---	No significative BP, CC, MF or Pathway	---	No significative BP, CC, MF or Pathway
Dextran 100ug/ml 48h Vs Control 48h (1292 genes)					
Category	**Term**	**Category**	**Term**	**Category**	**Term**
GOTERM CC	organelle membrane	GOTERM MF	transition metal ion binding	GOTERM MF	nucleotide binding
GOTERM MF	nucleotide binding	GOTERM MF	acid-amino acid ligase activity	GOTERM CC	nuclear lumen
GOTERM MF	transcription factor binding	GOTERM MF	ubiquitin-protein ligase activity	GOTERM CC	membrane-enclosed lumen
GOTERM MF	ribonucleotide binding	GOTERM BP	cellular protein catabolic process	GOTERM CC	organelle lumen
GOTERM MF	ATP binding	GOTERMBP	protein localization	GOTERM MF	ribonucleotide binding

Downregulated genes Upregulated genes Complete list

Figure 5.6 Microarray experiment - Top-5 most significant GO categories - Dextran 100µg/mL treated samples. Genes downregulated by Dextran 100µg/mL treatment seem to be involved in nucleotide binding, translation, MAPK signalling and Long-term depression pathways and processes at 6 and 48h (red panel). Upregulated genes were associated with GO categories related to RNA binding, ligase activity and protein catabolic processes at 6h and 48h (green panel). When the full lists of downregulated and upregulated genes were analysed, a similar enrichment of the same GO categories was seen. GO analysis was carried out using the lists of differentially expressed genes obtained from the microarray experiment, where wild-type BV2 cells were stimulated with Aβ1-42 fibrils, dextran 1µg/mL, dextran 100µg/mL, fibrinogen 1mg/mL and LPS (n=3).

Lastly, GO analysis of the gene lists generated for Dextran 100µg/mL treatment showed that downregulated genes were associated to processes related to binding to nucleotides, ribonucleotides and ATP (Figure 5.6). There was enrichment for genes associated with the MAPK pathway but only at 6h. Meanwhile, upregulated genes were associated to pathways related to RNA and metal ion binding, ligase activity and protein catabolic processes. Similar enrichments were seen when the full lists of genes were used for the analysis (Figure 5.6). Unexpectedly, it was not possible to identify any pathway enrichments for either down or upregulated genes at 24h, the same happened when the full list of differentially expressed genes was used.

5.3.5 **Microglial Markers and Microglial activation**

Many studies report the use of different cell markers for the identification of microglial cells. As such, this study explored how the different treatments used in our experiment affected the gene expression of these microglial markers. Table 5-3 shows some of the most common cell markers used in the study of microglial populations.

Table 5-3 Microglial cell markers differentially expressed by LPS treatment

Cell Marker	Differ. Expressed	Timepoint		
		6h	24h	48h
Cd11b (Itgam)	No	-	-	-
SFPi1	No	-	-	-
Cd68	No	-	-	-
Cd45 (PTPRC)	No	-	-	-
Cx3CR1	No	-	-	-
Iba1 (Aif1)	Yes	-	-	Downregulated
Cd14	Yes	Upregulated	Upregulated	Upregulated
CSF1	Yes	Upregulated	Upregulated	Upregulated
CSF1R	Yes	-	-	Upregulated
EMR1	Yes	-	Upregulated	Upregulated

Unexpectedly, only the LPS treatment was able to elicit differential expression of the revised genes. No other treatment (fibrinogen or dextran 100µg/mL) provoked differential gene expression on these genes. Of the 10 genes whose expression was assessed, 5 were not affected by the LPS treatment (or any other treatment). From the remaining 5, only Iba1 (Aif1) was downregulated when cells were stimulated with LPS.

Next, the gene expression of genes related to the M1 and/or M2 activation states was investigated in BV2 cells. Table 5-4 shows a list of cell markers which are associated with M1 and M2 activation states. This table shows results of analysis for the LPS treatment alone. Fibrinogen and dextran 100µg/mL had very little effect on gene expression of these M1/M2 cell markers. Fibrinogen only affected expression of 3 M1-related genes: H2-M2, Cd40 and TNF (all upregulated at 6h hours). Meanwhile, dextran sulphate 100µg/mL affected gene expression of 1 M1-related gene (IL6, downregulated at 24h) and 1 M2-related gene (VEGF(a), upregulated at 48h).

Table 5-4 Cell markers related to M1 or M2 activation states (LPS treatment)

Activation State	Cell Marker	Differ. Expressed	Timepoint		
			6h	24h	48h
M1	***MHCII (H2- family)***	Yes*	Upregulated	Upregulated	Upregulated
	CD40	Yes*	Upregulated	Upregulated	Upregulated
	IL1b	Yes	Upregulated	Upregulated	Upregulated
	IL6	Yes	Upregulated	Upregulated	Upregulated
	TNF	Yes	Upregulated	Upregulated	Upregulated
	IL18	Yes	Upregulated	-	-
	CCL2	Yes	Upregulated	Upregulated	Upregulated
	Cd80	No	-	-	-
	Il23	No	-	-	-
	Cd86	No	-	-	-
	Il12	Not passed QC	-	-	-
M2	***VEGF(a)***	Yes	-	-	Upregulated
	EGF	No	-	-	-
	TGFβ	No	-	-	-
	PDGF	No	-	-	-
	Il10	Not passed QC	-	-	-
	Arg1	Not passed QC	-	-	-

*** in top-5 differentially expressed genes**

As shown in Table 5-4, LPS treatment upregulates many M1-related genes at most timepoints and just one M2-related gene. From the upregulated genes, MHCII and CD40 genes were found among the top-5 differentially expressed genes for the whole of the experiment, highlighting their importance in the microglial response to LPS.

5.3.6 Differential expression of AD-related genes in response to LPS, dextran sulphate and fibrinogen

After studying the M1/M2 activation markers, the analysis focused on Alzheimer's disease related genes. In a recent paper, Karch et al. (2014) compiled a list of 31 genes which have been associated with AD risk. These 31 genes were analysed in the context of our experiment. Table 5-5 shows the results of this analysis for all treatments (without considering any particular timepoint).

Table 5-5 Differential gene expression of 31 AD-related genes

Name of Gene (mouse orthologue)	Present in Chip/Detected	Treatment effect
APP	Yes	***Upregulated by LPS***
APOE	Yes	***Downregulated by LPS Downregulated by Dextran 100µg/mL***
CD33	Yes	***Downregulated by LPS Downregulated by Fibrinogen***
CELF1 (CUGBP)	Yes	***CUGBP1 Upregulated by LPS CUGBP2 Downregulated by LPS***
MS4A6A (MS4A6D)	Yes	***MS4A6D Upregulated by LPS MS4A7A Upregulated by LPS MS4A7A Downregulated Fibrinogen***
INPP5D	Yes	***Downregulated by LPS***
MEF2C	Yes	
TREM2	Yes	
BIN1	Yes	*Downregulated by Dextran 100µg/mL*
PLD3	Yes	
RIN3	Yes	
PICALM	Yes	*Upregulated by Dextran 100µg/mL*
PTK2B	Yes	
ABCA7	Yes	*Not differentially expressed*
CASS4	Yes	
DSG2	Yes	
PSEN2	Yes	
SORL1	Yes	
ZCWPW1	Yes	
CR1 (Crry)	Yes	*Not passed QC*
PSEN1	Yes	
ADAM10	Not detected	-
CD2AP	Not detected	-
EPHA1	Not detected	-
FERMT2	Not detected	*Fermt3 Downregulated by Dextran 100µg/mL*
HLA-DRB5/HLA-DRB1 (H2-Eb1/H2-Eb1)	Not detected	*5 genes of H2-family Upreg. by LPS 1 gene of H2-family Upreg. by Fibrinogen*
MADD	Not detected	-
SLC24A4	Not detected	-
CLU	Not in the chip	-
NME8	Not in the chip	-
NYAP1	Not in the chip	-

As shown in Table 5-5, LPS can cause differential expression in as many as 8 genes (APP, APOE, CD33, CELF1 (CUGBP), INPP5D, MEF2C and *TREM2*) out of the 32 AD-related genes. Likewise, dextran sulphate 100μg/mL affected the expression of up to 6 genes (APOE, BIN1, PLD3, RIN3, PICALM and PTK2B) and fibrinogen only 1 gene (CD33). For individual gene expression profiles of AD-related genes see Supplementary Fig. 7.6.

Besides the 8 genes differentially expressed by LPS, 2 more genes (HLA-DRB5/HLA-DRB1 and MS4A6A) can be considered as affected by this treatment as other members of their same gene family were disrupted (Table 5-5). Similar observations were made for dextran sulphate and fibrinogen treatments (Table 5-5).

Additionally, analysis of the 31 AD-related genes revealed that many of them (7 in total) seem not to be expressed in microglial cells (Not detected) indicating that maybe they are expressed in other brain cell types. Similarly, 3 genes of the list were not included in the microarray (Not in microarray) and their involvement in microglial response to our treatments remains to be elucidated.

5.3.7 **Validation of *ApoE* and *Trem2* gene expression profiles by RT-qPCR**

Microarray data was validated by RT-qPCR in a new set of experiments. Validation of results was performed in a new set of five independent experiments (n=5) for two genes; *ApoE* and *Trem2*. Analogous to the microarray results, RT-qPCR analysis of these two genes showed a marked downregulation of their expression by the LPS treatment, reaching statistical significance at 48h in both cases (Figure 5.7, panels A and B). These results validate what was found in the microarray expression experiment and show that the same trends were replicated in a new set of experiments. Furthermore, RT-qPCR analysis found that fibrinogen could also modify ApoE gene expression, after 24h.

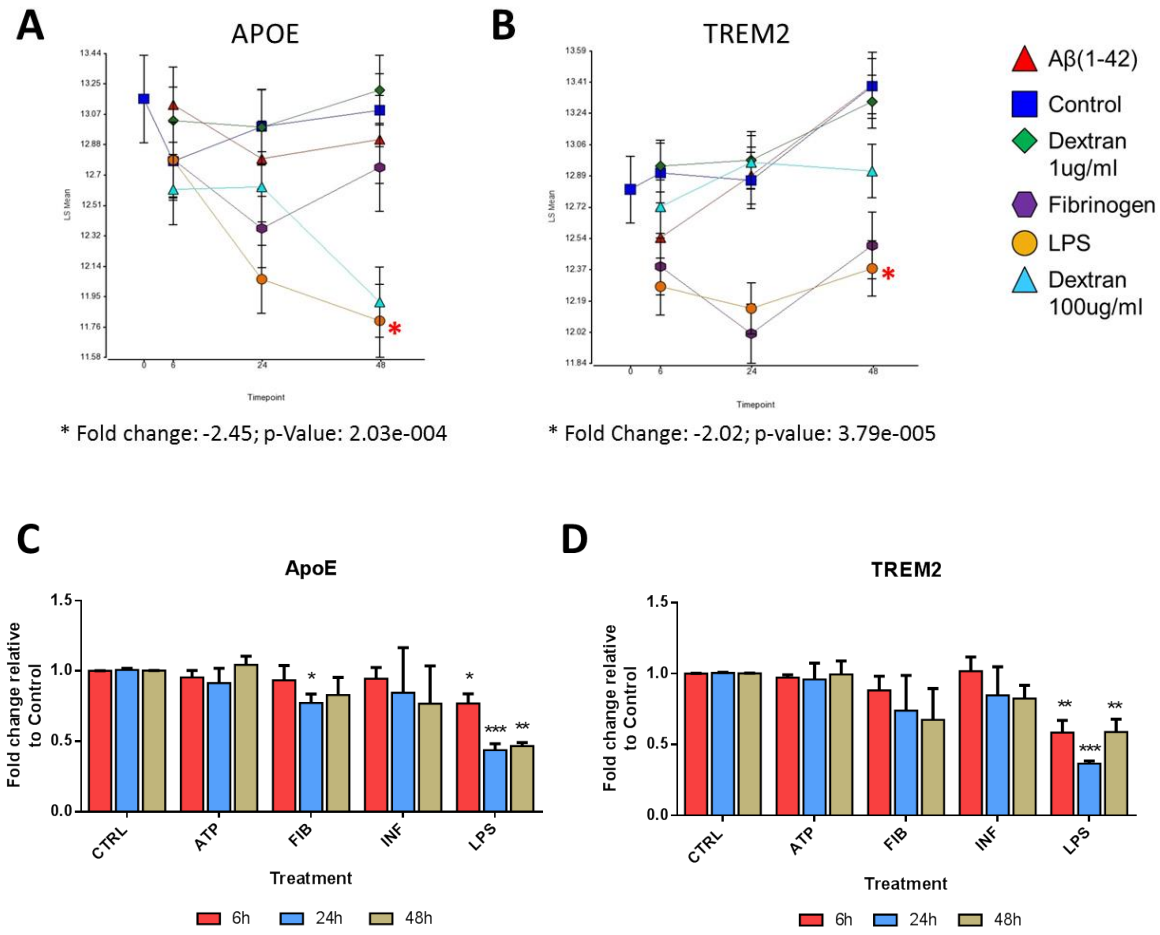

Figure 5.7 qPCR validation of *ApoE* and *Trem2* expression profiles in BV2 cells. Panels (A) and (B) show the gene expression profiles obtained from the microarray analysis using Partek Genomics Suite 6.6 (Interaction Plots) for *ApoE* and *Trem2* respectively. For panels A and B, results represent mean ± SD of three independent experiments (n=3). Asterisks (*) indicate which timepoints reached statistical significance, p-Values and fold change are shown below each panel. Panels (C) and (D) show the gene expression profiles obtained from the qPCR validation for *ApoE* and *Trem2* respectively. For panels C and D, results represent mean ± SD of five independent experiments (n=5). Statistical differences were calculated by 2-way ANOVA with Dunnett's correction for multiple comparisons, *p<0.05, **p<0.01, ***p<0.001.

5.4 RNAseq analysis of microglial activation states (M1, M2 or other) in BV2 cells

For this experiment, RNAseq was chosen for the analysis and comparison of the BV2 immune response to different microglial activators (M1 and M2) and Aβ1-42 species (monomers and oligomers). RNA sequencing has been shown to have many advantages over microarrays, including a higher sensitivity and wider dynamic range (Zhao et al., 2014).

Initially, the experiment focused on identifying the stimuli and dosages that modified the expression of genes linked to M1 and M2 activation. As such, dose response curves were prepared using known microglial activators: LPS, IL4, IL10 and TGFβ.

5.4.1 **Dose response curves for LPS, IL4, IL10 and TGFβ**

BV2 cells were seeded as per usual in 6-well plates (80 000cells/well) and left to rest for 24h before stimulation. After this, cells were stimulated with the aforementioned activators at a range of concentrations (from 0.1ng/mL to 1000ng/mL) and left for 6h before cell lysis and total RNA extraction. Dose response curves for the two Aβ1-42 species used in this experiment (oligomers and monomers) were not prepared, as the appropriate doses were obtained from previously published work by Zheng et al. (2016).

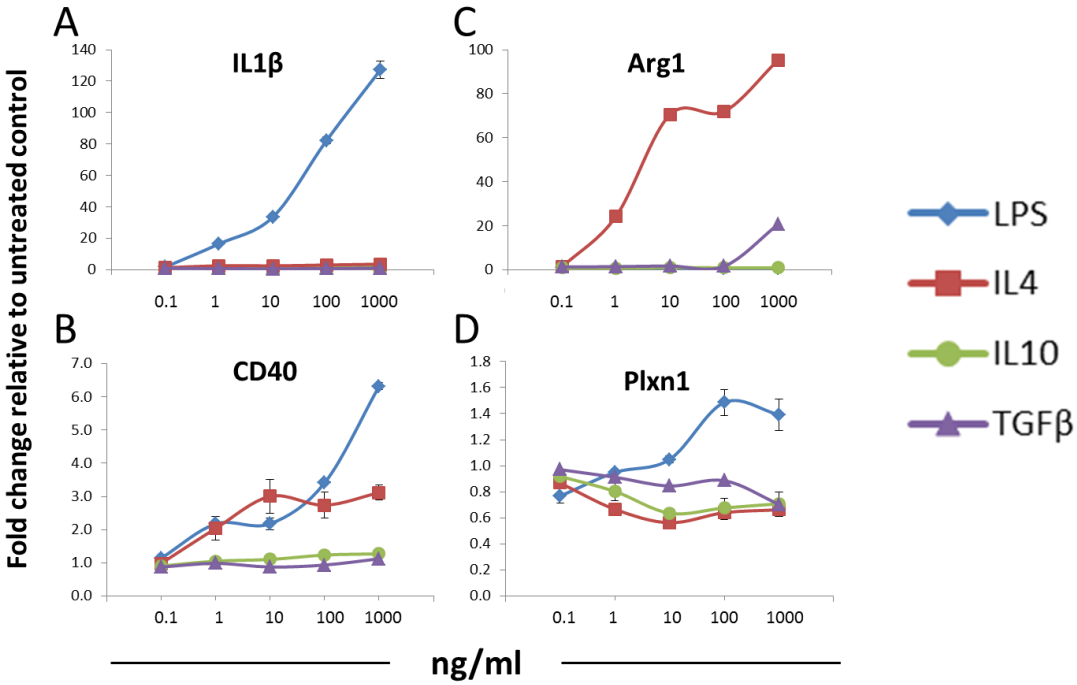

Figure 5.8 Dose-response curves for microglial activators M1 (LPS) and M2 (IL4, IL10 and TGFβ). BV2 cells were used to make dose-response curves for gene expression changes after stimulation with M1 and M2 microglial activators. BV2 cells were treated for 6 hours with the aforementioned stimulators at different concentrations (0.1ng/mL to 1000ng/mL) before lysating the cells for RNA extraction. Gene expression changes for **(A)** *IL1ß* **(B)** *Cd40* **(C)** *Arg1* and **(D)** *Plxn1* are shown**.** Ct values for each gene were normalised according to Table 2 8**.** Gene expression is expressed as fold change relative to the untreated control. Results represent mean ± SD of 3 technical replicates of a single experiment (n=1).

As shown in Figure 5.8, gene expression changes were evaluated in 4 genes (*IL1β, CD40, Arg1* and *Plxn1*) as a result of the BV2 stimulation with LPS, IL4, IL10 and TGFβ. For the dose response curves, *IL1β* was used as a marker of M1 activation. This gene had a clear increase in its expression in almost all the LPS concentrations assayed, being 1000ng/mL the dose which induced the highest upregulation of *IL1β*. As it was expected none of the M2 associated stimuli (IL4, IL10 and TGFβ) increased the expression of *IL1β* as dramatically as LPS. There were concerns in our group about the over-stimulation of BV2 cells with LPS (in our microarray experiment LPS was used at a concentration of 1000ng/mL). As a result, and considering the dose response curve

results, LPS was used at a concentration 100ng/mL (10 times lower than in our microarray experiment) for the RNAseq experiments. As observed in the microarray experiment, *Cd40* (another M1 marker) was among the top-5 differentially expressed genes by LPS treatment. Consequently, its expression was evaluated in the dose response curves. As expected, LPS stimulation had a dose dependent increase in its expression. Startlingly, an increase in the gene expression of *Cd40* in response to IL4 stimulation was observed, pointing to a more complex role of *Cd40* in BV2 activation. IL10 and TGFβ, on the other hand, had no effect over *Cd40* expression.

Arg1 is a typical marker for M2 activation in microglia/macrophages (Tang and Le, 2016). In our experiment, its expression had a dose dependent response to IL4, but not IL10 or TGFβ, the other M2 activators. Nevertheless, TGFβ could induce a modest change (compared to IL4) on the expression of *Arg1* at its highest concentration (1000ng/mL). Inconspicuously, there was no response to the LPS treatment. At this point, it was noticed that IL10 did not have any effect on M1 or M2 classical markers, reason why it was not used as stimulus in the RNAseq experiments. Using the data generated in this experiment, it will be worth to check the expression levels of the IL10 receptors in BV2 cells. The effect of the different M1 and M2 stimuli on the expression of *Plxna1*, a gene known to directly interact with *Trem2 (Takegahara et al., 2006)*, was also evaluated. As seen in Figure 5.8, the expression of this gene was slightly increased by LPS and was generally downregulated by M2 activators.

Considering the results seen during the dose response experiment, all stimuli used for the RNAseq experiment (LPS, IL4 and TFGβ) were used at a concentration of (100ng/mL). In this same experiment, the expression changes of other microglia-related genes (*Tnf, Trem2, ApoE, Dap12, CD33* and *Actin*) was also evaluated. For this part of the experiment only 3 stimuli were used; LPS, IL4 and IL10.

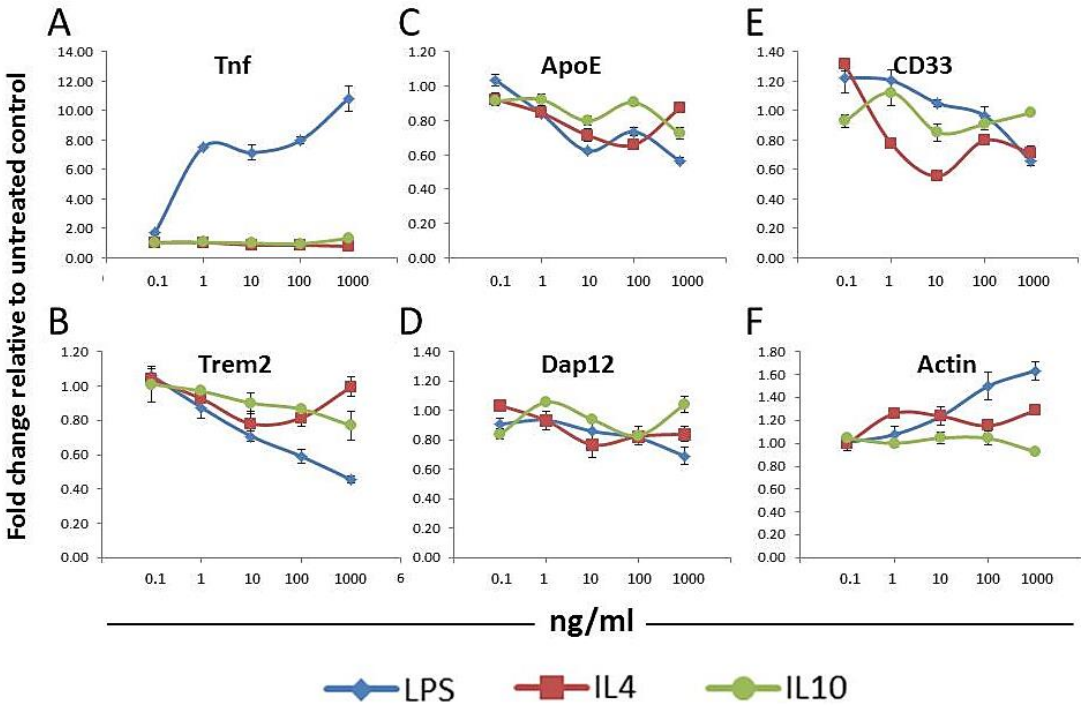

Figure 5.9 Dose-response curves of microglial activators M1 (LPS) and M2 (IL4 and IL10). Dose-response relationships for gene expression changes after stimulation with M1 and M2 microglial activators. BV2 cells were treated for 6 hours with the aforementioned stimulators at different concentrations before cell lysis and total RNA extraction. Gene expression changes for (A) *Tnf*; (B) *Trem2*; (C) *ApoE*; (D) *Dap12*; (E) *Cd33* and (F) *Actin* (*Actb*) are shown. Ct values for each gene were normalised according to **Table 2-8**.Gene expression is expressed as fold change relative to the untreated control. Results represent mean ± SD of 3 technical replicates of a single experiment (n=1).

As seen in Figure 5.9, gene expression changes in many microglia-related genes were evaluated in response to stimulation with different M1 and M2 activators. *Tnf* is a marker of M1 activation, and in our experiment its expression had a response that was dose dependent only for the LPS treatment (Figure 5.9, panel A). All other treatments showed no effect on its expression. The next gene studied was *Trem2*, its expression was modestly downregulated by IL4 and IL10. *Trem2* downregulation was less than 20% even at IL4's and IL10's highest concentrations. LPS, on the other hand, was able to downregulate *Trem2*'s expression in a dose-dependent manner. LPS reduced *Trem2* expression by 60% at the highest concentration used (1000ng/mL) (Figure 5.9, panel B). Downregulation of *TREM2* by LPS (and other classically pro-inflammatory molecules) has been reported previously (Jay et al., 2017), and it is probably associated with *TREM2´*s anti-inflammatory role. Several *in vitro* and *in vivo* studies have shown that TREM2 has an anti-inflammatory role in certain contexts. *TREM*2 deficient cell lines show higher levels of pro-inflammatory mediators (iNOS, TNFα, IL1β and IL6) in response to apoptotic neuronal membrane components and TLR ligands including LPS and Aβ42 (reviewed by Jay et al. (2017)). Conversely, classically anti-inflammatory molecules (such as vasoactive intestinal peptide and IL4) increase *TREM2* expression.

These results suggest that *TREM2* expression is dependent on the immune activation state of cells in response to pro- and anti-inflammatory stimuli.

ApoE expression did not seem to be greatly affected by IL4, IL10 or LPS stimulations, although both IL10 and LPS seemed to downregulate its expression (Figure 5.9, panel C). *Dap12* expression did not seem to be affected by any of the treatments, with expression values similar to those of the unstimulated control (Figure 5.9, panel D). *Cd33* expression was downregulated in dose dependent manner by both LPS and IL4. LPS downregulation of *Cd33* was clearly dose dependent, while IL4 downregulation plateaued at 10ng/mL. IL10 did not have any noticeable effect on *Cd33* expression (Figure 5.9, panel E). Finally, *Actin* gene (*Actb*) expression was not affected by either IL4 or IL10, but was upregulated by LPS in a dose dependent manner (Figure 5.9, panel F).

As shown in Figure 5.9, IL4, IL10 and LPS had different effects on the expression of microglia-associated genes. As expected, *Tnf* was only upregulated by LPS (M1) in a dose dependent manner. On the other hand, *Trem2* was downregulated by LPS (and IL10 to a lesser extend). All other genes had less clear responses to the stimuli used, although some trends in expression were noticeable (like in the case of *Actin* upregulation by LPS stimulation).

5.4.2 **Characterization of the different Aβ1-42 conformations by TEM (Transmission electron microscopy)**

AD is characterised pathologically by the formation of amyloid plaques and neurofibrillary tangles (Selkoe, 2001). The main components of the amyloid plaques are the fibrillar aggregates of Aβ peptides (39-43 amino acids) which are produced as a result of the of the enzymatic proteolysis of the APP protein (Shoji et al., 1992). The Aβ cascade hypothesis, suggests that oligomeric and fibrillar forms of these peptides are central to the pathogenesis and degeneration in AD (Selkoe, 1994, Hardy and Higgins, 1992). However, the precise role of Aβ in AD has yet to be clarified. Although there is a great body of literature that supports a central role for Aβ aggregation in AD pathogenesis, the debate is still very much open (Benilova et al., 2012).

Appropriate characterization of the different Aβ1-42 conformations used for experimentation was of great importance in this study. Jan et al. (2010) proposed the use of TEM for the morphological characterization of various Aβ1-42 conformations prepared using different protocols. This method was employed for the characterization of the Aβ1-42 monomeric, oligomeric and fibrillar preparations used in this study.

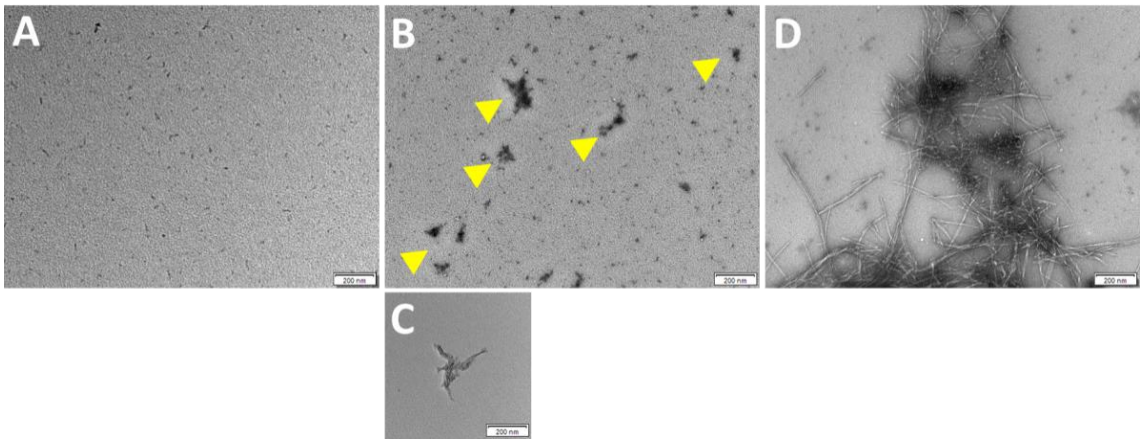

Figure 5.10 Morphological characterization of the different Aβ1-42 conformations used for the activation of BV2 cells using TEM. Representative TEM images of (A) monomeric, (B and C) oligomeric and (D) fibrillar Aβ1-42 preparations used for BV2 stimulation. Yellow arrowheads indicate oligomeric aggregates in panel B. Images are representative of 2 different Aβ1-42 batches (monomeric preparations) scale bar, 200nm.

Figure 5.10 shows the morphological characterization of the different Aβ1-42 conformations used in our BV2 activation experiments (RNAseq). As it is expected from monomeric Aβ1-42 preparations, it was not possible to detect any aggregates (Figure 5.10, panel A). Oligomeric preparations on the other hand showed structures of 5-200nm (Figure 5.10, panel B and C), which is consistent with high molecular weight metastable Aβ oligomers (protofibrils). Finally, Fibrillar preparations showed rod-like structures that were mainly >1μm in length and 8-12nm in diameter. These results are in accordance with what was described by Jan et al. (2010).

5.4.3 **Normalization and quality control of the RNA sequencing results**

BV2 WT cells (unmodified) were exposed to 6 different conditions under serum-free conditions; 1) untreated control (no stimulus), 2) IL4 100ng/mL, 3) LPS 100ng/mL, 4) Aβ1-42 monomers 500nM, 5) Aβ1-42 oligomers 500nM and 6) TGFβ 100ng/mL. Total mRNA was recovered from the stimulated cells at 6h, 24h and 48h after treatment. This experiment was repeated 3 times (n=3) using the same study design. RNA samples from the 3 biological repeats were prepared and sent together for RNAseq analysis by AROS Applied Biotechnology (described in Sections 2.6.1 and 2.6.2).

After RNA sequencing by AROS Applied Biotechnology, raw reads were sent back to us for analysis (fastq files). Raw sequencing results were normalised and quality control examined. After QC, 12 188 genes (out of all the genes in the Ensembl 86 reference) were included in the analysis. PCA analysis was used to identify outliers and to visualize the clustering of all samples; Partek® Flow™ software was used for this step.

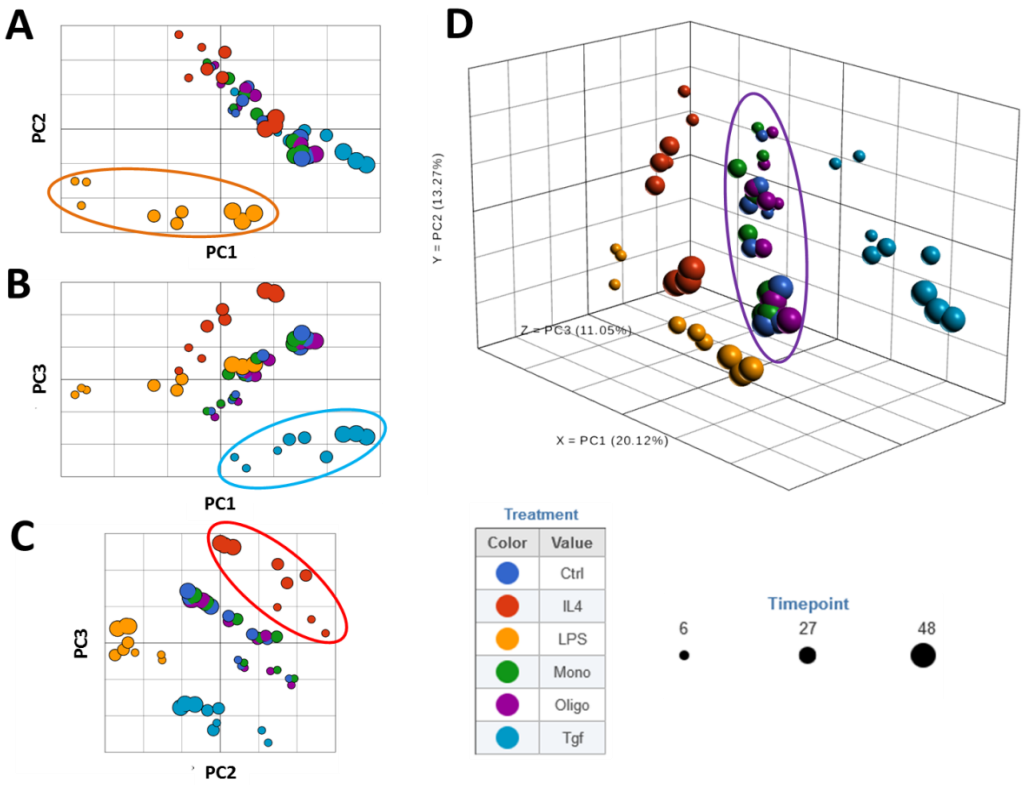

Figure 5.11 PCA scatter plot of RNAseq data – Effect of different M1 and M2 activators on BV2 activation. PCA was used to identify outliers and to visualize the clustering of all sequenced samples. Panels **A**, **B** and **C** show 2D representations of PC1 vs PC2, PC1 vs PC3 and PC2 vs PC3, respectively. Panel **D** shows a 3D representation of the 3 main PCs. No samples were excluded as a result of this analysis and it was possible to distinguish some clustering of samples. The orange oval in panel A highlights clustering of LPS (100ng/mL) treated cells. The sky-blue oval in panel B highlights clustering of TGFβ (100ng/mL) treated samples, the red oval highlights clustering of IL4 (100ng/mL) treated samples. Apart from those three well defined clusters all other samples – including Aβ1-42 oligomers (500nM), Aβ1-42 monomers (500nM) and untreated controls – were mixed up together third cluster, purple oval in panel D.

Figure 5.11 shows the PCA scatter plot of all samples submitted for RNA sequencing. Samples are coloured according to their treatment and the sizes of the spheres represent the different timepoints of each treatment. The Scatter plot already shows some clusters of samples which group according to the treatment used, that is the case LPS (orange oval in panel A), TGFβ (sky blue oval, panel B) and IL4 (red oval, Panel C). The rest of the samples (control, monomeric and oligomeric groups) were clustered together in a bigger group of samples with no obvious difference among them (purple oval, panel D). Sphere sizes also allowed us to distinguish clustering of samples according to their timepoint (within a same treatment). After, PCA none of the samples was discarded.

5.4.4 Identification of Differentially Expressed (DE) genes and generation of gene lists

Multi-factor ANOVA was used for the identification of differentially expressed (DE) genes. Statistical analysis was done using Partek® Flow™. The number of biological replicate (repeat or batch), timepoint, treatment and the interaction between timepoint and

treatment (treatment x timepoint) were used as the main sources of variation. Additionally, 18 contrasts (comparisons among samples) were set up to compare gene expression changes across treatments and timepoints (as shown in Table 5-6).

Table 5-6 Contrasts used for the multi-factor ANOVA – RNAseq Microglial activation experiment

	Control, 6h	Control, 24h	Control, 48h
Control, 6h			
Aβ monomers 500nM, 6h	**X**		
Aβ oligomers 500nM, 6h	**X**		
LPS 100ng/ml, 6h	**X**		
IL4 100ng/ml, 6h	**X**		
TGFβ 100ug/ml, 6h	**X**		
Control, 24h	**X**		
Aβ monomers 500nM, 24h		**X**	
Aβ oligomers 500nM, 24h		**X**	
LPS 100ng/ml, 24h		**X**	
IL4 100ng/ml, 24h		**X**	
TGFβ 100ug/ml, 24h		**X**	
Control, 48h	**X**	**X**	
Aβ monomers 500nM, 48h			**X**
Aβ oligomers 500nM, 48h			**X**
LPS 100ng/ml, 48h			**X**
IL4 100ng/ml, 48h			**X**
TGFβ 100ug/ml, 48h			**X**

Similar to the microarray experiment, each treatment was compared to its own control (untreated) for each timepoint. In the same way, all control samples (across timepoints) were compared with each other to investigate if gene expression wavered with time (timepoint).

Gene lists were created using a conservative FDR of 0.01 and a minimum fold change of ±1.5. Only 12 gene lists were generated (out of the 18 contrasts) as none of the treatments which involved either Aβ1-42 monomers or oligomers produced differentially expressed genes; except for Monomers at 6h which had Hapln3 as its only differentially expressed gene (downregulated). Considering this, less astringent conditions were used for the benefit of the Aβ1-42 treatments. The new conditions were FDR of 0.05 and a minimum fold change of ±1.5. Again, neither Aβ1-42 monomers nor oligomers generated lists of differentially expressed genes (again the exception was monomers at 6h which conserved Hapln3 as the only differentially expressed gene). This agrees with the results

obtained in section 5.3.3 of this thesis, where Aβ1-42 fibrils were not capable of inducing a response from BV2 cells.

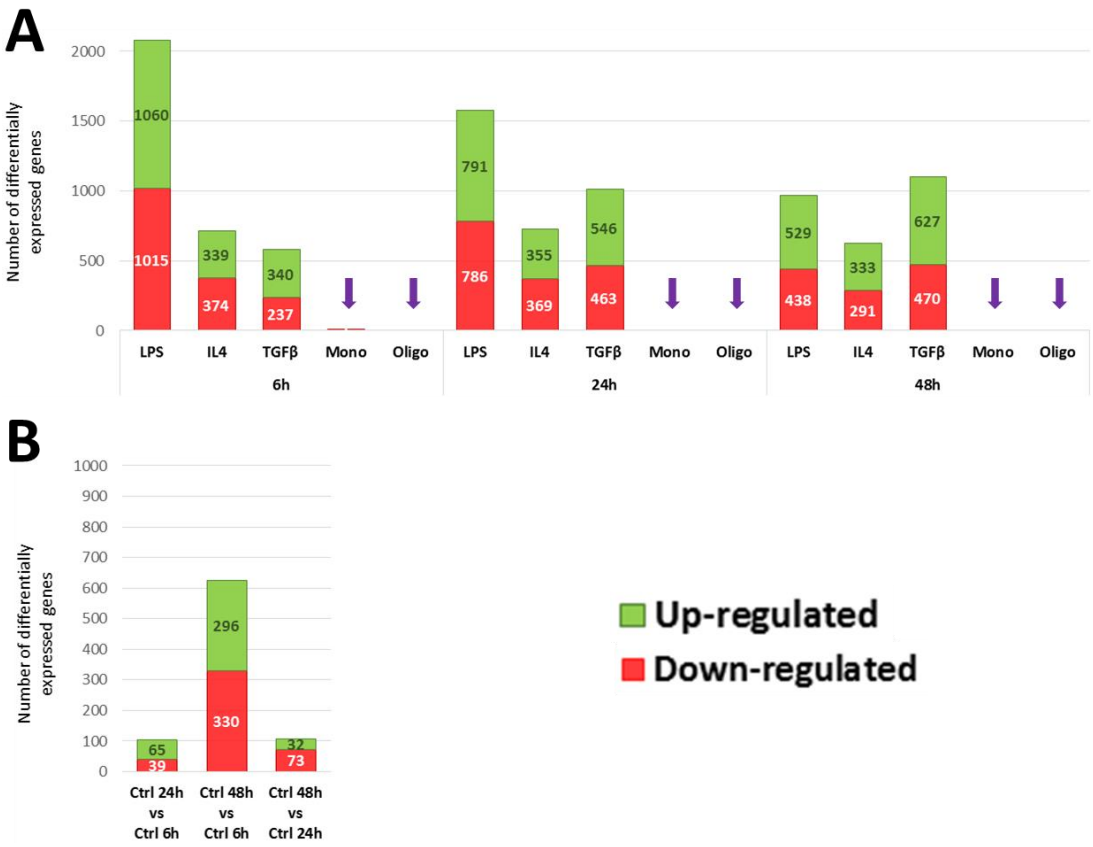

Figure 5.12 Number of differentially expressed genes - RNAseq *Trem2* deficiency effect on microglial activation. Following the ANOVA analysis, lists of differentially expressed genes were obtained. These lists were composed of genes whose expression was affected by any of the 5 treatments assayed: LPS (100ng/mL), IL4 (100ng/mL), TGFβ (100ng/mL) and Aβ1-42 monomers or oligomers (500nM) for 6h, 24h and 48hrs. **A)** Shows the number of differentially expressed genes per condition (treatment) and per timepoint compared to the control sample for its correspondent timepoint. Purple arrows indicate those treatments which did not generate lists of differentially expressed genes. **B)** Shows the number of differentially expressed genes in control samples at different timepoints.

Figure 5.12, panel A shows the number of differentially expressed genes for the 5 different (LPS, IL4, TGFβ, Aβ1-42 monomers and Aβ1-42 oligomers) at different timepoints. As mentioned before, none of the Aβ1-42 treatments (monomers or oligomers) generated lists of differentially expressed genes (indicated in panel A with purple arrows), the only exception being monomers at 6h which had 1 differentially expressed gene (Hapln3, downregulated). All the other treatments generated differentially expressed genes lists. A curious observation is the fact that the number of downregulated genes (red background) and the number of upregulated genes (green background) is almost the same (a 50-50% split) for each of the lists of differentially expressed genes.

As seen in Figure 5.12, panel A, the number of differentially expressed genes as a result of LPS stimulation was gradually lowered (2075>1577>967) as time passed (different timepoint) pointing to a resolution of inflammation in BV2 cells. Typically, inflammatory responses are divided in three phases: 1) inflammation, 2) resolution and 3) post-resolution. The inflammation phase is usually acute and finishes when the effector cells neutralize the inciting stimuli (usually within hours of the initial stimulation). The resolution phase is generally a longer process, taking between some hours to a couple of days. During this time cells remove the inflammatory stimuli (i.e. bacteria, LPS, etc.), remove death cells and debris and suspend the synthesis of pro-inflammatory mediators. The resolution phase serves to restore the functional homeostasis of the cells or tissue. Finally, the post-resolution phase serves as a bridge between innate and adaptive immunity (Fullerton and Gilroy, 2016). The reduction in the number of differentially expressed genes in our experiment points towards an attempt to return to the initial homeostatic state by suspending the expression of pro-inflammatory proteins and pathways. It should also be considered that the lowering of the effect of LPS in the BV2 transcriptional programme could be the result of phagocytic clearance of LPS as part of the resolution phase.

Meanwhile the number of differentially expressed genes by IL4 remained almost at the same levels throughout the experiment (between 724 and 624). For TGFβ, the number of differentially expressed genes increased as time went by (577<724<1097). These results demonstrate that all the treatments used in this experiment not only have varied effects on microglial expression but also have different temporal dynamics.

Figure 5.12, panel B shows the number of differentially expressed genes in control samples at different timepoints. As the panel shows, there were only 104 differentially expressed genes between the 24h control to 6h control. Similarly, there were only 105 differentially expressed genes between 48h control and 24h control. The largest number of differentially expressed genes, 626, was obtained when the 48h control was compared with the 6h control. This large number of differentially expressed genes suggests that BV2 cells experiment important changes in their gene expression programmes when they are kept in culture for longer times.

5.4.5 **Identification of enriched biological pathways – GO and Pathway analysis**

The ToppFun tool from the Toppgene suite (available at https://toppgene.cchmc.org/) was used for the identification of enriched GO categories and pathways in the generated gene lists of differentially expressed genes. Conditions of analysis were left as default and a FDR B&H (Benjamine-Hochberg) value of <0.05 was considered as statistically

significant for our analysis. Only the top-5 GO categories and pathways are shown for each gene list (condition), unless indicated differently.

1: GO: Molecular Function [Display Chart] 1771 annotations before applied cutoff / 18661 genes in category

	ID	Name	Source	pValue	FDR B&H	FDR B&Y	Bonferroni	Genes from Input	Genes in Annotation
1	GO:0030554	adenyl nucleotide binding		1.433E-7	1.442E-4	1.162E-3	2.538E-4	112	1530
2	GO:0032559	adenyl ribonucleotide binding		1.737E-7	1.442E-4	1.162E-3	3.076E-4	111	1518
3	GO:0005524	ATP binding		2.442E-7	1.442E-4	1.162E-3	4.325E-4	108	1475
4	GO:0008017	microtubule binding		3.809E-7	1.686E-4	1.359E-3	6.745E-4	28	214
5	GO:0015631	tubulin binding		3.338E-6	1.182E-3	9.525E-3	5.911E-3	32	293

Show 36 more annotations

2: GO: Biological Process [Display Chart] 7077 annotations before applied cutoff / 18623 genes in category

	ID	Name	Source	pValue	FDR B&H	FDR B&Y	Bonferroni	Genes from Input	Genes in Annotation
1	GO:0000278	mitotic cell cycle		2.571E-19	1.820E-15	1.718E-14	1.820E-15	113	1016
2	GO:0006955	immune response		9.900E-19	3.503E-15	3.307E-14	7.006E-15	149	1572
3	GO:0006954	inflammatory response		1.485E-18	3.503E-15	3.307E-14	1.051E-14	89	711
4	GO:1903047	mitotic cell cycle process		2.066E-18	3.655E-15	3.451E-14	1.462E-14	105	931
5	GO:0006952	defense response		3.480E-17	4.926E-14	4.651E-13	2.463E-13	150	1651

Show 45 more annotations

3: GO: Cellular Component [Display Chart] 685 annotations before applied cutoff / 19061 genes in category

	ID	Name	Source	pValue	FDR B&H	FDR B&Y	Bonferroni	Genes from Input	Genes in Annotation
1	GO:0005819	spindle		2.635E-11	1.805E-8	1.283E-7	1.805E-8	43	308
2	GO:0005876	spindle microtubule		5.610E-10	1.922E-7	1.366E-6	3.843E-7	17	60
3	GO:0000779	condensed chromosome, centromeric region		9.996E-10	2.282E-7	1.622E-6	6.847E-7	22	105
4	GO:0000922	spindle pole		4.225E-9	7.236E-7	5.143E-6	2.894E-6	24	133
5	GO:0000793	condensed chromosome		1.261E-8	1.505E-6	1.070E-5	8.638E-6	30	208

7: Pathway [Display Chart] 2240 annotations before applied cutoff / 12450 genes in category

	ID	Name	Source	pValue	FDR B&H	FDR B&Y	Bonferroni	Genes from Input	Genes in Annotation
1	138080	Aurora B signaling	BioSystems: Pathway Interaction Database	8.748E-13	1.960E-9	1.625E-8	1.960E-9	17	39
2	1269820	Mitotic Prometaphase	BioSystems: REACTOME	1.082E-10	1.212E-7	1.005E-6	2.424E-7	25	111
3	812256	TNF signaling pathway	BioSystems: KEGG	3.444E-10	2.263E-7	1.877E-6	7.715E-7	24	108
4	82973	Glutathione metabolism	BioSystems: KEGG	4.042E-10	2.263E-7	1.877E-6	9.054E-7	17	54
5	1269310	Cytokine Signaling in Immune system	BioSystems: REACTOME	9.223E-10	4.132E-7	3.426E-6	2.066E-6	77	763

Figure 5.13 RNAseq experiment - Top-5 most significant GO and Pathway categories - LPS treated samples, 48h. Representative image of the GO and pathway analysis for LPS treated samples. Lists of genes were submitted to the ToppFun online tool (part of the Toppgene Suite) to perform enrichment analysis.

1: GO: Molecular Function [Display Chart] 1946 annotations before applied cutoff / 18661 genes in category

	ID	Name	Source	pValue	FDR B&H	FDR B&Y	Bonferroni	Genes from Input	Genes in Annotation
1	GO:0038024	cargo receptor activity		1.565E-8	3.046E-5	2.483E-4	3.046E-5	18	71
2	GO:0001618	virus receptor activity		3.016E-6	2.780E-3	2.266E-2	5.869E-3	15	71
3	GO:0005102	receptor binding		4.285E-6	2.780E-3	2.266E-2	8.339E-3	124	1601
4	GO:0005044	scavenger receptor activity		2.258E-5	1.098E-2	8.953E-2	4.394E-2	11	47
5	GO:0005096	GTPase activator activity		3.287E-5	1.103E-2	8.989E-2	6.397E-2	32	283

Show 24 more annotations

2: GO: Biological Process [Display Chart] 7410 annotations before applied cutoff / 18623 genes in category

	ID	Name	Source	pValue	FDR B&H	FDR B&Y	Bonferroni	Genes from Input	Genes in Annotation
1	GO:0006955	immune response		3.170E-20	2.349E-16	2.228E-15	2.349E-16	170	1572
2	GO:0016477	cell migration		9.635E-16	3.570E-12	3.387E-11	7.139E-12	138	1300
3	GO:0040011	locomotion		2.597E-15	4.427E-12	4.200E-11	1.924E-11	168	1735
4	GO:0048870	cell motility		2.987E-15	4.427E-12	4.200E-11	2.213E-11	146	1428
5	GO:0051674	localization of cell		2.987E-15	4.427E-12	4.200E-11	2.213E-11	146	1428

Show 45 more annotations

3: GO: Cellular Component [Display Chart] 736 annotations before applied cutoff / 19061 genes in category

	ID	Name	Source	pValue	FDR B&H	FDR B&Y	Bonferroni	Genes from Input	Genes in Annotation
1	GO:0005764	lysosome		4.155E-15	1.529E-12	1.098E-11	3.058E-12	75	539
2	GO:0000323	lytic vacuole		4.155E-15	1.529E-12	1.098E-11	3.058E-12	75	539
3	GO:0005773	vacuole		4.774E-14	1.171E-11	8.408E-11	3.513E-11	126	1223
4	GO:0043202	lysosomal lumen		1.402E-12	2.581E-10	1.853E-9	1.032E-9	25	88
5	GO:0009897	external side of plasma membrane		2.566E-12	3.777E-10	2.712E-9	1.889E-9	49	310

7: Pathway [Display Chart] 2426 annotations before applied cutoff / 12450 genes in category

	ID	Name	Source	pValue	FDR B&H	FDR B&Y	Bonferroni	Genes from Input	Genes in Annotation
1	99052	Lysosome	BioSystems: KEGG	1.202E-14	2.916E-11	2.441E-10	2.916E-11	34	123
2	1457780	Neutrophil degranulation	BioSystems: REACTOME	8.761E-9	1.063E-5	8.896E-5	2.125E-5	62	492
3	153910	Phagosome	BioSystems: KEGG	7.803E-8	6.310E-5	5.283E-4	1.893E-4	28	154
4	1269203	Innate Immune System	BioSystems: REACTOME	1.295E-7	7.856E-5	6.577E-4	3.142E-4	122	1312
5	MAP00531 Glycosaminoglycan degradation	MAP00531 Glycosaminoglycan degradation	GenMAPP	2.448E-7	1.188E-4	9.942E-4	5.938E-4	7	10

Figure 5.14 RNAseq experiment - Top-5 most significant GO and Pathway categories - TGFβ treated samples, 48h. Representative image of the GO and pathway analysis for TGFβ treated samples. Lists of genes were submitted to the ToppFun online tool (part of the Toppgene Suite) to perform enrichment analysis.

1: GO: Molecular Function [Display Chart] 1414 annotations before applied cutoff / 18661 genes in category

	ID	Name	Source	pValue	FDR B&H	FDR B&Y	Bonferroni	Genes from Input	Genes in Annotation
1	GO:0004896	cytokine receptor activity		8.928E-9	1.262E-5	9.887E-5	1.262E-5	16	90
2	GO:0005102	receptor binding		8.767E-7	6.198E-4	4.854E-3	1.240E-3	82	1601
3	GO:0008329	signaling pattern recognition receptor activity		6.435E-6	2.275E-3	1.781E-2	9.099E-3	6	17
4	GO:0038187	pattern recognition receptor activity		6.435E-6	2.275E-3	1.781E-2	9.099E-3	6	17
5	GO:0042287	MHC protein binding		2.865E-5	7.927E-3	6.208E-2	4.052E-2	7	31

Show 6 more annotations

2: GO: Biological Process [Display Chart] 5847 annotations before applied cutoff / 18623 genes in category

	ID	Name	Source	pValue	FDR B&H	FDR B&Y	Bonferroni	Genes from Input	Genes in Annotation
1	GO:0006952	defense response		3.316E-16	1.939E-12	1.794E-11	1.939E-12	111	1651
2	GO:0002682	regulation of immune system process		2.986E-14	8.729E-11	8.075E-10	1.746E-10	100	1506
3	GO:0006954	inflammatory response		4.725E-14	9.209E-11	8.519E-10	2.763E-10	62	711
4	GO:0006955	immune response		6.797E-14	9.936E-11	9.192E-10	3.974E-10	102	1572
5	GO:0045321	leukocyte activation		1.384E-12	1.619E-9	1.498E-8	8.094E-9	65	828

Show 45 more annotations

3: GO: Cellular Component [Display Chart] 556 annotations before applied cutoff / 19061 genes in category

	ID	Name	Source	pValue	FDR B&H	FDR B&Y	Bonferroni	Genes from Input	Genes in Annotation
1	GO:0098552	side of membrane		2.384E-10	1.326E-7	9.146E-7	1.326E-7	44	510
2	GO:0009897	external side of plasma membrane		9.400E-10	2.613E-7	1.803E-6	5.227E-7	32	310
3	GO:0031226	intrinsic component of plasma membrane		3.173E-9	5.880E-7	4.057E-6	1.764E-6	94	1714
4	GO:0005887	integral component of plasma membrane		9.798E-9	1.362E-6	9.395E-6	5.448E-6	90	1651
5	GO:0009986	cell surface		1.146E-7	1.275E-5	8.794E-5	6.374E-5	55	873

7: Pathway [Display Chart] 1826 annotations before applied cutoff / 12450 genes in category

	ID	Name	Source	pValue	FDR B&H	FDR B&Y	Bonferroni	Genes from Input	Genes in Annotation
1	153910	Phagosome	BioSystems: KEGG	7.700E-7	1.406E-3	1.137E-2	1.406E-3	19	154
2	1269340	Hemostasis	BioSystems: REACTOME	1.680E-5	1.533E-2	1.240E-1	3.067E-2	42	640
3	MAP00330 Arginine and proline metabolism	MAP00330 Arginine and proline metabolism	GenMAPP	2.746E-5	1.671E-2	1.352E-1	5.014E-2	8	38
4	1457780	Neutrophil degranulation	BioSystems: REACTOME	3.975E-5	1.702E-2	1.377E-1	7.259E-2	34	492
5	1269171	Adaptive Immune System	BioSystems: REACTOME	4.661E-5	1.702E-2	1.377E-1	8.511E-2	49	826

Figure 5.15 RNAseq experiment - Top-5 most significant GO and Pathway categories - IL4 treated samples, 48h. Representative image of the GO and pathway analysis for IL4 treated samples. Lists of genes were submitted to the ToppFun online tool (part of the Toppgene Suite) to perform enrichment analysis.

Figure 5.13, Figure 5.14 and Figure 5.15 show representative images of the GO and pathway enrichment analysis performed using the lists of differentially expressed expressed genes in our experiment. The ToppFun application (from the Toppgene Suite) allows to perform up to 18 different gene enrichment analysis; this study focused on the 3 main GO categories; 1) Molecular Function (MF), 2) Biological Process (BP) and 3) Cellular Component (CC). In a similar way, this study focused on Pathway analysis (all of which are shown in Figure 5.13, Figure 5.15 and Figure 5.14). As seen before in the microarray experiment, LPS treatment of cells enriched GO categories related to cell division, immune and inflammatory responses and related to the cell cycle progression (Figure 5.13). Likewise, pathway analysis shows enrichment of pathways related to TNF signalling, glutathione metabolism and cytokine signalling. All related to immune activation of BV2 cells.

TGFβ stimulation (Figure 5.14) enriches categories related with receptor binding activity, immune response, cell migration and lysosomal function. Pathway analysis shows enrichment of lysosomal, phagosomal and innate immunity pathways. Finally, the IL4 (Figure 5.14) list of differentially expressed genes is enriched with terms related to cytokine signalling, pattern recognition receptors (PRRs), MHC binding, inflammatory and immune responses. Pathway analysis shows enrichment of a category related phagosome activity, neutrophil degranulation and adaptive immune response. As seen in the GO and Pathway analysis, many of the enriched terms were related to immune and inflammatory responses, which is consistent with the observations made in the microarray experiment. These results were expected as the experiment was carried out using immune cells.

The ToppFun application also allows to look for enrichment of terms and annotations in Disease databases, particularly 5 of them: 1) Clinical Variations, 2) DisGeNET BeFree, 3) DisGeNET Curated, 4) GWAS and 5) OMIM (Online Mendelian Inheritance in Man). Therefore, using this capability of the Toppfun application it was possible to look for enrichment of disease terms in the lists of differentially expressed genes. Disease pathway analysis focused primarily on the enrichment of the AD related pathways. Results from this analysis can be seen in Table 5-7.

Table 5-7 Association of microglial stimulators with AD pathway

Timepoint	Treatment	Enrichment of Disease terms for AD
6h	LPS	No
	IL4	Yes
	TGF	No
24h	LPS	No
	IL4	Yes
	TGF	No
48h	LPS	Yes
	IL4	Yes
	TGF	No

As it can be seen in Table 5-7, there is an enrichment of terms related to AD in IL4 activated cells at all timepoints in our experiment. Similarly, this same enrichment was seen for the LPS treated condition at 48h. These results support the involvement of microglial activation, either M2 or M1, in AD. A representative image of this Disease pathway analysis for IL4 at 48h can be seen in Supplementary Fig. 7.9.

5.4.6 Differential expression of microglial and immune activation markers

In the same way as the microarray experiment, the effect of the different treatments on the expression of microglial and immune activation markers was also investigated using the data from the RNAseq experiment.

As seen in Table 5.8, LPS, IL4 and TGFβ modified the gene expression of cell markers which are commonly used for the identification of microglial populations. Of interest is IBA1 (Aif1) which is routinely used as a marker of microglial cells in pathological studies. In our experiment, the expression of this gene was upregulated by LPS (M1) activation. This effect of M1 activators on IBA1 expression can lead to an over estimation of the microglial cell presence in pathological studies. Similarly, the use of any of the other microglial markers whose expression was modified by any of the three treatments can lead to inaccurate results. Of the list of 10 microglial markers only 5 were not modified by any of the 3 treatments: Cd11b (Itgam), SFPi1, CD68, CD45 (Ptprc) and EMR1. Considering these results, it would advisable to use any of these 5 markers in studies of microglial populations which might be activated.

In recent years, the transmembrane protein 119 (Tmem119), a cell-surface protein of unknown function, has emerged as a highly specific marker for microglia in both mouse and human (Bennett et al., 2016). The gene expression of this gene was also studied in our RNAseq experiment. This marker also changed in response to the three treatments; LPS (upregulated), IL4 (downregulated) and TGFβ (upregulated).

Table 5-8 Microglial cell markers differentially expressed by LPS, IL4 and TGFβ treatments

Cell Marker	LPS				IL4				TGFβ			
	Differ. Expressed	Timepoint			Differ. Expressed	Timepoint			Differ. Expressed	Timepoint		
		6h	24h	48h		6h	24h	48h		6h	24h	48h
Cd11b (Itgam)	No	-	-	-	No	-	-	-	No	-	-	-
SFPi1	No	-	-	-	No	-	-	-	No	-	-	-
Cd68	No	-	-	-	No	-	-	-	No	-	-	-
Cd45 (PTPRC)	No	-	-	-	No	-	-	-	No	-	-	-
Cx3CR1	No	-	-	-	No	-	-	-	Yes	-	Up-regulated	Up-regulated
Iba1 (Aif1)	Yes	-	-	Up-regulated	No	-	-	-	No	-	-	-
Cd14	Yes	Up-regulated	Up-regulated	-	Yes	Down-regulated	Down-regulated	Down-regulated	No	-	-	-
CSF1	Yes	Up-regulated	Up-regulated	Up-regulated	No	-	-	-	No	-	-	-
CSF1R	Yes	Up-regulated	Up-regulated	-	Yes	Up-regulated	-	-	Yes	Up-regulated	-	-
EMR1	No	-	-	-	No	-	-	-	No	-	-	-

Table 5-9 shows the analysis of the expression of M1 and M2 activation markers in response to LPS, IL4 and TGFβ in our experiment. M1 and M2 lists were derived from revision of literature including papers from: Tang and Le (2016), (Taylor et al., 2005) and Butovsky et al. (2005). As expected, LPS stimulation upregulated the expression of most genes associated with M1 activation, however it also caused the differential expression of 3 M2-related genes. This effect on the expression of M2 genes could be caused the anti-inflammatory response that is initiated by cells following M1 activation as a way to resolve inflammation. Surprisingly, IL4 treatment upregulated the expression of a considerable number of M1 associated genes (4 out of 11), while causing the differential expression of only 2 M2 markers (Pdgf(a) and Arg1). Finally, TGFβ stimulation was responsible for the differential expression of 3 M1-related markers: MHCII (upregulated), IL1β and CCL2 (both downregulated). At the same time, TGFβ caused the differential expression of 4 M2-related markers (Vegf(a), Pdgf(a), Il10 and Arg1).

The analysis of the expression of M1 and M2 markers shows a good response of BV2 cells to LPS with the concomitant upregulation of most M1 markers (9 out of 11). However, BV2 cells show a modest response to M2 activators (IL4 and TGFβ), since a small number of M2 markers was differentially expressed by any of these activators (2 and 4 out of 7, respectively). In this experiment, we did not see a clear upregulation of M2 markers in response to IL4 and TGFβ. One explanation for this could be the fact that under serum-free conditions cells were already immune deactivated (relaxed) and for that reason there was no room for gene expression changes of M2 markers, which could have been already expressed at high levels. Conversely, M1 markers had more “room” for differential expression since LPS can activate relaxed cells. Further studies should explore the possibility that in order to see a more pronounced response to IL4 and TGFβ, cells need to be pre-conditioned with an M1 activator.

Table 5-9 Cell markers of M1 and M2 activation are differentially expressed by LPS, IL4 and TGFβ

Activation State	Cell Marker	Differ. Expressed	LPS			Differ. Expressed	IL4			Differ. Expressed	TGF		
			Timepoint				Timepoint				Timepoint		
			6h	24h	48h		6h	24h	48h		6h	24h	48h
M1	*MHCII (H2-Oa)*	Yes	-	Up-regulated	Up-regulated	No	-	-	-	Yes	-	Up-regulated	Up-regulated
	CD40	Yes	Up-regulated	Up-regulated	-	Yes	Up-regulated	Up-regulated	Up-regulated	No	-	-	-
	IL1b	Yes	Up-regulated	Up-regulated	Up-regulated	Yes	Up-regulated	Up-regulated	Up-regulated	Yes	-	Down-regulated	Down-regulated
	IL6	Yes	Up-regulated	Up-regulated	Up-regulated	No	-	-	-	No	-	-	-
	TNF	Yes	Up-regulated	Up-regulated	Up-regulated	Yes	-	Down-regulated	-	No	-	-	-
	IL18	Yes	-	Down-regulated	-	No	-	-	-	No	-	-	-
	CCL2	Yes	Up-regulated	-	-	Yes	Up-regulated	Up-regulated	Up-regulated	Yes	-	Down-regulated	Down-regulated
	Cd80	Yes	Up-regulated	Up-regulated	-	No	-	-	-	No	-	-	-
	IL23	Yes	-	Up-regulated	Up-regulated	No	-	-	-	No	-	-	-
	Cd86	No	-	-	-	No	-	-	-	No	-	-	-
	IL12	No	-	-	-	No	-	-	-	No	-	-	-
M2	*VEGF(a)*	Yes	-	Up-regulated	Up-regulated	No	-	-	-	Yes	Up-regulated	Up-regulated	Up-regulated
	EGF	No	-	-	-	No	-	-	-	No	-	-	-
	TGFβ	Yes	Up-regulated	-	-	No	-	-	-	No	-	-	-
	PDGF(a)	No	-	-	-	No	-	-	-	Yes	Up-regulated	Up-regulated	Up-regulated
	PDGF(b)	Yes	Up-regulated	-	-	Yes	-	Down-regulated	Down-regulated	No	-	-	-
	IL10	No	-	-	-	No	-	-	-	Yes	Down-regulated	Down-regulated	Down-regulated
	Arg1	No	-	-	-	Yes	Up-regulated	Up-regulated	Up-regulated	Yes	-	-	Up-regulated

5.4.1 **Differential expression of AD-related genes by LPS, IL4 and TGFβ**

Table 5-10, shows the differential expression analysis of AD-related genes in BV2 cells treated with LPS, IL4 and TGFβ. Similarly to the microarray experiment, the analysis employed the list of AD-related genes compiled by Karch et al. (2014), plus two “extra” genes from a recent association study, which reported Abi3 and Plcg2 as new AD risk genes (Sims et al., 2017).

LPS stimulation caused the differential expression of 8 AD-related genes (ApoE, CD33, Inpp5d, Mef2c, *Trem2*, Ptk2b, Madd and Abi3). While IL4 and TGFβ stimulations caused the differential expression of 6 (CD33, Ms4a6a, Mef2c, Picalm, Clu and Abi3) and 8 (App, Apoe, Inpp5d, *Trem2*, Pld3, Cass4, Clu and Abi3) AD-related genes respectively. Similar to the results obtained in our microarray experiment, these results point to a significant effect of microglial activation status (M1 or M2) on the expression of genes which have been linked to AD pathogenesis.

Table 5-10 Differential gene expression of 33 AD-related genes

Cell Marker	Differ. Expressed	LPS			Differ. Expressed	IL4			Differ. Expressed	TGF		
		Timepoint				Timepoint				Timepoint		
		6h	24h	48h		6h	24h	48h		6h	24h	48h
APP	No	-	-	-	No	-	-	-	Yes	-	Up-regulated	-
APOE	Yes	-	Down-regulated	Down-regulated	No	-	-	-	Yes	-	Up-regulated	Up-regulated
CD33	Yes	Down-regulated	-	-	Yes	Down-regulated	Down-regulated	Down-regulated	No	-	-	-
CELF1 (CUGBP)	No	-	-	-	No	-	-	-	No	-	-	-
MS4A6A (MS4A6D)	No	-	-	-	Yes	Up-regulated	Up-regulated	Up-regulated	No	-	-	-
INPP5D	Yes	-	Down-regulated	-	No	-	-	-	Yes	Up-regulated	-	-
MEF2C	Yes	Down-regulated	Down-regulated	Down-regulated	Yes	Down-regulated	-	-	No	-	-	-
TREM2	Yes	-	Down-regulated	-	No	-	-	-	Yes	-	Up-regulated	Up-regulated
BIN1	No	-	-	-	No	-	-	-	No	-	-	-
PLD3	No	-	-	-	No	-	-	-	Yes	-	Up-regulated	Up-regulated
RIN3	No	-	-	-	No	-	-	-	No	-	-	-
PICALM	No	-	-	-	Yes	Up-regulated	-	-	No	-	-	-
PTK2B	Yes	-	Up-regulated	-	No	-	-	-	No	-	-	-
ABCA7	No	-	-	-	No	-	-	-	No	-	-	-
CASS4	No	-	-	-	No	-	-	-	Yes	Down-regulated	Down-regulated	Down-regulated
DSG2	No	-	-	-	No	-	-	-	No	-	-	-
PSEN2	No	-	-	-	No	-	-	-	No	-	-	-
SORL1	No	-	-	-	No	-	-	-	No	-	-	-

ZCWPW1	No	-	-	-	No	-	-	-	No	-	-	-
CR1 (Crry)	No	-	-	-	No	-	-	-	No	-	-	-
PSEN1	No	-	-	-	No	-	-	-	No	-	-	-
ADAM10	No	-	-	-	No	-	-	-	No	-	-	-
CD2AP	No	-	-	-	No	-	-	-	No	-	-	-
EPHA1	No	-	-	-	No	-	-	-	No	-	-	-
FERMT2	No	-	-	-	No	-	-	-	No	-	-	-
HLA-DRB5/ HLA-DRB1 (H2-Eb1/ H2-Eb1)	No	-	-	-	No	-	-	-	No	-	-	-
MADD	Yes	Down-regulated	-	-	No	-	-	-	No	-	-	-
SLC24A4	No	-	-	-	No	-	-	-	No	-	-	-
CLU	No	-	-	-	Yes	-	-	Down-regulated	Yes	-	Up-regulated	Up-regulated
NME8	No	-	-	-	No	-	-	-	No	-	-	-
NYAP1	No	-	-	-	No	-	-	-	No	-	-	-
Abi3	Yes	-	Down-regulated	-	Yes	-	Down-regulated	-	Yes	Up-regulated	-	Up-regulated
Plcg2	No	-	-	-	No	-	-	-	No	-	-	-

(Continued from previous page)

5.5 RNAseq analysis of the effect of *Trem2* deficiency on the activation of BV2 cells by LPS (M1)

5.5.1 Normalization and quality control

Similar to the activation experiments, RNA sequencing results were sent back from AROS Applied Biotechnology, as raw sequencing reads in fastq files. Raw sequencing results were normalised and quality control examined. After QC, 12 617 genes (out of all the genes in the Ensembl 86 reference) were included in the analysis. PCA analysis was carried out using the Partek® Flow™ software.

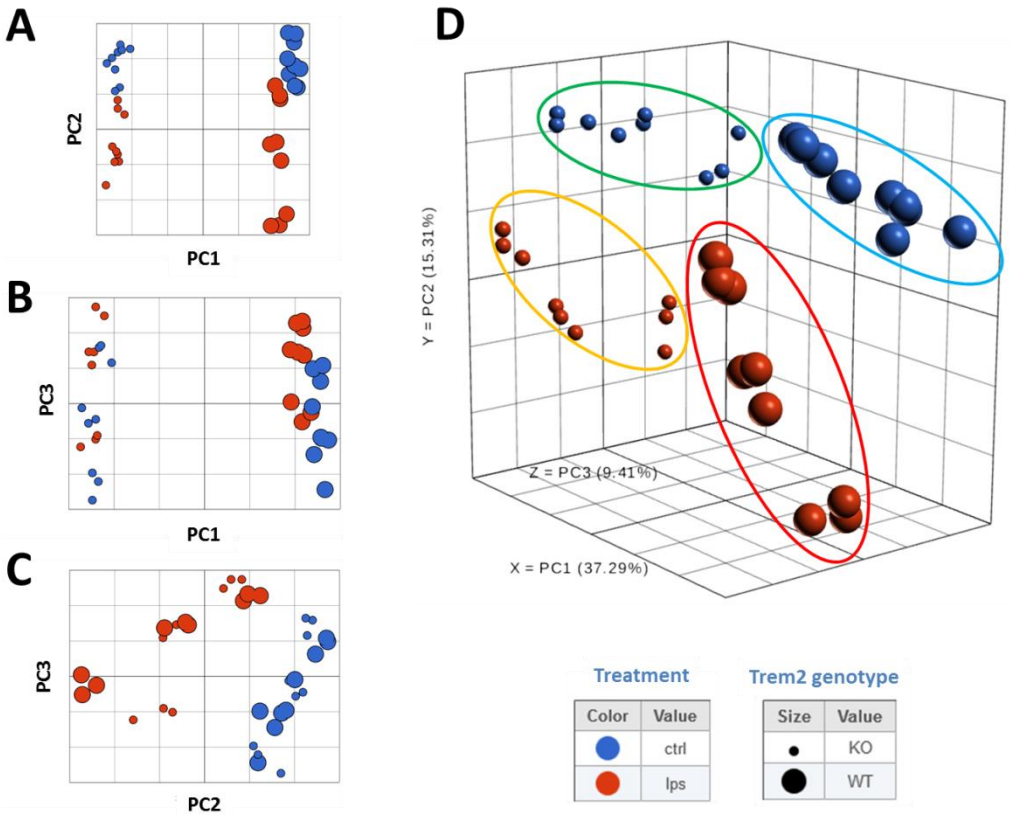

Figure 5.16 PCA scatter plot of RNAseq data – Effect of *Trem2* deficiency on BV2 activation. PCA was used to identify outliers and to visualize the clustering of all sequenced. Panels **A**, **B** and **C** show 2D representations of PC1vsPC2, PC1vsPC3 and PC2vsPC3, respectively. Panel **D** shows a 3D representation of the 3 main PC's. No samples were excluded as a result of this analysis and it was possible to distinguish some clustering of samples. Panel D, shows the clustering of 4 clear groups of samples: the sky blue oval highlights clustering of untreated WT cells (control), the red oval highlights clustering of LPS (100ng/mL) treated WT cells, the green oval highlights clustering of *Trem2* KO (B5 cell line) untreated cells and the orange oval highlights the clustering of *Trem2* KO LPS treated cells.

Figure 5.16 shows the PCA scatter plot of all samples used for the evaluation of the effect of *Trem2* deficiency on BV2 cell activation, M1 only. Samples are coloured according to their treatment and the sizes of the spheres represent the *Trem2* genotype. The scatter plot shows clear segregation of 4 different groups: 1) WT control (untreated, sky blue oval), 2) WT LPS treated (red oval), 3) *Trem2* KO control (untreated, green oval) and 4) *Trem2* LPS treated (orange oval). After, PCA none of the samples was discarded.

5.5.2 Identification of Differentially Expressed (DE) genes and generation of gene lists

Similar to the activation experiment, a Multi-factor ANOVA was used for the identification of differentially expressed genes. Partek® Flow™ was used for the statistical. For the statistical analysis the following criteria were used as the main sources of variation; number of biological replicate (repeat or batch), timepoint, treatment, *Trem2* genotype, timepoint x treatment, timepoint x *Trem2* genotype, treatment x *Trem2* genotype and timepoint x treatment x *Trem2* genotype. For comparison, 12 contrasts were set up to compare gene expression changes across treatments and timepoints (as shown in Table 5.6).

Table 5-11 Contrasts used for the multi-factor ANOVA – RNAseq effect of *Trem2* deficiency on the activation of BV2 cells by LPS (M1)

	WT x control, 6h	WT x control, 24h	WT x control, 48h	KO x control, 6h	KO x control, 24h	KO x control, 48h
WT x control, 6h						
WT x LPS 100ng/ml, 6h	X					
KO x control, 6h	X					
KO x LPS 100ng/ml, 6h	X			X		
WT x control, 24h						
WT x LPS 100ng/ml, 24h		X				
KO x control, 24h		X				
KO x LPS 100ng/ml, 24h		X			X	
WT x control, 48h						
WT x LPS 100ng/ml, 48h			X			
KO x control, 48h			X			
KO x LPS 100ng/ml, 48h			X			X

Analogous to the microarray and RNAseq (activation) experiments, each treatment condition was compared to its own untreated control for each timepoint. This time, control samples (across timepoints) were not compared with each other, since they have already been compared during the RNAseq microglial activation experiment. It is important to remember that the same control (untreated) samples were used for both RNAseq experiments as both experiments were done together as a single experiment.

The same conservative FDR of 0.01 and a minimum fold change of ±1.5 conditions were used for the generation of differentially expressed gene lists. 12 gene lists were created (one per contrast); all contrasts produced lists of differentially expressed genes.

Figure 5.17 Number of Differentially expressed genes - RNAseq *Trem2* deficiency effect on microglial activation. Following the ANOVA analysis, lists of differentially expressed genes were obtained. These lists were composed of genes whose expression was affected by *Trem2* deficiency and LPS (M1) activation of BV2 cells. **A)** Shows the number of differentially expressed genes per condition (genotype and treatment) and per timepoint compared to the control sample for its correspondent timepoint. **B)** Shows the number of differentially expressed genes in *Trem2* KO cells compared to BV2 unmodified (Control) per timepoint. WT=Wild type cells (BV2 unmodified), KO=*Trem2* KO (B5 cell line).

As seen in Figure 5.17, panel A, all conditions assayed in this experiment generated lists of differentially expressed genes. The first thing that sprung to our attention is the overall 50-50% split between up- and down-regulated genes for each list. This is interesting since there is a perception that during activation of immune cells, the number of upregulated genes is greater than the number of downregulated genes, which is not the case in our experiment. A second observation is the fact that the number of differentially expressed genes for the WT–LPS treated samples declined as time passed (1943>1435>797). This reduction in the number of differentially expressed genes points to a resolution of the inflammatory response to LPS.

Trem2 KO cells had a very different response to both untreated and LPS conditions, when compared to WT-untreated cells, in our experiment. For one, the number of differentially expressed genes in KO cells under untreated conditions (compared to WT

untreated for its correspondent timepoint) remained constant at ~4000 differentially expressed genes per timepoint, which was at least twice as many differentially expressed genes by LPS treatment of WT cells. This suggests that *Trem2* deficiency greatly disrupts BV2 gene expression and that this disturbance is constant as time passes by (different timepoints). Secondly, LPS treatment of KO cells had a small effect on the number of differentially expressed genes compared to the KO alone (4478>4595>4254) at any timepoint. Moreover, unlike the reduction seen in the number of differentially expressed genes for the LPS treatment of WT cells, the number of differentially expressed genes in KO cells treated with LPS remained almost constant (between 4595 and 4254). This result points to an impaired response to LPS treatment (not many genes were differentially expressed by LPS compared to the WT cells) and an impaired immune deactivation (resolution) in the KO cells (compared to the reduction in the number of differentially expressed genes seen in WT-LPS stimulated cells.

Figure 5.17, panel B, shows the comparison between the number of differentially expressed genes of WT and *Trem2* KO cells in response to LPS treatment for each timepoint. As seen in Figure 5.17, panel A, there were clear differences between the gene expression responses to LPS in WT and *Trem2* KO cells. These differences show a slight reduction as time goes by in the experiment (3867>3504>3497), but remain markedly different.

5.5.3 **Identification of enriched biological pathways – GO and Pathway analysis**

As before, identification of enriched GO categories and pathways was performed using the ToppFun tool from the Toppgene suite (available at https://toppgene.cchmc.org/). Conditions of analysis were left as default and a FDR B&H (Benjamine-Hochberg) value of <0.05 was considered as statistically significant for analysis. Only the top-5 GO categories and pathways for each gene list (condition) are shown, unless indicated otherwise.

1: GO: Molecular Function [Display Chart] 3071 annotations before applied cutoff / 18661 genes in category

	ID	Name	Source	pValue	FDR B&H	FDR B&Y	Bonferroni	Genes from Input	Genes in Annotation
1	GO:0019899	enzyme binding		1.429E-9	4.388E-6	3.777E-5	4.388E-6	441	1929
2	GO:0017076	purine nucleotide binding		4.264E-9	6.548E-6	5.636E-5	1.310E-5	428	1879
3	GO:0032553	ribonucleotide binding		6.521E-9	6.676E-6	5.746E-5	2.003E-5	427	1880
4	GO:0030554	adenyl nucleotide binding		9.207E-9	7.069E-6	6.084E-5	2.828E-5	356	1530
5	GO:0032555	purine ribonucleotide binding		1.233E-8	7.576E-6	6.521E-5	3.788E-5	422	1864

Show 25 more annotations

2: GO: Biological Process [Display Chart] 10565 annotations before applied cutoff / 18623 genes in category

	ID	Name	Source	pValue	FDR B&H	FDR B&Y	Bonferroni	Genes from Input	Genes in Annotation
1	GO:0002682	regulation of immune system process		2.019E-13	2.133E-9	2.100E-8	2.133E-9	378	1506
2	GO:0015031	protein transport		6.271E-13	3.313E-9	3.261E-8	6.625E-9	467	1948
3	GO:0006613	cotranslational protein targeting to membrane		8.009E-12	2.821E-8	2.776E-7	8.462E-8	48	101
4	GO:0070972	protein localization to endoplasmic reticulum		1.172E-11	3.097E-8	3.048E-7	1.239E-7	55	125
5	GO:0034613	cellular protein localization		2.022E-11	4.273E-8	4.205E-7	2.136E-7	401	1666

Show 45 more annotations

3: GO: Cellular Component [Display Chart] 1228 annotations before applied cutoff / 19061 genes in category

	ID	Name	Source	pValue	FDR B&H	FDR B&Y	Bonferroni	Genes from Input	Genes in Annotation
1	GO:0022626	cytosolic ribosome		1.006E-10	1.235E-7	9.498E-7	1.235E-7	51	119
2	GO:0044432	endoplasmic reticulum part		4.271E-10	2.623E-7	2.017E-6	5.245E-7	288	1177
3	GO:0005783	endoplasmic reticulum		3.122E-9	1.127E-6	8.666E-6	3.834E-6	390	1706
4	GO:0005789	endoplasmic reticulum membrane		4.687E-9	1.127E-6	8.666E-6	5.756E-6	245	994
5	GO:0022627	cytosolic small ribosomal subunit		5.256E-9	1.127E-6	8.666E-6	6.454E-6	25	44

7: Pathway [Display Chart] 3278 annotations before applied cutoff / 12450 genes in category

	ID	Name	Source	pValue	FDR B&H	FDR B&Y	Bonferroni	Genes from Input	Genes in Annotation
1	1268689	SRP-dependent cotranslational protein targeting to membrane	BioSystems: REACTOME	3.481E-13	1.141E-9	9.897E-9	1.141E-9	55	116
2	1269120	Viral mRNA Translation	BioSystems: REACTOME	2.030E-11	3.327E-8	2.885E-7	6.654E-8	45	93
3	1268691	Peptide chain elongation	BioSystems: REACTOME	8.697E-11	9.503E-8	8.241E-7	2.851E-7	44	93
4	1268692	Eukaryotic Translation Termination	BioSystems: REACTOME	1.213E-10	9.943E-8	8.623E-7	3.977E-7	45	97
5	1339156	Selenocysteine synthesis	BioSystems: REACTOME	3.177E-10	2.083E-7	1.807E-6	1.042E-6	44	96

18: Disease [Display Chart] 12640 annotations before applied cutoff / 16203 genes in category

	ID	Name	Source	pValue	FDR B&H	FDR B&Y	Bonferroni	Genes from Input	Genes in Annotation
1	C0023893	Liver Cirrhosis, Experimental	DisGeNET Curated	1.876E-20	2.372E-16	2.377E-15	2.372E-16	227	767
2	C0023467	Leukemia, Myelocytic, Acute	DisGeNET Curated	1.028E-13	6.494E-10	6.509E-9	1.299E-9	382	1646
3	C0023418	leukemia	DisGeNET Curated	8.453E-12	3.562E-8	3.569E-7	1.068E-7	412	1854
4	C4020899	Autosomal recessive predisposition	DisGeNET Curated	3.341E-11	1.056E-7	1.058E-6	4.223E-7	331	1445
5	C0003873	Rheumatoid Arthritis	DisGeNET Curated	8.978E-11	2.270E-7	2.275E-6	1.135E-6	366	1640
6	C0024299	Lymphoma	DisGeNET Curated	3.276E-10	6.902E-7	6.917E-6	4.141E-6	289	1253
7	C0524851	Neurodegenerative Disorders	DisGeNET Curated	1.131E-9	2.043E-6	2.047E-5	1.430E-5	179	710
8	C0027819	Neuroblastoma	DisGeNET Curated	2.592E-9	4.095E-6	4.104E-5	3.276E-5	367	1689
9	C0002395	Alzheimer's Disease	DisGeNET Curated	4.325E-9	5.789E-6	5.802E-5	5.466E-5	391	1825
10	C0002736	Amyotrophic Lateral Sclerosis	DisGeNET Curated	4.580E-9	5.789E-6	5.802E-5	5.789E-5	160	629
11	C0024138	Lupus Erythematosus, Discoid	DisGeNET Curated	6.335E-9	7.279E-6	7.295E-5	8.007E-5	90	303
12	C0024131	Lupus Vulgaris	DisGeNET BeFree	1.245E-8	1.312E-5	1.314E-4	1.574E-4	86	289
13	C0409974	Lupus Erythematosus	DisGeNET BeFree	1.946E-8	1.892E-5	1.896E-4	2.460E-4	87	296
14	C0151744	Myocardial Ischemia	DisGeNET Curated	2.265E-8	2.045E-5	2.049E-4	2.862E-4	114	421
15	C0023470	Myeloid Leukemia	DisGeNET Curated	2.731E-8	2.301E-5	2.306E-4	3.452E-4	127	484

Figure 5.18 Enrichment of GO and Pathway categories - *Trem2* KO vs WT, 6h. Representative image of the GO and pathway analysis for *Trem2* KO samples (6h). Lists of genes were submitted to the ToppFun online tool to perform enrichment analysis. The ToppFun report includes many enrichment categories, here only 5 of them are shown: Molecular Function (MF), Biological Process (BP), Cellular Component (CC), Pathway and Disease.

Figure 5.18 shows a representative image of the GO and Pathway analysis performed in the *Trem2* KO samples (similar results were obtained at 24h and 48h). GO terms enriched for the *Trem2* KO samples were related to nucleotide and ribonucleotide binding (MF); regulation of the immune response, protein localization and transport (BP); ribosome and endoplasmic reticulum (CC); peptide and protein translational processes

(Pathway). Interestingly, there was an enrichment of Disease terms related to Rheumatoid Arthritis (which could be related to the Nasu-Hakola phenotype), Neurodegenerative disorders and Alzheimer's disease.

5.5.4 **Differential expression of microglial and immune activation markers**

Similar to the past two gene expression experiments, this section examines the effect of *Trem2* deficiency on the expression of microglial and immune activation markers.

As seen in Table 5-12, LPS, IL4 and TGFβ were able to modify the gene expression of many cell markers which are used for the identification of microglial populations. Strikingly, Cd11b (Itgam) was upregulated in *Trem2* KO cells in all conditions and timepoints. This finding is a novel one to the best of our knowledge. Cd11b is a marker widely used for the study and identification of microglia. It is also part of the complement immune system. In flow cytometry assays for example, it is used to discriminate between, CD11b positive cells (meaning microglial cells) and Cd11b negative cells (meaning all other cell types of the brain)(Mazaheri et al., 2017). Interestingly, high expression of this marker has been associated with higher expression *Trem2* (Kim et al., 2017). The finding that Cd11b is upregulated in *Trem2* deficient cells can have implications for the study of the complement system in microglia. This system has already been shown to be disrupted in AD. An example of this is the upregulation of CR1, and other complement factors, which has been reported in affected regions of AD brains (Shen et al., 1997).

In a similar way, Iba1 (Aif1) is upregulated in KO cells (treated or LPS treated). The gene expression of this marker has already been shown to be disrupted in WT BV2 cells treated with LPS. Of the list of 10 microglial markers only 3 were not modified by either *Trem2* deficiency or the LPS treatment: SFPi1, CD45 (Ptprc) and EMR1. These 3 microglial markers have the only ones that have been shown not to be altered by any microglial challenge (this includes the microarray experiment and the 2 RNAseq experiments). Considering these results, it is strongly recommended to use any of these 3 markers for studies of microglial populations which might be activated or are *Trem2* deficient.

The expression of *Tmem119*, a highly specific marker for microglia (Bennett et al., 2016), in *Trem2* deficient BV2 cells was also examined in this study. Unsurprisingly, this marker was also upregulated by *Trem2* deficiency and in response to LPS stimulation (both in WT and *Trem2* KO cells).

Table 5-12 Microglial cell markers differentially expressed by *Trem2* deficiency

Cell Marker	KO-untreated				WT-LPS				KO-LPS			
	Differ.	Timepoint			Differ.	Timepoint			Differ.	Timepoint		
	Expressed	6h	24h	48h	Expressed	6h	24h	48h	Expressed	6h	24h	48h
Cd11b (Itgam)	Yes	Up-regulated	Up-regulated	Up-regulated	Yes	-	-	-	No	Up-regulated	Up-regulated	Up-regulated
SFPi1	No	-	-	-	No	-	-	-	No	-	-	-
Cd68	No	-	-	-	No	-	-	-	Yes	-	-	Down-regulated
Cd45 (PTPRC)	No	-	-	-	No	-	-	-	No	-	-	-
Cx3CR1	No	-	-	-	Yes	-	Up-regulated	Up-regulated	No	-	-	-
Iba1 (Aif1)	Yes	Down-regulated	Down-regulated	Down-regulated	Yes	Up-regulated	-	-	Yes	Down-regulated	Down-regulated	Down-regulated
Cd14	Yes	Down-regulated	Down-regulated	Down-regulated	Yes	Up-regulated	Up-regulated	-	No	-	-	-
CSF1	Yes	Down-regulated	Down-regulated		Yes	-	Up-regulated	Up-regulated	Yes	Down-regulated	Down-regulated	Down-regulated
CSF1R	Yes				Yes	Up-regulated	Up-regulated	-	Yes	Up-regulated	-	Up-regulated
EMR1	No	-	-	-	No	-	-	-	No	-	-	-

The analysis of the expression of M1 and M2 activation markers in *Trem2* KO cells is shown in Table 5-13. As shown in previous experiments, LPS stimulation of WT cells upregulated the expression of most genes associated with M1 activation, however it also caused the upregulation of 3 M2-related genes. Surprisingly, untreated *Trem2* KO cells caused the differential expression of 8 (out of 11) M1 associated genes. Additionally, these cells showed disruption on the expression of up to 7 (out of 7) M2 markers (3 downregulated and 4 upregulated). A similar pattern, of dysregulation on the expression of both M1 and M2 markers was seen in *Trem2* KO cells treated with LPS. This analysis of the expression of M1- and M2-related markers clearly shows a complete disruption on the expression of M1 and M2 markers in the *Trem2* KO cells under untreated and LPS treated conditions, compared to WT untreated cells.

Table 5-13 Cell markers of M1 and M2 activation are differentially expressed by *Trem2* deficiency and LPS.

Activation State	Cell Marker	Differ. Expressed	KO-Untreated			Differ. Expressed	WT-LPS			Differ. Expressed	KO-LPS		
			Timepoint				Timepoint				Timepoint		
			6h	24h	48h		6h	24h	48h		6h	24h	48h
M1	*MHCII (H2- Oa)*	Yes	-	-	Up-regulated	Yes	-	Up-regulated	Up-regulated	Yes	-	-	Up-regulated
	CD40	Yes	Up-regulated	Up-regulated	Up-regulated	Yes	Up-regulated	Up-regulated	-	Yes	Up-regulated	Up-regulated	Up-regulated
	IL1b	Yes	Up-regulated	Up-regulated	Up-regulated	Yes	Up-regulated	Up-regulated	Up-regulated	Yes	Up-regulated	Up-regulated	Up-regulated
	IL6	No	-	-	-	Yes	Up-regulated	Up-regulated	Up-regulated	No	-	-	-
	TNF	Yes	-	-	Up-regulated	Yes	Up-regulated	Up-regulated	Up-regulated	Yes	Up-regulated	Up-regulated	Up-regulated
	IL18	Yes	Up-regulated	Up-regulated	-	Yes	-	Down-regulated	-	Yes	Up-regulated	-	-
	CCL2	Yes	-	Down-regulated	-	Yes	Up-regulated	-	-	No	-	-	-
	Cd80	Yes	-	-	Up-regulated	Yes	Up-regulated	-	-	Yes	Up-regulated	Up-regulated	Up-regulated
	Il23(a)	Yes	Down-regulated	-	Up-regulated	Yes	-	Up-regulated	Up-regulated	Yes	-	Up-regulated	-
	Cd86	No	-	-	-	No	-	-	-	No	-	-	-
	Il12	No	-	-	-	No	-	-	-	No	-	-	-
M2	*VEGF(a)*	Yes	Up-regulated	Up-regulated	Up-regulated	Yes	-	Up-regulated	Up-regulated	Yes	Up-regulated	Up-regulated	Up-regulated
	EGF	Yes	Up-regulated	-	-	No	-	-	-	No	-	-	-
	TGFβ	Yes	-	Down-regulated	-	Yes	Up-regulated	-	-	No	-	-	-
	PDGF(a)	Yes	-	Up-regulated	-	No	-	-	-	No	-	-	-
	PDGF(b)	Yes	Down-regulated	Down-regulated	Down-regulated	Yes	Up-regulated	-	-	Yes	Down-regulated	Down-regulated	Down-regulated
	IL10	Yes	Down-regulated	Down-regulated	Down-regulated	No	-	-	-	Yes	-	Down-regulated	Down-regulated
	Arg1	Yes	Up-regulated	Up-regulated	Up-regulated	No	-	-	-	Yes	-	-	Up-regulated

5.5.5 Differential expression of AD-related genes in *Trem2* KO cells

Table 5.14 shows the analysis of the differential expression of AD-related genes in *Trem2* KO BV2 cells (untreated and LPS stimulated). Keeping in line with the previous RNAseq experiment, the same list of AD-related genes compiled by Karch et al. (2014) and the two "extra" genes (*Abi3* and *Plcg2*) from a recent association study (Sims et al., 2017) was used.

Trem2 deficiency causes the differential expression of 13 and 10 AD-related genes under untreated and LPS treated conditions, respectively. Meanwhile LPS activation of WT BV2 cells caused differentially expressed of only 8 genes (*ApoE, CD33, Inpp5d, Mef2c, Trem2, Ptk2b, Madd* and *Abi3*), which is consistent with the results obtained in the microarray study. The disruption in the gene expression patterns of a considerable number of AD-related genes in the *Trem2* KO cells suggests that *Trem2* plays an important role in the regulation of AD associated pathways.

Table 5-14 Differential gene expression of AD-related genes in *Trem2* KO cells.

Cell Marker	Differ. Expressed	*Trem2* KO-Untreated			Differ. Expressed	WT-LPS			Differ. Expressed	KO-LPS		
		Timepoint				Timepoint				Timepoint		
		6h	24h	48h		6h	24h	48h		6h	24h	48h
APP	No	-	-	-	No	-	-	-	No	-	-	-
APOE	Yes	Down-regulated	Down-regulated	Down-regulated	Yes	-	Down-regulated	Down-regulated	Yes	Down-regulated	Down-regulated	Down-regulated
CD33	Yes	-	Up-regulated	-	Yes	Down-regulated	-	-	No	-	-	-
CELF1 (CUGBP)	No	-	-	-	No	-	-	-	No	-	-	-
MS4A6A (MS4A6D)	No	-	-	-	No	-	-	-	No	-	-	-
INPP5D	No	-	-	-	Yes	Down-regulated	Down-regulated	-	No	-	-	-
MEF2C	Yes	Down-regulated	Down-regulated	Down-regulated	Yes	Down-regulated	Down-regulated	-	Yes	Down-regulated	Down-regulated	Down-regulated
TREM2	Yes	Down-regulated	Down-regulated	Down-regulated	Yes	-	Down-regulated	-	Yes	Down-regulated	Down-regulated	Down-regulated
BIN1	Yes	Up-regulated	Up-regulated	Up-regulated	No	-	-	-	Yes	Up-regulated	Up-regulated	Up-regulated
PLD3	No	-	-	-	No	-	-	-	No	-	-	-
RIN3	No	-	-	-	No	-	-	-	No	-	-	-
PICALM	Yes	Down-regulated	-	-	No	-	-	-	Yes	Down-regulated	-	-
PTK2B	No	-	-	-	Yes	Up-regulated	-	-	No	-	-	-
ABCA7	No	-	-	-	No	-	-	-	No	-	-	-
CASS4	Yes	-	-	Up-regulated	No	-	-	-	No	-	-	-
DSG2	No	-	-	-	No	-	-	-	No	-	-	-
PSEN2	Yes	Up-regulated	-	-	No	-	-	-	Yes	Up-regulated	-	-
SORL1	Yes	Up-regulated	Up-regulated	Up-regulated	No	-	-	-	Yes	Up-regulated	Up-regulated	Up-regulated
ZCWPW1	No	-	-	-	No	-	-	-	No	-	-	-

CR1 (Crry)	No	-	-	-	No	-	-	-	No	-	-	-
PSEN1	No	-	-	-	No	-	-	-	No	-	-	-
ADAM10	Yes	Down-regulated	Down-regulated	-	No	-	-	-	Yes	Down-regulated	Down-regulated	Down-regulated
CD2AP	No	-	-	-	No	-	-	-	Yes	Down-regulated	Down-regulated	-
EPHA1	No	-	-	-	No	-	-	-	No	-	-	-
FERMT2	No	-	-	-	No	-	-	-	No	-	-	-
HLA-DRB5/ HLA-DRB1 (H2-Eb1/ H2-Eb1)	No	-	-	-	No	-	-	-	No	-	-	-
MADD	Yes	-	Up-regulated	Up-regulated	Yes	Down-regulated	-	-	No	-	-	-
SLC24A4	No	-	-	-	No	-	-	-	No	-	-	-
CLU	Yes	Down-regulated	Down-regulated	Down-regulated	No	-	-		Yes	Down-regulated	Down-regulated	Down-regulated
NME8	No	-	-	-	No	-	-	-	No	-	-	-
NYAP1	No	-	-	-	No	-	-	-	No	-	-	-
Abi3	Yes	-	-	Up-regulated	Yes	-	Down-regulated	-	No	-	-	-
Plcg2	No	-	-	-	No	-	-	-	No	-	-	-

(Continued from previous page)

5.5.6 *Trem2 KO* effect on WT BV2 cells' gene expression programme

One of the aims of this chapter was to identify pathways which are disrupted by *Trem2* deficiency on BV2 cells. To this end, all the lists of differentially expressed genes obtained from the *Trem2* KO clone, irrespective of the timepoint, were compared with each other. This comparison allowed us to identify a list of genes which were disrupted by the *Trem2* deficiency regardless of the timepoint evaluated.

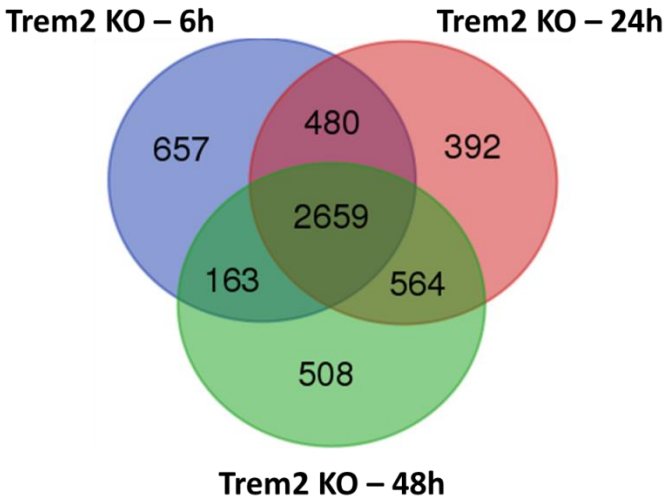

Figure 5.19 *Trem2* deficiency disrupts the expression of 2659 genes in BV2 microglia. The lists of differentially expressed genes generated from *Trem2* KO cells at each timepoint (6h, 24h and 48h) were compared with each other to identify those genes whose expression was disrupted by *Trem2* deficiency regardless of the timepoint. The number of genes shared by the 3 lists of differentially expressed genes was 2659.

As shown in Figure 5.19, *Trem2* deficiency disrupted the expression of 2659 genes in BV2 cells. This is a rather large number of genes which are disrupted and is equivalent to the number of genes disrupted by LPS stimulation on WT cells at 6 hours (1943 genes, see Figure 5.17). This list of 2659 genes was then used to look for enrichment of particular GO or Pathway categories.

A

1: GO: Molecular Function [Display Chart] 2616 annotations before applied cutoff / 18661 genes in category

	ID	Name	Source	pValue	FDR B&H	FDR B&Y	Bonferroni	Genes from Input	Genes in Annotation
1	GO:0017076	purine nucleotide binding		7.754E-9	8.564E-6	7.234E-5	2.028E-5	312	1879
2	GO:0030554	adenyl nucleotide binding		8.686E-9	8.564E-6	7.234E-5	2.272E-5	262	1530
3	GO:0032553	ribonucleotide binding		1.221E-8	8.564E-6	7.234E-5	3.193E-5	311	1880
4	GO:0032559	adenyl ribonucleotide binding		1.504E-8	8.564E-6	7.234E-5	3.935E-5	259	1518
5	GO:0032555	purine ribonucleotide binding		1.637E-8	8.564E-6	7.234E-5	4.282E-5	308	1864

Show 33 more annotations

B

2: GO: Biological Process [Display Chart] 9501 annotations before applied cutoff / 18623 genes in category

	ID	Name	Source	pValue	FDR B&H	FDR B&Y	Bonferroni	Genes from Input	Genes in Annotation
1	GO:0002682	regulation of immune system process		1.499E-14	1.424E-10	1.387E-9	1.424E-10	287	1506
2	GO:0006955	immune response		6.607E-13	3.138E-9	3.056E-8	6.277E-9	290	1572
3	GO:0006928	movement of cell or subcellular component		4.775E-9	1.512E-5	1.472E-4	4.536E-5	316	1882
4	GO:0001775	cell activation		7.533E-9	1.789E-5	1.742E-4	7.157E-5	186	1001
5	GO:0040011	locomotion		1.605E-8	2.559E-5	2.491E-4	1.525E-4	292	1735

Show 45 more annotations

C

3: GO: Cellular Component [Display Chart] 1078 annotations before applied cutoff / 19061 genes in category

	ID	Name	Source	pValue	FDR B&H	FDR B&Y	Bonferroni	Genes from Input	Genes in Annotation
1	GO:0009986	cell surface		5.848E-8	6.305E-5	4.767E-4	6.305E-5	160	873
2	GO:0098552	side of membrane		2.586E-7	1.394E-4	1.054E-3	2.788E-4	102	510
3	GO:0009897	external side of plasma membrane		4.306E-7	1.547E-4	1.170E-3	4.642E-4	69	310
4	GO:0005783	endoplasmic reticulum		6.070E-6	1.636E-3	1.237E-2	6.544E-3	267	1706
5	GO:0044432	endoplasmic reticulum part		1.155E-5	2.489E-3	1.882E-2	1.245E-2	192	1177

D

7: Pathway [Display Chart] 3063 annotations before applied cutoff / 12450 genes in category

	ID	Name	Source	pValue	FDR B&H	FDR B&Y	Bonferroni	Genes from Input	Genes in Annotation
1	1269203	Innate Immune System	BioSystems: REACTOME	9.213E-7	2.822E-3	2.428E-2	2.822E-3	221	1312
2	83048	MAPK signaling pathway	BioSystems: KEGG	3.516E-6	5.385E-3	4.634E-2	1.077E-2	58	255
3	1457780	Neutrophil degranulation	BioSystems: REACTOME	8.255E-6	8.428E-3	7.252E-2	2.528E-2	95	492
4	1404797	Platinum drug resistance	BioSystems: KEGG	5.421E-5	3.613E-2	3.109E-1	1.660E-1	22	73
5	82973	Glutathione metabolism	BioSystems: KEGG	5.898E-5	3.613E-2	3.109E-1	1.807E-1	18	54

E

18: Disease [Display Chart] 10889 annotations before applied cutoff / 16203 genes in category

	ID	Name	Source	pValue	FDR B&H	FDR B&Y	Bonferroni	Genes from Input	Genes in Annotation
1	C0023893	Liver Cirrhosis, Experimental	DisGeNET Curated	1.424E-18	1.550E-14	1.531E-13	1.550E-14	172	767
2	C0023467	Leukemia, Myelocytic, Acute	DisGeNET Curated	2.271E-12	1.236E-8	1.221E-7	2.473E-8	280	1646
3	C0023418	leukemia	DisGeNET Curated	3.242E-10	1.177E-6	1.162E-5	3.531E-6	298	1854
4	C0003873	Rheumatoid Arthritis	DisGeNET Curated	9.057E-10	2.466E-6	2.434E-5	9.863E-6	267	1640
5	C0002395	Alzheimer's Disease	DisGeNET Curated	3.109E-9	6.771E-6	6.685E-5	3.386E-5	289	1825

Figure 5.20 GO, Pathway and Disease enrichment analyses of BV2 genes disrupted by *Trem2* deficiency. GO, Pathway and Disease enrichment analysis was performed using the list of differentially expressed genes generated as a result *Trem2* deficiency (regardless of the timepoint); 2569 genes in total (see Figure 5.19). The analysis included 5 enrichment categories; 1) Molecular Function, 2) Biological Process, 3) Cellular component, 4) Pathway and 5) Disease pathways.

As seen in Figure 5.20, the list of genes differentially expressed as a consequence of *Trem2* deficiency shows an enrichment of terms associated with: binding to peptides, proteins, nucleotides, ATP, etc. (panel A, MF); cell activation, regulation of the immune response, cell migration and cytokine production (panel B, BP); cell surface, endoplasmic reticulum, endosome, etc. (pane C, CC); innate immune system and MAPK signalling pathway (Pathway). Additionally, there was an enrichment of terms associated with Rheumatoid arthritis and Alzheimer's disease in the Disease analysis (panel D). These results support the role of *TREM2* in cell activation and immune response, cell migration and cytokine production, while it offers a new link between *Trem2* deficiency and diseases like Rheumatoid arthritis and Alzheimer's disease. Pathway analysis showed enrichment of immune related pathways, such as innate immune system, MAPK

signalling pathways, Neutrophil degranulation and Glutathione metabolism. These results further confirm the role of *Trem2* in the regulation of immune responses (Yeh et al., 2017).

Curiously, there were some other members of the TREM family of genes among the 2659 genes differentially expressed as a consequence of *Trem2* deficiency. These genes included; *Trem3, Treml1* and *Treml4*. Remarkably, all of these genes were upregulated in the *Trem2* KO cell line compared to the WT cells. Parallel to these genes, *Trem1* was also differentially expressed by the lack *Trem2,* but only at the later timepoints (24h and 48h). These findings are interesting for 2 main reasons; 1) these group of genes are upregulated by the lack of *Trem2*, suggesting an interplay between members of the TREM family and, 2) TREM family members are all located in close proximity in the genome of both mouse and humans, as shown in Figure 5.21.

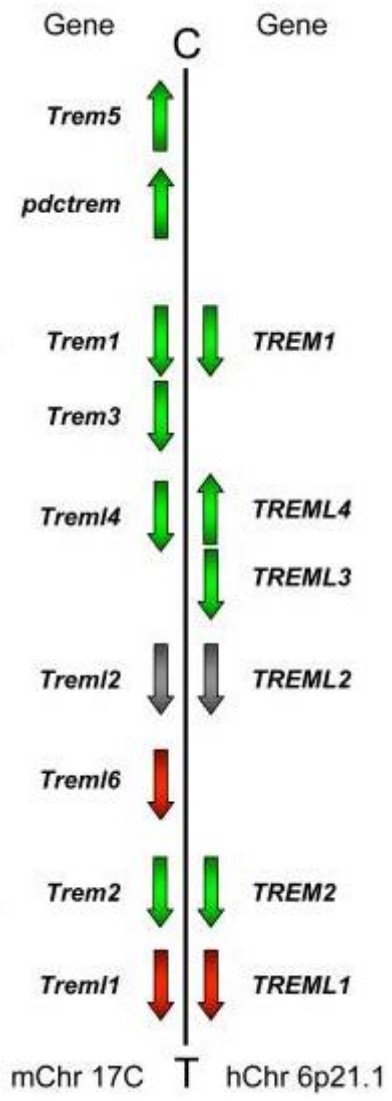

Figure 5.21 Localization of *TREM* genes on mouse chromosome 17C (left) and human chromosome 6p21.1 (right). Schematic of the relative position of TREM family members in both the mouse and human genomes. Genes shown in green are known or predicted to associate with *DAP12*, while those shown in red contain an ITIM (Immunoreceptor tyrosine-based inhibitory motif) motif(s). In contrast, *Treml2*, shown in gray, neither associates with *DAP12* nor has an *ITIM*. Modified from Ford and McVicar (2009).

5.6 Discussion

The aim of this chapter was to identify the immune/inflammatory activation mechanisms by which microglia may contribute to neurodegeneration, particularly in the case of AD. In this sense, this study aimed to dissect the microglial response to different immune activators and their correlation with stablished activation states (M1/M2 or other). As a possible link between AD and microglial activation, the microglial response to Aβ1-42 monomers, oligomers and fibrils was also evaluated. Another aim of this chapter was to investigate the relationship between the different microglial activation states and the expression of genes that have been associated with AD risk. Of particular interest was the role that *Trem2* might play in microglial activation and neurodegeneration. To this end, the response of *Trem2* KO cells (B5 cell line, obtained in Chapter 3) to the classical microglial activator LPS (M1) was also investigated.

At this point it is worth mentioning the importance of serum-starving microglial cells in order to immune downregulate them before stimulation/activation. Serum is rich in metabolites and growth factors, therefore it is universally used to supplement *in vitro* cell cultures, including microglial cells. Yet, it also contains many blood-borne molecules that are actively excluded from the CNS and that are not available to microglia in normal conditions. Serum supplementation of microglial cultures has been shown to alter their proliferative and phagocytic capacities, as well as their gene expression profile (Bohlen et al., 2017). Moreover, the morphology of BV2 cells is altered by the amount of serum in the culture medium. Cells grown in 10% serum are spherical, but when transferred into a serum-free culture medium these cells assume a more ramified appearance (Bohlen et al., 2017).

It is believed that increased autophagy, triggered by nutrient starvation conditions, is responsible for the immune downregulation of microglial cells grown in a serum-free medium (Bussi et al., 2017, Netea-Maier et al., 2016).There is evidence showing that autophagy controls immune processes in other tissues (for a review see Deretic et al. (2013)). Interestingly, microglial cells have been shown to undergo increased autophagy in both AD patients carrying *TREM2* risk variants and in *Trem2* deficient mouse models, highlighting the importance of *TREM2* in the cell's metabolic fitness (Ulland et al., 2017). Furthermore, there is evidence showing that degradation of extracellular soluble Aβ fibrils is dependent on autophagy mechanisms (Kitazawa et al., 2011).

Currently, most of the existing literature related to autophagy in the CNS (or AD for that matter) focuses on neurons with limited research exploring its effect on microglial function and immune activation (Arroyo et al., 2014, Plaza-Zabala et al., 2017). For this reason it is difficult to identify the effect that autophagy or serum starvation may have in

specific genes (such as *APOE* or *TREM2*). Nevertheless, there have been studies which have explored the effect of serum supplementation into serum-free cultures, which are starved and may undergo increased autophagy. In particular, Bohlen et al. (2017) showed that the addition of serum in microglial cultures lowered the expression levels of both *ApoE* and *Trem2* compared to serum-free cultures (supplementary information of the paper). Furthermore, the authors reported the upregulation of pathways involved in proliferation, amino acid metabolism and the complement immune system, while cytokine and lipid metabolism (*ApoE* is strongly associated with this pathway in the CNS) pathways are downregulated. The authors even observed a marked and sustained downregulation (by qPCR) of specific activation markers such as *Il1b, Tnf* and *Ccl2*, in primary microglial cells grown in serum-free conditions.

Conversely, Wang et al. (2017) have shown that the addition of 5% human serum (from healthy individuals or systemic lupus erythematosus patients) into BV2 cultures was able to upregulate the expression of MHCII and CD86 (the latter did not reach statistical significance), demonstrating clear microglial activation. However, in this study cells were not serum-starved (FBS was used for routine culture of cells) for any length of time before their stimulation with the human serum, which could affect the cells' sensitivity to stimuli. Altogether, serum supplementation has been shown to alter microglial cells in culture and for that reason it is common practice to avoid it before stimulation/activation.

Finally, it is worth discussing the role of the *APOE* gene in the immune response seen in AD in light of experimental results obtained. *APOE* is one of the many AD-risk genes related to neuroinflammation and there are numerous *in vitro* and *in vivo* studies that support this role (for a review Rebeck (2017)). For example, the different *APOE* isoforms have been shown to disturb inflammatory responses in microglia and astrocytes, with the *APOE4* isoform stimulating the strongest inflammatory phenotype (Lynch et al., 2003, Guo et al., 2004, Vitek et al., 2009). Conversely, APOE-based peptides signalling through the LRP1 receptor (Pocivavsek et al., 2009b), a known APOE receptor, have been shown to inhibit inflammatory processes in primary microglia (Pocivavsek et al., 2009a). APOE has also been shown to promote an anti-inflammatory phenotype in primary macrophages through binding to its receptors ApoER2 and VLDLR (Baitsch et al., 2011). Similarly, APOE-based peptides have been shown to alleviate and even prevent LPS-induced inflammation (Lynch et al., 2003), traumatic brain injury (Lynch et al., 2005), intracerebral haemorrhage (James et al., 2009) and focal ischemia (Wang et al., 2013) in mouse models. Remarkably, blocking inflammatory signalling can promote upregulation of APOE in microglia, suggesting that APOE levels and inflammation are in a negative feedback loop with APOE inhibiting inflammation and inflammation inhibiting APOE expression (Rebeck, 2017).

5.6.1 Microarray analysis of microglial activation: Different responses to LPS, Aβ1-42 (fibrils), dextran sulphate and fibrinogen.

To accomplish the first objective of this chapter, BV2 cells (murine microglial cell line) were exposed to six different stimuli; Aβ1-42 fibrils, dextran sulphate 1 and 100µg/mL, fibrinogen, LPS and an untreated control. Cells' responses were assessed in terms of whole gene expression using microarrays. Initial exploratory analysis of expression data, done during the quality control steps, already showed signs of sample clustering. PCA analysis (Figure 5.1) showed clustering of samples into three different groups; Dextran 100µg/mL, LPS and a third undefined cluster. Clustering of samples into 3 different groups indicated that these treatments produced markedly different gene expression responses in BV2 cells. Of particular interest was the third undefined cluster, which was composed of cells stimulated with Aβ1-42 fibrils, dextran sulphate 1µg/mL, fibrinogen and the untreated control, which suggested that these samples had similar genetic responses (or lack thereof) to those treatments.

To identify differences in the genetic responses to the different treatments, a multi-factor ANOVA was carried out. 21 comparisons (contrasts) were set up among conditions to be interrogated (Table 2.8) as part of the ANOVA. As shown in Table 5.2 and Figure 5.3, the only treatments that caused a statistically significant disruption in the gene expression programme of BV2 cells were: fibrinogen, LPS and dextran sulphate 100µg/mL.

The activation and disruption of the microglial gene expression profile by LPS was expected, as it is a well-known microglial activator which promotes the expression of several pro-inflammatory cytokines and enzymes that stimulate tissue inflammation (M1 activation) (Gonzalez et al., 2014, Nakamura et al., 1999). As seen in Figure 5.3, LPS disrupted the gene expression of 341, 420 and 516 genes at 6h, 24h and 48h after treatment, respectively.

Figure 5.3 also shows that fewer than 100 genes were differentially expressed when BV2 cells were treated with fibrinogen at any timepoint. A response to fibrinogen was expected as fibrinogen had already been shown to produce an inflammatory response in peripheral blood mononuclear cells (PBMCs). This response is driven by high levels of ROS, increased cytokine levels (TNFα, IL1β and IL6) and chemokine expression (CCL2, CCL3, CCL4, CXCL2) (Jensen et al., 2007). Yet, in the present study, fibrinogen only managed to downregulate *Tnfα* and *Cxcl2* at 6h (data not shown). It has been shown that fibrinogen can activate microglia via the αMβ2 integrin (ITGAM) (Jennewein et al., 2011).

Interestingly, infiltration of plasma proteins (including fibrinogen) into the CNS can activate microglial cells and trigger neurotoxic signalling cascades (Ryu and McLarnon, 2009, Hooper et al., 2009, Huang et al., 2008). Fibrinogen may enter into the brain through cerebral microbleeds or microhaemorrhages (Werring et al., 2010) which have been reported as an early event in AD (Sepehry et al., 2016). Elevated fibrinogen in plasma is also a risk factor for AD and vascular dementia (van Oijen et al., 2005, Xu et al., 2008) and a proposed CFS biomarker for AD (Lee et al., 2007).

Typically, the BBB (Blood-brain barrier) prevents fibrinogen from entering the brain; however, fibrinogen has been found in the brains of AD patients and mouse AD models (Cortes-Canteli et al., 2010, Jantaratnotai et al., 2010, Lipinski and Sajdel-Sulkowska, 2006, Viggars et al., 2011). BBB dysfunction, which has been reported in the brains of AD mice (Ujiie et al., 2003) and humans (Viggars et al., 2011), may explain the extravasation of fibrinogen into the brain parenchyma. BBB dysfunction can be caused by vascular factors associated with AD, including ischemia, ingestion of saturated fats or cholesterol, inflammation processes in the brain or hypertensive crises (Cortes-Canteli et al., 2012).

Interestingly, BBB dysfunction can also be caused by abnormal and excessive deposition of fibrinogen. *In vitro* studies have shown that high concentrations of fibrinogen can promote microvascular permeability by decreasing the levels of endothelial tight junction proteins (Patibandla et al., 2009). Similarly, BBB disruption can also be caused by cerebral amyloid angiopathy (CAA), which is characterised by the deposition of Aβ in the cortical and leptomeningeal vessel walls of arteries, arterioles and capillaries (Attems et al., 2011).

Dextran sulphate 100µg/mL disrupted the gene expression of 362, 186 and 1292 genes after 6h, 24h and 48h respectively (Figure 5.3). Dextran sulphate has been shown to be non-toxic and indigestible upon uptake by macrophages and it has also been shown not to disrupt cytolytic activity in macrophages (Hibbs, 1974). Remarkably, dextran sulphate is capable of simultaneously stimulating and suppressing cell-mediated immune responses (McCarthy and Babcock, 1978). In our study, dextran sulphate 100µg/mL promoted the biggest disruption in the genetic expression of BV2 cells, evidenced by the high number of differentially expressed genes.

In contrast, Aβ1-42 fibrils and dextran sulphate 1µg/mL did not have any effect on gene expression (Figure 5.3). As mentioned above, dextran sulphate is a non-toxic and indigestible molecule (Hibbs, 1974) and the lack of BV2 response when stimulated with dextran sulphate at 1µg/mL was not unexpected. On the other hand, there is evidence indicating that Aβ1-42 fibrils share receptors and intracellular signalling cascades with

LPS (Fassbender et al., 2004) and can induce an M1 activation of microglia, although less potently than oligomeric Aβ1-42 (Michelucci et al., 2009). Our results indicate that Aβ1-42 fibrils do not have any effect on BV2 gene expression at the concentration employed. A low Aβ1-42 fibril concentration was used in order to mimic the physiological concentration seen in the human brain. For subsequent experiments, it remains to be elucidated if higher Aβ1-42 fibril concentrations (or other Aβ1-42 conformations) can disrupt gene expression in BV2.

After identifying which treatments affected BV2 gene expression profiles, lists of differentially expressed genes for each treatment were obtained. GO analysis was performed using these gene lists and the DAVID (Database for Annotation, Visualization and Integrated Discovery) database. The first lists of differentially expressed genes to be analysed were those corresponding to the fibrinogen treatment. The lists of downregulated genes for all timepoints did not map to any pathway or GO category. Conversely, upregulated genes mapped into GO categories related DNA binding, transcription factor activity, biosynthetic processes related with the production of nucleobases and ribonucleobases. When the total number of differentially expressed genes was used for GO analysis, a similar result to the upregulated gene list was obtained, with no immune-related GO categories present. These results contrasted with previous studies in which fibrinogen induced an inflammatory response by PBMCs (Jennewein et al., 2011).

Next, GO analysis was carried out using the list of genes which were differentially expressed by the LPS treatment (Figure 5.5). Downregulated genes for 24h and 48h were associated with GO categories and pathways related to cell cycle progression, cell division, ribosomal activity and translation. This may suggest that prolonged LPS stimulation has an effect on cell division and proliferation in BV2 cells. Lists of upregulated genes for all three timepoints mapped to GO categories and pathways related with immune response, Toll-like and NOD-like signalling pathways and cytokine activity. LPS is a classical ligand of TLR4 (and others) and is known to induce M1 microglial activation (Tang and Le, 2015). As such, upregulation of immune associated pathways is in accordance with previous reports.

It is worth mentioning that there was a non-significant association between the LPS downregulated genes at 48h and an AD associated pathway (9 genes, Benjamini 0.073). This association became statistically significant (Figure 5.5) when the full list (up- and down-regulated genes) of differentially expressed genes (at 48h) was used (15 genes, Benjamini 0.012). Among these 15 associated genes are; *APOE, TNF, IL1β* and *APP* (Supplementary Fig. 7.7 and Supplementary Fig. 7.8). *APOE* (downregulated at 48h)

has been shown to bind Aβ peptides and influence Aβ aggregation and clearance of soluble Aβ (Liu et al., 2013, Castellano et al., 2011); consequently, downregulation of this gene can render microglia (and their surrounding cells) vulnerable to Aβ toxicity. On the other hand, higher levels of APP (upregulated at 48h) are associated with increased Aβ1-42 levels and fibril formation (Bettens et al., 2013). *TNF* and *IL1β* were also among the upregulated genes in this pathway. Interestingly, in mouse models of AD, increased levels of these two pro-inflammatory cytokines are associated with increased concentrations of Aβ (Patel et al., 2005, Lue et al., 2001a). These results suggest that M1 activation of microglia could decrease Aβ clearance and promote its accumulation together with increased expression of inflammation markers.

GO analysis was also carried out in the lists of differentially expressed genes by dextran sulphate 100μg/mL (Figure 5.6). Dextran sulphate seems to be able to disrupt the binding of essential molecules such as ATP, nucleotides, ribonucleotides and transcription factors, evidenced by the downregulation of such GO categories and pathways at 6h and 48h. Similarly, upregulated genes seem to affect RNA binding, metal ion binding and cellular ligase activity. Interpretation of the results from GO analysis at this point is difficult as there are no previous reports of similar studies in microglial cells to the best of our knowledge. Dextran sulphate is a nontoxic and indigestible molecule and has been shown not to affect macrophage activity (Hibbs, 1974). It has also been reported to stimulate and suppress cell-mediated immune responses (McCarthy and Babcock, 1978), but there is no information regarding their direct effect on cells. Interestingly, dextran sulphate 100μg/mL had the biggest number of differentially expressed genes; nonetheless, they do not seem to be associated with any immune response mechanisms.

It is well known that LPS stimulation of BV2 cells promotes M1 activation. To confirm this in our experiment, the expression of different M1 and M2 activation markers was evaluated in the lists of genes differentially expressed by LPS (Table 5.4). As anticipated, most M1 markers were upregulated. On the other hand, only one M2 marker (VEGF[a]) was upregulated, which confirmed our assumption regarding M1 activation of BV2 cells. These results are in agreement with what was reported by Michelucci et al. (2009) using primary microglial cells. Of note is the upregulation of the MHCII complex proteins and CD40 cell markers, both of which were among the 5-top differentially expressed genes in our experiment and are involved in the crosstalk with lymphocytes.

Another objective of this study was to investigate the effect of microglial activation (M1) on the genetic expression of specific genes which are commonly used as microglial cell markers. Out of the 10 genes assessed, 5 showed no differential expression throughout

the experiment (*Cd11b [Itgam], SFPi1, Cd68, Cd45 [PTPRC]* and *Cx3CR1*). The other 5 markers (*Iba1 [Aif1], Cd14, CSF1, CSF1R* and *EMR1*) were down- or upregulated at different timepoints. These results are significant as many studies use Iba1 to identify microglial cells in histological studies (Elmore et al., 2015, Zhang et al., 2014a). As shown in Table 5.3, prolonged M1 activation (48h) of microglial cells can promote downregulation of *Iba1,* giving rise to false negatives. The opposite can be said for the other 4 markers. As a result, it is highly recommended to use any of the 5 markers which were not differentially expressed during M1 activation of cells.

Finally, the expression of genes associated with increased AD risk was evaluated. Karch et al. (2014) put together a list of 31 genes that have been associated with AD in genetic studies. From this list, only 13 genes were differentially expressed in our experiment (Table 5.5). Fibrinogen caused the differential expression of only 2 genes (*CD33* and *Ms4a6a*), while dextran sulphate 100µg/mL caused differential expression of another 6 genes (*ApoE, Bin1, Pld3, Rin3, Picalm* and *Ptk2b*). Conversely, LPS caused the differential expression of 8 genes (*App, ApoE, CD33, Celf1 (Cucgbp), Ms4a6a (Ms4a6d), Inpp5d, Mef2c* and *Trem2*).

Stimulation of BV2 cells with fibrinogen and dextran sulphate 100µg/mL affected the expression of AD related genes for which there is limited functional information at the moment. This, coupled with the fact that there is little or no information regarding their effect on microglial activation, makes the interpretation of our results difficult at present. Nevertheless, it is clear that gene expression responses to these stimuli differ from that exerted by LPS (Figure 5.1). Interestingly, dextran sulphate has been proposed as a putative ligand of TREM2 (Daws et al., 2003) however neither of the two different doses used in our experiment had any effect on its gene expression (Table 5.5). Dextran sulphate is also able to reduce zymosan phagocytosis in both LPS-activated and non-activated RAW 264.7 cell lines (Sigola et al., 2016). In light of the effects of dextran sulphate on phagocytosis and its probable role as a TREM2 ligand, it would have been interesting to study the effect of *Trem2* deficiency on its uptake by BV2 cells. The opportunity to perform this assay in this thesis was missed as the models of *Trem2* deficiency were available. Future work should consider the use of the *Trem2*-deficient models in order to validate dextran sulphate as a TREM2 ligand.

In contrast, LPS treatment stimulated the differential expression of many AD-related genes. One of these genes is *App*; higher expression of *App* is linked to increased Aβ accumulation (Bettens et al., 2013) and in our experiment *App* was upregulated by LPS (M1 activation). This finding is a novel one, since *App* expression is mostly attributed to other cell types in the CNS (Zhang et al., 2014b). Another AD-related gene differentially

expressed by LPS is *ApoE*, which remains the strongest risk factor for AD. APOE is known to have a role in inflammation (Kim et al., 2009, Liu et al., 2013) and is able to influence aggregation and clearance of Aβ (Liu et al., 2013, Castellano et al., 2011). In consequence, downregulation of *ApoE*, as shown in our experiment, could favour Aβ accumulation and further disrupt inflammation mechanisms. In this regard, there are numerous *in vitro* and *in vivo* studies that support the role of APOE inflammation (for a review see Rebeck (2017)). For example, the different APOE isoforms have been shown to disturb inflammatory responses in microglia and astrocytes, with the APOE4 isoform stimulating the strongest inflammatory phenotype (Lynch et al., 2003, Guo et al., 2004, Vitek et al., 2009).

Conversely, APOE-based peptides have been shown to inhibit inflammatory processes in primary microglia (Pocivavsek et al., 2009a). Furthermore, APOE has also been shown to promote an anti-inflammatory phenotype in primary macrophages (Baitsch et al., 2011). Likewise, APOE-based peptides are able to alleviate and even prevent LPS induced inflammation (Lynch et al., 2003), traumatic brain injury (Lynch et al., 2005), intracerebral haemorrhage (James et al., 2009) and focal ischemia (Wang et al., 2013) in mouse models. Interestingly, blocking inflammatory signalling can promote upregulation of APOE in microglia (Pocivavsek and Rebeck, 2009), suggesting that APOE levels and inflammation are in a negative feedback loop (Rebeck, 2017).

CD33 is another gene which was differentially expressed by LPS; this gene is known to regulate innate immunity, neuroinflammatory processes and influence Aβ clearance (Malik et al., 2013, Jiang et al., 2014). Again, *CD33* downregulation could promote Aβ accumulation and dysregulation of immune mechanisms. Another gene downregulated by LPS is *Trem2*, a gene whose upregulation is known to stimulate phagocytosis and suppress inflammation (Rohn, 2013). As a result, *Trem2* downregulation could potentially exacerbate inflammation and reduce Aβ uptake by BV2 cells. *Trem2* downregulation by LPS (M1 activation) is in contrast with gene expression studies in brains from *App, Psen* and *App/Psen* transgenic mice, where there is upregulation of *Trem2* (Matarin et al., 2015). Remarkably, cells surrounding Aβ plaques in AD transgenic mice express high levels of *Trem2* (Frank et al., 2008) which, when compared with our results, suggests that microglial cells surrounding Aβ plaques have a different activation state to M1.

The results from this analysis suggest that M1 activation of microglial cells promotes the differential expression of AD-related genes which in turn promote the activation of different inflammatory mechanisms and the accumulation of Aβ peptides in the medium. Butovsky et al. (2005) and others have already published similar observations regarding

LPS stimulation; furthermore, they show that these effects can be partly resolved by stimulation with anti-inflammatory cytokines (including IL4 and TGFβ among others) *in vitro* and *in vivo* (for a review see Tang and Le (2016)).

The list of AD-related genes differentially expressed by LPS also includes; *Celf1 (CUGBP), Ms4a6a (Ms4a6d), Inpp5d* and *Mef2c*. The role of these genes in AD pathology remains largely unknown, but some of them may also be involved in the immune response: *Ms4a6a (Ms4a6d), Inpp5d* and *Mef2c* (Karch and Goate, 2015).

Validation of our microarray data was carried out using RT-qPCR quantification of *ApoE* and *Trem2* gene expression in a new set of experiments (Figure 5.7). The results of the validation closely replicated what was seen in the microarray data regarding fibrinogen and LPS activation and further showed that other stimuli such as ATP or IFNγ did not have similar effects on these two genes. It is worth keeping in mind that this first experiment was performed using microarrays, as they were ready available to our group. Statistical and expression analysis of results was relatively easy and not very time consuming (compared to NGS analysis). However, as mentioned in the introduction to this chapter, NGS RNAseq is becoming the method of choice for gene expression profiling studies as it offers a broader dynamic range and superior sensitivity (allowing the identification of new or tissue-specific transcripts). For example, some AD associated genes had no detection probes in the microarrays used, such as *CLU, NME8* and *NYAP1*. In the particular case of *CLU*, this gene was found to be differentially expressed by IL4 and TGFβ during the RNAseq experiment. Subsequent experiments were performed using NGS RNAseq to ensure that the lack of immune response seen in the fibrillary Aβ1-42 condition was not a result of the lower sensitivity of microarrays.

5.6.2 **RNAseq analysis of microglial activation: M1 and M2 activators**

In recent years, many studies have tried to unravel and expand the M1/M2 paradigm of microglial activation, as has been the case in macrophages (Martinez and Gordon, 2014). In AD, it is hypothesised that microglial activation is further complicated by the presence and microglial phagocytosis of Aβ plaques and tangles that are present in the extracellular space. Furthermore, changes in microglial activation status depend on the disease stage and severity; understanding the stage-specific changes in M1, M2 and other activation phenotypes may provide new insights into the pathogenic and degenerative mechanisms involved in neurodegenerative diseases (Tang and Le, 2016). This section attempts to expand the M1/M2 paradigm since many authors (Boche et al., 2013) consider it to be an over simplified, yet useful, model of microglial activation.

To this end BV2 cells were activated with 5 different stimuli (not including the untreated control): LPS (M1), TGFβ (M2), IL4 (M2), Aβ1-42 monomers and Aβ1-42 oligomers.

Changes in whole gene expression profiles were assessed at 3 different timepoints; 6h, 24h and 48h. As there are concerns regarding the proper characterization of Aβ1-42 species (Benilova et al., 2012), characterization of our preparations was performed using a morphological method based on TEM (Figure 5.10) (Jan et al., 2010).

Subsequently, whole genome expression changes were measured using an RNAseq approach. Initial exploratory analysis of normalised sequencing reads by PCA already showed clustering of samples according to their treatment and timepoint (Figure 5.11). Four distinctive sample clusters were seen: LPS, TGFβ, IL4 and Control-monomer-oligomer clusters. Clustering of samples points to significant differences between BV2 responses to the treatments, which were expected in the case of LPS, IL4 and TGFβ. Surprisingly, clustering of Aβ1-42 monomers and Aβ1-42 oligomers with the control (untreated) samples suggests very little effect (if any) of these treatments in the gene expression of BV2 cells.

Since all samples passed QC, they were all included in the ANOVA statistical analysis for the identification of differentially expressed genes. In this analysis 18 comparisons (contrasts) were set up (Table 5-6). As shown in Figure 5.12, not all treatments were able to disrupt gene expression in BV2 cells: Aβ1-42 monomers and oligomers had no effect on microglial gene expression. This result is again surprising since Aβ has been shown to activate microglia *in vitro*, through binding to PRRs, including RAGE (receptors for advanced glycation end products) (Yan et al., 1996), TLRs (Landreth and Reed-Geaghan, 2009), and scavenger receptors (El Khoury et al., 1996, Paresce et al., 1996).

Furthermore, activated microglia are closely associated with Aβ deposits in brains from AD patients and AD mouse models (Frautschy et al., 1998, McGeer et al., 1987). Aβ activated microglia show increased cytokine release and expression of inflammatory markers such as CD36, CD14, CD11c, MHCII and iNOS (Kamphuis et al., 2016, Martin et al., 2017). Interestingly, plaque associated microglia generally manifest M2 activation (as confirmed by YM1 staining) (Jimenez et al., 2008). This is an interesting fact, if we keep in mind that the phagocytic activity of microglia is attenuated by pro-inflammatory cytokines such as IFNγ, IL1β, and TNFα, which are associated with M1 microglia activation (Koenigsknecht-Talboo and Landreth, 2005).

In a similar study to ours, Walker et al. (2006) reported differential expression of more than 600 genes by post-mortem microglial cells from AD patients and matched control stimulated with 500nM and 2μM of oligomeric Aβ. They used microarrays (Human IB array) in their experiment. Nonetheless, in a recent report Das et al. (2016) demonstrated that BV2 cells have a reduced immune response triggered by LPS when compared to primary microglia. In light of both our microarray and RNAseq results regarding

differential expression of genes by Aβ1-42 stimulation, it is sensible to hypothesize that BV2 microglia may not be able to mount an immune response that can be detected by the methods used in this thesis. This lack of response can be explained by a myriad of reasons, and one of them could be the lack of appropriate receptors (Das et al., 2016) for the detection of Aβ1-42 molecules in BV2. A second probable reason for this lack of activation could be the low dose of Aβ peptides used. As an example, Walker et al. (2006) used a dose of 2μM Aβ oligomers to stimulate primary human microglia, while in this study we used concentrations of 20nM for fibrils and 500nM for monomers/oligomers. Stimulations with low Aβ doses were carried out to make our results comparable with the physiological doses of Aβ (~200pM) found in the brain (Koppensteiner et al., 2016). Finally, there is also the possibility that BV2 cells do not respond to Aβ1-42 molecules at all. However, Pan et al. (2011) have shown that oligomeric (and fibrillar to some extent) Aβ1-42 induce a potent inflammatory response in BV2 cells, though this was achieved with a dose of 1μM.

All other treatments (LPS, IL4 and TGFβ) influenced BV2 gene expression regardless of the timepoint. Lists of differentially expressed genes were generated for each condition after ANOVA. A remarkable observation at this stage was the almost perfect 50-50% split between the up- and down-regulated genes in each gene list. Remarkably, there was a decrease in the number of differentially expressed genes by LPS in the later timepoints. This was not the case for IL4 or TGFβ, which either maintained or increased the number of differentially expressed genes as time passed. These results suggest that BV2 cells have an acute and transient response to LPS, with a more prolonged and sustained response to IL4 and TGFβ (both M2 activators).

Gene ontology analyses of these three stimuli (performed for each timepoint) showed a clear enrichment of immune-associated GO categories and pathways (see Figure 5.13, Figure 5.14 and Figure 5.15). Interestingly, some of the differentially expressed gene lists were enriched with genes associated with AD (see Table 5-7 and Supplementary Fig. 9.9). Specifically, IL4 treatment showed enrichment of an AD disease pathway in all three timepoints evaluated. Meanwhile, LPS showed enrichment of terms associated with this AD disease pathway only at 48h, which is consistent with the previous findings reported in the microarray experiment (Figure 5.5).

After GO analysis, the changes in the gene expression of microglial and activation markers were assessed after stimulation with LPS, IL4 and TGFβ. As seen in Table 5-8, only 5 microglial markers were not disrupted by stimulation with any of the three microglial activators; *Cd11b (Itgam), SFPi1, CD68, CD45 (Ptprc)* and *EMR1*. Considering these results, it is advisable to use any of these 5 markers for studies of

microglial populations which might be activated. Among the microglial markers whose gene expression was disrupted is *Iba1 (Aif1)*, a gene which is widely used for the identification of microglial cells in pathological studies (Hellwig et al., 2015, Bachstetter et al., 2015). In the case of the microarray experiment, expression of *Iba1 (Aif1*) was downregulated by the LPS treatment at 48h, while in the RNAseq experiment this same gene was upregulated at 48h. These contradictory results suggest a highly dynamic expression of Iba1 (Aif1) in BV2 cells, which can lead either to an under- or over-estimation of the cell populations when used as a marker for the identification of microglia that could be M1 activated. Nevertheless, previous studies have shown that *Iba1 (Aif1*) is upregulated during microglial activation (Ito et al., 1998, Imai and Kohsaka, 2002, Sieber et al., 2013). IBA1 protein (Ionised calcium Binding Adapter molecule 1) is a member of the calcium-binding group of proteins (Korzhevskiy and Kirik, 2015). Little is known of the functions of IBA1. This protein has been shown to participate in cytoskeleton reorganization during phagocytosis (Ohsawa et al., 2000, Ohsawa et al., 2004). Its interaction with elements of the cytoskeleton is mediated through binding to ACTIN molecules (Sasaki et al., 2001).

Later, the effect of the 3 different microglial activators on the expression of M1- and M2-associated genes was investigated. As it was expected, LPS treatment upregulated the expression of most of the M1-associated genes and some M2-associated markers (VEGF(a), TGFβ, and PDGF). In this sense, upregulation of M2-associated genes like TGFβ could be part of the resolution response that microglia implements after LPS stimulation (Qian et al., 2008). Upregulation of M2 markers (such as VEGF(a)) by LPS in BV2 cells was also seen in the microarray study. Surprisingly, there were many M1-associated genes which were upregulated by IL4 (MHCII, CD40, IL1β and CCL2) and TGFβ (MHCII). Notably, IL4 reduced the expression of TNF, while TGFβ reduced the expression of IL1β and CCL2. As for M2 markers, IL4 upregulated the expression of *Arg1* and downregulated *PDGF*, while TGFβ upregulated the expression of *VEGF*(a), *PDGF* and *Arg1*. Upregulation of *Arg1* by both IL4 and TGFβ is consistent with M2 activation (Tang and Le, 2016). ARG1 participates in arginine metabolism and has been shown to protect neurons from injury by pro-inflammatory cytokines (Williams, 1997). Analysis of the differential expression of M1 and M2 markers in our experiment supports the observations made during the PCA (Figure 5.11); LPS, IL4 and TGFβ elicit very different responses in BV2 cells. Not only that, but despite IL4 and TGFβ both being M2 activators, they showed clear differences in their microglial responses, supporting the idea of a greater diversity in microglial responses than the dichotomy of the M1 and M2 activations (Tang and Le, 2016). This analysis also shows that the categorisation of markers according to the M1 and M2 activation states should only be used as a reference, since

genes like MHCII (classically associated with M1 activation) can be upregulated by LPS, IL4 and TGFβ. Finally, the timing of the stimulations should also be considered in this kind of analysis: for example, IL1β is upregulated by both in LPS and IL4 at 6h and 24h, but remains upregulated only by LPS at 48h.

The last step in the analysis of the microglial activation involved the study of the effect of different activators on the expression of AD-related genes. The list of AD-related genes used for this work was compiled by Karch et al. (2014) with the addition of two new AD-associated genes (*Abi3* and *Plcg2*) from a recent association study (Sims et al., 2017). As shown in Table 5.10 and similarly to what happened in the case of the microglial and activation markers, each of the treatments affects the expression of AD-related genes in different ways. For example, the newly reported gene *Abi3* is downregulated by LPS and IL4, and upregulated by TGFβ. *Abi3* has a role in the innate immune response via interferon-mediated signalling (Fairfax et al., 2014). *Trem2* is another gene whose expression is affected differently by these microglial activators. *Trem2* expression is downregulated by LPS (this same result was obtained in the microarray experiment, Table 5-5), it is not affected by IL4 (yet Turnbull et al. (2006) report an increase at the protein level) and is upregulated by TGFβ. Since *Trem2* upregulation is associated with increased phagocytosis capacity and suppression of inflammation (Rohn, 2013), stimulation of microglial cells with TGFβ could have a positive effect over amyloid plaque load without inflammation. *Trem2* downregulation caused by LPS (M1) could have the opposite effect, reducing Aβ phagocytosis while promoting a pro-inflammatory milieu. Upregulation of TREM2 protein in cells surrounding Aβ plaques in AD transgenic mice models (Frank et al., 2008) could be explained by a TGFβ-like activation of microglial cells in an attempt to resolve the plaques without inflammation.

Analogous to the microarray experiment, *ApoE* gene expression was downregulated by LPS. Meanwhile, its expression was not affected by IL4 and was upregulated by TGFβ. *ApoE* has been shown to influence aggregation and clearance of Aβ (Liu et al., 2013, Castellano et al., 2011) and its upregulation by TGFβ could have a positive effect, preventing Aβ aggregation and promoting its clearance. In this sense, Rebeck (2017) noted that APOE levels and inflammation are in a negative feedback loop, with APOE inhibiting inflammation and inflammation inhibiting APOE expression. This observation has been partially validated in our experiment as *Apoe* expression was downregulated by LPS (M1 activator) and upregulated by TGFβ (M2 activator), however IL4 (M2 activator) did not have any effect on their expression, further suggesting a greater complexity in the immune activation of BV2 cells and microglia in general.

Another important AD-associated gene which was differentially expressed by the different immune activators was *Clu*. Interestingly, *Clu* expression was only affected by M2 activators; IL4 and TGFβ. IL4 downregulated *Clu* expression at 48h only, while TGFβ upregulated its expression at 24h and 48h. CLU is a chaperone protein involved in apoptosis, complement regulation, lipid transport and cell-to-cell interactions (Jones and Jomary, 2002). Similarly to APOE, CLU has been shown to directly interact with Aβ and alter fibril formation *in vitro* (Reviewed by Li et al., 2014). Furthermore, there is evidence showing that both APOE and CLU can influence Aβ deposition and clearance *in vivo* (DeMattos et al., 2004). Moreover, CLU can modulate neuroinflammation by inhibiting the inflammatory response associated with complement activation (Nuutinen et al., 2009). Changes in *Clu* expression can have different effects on the progression of AD, either by inhibiting Aβ fibril formation, deposition and clearance or by regulating complement activation and lipid transport.

Interestingly, microglial cells in culture have been shown to require exogenous cholesterol for prolonged survival (Bohlen et al., 2017). Unlike macrophages in peripheral tissues, microglia do not have access to circulating lipoparticles from the blood or the CSF (Pfrieger and Ungerer, 2011). However, cholesterol is synthesised *de novo* within the CNS and it is transported via APOE and/or APOJ (CLU) proteins (Pfrieger and Ungerer, 2011, LaDu et al., 1998). Interestingly, TREM2 has recently been shown to participate in the binding and uptake of lipidated APOE and APOJ by microglial cells, with disease-associated TREM2 variants showing deficiencies in lipoparticle recognition and engulfment (Yeh et al., 2016). Furthermore, genetic variants in these three genes (*APOE*, *APOJ*, and *TREM2*) are among the strongest alleles linked to AD identified to date (Wes et al., 2016), and *APOE* variants alter Aβ clearance and microglial cholesterol content (Lee et al., 2012). These data highlights the importance of exogenous lipid species in microglial survival, suggesting that deficiencies (or the presence of AD-associated mutations) in these 3 genes in particular could result in a generalised microglial dysfunction related to insufficient delivery of cholesterol or other lipid species to the cells (Bohlen et al., 2017).

On the other hand, *CD33* was downregulated by both LPS and IL4, and was not affected by TGFβ. Importantly, in the microarray experiment *CD33* was also downregulated by LPS. CD33 is involved in the regulation of the innate immunity response, neuroinflammatory processes and can influence Aβ clearance (Malik et al., 2013, Jiang et al., 2014), its downregulation by LPS and IL4 can have detrimental effects on an AD context, by disrupting innate immune responses and Aβ clearance mechanisms. Other genes such as *INPP5D* and *MEF2C* were also shown to be downregulated by LPS in both the microarray and RNAseq experiments, validating these results. However genes

such as *APP, CELF1 and MS4A6A* were shown to be differentially expressed in the microarray experiment but showed no expression changes in the RNAseq experiment, showing that the different quantification platforms have different sensitivities and suggesting that a gene-by-gene validation may be needed in some cases. Future experiments should aim to validate or settle the differences seen between the two quantification platforms in the activation of microglial cells.

The analysis of the effect of LPS, IL4 and TGFβ in the gene expression of AD-related genes showed that both M1 and M2 activations can have beneficial and detrimental effects in an AD context. In order to harness the benefits of immune regulation of microglial cells in AD, and other neurodegenerative diseases, it is pivotal to understand the function of microglial genes and their expression changes in response to different immune activation states (Tang and Le, 2016).

5.6.3 **RNAseq analysis of microglial activation: Effect of *Trem2* deficiency on microglial gene expression and in response to LPS stimulation**

Identification of the *TREM2 R47H* rare variant as a strong genetic risk factor for AD (Guerreiro et al., 2013b, Jonsson et al., 2013) has certainly boosted interest in the role that microglia and neuroinflammation play in this disease. Emerging evidence has demonstrated the ability of TREM2 to promote anti-inflammatory responses in microglia (Hamerman et al., 2006, Turnbull et al., 2006). Furthermore, TREM2 has also been linked to the regulation of cell proliferation (Otero et al., 2012, Takahashi et al., 2005a), something that has not been observed in this thesis (see Section 4.3.1.3.2), another important cellular function for appropriate immune response. *In vivo* and *ex vivo* studies of microglial populations have shown that *Trem2* deficiency leads to an increase in pro-inflammatory cytokines such as IL1β and TNFα in response to LPS (Zheng et al., 2016), something that was also observed in this thesis (see Section 4.3.1.3.4) . *Trem2* deletion in murine alveolar macrophages resulted in enhanced expression of TLR4, TNFα and IL10 in response to LPS (Gao et al., 2013); we observed the opposite effect for IL10 in this thesis (see Section 4.3.1.3.4). However, the molecular mechanisms by which TREM2 could regulate microglial inflammatory responses remain unclear.

Chapters 3 and **4** describe the generation and characterization of isogenic BV2 cell lines which lacked the *Trem2* gene. These models were generated with the aim of investigating the molecular mechanisms that are disrupted in *Trem2's* absence. Identifying the molecular pathways which are disrupted by *Trem2* deficiency is the first step towards finding *Trem2*-specific pathway(s).

To this end, BV2 WT (*Trem2* +/+) and B5 (*Trem2* -/-) cells lines were treated with LPS (M1) and their gene expression responses were evaluated at three different timepoints (6h, 24h and 48h). Whole genome expression analysis was performed using an RNAseq approach. PCA of normalised sequencing reads already showed clustering of samples according to their *Trem2* genotype, treatment and timepoint (Figure 5.16). 4 distinctive sample clusters were seen: WT-untreated, WT-LPS treated, *Trem2* KO-untreated and *Trem2* KO-LPS treated clusters. Clear clustering of samples according to their *Trem2* genotype points to significant disruption of the gene expression of BV2 cells in the absence of *Trem2*. The clear divide between the WT and KO responses to LPS, suggests that these two cell lines also responded differently to this stimulus.

After QC of the RNAseq data, the next step was the identification of differentially expressed genes using an ANOVA analysis and 12 comparisons (contrasts) (Table 5-6). As shown in Figure 5.17, *Trem2* KO cells (LPS treated or untreated) showed a higher number of differentially expressed genes than untreated WT and LPS treated WT cells at any timepoint, which suggest an important disruption in the gene expression profile of BV2 cells. This result contrasts with a recent study by Mazaheri et al. (2017), where the authors report that the microglial homeostatic gene expression signature was not lost in *Trem2*-deficient cells. Although there are many technical differences between our studies (Mazaheri *et al.* used primary microglia from WT and *Trem2* -/- mice and the NanoString technology), there is enough evidence, mainly the large number of differentially expressed genes found in our study, to strongly suggest that *Trem2* deficiency has a major impact in the gene expression profile of BV2 cells.

A second observation, made during this part of the analysis, was the gradual reduction in the number of differentially expressed genes in LPS treated WT cells. This reduction suggests a steady de-activation of BV2 cells and inflammatory resolution. Meanwhile, *Trem2* KO cells showed a great number of differentially expressed genes when left untreated (almost twice the amount of differentially expressed genes seen in LPS treated WT cells). Furthermore, the number of differentially expressed genes increased at each timepoint when KO cells were treated with LPS. Moreover, these changes in expression don't appear to be an exaggerated immune response on the part of LPS-treated *Trem2* KO cells (>4250 genes), but rather show a high basal immune activation in these cells (*Trem2* KO untreated, ~4100 genes). Again, these results contrast with other studies which report an exaggerated response to inflammatory stimuli by *Trem2* deficient macrophages (Gawish et al., 2015a, Turnbull et al., 2006, Hamerman et al., 2006). In light of our results regarding the number of differentially expressed genes in *Trem2* KO cells, it can be concluded that the gene expression profile of BV2 cells is greatly disrupted by *Trem2* deficiency and this inevitably has detrimental effects on the cells' function,

including their immune response. A further observation is the impaired capacity of *Trem2* KO cells to gradually reduce the number of differentially expressed genes induced by LPS stimulation. The number of differentially expressed genes after LPS stimulation remained almost constant (between 4254 and 4595) throughout the experiment. These results contrast with other studies where the early inflammatory response seen in *Trem2* -/- mice was followed by an accelerated resolution of inflammation (Gawish et al., 2015a).

The next step in the analysis was the identification of GO and pathway enrichments in the generated gene lists. As was expected, most GO and pathway categories which showed enrichment of terms were related to already known immune and inflammatory mechanisms (Lue et al., 2015). Pathway analysis showed enrichment of terms related to peptide and protein translational processes, suggesting that *Trem2* could also have a role in protein translation. Interestingly, there was an enrichment of disease terms related to Rheumatoid Arthritis (which could be related to the Nasu-Hakola phenotype), neurodegenerative disorders and Alzheimer's disease, supporting the pathogenic role of *Trem2* in these diseases.

In contrast to what was done for the microarray experiments, GO analysis in the RNAseq data did not take into account the directionality of gene expression (i.e. whether a particular gene was down- or upregulated). Directional enrichment of gene lists and subsequent GO analysis has been shown to identify more efficiently those pathways and GO terms that are more pertinent to phenotypic differences. As a result, many researchers refer to the GO categories or pathways that are enriched for down- or upregulated genes as activating or inhibiting. Nevertheless, to consider those GO categories or pathways as activating or inhibiting based in their enrichment of down or upregulated genes may be inappropriate. Researchers must keep in mind that one of the most important limitations of gene enrichment analysis is that a "statistically" significant pathway (or category) only indicates a non-random disruption, but it does not advise about its biological implications (Hong et al., 2014). It is also worth keeping in mind that enrichment analysis, as used in this thesis, is based in the overrepresentation of genes associated with a particular GO term or pathway in our gene lists. If the goal of the enrichment analysis is to identify down or upregulated pathways in our gene lists, a different kind of analysis will be needed, namely GSEA (gene set enrichment analysis). This method starts from a list of gene-level statistics (such as fold change) and based on these statistics, calculates a gene set statistic for each gene set being analysed (Varemo et al., 2013). The results from the mRNAseq experiments (and microarray) will benefit from this kind of analysis which should be explored in order to gain new insights from microglial gene expression and *Trem2* deficiency.

After GO and pathway analysis, the effect of *Trem2* deficiency on the expression of microglial and activation markers was evaluated. As seen in Table 5.12, LPS, IL4 and TGFβ modified the gene expression of many cell markers which are widely used for the identification of microglial populations; these genes included *Cd11b* (*Itgam*), which is also a member of the Complement immune system. Remarkably, there seems to be a link between *Cd11b* and *Trem2* as high expression of this marker has been associated with higher expression *Trem2* (Kim et al., 2017). Nevertheless, in our experiment *Cd11b* was upregulated in *Trem2* deficient cells (untreated and LPS treated). It also important to remember *Cd11b's* role in the complement system as upregulation of CR1 and other complement factors have been reported in affected regions of AD brains (Shen et al., 1997). *ITGAM* encodes for the CD11b-integrin which pairs with the CD18-integrin to form a functional Mac-1-integrin (also known as CR3). Mac-1 is mainly expressed by myeloid cells (including macrophages, neutrophils and dendritic cells). Furthermore, CD11b expression is C5 (another member of the complement system) dependent in both granulocytes and monocytes. As shown in Section 4.3.1.3.4 and Supplementary figure 7.4, expression of C5a complement factor was upregulated in *Trem2*-deficient clones, suggesting an interaction between these two proteins. C5a is considered as a promiscuous receptor as it binds a great variety of ligands, including the complement protein iC3b and fibrinogen. Mac-1 mediates phagocytosis of iC3b-coated particles, such as apoptotic cells. It has also been shown to inhibit several immunological processes. In macrophages, Mac-1 modulates TLR signalling through Src/Syk signalling and is also capable of inducing expression of suppressor of cytokine signalling 3 (SOCS3) and protein A20, as well as IL10 (Fagerholm et al., 2013). Consequently, downregulation of *Cd11b* in microglia could reduce phagocytosis of apoptotic cells opsonised by iC3b and encourage TLR signalling and cytokine production.

Iba1 (*Aif1*), another classical microglial marker, was also upregulated in *Trem2* KO cells (untreated or LPS treated). Out of a list of 10 microglial markers, only 3 were not differentially expressed by *Trem2* deficiency or LPS treatment: *SFPi1, CD45 (Ptprc)* and *EMR1*. These 3 microglial markers are the only microglial markers that have not been differentially expressed by any of the stimuli used in any of the experiments carried out in this thesis. As a result, it is strongly suggested that these 3 proteins are routinely used as microglial markers to avoid over- or under-representation of different microglial populations. Changes on the expression of the novel microglial marker Tmem119 (Bennett et al., 2016) was also examined. As a result, this marker was found to be upregulated by *Trem2* deficiency and in response to LPS stimulation (both in WT and *Trem2* KO cells), which may lead to the erroneous identification or an over-estimation of

the number of microglial cells, caused by changes in the *Tmem119* gene expression rather than changes in cell number.

The effect of *Trem2* deficiency on the expression of M1 and M2 related markers was also scrutinised. Surprisingly, *Trem2* KO cells (untreated or LPS treated) had a large number of differentially expressed M1 and M2 markers, which suggest a major dysregulation of the microglial activation mechanisms. This result is consistent with observations made by other groups which report *Trem2* KO cells as having an altered inflammatory status. Although *Trem2* is usually considered to have an anti-inflammatory role in microglia, it is becoming increasingly clear that the *Trem2* immune modulatory role is more complex. The role of *Trem2* role in inflammatory responses is now believed to depend on the precise stimuli, strength, duration of stimulation and the cell context (Jay et al., 2017). Support for this concept comes from network analysis, in which *Trem2* was found to be co-expressed with both pro- and anti-inflammatory gene clusters (Forabosco et al., 2013).

The next step in our analysis was the evaluation of the effect of *Trem2* deficiency on the expression of AD-related genes. As seen in Table 5-14, *Trem2* deficiency caused disruption in the gene expression of 13 AD-related genes under untreated and 10 genes when *Trem2* KO cells were treated with LPS. Meanwhile LPS activation of WT BV2 cells caused the differential expression of only 8 genes. The 13 genes differentially expressed by the *Trem2* deficiency were: *ApoE, CD33, Mef2c, Trem2, Bin, Picalm, Cass4, Psen2, Sorl1, Adam10, Madd, Clu* and *Abi3*. As discussed before (microarray and RNAseq analysis of M1 and M2 responses), changes - particularly downregulation - on the expression of genes such *as ApoE, CD33, Trem2* and *Clu* can have negative effects in the context of AD pathology. Moreover, the disruption in the gene expression patterns of a considerable number (13 out of 33) of AD-related genes in the *Trem2* KO cells suggests that *Trem2* plays an important role in the regulation of AD associated pathways.

Finally, gene enrichment analysis of GO terms and pathways was carried out using only those genes which were differentially expressed because of *Trem2* KO regardless of the timepoint. To that end, all gene lists generated from untreated *Trem2* KO cells were compared to identify the group of genes that was differentially expressed as a result of *Trem2* deficiency at all timepoints (see Figure 5.19). Once those genes were identified, GO and pathway enrichment analysis was performed on this list. This list showed an enrichment of terms associated with: binding to peptides, proteins, nucleotides, ATP, etc. (MF); cell activation, regulation of the immune response, cell migration and cytokine production (BP); cell surface, endoplasmic reticulum, endosome, etc. (CC); innate immune system and MAPK signalling pathway (Pathway). Additionally, there was an

enrichment of terms associated with Rheumatoid arthritis and Alzheimer's disease in the disease analysis (Disease). These results support the role of *Trem2* in cell activation and immune response, cell migration and cytokine production (Sarlus and Heneka, 2017, Yeh et al., 2017), and they also point to a strong link between *Trem2* and Alzheimer's disease. Remarkably, in Chapter 4 of this thesis it was shown that BV2 cell migration had some degree of impairment (Section 4.3.1.3.3, more biological repeats of the migration experiment are needed to confirm this). Similarly, in the same chapter it has been shown that cytokine release was impaired in a *Trem2* dose response manner (Section 4.3.1.3.4). Conversely, we did not find any evidence, at the gene expression level, that pointed towards dysregulation in any phagocytosis related pathway or GO category at any timepoint. This observation is agreement with the results shown in Section 4.3.1.3.1, where TREM2 deficient cells showed no reduction of their phagocytic capacity compared to WT BV2 cells.

One final observation made during the expression analysis revealed that among the 2659 genes differentially expressed as a consequence of *Trem2* deficiency, there were some members of the *TREM* family, including: *Trem3, Treml1* and *Treml4*. Additionally, *Trem1* was differentially expressed but only at 24h and 48h. All the members of the TREM family, with the obvious exception of *Trem2*, were upregulated in the *Trem2* deficient cell line B5, which suggests that their functions are linked and co-regulated. TREM (and TREM-like) receptors are a family of structurally receptor proteins encoded by genes clustered together in chromosome 17 of mice or chromosome 6 of humans (as seen in Figure 5.21). These innate immune receptors are expressed mainly by myeloid cells (including monocytes, macrophages, microglia and osteoclasts among others) and are critical for the fine tuning of the immune response either by amplifying or dampening TLR-induced activation. Although these findings are very interesting, it is difficult to assess their relevance in the context of microglial activation, as neither their function nor their ligands are currently known. Interestingly, *Trem1* is the only exception since it has been identified as an amplifier of the inflammatory response in sepsis. Correspondingly, *Trem1* ligands have been detected on the surface of murine neutrophils and human platelets. However, the exact identity of this ligand remains unknown (reviewed by Ford and McVicar (2009)). Although a direct cross-talk between TREM1 and TREM2 signalling pathways has not been clearly defined, several studies have shown downregulation of cytokines such as TNFα by TREM2 suggesting opposing roles of these two receptors during immune activation (Roe et al., 2014).

6 CHAPTER 6: General Discussion and Conclusions

AD is the most common cause of dementia, accounting for 60-80% of all cases (Alzheimer's Association, 2014). It is characterised by progressive neuronal degeneration and synaptic loss, resulting in memory and motor impairment and an overall decline in cognitive function. It eventually leads to mental and functional incapacity and death (Mayeux, 2010). Currently, there is no treatment to slow or stop AD (Alzheimer's Association, 2014).

Pathologically, AD is characterised by extensive brain atrophy, accumulation of extracellular amyloid plaques, presence of intracellular neurofibrillary tangles (composed of abnormal tau protein) and significant neuronal loss (Mayeux, 2010). Another important pathological characteristic of AD is neuroinflammation (Rohn, 2013). It is well established that microglia, the brain's resident phagocytes, are pivotal for the inflammation/immune response in AD and other neurological diseases. Microglia act normally as sentinel cells, attacking and removing pathogens and cell debris (Wyss-Coray, 2006), but become reactive in AD (Pocock et al., 2002).

Recent GWAS studies have identified more than 20 (low risk) genetic variants associated with LOAD, the most prevalent form of AD. These variants have been associated with genes whose functions are involved in immune response, endocytosis and lipid biology. Many of these associated genes are highly expressed by microglia (Karch and Goate, 2015) further supporting the role of inflammation in AD pathology. The recent identification of a low frequency mutation in *TREM2* - a gene that confers increased risk of AD in LOAD cohorts - has brought neuroinflammation, and particularly the role of microglia, back to the centre of AD pathology (Guerreiro et al., 2013b, Jonsson et al., 2013).

The overriding aim of this thesis was to identify the immune/inflammatory mechanisms by which microglia may contribute to AD and other neurodegenerative diseases. This study was primarily focused on establishing links between microglial activation (M1/M2 or other) and stimulation with Aβ1-42 monomer, oligomers and/or fibrils. Of particular interest was the role that TREM2 might play in microglial activation and neurodegeneration. To this end, a second objective of this project was the generation and characterization of *Trem2* knock-out and *Trem2 R47H* knock-in BV2 cells for the study of *Trem2* function in the context of AD.

Chapter 3 of this thesis describes the use of the revolutionary gene editing technology CRISPR/Cas9 for the generation of: i) isogenic *Trem2* and *Dap12* knockout BV2 cells (Section 3.3.1) and ii) *Trem2 R47H* carrier BV2 cells. To generate isogenic *Trem2* and

Dap12 KO BV2 cells, commercially available CRISPR/Cas9 plasmids containing Cas9 nickases were used for gene editing as they confer higher specificity. Also, many different molecular biology techniques were employed for the isolation, clonal expansion and selection of cell clones carrying the mutated *Trem2* gene.

Unfortunately, during the first round of CRISPR/Cas9n editing, it was not possible to generate any *Trem2* or *Dap12* homozygous knockout clones. Instead, heterozygous *Trem2* knockout clones (*Trem2* haploinsufficient clones, or *Trem2* +/-) were obtained; of which only 2 were taken forward for further experimentation; namely clones A7 (carrying a 4bp deletion) and C8 (carrying a 34bp deletion). As for *Dap12*, it was not possible to obtain any kind of gene modification, which was the reason why all attempts to gene edit *Dap12* were terminated.

Interestingly, during the characterisation of clones A7 and C8 (*Trem2* +/-), *Trem2* expression was found to be reduced not only because of gene editing but also as a result of both the culture medium and stimuli used. Unexpectedly, addition of 10% FBS to the growth medium and LPS stimulation reduced *Trem2* expression by ~50% and ~75%, respectively (Figure 3.4). The same trend was observed in the gene edited cell lines. As previously discussed, these results were replicated in different sets of experiments and across multiple platforms (RT-qPCR, microarray and RNAseq). This prompted us to use supplementation of 10% FBS as a modulator of *Trem2* expression in other experiments.

Trem2´s downregulation in response to LPS is a well-documented phenomenon, although the exact inhibition mechanism still remains to be elucidated. Not many studies have explored the effect of serum supplementation on microglial activation and/or *Trem2* expression, yet Wang et al. (2017) reported that supplementation of 5% of BV2 culture medium with human serum from either healthy donors or systemic lupus erythematosus (SLE) patients was enough to activate microglia, which could in turn reduce *Trem2* expression. In light of their results and ours, it is hypothesised that serum supplementation (foetal calf serum or other) of BV2 cultures activates cells and further studies should explore the effects of such activation in terms of gene expression changes. Moreover, Bohlen et al. (2017) have shown that serum supplementation alter proliferation and phagocytic capacity of microglial cells; this is discussed in **Chapter 4**.

As mentioned above, a second round of CRISPR/Cas9 gene editing was necessary to generate homozygous *Trem2* knockout clones (*Trem2* -/-), of which B5 and G4 were taken forward for further characterization. It is suggested that the difficulty in obtaining such clones lies in the well-known BV2 cells' hard-to-transfect status (see **Chapter 3**). Future attempts to modify BV2 cells should therefore use a different approach, such as direct transfection of the Cas9 protein complexed together with the gRNA, among other

methods. Another limiting factor was the low survival rates seen after plasmid transfection. This can also be improved by using different transfection and CRISPR/Cas9 approaches, or by using newly developed and commercially available survival enhancing media.

To introduce the *Trem2 R47H* mutation into BV2 cells (Section 3.3.3), two different approaches were employed: CRISPR/Cas9n (nickases) and CRISPR/Cas9 (nuclease). In total, four attempts to introduce the mutation were made: one round using CRISPR/Cas9n and three rounds using CRISPR/Cas9. As a result, a total of 992 clones were screened. Unfortunately, gene editing was unsuccessful and it was not possible to generate any isogenic clones that carried the *Trem2 R47H* mutation either in heterozygosity or homozygosity. This result is not surprising given that the HDR mechanisms needed to introduce mutations are known to be less efficient than the non-templated NHEJ mechanism (see Section 3.4.1. for a detailed discussion). Future work should investigate new approaches to efficiently deliver the necessary components of the CRISPR/Cas9 system into this particular target cell line.

Chapter 4 describes the morphological and functional characterization of the *Trem2* +/- (A7 and C8) and *Trem2* -/- (B5 and G4) BV2 cell lines. To this end, the knockdown (of *Trem2* +/- clones) and knockout (of *Trem2* -/- clones) status of *Trem2* in the 4 genome edited cell lines was investigated. Characterization of the *Trem2* expression in these clones was carried out using RT-qPCR (Section 4.3.1.1), Western blot (Section 4.3.1.2.1), sTREM2 ELISA (Section 4.3.1.2.2) and immunostaining (Section 4.3.1.2.3).

In keeping with the results shown in Figure 3.4, *Trem2* mRNA expression data showed that it was not only affected by gene editing, but also by the serum content of cell culture medium and LPS stimulation. In this new set of experiments, *Trem2* expression was consistently downregulated by: FBS supplementation, LPS stimulation and the combination of both across all cell lines (Figure 4.1). As discussed in Section 4.4.1, serum supplementation and LPS stimulation have already been shown to downregulate *Trem2* in microglial cell cultures. Remarkably, during the characterization of the sTREM2 shedding by the CRISPR/Cas9 edited cell lines (Section 4.3.1.2.2), an interesting pattern of sTREM2 release was observed. In contrast to what was seen during the RT-qPCR expression analysis, release of sTREM2 was encouraged by serum supplementation alone or in combination with LPS. Meanwhile LPS alone, did not increase sTREM2 release (Figure 4.4). These results are interesting if we keep in mind that serum is both capable of reducing *Trem2* mRNA and increasing sTREM2 release, which combined can exhaust the cell's TREM2 protein reserve. Future experiments should investigate the effect of this TREM2 depletion on microglial function.

Notably, downregulation and knockout of the TREM2 protein was also confirmed by western blot analysis and immunostaining. Western blot analysis exhibited small levels of TREM2 expression in *Trem2* -/- clones, B5 and G4. It is hypothesised that low levels of expression were due to nonspecific binding of anti-TREM2 antibody used (AF1729, polyclonal sheep IgG). Detection of the mouse TREM2 protein expression with a different anti-TREM2 antibody might reduce the background signal and/or not detect TREM2 proteins in B5 and G4 clones. Interestingly, the same antibody was used for immunostaining, where no signs of TREM2 expression were seen in the *Trem2* -/- clones, but rather a high auto-fluorescence signal of these cells.

Once the genetic knockdown and knockout of *Trem2* was confirmed, the next step was the functional characterization of the genome edited cell lines (Section 4.3.1.3). The functional characterization of *Trem2* +/- and *Trem2* -/- clones was performed by testing their phagocytic capacity (using *E. coli* and *Zymosan* particles, Section 4.3.1.3.1), proliferation capacity (using KI67 and CFSE staining, Section 4.3.1.3.2), migration (using a modified Boyden chamber assay, Section 4.3.1.3.3), cytokine release (using proteome profiler arrays, Section 4.3.1.3.4) and the genetic expression of microglial associated genes (by RT-qPCR, Section 4.3.1.3.5).

Unlike previous reports (Kleinberger et al., 2014b, N'Diaye et al., 2009a, Atagi et al., 2015b, Xiang et al., 2016b), in this study, *Trem2* CRISPR/Cas9 clones (*Trem2* +/- or -/-) did not show a reduced phagocytic capacity of *E. coli* or Zymosan particles. It is hypothesised that these differences may be the result of dissimilarities between the culture conditions used in other studies and ours. In the present work, low-serum conditions were used (1% FBS), while most studies use 5 or 10% FBS in culture medium. This is particularly relevant in light of the results reported by Bohlen et al. (2017), which show that serum supplementation increases the phagocytic capacity of microglial cells. Similarly, there were no differences in the proliferation rates (speed) of WT and the *Trem2* CRISPR/Cas9 clones, also contradicting previous studies (Wang et al. (2016b)). Again, Bohlen et al. (2017) have shown that serum supplementation gives the impression of an apparent increase in survival over time. They go further to clarify that this apparent increase arises from two confounding factors: i) induction of rapid proliferation by serum supplementation (caused by unknown factors) and ii) accelerated clearance of dead cells in serum-containing cultures (probably caused by the accelerated phagocytosis promoted by serum).

On the other hand, there were some signs of impairment in the migration capacity of the *Trem2* CRISPR/Cas9 clones which is in agreement with the literature (Mazaheri et al. (2017)). There was also evidence of a compromised cytokine release capacity in the

Trem2 CRISPR/Cas9 clones (e.g. increased release IL10 and IL11 under unstimulated conditions or increased release of TNFα, IL1α and IL1β under LPS stimulation) and in response to the different stimuli (LPS, IL4 and TGFβ).

Interestingly, when WT cells were stimulated by either LPS, IL4 or TGFβ, there was a group of cytokine that were upregulated (green rectangle in Figure 4.12), pointing towards a common microglial cell activation mechanism. This group of cytokines was named "Microglial activation signature" and was also upregulated in the A7 (*Trem2* +/-) and B5 (*Trem2* -/-) cell lines under unstimulated conditions, implying that these cell lines are already activated even when left untreated. Importantly, this points to a possible role for TREM2 in microglial activation. This cytokine signature included IL11, IL12, FGF-21, CXCL9, IGFBP-3, IL10, IGFBP-5, leptin, FGF acidic, LIF, CXCL10, PDGF-BB and Pentraxin 2. Further studies on the expression and release of these cytokines during microglial activation are needed to validate their significance in the context of microglial activation. Unfortunately, the cytokine release experiment had two major limitations that should be taken into account for future work. First, in this thesis the experiment was only repeated once and more biological repeats will be needed to validate its results. Secondly, the cytokine arrays only provide us with relative quantification; further studies should seek to use methods that are capable of absolute quantification of cytokines.

Similarly, differences in the gene expression of many microglial associated genes (*Tnf, ApoE, CD40, CD33, Dap12* and *Plxna1*) were also detected by qPCR. None of these differences in the expression of the mentioned genes (i.e. *Tnf* or *ApoE*) was consistent with any *Trem2* genotype (*Trem2* +/- or -/-) and were associated with differences between the clonal cell lines. As a result, it can be concluded that *Trem2* deficiency does not affect the expression of *Tnf, ApoE, CD40, CD33, Dap12* and *Plxna1 in vitro*.

Chapter 5 describes the gene expression analysis of microglial activation in response to different stimuli including; LPS, dextran sulphate, fibrinogen, IL4, TGFβ and Aβ1-42 (as monomers, oligomers and fibrils). For the analysis of the gene expression changes during microglial activation, two different approaches were used: gene expression microarrays (Section 5.3) and RNA sequencing (Section 5.4). In both analyses, differentially expressed genes were identified using Partek Suite and Partek Flow software. Once the differentially expressed genes were identified for each treatment, GO and Pathway enrichment analysis were carried out.

Concurrently, the effect of the different stimuli on the expression of microglial and immune activation markers as well as AD-associated genes was investigated. Significant differences were found among most treatments, but strikingly there was no evidence of immune activation by any of the three Aβ1-42 conformations (monomers, oligomers or

fibrils). This was despite a careful morphological characterization of the different Aβ1-42 conformations by TEM (Section 5.4.2). These results contrast with previous reports where Aβ1-42 was able to activate microglial cells (Tang and Le, 2016, Michelucci et al., 2009). Walker et al. (2006) reported inflammatory activation of primary microglia with 2μM aggregated Aβ (fibrils and oligomers) in serum-free medium. Meanwhile, Maezawa et al. (2011) reported a unique activation signature of microglial cells with Aβ oligomers at 20nM. In our study, we used a concentration of 500nM for both oligomers and monomers (and 20nM of Aβ fibrils for the microarray experiment); however, none of the Aβ conformations managed to activate microglial cells. Forthcoming studies should use different (higher) Aβ doses to stimulate microglial cells in order to study their effect on microglial activation.

Importantly, both the microarray and RNAseq experiments found that LPS stimulation of BV2 cells caused the disruption of many AD-related genes. The microarray and RNAseq experiments showed that for both approaches, an average of 25% of AD-related genes were differentially expressed by this treatment.

It is of note that there were some small discrepancies between the results obtained using both platforms. For example, *App* was reported to be upregulated by LPS treatment in the microarray experiment, but showed no differential expression in the RNAseq experiment. Similarly, *CELF1* (*Gugbp*) and *MS4A6A* (*Ms4a6d*) were upregulated in the microarray experiment but showed no signs of differential expression in the RNAseq experiment. In contrast, RNAseq data showed that in response to LPS, *Ptk2b* and *Madd* were upregulated and downregulated, respectively; this was not observed in the microarray data. These small discrepancies could be the result of differences in library preparation methods and/or the specificity of both platforms.

In contrast, concurring results were found in the case of *ApoE, Cd33, Inpp5d, Mef2c* and *Trem2*. The importance of the expression changes seen in these genes, in the context of microglial activation, needs to be explored in future studies. Notably, changes in the expression of *ApoE* and *Trem2* in response to LPS have been validated by RT-QPCR in this thesis (for reference see Figure 4.1 and Figure 4.13), further confirming their role in microglial activation.

With regards to IL4 and TGFβ stimulations, differential expression of 6 (*Cd33, Ms4a6a, Mef2c, Picalm, Clu* and *Abi3*) and 8 (*App, Apoe, Inpp5d, Trem2, Pld3, Cass4, Clu* and *Abi3*) AD-related genes was observed, respectively. Altogether, these results point to a significant effect of microglial activation (M1 or M2) on the expression of genes which have been linked to AD.

Finally, **Chapter 5** also describes the gene expression analysis carried out to compare the gene expression profile of WT and B5 (*Trem2* -/-) BV2 cell lines under untreated and LPS conditions (Section 5.5). This comparison allowed us to identify clear differences between the gene expression profiles of *Trem2* +/+ and *Trem2* -/- cells and detect some of the molecular functions and pathways disrupted as a result of *Trem2* deficiency. Post-ANOVA lists of differentially expressed genes were generated for all conditions assayed (see Figure 5.17). A striking first observation was the huge number of differentially expressed genes observed in the *Trem2* -/- cell line: almost 4000 at any timepoint for the untreated *Trem2* -/- cells. This is almost twice as much as the number of differentially expressed genes in WT cells stimulated with LPS at 6h. Such a great number of differentially expressed genes in untreated cells points towards an important disruption in the gene expression programme of BV2 cells.

Depending on the timepoint, LPS stimulation of B5 cells increased the number of differentially expressed genes in a range of 360 to 520, , compared to untreated *Trem2* -/- cells. Another important observation was that WT cells stimulated with LPS seemed to resolve the inflammatory insult as time progressed. This could be evidenced by the lowering in the number of differentially expressed genes in this treatment group. Such reduction was not as noticeable in *Trem2* -/- cells, therefore suggesting they might have an impaired resolution response to inflammatory insults, such as LPS.

During the GO analysis, *Trem2* -/- cells showed enrichment of terms associated with regulation of the immune response and protein transport (BF) among others. It also showed enrichment of disease terms associated with Rheumatoid Arthritis, Neurodegenerative disorders and Alzheimer's disease, all of which have been shown to have an immune pathogenic component.

Regarding the analysis of the effect of the *Trem2* deficiency in the expression of AD-associated clones (Section 5.5.5), we showed that as many as 13 were differentially expressed as a consequence of the genetic knockout (*ApoE, Cd33, Mef2c, Trem2, Bin, Picalm, Cass4, Psen, Sorl1, Adam10, Madd, Clu* and *Abi3*). This disruption was even bigger than that of LPS stimulation of WT BV2 cells, which only disrupted the expression of 8 genes (*ApoE, CD33, Inpp5d, Mef2c, Trem2, Ptk2b, Madd* and *Abi3*). Again, this bigger number of differentially expressed genes suggests an important dysregulation in the gene expression programme of genes, and possibly pathways, associated with AD.

Overall, the present study has achieved its main goal of gaining a better understanding of microglial activation in response to different stimuli, including Aβ1-42 in three different conformations. Furthermore, by using the CRISPR/Cas9 technology to modify BV2 cells, 4 new *in vitro* models for the study of TREM2 function were created. These *in vitro*

models were functionally characterised with regards to their phagocytic, proliferative, migratory and cytokine release capacities. Although investigation of said capacities produced data that were in accordance with the literature, some contradicting results were also obtained concerning both phagocytosis and proliferation in BV2 modified cells. Additionally, the comparison of the gene expression profile of the newly generated B5 (*Trem2* -/-) cell line with the wild-type has allowed the identification of specific genes whose expression profiles were disrupted in the absence of *Trem2*. Our findings thus provide new insights into microglial activation mechanisms and *Trem2* function in microglial cells.

6.1 **Future work**

Forthcoming studies of microglial activation and *Trem2's* function will benefit from the use of primary microglia or iPSC-derived-microglia. Immortalised microglial cell lines (BV2, N9 and HM06) are good models for microglial research; nevertheless, many gene expression and functional studies have found major differences between primary microglia and these immortalised cell lines, including BV2s (Horvath et al., 2008).

New protocols for the differentiation of iPSCs into virtually all somatic cell types, including microglia (Muffat et al., 2016, Abud et al., 2017), are being developed constantly, providing us with useful tools for human disease modelling. Fortunately, iPSC are also amenable to CRISPR/Cas9 genome editing for *Trem2* knockout or knock-in. Comparison and validation of the gene expression results obtained in the RNAseq experiment using either primary microglial cells or human iPSC-derived microglia will be valuable to the study of TREM2 function. Having already acquired the expertise on CRISPR/Cas9 *in vitro* modification of cell lines, it would be reasonable to re-attempt to knockout relevant genes, including *Dap12, ApoE* and *Clu* in BV2 cells in order to investigate their effects on microglial function and assess their role in neurodegeneration.

Future work using BV2 cells should also explore the effect of serum supplementation as an immune activator. Work by Wang et al. (2017) and others has suggested that this kind of supplementation can immune-modulate microglial cultures. This is particularly relevant since microglial cells *in vivo* are isolated from serum proteins in the CNS. Moreover, FBS supplementation has been shown to reduce mRNA expression of *Trem2* and increase sTREM2 release, which could potentially deplete TREM2 in microglial cells. This reduction of the available TREM2 protein as a result of FBS supplementation should be studied in terms of its functional implications for microglial cells.

In this thesis, cytokine release assay was done using a semi-quantitative platform (Proteome Profiler Mouse XL Cytokine Array) in order to identify differences between the WT cells and the *Trem2* edited clones, particularly differences in the secretion of M1-

associated cytokines and components of the complement system. This assay also allowed the identification of an activation signature, a group of cytokines that was downregulated when cells were activated by either M1 or M2 activators. Nevertheless, it would be beneficial to use a quantitative platform such as the Luminex Bead-based Multiplex Assay in future experiments. Finally, RNAseq data could be re-analysed using a different pipeline for transcript analysis (different isoforms from the same gene) instead of the gene expression analysis reported in Chapter 5, as the former allows the interrogation of different isoforms from the same gene. Certainly, this would be more informative for both the microglial activation and the *Trem2* KO experiments, and also offers the possibility to discover new microglial specific gene transcripts.

7 SUPPLEMENTARY FIGURES

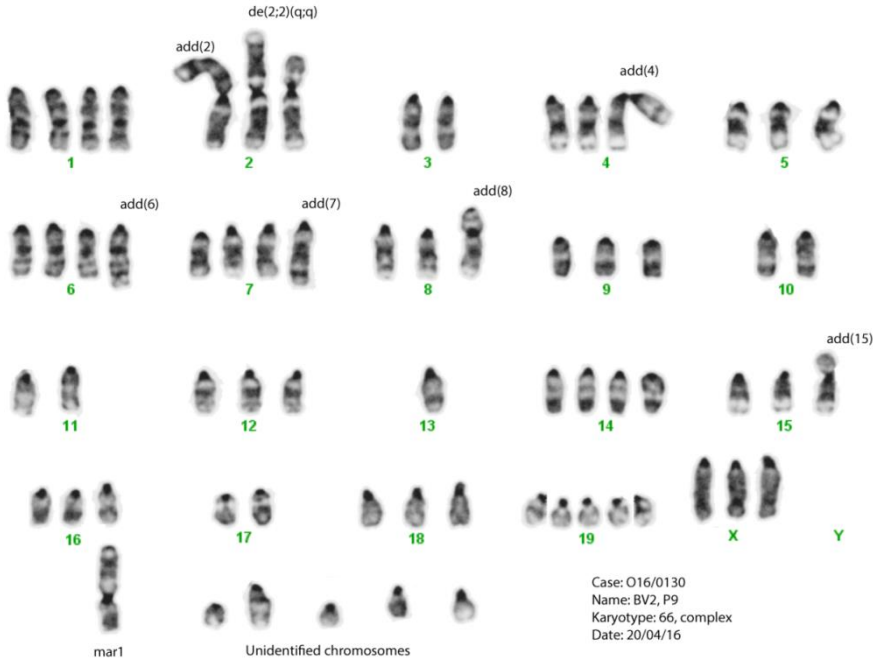

Supplementary Fig. 7.1 BV2 WT cells' Karyotype. Unmodified BV2 cells were karyotyped commercially (CELL Guidance Systems Genetics Service, Cambridge, UK) and were found to have a "Grossly abnormal mouse karyotype", with 62-66 chromosomes. Mouse normal karyotype (2n) is made of 40 chromosomes (Nachman and Searle, 1995). Chromosome 17 (*Trem2*'s location) was found to have 2-4 copies in these cells.

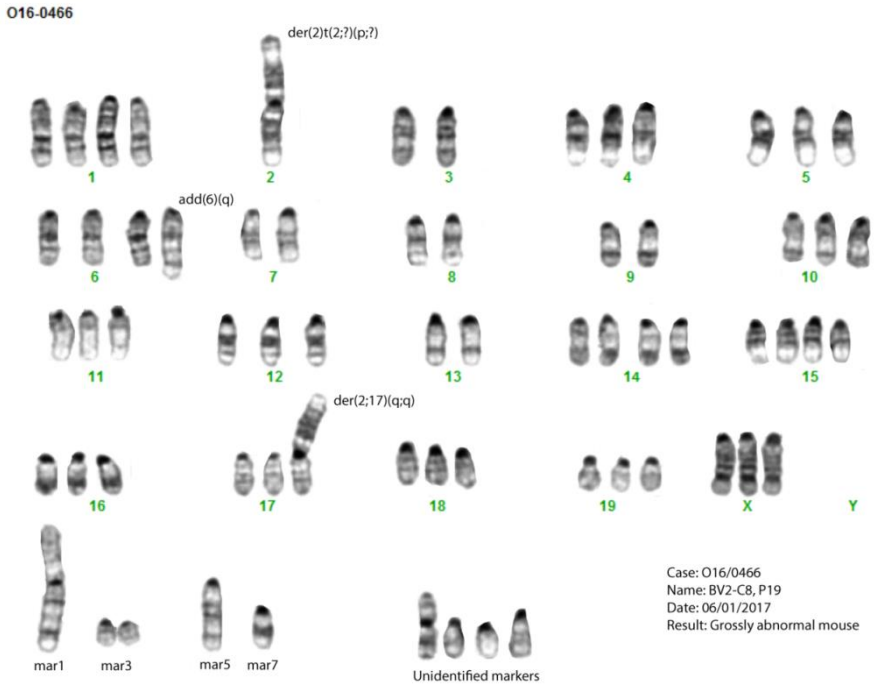

Supplementary Fig. 7.2 BV2 C4 (*Trem2* +/-) cell line Karyotype. CRISPR/Cas9 modified C8 cells were karyotyped commercially (CELL Guidance Systems Genetics Service, Cambridge, UK) and were found to have a "Grossly abnormal mouse karyotype", with 62-66 chromosomes. Mouse normal karyotype (2n) is made of 40 chromosomes (Nachman and Searle, 1995). Chromosome 17 (*Trem2*'s location) was found to have 3 copies in these cells.

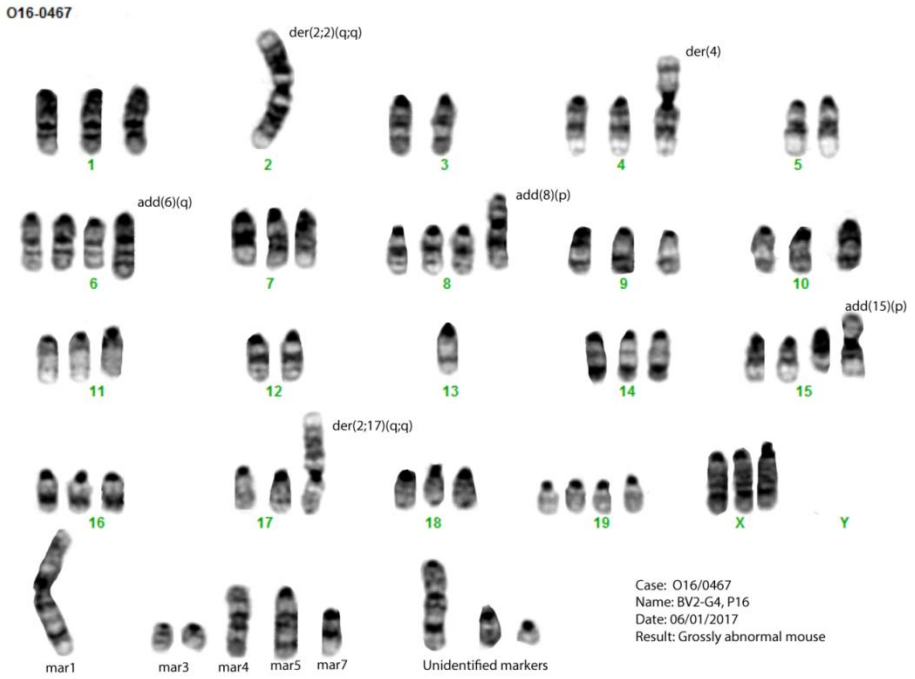

Supplementary Fig. 7.3 BV2 G4 (*Trem2* -/-) cell line Karyotype. CRISPR/Cas9 modified G4 cells were karyotyped commercially (CELL Guidance Systems Genetics Service, Cambridge, UK) and were found to have a "Grossly abnormal mouse karyotype", with 62-66 chromosomes. Mouse normal karyotype (2n) is made of 40 chromosomes (Nachman and Searle, 1995). Chromosome 17 (*Trem2*'s location) was found to have 3-4 copies in these cells.

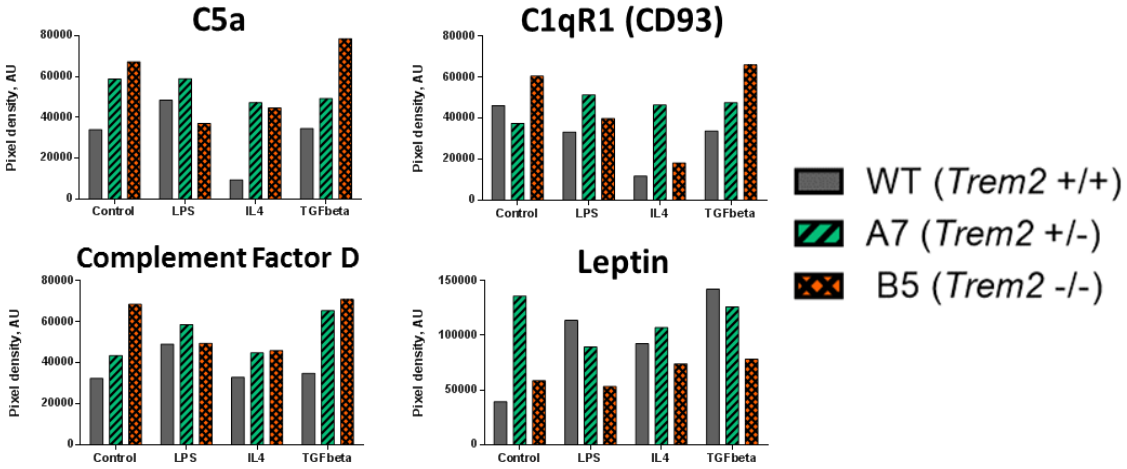

Supplementary Fig. 7.4 Effect of *Trem2* deficiency on complement system associated cytokine and Leptin. Semi-quantitative cytokine detection was performed using Proteome Profiler Antibody Arrays (R&D; ARY028) for 111 different analytes according to manufacturer's instructions. Only 3 cell lines were used for this experiment; WT, A7 (*Trem2* +/-) and B5 (*Trem2* -/-). Cell lines were exposed to 4 different treatments; Control (untreated), LPS, IL4 and TGFβ for 24h. Individual plots of Complement associated cytokines (C5a, C1qR1 and Complement Factor D) and Leptin.

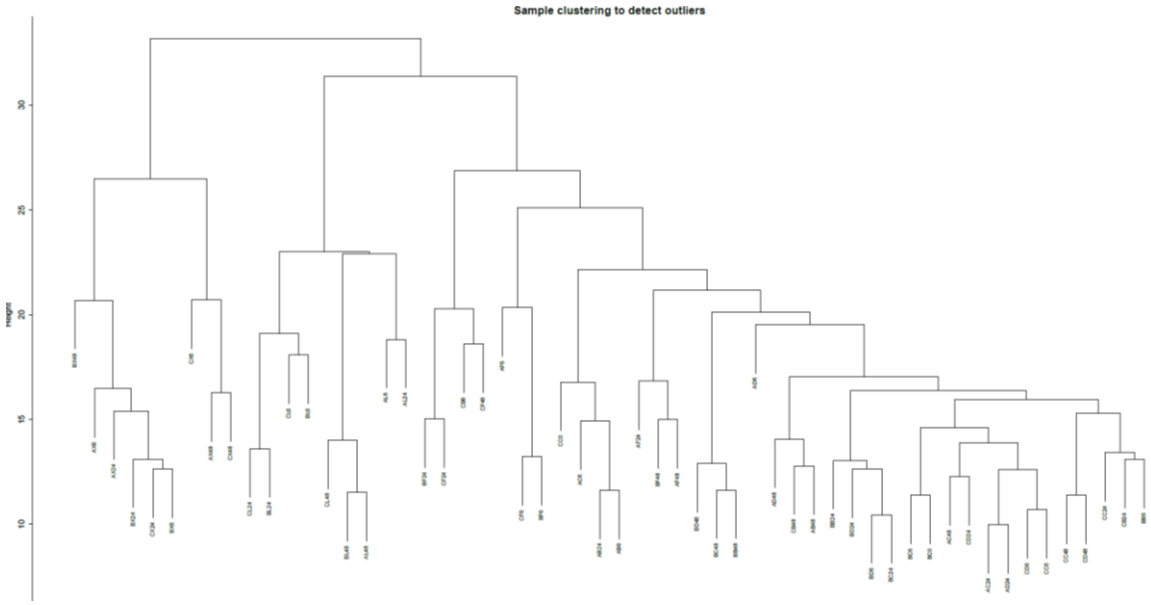

Supplementary Fig. 7.5 Non-supervised hierarchical clustering. Unsupervised clustering was performed to determine phylogenetic distances between samples for detection of potential outliers. No outliers were identified for this experiment.

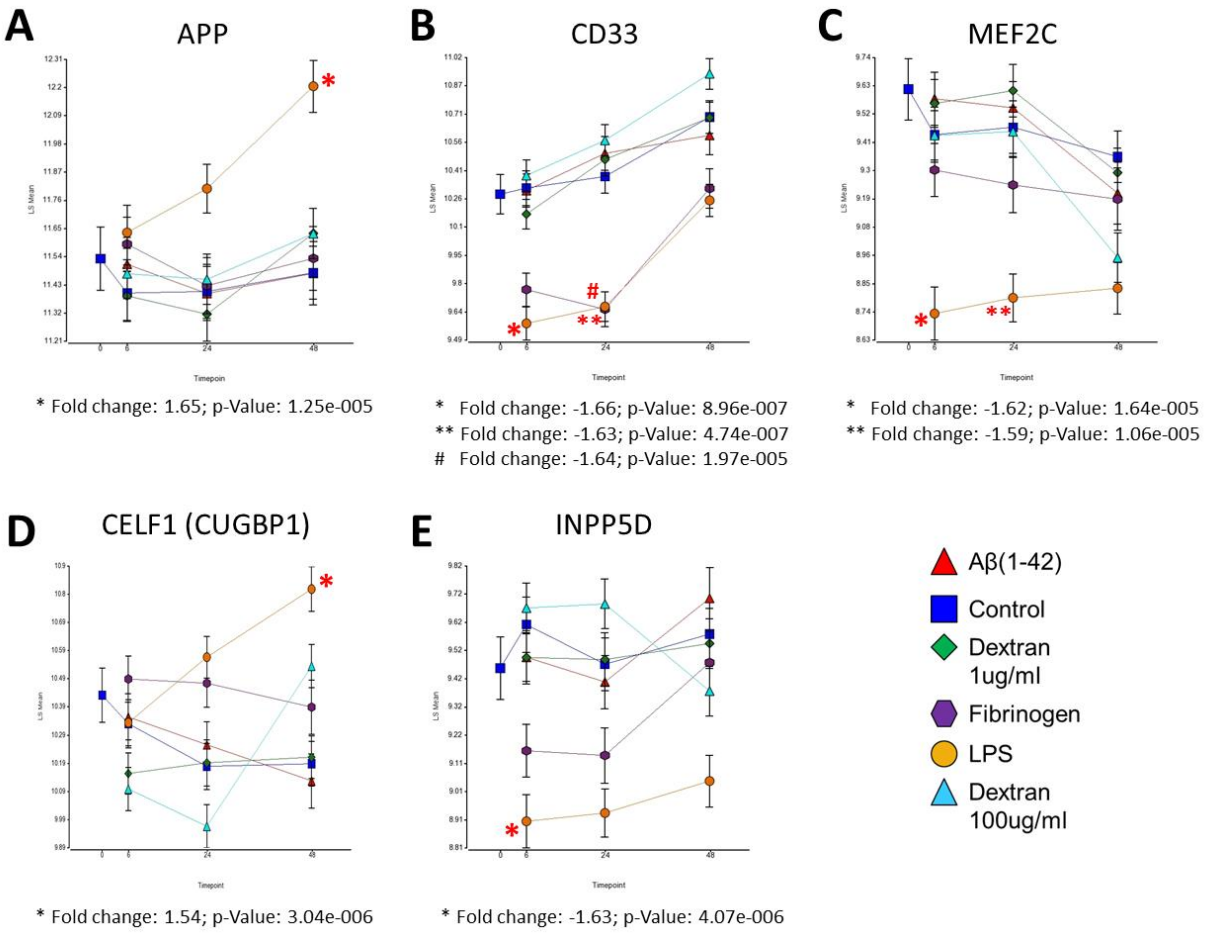

Supplementary Fig. 7.6 AD-related genes differentially expressed in response to LPS treatment. In addition to APOE and *TREM2*, 5 more genes were differentially expressed by microglia in response to LPS treatment; APP, CD33, MEF2C, CELF1 (CUGBP) and INPP5D. * and ** represent statistical significance for LPS treatment and # represents statistical significance for fibrinogen treatment.

SUPPLEMENTARY FIGURES

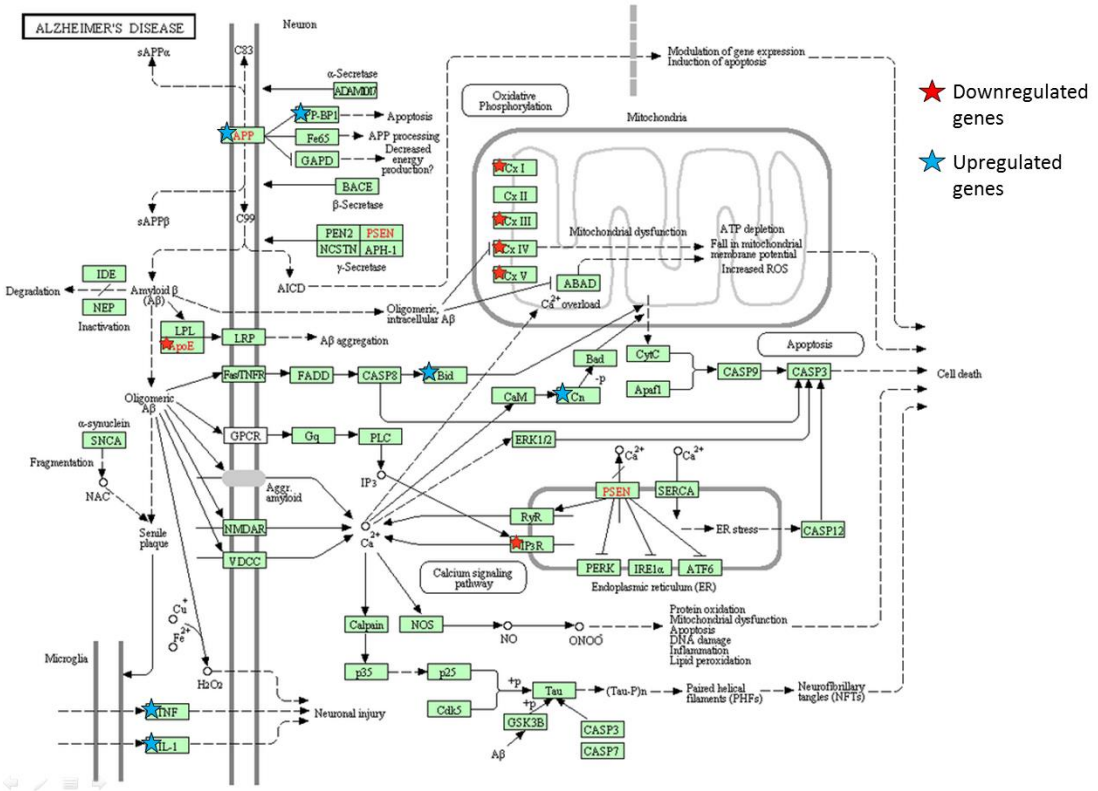

Supplementary Fig. 7.7 AD-related KEGG pathway associated with differentially expressed genes obtained with LPS treatment (48h). GO analysis of differentially expressed genes identified a significant association between and AD-related pathway and 15 genes in the list (Benjamini 0.012). Upregulated genes (blue stars) correspond to 6 genes (including APP, TNF and IL1β), while downregulated genes (red stars) correspond to 9 genes (including APOE). GO analysis of only the downregulated genes also showed an association with this same AD-related pathway but it was not statistically significant (Benjamini 0.073).

Full list of differentially expressed genes by LPS	Downregulated genes by LPS
NADH dehydrogenase (ubiquinone) 1 beta subcomplex 3; predicted gene 3192	NADH dehydrogenase (ubiquinone) 1 beta subcomplex 3; predicted gene 3192
NADH dehydrogenase (ubiquinone) 1 beta subcomplex 8	NADH dehydrogenase (ubiquinone) 1 beta subcomplex 8
NADH dehydrogenase (ubiquinone) 1 beta subcomplex 7	NADH dehydrogenase (ubiquinone) 1 beta subcomplex 7
NADH dehydrogenase (ubiquinone) Fe-S protein 7	NADH dehydrogenase (ubiquinone) Fe-S protein 7
Apolipoprotein E (APOE)	Apolipoprotein E (APOE)
Cytochrome c oxidase, subunit VIIa 1	Cytochrome c oxidase, subunit VIIa 1
Inositol 1,4,5-triphosphate receptor 3 (IP3R)	Inositol 1,4,5-triphosphate receptor 3 (IP3R)
Predicted gene 14088; ubiquinol-cytochrome c reductase hinge protein	Predicted gene 14088; ubiquinol-cytochrome c reductase hinge protein
Predicted gene 10231; similar to ATP synthase, H+ transporting, mitochondrial F0 complex, subunit c (subunit 9); predicted gene 10175; predicted gene 5911; ATP synthase, H+ transporting, mitochondrial F0 complex, subunit c (subunit 9), isoform 2	Predicted gene 10231; similar to ATP synthase, H+ transporting, mitochondrial F0 complex, subunit c (subunit 9); predicted gene 10175; predicted gene 5911; ATP synthase, H+ transporting, mitochondrial F0 complex, subunit c (subunit 9), isoform 2
BH3 interacting domain death agonist (Bid)	
Amyloid beta (A4) precursor protein (APP)	
Interleukin 1 beta (IL1β)	
Protein phosphatase 3, catalytic subunit, gamma isoform	
Similar to Amyloid beta precursor protein binding protein 1; NEDD8 activating enzyme E1 subunit 1 (APP-BP1)	
Tumor necrosis factor (TNF)	

Downregulated genes Upregulated genes

Supplementary Fig. 7.8 Lists of genes associated with the AD-related KEGG pathway (LPS treatment, 48h). GO analysis of differentially expressed genes identified a significant association between an AD-related pathway and 15 genes (left panel). Out of these 15 genes, 9 were downregulated (red background) by the LPS treatment (including APOE) while 6 were upregulated (green background) by this treatment (including APP, TNF and IL1β). GO analysis of only the downregulated genes also showed an association with this same AD-related pathway (right panel) but it was not statistically significant (Benjamini 0.073).

18: Disease [Display Chart] 5486 annotations before applied cutoff / 16203 genes in category

	ID	Name	Source	pValue	FDR B&H	FDR B&Y	Bonferroni	Genes from Input	Genes in Annotation
1	C0003864	Arthritis	DisGeNET Curated	1.468E-11	8.053E-8	7.399E-7	8.053E-8	52	606
2	C0026769	Multiple Sclerosis	DisGeNET Curated	6.624E-11	1.817E-7	1.669E-6	3.634E-7	66	920
3	C0004364	Autoimmune Diseases	DisGeNET Curated	2.556E-10	4.674E-7	4.295E-6	1.402E-6	70	1038
4	C0032285	Pneumonia	DisGeNET Curated	6.474E-10	8.880E-7	8.158E-6	3.552E-6	42	476
5	C0003873	Rheumatoid Arthritis	DisGeNET Curated	2.156E-9	2.011E-6	1.848E-5	1.183E-5	93	1640
6	C0409974	Lupus Erythematosus	DisGeNET BeFree	2.200E-9	2.011E-6	1.848E-5	1.207E-5	31	296
7	C0024138	Lupus Erythematosus, Discoid	DisGeNET Curated	3.872E-9	3.014E-6	2.769E-5	2.124E-5	31	303
8	C0024141	Lupus Erythematosus, Systemic	DisGeNET Curated	4.517E-9	3.014E-6	2.769E-5	2.478E-5	63	951
9	C0024131	Lupus Vulgaris	DisGeNET BeFree	4.945E-9	3.014E-6	2.769E-5	2.713E-5	30	289
10	C3714636	Pneumonitis	DisGeNET BeFree	6.195E-9	3.398E-6	3.122E-5	3.398E-5	31	309
11	C0023893	Liver Cirrhosis, Experimental	DisGeNET Curated	8.218E-9	4.098E-6	3.765E-5	4.508E-5	54	767
12	C0038454	Cerebrovascular accident	DisGeNET Curated	1.959E-8	8.955E-6	8.227E-5	1.075E-4	49	679
13	C0023434	Chronic Lymphocytic Leukemia	DisGeNET Curated	3.941E-8	1.663E-5	1.528E-4	2.162E-4	66	1077
14	C0004096	Asthma	DisGeNET Curated	5.049E-8	1.979E-5	1.818E-4	2.770E-4	69	1155
15	C0027051	Myocardial Infarction	DisGeNET Curated	1.157E-7	4.231E-5	3.887E-4	6.346E-4	51	763
16	C0009324	Ulcerative Colitis	DisGeNET Curated	2.727E-7	9.229E-5	8.479E-4	1.496E-3	50	762
17	C0014070	Encephalomyelitis	DisGeNET BeFree	3.022E-7	9.229E-5	8.479E-4	1.658E-3	30	347
18	C0162820	Dermatitis, Allergic Contact	DisGeNET Curated	3.028E-7	9.229E-5	8.479E-4	1.661E-3	15	99
19	C0023418	leukemia	DisGeNET Curated	3.924E-7	1.133E-4	1.041E-3	2.153E-3	94	1854
20	C0004153	Atherosclerosis	DisGeNET Curated	4.332E-7	1.188E-4	1.092E-3	2.377E-3	62	1053
21	C0003850	Arteriosclerosis	DisGeNET Curated	6.798E-7	1.776E-4	1.631E-3	3.729E-3	62	1067
22	C0026764	Multiple Myeloma	DisGeNET Curated	7.513E-7	1.798E-4	1.652E-3	4.122E-3	69	1241
23	C0023467	Leukemia, Myelocytic, Acute	DisGeNET Curated	7.540E-7	1.798E-4	1.652E-3	4.136E-3	85	1646
24	C0009319	Colitis	DisGeNET Curated	8.232E-7	1.882E-4	1.729E-3	4.516E-3	40	569
25	C0024117	Chronic Obstructive Airway Disease	DisGeNET Curated	1.253E-6	2.634E-4	2.420E-3	6.873E-3	39	557
26	C0042344	Varicose Ulcer	DisGeNET BeFree	1.281E-6	2.634E-4	2.420E-3	7.025E-3	8	28
27	C0033860	Psoriasis	DisGeNET Curated	1.296E-6	2.634E-4	2.420E-3	7.112E-3	42	623
28	C0243026	Sepsis	DisGeNET Curated	1.561E-6	3.058E-4	2.809E-3	8.562E-3	36	498
29	C0002395	Alzheimer's Disease	DisGeNET Curated	2.387E-6	4.515E-4	4.148E-3	1.309E-2	90	1825
30	C0340288	Stable angina	DisGeNET Curated	2.973E-6	5.436E-4	4.994E-3	1.631E-2	12	76
31	C0011860	Diabetes Mellitus, Non-Insulin-Dependent	DisGeNET Curated	3.830E-6	6.778E-4	6.228E-3	2.101E-2	74	1427
32	C0010346	Crohn Disease	DisGeNET Curated	4.382E-6	7.512E-4	6.901E-3	2.404E-2	45	722
33	C0010068	Coronary heart disease	DisGeNET Curated	5.729E-6	9.396E-4	8.632E-3	3.143E-2	47	776
34	C0079731	B-Cell Lymphomas	DisGeNET Curated	5.823E-6	9.396E-4	8.632E-3	3.195E-2	43	684
35	C0023487	Acute Promyelocytic Leukemia	DisGeNET Curated	7.248E-6	1.136E-3	1.044E-2	3.976E-2	33	468
36	C0021390	Inflammatory Bowel Diseases	DisGeNET Curated	1.048E-5	1.580E-3	1.451E-2	5.750E-2	45	747
37	C0239946	Fibrosis, Liver	DisGeNET Curated	1.065E-5	1.580E-3	1.451E-2	5.845E-2	31	434
38	C0019693	HIV Infections	DisGeNET Curated	1.230E-5	1.775E-3	1.631E-2	6.747E-2	47	799
39	C0023895	Liver diseases	DisGeNET Curated	1.663E-5	2.340E-3	2.150E-2	9.125E-2	37	576
40	C0023890	Liver Cirrhosis	DisGeNET Curated	1.897E-5	2.602E-3	2.390E-2	1.041E-1	39	625
41	C0039103	Synovitis	DisGeNET Curated	2.014E-5	2.695E-3	2.476E-2	1.105E-1	13	106
42	C0036690	Septicemia	DisGeNET Curated	2.165E-5	2.813E-3	2.584E-2	1.188E-1	31	450
43	C0007222	Cardiovascular Diseases	DisGeNET Curated	2.211E-5	2.813E-3	2.584E-2	1.213E-1	44	746
44	C0010054	Coronary Arteriosclerosis	DisGeNET Curated	2.256E-5	2.813E-3	2.584E-2	1.238E-1	43	723
45	C0149678	Epstein-Barr Virus Infections	DisGeNET BeFree	2.334E-5	2.826E-3	2.596E-2	1.281E-1	20	228
46	C1956346	Coronary Artery Disease	DisGeNET Curated	2.383E-5	2.826E-3	2.596E-2	1.307E-1	46	796
47	C0004943	Behcet Syndrome	DisGeNET Curated	2.421E-5	2.826E-3	2.596E-2	1.328E-1	19	210
48	C0019196	Hepatitis C	DisGeNET Curated	2.597E-5	2.968E-3	2.727E-2	1.425E-1	44	751
49	C0155877	Allergic asthma	DisGeNET BeFree	3.461E-5	3.875E-3	3.560E-2	1.899E-1	18	197
50	C1140680	Malignant neoplasm of ovary	DisGeNET Curated	4.476E-5	4.818E-3	4.426E-2	2.455E-1	88	1911

Supplementary Fig. 7.9 Disease pathway enrichment analysis – IL4, 48h. Representative image of the Disease pathway analysis showing the enrichment of the AD related Disease pathway.

SUPPLEMENTARY FIGURES

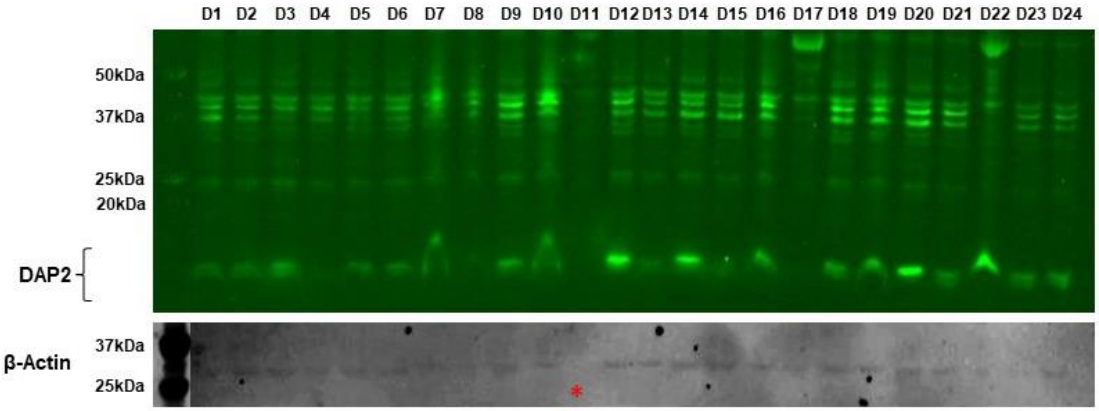

Supplementary Fig. 7.10 DAP12 Western blot for the identification of DAP12 KO BV2 clones. All *Dap12* CRISPR/Cas9 clones were analysed by Western blot to identify if there was a reduction on the expression of DAP12 protein (10-12kDa). The figure only shows 24 out of the 30 surviving *Dap12* CRISPR/Cas9 clones. The amount of protein lysate in each lane varies (approximately 20ug) as protein content was not quantified prior to electrophoresis. DAP12 was detected using a rabbit monoclonal anti-DAP12 antibody (Cell Signalling, Cat# 12492, 1:500 dilution). None of the clones seemed to have lost expression of DAP12 on whole cell lysates. β-actin (45kDa) was used as a loading control and was detected using a mouse monoclonal ant-β-actin antibody (Sigma, Cat# A5441, 1:10 000 dilution). Clone D11 (*) did not seem to have enough protein for Western blot detection as β-actin loading control did not showed a detectable signal. Clone D17, had a very faint DAP12 band which is not visible in this figure.

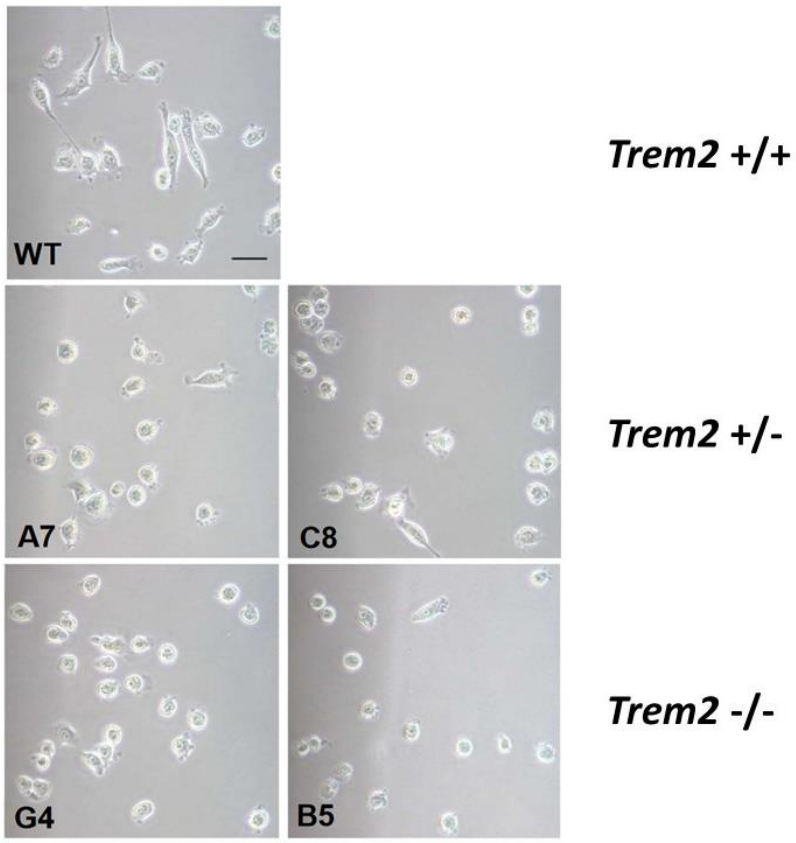

Supplementary Fig. 7.11 The effect of *Trem2* deficiency on the morphology of BV2 cells. Representative phase contrast images of WT (unmodified) and CRISPR/Cas9-edited BV2 cell lines grown in serum containing medium for 24h. Scale bar represents 100µm. Photographs were taken by Dr. Alexandra Phillips, Dept. of Neuroinflammation, UCL Institute of Neurology.

8 REFERENCES

ABUD, E. M., RAMIREZ, R. N., MARTINEZ, E. S., HEALY, L. M., NGUYEN, C. H. H., NEWMAN, S. A., YEROMIN, A. V., SCARFONE, V. M., MARSH, S. E., FIMBRES, C., CARAWAY, C. A., FOTE, G. M., MADANY, A. M., AGRAWAL, A., KAYED, R., GYLYS, K. H., CAHALAN, M. D., CUMMINGS, B. J., ANTEL, J. P., MORTAZAVI, A., CARSON, M. J., POON, W. W. & BLURTON-JONES, M. 2017. iPSC-Derived Human Microglia-like Cells to Study Neurological Diseases. *Neuron,* 94**,** 278-293 e9.

ADAMS, R. A., BAUER, J., FLICK, M. J., SIKORSKI, S. L., NURIEL, T., LASSMANN, H., DEGEN, J. L. & AKASSOGLOU, K. 2007. The fibrin-derived gamma377-395 peptide inhibits microglia activation and suppresses relapsing paralysis in central nervous system autoimmune disease. *J Exp Med,* 204**,** 571-82.

AKBARALY, T. N., PORTET, F., FUSTINONI, S., DARTIGUES, J. F., ARTERO, S., ROUAUD, O., TOUCHON, J., RITCHIE, K. & BERR, C. 2009. Leisure activities and the risk of dementia in the elderly: results from the Three-City Study. *Neurology,* 73**,** 854-61.

ALOE, L. & ROCCO, M. L. 2015. NGF and therapeutic prospective: what have we learned from the NGF transgenic models? *Ann Ist Super Sanita,* 51**,** 5-10.

ALZHEIMER'S ASSOCIATION 2013. Alzheimer's disease facts and figures. *Alzheimer's & Dementia: The Journal of the Alzheimer's Association,* 9**,** 208-45.

ALZHEIMER'S ASSOCIATION 2014. Alzheimer's disease facts and figures. *Alzheimer's & Dementia: The Journal of the Alzheimer's Association,* 10**,** e47-92.

ALZHEIMER'S ASSOCIATION 2018. Alzheimer's disease facts and figures. *Alzheimer's & Dementia: The Journal of the Alzheimer's Association,* 14**,** 367-429.

ANGGONO, V., TSAI, L. H. & GOTZ, J. 2016. Glutamate Receptors in Alzheimer's Disease: Mechanisms and Therapies. *Neural Plast,* 2016**,** 8256196.

AOUIDA, M., EID, A., ALI, Z., CRADICK, T., LEE, C., DESHMUKH, H., ATEF, A., ABUSAMRA, D., GADHOUM, S. Z., MERZABAN, J., BAO, G. & MAHFOUZ, M. 2015. Efficient fdCas9 Synthetic Endonuclease with Improved Specificity for Precise Genome Engineering. *PLoS One,* 10**,** e0133373.

ARROYO, D. S., GAVIGLIO, E. A., PERALTA RAMOS, J. M., BUSSI, C., RODRIGUEZ-GALAN, M. C. & IRIBARREN, P. 2014. Autophagy in inflammation, infection, neurodegeneration and cancer. *Int Immunopharmacol,* 18**,** 55-65.

ASPLUND, A., PRADIP, A., VAN GIEZEN, M., ASPEGREN, A., CHOUKAIR, H., REHNSTROM, M., JACOBSSON, S., GHOSHEH, N., EL HAJJAM, D., HOLMGREN, S., LARSSON, S., BENECKE, J., BUTRON, M., WIGANDER, A., NOAKSSON, K., SARTIPY, P., BJORQUIST, P., EDSBAGGE, J. & KUPPERS-MUNTHER, B. 2016. One Standardized Differentiation Procedure Robustly Generates Homogenous Hepatocyte Cultures Displaying Metabolic Diversity from a Large Panel of Human Pluripotent Stem Cells. *Stem Cell Rev,* 12**,** 90-104.

ATAGI, Y., LIU, C. C., PAINTER, M. M., CHEN, X. F., VERBEECK, C., ZHENG, H., LI, X., RADEMAKERS, R., KANG, S. S., XU, H., YOUNKIN, S., DAS, P., FRYER, J. D. & BU, G. 2015a. Apolipoprotein E Is a Ligand for Triggering Receptor Expressed on Myeloid Cells 2 (TREM2). *J Biol Chem,* 290**,** 26043-50.

ATAGI, Y., LIU, C. C., PAINTER, M. M., CHEN, X. F., VERBEECK, C., ZHENG, H. H., LI, X., RADEMAKERS, R., KANG, S. S., XU, H. X., YOUNKIN, S., DAS, P., FRYER, J. D. & BU, G. J. 2015b. Apolipoprotein E Is a Ligand for Triggering Receptor Expressed on Myeloid Cells 2 (TREM2). *Journal of Biological Chemistry,* 290**,** 26043-26050.

ATTEMS, J., JELLINGER, K., THAL, D. R. & VAN NOSTRAND, W. 2011. Review: sporadic cerebral amyloid angiopathy. *Neuropathol Appl Neurobiol,* 37**,** 75-93.

AVDIC, S., CAO, J. Z., MCSHARRY, B. P., CLANCY, L. E., BROWN, R., STEAIN, M., GOTTLIEB, D. J., ABENDROTH, A. & SLOBEDMAN, B. 2013. Human cytomegalovirus interleukin-10 polarizes monocytes toward a deactivated M2c phenotype to repress host immune responses. *J Virol,* 87**,** 10273-82.

REFERENCES

AVRAMOVICH, Y., AMIT, T. & YOUDIM, M. B. 2002. Non-steroidal anti-inflammatory drugs stimulate secretion of non-amyloidogenic precursor protein. *J Biol Chem,* 277**,** 31466-73.

BACHSTETTER, A. D., VAN ELDIK, L. J., SCHMITT, F. A., NELTNER, J. H., IGHODARO, E. T., WEBSTER, S. J., PATEL, E., ABNER, E. L., KRYSCIO, R. J. & NELSON, P. T. 2015. Disease-related microglia heterogeneity in the hippocampus of Alzheimer's disease, dementia with Lewy bodies, and hippocampal sclerosis of aging. *Acta Neuropathol Commun,* 3**,** 32.

BAGASRA, O., MICHAELS, F. H., ZHENG, Y. M., BOBROSKI, L. E., SPITSIN, S. V., FU, Z. F., TAWADROS, R. & KOPROWSKI, H. 1995. Activation of the inducible form of nitric oxide synthase in the brains of patients with multiple sclerosis. *Proc Natl Acad Sci U S A,* 92**,** 12041-5.

BAILEY, C. C., DEVAUX, L. B. & FARZAN, M. 2015. The Triggering Receptor Expressed on Myeloid Cells 2 Binds Apolipoprotein E. *J Biol Chem,* 290**,** 26033-42.

BAITSCH, D., BOCK, H. H., ENGEL, T., TELGMANN, R., MULLER-TIDOW, C., VARGA, G., BOT, M., HERZ, J., ROBENEK, H., VON ECKARDSTEIN, A. & NOFER, J. R. 2011. Apolipoprotein E induces antiinflammatory phenotype in macrophages. *Arterioscler Thromb Vasc Biol,* 31**,** 1160-8.

BAKKER, A. B., HOEK, R. M., CERWENKA, A., BLOM, B., LUCIAN, L., MCNEIL, T., MURRAY, R., PHILLIPS, L. H., SEDGWICK, J. D. & LANIER, L. L. 2000. DAP12-deficient mice fail to develop autoimmunity due to impaired antigen priming. *Immunity,* 13**,** 345-53.

BAL-PRICE, A., MATTHIAS, A. & BROWN, G. C. 2002. Stimulation of the NADPH oxidase in activated rat microglia removes nitric oxide but induces peroxynitrite production. *J Neurochem,* 80**,** 73-80.

BAMBERGER, M. E., HARRIS, M. E., MCDONALD, D. R., HUSEMANN, J. & LANDRETH, G. E. 2003. A cell surface receptor complex for fibrillar beta-amyloid mediates microglial activation. *J Neurosci,* 23**,** 2665-74.

BARRANGOU, R., BIRMINGHAM, A., WIEMANN, S., BEIJERSBERGEN, R. L., HORNUNG, V. & SMITH, A. 2015. Advances in CRISPR-Cas9 genome engineering: lessons learned from RNA interference. *Nucleic Acids Res,* 43**,** 3407-19.

BAYER, T. A., CAPPAI, R., MASTERS, C. L., BEYREUTHER, K. & MULTHAUP, G. 1999. It all sticks together--the APP-related family of proteins and Alzheimer's disease. *Mol Psychiatry,* 4**,** 524-8.

BECKER, L., LIU, N. C., AVERILL, M. M., YUAN, W., PAMIR, N., PENG, Y., IRWIN, A. D., FU, X., BORNFELDT, K. E. & HEINECKE, J. W. 2012. Unique proteomic signatures distinguish macrophages and dendritic cells. *PLoS One,* 7**,** e33297.

BEINS, E., ULAS, T., TERNES, S., NEUMANN, H., SCHULTZE, J. L. & ZIMMER, A. 2016. Characterization of inflammatory markers and transcriptome profiles of differentially activated embryonic stem cell-derived microglia. *Glia,* 64**,** 1007-20.

BELL, C. C., MAGOR, G. W., GILLINDER, K. R. & PERKINS, A. C. 2014. A high-throughput screening strategy for detecting CRISPR-Cas9 induced mutations using next-generation sequencing. *BMC Genomics,* 15**,** 1002.

BELL, K. F., DUCATENZEILER, A., RIBEIRO-DA-SILVA, A., DUFF, K., BENNETT, D. A. & CUELLO, A. C. 2006. The amyloid pathology progresses in a neurotransmitter-specific manner. *Neurobiol Aging,* 27**,** 1644-57.

BENILOVA, I., KARRAN, E. & DE STROOPER, B. 2012. The toxic Abeta oligomer and Alzheimer's disease: an emperor in need of clothes. *Nat Neurosci,* 15**,** 349-57.

BENJAMINI, Y. & HOCHBERG, Y. 1995. Controlling the False Discovery Rate: A Practical and Powerful Approach to Multiple Testing. *Journal of the Royal Statistical Society. Series B (Methodological),* 57**,** 289-300.

BENNETT, M. L., BENNETT, F. C., LIDDELOW, S. A., AJAMI, B., ZAMANIAN, J. L., FERNHOFF, N. B., MULINYAWE, S. B., BOHLEN, C. J., ADIL, A., TUCKER, A., WEISSMAN, I. L., CHANG, E. F., LI, G., GRANT, G. A., HAYDEN GEPHART, M. G. & BARRES, B. A. 2016. New tools for

studying microglia in the mouse and human CNS. *Proc Natl Acad Sci U S A,* 113**,** E1738-46.

BHAYA, D., DAVISON, M. & BARRANGOU, R. 2011. CRISPR-Cas systems in bacteria and archaea: versatile small RNAs for adaptive defense and regulation. *Annu Rev Genet,* 45**,** 273-97.

BISCARO, B., LINDVALL, O., TESCO, G., EKDAHL, C. T. & NITSCH, R. M. 2012. Inhibition of microglial activation protects hippocampal neurogenesis and improves cognitive deficits in a transgenic mouse model for Alzheimer's disease. *Neurodegener Dis,* 9**,** 187-98.

BLALOCK, E. M., GEDDES, J. W., CHEN, K. C., PORTER, N. M., MARKESBERY, W. R. & LANDFIELD, P. W. 2004. Incipient Alzheimer's disease: microarray correlation analyses reveal major transcriptional and tumor suppressor responses. *Proc Natl Acad Sci U S A,* 101**,** 2173-8.

BLASI, E., BARLUZZI, R., BOCCHINI, V., MAZZOLLA, R. & BISTONI, F. 1990. Immortalization of murine microglial cells by a v-raf/v-myc carrying retrovirus. *J Neuroimmunol,* 27**,** 229-37.

BLASKO, I., MARX, F., STEINER, E., HARTMANN, T. & GRUBECK-LOEBENSTEIN, B. 1999. TNFalpha plus IFNgamma induce the production of Alzheimer beta-amyloid peptides and decrease the secretion of APPs. *FASEB J,* 13**,** 63-8.

BLOUDEK, L. M., SPACKMAN, D. E., BLANKENBURG, M. & SULLIVAN, S. D. 2011. Review and meta-analysis of biomarkers and diagnostic imaging in Alzheimer's disease. *J Alzheimers Dis,* 26**,** 627-45.

BOCHE, D., PERRY, V. H. & NICOLL, J. A. 2013. Review: activation patterns of microglia and their identification in the human brain. *Neuropathol Appl Neurobiol,* 39**,** 3-18.

BOETTCHER, M. & MCMANUS, M. T. 2015. Choosing the Right Tool for the Job: RNAi, TALEN, or CRISPR. *Mol Cell,* 58**,** 575-85.

BOGDANOVE, A. J., SCHORNACK, S. & LAHAYE, T. 2010. TAL effectors: finding plant genes for disease and defense. *Curr Opin Plant Biol,* 13**,** 394-401.

BOGDANOVE, A. J. & VOYTAS, D. F. 2011. TAL effectors: customizable proteins for DNA targeting. *Science,* 333**,** 1843-6.

BOHLEN, C. J., BENNETT, F. C., TUCKER, A. F., COLLINS, H. Y., MULINYAWE, S. B. & BARRES, B. A. 2017. Diverse Requirements for Microglial Survival, Specification, and Function Revealed by Defined-Medium Cultures. *Neuron,* 94**,** 759-773 e8.

BOUTAJANGOUT, A. & WISNIEWSKI, T. 2013. The innate immune system in Alzheimer's disease. *Int J Cell Biol,* 2013**,** 576383.

BRADFORD, M. M. 1976. A rapid and sensitive method for the quantitation of microgram quantities of protein utilizing the principle of protein-dye binding. *Anal Biochem,* 72**,** 248-54.

BRADSHAW, E. M., CHIBNIK, L. B., KEENAN, B. T., OTTOBONI, L., RAJ, T., TANG, A., ROSENKRANTZ, L. L., IMBOYWA, S., LEE, M., VON KORFF, A., ALZHEIMER DISEASE NEUROIMAGING, I., MORRIS, M. C., EVANS, D. A., JOHNSON, K., SPERLING, R. A., SCHNEIDER, J. A., BENNETT, D. A. & DE JAGER, P. L. 2013. CD33 Alzheimer's disease locus: altered monocyte function and amyloid biology. *Nat Neurosci,* 16**,** 848-50.

BRADT, B. M., KOLB, W. P. & COOPER, N. R. 1998. Complement-dependent proinflammatory properties of the Alzheimer's disease beta-peptide. *J Exp Med,* 188**,** 431-8.

BRANDENBURG, L. O., KONRAD, M., WRUCK, C. J., KOCH, T., LUCIUS, R. & PUFE, T. 2010. Functional and physical interactions between formyl-peptide-receptors and scavenger receptor MARCO and their involvement in amyloid beta 1-42-induced signal transduction in glial cells. *J Neurochem,* 113**,** 749-60.

BRETELER, M. M., CLAUS, J. J., GROBBEE, D. E. & HOFMAN, A. 1994. Cardiovascular disease and distribution of cognitive function in elderly people: the Rotterdam Study. *BMJ,* 308**,** 1604-8.

BRINKMAN, E. K., CHEN, T., AMENDOLA, M. & VAN STEENSEL, B. 2014. Easy quantitative assessment of genome editing by sequence trace decomposition. *Nucleic Acids Res,* 42**,** e168.

REFERENCES

BROOKMEYER, R., GRAY, S. & KAWAS, C. 1998. Projections of Alzheimer's disease in the United States and the public health impact of delaying disease onset. *Am J Public Health,* 88**,** 1337-42.

BROOKMEYER, R., JOHNSON, E., ZIEGLER-GRAHAM, K. & ARRIGHI, H. M. 2007. Forecasting the global burden of Alzheimer's disease. *Alzheimers Dement,* 3**,** 186-91.

BROSSERON, F., KRAUTHAUSEN, M., KUMMER, M. & HENEKA, M. T. 2014. Body fluid cytokine levels in mild cognitive impairment and Alzheimer's disease: a comparative overview. *Mol Neurobiol,* 50**,** 534-44.

BROWN, G. C. & NEHER, J. J. 2010. Inflammatory neurodegeneration and mechanisms of microglial killing of neurons. *Mol Neurobiol,* 41**,** 242-7.

BROWN, G. C. & NEHER, J. J. 2012. Eaten alive! Cell death by primary phagocytosis: 'phagoptosis'. *Trends in Biochemical Sciences,* 37**,** 325-332.

BROWN, G. D. & GORDON, S. 2001. Immune recognition. A new receptor for beta-glucans. *Nature,* 413**,** 36-7.

BROWN, G. D., TAYLOR, P. R., REID, D. M., WILLMENT, J. A., WILLIAMS, D. L., MARTINEZ-POMARES, L., WONG, S. Y. & GORDON, S. 2002. Dectin-1 is a major beta-glucan receptor on macrophages. *J Exp Med,* 196**,** 407-12.

BROWNE, T. C., MCQUILLAN, K., MCMANUS, R. M., O'REILLY, J. A., MILLS, K. H. & LYNCH, M. A. 2013. IFN-gamma Production by amyloid beta-specific Th1 cells promotes microglial activation and increases plaque burden in a mouse model of Alzheimer's disease. *J Immunol,* 190**,** 2241-51.

BURGUILLOS, M. A., DEIERBORG, T., KAVANAGH, E., PERSSON, A., HAJJI, N., GARCIA-QUINTANILLA, A., CANO, J., BRUNDIN, P., ENGLUND, E., VENERO, J. L. & JOSEPH, B. 2011. Caspase signalling controls microglia activation and neurotoxicity. *Nature,* 472**,** 319-24.

BUSSI, C., PERALTA RAMOS, J. M., ARROYO, D. S., GAVIGLIO, E. A., GALLEA, J. I., WANG, J. M., CELEJ, M. S. & IRIBARREN, P. 2017. Autophagy down regulates pro-inflammatory mediators in BV2 microglial cells and rescues both LPS and alpha-synuclein induced neuronal cell death. *Sci Rep,* 7**,** 43153.

BUTOVSKY, O., TALPALAR, A. E., BEN-YAAKOV, K. & SCHWARTZ, M. 2005. Activation of microglia by aggregated beta-amyloid or lipopolysaccharide impairs MHC-II expression and renders them cytotoxic whereas IFN-gamma and IL-4 render them protective. *Mol Cell Neurosci,* 29**,** 381-93.

BUTTERFIELD, D. A., REED, T. T., PERLUIGI, M., DE MARCO, C., COCCIA, R., KELLER, J. N., MARKESBERY, W. R. & SULTANA, R. 2007. Elevated levels of 3-nitrotyrosine in brain from subjects with amnestic mild cognitive impairment: implications for the role of nitration in the progression of Alzheimer's disease. *Brain Res,* 1148**,** 243-8.

CACACE, R., SLEEGERS, K. & VAN BROECKHOVEN, C. 2016. Molecular genetics of early-onset Alzheimer's disease revisited. *Alzheimers Dement,* 12**,** 733-48.

CALDERON-GARCIDUENAS, A. L. & DUYCKAERTS, C. 2017. Alzheimer disease. *Handb Clin Neurol,* 145**,** 325-337.

CANNON, J. P., O'DRISCOLL, M. & LITMAN, G. W. 2012. Specific lipid recognition is a general feature of CD300 and TREM molecules. *Immunogenetics,* 64**,** 39-47.

CANTONI, C., BOLLMAN, B., LICASTRO, D., XIE, M. Q., MIKESELL, R., SCHMIDT, R., YUEDE, C. M., GALIMBERTI, D., OLIVECRONA, G., KLEIN, R. S., CROSS, A. H., OTERO, K. & PICCIO, L. 2015. TREM2 regulates microglial cell activation in response to demyelination in vivo. *Acta Neuropathologica,* 129**,** 429-447.

CARLSON, M. C., HELMS, M. J., STEFFENS, D. C., BURKE, J. R., POTTER, G. G. & PLASSMAN, B. L. 2008. Midlife activity predicts risk of dementia in older male twin pairs. *Alzheimers Dement,* 4**,** 324-31.

CARMONA, S., HARDY, J. & GUERREIRO, R. 2018. The genetic landscape of Alzheimer disease. *Handb Clin Neurol,* 148**,** 395-408.

CARROLL, D. 2011. Genome engineering with zinc-finger nucleases. *Genetics,* 188**,** 773-82.

CASTELLANO, J. M., KIM, J., STEWART, F. R., JIANG, H., DEMATTOS, R. B., PATTERSON, B. W., FAGAN, A. M., MORRIS, J. C., MAWUENYEGA, K. G., CRUCHAGA, C., GOATE, A. M., BALES, K. R., PAUL, S. M., BATEMAN, R. J. & HOLTZMAN, D. M. 2011. Human apoE isoforms differentially regulate brain amyloid-beta peptide clearance. *Sci Transl Med,* 3**,** 89ra57.

CAUWELS, A., ROGGE, E., VANDENDRIESSCHE, B., SHIVA, S. & BROUCKAERT, P. 2014. Extracellular ATP drives systemic inflammation, tissue damage and mortality. *Cell Death Dis,* 5**,** e1102.

CHAKRABARTY, P., TIANBAI, L., HERRING, A., CEBALLOS-DIAZ, C., DAS, P. & GOLDE, T. E. 2012. Hippocampal expression of murine IL-4 results in exacerbation of amyloid deposition. *Mol Neurodegener,* 7**,** 36.

CHAN, S. L., KIM, W. S., KWOK, J. B., HILL, A. F., CAPPAI, R., RYE, K. A. & GARNER, B. 2008. ATP-binding cassette transporter A7 regulates processing of amyloid precursor protein in vitro. *J Neurochem,* 106**,** 793-804.

CHANG, C. F., WAN, J., LI, Q., RENFROE, S. C., HELLER, N. M. & WANG, J. 2017. Alternative activation-skewed microglia/macrophages promote hematoma resolution in experimental intracerebral hemorrhage. *Neurobiol Dis,* 103**,** 54-69.

CHEN, B., GILBERT, L. A., CIMINI, B. A., SCHNITZBAUER, J., ZHANG, W., LI, G. W., PARK, J., BLACKBURN, E. H., WEISSMAN, J. S., QI, L. S. & HUANG, B. 2013a. Dynamic imaging of genomic loci in living human cells by an optimized CRISPR/Cas system. *Cell,* 155**,** 1479-91.

CHEN, L. C., LASKIN, J. D., GORDON, M. K. & LASKIN, D. L. 2008. Regulation of TREM expression in hepatic macrophages and endothelial cells during acute endotoxemia. *Experimental and Molecular Pathology,* 84**,** 145-155.

CHEN, Q., ZHANG, K., JIN, Y., ZHU, T., CHENG, B., SHU, Q. & FANG, X. 2013b. Triggering receptor expressed on myeloid cells-2 protects against polymicrobial sepsis by enhancing bacterial clearance. *Am J Respir Crit Care Med,* 188**,** 201-12.

CHERRY, J. D., OLSCHOWKA, J. A. & O'BANION, M. K. 2014. Neuroinflammation and M2 microglia: the good, the bad, and the inflamed. *J Neuroinflammation,* 11**,** 98.

CHIANG, T. W., LE SAGE, C., LARRIEU, D., DEMIR, M. & JACKSON, S. P. 2016. CRISPR-Cas9(D10A) nickase-based genotypic and phenotypic screening to enhance genome editing. *Sci Rep,* 6**,** 24356.

CHINETTI-GBAGUIDI, G. & STAELS, B. 2011. Macrophage polarization in metabolic disorders: functions and regulation. *Curr Opin Lipidol,* 22**,** 365-72.

CHRISTIAN, M., CERMAK, T., DOYLE, E. L., SCHMIDT, C., ZHANG, F., HUMMEL, A., BOGDANOVE, A. J. & VOYTAS, D. F. 2010. Targeting DNA double-strand breaks with TAL effector nucleases. *Genetics,* 186**,** 757-61.

CLONTECH LABORATORIES, I. 2016. Superior Single-Cell Cloning of iPS Cells with the Cellartis® DEF-CS™ 500 Culture System. US.

COLANGELO, V., SCHURR, J., BALL, M. J., PELAEZ, R. P., BAZAN, N. G. & LUKIW, W. J. 2002. Gene expression profiling of 12633 genes in Alzheimer hippocampal CA1: transcription and neurotrophic factor down-regulation and up-regulation of apoptotic and pro-inflammatory signaling. *J Neurosci Res,* 70**,** 462-73.

COLONNA, M. 2003. TREMs in the immune system and beyond. *Nat Rev Immunol,* 3**,** 445-53.

COLONNA, M. & BUTOVSKY, O. 2017. Microglia Function in the Central Nervous System During Health and Neurodegeneration. *Annu Rev Immunol,* 35**,** 441-468.

COLONNA, M. & WANG, Y. 2016. TREM2 variants: new keys to decipher Alzheimer disease pathogenesis. *Nat Rev Neurosci,* 17**,** 201-7.

COLTON, C. & WILCOCK, D. M. 2010. Assessing activation states in microglia. *CNS Neurol Disord Drug Targets,* 9**,** 174-91.

COLTON, C. A., MOTT, R. T., SHARPE, H., XU, Q., VAN NOSTRAND, W. E. & VITEK, M. P. 2006. Expression profiles for macrophage alternative activation genes in AD and in mouse models of AD. *J Neuroinflammation,* 3**,** 27.

COMBS, C. K., KARLO, J. C., KAO, S. C. & LANDRETH, G. E. 2001. beta-Amyloid stimulation of microglia and monocytes results in TNFalpha-dependent expression of inducible nitric oxide synthase and neuronal apoptosis. *J Neurosci,* 21**,** 1179-88.

CORDELL, C. B., BORSON, S., BOUSTANI, M., CHODOSH, J., REUBEN, D., VERGHESE, J., THIES, W., FRIED, L. B. & MEDICARE DETECTION OF COGNITIVE IMPAIRMENT, W. 2013. Alzheimer's Association recommendations for operationalizing the detection of cognitive impairment during the Medicare Annual Wellness Visit in a primary care setting. *Alzheimers Dement,* 9**,** 141-50.

CORDER, E. H., SAUNDERS, A. M., STRITTMATTER, W. J., SCHMECHEL, D. E., GASKELL, P. C., SMALL, G. W., ROSES, A. D., HAINES, J. L. & PERICAK-VANCE, M. A. 1993. Gene dose of apolipoprotein E type 4 allele and the risk of Alzheimer's disease in late onset families. *Science,* 261**,** 921-3.

CORNU, T. I., THIBODEAU-BEGANNY, S., GUHL, E., ALWIN, S., EICHTINGER, M., JOUNG, J. K. & CATHOMEN, T. 2008. DNA-binding specificity is a major determinant of the activity and toxicity of zinc-finger nucleases. *Mol Ther,* 16**,** 352-8.

CORTES-CANTELI, M., PAUL, J., NORRIS, E. H., BRONSTEIN, R., AHN, H. J., ZAMOLODCHIKOV, D., BHUVANENDRAN, S., FENZ, K. M. & STRICKLAND, S. 2010. Fibrinogen and beta-amyloid association alters thrombosis and fibrinolysis: a possible contributing factor to Alzheimer's disease. *Neuron,* 66**,** 695-709.

CORTES-CANTELI, M., ZAMOLODCHIKOV, D., AHN, H. J., STRICKLAND, S. & NORRIS, E. H. 2012. Fibrinogen and altered hemostasis in Alzheimer's disease. *J Alzheimers Dis,* 32**,** 599-608.

CREHAN, H., HARDY, J. & POCOCK, J. 2013. Blockage of CR1 prevents activation of rodent microglia. *Neurobiol Dis,* 54**,** 139-49.

CRUCHAGA, C., KARCH, C. M., JIN, S. C., BENITEZ, B. A., CAI, Y., GUERREIRO, R., HARARI, O., NORTON, J., BUDDE, J., BERTELSEN, S., JENG, A. T., COOPER, B., SKORUPA, T., CARRELL, D., LEVITCH, D., HSU, S., CHOI, J., RYTEN, M., SASSI, C., BRAS, J., GIBBS, R. J., HERNANDEZ, D. G., LUPTON, M. K., POWELL, J., FORABOSCO, P., RIDGE, P. G., CORCORAN, C. D., TSCHANZ, J. T., NORTON, M. C., MUNGER, R. G., SCHMUTZ, C., LEARY, M., DEMIRCI, F. Y., BAMNE, M. N., WANG, X., LOPEZ, O. L., GANGULI, M., MEDWAY, C., TURTON, J., LORD, J., BRAAE, A., BARBER, I., BROWN, K., ALZHEIMER'S RESEARCH, U. K. C., PASTOR, P., LORENZO-BETANCOR, O., BRKANAC, Z., SCOTT, E., TOPOL, E., MORGAN, K., ROGAEVA, E., SINGLETON, A., HARDY, J., KAMBOH, M. I., GEORGE-HYSLOP, P. S., CAIRNS, N., MORRIS, J. C., KAUWE, J. S. K. & GOATE, A. M. 2014. Rare coding variants in the phospholipase D3 gene confer risk for Alzheimer's disease. *Nature,* 505**,** 550-554.

DAHLGREN, K. N., MANELLI, A. M., STINE, W. B., JR., BAKER, L. K., KRAFFT, G. A. & LADU, M. J. 2002. Oligomeric and fibrillar species of amyloid-beta peptides differentially affect neuronal viability. *J Biol Chem,* 277**,** 32046-53.

DAI, X. J., LI, N., YU, L., CHEN, Z. Y., HUA, R., QIN, X. & ZHANG, Y. M. 2015. Activation of BV2 microglia by lipopolysaccharide triggers an inflammatory reaction in PC12 cell apoptosis through a toll-like receptor 4-dependent pathway. *Cell Stress Chaperones,* 20**,** 321-31.

DARDALHON, V., KORN, T., KUCHROO, V. K. & ANDERSON, A. C. 2008. Role of Th1 and Th17 cells in organ-specific autoimmunity. *J Autoimmun,* 31**,** 252-6.

DARIA, A., COLOMBO, A., LLOVERA, G., HAMPEL, H., WILLEM, M., LIESZ, A., HAASS, C. & TAHIROVIC, S. 2017. Young microglia restore amyloid plaque clearance of aged microglia. *EMBO J,* 36**,** 583-603.

DARZYNKIEWICZ, Z., ZHAO, H., ZHANG, S., LEE, M. Y., LEE, E. Y. & ZHANG, Z. 2015. Initiation and termination of DNA replication during S phase in relation to cyclins D1, E and A, p21WAF1, Cdt1 and the p12 subunit of DNA polymerase delta revealed in individual cells by cytometry. *Oncotarget,* 6**,** 11735-50.

DAS, A., KIM, S. H., ARIFUZZAMAN, S., YOON, T., CHAI, J. C., LEE, Y. S., PARK, K. S., JUNG, K. H. & CHAI, Y. G. 2016. Transcriptome sequencing reveals that LPS-triggered transcriptional responses in established microglia BV2 cell lines are poorly representative of primary microglia. *J Neuroinflammation,* 13**,** 182.

DAWS, M. R., SULLAM, P. M., NIEMI, E. C., CHEN, T. T., TCHAO, N. K. & SEAMAN, W. E. 2003. Pattern recognition by TREM-2: binding of anionic ligands. *J Immunol,* 171**,** 594-9.

DE SIMONE, R., AMBROSINI, E., CARNEVALE, D., AJMONE-CAT, M. A. & MINGHETTI, L. 2007. NGF promotes microglial migration through the activation of its high affinity receptor: modulation by TGF-beta. *J Neuroimmunol,* 190**,** 53-60.

DEMATTOS, R. B., CIRRITO, J. R., PARSADANIAN, M., MAY, P. C., O'DELL, M. A., TAYLOR, J. W., HARMONY, J. A., ARONOW, B. J., BALES, K. R., PAUL, S. M. & HOLTZMAN, D. M. 2004. ApoE and clusterin cooperatively suppress Abeta levels and deposition: evidence that ApoE regulates extracellular Abeta metabolism in vivo. *Neuron,* 41**,** 193-202.

DERETIC, V., SAITOH, T. & AKIRA, S. 2013. Autophagy in infection, inflammation and immunity. *Nat Rev Immunol,* 13**,** 722-37.

DEWITT, M. A., CORN, J. E. & CARROLL, D. 2017. Genome editing via delivery of Cas9 ribonucleoprotein. *Methods,* 121-122**,** 9-15.

DING, Q., LEE, Y. K., SCHAEFER, E. A., PETERS, D. T., VERES, A., KIM, K., KUPERWASSER, N., MOTOLA, D. L., MEISSNER, T. B., HENDRIKS, W. T., TREVISAN, M., GUPTA, R. M., MOISAN, A., BANKS, E., FRIESEN, M., SCHINZEL, R. T., XIA, F., TANG, A., XIA, Y., FIGUEROA, E., WANN, A., AHFELDT, T., DAHERON, L., ZHANG, F., RUBIN, L. L., PENG, L. F., CHUNG, R. T., MUSUNURU, K. & COWAN, C. A. 2013. A TALEN genome-editing system for generating human stem cell-based disease models. *Cell Stem Cell,* 12**,** 238-51.

DOENS, D. & FERNANDEZ, P. L. 2014. Microglia receptors and their implications in the response to amyloid beta for Alzheimer's disease pathogenesis. *J Neuroinflammation,* 11**,** 48.

DORE, J. J., JR., EDENS, M., GARAMSZEGI, N. & LEOF, E. B. 1998. Heteromeric and homomeric transforming growth factor-beta receptors show distinct signaling and endocytic responses in epithelial cells. *J Biol Chem,* 273**,** 31770-7.

DOW, L. E. 2015. Modeling Disease In Vivo With CRISPR/Cas9. *Trends Mol Med,* 21**,** 609-621.

DU, P., KIBBE, W. A. & LIN, S. M. 2008. lumi: a pipeline for processing Illumina microarray. *Bioinformatics,* 24**,** 1547-8.

DUCY, P., AMLING, M., TAKEDA, S., PRIEMEL, M., SCHILLING, A. F., BEIL, F. T., SHEN, J., VINSON, C., RUEGER, J. M. & KARSENTY, G. 2000. Leptin inhibits bone formation through a hypothalamic relay: a central control of bone mass. *Cell,* 100**,** 197-207.

EID, A. & MAHFOUZ, M. M. 2016. Genome editing: the road of CRISPR/Cas9 from bench to clinic. *Exp Mol Med,* 48**,** e265.

EL KHOURY, J., HICKMAN, S. E., THOMAS, C. A., CAO, L., SILVERSTEIN, S. C. & LOIKE, J. D. 1996. Scavenger receptor-mediated adhesion of microglia to beta-amyloid fibrils. *Nature,* 382**,** 716-9.

ENGELHART, M. J., GEERLINGS, M. I., RUITENBERG, A., VAN SWIETEN, J. C., HOFMAN, A., WITTEMAN, J. C. & BRETELER, M. M. 2002. Diet and risk of dementia: Does fat matter?: The Rotterdam Study. *Neurology,* 59**,** 1915-21.

EVANS, D. A., FUNKENSTEIN, H. H., ALBERT, M. S., SCHERR, P. A., COOK, N. R., CHOWN, M. J., HEBERT, L. E., HENNEKENS, C. H. & TAYLOR, J. O. 1989. Prevalence of Alzheimer's disease in a community population of older persons. Higher than previously reported. *JAMA,* 262**,** 2551-6.

FAGERHOLM, S. C., MACPHERSON, M., JAMES, M. J., SEVIER-GUY, C. & LAU, C. S. 2013. The CD11b-integrin (ITGAM) and systemic lupus erythematosus. *Lupus,* 22**,** 657-63.

FAIRFAX, B. P., HUMBURG, P., MAKINO, S., NARANBHAI, V., WONG, D., LAU, E., JOSTINS, L., PLANT, K., ANDREWS, R., MCGEE, C. & KNIGHT, J. C. 2014. Innate immune activity conditions the effect of regulatory variants upon monocyte gene expression. *Science,* 343**,** 1246949.

FAZZARI, P., HORRE, K., ARRANZ, A. M., FRIGERIO, C. S., SAITO, T., SAIDO, T. C. & DE STROOPER, B. 2017. PLD3 gene and processing of APP. *Nature,* 541**,** E1-E2.

FELLMANN, C., GOWEN, B. G., LIN, P. C., DOUDNA, J. A. & CORN, J. E. 2017. Cornerstones of CRISPR-Cas in drug discovery and therapy. *Nat Rev Drug Discov,* 16**,** 89-100.

FENG, Q., SHABRANI, N., THON, J. N., HUO, H., THIEL, A., MACHLUS, K. R., KIM, K., BROOKS, J., LI, F., LUO, C., KIMBREL, E. A., WANG, J., KIM, K. S., ITALIANO, J., CHO, J., LU, S. J. & LANZA, R. 2014. Scalable generation of universal platelets from human induced pluripotent stem cells. *Stem Cell Reports,* 3**,** 817-31.

FERNANDES, A., MILLER-FLEMING, L. & PAIS, T. F. 2014. Microglia and inflammation: conspiracy, controversy or control? *Cell Mol Life Sci,* 71**,** 3969-85.

FLEMINGER, S., OLIVER, D. L., LOVESTONE, S., RABE-HESKETH, S. & GIORA, A. 2003. Head injury as a risk factor for Alzheimer's disease: the evidence 10 years on; a partial replication. *J Neurol Neurosurg Psychiatry,* 74**,** 857-62.

FLICK, M. J., DU, X., WITTE, D. P., JIROUSKOVA, M., SOLOVIEV, D. A., BUSUTTIL, S. J., PLOW, E. F. & DEGEN, J. L. 2004. Leukocyte engagement of fibrin(ogen) via the integrin receptor alphaMbeta2/Mac-1 is critical for host inflammatory response in vivo. *J Clin Invest,* 113**,** 1596-606.

FORABOSCO, P., RAMASAMY, A., TRABZUNI, D., WALKER, R., SMITH, C., BRAS, J., LEVINE, A. P., HARDY, J., POCOCK, J. M., GUERREIRO, R., WEALE, M. E. & RYTEN, M. 2013. Insights into TREM2 biology by network analysis of human brain gene expression data. *Neurobiol Aging,* 34**,** 2699-714.

FORD, J. W. & MCVICAR, D. W. 2009. TREM and TREM-like receptors in inflammation and disease. *Curr Opin Immunol,* 21**,** 38-46.

FRANK, S., BURBACH, G. J., BONIN, M., WALTER, M., STREIT, W., BECHMANN, I. & DELLER, T. 2008. TREM2 is upregulated in amyloid plaque-associated microglia in aged APP23 transgenic mice. *Glia,* 56**,** 1438-47.

FRANKOLA, K. A., GREIG, N. H., LUO, W. & TWEEDIE, D. 2011. Targeting TNF-alpha to elucidate and ameliorate neuroinflammation in neurodegenerative diseases. *CNS Neurol Disord Drug Targets,* 10**,** 391-403.

FRATIGLIONI, L. & WANG, H. X. 2007. Brain reserve hypothesis in dementia. *J Alzheimers Dis,* 12**,** 11-22.

FRAUTSCHY, S. A., YANG, F., IRRIZARRY, M., HYMAN, B., SAIDO, T. C., HSIAO, K. & COLE, G. M. 1998. Microglial response to amyloid plaques in APPsw transgenic mice. *Am J Pathol,* 152**,** 307-17.

FRICKER, M., TOLKOVSKY, A. M., BORUTAITE, V., COLEMAN, M. & BROWN, G. C. 2018. Neuronal Cell Death. *Physiol Rev,* 98**,** 813-880.

FU, R., SHEN, Q., XU, P., LUO, J. J. & TANG, Y. 2014. Phagocytosis of microglia in the central nervous system diseases. *Mol Neurobiol,* 49**,** 1422-34.

FU, Y., FODEN, J. A., KHAYTER, C., MAEDER, M. L., REYON, D., JOUNG, J. K. & SANDER, J. D. 2013. High-frequency off-target mutagenesis induced by CRISPR-Cas nucleases in human cells. *Nat Biotechnol,* 31**,** 822-6.

FULLERTON, J. N. & GILROY, D. W. 2016. Resolution of inflammation: a new therapeutic frontier. *Nat Rev Drug Discov,* 15**,** 551-67.

GANTNER, B. N., SIMMONS, R. M., CANAVERA, S. J., AKIRA, S. & UNDERHILL, D. M. 2003. Collaborative induction of inflammatory responses by dectin-1 and Toll-like receptor 2. *J Exp Med,* 197**,** 1107-17.

GAO, H. M., ZHOU, H., ZHANG, F., WILSON, B. C., KAM, W. & HONG, J. S. 2011. HMGB1 acts on microglia Mac1 to mediate chronic neuroinflammation that drives progressive neurodegeneration. *J Neurosci,* 31**,** 1081-92.

GAO, X., DONG, Y., LIU, Z. & NIU, B. 2013. Silencing of triggering receptor expressed on myeloid cells-2 enhances the inflammatory responses of alveolar macrophages to lipopolysaccharide. *Mol Med Rep,* 7**,** 921-6.

GASIUNAS, G., BARRANGOU, R., HORVATH, P. & SIKSNYS, V. 2012. Cas9-crRNA ribonucleoprotein complex mediates specific DNA cleavage for adaptive immunity in bacteria. *Proc Natl Acad Sci U S A,* 109**,** E2579-86.

GAWISH, R., MARTINS, R., BOHM, B., WIMBERGER, T., SHARIF, O., LAKOVITS, K., SCHMIDT, M. & KNAPP, S. 2015a. Triggering receptor expressed on myeloid cells-2 fine-tunes inflammatory responses in murine Gram-negative sepsis. *FASEB J,* 29**,** 1247-57.

GAWISH, R., MARTINS, R., BOHM, B., WIMBERGER, T., SHARIF, O., LAKOVITS, K., SCHMIDT, M. & KNAPP, S. 2015b. Triggering receptor expressed on myeloid cells-2 fine-tunes inflammatory responses in murine Gram-negative sepsis. *Faseb Journal,* 29**,** 1247-1257.

GHOSH, S., WU, M. D., SHAFTEL, S. S., KYRKANIDES, S., LAFERLA, F. M., OLSCHOWKA, J. A. & O'BANION, M. K. 2013. Sustained interleukin-1beta overexpression exacerbates tau pathology despite reduced amyloid burden in an Alzheimer's mouse model. *J Neurosci,* 33**,** 5053-64.

GLASS, C. K., SAIJO, K., WINNER, B., MARCHETTO, M. C. & GAGE, F. H. 2010. Mechanisms underlying inflammation in neurodegeneration. *Cell,* 140**,** 918-34.

GLENN, H. L., MESSNER, J. & MELDRUM, D. R. 2016. A simple non-perturbing cell migration assay insensitive to proliferation effects. *Sci Rep,* 6**,** 31694.

GOATE, A., CHARTIER-HARLIN, M. C., MULLAN, M., BROWN, J., CRAWFORD, F., FIDANI, L., GIUFFRA, L., HAYNES, A., IRVING, N., JAMES, L. & ET AL. 1991. Segregation of a missense mutation in the amyloid precursor protein gene with familial Alzheimer's disease. *Nature,* 349**,** 704-6.

GOLDE, T. E., ECKMAN, C. B. & YOUNKIN, S. G. 2000. Biochemical detection of Abeta isoforms: implications for pathogenesis, diagnosis, and treatment of Alzheimer's disease. *Biochim Biophys Acta,* 1502**,** 172-87.

GOMES, C., FERREIRA, R., GEORGE, J., SANCHES, R., RODRIGUES, D. I., GONCALVES, N. & CUNHA, R. A. 2013. Activation of microglial cells triggers a release of brain-derived neurotrophic factor (BDNF) inducing their proliferation in an adenosine A(2A) receptor-dependent manner: A(2A) receptor blockade prevents BDNF release and proliferation of microglia. *Journal of Neuroinflammation,* 10.

GONZALEZ, H., ELGUETA, D., MONTOYA, A. & PACHECO, R. 2014. Neuroimmune regulation of microglial activity involved in neuroinflammation and neurodegenerative diseases. *J Neuroimmunol,* 274**,** 1-13.

GONZALEZ, H. & PACHECO, R. 2014. T-cell-mediated regulation of neuroinflammation involved in neurodegenerative diseases. *J Neuroinflammation,* 11**,** 201.

GORDON, S. 2003. Alternative activation of macrophages. *Nat Rev Immunol,* 3**,** 23-35.

GRICIUC, A., SERRANO-POZO, A., PARRADO, A. R., LESINSKI, A. N., ASSELIN, C. N., MULLIN, K., HOOLI, B., CHOI, S. H., HYMAN, B. T. & TANZI, R. E. 2013. Alzheimer's disease risk gene CD33 inhibits microglial uptake of amyloid beta. *Neuron,* 78**,** 631-43.

GROOT, C., HOOGHIEMSTRA, A. M., RAIJMAKERS, P. G., VAN BERCKEL, B. N., SCHELTENS, P., SCHERDER, E. J., VAN DER FLIER, W. M. & OSSENKOPPELE, R. 2016. The effect of physical activity on cognitive function in patients with dementia: A meta-analysis of randomized control trials. *Ageing Res Rev,* 25**,** 13-23.

GROVES, E., DART, A. E., COVARELLI, V. & CARON, E. 2008. Molecular mechanisms of phagocytic uptake in mammalian cells. *Cell Mol Life Sci,* 65**,** 1957-76.

GUERREIRO, R., BRAS, J. & HARDY, J. 2013a. SnapShot: genetics of Alzheimer's disease. *Cell,* 155**,** 968-968 e1.

GUERREIRO, R., WOJTAS, A., BRAS, J., CARRASQUILLO, M., ROGAEVA, E., MAJOUNIE, E., CRUCHAGA, C., SASSI, C., KAUWE, J. S., YOUNKIN, S., HAZRATI, L., COLLINGE, J., POCOCK, J., LASHLEY, T., WILLIAMS, J., LAMBERT, J. C., AMOUYEL, P., GOATE, A., RADEMAKERS, R., MORGAN, K., POWELL, J., ST GEORGE-HYSLOP, P., SINGLETON, A., HARDY, J. & ALZHEIMER GENETIC ANALYSIS, G. 2013b. TREM2 variants in Alzheimer's disease. *N Engl J Med,* 368**,** 117-27.

GUERREIRO, R. J., GUSTAFSON, D. R. & HARDY, J. 2012. The genetic architecture of Alzheimer's disease: beyond APP, PSENs and APOE. *Neurobiol Aging,* 33**,** 437-56.

GUERREIRO, R. J., LOHMANN, E., BRAS, J. M., GIBBS, J. R., ROHRER, J. D., GURUNLIAN, N., DURSUN, B., BILGIC, B., HANAGASI, H., GURVIT, H., EMRE, M., SINGLETON, A. & HARDY, J. 2013c. Using exome sequencing to reveal mutations in TREM2 presenting as a frontotemporal dementia-like syndrome without bone involvement. *JAMA Neurol,* 70**,** 78-84.

GUILINGER, J. P., THOMPSON, D. B. & LIU, D. R. 2014. Fusion of catalytically inactive Cas9 to FokI nuclease improves the specificity of genome modification. *Nat Biotechnol,* 32**,** 577-582.

GUO, L., LADU, M. J. & VAN ELDIK, L. J. 2004. A dual role for apolipoprotein e in neuroinflammation: anti- and pro-inflammatory activity. *J Mol Neurosci,* 23**,** 205-12.

GUO, R. F. & WARD, P. A. 2005. Role of C5a in inflammatory responses. *Annu Rev Immunol,* 23**,** 821-52.

GUSTAFSSON, C., MJOSBERG, J., MATUSSEK, A., GEFFERS, R., MATTHIESEN, L., BERG, G., SHARMA, S., BUER, J. & ERNERUDH, J. 2008. Gene expression profiling of human decidual macrophages: evidence for immunosuppressive phenotype. *PLoS One,* 3**,** e2078.

HALL, T. A. 1999. BioEdit: a user-friendly biological sequence alignment editor and analysis program for Windows 95/98/NT. *Nucleic Acids Symposium Series***,** 95-98.

HAMERMAN, J. A., JARJOURA, J. R., HUMPHREY, M. B., NAKAMURA, M. C., SEAMAN, W. E. & LANIER, L. L. 2006. Cutting edge: inhibition of TLR and FcR responses in macrophages by triggering receptor expressed on myeloid cells (TREM)-2 and DAP12. *J Immunol,* 177**,** 2051-5.

HAMERMAN, J. A., TCHAO, N. K., LOWELL, C. A. & LANIER, L. L. 2005. Enhanced Toll-like receptor responses in the absence of signaling adaptor DAP12. *Nat Immunol,* 6**,** 579-86.

HARDY, J. & ALLSOP, D. 1991. Amyloid deposition as the central event in the aetiology of Alzheimer's disease. *Trends Pharmacol Sci,* 12**,** 383-8.

HARDY, J. A. & HIGGINS, G. A. 1992. Alzheimer's disease: the amyloid cascade hypothesis. *Science,* 256**,** 184-5.

HAROLD, D., ABRAHAM, R., HOLLINGWORTH, P., SIMS, R., GERRISH, A., HAMSHERE, M. L., PAHWA, J. S., MOSKVINA, V., DOWZELL, K., WILLIAMS, A., JONES, N., THOMAS, C., STRETTON, A., MORGAN, A. R., LOVESTONE, S., POWELL, J., PROITSI, P., LUPTON, M. K., BRAYNE, C., RUBINSZTEIN, D. C., GILL, M., LAWLOR, B., LYNCH, A., MORGAN, K., BROWN, K. S., PASSMORE, P. A., CRAIG, D., MCGUINNESS, B., TODD, S., HOLMES, C., MANN, D., SMITH, A. D., LOVE, S., KEHOE, P. G., HARDY, J., MEAD, S., FOX, N., ROSSOR, M., COLLINGE, J., MAIER, W., JESSEN, F., SCHURMANN, B., HEUN, R., VAN DEN BUSSCHE, H., HEUSER, I., KORNHUBER, J., WILTFANG, J., DICHGANS, M., FROLICH, L., HAMPEL, H., HULL, M., RUJESCU, D., GOATE, A. M., KAUWE, J. S., CRUCHAGA, C., NOWOTNY, P., MORRIS, J. C., MAYO, K., SLEEGERS, K., BETTENS, K., ENGELBORGHS, S., DE DEYN, P. P., VAN BROECKHOVEN, C., LIVINGSTON, G., BASS, N. J., GURLING, H., MCQUILLIN, A., GWILLIAM, R., DELOUKAS, P., AL-CHALABI, A., SHAW, C. E., TSOLAKI, M., SINGLETON, A. B., GUERREIRO, R., MUHLEISEN, T. W., NOTHEN, M. M., MOEBUS, S., JOCKEL, K. H., KLOPP, N., WICHMANN, H. E., CARRASQUILLO, M. M., PANKRATZ, V. S., YOUNKIN, S. G., HOLMANS, P. A., O'DONOVAN, M., OWEN, M. J. & WILLIAMS, J. 2009. Genome-wide association study identifies variants at CLU and PICALM associated with Alzheimer's disease. *Nat Genet,* 41**,** 1088-93.

HARROD, A., FULTON, J., NGUYEN, V. T. M., PERIYASAMY, M., RAMOS-GARCIA, L., LAI, C. F., METODIEVA, G., DE GIORGIO, A., WILLIAMS, R. L., SANTOS, D. B., GOMEZ, P. J., LIN, M. L., METODIEV, M. V., STEBBING, J., CASTELLANO, L., MAGNANI, L., COOMBES, R. C., BULUWELA, L. & ALI, S. 2017. Genomic modelling of the ESR1 Y537S mutation for

evaluating function and new therapeutic approaches for metastatic breast cancer. *Oncogene,* 36**,** 2286-2296.

HARTLEY, D., BLUMENTHAL, T., CARRILLO, M., DIPAOLO, G., ESRALEW, L., GARDINER, K., GRANHOLM, A. C., IQBAL, K., KRAMS, M., LEMERE, C., LOTT, I., MOBLEY, W., NESS, S., NIXON, R., POTTER, H., REEVES, R., SABBAGH, M., SILVERMAN, W., TYCKO, B., WHITTEN, M. & WISNIEWSKI, T. 2015. Down syndrome and Alzheimer's disease: Common pathways, common goals. *Alzheimers Dement,* 11**,** 700-9.

HASELMAYER, P., GROSSE-HOVEST, L., VON LANDENBERG, P., SCHILD, H. & RADSAK, M. P. 2007. TREM-1 ligand expression on platelets enhances neutrophil activation. *Blood,* 110**,** 1029-35.

HAYASHI, M., NAKASHIMA, T., TANIGUCHI, M., KODAMA, T., KUMANOGOH, A. & TAKAYANAGI, H. 2012. Osteoprotection by semaphorin 3A. *Nature,* 485**,** 69-74.

HELLWIG, S., MASUCH, A., NESTEL, S., KATZMARSKI, N., MEYER-LUEHMANN, M. & BIBER, K. 2015. Forebrain microglia from wild-type but not adult 5xFAD mice prevent amyloid-beta plaque formation in organotypic hippocampal slice cultures. *Sci Rep,* 5**,** 14624.

HENEKA, M. T., CARSON, M. J., EL KHOURY, J., LANDRETH, G. E., BROSSERON, F., FEINSTEIN, D. L., JACOBS, A. H., WYSS-CORAY, T., VITORICA, J., RANSOHOFF, R. M., HERRUP, K., FRAUTSCHY, S. A., FINSEN, B., BROWN, G. C., VERKHRATSKY, A., YAMANAKA, K., KOISTINAHO, J., LATZ, E., HALLE, A., PETZOLD, G. C., TOWN, T., MORGAN, D., SHINOHARA, M. L., PERRY, V. H., HOLMES, C., BAZAN, N. G., BROOKS, D. J., HUNOT, S., JOSEPH, B., DEIGENDESCH, N., GARASCHUK, O., BODDEKE, E., DINARELLO, C. A., BREITNER, J. C., COLE, G. M., GOLENBOCK, D. T. & KUMMER, M. P. 2015. Neuroinflammation in Alzheimer's disease. *Lancet Neurol,* 14**,** 388-405.

HENEKA, M. T., KUMMER, M. P., STUTZ, A., DELEKATE, A., SCHWARTZ, S., VIEIRA-SAECKER, A., GRIEP, A., AXT, D., REMUS, A., TZENG, T. C., GELPI, E., HALLE, A., KORTE, M., LATZ, E. & GOLENBOCK, D. T. 2013. NLRP3 is activated in Alzheimer's disease and contributes to pathology in APP/PS1 mice. *Nature,* 493**,** 674-8.

HENG, T. S., PAINTER, M. W. & IMMUNOLOGICAL GENOME PROJECT, C. 2008. The Immunological Genome Project: networks of gene expression in immune cells. *Nat Immunol,* 9**,** 1091-4.

HENJUM, K., ALMDAHL, I. S., ARSKOG, V., MINTHON, L., HANSSON, O., FLADBY, T. & NILSSON, L. N. 2016. Cerebrospinal fluid soluble TREM2 in aging and Alzheimer's disease. *Alzheimers Res Ther,* 8**,** 17.

HESLEGRAVE, A., HEYWOOD, W., PATERSON, R., MAGDALINOU, N., SVENSSON, J., JOHANSSON, P., OHRFELT, A., BLENNOW, K., HARDY, J., SCHOTT, J., MILLS, K. & ZETTERBERG, H. 2016. Increased cerebrospinal fluid soluble TREM2 concentration in Alzheimer's disease. *Molecular Neurodegeneration,* 11.

HICKMAN, R. A., FAUSTIN, A. & WISNIEWSKI, T. 2016. Alzheimer Disease and Its Growing Epidemic: Risk Factors, Biomarkers, and the Urgent Need for Therapeutics. *Neurol Clin,* 34**,** 941-953.

HICKMAN, S. E., KINGERY, N. D., OHSUMI, T. K., BOROWSKY, M. L., WANG, L. C., MEANS, T. K. & EL KHOURY, J. 2013. The microglial sensome revealed by direct RNA sequencing. *Nat Neurosci,* 16**,** 1896-905.

HOLLINGWORTH, P., HAROLD, D., SIMS, R., GERRISH, A., LAMBERT, J. C., CARRASQUILLO, M. M., ABRAHAM, R., HAMSHERE, M. L., PAHWA, J. S., MOSKVINA, V., DOWZELL, K., JONES, N., STRETTON, A., THOMAS, C., RICHARDS, A., IVANOV, D., WIDDOWSON, C., CHAPMAN, J., LOVESTONE, S., POWELL, J., PROITSI, P., LUPTON, M. K., BRAYNE, C., RUBINSZTEIN, D. C., GILL, M., LAWLOR, B., LYNCH, A., BROWN, K. S., PASSMORE, P. A., CRAIG, D., MCGUINNESS, B., TODD, S., HOLMES, C., MANN, D., SMITH, A. D., BEAUMONT, H., WARDEN, D., WILCOCK, G., LOVE, S., KEHOE, P. G., HOOPER, N. M., VARDY, E. R., HARDY, J., MEAD, S., FOX, N. C., ROSSOR, M., COLLINGE, J., MAIER, W., JESSEN, F., RUTHER, E., SCHURMANN, B., HEUN, R., KOLSCH, H., VAN DEN BUSSCHE, H., HEUSER, I., KORNHUBER, J., WILTFANG, J., DICHGANS, M., FROLICH, L., HAMPEL, H.,

GALLACHER, J., HULL, M., RUJESCU, D., GIEGLING, I., GOATE, A. M., KAUWE, J. S., CRUCHAGA, C., NOWOTNY, P., MORRIS, J. C., MAYO, K., SLEEGERS, K., BETTENS, K., ENGELBORGHS, S., DE DEYN, P. P., VAN BROECKHOVEN, C., LIVINGSTON, G., BASS, N. J., GURLING, H., MCQUILLIN, A., GWILLIAM, R., DELOUKAS, P., AL-CHALABI, A., SHAW, C. E., TSOLAKI, M., SINGLETON, A. B., GUERREIRO, R., MUHLEISEN, T. W., NOTHEN, M. M., MOEBUS, S., JOCKEL, K. H., KLOPP, N., WICHMANN, H. E., PANKRATZ, V. S., SANDO, S. B., AASLY, J. O., BARCIKOWSKA, M., WSZOLEK, Z. K., DICKSON, D. W., GRAFF-RADFORD, N. R., PETERSEN, R. C., et al. 2011. Common variants at ABCA7, MS4A6A/MS4A4E, EPHA1, CD33 and CD2AP are associated with Alzheimer's disease. *Nat Genet,* 43**,** 429-35.

HOLTZMAN, D. M., HERZ, J. & BU, G. 2012. Apolipoprotein E and apolipoprotein E receptors: normal biology and roles in Alzheimer disease. *Cold Spring Harb Perspect Med,* 2**,** a006312.

HOLTZMAN, D. M., MORRIS, J. C. & GOATE, A. M. 2011. Alzheimer's disease: the challenge of the second century. *Sci Transl Med,* 3**,** 77sr1.

HONG, G., ZHANG, W., LI, H., SHEN, X. & GUO, Z. 2014. Separate enrichment analysis of pathways for up- and downregulated genes. *J R Soc Interface,* 11**,** 20130950.

HOOPER, C., PINTEAUX-JONES, F., FRY, V. A., SEVASTOU, I. G., BAKER, D., HEALES, S. J. & POCOCK, J. M. 2009. Differential effects of albumin on microglia and macrophages; implications for neurodegeneration following blood-brain barrier damage. *J Neurochem,* 109**,** 694-705.

HORNSTEIN, B. D., ROMAN, D., AREVALO-SOLIZ, L. M., ENGEVIK, M. A. & ZECHIEDRICH, L. 2016. Effects of Circular DNA Length on Transfection Efficiency by Electroporation into HeLa Cells. *PLoS One,* 11**,** e0167537.

HORVATH, P. & BARRANGOU, R. 2010. CRISPR/Cas, the immune system of bacteria and archaea. *Science,* 327**,** 167-70.

HORVATH, R. J., NUTILE-MCMENEMY, N., ALKAITIS, M. S. & DELEO, J. A. 2008. Differential migration, LPS-induced cytokine, chemokine, and NO expression in immortalized BV-2 and HAPI cell lines and primary microglial cultures. *J Neurochem,* 107**,** 557-69.

HOSACK, D. A., DENNIS, G., JR., SHERMAN, B. T., LANE, H. C. & LEMPICKI, R. A. 2003. Identifying biological themes within lists of genes with EASE. *Genome Biol,* 4**,** R70.

HSIEH, C. L., KOIKE, M., SPUSTA, S. C., NIEMI, E. C., YENARI, M., NAKAMURA, M. C. & SEAMAN, W. E. 2009. A role for TREM2 ligands in the phagocytosis of apoptotic neuronal cells by microglia. *J Neurochem,* 109**,** 1144-56.

HSU, P. D. & ZHANG, F. 2012. Dissecting neural function using targeted genome engineering technologies. *ACS Chem Neurosci,* 3**,** 603-10.

HUANG, C. F., LI, G., MA, R., SUN, S. G. & CHEN, J. G. 2008. Thrombin-induced microglial activation contributes to the degeneration of nigral dopaminergic neurons in vivo. *Neurosci Bull,* 24**,** 66-72.

HUMPHREY, M. B. & NAKAMURA, M. C. 2016. A Comprehensive Review of Immunoreceptor Regulation of Osteoclasts. *Clinical Reviews in Allergy & Immunology,* 51**,** 48-58.

HUNTER, J. M., KWAN, J., MALEK-AHMADI, M., MAAROUF, C. L., KOKJOHN, T. A., BELDEN, C., SABBAGH, M. N., BEACH, T. G. & ROHER, A. E. 2012. Morphological and pathological evolution of the brain microcirculation in aging and Alzheimer's disease. *PLoS One,* 7**,** e36893.

ILIFF, J. J., WANG, M., LIAO, Y., PLOGG, B. A., PENG, W., GUNDERSEN, G. A., BENVENISTE, H., VATES, G. E., DEANE, R., GOLDMAN, S. A., NAGELHUS, E. A. & NEDERGAARD, M. 2012. A paravascular pathway facilitates CSF flow through the brain parenchyma and the clearance of interstitial solutes, including amyloid beta. *Sci Transl Med,* 4**,** 147ra111.

IMAI, Y. & KOHSAKA, S. 2002. Intracellular signaling in M-CSF-induced microglia activation: role of Iba1. *Glia,* 40**,** 164-74.

ISHIZUKA, K., KIMURA, T., IGATA-YI, R., KATSURAGI, S., TAKAMATSU, J. & MIYAKAWA, T. 1997. Identification of monocyte chemoattractant protein-1 in senile plaques and reactive microglia of Alzheimer's disease. *Psychiatry Clin Neurosci,* 51**,** 135-8.

ITO, D., IMAI, Y., OHSAWA, K., NAKAJIMA, K., FUKUUCHI, Y. & KOHSAKA, S. 1998. Microglia-specific localisation of a novel calcium binding protein, Iba1. *Brain Res Mol Brain Res,* 57**,** 1-9.

ITO, H. & HAMERMAN, J. A. 2012. TREM-2, triggering receptor expressed on myeloid cell-2, negatively regulates TLR responses in dendritic cells. *Eur J Immunol,* 42**,** 176-85.

IULITA, M. F. & CUELLO, A. C. 2016. The NGF Metabolic Pathway in the CNS and its Dysregulation in Down Syndrome and Alzheimer's Disease. *Curr Alzheimer Res,* 13**,** 53-67.

JAMES, M. L., SULLIVAN, P. M., LASCOLA, C. D., VITEK, M. P. & LASKOWITZ, D. T. 2009. Pharmacogenomic effects of apolipoprotein e on intracerebral hemorrhage. *Stroke,* 40**,** 632-9.

JAN, A., HARTLEY, D. M. & LASHUEL, H. A. 2010. Preparation and characterization of toxic Abeta aggregates for structural and functional studies in Alzheimer's disease research. *Nat Protoc,* 5**,** 1186-209.

JANTARATNOTAI, N., SCHWAB, C., RYU, J. K., MCGEER, P. L. & MCLARNON, J. G. 2010. Converging perturbed microvasculature and microglial clusters characterize Alzheimer disease brain. *Curr Alzheimer Res,* 7**,** 625-36.

JAROSZ-GRIFFITHS, H. H., NOBLE, E., RUSHWORTH, J. V. & HOOPER, N. M. 2016. Amyloid-beta Receptors: The Good, the Bad, and the Prion Protein. *J Biol Chem,* 291**,** 3174-83.

JAY, T. R., MILLER, C. M., CHENG, P. J., GRAHAM, L. C., BEMILLER, S., BROIHIER, M. L., XU, G., MARGEVICIUS, D., KARLO, J. C., SOUSA, G. L., COTLEUR, A. C., BUTOVSKY, O., BEKRIS, L., STAUGAITIS, S. M., LEVERENZ, J. B., PIMPLIKAR, S. W., LANDRETH, G. E., HOWELL, G. R., RANSOHOFF, R. M. & LAMB, B. T. 2015. TREM2 deficiency eliminates TREM2+ inflammatory macrophages and ameliorates pathology in Alzheimer's disease mouse models. *J Exp Med,* 212**,** 287-95.

JAY, T. R., VON SAUCKEN, V. E. & LANDRETH, G. E. 2017. TREM2 in Neurodegenerative Diseases. *Mol Neurodegener,* 12**,** 56.

JEHLE, A. W., GARDAI, S. J., LI, S., LINSEL-NITSCHKE, P., MORIMOTO, K., JANSSEN, W. J., VANDIVIER, R. W., WANG, N., GREENBERG, S., DALE, B. M., QIN, C., HENSON, P. M. & TALL, A. R. 2006. ATP-binding cassette transporter A7 enhances phagocytosis of apoptotic cells and associated ERK signaling in macrophages. *J Cell Biol,* 174**,** 547-56.

JENSEN, T., KIERULF, P., SANDSET, P. M., KLINGENBERG, O., JOO, G. B., GODAL, H. C. & SKJONSBERG, O. H. 2007. Fibrinogen and fibrin induce synthesis of proinflammatory cytokines from isolated peripheral blood mononuclear cells. *Thromb Haemost,* 97**,** 822-9.

JIANG, T., YU, J. T., HU, N., TAN, M. S., ZHU, X. C. & TAN, L. 2014. CD33 in Alzheimer's disease. *Mol Neurobiol,* 49**,** 529-35.

JIMENEZ, S., BAGLIETTO-VARGAS, D., CABALLERO, C., MORENO-GONZALEZ, I., TORRES, M., SANCHEZ-VARO, R., RUANO, D., VIZUETE, M., GUTIERREZ, A. & VITORICA, J. 2008. Inflammatory response in the hippocampus of PS1M146L/APP751SL mouse model of Alzheimer's disease: age-dependent switch in the microglial phenotype from alternative to classic. *J Neurosci,* 28**,** 11650-61.

JIN, S. C., BENITEZ, B. A., KARCH, C. M., COOPER, B., SKORUPA, T., CARRELL, D., NORTON, J. B., HSU, S., HARARI, O., CAI, Y., BERTELSEN, S., GOATE, A. M. & CRUCHAGA, C. 2014. Coding variants in TREM2 increase risk for Alzheimer's disease. *Hum Mol Genet,* 23**,** 5838-46.

JINEK, M., CHYLINSKI, K., FONFARA, I., HAUER, M., DOUDNA, J. A. & CHARPENTIER, E. 2012. A programmable dual-RNA-guided DNA endonuclease in adaptive bacterial immunity. *Science,* 337**,** 816-21.

JINEK, M., EAST, A., CHENG, A., LIN, S., MA, E. & DOUDNA, J. 2013. RNA-programmed genome editing in human cells. *Elife,* 2**,** e00471.

JOHNSON, V. E., STEWART, J. E., BEGBIE, F. D., TROJANOWSKI, J. Q., SMITH, D. H. & STEWART, W. 2013. Inflammation and white matter degeneration persist for years after a single traumatic brain injury. *Brain,* 136**,** 28-42.

JOLLIFE, I. T. 2002. *Principal Component Analysis* Springer-Verlag New York.

JONES, S. E. & JOMARY, C. 2002. Clusterin. *Int J Biochem Cell Biol,* 34**,** 427-31.

JONSSON, T., STEFANSSON, H., STEINBERG, S., JONSDOTTIR, I., JONSSON, P. V., SNAEDAL, J., BJORNSSON, S., HUTTENLOCHER, J., LEVEY, A. I., LAH, J. J., RUJESCU, D., HAMPEL, H., GIEGLING, I., ANDREASSEN, O. A., ENGEDAL, K., ULSTEIN, I., DJUROVIC, S., IBRAHIM-VERBAAS, C., HOFMAN, A., IKRAM, M. A., VAN DUIJN, C. M., THORSTEINSDOTTIR, U., KONG, A. & STEFANSSON, K. 2013. Variant of TREM2 associated with the risk of Alzheimer's disease. *N Engl J Med,* 368**,** 107-16.

KAIFU, T., NAKAHARA, J., INUI, M., MISHIMA, K., MOMIYAMA, T., KAJI, M., SUGAHARA, A., KOITO, H., UJIKE-ASAI, A., NAKAMURA, A., KANAZAWA, K., TAN-TAKEUCHI, K., IWASAKI, K., YOKOYAMA, W. M., KUDO, A., FUJIWARA, M., ASOU, H. & TAKAI, T. 2003. Osteopetrosis and thalamic hypomyelinosis with synaptic degeneration in DAP12-deficient mice. *J Clin Invest,* 111**,** 323-32.

KALARIA, R. N. 2010. Vascular basis for brain degeneration: faltering controls and risk factors for dementia. *Nutr Rev,* 68 Suppl 2**,** S74-87.

KALMIJN, S., LAUNER, L. J., OTT, A., WITTEMAN, J. C., HOFMAN, A. & BRETELER, M. M. 1997. Dietary fat intake and the risk of incident dementia in the Rotterdam Study. *Ann Neurol,* 42**,** 776-82.

KAMPHUIS, W., KOOIJMAN, L., SCHETTERS, S., ORRE, M. & HOL, E. M. 2016. Transcriptional profiling of CD11c-positive microglia accumulating around amyloid plaques in a mouse model for Alzheimer's disease. *Biochim Biophys Acta,* 1862**,** 1847-60.

KANEKIYO, T., XU, H. & BU, G. 2014. ApoE and Abeta in Alzheimer's disease: accidental encounters or partners? *Neuron,* 81**,** 740-54.

KANG, S. S., KURTI, A., BAKER, K. E., LIU, C. C., COLONNA, M., ULRICH, J. D., HOLTZMAN, D. M., BU, G. & FRYER, J. D. 2018. Behavioral and transcriptomic analysis of Trem2-null mice: not all knockout mice are created equal. *Hum Mol Genet,* 27**,** 211-223.

KAPELLOS, T. S., TAYLOR, L., LEE, H., COWLEY, S. A., JAMES, W. S., IQBAL, A. J. & GREAVES, D. R. 2016. A novel real time imaging platform to quantify macrophage phagocytosis. *Biochem Pharmacol,* 116**,** 107-19.

KARCH, C. M., CRUCHAGA, C. & GOATE, A. M. 2014. Alzheimer's disease genetics: from the bench to the clinic. *Neuron,* 83**,** 11-26.

KARCH, C. M. & GOATE, A. M. 2015. Alzheimer's disease risk genes and mechanisms of disease pathogenesis. *Biol Psychiatry,* 77**,** 43-51.

KARCH, C. M., JENG, A. T., NOWOTNY, P., CADY, J., CRUCHAGA, C. & GOATE, A. M. 2012. Expression of novel Alzheimer's disease risk genes in control and Alzheimer's disease brains. *PLoS One,* 7**,** e50976.

KATO, T. & TAKADA, S. 2017. In vivo and in vitro disease modeling with CRISPR/Cas9. *Brief Funct Genomics,* 16**,** 13-24.

KICHEV, A., EEDE, P., GRESSENS, P., THORNTON, C. & HAGBERG, H. 2017. Implicating Receptor Activator of NF-kappaB (RANK)/RANK Ligand Signalling in Microglial Responses to Toll-Like Receptor Stimuli. *Dev Neurosci,* 39**,** 192-206.

KIM, C., HO, D. H., SUK, J. E., YOU, S., MICHAEL, S., KANG, J., JOONG LEE, S., MASLIAH, E., HWANG, D., LEE, H. J. & LEE, S. J. 2013a. Neuron-released oligomeric alpha-synuclein is an endogenous agonist of TLR2 for paracrine activation of microglia. *Nat Commun,* 4**,** 1562.

KIM, H. S., BERNITZ, J. M., LEE, D. F. & LEMISCHKA, I. R. 2014. Genomic editing tools to model human diseases with isogenic pluripotent stem cells. *Stem Cells Dev,* 23**,** 2673-86.

KIM, J., BASAK, J. M. & HOLTZMAN, D. M. 2009. The role of apolipoprotein E in Alzheimer's disease. *Neuron,* 63**,** 287-303.

KIM, S. M., MUN, B. R., LEE, S. J., JOH, Y., LEE, H. Y., JI, K. Y., CHOI, H. R., LEE, E. H., KIM, E. M., JANG, J. H., SONG, H. W., MOOK-JUNG, I., CHOI, W. S. & KANG, H. S. 2017. TREM2 promotes Abeta phagocytosis by upregulating C/EBPalpha-dependent CD36 expression in microglia. *Sci Rep,* 7**,** 11118.

KIM, W. S., GUILLEMIN, G. J., GLAROS, E. N., LIM, C. K. & GARNER, B. 2006. Quantitation of ATP-binding cassette subfamily-A transporter gene expression in primary human brain cells. *Neuroreport,* 17**,** 891-6.

KIM, W. S., LI, H., RUBERU, K., CHAN, S., ELLIOTT, D. A., LOW, J. K., CHENG, D., KARL, T. & GARNER, B. 2013b. Deletion of Abca7 increases cerebral amyloid-beta accumulation in the J20 mouse model of Alzheimer's disease. *J Neurosci,* 33**,** 4387-94.

KIM, Y. G., CHA, J. & CHANDRASEGARAN, S. 1996. Hybrid restriction enzymes: zinc finger fusions to Fok I cleavage domain. *Proc Natl Acad Sci U S A,* 93**,** 1156-60.

KITAZAWA, M., CHENG, D., TSUKAMOTO, M. R., KOIKE, M. A., WES, P. D., VASILEVKO, V., CRIBBS, D. H. & LAFERLA, F. M. 2011. Blocking IL-1 signaling rescues cognition, attenuates tau pathology, and restores neuronal beta-catenin pathway function in an Alzheimer's disease model. *J Immunol,* 187**,** 6539-49.

KLEINBERGER, G., YAMANISHI, Y., SUAREZ-CALVET, M., CZIRR, E., LOHMANN, E., CUYVERS, E., STRUYFS, H., PETTKUS, N., WENNINGER-WEINZIERL, A., MAZAHERI, F., TAHIROVIC, S., LLEO, A., ALCOLEA, D., FORTEA, J., WILLEM, M., LAMMICH, S., MOLINUEVO, J. L., SANCHEZ-VALLE, R., ANTONELL, A., RAMIREZ, A., HENEKA, M. T., SLEEGERS, K., VAN DER ZEE, J., MARTIN, J. J., ENGELBORGHS, S., DEMIRTAS-TATLIDEDE, A., ZETTERBERG, H., VAN BROECKHOVEN, C., GURVIT, H., WYSS-CORAY, T., HARDY, J., COLONNA, M. & HAASS, C. 2014a. TREM2 mutations implicated in neurodegeneration impair cell surface transport and phagocytosis. *Sci Transl Med,* 6**,** 243ra86.

KLEINBERGER, G., YAMANISHI, Y., SUAREZ-CALVET, M., CZIRR, E., LOHMANN, E., CUYVERS, E., STRUYFS, H., PETTKUS, N., WENNINGER-WEINZIERL, A., MAZAHERI, F., TAHIROVIC, S., LLEO, A., ALCOLEA, D., FORTEA, J., WILLEM, M., LAMMICH, S., MOLINUEVO, J. L., SANCHEZ-VALLE, R., ANTONELL, A., RAMIREZ, A., HENEKA, M. T., SLEEGERS, K., VAN DER ZEE, J., MARTIN, J. J., ENGELBORGHS, S., DEMIRTAS-TATLIDEDE, A., ZETTERBERG, H., VAN BROECKHOVEN, C., GURVIT, H., WYSS-CORAY, T., HARDY, J., COLONNA, M. & HAASS, C. 2014b. TREM2 mutations implicated in neurodegeneration impair cell surface transport and phagocytosis. *Science Translational Medicine,* 6.

KLESNEY-TAIT, J., TURNBULL, I. R. & COLONNA, M. 2006. The TREM receptor family and signal integration. *Nat Immunol,* 7**,** 1266-73.

KLOS, A., WENDE, E., WAREHAM, K. J. & MONK, P. N. 2013. International Union of Basic and Clinical Pharmacology. [corrected]. LXXXVII. Complement peptide C5a, C4a, and C3a receptors. *Pharmacol Rev,* 65**,** 500-43.

KLUNEMANN, H. H., RIDHA, B. H., MAGY, L., WHERRETT, J. R., HEMELSOET, D. M., KEEN, R. W., DE BLEECKER, J. L., ROSSOR, M. N., MARIENHAGEN, J., KLEIN, H. E., PELTONEN, L. & PALONEVA, J. 2005. The genetic causes of basal ganglia calcification, dementia, and bone cysts: DAP12 and TREM2. *Neurology,* 64**,** 1502-7.

KOBER, D. L., ALEXANDER-BRETT, J. M., KARCH, C. M., CRUCHAGA, C., COLONNA, M., HOLTZMAN, M. J. & BRETT, T. J. 2016. Neurodegenerative disease mutations in TREM2 reveal a functional surface and distinct loss-of-function mechanisms. *Elife,* 5.

KOENIGSKNECHT-TALBOO, J. & LANDRETH, G. E. 2005. Microglial phagocytosis induced by fibrillar beta-amyloid and IgGs are differentially regulated by proinflammatory cytokines. *J Neurosci,* 25**,** 8240-9.

KOONIN, E. V., MAKAROVA, K. S. & ZHANG, F. 2017. Diversity, classification and evolution of CRISPR-Cas systems. *Curr Opin Microbiol,* 37**,** 67-78.

KOPPENSTEINER, P., TRINCHESE, F., FA, M., PUZZO, D., GULISANO, W., YAN, S., POUSSIN, A., LIU, S., OROZCO, I., DALE, E., TEICH, A. F., PALMERI, A., NINAN, I., BOEHM, S. &

ARANCIO, O. 2016. Time-dependent reversal of synaptic plasticity induced by physiological concentrations of oligomeric Abeta42: an early index of Alzheimer's disease. *Sci Rep,* 6**,** 32553.

KORZHEVSKIY, D. E. & KIRIK, O. V. 2015. [Cerebral Microglia and Microglial Markers]. *Morfologiia,* 147**,** 37-44.

KRESO, A., O'BRIEN, C. A., VAN GALEN, P., GAN, O. I., NOTTA, F., BROWN, A. M., NG, K., MA, J., WIENHOLDS, E., DUNANT, C., POLLETT, A., GALLINGER, S., MCPHERSON, J., MULLIGHAN, C. G., SHIBATA, D. & DICK, J. E. 2013. Variable clonal repopulation dynamics influence chemotherapy response in colorectal cancer. *Science,* 339**,** 543-8.

KULLER, L. H., SHEMANSKI, L., MANOLIO, T., HAAN, M., FRIED, L., BRYAN, N., BURKE, G. L., TRACY, R. & BHADELIA, R. 1998. Relationship between ApoE, MRI findings, and cognitive function in the Cardiovascular Health Study. *Stroke,* 29**,** 388-98.

KUMMER, M. P., HERMES, M., DELEKARTE, A., HAMMERSCHMIDT, T., KUMAR, S., TERWEL, D., WALTER, J., PAPE, H. C., KONIG, S., ROEBER, S., JESSEN, F., KLOCKGETHER, T., KORTE, M. & HENEKA, M. T. 2011. Nitration of tyrosine 10 critically enhances amyloid beta aggregation and plaque formation. *Neuron,* 71**,** 833-44.

LABZIN, L. I., HENEKA, M. T. & LATZ, E. 2018. Innate Immunity and Neurodegeneration. *Annu Rev Med,* 69**,** 437-449.

LACEY, D. C., ACHUTHAN, A., FLEETWOOD, A. J., DINH, H., ROINIOTIS, J., SCHOLZ, G. M., CHANG, M. W., BECKMAN, S. K., COOK, A. D. & HAMILTON, J. A. 2012. Defining GM-CSF- and macrophage-CSF-dependent macrophage responses by in vitro models. *J Immunol,* 188**,** 5752-65.

LADU, M. J., GILLIGAN, S. M., LUKENS, J. R., CABANA, V. G., REARDON, C. A., VAN ELDIK, L. J. & HOLTZMAN, D. M. 1998. Nascent astrocyte particles differ from lipoproteins in CSF. *J Neurochem,* 70**,** 2070-81.

LAHIRI, D. K., CHEN, D., VIVIEN, D., GE, Y. W., GREIG, N. H. & ROGERS, J. T. 2003a. Role of cytokines in the gene expression of amyloid beta-protein precursor: identification of a 5'-UTR-binding nuclear factor and its implications in Alzheimer's disease. *J Alzheimers Dis,* 5**,** 81-90.

LAHIRI, D. K., FARLOW, M. R., SAMBAMURTI, K., GREIG, N. H., GIACOBINI, E. & SCHNEIDER, L. S. 2003b. A critical analysis of new molecular targets and strategies for drug developments in Alzheimer's disease. *Curr Drug Targets,* 4**,** 97-112.

LAMBERT, J. C., HEATH, S., EVEN, G., CAMPION, D., SLEEGERS, K., HILTUNEN, M., COMBARROS, O., ZELENIKA, D., BULLIDO, M. J., TAVERNIER, B., LETENNEUR, L., BETTENS, K., BERR, C., PASQUIER, F., FIEVET, N., BARBERGER-GATEAU, P., ENGELBORGHS, S., DE DEYN, P., MATEO, I., FRANCK, A., HELISALMI, S., PORCELLINI, E., HANON, O., EUROPEAN ALZHEIMER'S DISEASE INITIATIVE, I., DE PANCORBO, M. M., LENDON, C., DUFOUIL, C., JAILLARD, C., LEVEILLARD, T., ALVAREZ, V., BOSCO, P., MANCUSO, M., PANZA, F., NACMIAS, B., BOSSU, P., PICCARDI, P., ANNONI, G., SERIPA, D., GALIMBERTI, D., HANNEQUIN, D., LICASTRO, F., SOININEN, H., RITCHIE, K., BLANCHE, H., DARTIGUES, J. F., TZOURIO, C., GUT, I., VAN BROECKHOVEN, C., ALPEROVITCH, A., LATHROP, M. & AMOUYEL, P. 2009. Genome-wide association study identifies variants at CLU and CR1 associated with Alzheimer's disease. *Nat Genet,* 41**,** 1094-9.

LAMBERT, J. C., IBRAHIM-VERBAAS, C. A., HAROLD, D., NAJ, A. C., SIMS, R., BELLENGUEZ, C., DESTAFANO, A. L., BIS, J. C., BEECHAM, G. W., GRENIER-BOLEY, B., RUSSO, G., THORTON-WELLS, T. A., JONES, N., SMITH, A. V., CHOURAKI, V., THOMAS, C., IKRAM, M. A., ZELENIKA, D., VARDARAJAN, B. N., KAMATANI, Y., LIN, C. F., GERRISH, A., SCHMIDT, H., KUNKLE, B., DUNSTAN, M. L., RUIZ, A., BIHOREAU, M. T., CHOI, S. H., REITZ, C., PASQUIER, F., CRUCHAGA, C., CRAIG, D., AMIN, N., BERR, C., LOPEZ, O. L., DE JAGER, P. L., DERAMECOURT, V., JOHNSTON, J. A., EVANS, D., LOVESTONE, S., LETENNEUR, L., MORON, F. J., RUBINSZTEIN, D. C., EIRIKSDOTTIR, G., SLEEGERS, K., GOATE, A. M., FIEVET, N., HUENTELMAN, M. W., GILL, M., BROWN, K., KAMBOH, M. I., KELLER, L., BARBERGER-GATEAU, P., MCGUINESS, B., LARSON, E. B., GREEN, R., MYERS,

A. J., DUFOUIL, C., TODD, S., WALLON, D., LOVE, S., ROGAEVA, E., GALLACHER, J., ST GEORGE-HYSLOP, P., CLARIMON, J., LLEO, A., BAYER, A., TSUANG, D. W., YU, L., TSOLAKI, M., BOSSU, P., SPALLETTA, G., PROITSI, P., COLLINGE, J., SORBI, S., SANCHEZ-GARCIA, F., FOX, N. C., HARDY, J., DENIZ NARANJO, M. C., BOSCO, P., CLARKE, R., BRAYNE, C., GALIMBERTI, D., MANCUSO, M., MATTHEWS, F., EUROPEAN ALZHEIMER'S DISEASE, I., GENETIC, ENVIRONMENTAL RISK IN ALZHEIMER'S, D., ALZHEIMER'S DISEASE GENETIC, C., COHORTS FOR, H., AGING RESEARCH IN GENOMIC, E., MOEBUS, S., MECOCCI, P., DEL ZOMPO, M., MAIER, W., HAMPEL, H., PILOTTO, A., BULLIDO, M., PANZA, F., CAFFARRA, P., et al. 2013. Meta-analysis of 74,046 individuals identifies 11 new susceptibility loci for Alzheimer's disease. *Nat Genet,* 45**,** 1452-8.

LANDLINGER, C., OBERLEITNER, L., GRUBER, P., NOIGES, B., YATSYK, K., SANTIC, R., MANDLER, M. & STAFFLER, G. 2015. Active immunization against complement factor C5a: a new therapeutic approach for Alzheimer's disease. *J Neuroinflammation,* 12**,** 150.

LANDRETH, G. E. & REED-GEAGHAN, E. G. 2009. Toll-like receptors in Alzheimer's disease. *Curr Top Microbiol Immunol,* 336**,** 137-53.

LASKIN, D. L. 2009. Macrophages and inflammatory mediators in chemical toxicity: a battle of forces. *Chem Res Toxicol,* 22**,** 1376-85.

LATTANTE, S., LE BER, I., CAMUZAT, A., DAYAN, S., GODARD, C., VAN BORTEL, I., DE SEPTENVILLE, A., CIURA, S., BRICE, A., KABASHI, E., FRENCH RESEARCH NETWORK ON, F. T. D. & FTD, A. L. S. 2013. TREM2 mutations are rare in a French cohort of patients with frontotemporal dementia. *Neurobiol Aging,* 34**,** 2443 e1-2.

LEDEBOER, A., BREVE, J. J., POOLE, S., TILDERS, F. J. & VAN DAM, A. M. 2000. Interleukin-10, interleukin-4, and transforming growth factor-beta differentially regulate lipopolysaccharide-induced production of pro-inflammatory cytokines and nitric oxide in co-cultures of rat astroglial and microglial cells. *Glia,* 30**,** 134-42.

LEDFORD, H. 2016. CRISPR: gene editing is just the beginning. *Nature,* 531**,** 156-9.

LEE, C. K., WEINDRUCH, R. & PROLLA, T. A. 2000. Gene-expression profile of the ageing brain in mice. *Nat Genet,* 25**,** 294-7.

LEE, C. Y., TSE, W., SMITH, J. D. & LANDRETH, G. E. 2012. Apolipoprotein E promotes beta-amyloid trafficking and degradation by modulating microglial cholesterol levels. *J Biol Chem,* 287**,** 2032-44.

LEE, J. W., NAMKOONG, H., KIM, H. K., KIM, S., HWANG, D. W., NA, H. R., HA, S. A., KIM, J. R. & KIM, J. W. 2007. Fibrinogen gamma-A chain precursor in CSF: a candidate biomarker for Alzheimer's disease. *BMC Neurol,* 7**,** 14.

LEHNARDT, S., SCHOTT, E., TRIMBUCH, T., LAUBISCH, D., KRUEGER, C., WULCZYN, G., NITSCH, R. & WEBER, J. R. 2008. A vicious cycle involving release of heat shock protein 60 from injured cells and activation of toll-like receptor 4 mediates neurodegeneration in the CNS. *J Neurosci,* 28**,** 2320-31.

LEIBSON, C. L., ROCCA, W. A., HANSON, V. A., CHA, R., KOKMEN, E., O'BRIEN, P. C. & PALUMBO, P. J. 1997. The risk of dementia among persons with diabetes mellitus: a population-based cohort study. *Ann N Y Acad Sci,* 826**,** 422-7.

LEVY-LAHAD, E., WASCO, W., POORKAJ, P., ROMANO, D. M., OSHIMA, J., PETTINGELL, W. H., YU, C. E., JONDRO, P. D., SCHMIDT, S. D., WANG, K. & ET AL. 1995. Candidate gene for the chromosome 1 familial Alzheimer's disease locus. *Science,* 269**,** 973-7.

LI, N., LIU, B. W., REN, W. Z., LIU, J. X., LI, S. N., FU, S. P., ZENG, Y. L., XU, S. Y., YAN, X., GAO, Y. J., LIU, D. F. & WANG, W. 2016. GLP-2 Attenuates LPS-Induced Inflammation in BV-2 Cells by Inhibiting ERK1/2, JNK1/2 and NF-kappaB Signaling Pathways. *Int J Mol Sci,* 17**,** 190.

LI, X., KROIN, J. S., KC, R., GIBSON, G., CHEN, D., CORBETT, G. T., PAHAN, K., FAYYAZ, S., KIM, J. S., VAN WIJNEN, A. J., SUH, J., KIM, S. G. & IM, H. J. 2013. Altered spinal microRNA-146a and the microRNA-183 cluster contribute to osteoarthritic pain in knee joints. *J Bone Miner Res,* 28**,** 2512-22.

LI, X., MA, Y., WEI, X., LI, Y., WU, H., ZHUANG, J. & ZHAO, Z. 2014. Clusterin in Alzheimer's disease: a player in the biological behavior of amyloid-beta. *Neurosci Bull,* 30**,** 162-8.

LI, X., MONTINE, K. S., KEENE, C. D. & MONTINE, T. J. 2015. Different mechanisms of apolipoprotein E isoform-dependent modulation of prostaglandin E2 production and triggering receptor expressed on myeloid cells 2 (TREM2) expression after innate immune activation of microglia. *FASEB J,* 29**,** 1754-62.

LIANG, X., POTTER, J., KUMAR, S., ZOU, Y., QUINTANILLA, R., SRIDHARAN, M., CARTE, J., CHEN, W., ROARK, N., RANGANATHAN, S., RAVINDER, N. & CHESNUT, J. D. 2015. Rapid and highly efficient mammalian cell engineering via Cas9 protein transfection. *J Biotechnol,* 208**,** 44-53.

LIAO, Y. F., WANG, B. J., CHENG, H. T., KUO, L. H. & WOLFE, M. S. 2004. Tumor necrosis factor-alpha, interleukin-1beta, and interferon-gamma stimulate gamma-secretase-mediated cleavage of amyloid precursor protein through a JNK-dependent MAPK pathway. *J Biol Chem,* 279**,** 49523-32.

LIEB, W., BEISER, A. S., VASAN, R. S., TAN, Z. S., AU, R., HARRIS, T. B., ROUBENOFF, R., AUERBACH, S., DECARLI, C., WOLF, P. A. & SESHADRI, S. 2009. Association of plasma leptin levels with incident Alzheimer disease and MRI measures of brain aging. *JAMA,* 302**,** 2565-72.

LIN, S., STAAHL, B. T., ALLA, R. K. & DOUDNA, J. A. 2014. Enhanced homology-directed human genome engineering by controlled timing of CRISPR/Cas9 delivery. *Elife,* 3**,** e04766.

LIPINSKI, B. & SAJDEL-SULKOWSKA, E. M. 2006. New insight into Alzheimer disease: demonstration of fibrin(ogen)-serum albumin insoluble deposits in brain tissue. *Alzheimer Dis Assoc Disord,* 20**,** 323-6.

LIU, C. C., LIU, C. C., KANEKIYO, T., XU, H. & BU, G. 2013. Apolipoprotein E and Alzheimer disease: risk, mechanisms and therapy. *Nat Rev Neurol,* 9**,** 106-18.

LIU, D. & NIU, Z. X. 2009. The structure, genetic polymorphisms, expression and biological functions of complement receptor type 1 (CR1/CD35). *Immunopharmacol Immunotoxicol,* 31**,** 524-35.

LIVAK, K. J. & SCHMITTGEN, T. D. 2001. Analysis of relative gene expression data using real-time quantitative PCR and the 2(-Delta Delta C(T)) Method. *Methods,* 25**,** 402-8.

LORENZO, A. & YANKNER, B. A. 1994. Beta-amyloid neurotoxicity requires fibril formation and is inhibited by congo red. *Proc Natl Acad Sci U S A,* 91**,** 12243-7.

LUCHSINGER, J. A., TANG, M. X., STERN, Y., SHEA, S. & MAYEUX, R. 2001. Diabetes mellitus and risk of Alzheimer's disease and dementia with stroke in a multiethnic cohort. *Am J Epidemiol,* 154**,** 635-41.

LUCIN, K. M. & WYSS-CORAY, T. 2009. Immune activation in brain aging and neurodegeneration: too much or too little? *Neuron,* 64**,** 110-22.

LUE, L. F., KUO, Y. M., BEACH, T. & WALKER, D. G. 2010. Microglia activation and anti-inflammatory regulation in Alzheimer's disease. *Mol Neurobiol,* 41**,** 115-28.

LUE, L. F., RYDEL, R., BRIGHAM, E. F., YANG, L. B., HAMPEL, H., MURPHY, G. M., JR., BRACHOVA, L., YAN, S. D., WALKER, D. G., SHEN, Y. & ROGERS, J. 2001a. Inflammatory repertoire of Alzheimer's disease and nondemented elderly microglia in vitro. *Glia,* 35**,** 72-9.

LUE, L. F., SCHMITZ, C. & WALKER, D. G. 2015. What happens to microglial TREM2 in Alzheimer's disease: Immunoregulatory turned into immunopathogenic? *Neuroscience,* 302**,** 138-50.

LUE, L. F., WALKER, D. G. & ROGERS, J. 2001b. Modeling microglial activation in Alzheimer's disease with human postmortem microglial cultures. *Neurobiol Aging,* 22**,** 945-56.

LUO, X. G. & CHEN, S. D. 2012. The changing phenotype of microglia from homeostasis to disease. *Transl Neurodegener,* 1**,** 9.

LYNCH, J. R., TANG, W., WANG, H., VITEK, M. P., BENNETT, E. R., SULLIVAN, P. M., WARNER, D. S. & LASKOWITZ, D. T. 2003. APOE genotype and an ApoE-mimetic peptide modify the

systemic and central nervous system inflammatory response. *J Biol Chem,* 278**,** 48529-33.

LYNCH, J. R., WANG, H., MACE, B., LEINENWEBER, S., WARNER, D. S., BENNETT, E. R., VITEK, M. P., MCKENNA, S. & LASKOWITZ, D. T. 2005. A novel therapeutic derived from apolipoprotein E reduces brain inflammation and improves outcome after closed head injury. *Exp Neurol,* 192**,** 109-16.

LYONS, A. B. & PARISH, C. R. 1994. Determination of lymphocyte division by flow cytometry. *J Immunol Methods,* 171**,** 131-7.

MAESS, M. B., WITTIG, B. & LORKOWSKI, S. 2014. Highly efficient transfection of human THP-1 macrophages by nucleofection. *J Vis Exp***,** e51960.

MAEZAWA, I., ZIMIN, P. I., WULFF, H. & JIN, L. W. 2011. Amyloid-beta protein oligomer at low nanomolar concentrations activates microglia and induces microglial neurotoxicity. *J Biol Chem,* 286**,** 3693-706.

MAHESHWARI, A., JANSSENS, K., BOGIE, J., VAN DEN HAUTE, C., STRUYS, T., LAMBRICHTS, I., BAEKELANDT, V., STINISSEN, P., HENDRIKS, J. J., SLAETS, H. & HELLINGS, N. 2013. Local overexpression of interleukin-11 in the central nervous system limits demyelination and enhances remyelination. *Mediators Inflamm,* 2013**,** 685317.

MAHFOUZ, M. M., LI, L., SHAMIMUZZAMAN, M., WIBOWO, A., FANG, X. & ZHU, J. K. 2011. De novo-engineered transcription activator-like effector (TALE) hybrid nuclease with novel DNA binding specificity creates double-strand breaks. *Proc Natl Acad Sci U S A,* 108**,** 2623-8.

MAIRUAE, N. & CHEEPSUNTHORN, P. 2018. Valproic acid attenuates nitric oxide and interleukin-1beta production in lipopolysaccharide-stimulated iron-rich microglia. *Biomed Rep,* 8**,** 359-364.

MALI, P., YANG, L., ESVELT, K. M., AACH, J., GUELL, M., DICARLO, J. E., NORVILLE, J. E. & CHURCH, G. M. 2013. RNA-guided human genome engineering via Cas9. *Science,* 339**,** 823-6.

MALIK, M., SIMPSON, J. F., PARIKH, I., WILFRED, B. R., FARDO, D. W., NELSON, P. T. & ESTUS, S. 2013. CD33 Alzheimer's risk-altering polymorphism, CD33 expression, and exon 2 splicing. *J Neurosci,* 33**,** 13320-5.

MANTOVANI, A., SOZZANI, S., LOCATI, M., ALLAVENA, P. & SICA, A. 2002. Macrophage polarization: tumor-associated macrophages as a paradigm for polarized M2 mononuclear phagocytes. *Trends Immunol,* 23**,** 549-55.

MARIONI, J. C., MASON, C. E., MANE, S. M., STEPHENS, M. & GILAD, Y. 2008. RNA-seq: an assessment of technical reproducibility and comparison with gene expression arrays. *Genome Res,* 18**,** 1509-17.

MARTIN, E., BOUCHER, C., FONTAINE, B. & DELARASSE, C. 2017. Distinct inflammatory phenotypes of microglia and monocyte-derived macrophages in Alzheimer's disease models: effects of aging and amyloid pathology. *Aging Cell,* 16**,** 27-38.

MARTINEZ, F. O. & GORDON, S. 2014. The M1 and M2 paradigm of macrophage activation: time for reassessment. *F1000Prime Rep,* 6**,** 13.

MARTINEZ, F. O., GORDON, S., LOCATI, M. & MANTOVANI, A. 2006. Transcriptional profiling of the human monocyte-to-macrophage differentiation and polarization: new molecules and patterns of gene expression. *J Immunol,* 177**,** 7303-11.

MARUYAMA, T., DOUGAN, S. K., TRUTTMANN, M. C., BILATE, A. M., INGRAM, J. R. & PLOEGH, H. L. 2015. Increasing the efficiency of precise genome editing with CRISPR-Cas9 by inhibition of nonhomologous end joining. *Nat Biotechnol,* 33**,** 538-42.

MATARIN, M., SALIH, D. A., YASVOINA, M., CUMMINGS, D. M., GUELFI, S., LIU, W., NAHABOO SOLIM, M. A., MOENS, T. G., PAUBLETE, R. M., ALI, S. S., PERONA, M., DESAI, R., SMITH, K. J., LATCHAM, J., FULLEYLOVE, M., RICHARDSON, J. C., HARDY, J. & EDWARDS, F. A. 2015. A genome-wide gene-expression analysis and database in transgenic mice during development of amyloid or tau pathology. *Cell Rep,* 10**,** 633-44.

MAWUENYEGA, K. G., SIGURDSON, W., OVOD, V., MUNSELL, L., KASTEN, T., MORRIS, J. C., YARASHESKI, K. E. & BATEMAN, R. J. 2010. Decreased clearance of CNS beta-amyloid in Alzheimer's disease. *Science,* 330**,** 1774.

MAYEUX, R. 2010. Clinical practice. Early Alzheimer's disease. *N Engl J Med,* 362**,** 2194-201.

MAZAHERI, F., SNAIDERO, N., KLEINBERGER, G., MADORE, C., DARIA, A., WERNER, G., KRASEMANN, S., CAPELL, A., TRUMBACH, D., WURST, W., BRUNNER, B., BULTMANN, S., TAHIROVIC, S., KERSCHENSTEINER, M., MISGELD, T., BUTOVSKY, O. & HAASS, C. 2017. TREM2 deficiency impairs chemotaxis and microglial responses to neuronal injury. *EMBO Rep,* 18**,** 1186-1198.

MCGEER, P. L., AKIYAMA, H., ITAGAKI, S. & MCGEER, E. G. 1989. Activation of the classical complement pathway in brain tissue of Alzheimer patients. *Neurosci Lett,* 107**,** 341-6.

MCGEER, P. L., ITAGAKI, S., BOYES, B. E. & MCGEER, E. G. 1988. Reactive microglia are positive for HLA-DR in the substantia nigra of Parkinson's and Alzheimer's disease brains. *Neurology,* 38**,** 1285-91.

MCGEER, P. L., ITAGAKI, S., TAGO, H. & MCGEER, E. G. 1987. Reactive microglia in patients with senile dementia of the Alzheimer type are positive for the histocompatibility glycoprotein HLA-DR. *Neurosci Lett,* 79**,** 195-200.

MEDEIROS, R. & LAFERLA, F. M. 2013. Astrocytes: conductors of the Alzheimer disease neuroinflammatory symphony. *Exp Neurol,* 239**,** 133-8.

MEDWAY, C. & MORGAN, K. 2014. Review: The genetics of Alzheimer's disease; putting flesh on the bones. *Neuropathol Appl Neurobiol,* 40**,** 97-105.

MELCHIOR, B., GARCIA, A. E., HSIUNG, B. K., LO, K. M., DOOSE, J. M., THRASH, J. C., STALDER, A. K., STAUFENBIEL, M., NEUMANN, H. & CARSON, M. J. 2010. Dual induction of TREM2 and tolerance-related transcript, Tmem176b, in amyloid transgenic mice: implications for vaccine-based therapies for Alzheimer's disease. *ASN Neuro,* 2**,** e00037.

MEYER-LUEHMANN, M., SPIRES-JONES, T. L., PRADA, C., GARCIA-ALLOZA, M., DE CALIGNON, A., ROZKALNE, A., KOENIGSKNECHT-TALBOO, J., HOLTZMAN, D. M., BACSKAI, B. J. & HYMAN, B. T. 2008. Rapid appearance and local toxicity of amyloid-beta plaques in a mouse model of Alzheimer's disease. *Nature,* 451**,** 720-4.

MICHELUCCI, A., HEURTAUX, T., GRANDBARBE, L., MORGA, E. & HEUSCHLING, P. 2009. Characterization of the microglial phenotype under specific pro-inflammatory and anti-inflammatory conditions: Effects of oligomeric and fibrillar amyloid-beta. *J Neuroimmunol,* 210**,** 3-12.

MILLER, J. A., WOLTJER, R. L., GOODENBOUR, J. M., HORVATH, S. & GESCHWIND, D. H. 2013. Genes and pathways underlying regional and cell type changes in Alzheimer's disease. *Genome Med,* 5**,** 48.

MOLLER, H. J. & GRAEBER, M. B. 1998. The case described by Alois Alzheimer in 1911. Historical and conceptual perspectives based on the clinical record and neurohistological sections. *Eur Arch Psychiatry Clin Neurosci,* 248**,** 111-22.

MONIF, M., BURNSTOCK, G. & WILLIAMS, D. A. 2010. Microglia: proliferation and activation driven by the P2X7 receptor. *Int J Biochem Cell Biol,* 42**,** 1753-6.

MONSONEGO, A., IMITOLA, J., PETROVIC, S., ZOTA, V., NEMIROVSKY, A., BARON, R., FISHER, Y., OWENS, T. & WEINER, H. L. 2006. Abeta-induced meningoencephalitis is IFN-gamma-dependent and is associated with T cell-dependent clearance of Abeta in a mouse model of Alzheimer's disease. *Proc Natl Acad Sci U S A,* 103**,** 5048-53.

MORE, S. V., KUMAR, H., KIM, I. S., KOPPULLA, S., KIM, B. W. & CHOI, D. K. 2013. Strategic selection of neuroinflammatory models in Parkinson's disease: evidence from experimental studies. *CNS Neurol Disord Drug Targets,* 12**,** 680-97.

MORGANTI, J. M., NASH, K. R., GRIMMIG, B. A., RANJIT, S., SMALL, B., BICKFORD, P. C. & GEMMA, C. 2012. The soluble isoform of CX3CL1 is necessary for neuroprotection in a mouse model of Parkinson's disease. *J Neurosci,* 32**,** 14592-601.

MOUT, R., RAY, M., LEE, Y. W., SCALETTI, F. & ROTELLO, V. M. 2017. In Vivo Delivery of CRISPR/Cas9 for Therapeutic Gene Editing: Progress and Challenges. *Bioconjug Chem,* 28**,** 880-884.

MRDJEN, D., PAVLOVIC, A., HARTMANN, F. J., SCHREINER, B., UTZ, S. G., LEUNG, B. P., LELIOS, I., HEPPNER, F. L., KIPNIS, J., MERKLER, D., GRETER, M. & BECHER, B. 2018. High-Dimensional Single-Cell Mapping of Central Nervous System Immune Cells Reveals Distinct Myeloid Subsets in Health, Aging, and Disease. *Immunity,* 48**,** 599.

MUFFAT, J., LI, Y., YUAN, B., MITALIPOVA, M., OMER, A., CORCORAN, S., BAKIASI, G., TSAI, L. H., AUBOURG, P., RANSOHOFF, R. M. & JAENISCH, R. 2016. Efficient derivation of microglia-like cells from human pluripotent stem cells. *Nat Med,* 22**,** 1358-1367.

MURRAY, C. E., KING, A., TROAKES, C., HODGES, A. & LASHLEY, T. 2018. APOE epsilon4 is also required in TREM2 R47H variant carriers for Alzheimer's disease to develop. *Neuropathol Appl Neurobiol*.

N'DIAYE, E. N., BRANDA, C. S., BRANDA, S. S., NEVAREZ, L., COLONNA, M., LOWELL, C., HAMERMAN, J. A. & SEAMAN, W. E. 2009a. TREM-2 (triggering receptor expressed on myeloid cells 2) is a phagocytic receptor for bacteria. *Journal of Cell Biology,* 184**,** 215-223.

N'DIAYE, E. N., BRANDA, C. S., BRANDA, S. S., NEVAREZ, L., COLONNA, M., LOWELL, C., HAMERMAN, J. A. & SEAMAN, W. E. 2009b. TREM-2 (triggering receptor expressed on myeloid cells 2) is a phagocytic receptor for bacteria. *J Cell Biol,* 184**,** 215-23.

NACHMAN, M. W. & SEARLE, J. B. 1995. Why is the house mouse karyotype so variable? *Trends Ecol Evol,* 10**,** 397-402.

NAJ, A. C., JUN, G., BEECHAM, G. W., WANG, L. S., VARDARAJAN, B. N., BUROS, J., GALLINS, P. J., BUXBAUM, J. D., JARVIK, G. P., CRANE, P. K., LARSON, E. B., BIRD, T. D., BOEVE, B. F., GRAFF-RADFORD, N. R., DE JAGER, P. L., EVANS, D., SCHNEIDER, J. A., CARRASQUILLO, M. M., ERTEKIN-TANER, N., YOUNKIN, S. G., CRUCHAGA, C., KAUWE, J. S., NOWOTNY, P., KRAMER, P., HARDY, J., HUENTELMAN, M. J., MYERS, A. J., BARMADA, M. M., DEMIRCI, F. Y., BALDWIN, C. T., GREEN, R. C., ROGAEVA, E., ST GEORGE-HYSLOP, P., ARNOLD, S. E., BARBER, R., BEACH, T., BIGIO, E. H., BOWEN, J. D., BOXER, A., BURKE, J. R., CAIRNS, N. J., CARLSON, C. S., CARNEY, R. M., CARROLL, S. L., CHUI, H. C., CLARK, D. G., CORNEVEAUX, J., COTMAN, C. W., CUMMINGS, J. L., DECARLI, C., DEKOSKY, S. T., DIAZ-ARRASTIA, R., DICK, M., DICKSON, D. W., ELLIS, W. G., FABER, K. M., FALLON, K. B., FARLOW, M. R., FERRIS, S., FROSCH, M. P., GALASKO, D. R., GANGULI, M., GEARING, M., GESCHWIND, D. H., GHETTI, B., GILBERT, J. R., GILMAN, S., GIORDANI, B., GLASS, J. D., GROWDON, J. H., HAMILTON, R. L., HARRELL, L. E., HEAD, E., HONIG, L. S., HULETTE, C. M., HYMAN, B. T., JICHA, G. A., JIN, L. W., JOHNSON, N., KARLAWISH, J., KARYDAS, A., KAYE, J. A., KIM, R., KOO, E. H., KOWALL, N. W., LAH, J. J., LEVEY, A. I., LIEBERMAN, A. P., LOPEZ, O. L., MACK, W. J., MARSON, D. C., MARTINIUK, F., MASH, D. C., MASLIAH, E., MCCORMICK, W. C., MCCURRY, S. M., MCDAVID, A. N., MCKEE, A. C., MESULAM, M., MILLER, B. L., et al. 2011. Common variants at MS4A4/MS4A6E, CD2AP, CD33 and EPHA1 are associated with late-onset Alzheimer's disease. *Nat Genet,* 43**,** 436-41.

NAKAMURA, Y., SI, Q. S. & KATAOKA, K. 1999. Lipopolysaccharide-induced microglial activation in culture: temporal profiles of morphological change and release of cytokines and nitric oxide. *Neurosci Res,* 35**,** 95-100.

NATHAN, C., CALINGASAN, N., NEZEZON, J., DING, A., LUCIA, M. S., LA PERLE, K., FUORTES, M., LIN, M., EHRT, S., KWON, N. S., CHEN, J., VODOVOTZ, Y., KIPIANI, K. & BEAL, M. F. 2005. Protection from Alzheimer's-like disease in the mouse by genetic ablation of inducible nitric oxide synthase. *J Exp Med,* 202**,** 1163-9.

NEGGERS, J. E., VERCRUYSSE, T., JACQUEMYN, M., VANSTREELS, E., BALOGLU, E., SHACHAM, S., CROCHIERE, M., LANDESMAN, Y. & DAELEMANS, D. 2015. Identifying drug-target selectivity of small-molecule CRM1/XPO1 inhibitors by CRISPR/Cas9 genome editing. *Chem Biol,* 22**,** 107-16.

NEHER, J. J., NENISKYTE, U., ZHAO, J. W., BAL-PRICE, A., TOLKOVSKY, A. M. & BROWN, G. C. 2011. Inhibition of microglial phagocytosis is sufficient to prevent inflammatory neuronal death. *J Immunol,* 186**,** 4973-83.

NENISKYTE, U., FRICKER, M. & BROWN, G. C. 2016. Amyloid beta induces microglia to phagocytose neurons via activation of protein kinase Cs and NADPH oxidase. *Int J Biochem Cell Biol,* 81**,** 346-355.

NENISKYTE, U., NEHER, J. J. & BROWN, G. C. 2011. Neuronal death induced by nanomolar amyloid beta is mediated by primary phagocytosis of neurons by microglia. *J Biol Chem,* 286**,** 39904-13.

NETEA-MAIER, R. T., PLANTINGA, T. S., VAN DE VEERDONK, F. L., SMIT, J. W. & NETEA, M. G. 2016. Modulation of inflammation by autophagy: Consequences for human disease. *Autophagy,* 12**,** 245-60.

NICE 2018. Dementia - assessment, management and support for people living with dementia and their carers.

NUUTINEN, T., SUURONEN, T., KAUPPINEN, A. & SALMINEN, A. 2009. Clusterin: a forgotten player in Alzheimer's disease. *Brain Res Rev,* 61**,** 89-104.

O'BRIEN, R. J. & WONG, P. C. 2011. Amyloid precursor protein processing and Alzheimer's disease. *Annu Rev Neurosci,* 34**,** 185-204.

OHSAWA, K., IMAI, Y., KANAZAWA, H., SASAKI, Y. & KOHSAKA, S. 2000. Involvement of Iba1 in membrane ruffling and phagocytosis of macrophages/microglia. *J Cell Sci,* 113 (Pt 17)**,** 3073-84.

OHSAWA, K., IMAI, Y., SASAKI, Y. & KOHSAKA, S. 2004. Microglia/macrophage-specific protein Iba1 binds to fimbrin and enhances its actin-bundling activity. *J Neurochem,* 88**,** 844-56.

OLABARRIA, M., NORISTANI, H. N., VERKHRATSKY, A. & RODRIGUEZ, J. J. 2010. Concomitant astroglial atrophy and astrogliosis in a triple transgenic animal model of Alzheimer's disease. *Glia,* 58**,** 831-8.

OLIVE, J. F., QIN, Y., DECRISTO, M. J., LASZEWSKI, T., GREATHOUSE, F. & MCALLISTER, S. S. 2018. Accounting for tumor heterogeneity when using CRISPR-Cas9 for cancer progression and drug sensitivity studies. *PLoS One,* 13**,** e0198790.

OLMOS, G. & LLADO, J. 2014. Tumor necrosis factor alpha: a link between neuroinflammation and excitotoxicity. *Mediators Inflamm,* 2014**,** 861231.

OPAL, S. M. & DEPALO, V. A. 2000. Anti-inflammatory cytokines. *Chest,* 117**,** 1162-72.

ORCHARD, R. C., WILEN, C. B., DOENCH, J. G., BALDRIDGE, M. T., MCCUNE, B. T., LEE, Y. C., LEE, S., PRUETT-MILLER, S. M., NELSON, C. A., FREMONT, D. H. & VIRGIN, H. W. 2016. Discovery of a proteinaceous cellular receptor for a norovirus. *Science,* 353**,** 933-6.

ORIGLIA, N., BONADONNA, C., ROSELLINI, A., LEZNIK, E., ARANCIO, O., YAN, S. S. & DOMENICI, L. 2010. Microglial receptor for advanced glycation end product-dependent signal pathway drives beta-amyloid-induced synaptic depression and long-term depression impairment in entorhinal cortex. *J Neurosci,* 30**,** 11414-25.

ORIHUELA, R., MCPHERSON, C. A. & HARRY, G. J. 2016. Microglial M1/M2 polarization and metabolic states. *Br J Pharmacol,* 173**,** 649-65.

OTERO, K., SHINOHARA, M., ZHAO, H., CELLA, M., GILFILLAN, S., COLUCCI, A., FACCIO, R., ROSS, F. P., TEITELBAUM, S. L., TAKAYANAGI, H. & COLONNA, M. 2012. TREM2 and beta-catenin regulate bone homeostasis by controlling the rate of osteoclastogenesis. *J Immunol,* 188**,** 2612-21.

OTERO, K., TURNBULL, I. R., POLIANI, P. L., VERMI, W., CERUTTI, E., AOSHI, T., TASSI, I., TAKAI, T., STANLEY, S. L., MILLER, M., SHAW, A. S. & COLONNA, M. 2009. Macrophage colony-stimulating factor induces the proliferation and survival of macrophages via a pathway involving DAP12 and beta-catenin. *Nat Immunol,* 10**,** 734-43.

OTERO, M., LAGO, R., LAGO, F., REINO, J. J. & GUALILLO, O. 2005. Signalling pathway involved in nitric oxide synthase type II activation in chondrocytes: synergistic effect of leptin with interleukin-1. *Arthritis Res Ther,* 7**,** R581-91.

OTT, A., STOLK, R. P., VAN HARSKAMP, F., POLS, H. A., HOFMAN, A. & BRETELER, M. M. 1999. Diabetes mellitus and the risk of dementia: The Rotterdam Study. *Neurology,* 53**,** 1937-42.

OZINSKY, A., UNDERHILL, D. M., FONTENOT, J. D., HAJJAR, A. M., SMITH, K. D., WILSON, C. B., SCHROEDER, L. & ADEREM, A. 2000. The repertoire for pattern recognition of pathogens by the innate immune system is defined by cooperation between toll-like receptors. *Proc Natl Acad Sci U S A,* 97**,** 13766-71.

PAGLINAWAN, R., MALIPIERO, U., SCHLAPBACH, R., FREI, K., REITH, W. & FONTANA, A. 2003. TGFbeta directs gene expression of activated microglia to an anti-inflammatory phenotype strongly focusing on chemokine genes and cell migratory genes. *Glia,* 44**,** 219-31.

PAINTER, M. M., ATAGI, Y., LIU, C. C., RADEMAKERS, R., XU, H., FRYER, J. D. & BU, G. 2015. TREM2 in CNS homeostasis and neurodegenerative disease. *Mol Neurodegener,* 10**,** 43.

PALONEVA, J., KESTILA, M., WU, J., SALMINEN, A., BOHLING, T., RUOTSALAINEN, V., HAKOLA, P., BAKKER, A. B., PHILLIPS, J. H., PEKKARINEN, P., LANIER, L. L., TIMONEN, T. & PELTONEN, L. 2000. Loss-of-function mutations in TYROBP (DAP12) result in a presenile dementia with bone cysts. *Nat Genet,* 25**,** 357-61.

PALONEVA, J., MANNINEN, T., CHRISTMAN, G., HOVANES, K., MANDELIN, J., ADOLFSSON, R., BIANCHIN, M., BIRD, T., MIRANDA, R., SALMAGGI, A., TRANEBJAERG, L., KONTTINEN, Y. & PELTONEN, L. 2002. Mutations in two genes encoding different subunits of a receptor signaling complex result in an identical disease phenotype. *Am J Hum Genet,* 71**,** 656-62.

PAN, X. D., ZHU, Y. G., LIN, N., ZHANG, J., YE, Q. Y., HUANG, H. P. & CHEN, X. C. 2011. Microglial phagocytosis induced by fibrillar beta-amyloid is attenuated by oligomeric beta-amyloid: implications for Alzheimer's disease. *Mol Neurodegener,* 6**,** 45.

PARADOWSKA-GORYCKA, A. & JURKOWSKA, M. 2013. Structure, expression pattern and biological activity of molecular complex TREM-2/DAP12. *Hum Immunol,* 74**,** 730-7.

PARESCE, D. M., GHOSH, R. N. & MAXFIELD, F. R. 1996. Microglial cells internalize aggregates of the Alzheimer's disease amyloid beta-protein via a scavenger receptor. *Neuron,* 17**,** 553-65.

PARK, J. S., JI, I. J., AN, H. J., KANG, M. J., KANG, S. W., KIM, D. H. & YOON, S. Y. 2015. Disease-Associated Mutations of TREM2 Alter the Processing of N-Linked Oligosaccharides in the Golgi Apparatus. *Traffic,* 16**,** 510-8.

PARK, K. W., LEE, D. Y., JOE, E. H., KIM, S. U. & JIN, B. K. 2005. Neuroprotective role of microglia expressing interleukin-4. *J Neurosci Res,* 81**,** 397-402.

PATEL, N. S., PARIS, D., MATHURA, V., QUADROS, A. N., CRAWFORD, F. C. & MULLAN, M. J. 2005. Inflammatory cytokine levels correlate with amyloid load in transgenic mouse models of Alzheimer's disease. *J Neuroinflammation,* 2**,** 9.

PATIBANDLA, P. K., TYAGI, N., DEAN, W. L., TYAGI, S. C., ROBERTS, A. M. & LOMINADZE, D. 2009. Fibrinogen induces alterations of endothelial cell tight junction proteins. *J Cell Physiol,* 221**,** 195-203.

PEKNY, M., WILHELMSSON, U. & PEKNA, M. 2014. The dual role of astrocyte activation and reactive gliosis. *Neurosci Lett,* 565**,** 30-8.

PENG, R., LIN, G. & LI, J. 2016. Potential pitfalls of CRISPR/Cas9-mediated genome editing. *FEBS J,* 283**,** 1218-31.

PENG, Y., CLARK, K. J., CAMPBELL, J. M., PANETTA, M. R., GUO, Y. & EKKER, S. C. 2014. Making designer mutants in model organisms. *Development,* 141**,** 4042-54.

PERL, D. P. 2010. Neuropathology of Alzheimer's disease. *Mt Sinai J Med,* 77**,** 32-42.

PFRIEGER, F. W. & UNGERER, N. 2011. Cholesterol metabolism in neurons and astrocytes. *Prog Lipid Res,* 50**,** 357-71.

PICCIO, L., BUONSANTI, C., CELLA, M., TASSI, I., SCHMIDT, R. E., FENOGLIO, C., RINKER, J., 2ND, NAISMITH, R. T., PANINA-BORDIGNON, P., PASSINI, N., GALIMBERTI, D., SCARPINI, E.,

COLONNA, M. & CROSS, A. H. 2008. Identification of soluble TREM-2 in the cerebrospinal fluid and its association with multiple sclerosis and CNS inflammation. *Brain,* 131**,** 3081-91.

PICCIO, L., DEMING, Y., DEL-AGUILA, J. L., GHEZZI, L., HOLTZMAN, D. M., FAGAN, A. M., FENOGLIO, C., GALIMBERTI, D., BORRONI, B. & CRUCHAGA, C. 2016. Cerebrospinal fluid soluble TREM2 is higher in Alzheimer disease and associated with mutation status. *Acta Neuropathol,* 131**,** 925-33.

PICKERING, M. & O'CONNOR, J. J. 2007. Pro-inflammatory cytokines and their effects in the dentate gyrus. *Prog Brain Res,* 163**,** 339-54.

PIEHLER, A. P., GRIMHOLT, R. M., OVSTEBO, R. & BERG, J. P. 2010. Gene expression results in lipopolysaccharide-stimulated monocytes depend significantly on the choice of reference genes. *BMC Immunol,* 11**,** 21.

PLASSMAN, B. L., HAVLIK, R. J., STEFFENS, D. C., HELMS, M. J., NEWMAN, T. N., DROSDICK, D., PHILLIPS, C., GAU, B. A., WELSH-BOHMER, K. A., BURKE, J. R., GURALNIK, J. M. & BREITNER, J. C. 2000. Documented head injury in early adulthood and risk of Alzheimer's disease and other dementias. *Neurology,* 55**,** 1158-66.

PLAZA-ZABALA, A., SIERRA-TORRE, V. & SIERRA, A. 2017. Autophagy and Microglia: Novel Partners in Neurodegeneration and Aging. *Int J Mol Sci,* 18.

POCIVAVSEK, A., BURNS, M. P. & REBECK, G. W. 2009a. Low-density lipoprotein receptors regulate microglial inflammation through c-Jun N-terminal kinase. *Glia,* 57**,** 444-53.

POCIVAVSEK, A., MIKHAILENKO, I., STRICKLAND, D. K. & REBECK, G. W. 2009b. Microglial low-density lipoprotein receptor-related protein 1 modulates c-Jun N-terminal kinase activation. *J Neuroimmunol,* 214**,** 25-32.

POCIVAVSEK, A. & REBECK, G. W. 2009. Inhibition of c-Jun N-terminal kinase increases apoE expression in vitro and in vivo. *Biochem Biophys Res Commun,* 387**,** 516-20.

POCOCK, J. M., LIDDLE, A. C., HOOPER, C., TAYLOR, D. L., DAVENPORT, C. M. & MORGAN, S. C. 2002. Activated microglia in Alzheimer's disease and stroke. *Ernst Schering Res Found Workshop***,** 105-32.

POLIANI, P. L., WANG, Y., FONTANA, E., ROBINETTE, M. L., YAMANISHI, Y., GILFILLAN, S. & COLONNA, M. 2015. TREM2 sustains microglial expansion during aging and response to demyelination. *J Clin Invest,* 125**,** 2161-70.

PONOMAREV, E. D., SHRIVER, L. P. & DITTEL, B. N. 2006. CD40 expression by microglial cells is required for their completion of a two-step activation process during central nervous system autoimmune inflammation. *J Immunol,* 176**,** 1402-10.

POON, V. Y., CHOI, S. & PARK, M. 2013. Growth factors in synaptic function. *Front Synaptic Neurosci,* 5**,** 6.

POPP, M. W. & MAQUAT, L. E. 2016. Leveraging Rules of Nonsense-Mediated mRNA Decay for Genome Engineering and Personalized Medicine. *Cell,* 165**,** 1319-1322.

POTTIER, C., RAVENSCROFT, T. A., BROWN, P. H., FINCH, N. A., BAKER, M., PARSONS, M., ASMANN, Y. W., REN, Y., CHRISTOPHER, E., LEVITCH, D., VAN BLITTERSWIJK, M., CRUCHAGA, C., CAMPION, D., NICOLAS, G., RICHARD, A. C., GUERREIRO, R., BRAS, J. T., ZUCHNER, S., GONZALEZ, M. A., BU, G., YOUNKIN, S., KNOPMAN, D. S., JOSEPHS, K. A., PARISI, J. E., PETERSEN, R. C., ERTEKIN-TANER, N., GRAFF-RADFORD, N. R., BOEVE, B. F., DICKSON, D. W. & RADEMAKERS, R. 2016. TYROBP genetic variants in early-onset Alzheimer's disease. *Neurobiol Aging,* 48**,** 222 e9-222 e15.

PRADA, I., ONGANIA, G. N., BUONSANTI, C., PANINA-BORDIGNON, P. & MELDOLESI, J. 2006. Triggering receptor expressed in myeloid cells 2 (TREM2) trafficking in microglial cells: Continuous shuttling to and from the plasma membrane regulated by cell stimulation. *Neuroscience,* 140**,** 1139-1148.

PRINCE, M., WIMO, A., GUERCHET, M., ALI, G., WU, Y. & PRINA, M. 2015. World Alzheimer Report 2015: The Global Impact of Dementia. *In:* (ADI), A. S. D. I. (ed.). London.

PRINCE, M. A., E.; GUERCHET, M.; PRINA, M. 2014. World Alzheimer Report 2014: Dementia and Risk Reduction an Analysis of Protective and Modifiable Factors, 2014.

PROITSI, P., LEE, S. H., LUNNON, K., KEOHANE, A., POWELL, J., TROAKES, C., AL-SARRAJ, S., FURNEY, S., SOININEN, H., KLOSZEWSKA, I., MECOCCI, P., TSOLAKI, M., VELLAS, B., LOVESTONE, S., HODGES, A. & ADDNEUROMED, C. 2014. Alzheimer's disease susceptibility variants in the MS4A6A gene are associated with altered levels of MS4A6A expression in blood. *Neurobiol Aging,* 35**,** 279-90.

QI, L. S., LARSON, M. H., GILBERT, L. A., DOUDNA, J. A., WEISSMAN, J. S., ARKIN, A. P. & LIM, W. A. 2013. Repurposing CRISPR as an RNA-guided platform for sequence-specific control of gene expression. *Cell,* 152**,** 1173-83.

QIAN, L., WEI, S. J., ZHANG, D., HU, X., XU, Z., WILSON, B., EL-BENNA, J., HONG, J. S. & FLOOD, P. M. 2008. Potent anti-inflammatory and neuroprotective effects of TGF-beta1 are mediated through the inhibition of ERK and p47phox-Ser345 phosphorylation and translocation in microglia. *J Immunol,* 181**,** 660-8.

QIN, L., LIU, Y., WANG, T., WEI, S. J., BLOCK, M. L., WILSON, B., LIU, B. & HONG, J. S. 2004. NADPH oxidase mediates lipopolysaccharide-induced neurotoxicity and proinflammatory gene expression in activated microglia. *J Biol Chem,* 279**,** 1415-21.

QIN, S., JIANG, F., ZHOU, Y., ZHOU, G., YE, P. & JI, Y. 2017. Local knockdown of Nav1.6 relieves pain behaviors induced by BmK I. *Acta Biochim Biophys Sin (Shanghai),* 49**,** 713-721.

RAGHAVACHARI, N., BARB, J., YANG, Y., LIU, P., WOODHOUSE, K., LEVY, D., O'DONNELL, C. J., MUNSON, P. J. & KATO, G. J. 2012. A systematic comparison and evaluation of high density exon arrays and RNA-seq technology used to unravel the peripheral blood transcriptome of sickle cell disease. *BMC Med Genomics,* 5**,** 28.

RAN, F. A., HSU, P. D., LIN, C. Y., GOOTENBERG, J. S., KONERMANN, S., TREVINO, A. E., SCOTT, D. A., INOUE, A., MATOBA, S., ZHANG, Y. & ZHANG, F. 2013a. Double nicking by RNA-guided CRISPR Cas9 for enhanced genome editing specificity. *Cell,* 154**,** 1380-9.

RAN, F. A., HSU, P. D., WRIGHT, J., AGARWALA, V., SCOTT, D. A. & ZHANG, F. 2013b. Genome engineering using the CRISPR-Cas9 system. *Nat Protoc,* 8**,** 2281-2308.

RANSOHOFF, R. M. 2016. A polarizing question: do M1 and M2 microglia exist? *Nat Neurosci,* 19**,** 987-91.

RANSOHOFF, R. M. & CARDONA, A. E. 2010. The myeloid cells of the central nervous system parenchyma. *Nature,* 468**,** 253-62.

RAO, S., MORALES, A. A. & PEARSE, D. D. 2015. The Comparative Utility of Viromer RED and Lipofectamine for Transient Gene Introduction into Glial Cells. *Biomed Res Int,* 2015**,** 458624.

RAYAPROLU, S., MULLEN, B., BAKER, M., LYNCH, T., FINGER, E., SEELEY, W. W., HATANPAA, K. J., LOMEN-HOERTH, C., KERTESZ, A., BIGIO, E. H., LIPPA, C., JOSEPHS, K. A., KNOPMAN, D. S., WHITE, C. L., 3RD, CASELLI, R., MACKENZIE, I. R., MILLER, B. L., BOCZARSKA-JEDYNAK, M., OPALA, G., KRYGOWSKA-WAJS, A., BARCIKOWSKA, M., YOUNKIN, S. G., PETERSEN, R. C., ERTEKIN-TANER, N., UITTI, R. J., MESCHIA, J. F., BOYLAN, K. B., BOEVE, B. F., GRAFF-RADFORD, N. R., WSZOLEK, Z. K., DICKSON, D. W., RADEMAKERS, R. & ROSS, O. A. 2013. TREM2 in neurodegeneration: evidence for association of the p.R47H variant with frontotemporal dementia and Parkinson's disease. *Mol Neurodegener,* 8**,** 19.

REBECK, G. W. 2017. The role of APOE on lipid homeostasis and inflammation in normal brains. *J Lipid Res,* 58**,** 1493-1499.

REED-GEAGHAN, E. G., SAVAGE, J. C., HISE, A. G. & LANDRETH, G. E. 2009. CD14 and toll-like receptors 2 and 4 are required for fibrillar A{beta}-stimulated microglial activation. *J Neurosci,* 29**,** 11982-92.

REITZ, C. & MAYEUX, R. 2014. Alzheimer disease: epidemiology, diagnostic criteria, risk factors and biomarkers. *Biochem Pharmacol,* 88**,** 640-51.

RESENDE, R., FERREIRO, E., PEREIRA, C. & RESENDE DE OLIVEIRA, C. 2008. Neurotoxic effect of oligomeric and fibrillar species of amyloid-beta peptide 1-42: involvement of endoplasmic reticulum calcium release in oligomer-induced cell death. *Neuroscience,* 155**,** 725-37.

REYNOLDS, A. D., STONE, D. K., HUTTER, J. A., BENNER, E. J., MOSLEY, R. L. & GENDELMAN, H. E. 2010. Regulatory T cells attenuate Th17 cell-mediated nigrostriatal dopaminergic neurodegeneration in a model of Parkinson's disease. *J Immunol,* 184**,** 2261-71.

ROBERTS, R. O., CERHAN, J. R., GEDA, Y. E., KNOPMAN, D. S., CHA, R. H., CHRISTIANSON, T. J., PANKRATZ, V. S., IVNIK, R. J., O'CONNOR, H. M. & PETERSEN, R. C. 2010. Polyunsaturated fatty acids and reduced odds of MCI: the Mayo Clinic Study of Aging. *J Alzheimers Dis,* 21**,** 853-65.

ROBERTSON, N., RAPPAS, M., DORE, A. S., BROWN, J., BOTTEGONI, G., KOGLIN, M., CANSFIELD, J., JAZAYERI, A., COOKE, R. M. & MARSHALL, F. H. 2018. Structure of the complement C5a receptor bound to the extra-helical antagonist NDT9513727. *Nature,* 553**,** 111-114.

ROE, K., GIBOT, S. & VERMA, S. 2014. Triggering receptor expressed on myeloid cells-1 (TREM-1): a new player in antiviral immunity? *Front Microbiol,* 5**,** 627.

ROGERS, J., LI, R., MASTROENI, D., GROVER, A., LEONARD, B., AHERN, G., CAO, P., KOLODY, H., VEDDERS, L., KOLB, W. P. & SABBAGH, M. 2006. Peripheral clearance of amyloid beta peptide by complement C3-dependent adherence to erythrocytes. *Neurobiol Aging,* 27**,** 1733-9.

ROGERS, J. T., LEITER, L. M., MCPHEE, J., CAHILL, C. M., ZHAN, S. S., POTTER, H. & NILSSON, L. N. 1999. Translation of the alzheimer amyloid precursor protein mRNA is up-regulated by interleukin-1 through 5'-untranslated region sequences. *J Biol Chem,* 274**,** 6421-31.

ROGERS, J. T., RANDALL, J. D., CAHILL, C. M., EDER, P. S., HUANG, X., GUNSHIN, H., LEITER, L., MCPHEE, J., SARANG, S. S., UTSUKI, T., GREIG, N. H., LAHIRI, D. K., TANZI, R. E., BUSH, A. I., GIORDANO, T. & GULLANS, S. R. 2002. An iron-responsive element type II in the 5'-untranslated region of the Alzheimer's amyloid precursor protein transcript. *J Biol Chem,* 277**,** 45518-28.

ROHN, T. T. 2013. The triggering receptor expressed on myeloid cells 2: "TREM-ming" the inflammatory component associated with Alzheimer's disease. *Oxid Med Cell Longev,* 2013**,** 860959.

ROHN, T. T., KOKOULINA, P., EATON, C. R. & POON, W. W. 2009. Caspase activation in transgenic mice with Alzheimer-like pathology: results from a pilot study utilizing the caspase inhibitor, Q-VD-OPh. *Int J Clin Exp Med,* 2**,** 300-8.

ROSSI, S., MOTTA, C., STUDER, V., MACCHIARULO, G., VOLPE, E., BARBIERI, F., RUOCCO, G., BUTTARI, F., FINARDI, A., MANCINO, R., WEISS, S., BATTISTINI, L., MARTINO, G., FURLAN, R., DRULOVIC, J. & CENTONZE, D. 2014. Interleukin-1beta causes excitotoxic neurodegeneration and multiple sclerosis disease progression by activating the apoptotic protein p53. *Mol Neurodegener,* 9**,** 56.

ROUSSOS, P., KATSEL, P., FAM, P., TAN, W., PUROHIT, D. P. & HAROUTUNIAN, V. 2015. The triggering receptor expressed on myeloid cells 2 (TREM2) is associated with enhanced inflammation, neuropathological lesions and increased risk for Alzheimer's dementia. *Alzheimers Dement,* 11**,** 1163-70.

ROVIO, S., KAREHOLT, I., HELKALA, E. L., VIITANEN, M., WINBLAD, B., TUOMILEHTO, J., SOININEN, H., NISSINEN, A. & KIVIPELTO, M. 2005. Leisure-time physical activity at midlife and the risk of dementia and Alzheimer's disease. *Lancet Neurol,* 4**,** 705-11.

RYU, J. K. & MCLARNON, J. G. 2009. A leaky blood-brain barrier, fibrinogen infiltration and microglial reactivity in inflamed Alzheimer's disease brain. *J Cell Mol Med,* 13**,** 2911-25.

SAFAIYAN, S., KANNAIYAN, N., SNAIDERO, N., BRIOSCHI, S., BIBER, K., YONA, S., EDINGER, A. L., JUNG, S., ROSSNER, M. J. & SIMONS, M. 2016. Age-related myelin degradation burdens the clearance function of microglia during aging. *Nat Neurosci,* 19**,** 995-8.

SAKARAM, S., CRAIG, M. P., HILL, N. T., ALJAGTHMI, A., GARRIDO, C., PALIY, O., BOTTOMLEY, M., RAYMER, M. & KADAKIA, M. P. 2018. Identification of novel DeltaNp63alpha-regulated miRNAs using an optimized small RNA-Seq analysis pipeline. *Sci Rep,* 8**,** 10069.

SALEH-GOHARI, N. & HELLEDAY, T. 2004. Conservative homologous recombination preferentially repairs DNA double-strand breaks in the S phase of the cell cycle in human cells. *Nucleic Acids Res,* 32**,** 3683-8.

SALMINEN, A., OJALA, J., KAUPPINEN, A., KAARNIRANTA, K. & SUURONEN, T. 2009. Inflammation in Alzheimer's disease: amyloid-beta oligomers trigger innate immunity defence via pattern recognition receptors. *Prog Neurobiol,* 87**,** 181-94.

SALSMAN, J. & DELLAIRE, G. 2017. Precision genome editing in the CRISPR era. *Biochem Cell Biol,* 95**,** 187-201.

SANDER, J. D. & JOUNG, J. K. 2014. CRISPR-Cas systems for editing, regulating and targeting genomes. *Nat Biotechnol,* 32**,** 347-55.

SARLUS, H. & HENEKA, M. T. 2017. Microglia in Alzheimer's disease. *J Clin Invest,* 127**,** 3240-3249.

SASAKI, Y., OHSAWA, K., KANAZAWA, H., KOHSAKA, S. & IMAI, Y. 2001. Iba1 is an actin-cross-linking protein in macrophages/microglia. *Biochem Biophys Res Commun,* 286**,** 292-7.

SASSI, C., NALLS, M. A., RIDGE, P. G., GIBBS, J. R., DING, J., LUPTON, M. K., TROAKES, C., LUNNON, K., AL-SARRAJ, S., BROWN, K. S., MEDWAY, C., CLEMENT, N., LORD, J., TURTON, J., BRAS, J., ALMEIDA, M. R., CONSORTIUM, A., HOLSTEGE, H., LOUWERSHEIMER, E., VAN DER FLIER, W. M., SCHELTENS, P., VAN SWIETEN, J. C., SANTANA, I., OLIVEIRA, C., MORGAN, K., POWELL, J. F., KAUWE, J. S., CRUCHAGA, C., GOATE, A. M., SINGLETON, A. B., GUERREIRO, R. & HARDY, J. 2016. ABCA7 p.G215S as potential protective factor for Alzheimer's disease. *Neurobiol Aging,* 46**,** 235 e1-9.

SCHAFFER, C., SARAD, N., DECRUMPE, A., GOSWAMI, D., HERRMANN, S., MORALES, J., PATEL, P. & OSBORNE, J. 2015. Biomarkers in the Diagnosis and Prognosis of Alzheimer's Disease. *J Lab Autom,* 20**,** 589-600.

SCHARF, I., BIERBAUMER, L., HUBER, H., WITTMANN, P., HAIDER, C., PIRKER, C., BERGER, W. & MIKULITS, W. 2018. Dynamics of CRISPR/Cas9-mediated genomic editing of the AXL locus in hepatocellular carcinoma cells. *Oncol Lett,* 15**,** 2441-2450.

SCHLIWA, M. 1982. Action of cytochalasin D on cytoskeletal networks. *J Cell Biol,* 92**,** 79-91.

SCHMID, C. D., SAUTKULIS, L. N., DANIELSON, P. E., COOPER, J., HASEL, K. W., HILBUSH, B. S., SUTCLIFFE, J. G. & CARSON, M. J. 2002. Heterogeneous expression of the triggering receptor expressed on myeloid cells-2 on adult murine microglia. *J Neurochem,* 83**,** 1309-20.

SCHNELLER, J. L., LEE, C. M., BAO, G. & VENDITTI, C. P. 2017. Genome editing for inborn errors of metabolism: advancing towards the clinic. *BMC Med,* 15**,** 43.

SCHULTZE, J. L., FREEMAN, T., HUME, D. A. & LATZ, E. 2015. A transcriptional perspective on human macrophage biology. *Semin Immunol,* 27**,** 44-50.

SELKOE, D. J. 1991. The molecular pathology of Alzheimer's disease. *Neuron,* 6**,** 487-98.

SELKOE, D. J. 1994. Alzheimer's disease: a central role for amyloid. *J Neuropathol Exp Neurol,* 53**,** 438-47.

SELKOE, D. J. 2001. Alzheimer's disease: genes, proteins, and therapy. *Physiol Rev,* 81**,** 741-66.

SELKOE, D. J. 2002. Alzheimer's disease is a synaptic failure. *Science,* 298**,** 789-91.

SEPEHRY, A. A., LANG, D., HSIUNG, G. Y. & RAUSCHER, A. 2016. Prevalence of Brain Microbleeds in Alzheimer Disease: A Systematic Review and Meta-Analysis on the Influence of Neuroimaging Techniques. *AJNR Am J Neuroradiol,* 37**,** 215-22.

SESHADRI, S., FITZPATRICK, A. L., IKRAM, M. A., DESTEFANO, A. L., GUDNASON, V., BOADA, M., BIS, J. C., SMITH, A. V., CARASSQUILLO, M. M., LAMBERT, J. C., HAROLD, D., SCHRIJVERS, E. M., RAMIREZ-LORCA, R., DEBETTE, S., LONGSTRETH, W. T., JR., JANSSENS, A. C., PANKRATZ, V. S., DARTIGUES, J. F., HOLLINGWORTH, P., ASPELUND, T., HERNANDEZ, I., BEISER, A., KULLER, L. H., KOUDSTAAL, P. J., DICKSON, D. W., TZOURIO, C., ABRAHAM, R., ANTUNEZ, C., DU, Y., ROTTER, J. I., AULCHENKO, Y. S., HARRIS, T. B., PETERSEN, R. C., BERR, C., OWEN, M. J., LOPEZ-ARRIETA, J., VARADARAJAN, B. N., BECKER, J. T., RIVADENEIRA, F., NALLS, M. A., GRAFF-RADFORD, N. R., CAMPION, D., AUERBACH, S., RICE, K., HOFMAN, A., JONSSON, P. V., SCHMIDT,

H., LATHROP, M., MOSLEY, T. H., AU, R., PSATY, B. M., UITTERLINDEN, A. G., FARRER, L. A., LUMLEY, T., RUIZ, A., WILLIAMS, J., AMOUYEL, P., YOUNKIN, S. G., WOLF, P. A., LAUNER, L. J., LOPEZ, O. L., VAN DUIJN, C. M., BRETELER, M. M., CONSORTIUM, C., CONSORTIUM, G. & CONSORTIUM, E. 2010. Genome-wide analysis of genetic loci associated with Alzheimer disease. *JAMA,* 303**,** 1832-40.

SESSA, G., PODINI, P., MARIANI, M., MERONI, A., SPREAFICO, R., SINIGAGLIA, F., COLONNA, M., PANINA, P. & MELDOLESI, J. 2004. Distribution and signaling of TREM2/DAP12, the receptor system mutated in human polycystic lipomembraneous osteodysplasia with sclerosing leukoencephalopathy dementia. *European Journal of Neuroscience,* 20**,** 2617-2628.

SHAFTEL, S. S., GRIFFIN, W. S. & O'BANION, M. K. 2008. The role of interleukin-1 in neuroinflammation and Alzheimer disease: an evolving perspective. *J Neuroinflammation,* 5**,** 7.

SHAFTEL, S. S., KYRKANIDES, S., OLSCHOWKA, J. A., MILLER, J. N., JOHNSON, R. E. & O'BANION, M. K. 2007. Sustained hippocampal IL-1 beta overexpression mediates chronic neuroinflammation and ameliorates Alzheimer plaque pathology. *J Clin Invest,* 117**,** 1595-604.

SHARPE, J. J. & COOPER, T. A. 2017. Unexpected consequences: exon skipping caused by CRISPR-generated mutations. *Genome Biol,* 18**,** 109.

SHEN, B., ZHANG, W., ZHANG, J., ZHOU, J., WANG, J., CHEN, L., WANG, L., HODGKINS, A., IYER, V., HUANG, X. & SKARNES, W. C. 2014. Efficient genome modification by CRISPR-Cas9 nickase with minimal off-target effects. *Nat Methods,* 11**,** 399-402.

SHEN, Y., LI, R., MCGEER, E. G. & MCGEER, P. L. 1997. Neuronal expression of mRNAs for complement proteins of the classical pathway in Alzheimer brain. *Brain Res,* 769**,** 391-5.

SHEN, Y., LUE, L., YANG, L., ROHER, A., KUO, Y., STROHMEYER, R., GOUX, W. J., LEE, V., JOHNSON, G. V., WEBSTER, S. D., COOPER, N. R., BRADT, B. & ROGERS, J. 2001. Complement activation by neurofibrillary tangles in Alzheimer's disease. *Neurosci Lett,* 305**,** 165-8.

SHERRINGTON, R., ROGAEV, E. I., LIANG, Y., ROGAEVA, E. A., LEVESQUE, G., IKEDA, M., CHI, H., LIN, C., LI, G., HOLMAN, K., TSUDA, T., MAR, L., FONCIN, J. F., BRUNI, A. C., MONTESI, M. P., SORBI, S., RAINERO, I., PINESSI, L., NEE, L., CHUMAKOV, I., POLLEN, D., BROOKES, A., SANSEAU, P., POLINSKY, R. J., WASCO, W., DA SILVA, H. A., HAINES, J. L., PERKICAK-VANCE, M. A., TANZI, R. E., ROSES, A. D., FRASER, P. E., ROMMENS, J. M. & ST GEORGE-HYSLOP, P. H. 1995. Cloning of a gene bearing missense mutations in early-onset familial Alzheimer's disease. *Nature,* 375**,** 754-60.

SHIVELY, S., SCHER, A. I., PERL, D. P. & DIAZ-ARRASTIA, R. 2012. Dementia resulting from traumatic brain injury: what is the pathology? *Arch Neurol,* 69**,** 1245-51.

SHOJI, M., GOLDE, T. E., GHISO, J., CHEUNG, T. T., ESTUS, S., SHAFFER, L. M., CAI, X. D., MCKAY, D. M., TINTNER, R., FRANGIONE, B. & ET AL. 1992. Production of the Alzheimer amyloid beta protein by normal proteolytic processing. *Science,* 258**,** 126-9.

SICA, A. & MANTOVANI, A. 2012. Macrophage plasticity and polarization: in vivo veritas. *J Clin Invest,* 122**,** 787-95.

SIEBER, M. W., JAENISCH, N., BREHM, M., GUENTHER, M., LINNARTZ-GERLACH, B., NEUMANN, H., WITTE, O. W. & FRAHM, C. 2013. Attenuated inflammatory response in triggering receptor expressed on myeloid cells 2 (TREM2) knock-out mice following stroke. *PLoS One,* 8**,** e52982.

SIGOLA, L. B., FUENTES, A. L., MILLIS, L. M., VAPENIK, J. & MURIRA, A. 2016. Effects of Toll-like receptor ligands on RAW 264.7 macrophage morphology and zymosan phagocytosis. *Tissue Cell,* 48**,** 389-96.

SIMS, R., VAN DER LEE, S. J., NAJ, A. C., BELLENGUEZ, C., BADARINARAYAN, N., JAKOBSDOTTIR, J., KUNKLE, B. W., BOLAND, A., RAYBOULD, R., BIS, J. C., MARTIN, E. R., GRENIER-BOLEY, B., HEILMANN-HEIMBACH, S., CHOURAKI, V., KUZMA, A. B., SLEEGERS, K.,

VRONSKAYA, M., RUIZ, A., GRAHAM, R. R., OLASO, R., HOFFMANN, P., GROVE, M. L., VARDARAJAN, B. N., HILTUNEN, M., NOTHEN, M. M., WHITE, C. C., HAMILTON-NELSON, K. L., EPELBAUM, J., MAIER, W., CHOI, S. H., BEECHAM, G. W., DULARY, C., HERMS, S., SMITH, A. V., FUNK, C. C., DERBOIS, C., FORSTNER, A. J., AHMAD, S., LI, H., BACQ, D., HAROLD, D., SATIZABAL, C. L., VALLADARES, O., SQUASSINA, A., THOMAS, R., BRODY, J. A., QU, L., SANCHEZ-JUAN, P., MORGAN, T., WOLTERS, F. J., ZHAO, Y., GARCIA, F. S., DENNING, N., FORNAGE, M., MALAMON, J., NARANJO, M. C. D., MAJOUNIE, E., MOSLEY, T. H., DOMBROSKI, B., WALLON, D., LUPTON, M. K., DUPUIS, J., WHITEHEAD, P., FRATIGLIONI, L., MEDWAY, C., JIAN, X., MUKHERJEE, S., KELLER, L., BROWN, K., LIN, H., CANTWELL, L. B., PANZA, F., MCGUINNESS, B., MORENO-GRAU, S., BURGESS, J. D., SOLFRIZZI, V., PROITSI, P., ADAMS, H. H., ALLEN, M., SERIPA, D., PASTOR, P., CUPPLES, L. A., PRICE, N. D., HANNEQUIN, D., FRANK-GARCIA, A., LEVY, D., CHAKRABARTY, P., CAFFARRA, P., GIEGLING, I., BEISER, A. S., GIEDRAITIS, V., HAMPEL, H., GARCIA, M. E., WANG, X., LANNFELT, L., MECOCCI, P., EIRIKSDOTTIR, G., CRANE, P. K., PASQUIER, F., BOCCARDI, V., et al. 2017. Rare coding variants in PLCG2, ABI3, and TREM2 implicate microglial-mediated innate immunity in Alzheimer's disease. *Nat Genet,* 49**,** 1373-1384.

SINGH, P., SCHIMENTI, J. C. & BOLCUN-FILAS, E. 2015. A mouse geneticist's practical guide to CRISPR applications. *Genetics,* 199**,** 1-15.

SINGH, V., BRADDICK, D. & DHAR, P. K. 2017. Exploring the potential of genome editing CRISPR-Cas9 technology. *Gene,* 599**,** 1-18.

SLATTERY, C. F., BECK, J. A., HARPER, L., ADAMSON, G., ABDI, Z., UPHILL, J., CAMPBELL, T., DRUYEH, R., MAHONEY, C. J., ROHRER, J. D., KENNY, J., LOWE, J., LEUNG, K. K., BARNES, J., CLEGG, S. L., BLAIR, M., NICHOLAS, J. M., GUERREIRO, R. J., ROWE, J. B., PONTO, C., ZERR, I., KRETZSCHMAR, H., GAMBETTI, P., CRUTCH, S. J., WARREN, J. D., ROSSOR, M. N., FOX, N. C., COLLINGE, J., SCHOTT, J. M. & MEAD, S. 2014. R47H TREM2 variant increases risk of typical early-onset Alzheimer's disease but not of prion or frontotemporal dementia. *Alzheimers Dement,* 10**,** 602-608 e4.

SMITH, C., GENTLEMAN, S. M., LECLERCQ, P. D., MURRAY, L. S., GRIFFIN, W. S., GRAHAM, D. I. & NICOLL, J. A. 2013. The neuroinflammatory response in humans after traumatic brain injury. *Neuropathol Appl Neurobiol,* 39**,** 654-66.

SOLDNER, F., LAGANIERE, J., CHENG, A. W., HOCKEMEYER, D., GAO, Q., ALAGAPPAN, R., KHURANA, V., GOLBE, L. I., MYERS, R. H., LINDQUIST, S., ZHANG, L., GUSCHIN, D., FONG, L. K., VU, B. J., MENG, X., URNOV, F. D., REBAR, E. J., GREGORY, P. D., ZHANG, H. S. & JAENISCH, R. 2011. Generation of isogenic pluripotent stem cells differing exclusively at two early onset Parkinson point mutations. *Cell,* 146**,** 318-31.

SONG, W., HOOLI, B., MULLIN, K., JIN, S. C., CELLA, M., ULLAND, T. K., WANG, Y., TANZI, R. E. & COLONNA, M. 2017. Alzheimer's disease-associated TREM2 variants exhibit either decreased or increased ligand-dependent activation. *Alzheimers Dement,* 13**,** 381-387.

SRINIVASAN, K., FRIEDMAN, B. A., LARSON, J. L., LAUFFER, B. E., GOLDSTEIN, L. D., APPLING, L. L., BORNEO, J., POON, C., HO, T., CAI, F., STEINER, P., VAN DER BRUG, M. P., MODRUSAN, Z., KAMINKER, J. S. & HANSEN, D. V. 2016. Untangling the brain's neuroinflammatory and neurodegenerative transcriptional responses. *Nat Commun,* 7**,** 11295.

STERNBERG, S. H. & DOUDNA, J. A. 2015. Expanding the Biologist's Toolkit with CRISPR-Cas9. *Mol Cell,* 58**,** 568-74.

STREIT, W. J. 2005. Microglia and neuroprotection: implications for Alzheimer's disease. *Brain Res Brain Res Rev,* 48**,** 234-9.

STREIT, W. J., BRAAK, H., XUE, Q. S. & BECHMANN, I. 2009. Dystrophic (senescent) rather than activated microglial cells are associated with tau pathology and likely precede neurodegeneration in Alzheimer's disease. *Acta Neuropathol,* 118**,** 475-85.

STREIT, W. J., MRAK, R. E. & GRIFFIN, W. S. 2004. Microglia and neuroinflammation: a pathological perspective. *J Neuroinflammation,* 1**,** 14.

STROHMEYER, R., RAMIREZ, M., COLE, G. J., MUELLER, K. & ROGERS, J. 2002. Association of factor H of the alternative pathway of complement with agrin and complement receptor 3 in the Alzheimer's disease brain. *J Neuroimmunol,* 131**,** 135-46.

SUAREZ-CALVET, M., ARAQUE CABALLERO, M. A., KLEINBERGER, G., BATEMAN, R. J., FAGAN, A. M., MORRIS, J. C., LEVIN, J., DANEK, A., EWERS, M., HAASS, C. & DOMINANTLY INHERITED ALZHEIMER, N. 2016. Early changes in CSF sTREM2 in dominantly inherited Alzheimer's disease occur after amyloid deposition and neuronal injury. *Sci Transl Med,* 8**,** 369ra178.

SUH, H. S., ZHAO, M. L., DERICO, L., CHOI, N. & LEE, S. C. 2013. Insulin-like growth factor 1 and 2 (IGF1, IGF2) expression in human microglia: differential regulation by inflammatory mediators. *J Neuroinflammation,* 10**,** 37.

SWARDFAGER, W., LANCTOT, K., ROTHENBURG, L., WONG, A., CAPPELL, J. & HERRMANN, N. 2010. A meta-analysis of cytokines in Alzheimer's disease. *Biol Psychiatry,* 68**,** 930-41.

TACHIDA, Y., NAKAGAWA, K., SAITO, T., SAIDO, T. C., HONDA, T., SAITO, Y., MURAYAMA, S., ENDO, T., SAKAGUCHI, G., KATO, A., KITAZUME, S. & HASHIMOTO, Y. 2008. Interleukin-1 beta up-regulates TACE to enhance alpha-cleavage of APP in neurons: resulting decrease in Abeta production. *J Neurochem,* 104**,** 1387-93.

TAI, L. M., GHURA, S., KOSTER, K. P., LIAKAITE, V., MAIENSCHEIN-CLINE, M., KANABAR, P., COLLINS, N., BEN-AISSA, M., LEI, A. Z., BAHROOS, N., GREEN, S. J., HENDRICKSON, B., VAN ELDIK, L. J. & LADU, M. J. 2015. APOE-modulated Abeta-induced neuroinflammation in Alzheimer's disease: current landscape, novel data, and future perspective. *J Neurochem,* 133**,** 465-88.

TAKAHASHI, K., PRINZ, M., STAGI, M., CHECHNEVA, O. & NEUMANN, H. 2007. TREM2-transduced myeloid precursors mediate nervous tissue debris clearance and facilitate recovery in an animal model of multiple sclerosis. *PLoS Med,* 4**,** e124.

TAKAHASHI, K., ROCHFORD, C. D. & NEUMANN, H. 2005a. Clearance of apoptotic neurons without inflammation by microglial triggering receptor expressed on myeloid cells-2. *J Exp Med,* 201**,** 647-57.

TAKAHASHI, K., ROCHFORD, C. D. P. & NEUMANN, H. 2005b. Clearance of apoptotic neurons without inflammation by microglial triggering receptor expressed on myeloid cells-2. *Journal of Experimental Medicine,* 201**,** 647-657.

TAKATA, K., KITAMURA, Y., SAEKI, M., TERADA, M., KAGITANI, S., KITAMURA, R., FUJIKAWA, Y., MAELICKE, A., TOMIMOTO, H., TANIGUCHI, T. & SHIMOHAMA, S. 2010. Galantamine-induced amyloid-{beta} clearance mediated via stimulation of microglial nicotinic acetylcholine receptors. *J Biol Chem,* 285**,** 40180-91.

TAKEGAHARA, N., TAKAMATSU, H., TOYOFUKU, T., TSUJIMURA, T., OKUNO, T., YUKAWA, K., MIZUI, M., YAMAMOTO, M., PRASAD, D. V., SUZUKI, K., ISHII, M., TERAI, K., MORIYA, M., NAKATSUJI, Y., SAKODA, S., SATO, S., AKIRA, S., TAKEDA, K., INUI, M., TAKAI, T., IKAWA, M., OKABE, M., KUMANOGOH, A. & KIKUTANI, H. 2006. Plexin-A1 and its interaction with DAP12 in immune responses and bone homeostasis. *Nat Cell Biol,* 8**,** 615-22.

TAKEUCHI, O., HOSHINO, K., KAWAI, T., SANJO, H., TAKADA, H., OGAWA, T., TAKEDA, K. & AKIRA, S. 1999. Differential roles of TLR2 and TLR4 in recognition of gram-negative and gram-positive bacterial cell wall components. *Immunity,* 11**,** 443-51.

TANG, Y. & LE, W. 2016. Differential Roles of M1 and M2 Microglia in Neurodegenerative Diseases. *Mol Neurobiol,* 53**,** 1181-94.

TARKOWSKI, E., LILJEROTH, A. M., MINTHON, L., TARKOWSKI, A., WALLIN, A. & BLENNOW, K. 2003. Cerebral pattern of pro- and anti-inflammatory cytokines in dementias. *Brain Res Bull,* 61**,** 255-60.

TAYLOR, P. R., MARTINEZ-POMARES, L., STACEY, M., LIN, H. H., BROWN, G. D. & GORDON, S. 2005. Macrophage receptors and immune recognition. *Annu Rev Immunol,* 23**,** 901-44.

THORVALDSDOTTIR, H., ROBINSON, J. T. & MESIROV, J. P. 2013. Integrative Genomics Viewer (IGV): high-performance genomics data visualization and exploration. *Brief Bioinform,* 14**,** 178-92.

TOGO, T., AKIYAMA, H., ISEKI, E., KONDO, H., IKEDA, K., KATO, M., ODA, T., TSUCHIYA, K. & KOSAKA, K. 2002. Occurrence of T cells in the brain of Alzheimer's disease and other neurological diseases. *J Neuroimmunol,* 124**,** 83-92.

TOMASELLO, E., DESMOULINS, P. O., CHEMIN, K., GUIA, S., CREMER, H., ORTALDO, J., LOVE, P., KAISERLIAN, D. & VIVIER, E. 2000. Combined natural killer cell and dendritic cell functional deficiency in KARAP/DAP12 loss-of-function mutant mice. *Immunity,* 13**,** 355-64.

TROWSDALE, J. & KNIGHT, J. C. 2013. Major histocompatibility complex genomics and human disease. *Annu Rev Genomics Hum Genet,* 14**,** 301-23.

TURNBULL, I. R. & COLONNA, M. 2007. Activating and inhibitory functions of DAP12. *Nat Rev Immunol,* 7**,** 155-61.

TURNBULL, I. R., GILFILLAN, S., CELLA, M., AOSHI, T., MILLER, M., PICCIO, L., HERNANDEZ, M. & COLONNA, M. 2006. Cutting edge: TREM-2 attenuates macrophage activation. *J Immunol,* 177**,** 3520-4.

UJIIE, M., DICKSTEIN, D. L., CARLOW, D. A. & JEFFERIES, W. A. 2003. Blood-brain barrier permeability precedes senile plaque formation in an Alzheimer disease model. *Microcirculation,* 10**,** 463-70.

ULLAND, T. K., SONG, W. M., HUANG, S. C., ULRICH, J. D., SERGUSHICHEV, A., BEATTY, W. L., LOBODA, A. A., ZHOU, Y., CAIRNS, N. J., KAMBAL, A., LOGINICHEVA, E., GILFILLAN, S., CELLA, M., VIRGIN, H. W., UNANUE, E. R., WANG, Y., ARTYOMOV, M. N., HOLTZMAN, D. M. & COLONNA, M. 2017. TREM2 Maintains Microglial Metabolic Fitness in Alzheimer's Disease. *Cell,* 170**,** 649-663 e13.

UNITED NATIONS, DEPARTMENT OF ECONOMIC AND SOCIAL AFFAIRS, POPULATION DIVISION 2015. World Population Ageing 2015 New York.

VAN CAUWENBERGHE, C., VAN BROECKHOVEN, C. & SLEEGERS, K. 2016. The genetic landscape of Alzheimer disease: clinical implications and perspectives. *Genet Med,* 18**,** 421-30.

VAN OIJEN, M., WITTEMAN, J. C., HOFMAN, A., KOUDSTAAL, P. J. & BRETELER, M. M. 2005. Fibrinogen is associated with an increased risk of Alzheimer disease and vascular dementia. *Stroke,* 36**,** 2637-41.

VAN RIET, E., EVERTS, B., RETRA, K., PHYLIPSEN, M., VAN HELLEMOND, J. J., TIELENS, A. G., VAN DER KLEIJ, D., HARTGERS, F. C. & YAZDANBAKHSH, M. 2009. Combined TLR2 and TLR4 ligation in the context of bacterial or helminth extracts in human monocyte derived dendritic cells: molecular correlates for Th1/Th2 polarization. *BMC Immunol,* 10**,** 9.

VAREMO, L., NIELSEN, J. & NOOKAEW, I. 2013. Enriching the gene set analysis of genome-wide data by incorporating directionality of gene expression and combining statistical hypotheses and methods. *Nucleic Acids Res,* 41**,** 4378-91.

VARNUM, M. M., CLAYTON, K. A., YOSHII-KITAHARA, A., YONEMOTO, G., KORO, L., IKEZU, S. & IKEZU, T. 2017. A split-luciferase complementation, real-time reporting assay enables monitoring of the disease-associated transmembrane protein TREM2 in live cells. *Journal of Biological Chemistry,* 292**,** 10651-10663.

VIGGARS, A. P., WHARTON, S. B., SIMPSON, J. E., MATTHEWS, F. E., BRAYNE, C., SAVVA, G. M., GARWOOD, C., DREW, D., SHAW, P. J. & INCE, P. G. 2011. Alterations in the blood brain barrier in ageing cerebral cortex in relationship to Alzheimer-type pathology: a study in the MRC-CFAS population neuropathology cohort. *Neurosci Lett,* 505**,** 25-30.

VITEK, M. P., BROWN, C. M. & COLTON, C. A. 2009. APOE genotype-specific differences in the innate immune response. *Neurobiol Aging,* 30**,** 1350-60.

VODOVOTZ, Y., LUCIA, M. S., FLANDERS, K. C., CHESLER, L., XIE, Q. W., SMITH, T. W., WEIDNER, J., MUMFORD, R., WEBBER, R., NATHAN, C., ROBERTS, A. B., LIPPA, C. F. & SPORN, M. B. 1996. Inducible nitric oxide synthase in tangle-bearing neurons of patients with Alzheimer's disease. *J Exp Med,* 184**,** 1425-33.

VUOLTEENAHO, K., KOSKINEN, A., KUKKONEN, M., NIEMINEN, R., PAIVARINTA, U., MOILANEN, T. & MOILANEN, E. 2009. Leptin enhances synthesis of proinflammatory mediators in human osteoarthritic cartilage--mediator role of NO in leptin-induced PGE2, IL-6, and IL-8 production. *Mediators Inflamm,* 2009**,** 345838.

WALKER, D. G., LINK, J., LUE, L. F., DALSING-HERNANDEZ, J. E. & BOYES, B. E. 2006. Gene expression changes by amyloid beta peptide-stimulated human postmortem brain microglia identify activation of multiple inflammatory processes. *J Leukoc Biol,* 79**,** 596-610.

WALTER, J. 2016. The Triggering Receptor Expressed on Myeloid Cells 2: A Molecular Link of Neuroinflammation and Neurodegenerative Diseases. *J Biol Chem,* 291**,** 4334-41.

WANG, H., ANDERSON, L. G., LASCOLA, C. D., JAMES, M. L., VENKATRAMAN, T. N., BENNETT, E. R., ACHESON, S. K., VITEK, M. P. & LASKOWITZ, D. T. 2013. ApolipoproteinE mimetic peptides improve outcome after focal ischemia. *Exp Neurol,* 241**,** 67-74.

WANG, J., YANG, C., ZHAO, Q., ZHU, Z., LI, Y. & YANG, P. 2017. Microglia activation induced by serum of SLE patients. *J Neuroimmunol,* 310**,** 135-142.

WANG, J., YU, J. T. & TAN, L. 2015a. PLD3 in Alzheimer's disease. *Mol Neurobiol,* 51**,** 480-6.

WANG, R. & REDDY, P. H. 2017. Role of Glutamate and NMDA Receptors in Alzheimer's Disease. *J Alzheimers Dis,* 57**,** 1041-1048.

WANG, W. Y., TAN, M. S., YU, J. T. & TAN, L. 2015b. Role of pro-inflammatory cytokines released from microglia in Alzheimer's disease. *Ann Transl Med,* 3**,** 136.

WANG, X. Q., TAO, B. B., LI, B., WANG, X. H., ZHANG, W. C., WAN, L., HUA, X. M. & LI, S. T. 2016a. Overexpression of TREM2 enhances glioma cell proliferation and invasion: a therapeutic target in human glioma. *Oncotarget,* 7**,** 2354-2366.

WANG, Y., CELLA, M., MALLINSON, K., ULRICH, J. D., YOUNG, K. L., ROBINETTE, M. L., GILFILLAN, S., KRISHNAN, G. M., SUDHAKAR, S., ZINSELMEYER, B. H., HOLTZMAN, D. M., CIRRITO, J. R. & COLONNA, M. 2015c. TREM2 lipid sensing sustains the microglial response in an Alzheimer's disease model. *Cell,* 160**,** 1061-71.

WANG, Y., JIN, S., SONOBE, Y., CHENG, Y., HORIUCHI, H., PARAJULI, B., KAWANOKUCHI, J., MIZUNO, T., TAKEUCHI, H. & SUZUMURA, A. 2014. Interleukin-1beta induces blood-brain barrier disruption by downregulating Sonic hedgehog in astrocytes. *PLoS One,* 9**,** e110024.

WANG, Y., ULLAND, T. K., ULRICH, J. D., SONG, W., TZAFERIS, J. A., HOLE, J. T., YUAN, P., MAHAN, T. E., SHI, Y., GILFILLAN, S., CELLA, M., GRUTZENDLER, J., DEMATTOS, R. B., CIRRITO, J. R., HOLTZMAN, D. M. & COLONNA, M. 2016b. TREM2-mediated early microglial response limits diffusion and toxicity of amyloid plaques. *J Exp Med,* 213**,** 667-75.

WERRING, D. J., GREGOIRE, S. M. & CIPOLOTTI, L. 2010. Cerebral microbleeds and vascular cognitive impairment. *J Neurol Sci,* 299**,** 131-5.

WES, P. D., SAYED, F. A., BARD, F. & GAN, L. 2016. Targeting microglia for the treatment of Alzheimer's Disease. *Glia,* 64**,** 1710-32.

WHITEHOUSE, P. J., PRICE, D. L., CLARK, A. W., COYLE, J. T. & DELONG, M. R. 1981. Alzheimer disease: evidence for selective loss of cholinergic neurons in the nucleus basalis. *Ann Neurol,* 10**,** 122-6.

WILCOCK, D. M., ZHAO, Q., MORGAN, D., GORDON, M. N., EVERHART, A., WILSON, J. G., LEE, J. E. & COLTON, C. A. 2011. Diverse inflammatory responses in transgenic mouse models of Alzheimer's disease and the effect of immunotherapy on these responses. *ASN Neuro,* 3**,** 249-58.

WILKINSON, K. & EL KHOURY, J. 2012. Microglial scavenger receptors and their roles in the pathogenesis of Alzheimer's disease. *Int J Alzheimers Dis,* 2012**,** 489456.

WILLIAMS, K. 1997. Interactions of polyamines with ion channels. *Biochem J,* 325 (Pt 2)**,** 289-97.

WIMO, A., JONSSON, L., BOND, J., PRINCE, M., WINBLAD, B. & ALZHEIMER DISEASE, I. 2013. The worldwide economic impact of dementia 2010. *Alzheimers Dement,* 9**,** 1-11 e3.

WONG, T. P., DEBEIR, T., DUFF, K. & CUELLO, A. C. 1999. Reorganization of cholinergic terminals in the cerebral cortex and hippocampus in transgenic mice carrying mutated presenilin-1 and amyloid precursor protein transgenes. *J Neurosci,* 19**,** 2706-16.

WOODRUFF, T. M., NANDAKUMAR, K. S. & TEDESCO, F. 2011. Inhibiting the C5-C5a receptor axis. *Mol Immunol,* 48**,** 1631-42.

WU, K., BYERS, D. E., JIN, X., AGAPOV, E., ALEXANDER-BRETT, J., PATEL, A. C., CELLA, M., GILFILAN, S., COLONNA, M., KOBER, D. L., BRETT, T. J. & HOLTZMAN, M. J. 2015a. TREM-2 promotes macrophage survival and lung disease after respiratory viral infection. *J Exp Med,* 212**,** 681-97.

WU, K., BYERS, D. E., JIN, X. H., AGAPOV, E., ALEXANDER-BRETT, J., PATEL, A. C., CELLA, M., GILFILAN, S., COLONNA, M., KOBER, D. L., BRETT, T. J. & HOLTZMAN, M. J. 2015b. TREM-2 promotes macrophage survival and lung disease after respiratory viral infection. *Journal of Experimental Medicine,* 212**,** 681-697.

WUNDERLICH, P., GLEBOV, K., KEMMERLING, N., TIEN, N. T., NEUMANN, H. & WALTER, J. 2013. Sequential proteolytic processing of the triggering receptor expressed on myeloid cells-2 (TREM2) protein by ectodomain shedding and gamma-secretase-dependent intramembranous cleavage. *J Biol Chem,* 288**,** 33027-36.

WYSS-CORAY, T. 2006. Inflammation in Alzheimer disease: driving force, bystander or beneficial response? *Nat Med,* 12**,** 1005-15.

WYSS-CORAY, T., LOIKE, J. D., BRIONNE, T. C., LU, E., ANANKOV, R., YAN, F., SILVERSTEIN, S. C. & HUSEMANN, J. 2003. Adult mouse astrocytes degrade amyloid-beta in vitro and in situ. *Nat Med,* 9**,** 453-7.

XIA, M. Q., QIN, S. X., WU, L. J., MACKAY, C. R. & HYMAN, B. T. 1998. Immunohistochemical study of the beta-chemokine receptors CCR3 and CCR5 and their ligands in normal and Alzheimer's disease brains. *Am J Pathol,* 153**,** 31-7.

XIANG, X., WERNER, G., BOHRMANN, B., LIESZ, A., MAZAHERI, F., CAPELL, A., FEEDERLE, R., KNUESEL, I., KLEINBERGER, G. & HAASS, C. 2016a. TREM2 deficiency reduces the efficacy of immunotherapeutic amyloid clearance. *EMBO Mol Med,* 8**,** 992-1004.

XIANG, X. Y., WERNER, G., BOHRMANN, B., LIESZ, A., MAZAHERI, F., CAPELL, A., FEEDERLE, R., KNUESEL, I., KLEINBERGER, G. & HAASS, C. 2016b. TREM2 deficiency reduces the efficacy of immunotherapeutic amyloid clearance. *Embo Molecular Medicine,* 8**,** 992-1004.

XING, J., TITUS, A. R. & HUMPHREY, M. B. 2015. The TREM2-DAP12 signaling pathway in Nasu-Hakola disease: a molecular genetics perspective. *Res Rep Biochem,* 5**,** 89-100.

XU, G., ZHANG, H., ZHANG, S., FAN, X. & LIU, X. 2008. Plasma fibrinogen is associated with cognitive decline and risk for dementia in patients with mild cognitive impairment. *Int J Clin Pract,* 62**,** 1070-5.

XUE, J., SCHMIDT, S. V., SANDER, J., DRAFFEHN, A., KREBS, W., QUESTER, I., DE NARDO, D., GOHEL, T. D., EMDE, M., SCHMIDLEITHNER, L., GANESAN, H., NINO-CASTRO, A., MALLMANN, M. R., LABZIN, L., THEIS, H., KRAUT, M., BEYER, M., LATZ, E., FREEMAN, T. C., ULAS, T. & SCHULTZE, J. L. 2014. Transcriptome-based network analysis reveals a spectrum model of human macrophage activation. *Immunity,* 40**,** 274-88.

YAN, S. D., CHEN, X., FU, J., CHEN, M., ZHU, H., ROHER, A., SLATTERY, T., ZHAO, L., NAGASHIMA, M., MORSER, J., MIGHELI, A., NAWROTH, P., STERN, D. & SCHMIDT, A. M. 1996. RAGE and amyloid-beta peptide neurotoxicity in Alzheimer's disease. *Nature,* 382**,** 685-91.

YANG, H., YANG, H., XIE, Z., WEI, L. & BI, J. 2013. Systemic transplantation of human umbilical cord derived mesenchymal stem cells-educated T regulatory cells improved the impaired cognition in AbetaPPswe/PS1dE9 transgenic mice. *PLoS One,* 8**,** e69129.

YAO, L., KAN, E. M., LU, J., HAO, A., DHEEN, S. T., KAUR, C. & LING, E. A. 2013. Toll-like receptor 4 mediates microglial activation and production of inflammatory mediators in neonatal rat brain following hypoxia: role of TLR4 in hypoxic microglia. *J Neuroinflammation,* 10**,** 23.

YE, S. M. & JOHNSON, R. W. 2001. An age-related decline in interleukin-10 may contribute to the increased expression of interleukin-6 in brain of aged mice. *Neuroimmunomodulation,* 9**,** 183-92.

YEH, F. L., HANSEN, D. V. & SHENG, M. 2017. TREM2, Microglia, and Neurodegenerative Diseases. *Trends Mol Med,* 23**,** 512-533.

YEH, F. L., WANG, Y., TOM, I., GONZALEZ, L. C. & SHENG, M. 2016. TREM2 Binds to Apolipoproteins, Including APOE and CLU/APOJ, and Thereby Facilitates Uptake of Amyloid-Beta by Microglia. *Neuron,* 91**,** 328-40.

YU, X., LIANG, X., XIE, H., KUMAR, S., RAVINDER, N., POTTER, J., DE MOLLERAT DU JEU, X. & CHESNUT, J. D. 2016. Improved delivery of Cas9 protein/gRNA complexes using lipofectamine CRISPRMAX. *Biotechnol Lett,* 38**,** 919-29.

YUAN, P., CONDELLO, C., KEENE, C. D., WANG, Y., BIRD, T. D., PAUL, S. M., LUO, W., COLONNA, M., BADDELEY, D. & GRUTZENDLER, J. 2016. TREM2 Haplodeficiency in Mice and Humans Impairs the Microglia Barrier Function Leading to Decreased Amyloid Compaction and Severe Axonal Dystrophy. *Neuron,* 92**,** 252-264.

ZHANG, Y., CHEN, K., SLOAN, S. A., BENNETT, M. L., SCHOLZE, A. R., O'KEEFFE, S., PHATNANI, H. P., GUARNIERI, P., CANEDA, C., RUDERISCH, N., DENG, S., LIDDELOW, S. A., ZHANG, C., DANEMAN, R., MANIATIS, T., BARRES, B. A. & WU, J. Q. 2014. An RNA-sequencing transcriptome and splicing database of glia, neurons, and vascular cells of the cerebral cortex. *J Neurosci,* 34**,** 11929-47.

ZHAO, M., CRIBBS, D. H., ANDERSON, A. J., CUMMINGS, B. J., SU, J. H., WASSERMAN, A. J. & COTMAN, C. W. 2003. The induction of the TNFalpha death domain signaling pathway in Alzheimer's disease brain. *Neurochem Res,* 28**,** 307-18.

ZHAO, S., FUNG-LEUNG, W. P., BITTNER, A., NGO, K. & LIU, X. 2014. Comparison of RNA-Seq and microarray in transcriptome profiling of activated T cells. *PLoS One,* 9**,** e78644.

ZHAO, W., XIE, W., XIAO, Q., BEERS, D. R. & APPEL, S. H. 2006. Protective effects of an anti-inflammatory cytokine, interleukin-4, on motoneuron toxicity induced by activated microglia. *J Neurochem,* 99**,** 1176-87.

ZHAO, Y., WU, X., LI, X., JIANG, L. L., GUI, X., LIU, Y., SUN, Y., ZHU, B., PINA-CRESPO, J. C., ZHANG, M., ZHANG, N., CHEN, X., BU, G., AN, Z., HUANG, T. Y. & XU, H. 2018. TREM2 Is a Receptor for beta-Amyloid that Mediates Microglial Function. *Neuron,* 97**,** 1023-1031 e7.

ZHENG, H., LIU, C. C., ATAGI, Y., CHEN, X. F., JIA, L., YANG, L., HE, W., ZHANG, X., KANG, S. S., ROSENBERRY, T. L., FRYER, J. D., ZHANG, Y. W., XU, H. & BU, G. 2016. Opposing roles of the triggering receptor expressed on myeloid cells 2 and triggering receptor expressed on myeloid cells-like transcript 2 in microglia activation. *Neurobiol Aging,* 42**,** 132-41.

ZHONG, L., CHEN, X. F., ZHANG, Z. L., WANG, Z., SHI, X. Z., XU, K., ZHANG, Y. W., XU, H. & BU, G. 2015. DAP12 Stabilizes the C-terminal Fragment of the Triggering Receptor Expressed on Myeloid Cells-2 (TREM2) and Protects against LPS-induced Pro-inflammatory Response. *J Biol Chem,* 290**,** 15866-77.

ZHOU, K., ZHONG, Q., WANG, Y. C., XIONG, X. Y., MENG, Z. Y., ZHAO, T., ZHU, W. Y., LIAO, M. F., WU, L. R., YANG, Y. R., LIU, J., DUAN, C. M., LI, J., GONG, Q. W., LIU, L., YANG, M. H., XIONG, A., WANG, J. & YANG, Q. W. 2017. Regulatory T cells ameliorate intracerebral hemorrhage-induced inflammatory injury by modulating microglia/macrophage polarization through the IL-10/GSK3beta/PTEN axis. *J Cereb Blood Flow Metab,* 37**,** 967-979.

ZHOU, X., SPITTAU, B. & KRIEGLSTEIN, K. 2012. TGFbeta signalling plays an important role in IL4-induced alternative activation of microglia. *J Neuroinflammation,* 9**,** 210.

ZUCCOLO, J., BAU, J., CHILDS, S. J., GOSS, G. G., SENSEN, C. W. & DEANS, J. P. 2010. Phylogenetic analysis of the MS4A and TMEM176 gene families. *PLoS One,* 5**,** e9369.